LASER SPECTROSCOPY OF ALKALINE EARTH OXIDE FLAMES AND DEPERTURBATION OF DIATOMIC MOLECULAR SPECTRA

by

Richard Alan Gottscho
B.S. The Pennsylvania State University
(1974)

SUBMITTED IN PARTIAL FULFILLMENT
OF THE REQUIREMENTS FOR THE
DEGREE OF
DOCTOR OF PHILOSOPHY

at the

MASSACHUSETTS INSTITUTE OF TECHNOLOGY
(February, 1979)

Signature of the Author . . . . . Signature redacted
Department of Chemistry
February 8, 1979

Certified by. . . . . Signature redacted
Thesis Supervisor

Accepted by . . . . . Signature redacted
Departmental Committee on
Graduate Students

This Doctoral Thesis has been examined by a Committee of the Department of Chemistry as follows:

Professor Robert Silbey — Signature redacted
Chairman of Thesis Committee

Professor James Kinsey — Signature redacted

Professor Robert Field — Signature redacted
Thesis Supervisor

LASER SPECTROSCOPY OF ALKALINE EARTH OXIDE FLAMES AND DEPERTURBATION OF DIATOMIC MOLECULAR SPECTRA

by

Richard Alan Gottscho

Submitted to the Department of Chemistry on February 8, 1979, in partial fulfillment of the requirements for the Degree of Doctor of Philosophy.

ABSTRACT

Optical-optical double resonance (OODR) spectroscopy using two tunable dye lasers is used to systematically analyze the high lying and low lying electronic states of BaO. Three new electronic states - $D^1\Sigma^+$, $E^1\Sigma^+$, and $a^3\Sigma^+$ - are observed directly for the first time. Numerous perturbations are observed in both high lying and low lying states. a $^3\Sigma^+$ is shown to be the lowest excited electronic state of BaO from the vibrational dependence of $a^3\Sigma^+ \sim A'^1\Pi$ spin-orbit interaction matrix elements. Improved spectroscopic constants for every BaO electronic state except $X^1\Sigma^+$ are obtained from separate deperturbation of the low and high lying states.

$C^1\Sigma^+$-$a^3\Sigma^+$, $C^1\Sigma^+$-$b^3\Pi$, and $C^1\Sigma^+$-$A'^1\Pi$ band systems are proposed as a viable means to determine nascent populations in these metastable, reservoir BaO states.

Sub-Doppler OODR excitation spectra are used to simultaneously monitor BaO ($A^1\Sigma^+$) rotational, translational, and angular momentum orientational relaxation with Ar and CO_2 collision partners. OODR collisional satellite line widths are interpreted in terms of moments of the center of mass scattering angle. Propensities for small changes in J and small angle scattering are observed and qualitatively understood in terms of a long range, weak collision model. A cross section for $J = 1$, $M = 0 \rightarrow J = 1$, $|M| = 1$ reorientation of 4.2 ± 1.2 Å^2 is measured when BaO collides with CO_2. $J = 1 \rightarrow J = 2$ transfer is also accompanied by significant reorientation of the J vector with respect to space-fixed axes.

Ar^+ and dye laser excitation of CaO is also reported. These spectra prove unambiguously that the $a^3\Pi$ and $A'^1\Pi$ states of CaO are lower levels for at least part of the orange and green band systems.

To My Family

ACKNOWLEDGEMENTS

First of all, I thank Professor Robert Field for his generous support and encouragement during the last four and a half years. Many of the ideas expressed by this work were originally his.

Conversations with Professors James Kinsey of the Chemistry Department and David Pritchard of the Physics Department are always enlightening and have been particularly helpful in interpreting the results in Chapter 5. Working with Dr. Roger Bacis and Professor Stuart Silvers on the energy transfer experiments described in Chapters 5 and 6 was exhilarating. I am most grateful for the generous experimental assistance received from Professor John Lombardi, Phil Brucat, Jeff Manni, Mike Dulick, and Paul Weiss. Conversations with Tony Kotlar on least squares fitting were informative and I am glad he modified the fitting routine.

Conversations with Professor J. Gary Pruett, Afranio Torres-Filho, Professor Paul Dagdigian, Louise Pasternack, Jim Reuther, and Tim Brunner have been stimulating. I also thank these people for giving me results of their work prior to publication.

Carter Kittrell and Professor Robert Bernheim first introduced me to laser spectroscopy.

professor Robert Silbey will never be forgotten for his colorful quantum mechanics lectures, for which I commute his sentence to life(see C.C.Jenson, MIT, Ph.D.,1979).

While in France for two months, I was warmly entertained and educated by Drs. Hélène Lefebvre-Brion, Joëlle Rostas, Marcel Horani, Joël Schamps, Jean-Michel Robbe, Roger Bacis, Jean d'Incan, Rene Stringat and Christian Arthénour. I thank them all and hope to reciprocate repeatedly in the future.

Ray Dove and Murray Somerville are in no small way responsible for the success of these experiments by their prompt response to my pleas for help.

Without Maureen Frangioso, this thesis would not have been submitted for at least two more months. I hope that she doesn't have to type another table for at least three weeks.

Brooke Koffend is responsible for much of the deperturbation work in Chapter 3 as well as development of the home built lasers. His ever constant enthusiasm for his work has been an inspiration to me.

Ron Marks' friendship and creative wit have helped me to endure the many hours of writing. I wish him continued success on and a speedy conclusion to the CaO green and orange band analyses.

To Craig Jensen, Chief Space Cadet, and the

Rolling Stones, I am indebted for their alleviation of my states of depression and amplification of my states of mania.

Bill Browder and Isaac Asimov have the dubious distinction of being responsible for this work in that they first turned me on to science and science fiction.

Finally, I thank my family, to whom this thesis is dedicated, for their unfailing love and faith.

TABLE OF CONTENTS

TABLE OF CONTENTS (Cont.)

TABLE OF CONTENTS (Cont.)

TABLE OF CONTENTS (Cont.)

LIST OF FIGURES

LIST OF FIGURES (cont.)

List of Tables

List of Tables (cont.)

Volume I.

Chapter 1: Introduction

This thesis represents an extensive study of alkaline earth oxide structure and dynamics in low pressure flames. Specifically, BaO formed in the reaction

$$Ba + CO_2 + Ar \rightarrow BaO + CO + Ar \qquad (1.1)$$

and CaO formed by

$$Ca + N_2O + Ar \rightarrow CaO + N_2 + Ar \qquad (1.2)$$

are studied by laser spectroscopy. The results obtained include: (1) discovery of a new, low-lying, metastable electronic state of BaO, $a^3\Sigma^+$; (2) development of a spectroscopic map by which the nascent populations of low lying metastable BaO electronic states can be monitored; (3) unambiguous assignment of two lower states in the complex and controversial orange and green band systems of CaO as $A'^1\Pi$ and $a^3\Pi$; (4) simultaneous monitoring of BaO rotational and translational relaxation in BaO $\sim$ Ar and BaO $\sim$ CO_2 collisions; (5) interpretation of velocity changing collisions in terms of a simple kinematic picture whereby OODR line widths are related to moments of the center of mass scattering angle; and (6) measurements of collision induced angular momentum reorientation in low J levels of excited BaO ($A^1\Sigma^+$).

Interest in alkaline-earth oxide flames stems from the range of chemiluminescent photon yields observed

for different metal atom-oxidant combinations.[1-8] For example, at total pressures of ≈ 1 torr, photon yields for reactions of N_2O with Ca, Sr, and Ba are, respectively, 1.2%,[4] 6.6%[5], and 15%.[2] Moreover, these yields are observed to be strongly pressure dependent: in the Ba + N_2O reaction the photon yield varies from 0.2% at 3 x 10^{-3} torr to 23% at 10 torr.[2,3] The pressure dependence of these photon yields has been interpreted as evidence for a precursor to $A^1\Sigma^+ \rightarrow X^1\Sigma^+$ chemiluminescence.[3,5-7,9,10]

Although there is a consensus that a metastable, reservoir state acts as precursor to chemiluminescence, the identity of this state has been the subject of controversy: both $b^3\Pi$[3,5,6,9-11,†] and high vibrational levels of $X^1\Sigma^+$ [7,12] have been suggested. Evidence for $b^3\Pi$ comes from the observation that $A^1\Sigma^+$ vibrational levels perturbed by $b^3\Pi$ (via spin-orbit interaction) exhibit greater photon yields than do unperturbed $A^1\Sigma^+$ vibrational levels.[9,10] The primary argument invoked for $X^1\Sigma^+$ is spin-conservation: the ground states of Ba and N_2O are, respectively, ^1S and $\underset{\sim}{X}^1\Sigma^+$ so that chemical production of $b^3\Pi$ would violate the spin-conservation rule.[7,21] On the other hand, the spin-forbidden reaction

† In BaO this state has recently been renamed as $b^{3'}\Pi$ in light of the discovery of the lower lying $a^{3'}\Sigma^+$ state (Appendix 6). In all other alkaline-earth oxides it is called $a^3\Pi$.

$$Ba(^1S) + SO_2(\tilde{X}^1A) \rightarrow BaO(X^1\Sigma^+) + SO(X^3\Sigma^-), \qquad (1.3)$$

where the reaction exothermicity is insufficient to populate either the lowest BaO triplet state or the lowest SO singlet state, is found to proceed four times more rapidly than the spin-allowed reaction:[13,14]

$$Ba(^1S) + CO_2(\tilde{X}^1\Sigma^+) \rightarrow BaO(X^1\Sigma^+) + CO(X^1\Sigma^+). \qquad (1.4)$$

The role of intramolecular perturbations in efficient intersystem transfer is well established.[15-19] Perturbations arise from mixing of Born-Oppenheimer basis states and a sharing of structural properties. Thus, perturbations between $b^3\Pi$ and $A^1\Sigma^+$ result in the loss of spin as a good quantum number and intersystem transfer rates comparable to those for rotational energy transfer. It is certain therefore, that $b^3\Pi$ is a precursor to $A^1\Sigma^+$ but the question remains as to which state, $X^1\Sigma^+$ or $b^3\Pi$, is initially formed in the reaction. Recently, Reuther and Palmer have demonstrated from the vibrational dependence of $A^1\Sigma^+$ photon yields measured over a pressure range of several orders of magnitude that high vibrational levels of $X^1\Sigma^+$ are initially formed and transfer to $b^3\Pi$ occurs subsequently via $b^3\Pi \sim X^1\Sigma^+$ perturbations.[20]

The role of excited state metal reactants in these reactions has also been investigated both experimentally[21-23] and theoretically.[12,24] The reactions appear to be well

suited to the study of laser induced excited state chemistry.

The addition of CO results in production of excited, metastable metal atoms.[25,26] This reaction has been proposed as an efficient generator for atomic metastables to be used in alkali-akaline-earth excimer lasers.[27]

Spectroscopic questions relative to the chemistry discussed above are: (1) where are the low lying, energy reservoir states; (2) where do these metastable states cross and perturb $X^1\Sigma^+$ and $A^1\Sigma^+$; and (3)what is the high energy electronic structure of the alkaline-earth oxides? The first two questions are relevant to ground state reactions as shown above and the third question to excited state reactions. If the high energy structure is known, populations can be probed and the energy flow pathways established unambiguously. To an extent, these spectroscopic questions are answered for BaO by this thesis. Some of the results have already been employed by Torres-Filho and Pruett in probing populations in high vibrational levels of $X^1\Sigma^+$ and low levels of $A'^1\Pi$ and $b^3\Pi$.[28]

The technique employed to characterize both the high lying and low lying states of BaO is OODR. Appendix 5 reported the first observations of OODR excitation into

$C^1\Sigma^+$ and subsequent fluorescence into $b^3\Pi$ and $A'^1\Pi$. Appendix 6 reports the first observation of $a^3\Sigma^+$, also via OODR induced $C^1\Sigma^+$ fluorescence. Appendix 7 describes the ease with which extra lines in the OODR excitation spectrum can be recognized by virtue of their narrower power broadened line widths. The OODR technique, excitation spectra, fluorescence spectra, and the deperturbation analysis employed in characterizing all of these states is described in detail in Chapter 3.

Chapter 2 of this thesis summarizes the methods and utility of deperturbation. The principles are further illustrated in Appendices 1, 3, and 4. The computer programs as well as sample output are given in Appendix 2.

Chapter 4 presents preliminary results of Ar^+ and dye laser excitation of CaO where the orange and green band systems of this molecule are established as potential population probes for $a^3\Pi$ and $A'^1\Pi$. These bands should also permit the characterization of $a^3\Pi \sim X^1\Sigma^+$ and $A'^1\Pi \sim X^1\Sigma^+$ perturbations.

In Chapters 5 and 6 OODR is shown to be a powerful means by which energy transfer processes subsequent to chemical reaction can be monitored. Specifically, a single $A^1\Sigma^+$ rovibronic level is prepared with a narrow distribution of speeds along the laser propagation

direction as well as a specific orientation of the total angular momentum with respect to space fixed axes. Rotational,translational, and orientational relaxation is then monitored simultaneously via excitation to $C^1\Sigma^+$ while $C^1\Sigma^+ \rightarrow X^1\Sigma^+$ UV fluorescence is detected. Chapter 5 presents the rotational and translational relaxation results. The latter are interpreted in terms of moments of the center of mass scattering angle. Depolarization, or orientational relaxation,is discussed in Chapter 6.

I will state several times in this thesis that a spectroscopic assignment is straightforward (in fact, embarrassingly so). Simplicity is the virtue of double resonance laser spectroscopy.

References for Chapter 1

1. D.J. Eckstrom, S.A. Edelstein, and S.W. Benson, J. Chem. Phys. 60, 2930 (1974).
2. C.R. Jones and H.P. Broida, J. Chem. Phys. 60, 4373 (1974)
3. C.J. Hsu, W.D. Krugh, and H.B. Palmer, J. Chem. Phys. 60, 5118 (1974).
4. G.A. Capelle, C.R. Jones, J. Zorskie, and H.P. Broida, J. Chem. Phys. 61, 4777 (1974).
5. H.B. Palmer, W.D. Krugh, and C.J. Hsu, Symp. Combust., 15th, Tokyo, Japan, 1974 (1975), p. 951.
6. G.A. Capelle, H.P. Broida, and R.W. Field, J. Chem. Phys. 62, 3131 (1975).
7. D.J. Eckstrom, S.A. Edelstein, D.L. Huestis, B.E. Perry, and S.W. Benson, J. Chem. Phys. 63, 3828 (1975).
8. P.J. Dagdigian, Chem. Phys. Lett. 55, 239 (1978).
9. R.W. Field, C.R. Jones, and H.P. Broida, J. Chem. Phys. 60, 4377 (1974).
10. R.W. Field, "Long-Lived, Energetic Products of Chemical Reactions: Ba + N_2O, A Case Study", in Molecular Spectroscopy: Modern Research Volume II (Academic Press, New York, 1976), ed. N.K. Rao, p. 261.

11. R.W. Field, C.R. Jones, and H.P. Broida, J. Chem. Phys. 62, 2012 (1975).

12. D. Husain and J.R. Wiesenfeld, J. Chem. Phys. 62, 2010 (1975).

13. G.P. Smith and R.N. Zare, J. Am. Chem. Soc. 97, 1985 (1975).

14. R. Behrens, Jr., A. Freedman, R.R. Herm, and T.P. Parr, J. Am. Chem. Soc. 98, 294 (1976).

15. A.T. Wager, Phys. Rev. 64, 18 (1943).

16. H.P. Broida and S. Golden, Can. J. Chem. 38, 1666 (1960).

17. H.E. Radford and H.P. Broida, J. Chem. Phys. 38, 644 (1963).

18. W.M. Gelbart and K.F. Freed, Chem. Phys. Lett. 18, 470 (1973).

19. D. Grimbert, M. Lavollee, A. Nitzan, and A. Tramer, Chem. Phys. Lett. 57, 45 (1978).

20. J.J. Reuther and H.B. Palmer, 33rd Symposium on Molecular Spectroscopy, Ohio State University, Columbus, Ohio, 1978. Talk RF11.

21. B.G. Wicke, M.A. Revelli, and D.O. Harris, J. Chem. Phys. 63, 3120 (1975).

22. S.A. Johnson, R.W. Solarz, J.W. Dubrin, and R. Brotzmann, American Chemical Society Meeting, Anaheim, Ca., 1978.

23. L. Pasternack and P.J. Dagdigian, Chem. Phys. (in press).

24. M.H. Alexander and P.J. Dagdigian, Chem. Phys. (in press).

25. D.J. Benard, W.D. Slafer, and P.H. Lee, Chem. Phys. Lett. 43, 69 (1976).

26. D.J. Benard, W.D. Slafer, J. Hecht, and P.H. Lee, Electronic Transition Lasers II, eds. L.E. Wilson, S.N. Suchard, J.I. Steinfeld, M.I.T. Press, Cambridge, Mass., 1977, Chapter II-8.

27. D.J. Benard, P.J. Love, and W.D. Slafer, Chem. Phys. Lett. 48, 321 (1977).

28. A. Torres-Filho and J.G. Pruett, J. Chem. Phys. (in press).

29. R.W. Field, J. Chem. Phys. 60, 2400 (1974).

Chapter 2: Deperturbation of Diatomic Band Spectra

I. Introduction

The regular patterns exhibited by diatomic band spectra are often interrupted by missing, shifted and extra lines. These phenomena are collectively referred to as perturbations and result from mixing of Born-Oppenheimer basis states via interactions in the molecular Hamiltonian. These interactions can ordinarily be neglected but are significant when the energy separation between mutually interacting levels becomes comparable to the interaction matrix element.

Often, one of the interacting states is not readily observed owing to electric dipole selection rules (e.g. a low lying triplet state). Although perturbations complicate spectral analysis, they can provide a wealth of information on the structure of such dark states.

The goal of deperturbation is to express observed eigenvalues in terms of basis state properties and mixing coefficients. This allows the calculation of both static and dynamic molecular properties in both perturbed and unperturbed spectral regions. For example, intersystem crossing has been shown to proceed principally via levels which share the properties of both electronic states; the branching ratio from one state to another can be calculated from

the perturbed level mixing coefficients.[1-4]

The purpose of this chapter is to outline the techniques of deperturbation employed in Appendix 1 on the First Negative Group of N_2^+, $B^2\Sigma_u^+ - X^2\Sigma_g^+$, and in Chapter 3 on the high and low lying states of BaO. The computer programs used for these works are listed in Appendix 2 and are described below.

II. Method

The techniques of deperturbation are not new.[5-19] First, a model is chosen by selecting a basis set of electronic states and then by setting up the Hamiltonian matrix, whose off-diagonal elements connect different basis states and are responsible for spectroscopic perturbations. Methods for deriving the Hamiltonian can be found in Refs. 5 through 24. An excellent review of the perturbations found in diatomic molecules has been written by Lefebvre-Brion.[25] The matrix elements are expressed in terms of parameters, such as energies, rotational constants and perturbation matrix elements, which are to be least squares fitted.

Initial guesses for the parameters are made, the Hamiltonian is numerically diagonalized, and differences between eigenvalues are calculated to obtain transition frequencies. These are then compared to experimental frequencies and the parameters are varied to obtain the best fit to the data. This is the so-called direct approach to determining molecular constants.[27-30] In order to deal with small matrices and avoid computer storage problems, each band is usually fit individually and the results from each band-fit are subsequently merged in a statistically rigorous fashion by taking into account correlations

between different parameters.[26,31,32,†]

Although this method works well for unperturbed systems where all non-zero constants can be determined, deperturbation usually suffers from incomplete information on the perturbing state so that many parameters must be held fixed at estimated values. If uncertainties in these parameters and correlations with other parameters, both varied and fixed, are not considered, the merge procedure is not statistically rigorous and may fail (see Appendix 1 for further discussion).

Fixing parameters which cannot be determined by least squares adjustment is essential in obtaining fitted parameters which are physically significantly. For example, if one spin component of a $^2\Pi$ state perturbs a $^2\Sigma^+$ state with larger rotational constant,but the other component lies below the $^2\Sigma^+$ origin and does not perturb $^2\Sigma^+$ significantly, the $^2\Pi$ spin-orbit constant, A_Π, cannot be determined. However, if A_Π is fixed at zero, the energy obtained for the $^2\Pi$ level will be incorrect by an amount comparable to A_Π. Generally, it is useful to calculate and fix perturbation matrix elements which cannot be determined in order to

---

†An alternative to band by band fitting is to fit all bands simultaneously. Athénour has developed an algorithm for this global fit approach which does not used a prohibitive amount of computer storage.[33]

obtain physically significant rotational and centrifugal distortion constants.

After preliminary fits to the data, energies and rotational constants are obtained which are used to construct a Rydberg Klein Rees (RKR)[34] potential energy curve which is in turn used to calculate second order perturbation parameters,centrifugal distortion constants, and correct initial guesses for fixed interaction matrix elements (see below, Appendix 1, and Refs. 35-37). The above procedure is repeated until self-consistency is attained.

Two criteria are used to define complete deperturbation: (1) observed minus calculated transition frequencies must be random and comparable to experimental error and (2) perturbation matrix elements and second-order constants such as centrifugal distortion must be internally consistent. When the data are fit band by band, as opposed to a global fit of all bands simultaneously, an additional criterion for complete deperturbation is employed: vibrational intervals and rotational constants must decrease monotonically in a regular fashion with increasing vibrational quantum number. If these criteria are not met, either the data are systematically in error or the model Hamiltonian is incomplete.

Appendix 1 illustrates these principles in the deperturbation of the N_2^+ $B^2\Sigma_u^+ - X^2\Sigma_g^+$ band system.

III. Computer Programs

The two programs used in Appendix 1 and Chapter 3 are listed in Appendix 2. The second program consists of a main, calling routine, LSQ, and subroutines NEWFIT, DMFSD, DSINV, TRED2, TQL2, PRINT, PRINTA, PUNCH, PLOT, NAMEIT, LEVEL, SETUP, and MATRIX. NEWFIT is a non-linear least squares algorithm based on the work by Wentworth[38] and Marquardt[39] and was originally written by R. Stern and T. Bergeman with modifications made by A. Kotlar and myself. The DMFSD and DSINV routines are standard matrix inversion algorithms. TRED2 and TQL2 are matrix diagonalization routines: PRINT, PRINTA, PUNCH, and PLOT are all output subprograms.

The subroutines NAMEIT, LEVEL, SETUP, and MATRIX are unique to a specific deperturbation problem and separate routines are given for N_2^+ $B^2\Sigma_u^+ - X^2\Sigma_g^+$, BaO high lying state, and BaO low lying state deperturbation. NAMEIT simply assigns names to parameters in MATRIX. The order of these names corresponds to a code used to input the initial guesses; the parameters for each deperturbation model are listed in Appendix 2 along with their physical origin. LEVEL is a calling routine for the calculation of energy levels and transition frequencies: it first calls SETUP to calculate J independent factors in MATRIX, then calls MATRIX to calculate all non-

zero matrix elements, and then calls TRED2 and TQL2 to diagonalize MATRIX.

Sample output for a fit to the BaO $A^1\Sigma^+ - X^1\Sigma^+$ (0,0) band is given in Appendix 2. The output consists of initial, intermediate, and final parameters followed by a listing of the covariance and correlation matrices and eigenvalues and eigenvectors of the scaled curvature matrix. The latter may be used in diagnostic least squares[40] but are not used here. The observed transitions, or energies, are then compared to calculated values. Each transition is labeled by upper and lower level rotational quantum numbers, ranks, and parities; if energies are fitted, the lower level labels are set equal to zero. The rank is an energy ordering index: 1 corresponds to highest energy. Following this is a plot of the residuals and then a table of term values, beneath which mixing fractions are given. In the doublet fitting routines, fractional Π character corresponds to $^2\Pi_{3/2}$; the difference between the sum of the Σ fraction and Π fraction from unity is, therefore, the $^2\Pi_{1/2}$ fractional character. In the BaO low lying state fitter, Π character represents $^1\Pi$ and Σ character represents total Σ character. In the BaO high lying state fitter, Π character represents state #3 in the Hamiltonian, Σ character represents state #1. The specification of Σ and Π character to be

output is done in LEVEL by squaring and summing elements of the unitary matrix which diagonalizes MATRIX.

The first program in Appendix 2 is called CALC and calculates frequencies for perturbed $^2\Sigma^+$ - $^2\Sigma^+$ and $^2\Pi$ - $^2\Sigma^+$ band systems. The ground state must always be $^2\Sigma^+$. It requires subroutines MATRIX, SETUP, NAMEIT, TQL2, and TRED2 from the doublet fitter. This program was used in the deperturbation of N_2^+ $B^2\Sigma_u^+$ - $X^2\Sigma_g^+$ (Appendix 1) to aid in extending rotational analyses as well as predict positions and relative intensities (from mixing fractions) of extra lines. Sample output is included (the $B^2\Sigma_u^+$ - $X^2\Sigma_g^+$ (3,5) band) and is self-explanatory.

IV. Interpretation and use of perturbation matrix elements

Besides deperturbed energies and rotational constants which permit the construction of basis state potential energy curves, perturbation matrix elements are obtained. These can be used to determine second order constants, perturbing state absolute vibrational numberings, and an LCAO description of the molecular bonding.

These principles are illustrated in Appendices 1 and 6. In Appendix 1, N_2^+ $A^2\Pi_u \sim B^2\Sigma_u^+$ vibronic rotation-electronic and spin-orbit interaction matrix elements are factored into vibrational and electronic parts. From calculated vibrational integrals, obtained from deperturbed RKR curves, a constant electronic matrix element is obtained. The validity of this factorization is discussed in Refs. 41 and 42. These electronic factors can then be used with different calculated vibrational integrals to generate vibronic matrix elments which are otherwise indeterminate. Moreover, perturbation sums can be evaluated in the calculation of second order constants. For example, the N_2^+ $B^2\Sigma_u^+$ spin-rotation constant, γ, for a given vibrational level is calculable from second-order spin-orbit interactions with all $A^2\Pi_u$ vibrational levels

not included in the deperturbation model Hamiltonian (see Appendix 1). Agreement between calculated and fitted second order constants is used as a criterion for complete deperturbation.

More importantly, factorization of perturbation matrix elements has been used to determine absolute vibrational numberings for perturbing states[18,43] (Appendix 6). When the absolute numbering is unknown, deperturbed energies and rotational constants yield a family of potential energy curves, corresponding to different v numberings, with different fundamental vibrational frequencies and internuclear distances. However, vibrational integrals between mutually interacting states are generally different for each member of the family of perturbing state curves. By choosing trial numberings, calculating vibrational factors, and then checking for constancy in the electronic factor, the correct numbering is determined.

By representing each interacting state by a molecular orbital configuration and perturbation operators by sums or products of one-electron operators, electronic perturbation matrix elements can be written in terms of one-electron integrals.[25,44,45] These principles are applied in Appendices 1, 3, and 5. One-electron molecular integrals can, in turn, be further reduced to sums of atomic one-electronic integrals by the

LCAO-MO method.[25,46-48] When the atomic integrals are known, this procedure can be inverted to obtain descriptions of the molecular orbitals in terms of atomic orbitals. In Appendix 1, for example, atomic and ionic nitrogen spin-orbit splittings are used to show that the valence $1\pi_u$ and $2\sigma_u$ orbitals are comprised of ≈ 100% and ≈ 33% 2p atomic orbital character, respectively. When electronic perturbation matrix elements are unknown, these semi-empirical techniques provide the experimentalist with crucial estimates of interaction matrix elements and spin-orbit constants with which he can begin to analyze a perturbed spectrum.

Finally, the importance of ab initio calculations in deperturbation is noted. Ab initio calculations are not only an alternative to semi-empirical estimates but more importantly provide estimates of parameters where semi-empirical estimates do not exist or are expected to be unreliable. These principles are exemplified in Refs. 41,49 through 54 and in Appendix 4. For example, Λ-doubling in CH was calculated ab initio by Hammersley and Richards to within 1% of experimental values and is in better agreement with the astronomical value than are terrestrial experimental values.[50]

V. Conclusion

In summary, deperturbation yields a characterization of band spectra in terms of a physically meaningful model which in turn may be used to calculate a variety of molecular properties as well as extend band analyses. This should be contrasted with the fitting of spectroscopic data to an arbitrary model which can merely result in reproduction of the experimental data and has no useful predictive power.

References for Chapter 2

1. A.T. Wager, Phys. Rev. 64, 18 (1943).
2. H.P. Broida and S. Golden, Can. J. Chem. 38, 1666 (1960).
3. H.E. Radford and H.P. Broida, J. Chem. Phys. 38, 644 (1963).
4. W.M. Gelbart and K.F. Freed, Chem. Phys. Lett. 18, 470 (1973).
5. A. Lagerqvist and E. Miescher, Helv. Phys. Acta 31, 221 (1958).
6. P. Felenbok and H. Lefebvre-Brion, Can. J. Phys. 44, 1677 (1965).
7. A. Lagerqvist and E. Miescher, Can. J. Phys. 44, 1525-1539 (1966).
8. H. Lefebvre-Brion, Can. J. Phys. 47, 541 (1969).
9. K. Dressler, Can. J. Phys. 47, 547 (1969).
10. R.W. Field and T.H. Bergeman, J. Chem. Phys. 54, 2936 (1971).
11. a) M. Leoni and K. Dressler, J. Appl. Math. Phys. 22, 794 (1971).
    b) E. Bartholdi, M. Leoni, and K. Dressler, J. Appl. Math. Phys. 22, 797 (1971).
12. M. Leoni and K. Dressler, Helv. Phys. Acta 45, 959 (1972).

13. R.W. Field, S.G. Tilford, R.A. Howard, and J.D. Simmons; J. Mol. Spectrosc. 44, 347 (1972).

14. R.W. Field, B.G. Wicke, J.D. Simmons, and S.G. Tilford, J. Mol. Spectrosc. 44, 383 (1972).

15. R.W. Martin and A.J. Merer, Can. J. Phys. 51, 125 (1973).

16. A.J. Merer, D.N. Malm, R.W. Martin, M. Horani, and J. Rostas, Can. J. Phys. 53, 251 (1975).

17. D. Cossart and T. Bergeman, J. Chem. Phys. 65, 5462 (1976).

18. R.W. Field, A. Lagerqvist, and I. Renhorn, Phys. Scripta 14, 298 (1976).

19. D. Cossart, M. Horani, and J. Rostas, J. Mol. Spectrosc. 67, 283 (1977).

20. K.F. Freed, J. Chem. Phys. 45, 4214 (1966).

21. I. Kovács, Rotational Structure in the Spectra of Diatomic Molecules (American Elsevier, New York, 1969).

22. J.T. Hougen, Natl. Bureau Stand. U.S. Monogr. 115 (1970).

23. T.E.H. Walker, Mol. Phys. 23, 489 (1972).

24. L. Klynning, "Multiplet Structure of Spectra of Diatomic Molecules", in Atoms, Molecules, and Lasers, International Atomic Energy Agency (Vienna, 1974), p. 449.

25. H. Lefebvre-Brion, "Perturbations in the Spectra of Diatomic Molecules" in Atoms, Molecules, and Lasers, International Atomic Energy Agency (Vienna, 1974), p. 411.

26. For a review see, D.L. Albritton, A.L. Schmeltekopf, and R.N. Zare, "An introduction to the least-squares fitting of spectroscopic data" in Modern Spectroscopy, Modern Research II (K. Narahari Rao, Ed.) pp. 1-67, Academic Press, New York, 1976.

27. R.N. Zare, A.L. Schmeltekopf, W.J.Harrop, and D.L. Albritton; J. Mol. Spectrosc. 46, 37-66 (1973).

28. D.L. Albritton, W.J.Harrop, and A.L. Schmeltekopf, R.N. Zare, and E.L. Crow, J. Mol. Spectrosc. 46, 67 (1973).

29. D.L. Albritton, W.J.Harrop, and A.L. Schmeltekopf, and R.N. Zare, J. Mol. Spectrosc. 46, 103 (1973).

30. J.A. Coxon, J. Mol. Spectrosc. 58, 1 (1975).

31. D.L. Albritton, A.L. Schmeltekopf, and R.N. Zare; J. Mol. Spectrosc. 67, 132 (1977).

32. D.L. Albritton, A.L. Schmeltekopf, W.J.Harrop, R.N. Zare, and J. Czarny, J. Mol. Spectrosc. 67, 157 (1977).

33. C. Athénour, Ph.D. thesis, University of Nice, France, 1975.

34. R. Rydberg, Z. Physik 73, 376 (1931); 80, 514 (1933); O. Klein, Z. Physik 76, 226 (1932); and A.L.G. Rees, Proc. Phys. Soc. 59, 998 (1947).

35. D.L. Albritton, W.J. Harrop, A.L. Schmeltekopf, and R.N. Zare, J. Mol. Spectrosc. 46, 25 (1973).

36. W.M. Kosman and J. Hinze, J. Mol. Spectrosc. 56, 93 (1975).

37. J. Tellinghuisen and D.L. Albritton, J. Mol. Spectrosc. 57, 160 (1975).

38. W.E. Wentworth, J. Chem. Ed. 42, 96-103 (1965).

39. D.W. Marquardt, J. Soc. Indust. Appl. Math. 11, 431 (1963).

40. R.F. Curl, Jr., J. Comp. Phys. 6, 367 (1970).

41. J.A. Hall, J. Schamps, J.M. Robbe, and H. Lefebvre-Brion, J. Chem. Phys. 59, 3271 (1973).

42. J. Schamps, J. Quant. Spectrosc. Radiat. Transfer 17, 685 (1977).

43. R.W. Field, J. Chem. Phys. 60, 2400 (1974).

44. E.U. Condon and G.H. Shortley, The Theory of Atomic Spectra, Cambridge University Press, Cambridge, 1951.

45. M. Tinkham, Group Theory and Quantum Mechanics, McGraw-Hill (New York, 1964).

46. H. Lefebvre-Brion and C.M. Moser, J. Chem. Phys. 44, 2951 (1966).

47. E. Ishiguro and M. Kobori, J. Phys. Soc. Japan 22, 263 (1967).

48. S. Leach, Act. Phys. Polon. 34, 705 (1968).

49. T.E.H. Walker and W.G. Richards, Phys. Rev. 177, 100 (1969).

50. R.E. Hammersley and W.G. Richards, Nature 251, 598 (1974).

51. I.D.L. Wilson and W.G. Richards, Nature 258, 133 (1975).

52. J.A. Coxon and R.E. Hammersley, J. Mol. Spectrosc. 58, 29 (1975).

53. J.M. Robbe and J. Schamps, J. Chem. Phys. 65, 5420 (1976).

54. S. Green and R.N. Zare, J. Mol. Spectrosc. 64, 217 (1977).

Chapter 3: Optical-Optical Double Resonance Spectroscopy of BaO

I. Introduction

As discussed in Chapter 1, the spectroscopic characterization of low lying, long lived, electronic states is essential to the understanding of alkaline-earth oxide flame dynamics. This chapter describes the results of optical-optical double resonance (OODR) experiments on BaO used to detect and characterize not only $a^3\Sigma^+$, $b^3\Pi$, and $A'^1\Pi$ but also three high lying states-$D^1\Sigma^+$, $C^1\Sigma^+$, and $E^1\Sigma^+$-which can be used to probe lower level populations.

OODR is defined as stepwise excitation from an initial to a final via a real intermediate level: in these experiments $A^1\Sigma^+ \leftarrow X^1\Sigma^+$ is pumped and $* \leftarrow A^1\Sigma^+$, where * denotes $D^1\Sigma^+$, $C^1\Sigma^+$, or $E^1\Sigma^+$, is subsequently probed using two tunable dye lasers. OODR transitions are detected by $* \rightarrow X^1\Sigma^+$ UV fluorescence or by decreases in $A^1\Sigma^+ \rightarrow X^1\Sigma^+$ pump laser induced fluorescence (Fig. 3.1). Two types of dye lasers - broad bandwidth ($\Delta\nu_{FWHM} \approx 1$ cm^{-1}) and frequency stabilized, narrow bandwidth ($\Delta\nu_{FWHM} \approx 3 \times 10^{-5}$ cm^{-1}) - are used. Broad bandwidth lasers are employed for survey spectra and low resolution characterization of $D^1\Sigma^+$ (v = 4-6), $C^1\Sigma^+$ (v = 0 and 4), and $E^1\Sigma^+$ (v = ?).

OODR with two narrow spectral width lasers yields (1) sub-Doppler excitation spectra ($* \rightarrow X^1\Sigma^+$ UV fluorescence

Figure 3.1: OODR excitation spectrum illustrating the two means of detection: (1) decrease in A → X fluorescence (upper trace) and (2) increase in C → X UV fluorescence (lower trace). $A^1\Sigma^+ \leftarrow X^1\Sigma^+$ (1,0) P(1) is pumped while $C^1\Sigma^+ \leftarrow A^1\Sigma^+$ (3,1) R(0) is probed. The upper trace is slightly broadened instrumentally; the lower trace line width is determined solely from homogeneous broadening mechanisms (Chapter 5).

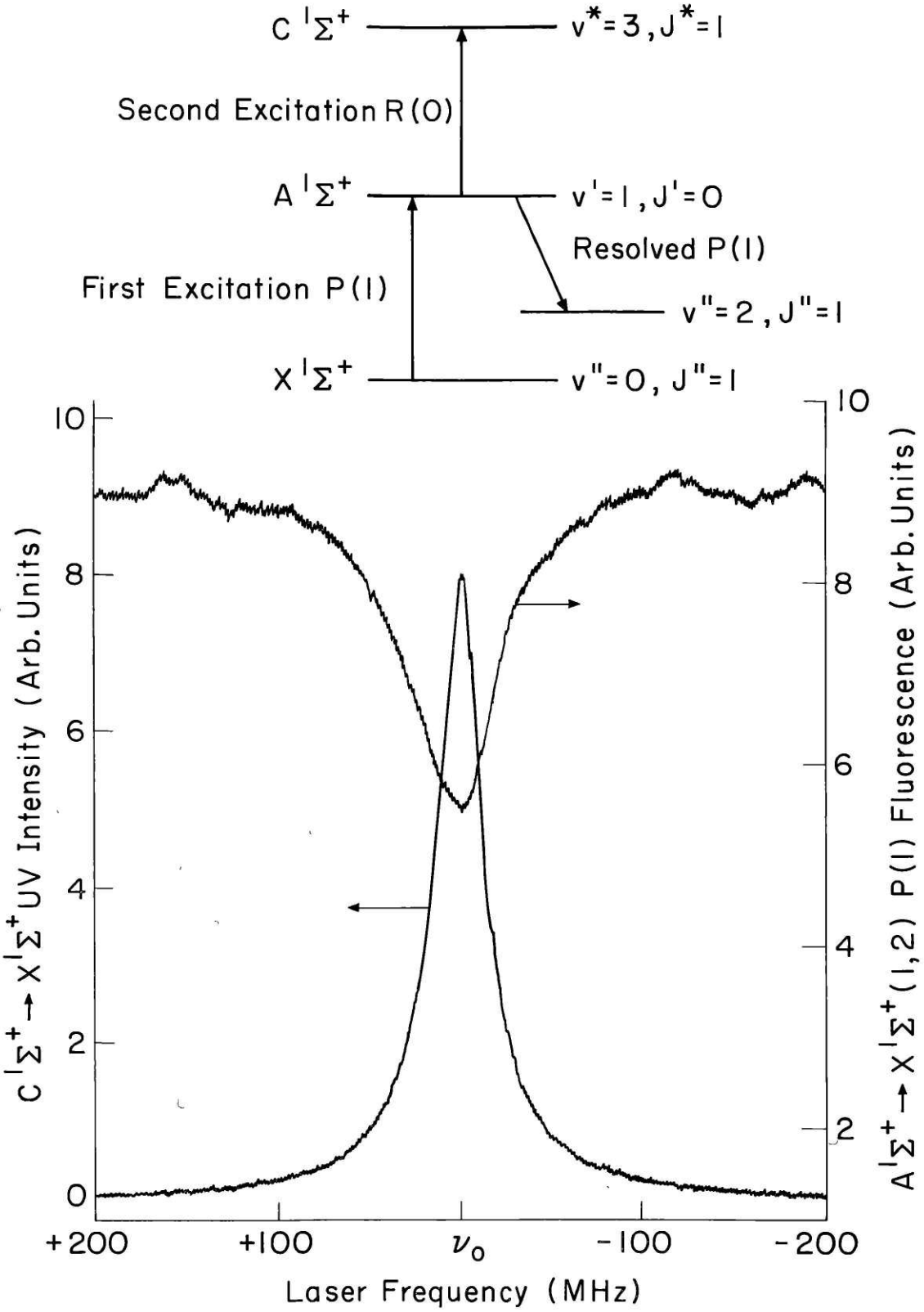
C $^1\Sigma^+$
v*=3, J*=1
Second Excitation R(0)
A $^1\Sigma^+$
v'=1, J'=0
Resolved P(1)
First Excitation P(1)
v"=2, J"=1
X $^1\Sigma^+$
v"=0, J"=1
C $^1\Sigma^+ \rightarrow$ X $^1\Sigma^+$ UV Intensity (Arb. Units)
A $^1\Sigma^+ \rightarrow$ X $^1\Sigma^+$(1,2) P(1) Fluorescence (Arb. Units)
0
2
4
6
8
10
+200
+100
ν_0
-100
-200
Laser Frequency (MHz)

Figure 3.1

vs. probe laser frequency) and (2) enhances $* \leftarrow A^1\Sigma^+ \leftarrow X^1\Sigma^+$ pumping efficiency. The former results in $C^1\Sigma^+ - A^1\Sigma^+$ (1,0), (2,1), and (3,1)† transition frequencies measured to a precision of 3×10^{-3} cm^{-1} and unambiguous detection of extra lines at perturbations (Appendix 7). Enhanced OODR pumping makes $C^1\Sigma^+ \rightarrow a^3\Sigma^+$ and $b^3\Pi_o$ emission detectable and improves the $* \rightarrow X^1\Sigma^+$ emission signal to noise ratio (S/N) by a factor of $\approx$ 50.

Previous OODR experiments employed broad bandwidth or unstabilized, narrow bandwidth or fixed frequency lasers in demonstrating the utility of OODR in simplfying excitation spectra and in accessing states with nominally zero transition moments to the ground state[1-5] (Appendix 5). A review of double resonance spectroscopy including OODR has recently been published by Steinfeld and Houston.[6]

Previous spectroscopic studies of the low lying (T_e < 20,000 cm^{-1}) states of BaO dealt with $X^1\Sigma^+$, $A^1\Sigma^+$, $b^3\Pi$, and $A'^1\Pi$. Until this work $a^3\Sigma^+$ had not been detected (Appendix 6). Mahanti[7] was the first to correctly analyze $A^1\Sigma^+ - X^1\Sigma^+$ vibrational structure. Lagerqvist, Lind, and Barrow 8 (LLB) rotationally analyzed eleven bands (through

---

†(v*,v') where v* and v' denote the $C^1\Sigma^+$ and $A^1\Sigma^+$ vibrational quantum numbers, respectively. v" and v are reserved for $X^1\Sigma^+$ and the final level of OODR induced * fluorescence, respectively.

v' = 5) of the $A^1\Sigma^+ - X^1\Sigma^+$ system and detected numerous perturbations but were not able to definitely determine the perturbing state symmetries. Field[9] re-examined LLB's data and from perturbation patterns and magnitudes as well as the vibrational variation of interaction matrix elements not only assigned the perturbing state symmetries as $b^3\Pi$ and $A'^1\Pi$ but also determined the zero vibration energies of these states with respect to $X^1\Sigma^+$. Field's analysis was subsequently verified by the detection of $A'^1\Pi \rightarrow X^1\Sigma^+$ chemiluminescence[10,11], time-resolved laser induced $A'^1\Pi \rightarrow X^1\Sigma^+$ fluorescence,[12] and broad bandwidth OODR induced $C^1\Sigma^+ \rightarrow A'^1\Pi$ and $b^3\Pi_1$ fluorescence (Appendix 5). Microwave[13-15] and microwave-optical double resonance (MODR)[17-20] experiments have provided precise $X^1\Sigma^+$ and $A^1\Sigma^+$ rotational constants and dipole moments.

Higher lying states (T_e > 20,000 cm^{-1}) of BaO were first observed by Parkinson[21] who vibrationally analyzed bands observed in shock tube absorption between 290 and 390 nm and assigned the lower state as $X^1\Sigma^+$ but he could not determine the upper state electronic symmetry. Parker[22] re-examined this spectral region, extended Parkinson's analysis, and corrected Parkinson's upper state vibrational constants which were inexplicably in error. The upper electronic state of this Parkinson band system was established as $C^1\Sigma^+$ in OODR experiments described in Appendix 5. Field, Capelle, and Revelli[3], using an Ar^+

laser to pump $A^1\Sigma^+ \leftarrow X^1\Sigma^+$ and a broadband dye laser to probe $* \leftarrow A^1\Sigma^+$, detected excitation into nineteen * vibrational levels but could not unambiguously group these levels into electronic states owing to irregular energy and rotational constant variations. However, every level observed exhibited $^1\Sigma^+$ electronic symmetry.[3] Recently, Torres-Filho and Pruett[23] (TP) observed and vibrationally assigned over one hundred $C^1\Sigma^+ - X^1\Sigma^+$ bands by pulsed dye laser excitation from high $X^1\Sigma^+$ vibrational levels (v" = 7 through 33); TP also noted irregular $C^1\Sigma^+$ vibrational intervals signalling the presence of perturbations. In fact, these perturbations are primarily responsible for the finite electric dipole $C \rightarrow a$ and b transition moments.

This work reports observation of two additional high lying electronic states, $D^1\Sigma^+$ and $E^1\Sigma^+$, and partial deperturbation of $C^1\Sigma^+$ v = 0, 1, 2, and 3 (Section III.A.).

$C\,^1\Sigma^+$ emission into $a^3\Sigma^+$, $A^1\Sigma^+$, $b^3\Pi$, and $A'^1\Pi$ is analyzed and combined with data from Refs. 8 and 19 in deperturbation and improved spectroscopic constants for these low lying states are obtained (Section III.B.). The results of this deperturbation, discussed in Section IV, suggest that another low lying, hitherto unseen electronic state of BaO exists in this energy region.

The known electronic structure of BaO and means by which low lying level populations can be monitored

are reviewed and discussed in Section IV.

In Section II, experimental details of the OODR experiment are presented.

II. Experimental

The method for producing diatomic metal oxides has been described in detail elsewhere.[24,25] Briefly, Ba metal (Alfa, 99.999% purity) was placed into an alumina crucible (Mathis) which was, in turn, inserted into a tungsten basket heater (Mathis) and then resistively heated (≈ 50 amps at ≈ 3-6 VAC) until the metal melted. Ba vapor was then entrained in a flow of Ar carrier gas (Airco, 99.998% purity) and mixed with CO_2 (Airco, 99.8% purity) to spontaneously form BaO. A weak, red chemiluminescent flame was observed initially but was no longer visible to the eye after about one hour. Steady state operating pressures were typically 0.5 - 4 torr Ar, 0.05 torr CO_2 and 1 x 10^{-4} torr Ba.

From an Ar flow rate of ≈ 10 $cm^3 sec^{-1}$, measured (using a Matheson #603 calibrated flow tube) before expansion, and knowledge of the flame pressure, a flow rate in the flame of ≈ 5 x 10^2 cm sec^{-1} is estimated. This produces a negligible Doppler shift in C ← A excitation spectra.

Fig. 3.2 illustrates the optical arrangement for narrow bandwidth OODR. A Coherent Radiation CR10 Ar^+ laser operating at 514.5 nm with 4.4W output power was used to simultaneously pump two Coherent Radiation CR599-21 dye lasers. Dye laser outputs were typically

Figure 3.2: Optical schematic diagram of OODR apparatus. The focussing lens 2 was sometimes removed (see Chapter 5). See text for discussion of components and filters used.

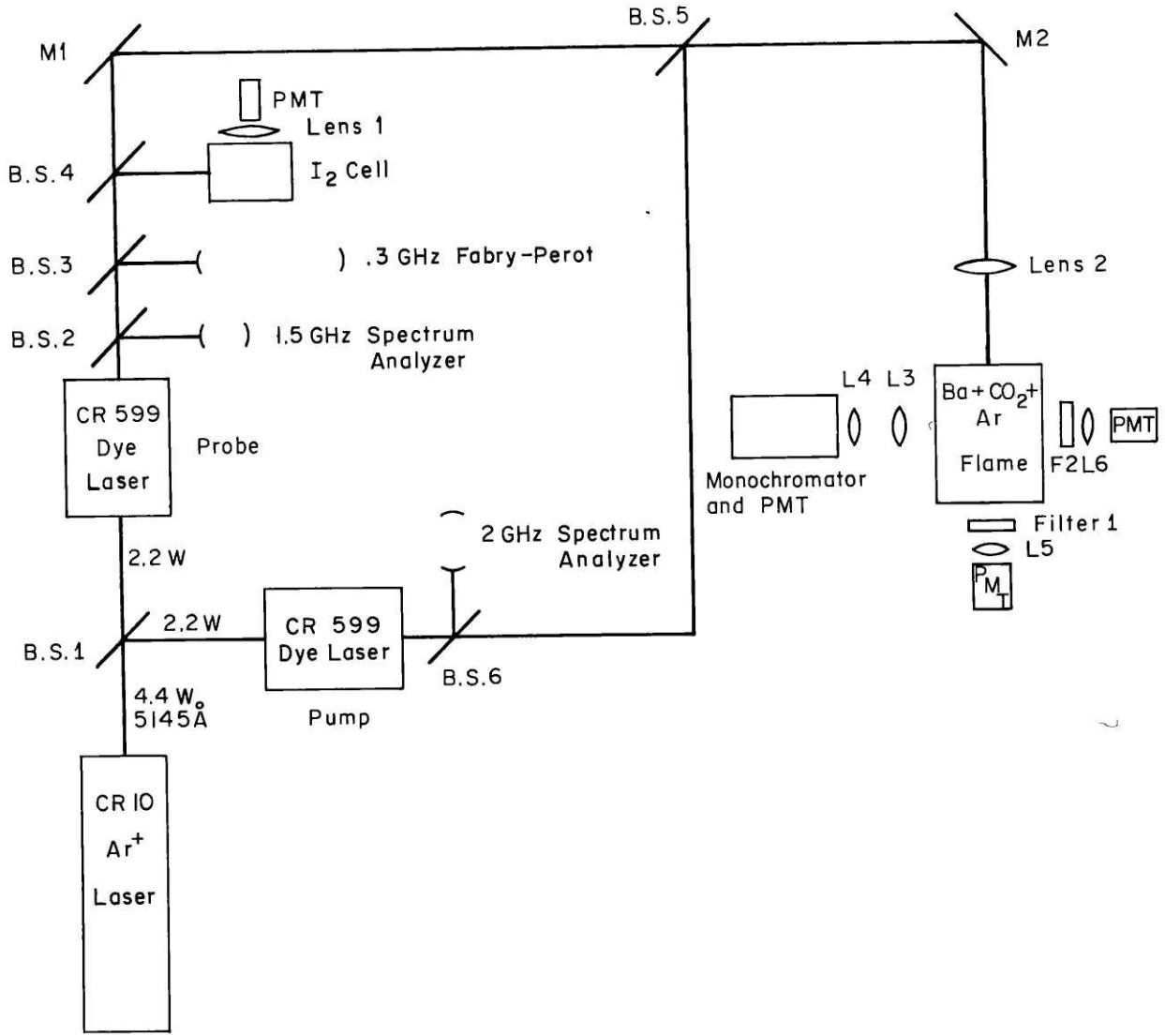
M1
B.S.5
M2
PMT
Lens 1
B.S.4
I_2 Cell
B.S.3
) .3 GHz Fabry-Perot
B.S.2
) 1.5 GHz Spectrum Analyzer
Lens 2
L4 L3
Ba+CO_2+ Ar Flame
PMT
F2L6
CR 599 Dye Laser
Probe
Monochromator and PMT
Filter 1
L5
PMT
2 GHz Spectrum Analyzer
2.2 W
2.2W
CR 599 Dye Laser
B.S.1
B.S.6
4.4 W 5145Å
Pump
CR 10 Ar^+ Laser

Figure 3.2

100 mW single mode ($\Delta\nu_{FWHM} \approx$ 1 MHz) and frequency stabilized at $\lambda \approx$ 600 nm. The pump laser frequency was monitored using a Spectra Physics 2 GHZ free spectral range (FSR) spectrum analyzer; the probe laser was monitored using a Tropel 1.5 GHz FSR spectrum analyzer, a 300 MHZ FSR fixed length semi-confocal Fabry-Perot etalon, and an I_2 cell. I_2 fluorescence excited by the probe laser was detected perpendicular to the laser propagation direction through a Corning 2-60 color glass filter by a Hamamatsu R372 photomultiplier tube (PMT) operated at - 600 VDC; the PMT current was measured using a Hewlett Packard 425 microammeter. Pump and probe lasers were combined at beam splitter 5 so that they propagated collinearly (Fig. 3.2). The beam splitter resulted in $\approx$ 50% loss in each beam[†]. The lasers were then focussed into the oven chamber using a 2 in. diameter, 12 in., focal length quartz lens (this lens was sometimes removed for experiments described in Chapters 5 and 6). The minimum beam waists (1/e intensity points) were estimated to be $\approx$ 50 μm at the focal point which was $\approx$ 1 in. below flame center. These conditions resulted in optimum S/N of $\approx$ 200. Pump laser

[†]Alternatively, beam splitter 5 in Fig. 3.2 could be eliminated and the lasers crossed via lens 2; the same S/N results.

induced $A^1\Sigma^+ \rightarrow X^1\Sigma^+$ fluorescence was monitored perpendicular to the laser propagation direction through Corning glass color and Ditric Optics 10 nm bandpass interference filters: for A → X (0,2) emission, Corning 2-61 and Ditric 650 nm (center frequency); for A → X (1,2) emission, Corning 2-62 and Ditric 630 nm; for A → X (2,1), Corning 3-66 and Ditric 590 nm; and for A → X (3,1), Corning 3-67 and Ditric 570 nm. $* \rightarrow X^1\Sigma^+$ UV fluorescence was monitored through a Corning glass 7-37 color filter and a Ditric Optics 480 nm cut-off (short λ passing) interference filter. Both A→X and *→X fluorescence were focussed using 2 in. diameter, 2.5 in. focal length quartz lenses onto Hamamatsu R372 and R212 PMTs, respectively. PMTs were operated at -600 VDC and currents were measured using Keithley 417 fast picoammeters. Resolved spectra were obtained by collimating the fluorescence with a 2 in. diameter, 4 in. focal length lens and then focussing with a 2 in. diameter, 8 in. focal length lens onto the entrance slit of a Spex 1802 monochromator equipped with a 1200 groove/mm classical grating blazed at 1.2μ. Monochromator output was monitored using an RCA C31034A PMT cooled to - 20.0°C (Products for Research) and operated at - 1400 VDC. The C31034A output was subsequently measured using Ortec photon counting equipment (9301 preamplifier, AN302/N quad amplifier, T105/NL dual

discriminator, 416A gate and delay generator, 441 rate-meter, and M250/N nimbin). Typical $*\rightarrow X^1\Sigma^+$ total UV fluorescence signals were $1x10^{-7}$ amps. $A^1\Sigma^+\rightarrow X^1\Sigma^+$, $*\rightarrow X^1\Sigma^+$, I_2 fluorescence, and the 300 MHz Fabry-Perot transmission peaks were simultaneously recorded on a four pen Esterline-Angus strip chart recorder. I_2 excitation spectra were used for absolute frequency calibration[26] to .003 cm^{-1} and the 300 MHz Fabry-Perot transmissions were used for relative frequency calibration to .003 cm^{-1}.

Exciton 590 dye was used in the CR599-21 probe laser always and in the CR599-21 pump laser for $A^1\Sigma^+ \leftarrow X^1\Sigma^+$ (0,0) and (1,0) excitation. $A^1\Sigma^+ \leftarrow X^1\Sigma^+$ (2,0) and (3,1) were pumped with a broad bandwidth dye laser with Exciton 540 dye.

The broad bandwidth lasers (home-made) exhibited a spectral width (FWHM) of $\approx$ 1 cm^{-1} with a three stage birefringent filter inserted in the laser cavity.[27-30] Typical output powers were 0.5-1W. The optical arrangement was identical to that described above except that spectrum analyzers and an I_2 cell were not used and the 300 MHz Fabry-Perot was relaced by a 3.057 cm^{-1} FSR solid quartz etalon, which provided a relative precision of 0.2 cm^{-1}. Absolute frequency calibration to 0.5 cm^{-1} was obtained by passing the probe laser through the monochromator along with Ne emission from an Oriel pen lamp.[31]

The OODR experiment would proceed by tuning

the pump laser to an A ← X transition and monitoring resolved $A^1\Sigma^+ \rightarrow X^1\Sigma^+$ fluorescence through the monochromator in both thepumped band and in at least one additional band; separations between fluorescence lines correspond to known[8,15,16] ground state combination differences and were thus used to determine J'.[32,33] Knowledge of the laser frequency was sufficient to determine the $A^1\Sigma^+ - X^1\Sigma^+$ band excited.[7,8] For narrow bandwidth excitation, only the most abundant isotope, $^{138}Ba^{16}O$ was selected (Fig. 3.3), but the shifts corresponding to different isotopes of Ba were unresolvable when broad bandwidth excitation was employed. Broad bandwidth pumping usually resulted in excitation of two lines corresponding to different values of J' but the fluorescence could always be resolved in an $A^1\Sigma^+ \rightarrow X^1\Sigma^+$ band other than the one pumped and the transitions were thereby unambiguously assigned. The pump laser frequency was then fixed while the probe laser was scanned to obtain $* \leftarrow A^1\Sigma^+$ excitation spectra.

Figure 3.3: $A^1\Sigma^+ \leftarrow X^1\Sigma^+$ (1,0) excitation spectrum (probe laser blocked) illustrating the isotopic selectivity of single mode pumping. Lines corresponding to the most abundant isotope, $^{138}Ba^{16}O$ (71.7%), are labeled only by the rotational transition. Note the intensity of P(1) relative to $^{135}Ba^{16}O$ (6.6%) R(11).

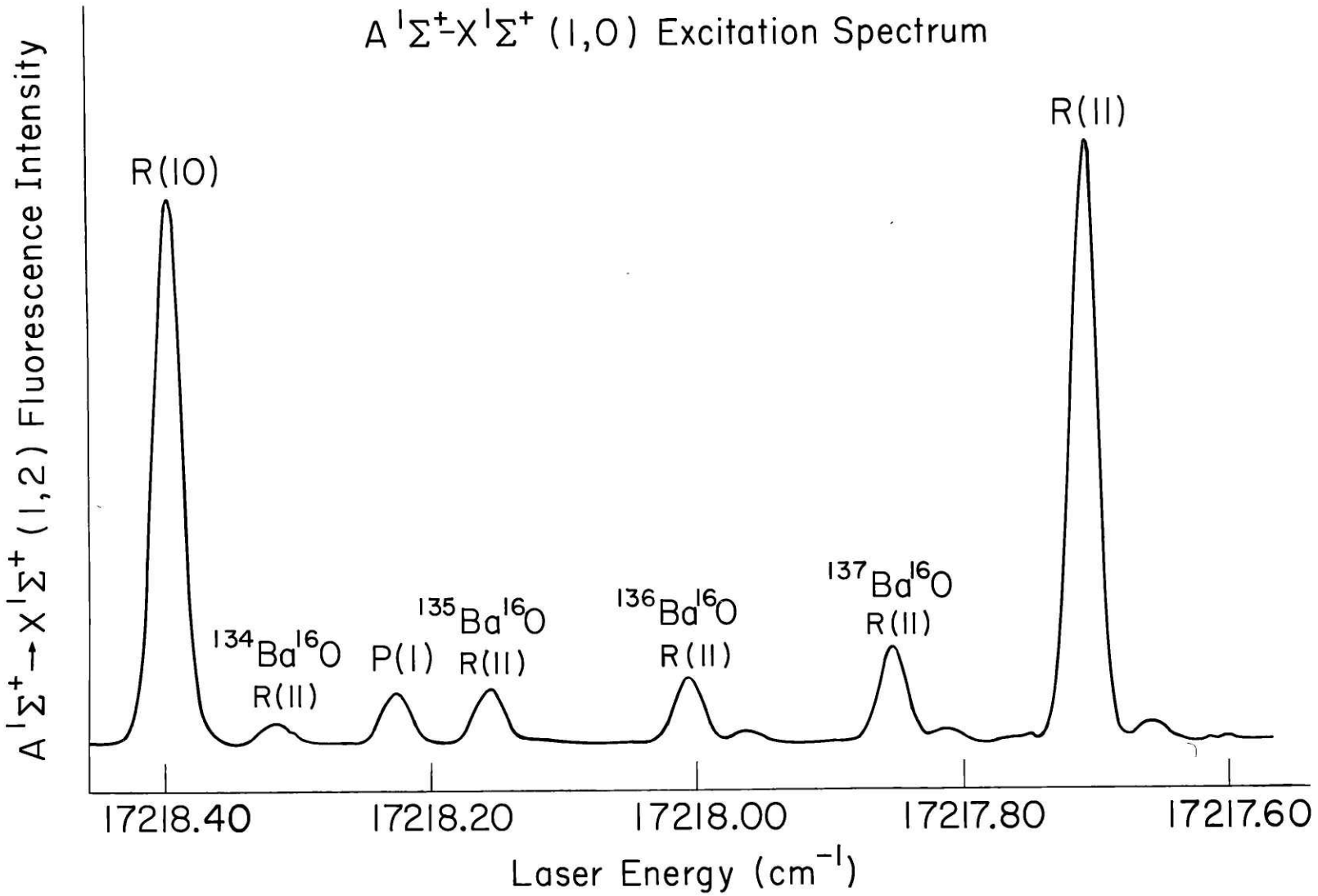
A ¹Σ⁺-X ¹Σ⁺ (1,0) Excitation Spectrum
A ¹Σ⁺ → X ¹Σ⁺ (1,2) Fluorescence Intensity
R(10)
R(11)
¹³⁴Ba¹⁶O R(11)
P(1)
¹³⁵Ba¹⁶O R(11)
¹³⁶Ba¹⁶O R(11)
¹³⁷Ba¹⁶O R(11)
17218.40
17218.20
17218.00
17217.80
17217.60
Laser Energy (cm⁻¹)

Figure 3.3

III. Results

A. * ← $A^1\Sigma^+$ Excitation Spectra

1. Electronic and Vibrational Structure

* ← $A^1\Sigma^+$ band heads observed here are given in Table 3.1. * state vibrational assignments are made by counting nodes in resolved * → $X^1\Sigma^+$ UV fluorescence spectra (Fig. 3.4): because the * state equilibrium internuclear distances (R_e) are ≈ 1.14 times R_e ($X^1\Sigma^+$) (see below), Franck-Condon intensity distributions for emission from a single * vibrational level are reflections of * vibrational wave functions.[34,35] Fluorescence from the $E^1\Sigma^+$ and c levels in Table 3.1 is too weak to provide reliable node counts.

$C^1\Sigma^+(v^* = 1)$ is strongly perturbed at low J (see below) so that an extra band head is observed (Table 3.1). Fluorescence from this extra band exhibits the same Franck-Condon intensity distribution as the main band indicating that the extra band fluorescence intensity is borrowed from the main band; this precludes a vibrational assignment by the above method for the perturbing level.

It should be noted that the vibrational assignments in Table 3.1 indicate that $D^1\Sigma^+$ lies below $C^1\Sigma^+$ but since $C^1\Sigma^+$ was discovered[21] and named previously (Appendix 5) it seems undesirable to re-name these states here.

Table 3.1: $* \leftarrow A^1\Sigma^+$ Band Heads[a]

*	(v*,v')	λ^{Air}_{Head}(nm)	σ_{Head}(cm^{-1})	$A^1\Sigma^+ \leftarrow X^1\Sigma^+$ Band Pumped (v',v")
$C^1\Sigma^+$	(0,0)	623.58(2)	16032.0(5)	(0,1), (0,0)
$C^1\Sigma^+$	(1,0) main	607.7585(11)	16449.359(3)	(0,0)
	(1,0) extra	606.4684(11)	16484.352(3)	
$C^1\Sigma^+$	(2,1)	609.2764(11)	16408.380(3)	(1,0)
$C^1\Sigma^+$	(3,1)	594.0521(20)	16828.894(6)	(1,0)
c	(c+2,1)	593.4745(10)	16845.268(3)	
$C^1\Sigma^+$	(3,2)	611.64(4)	16345.(1)	(2,0)
$C^1\Sigma^+$	(4,2)	596.28(4)	16766.(1)	(2,0)
$C^1\Sigma^+$	(5,3)	598.35(2)	16708.1(5)	(3,1)
$D^1\Sigma^+$	(3,2)	618.83(4)	16155.(1)	(2,0)
$D^1\Sigma^+$	(4,2)	604.83(4)	16529.(1)	(2,0)
$D^1\Sigma^+$	(5,3)	609.39(2)	16405.3(5)	(3,1)
$D^1\Sigma^+$	(6,3)	595.71(2)	16782.1(5)	(3,1)
$E^1\Sigma^+$	(e,2)	605.31(4)	16516.(1)	(2,0)
c	(c+4,3)	600.25(2)	16655.2(5)	(3,1)

[a]Uncertainties of 1σ in the last digit are given in parentheses.

Figure 3.4: $C^1\Sigma^+ \rightarrow X^1\Sigma^+$ resolved UV fluorescence
The number of nodes in the Franck-Condon intensity distribution indicates that $v^* = 4$. Each band consists of a P and R doublet.

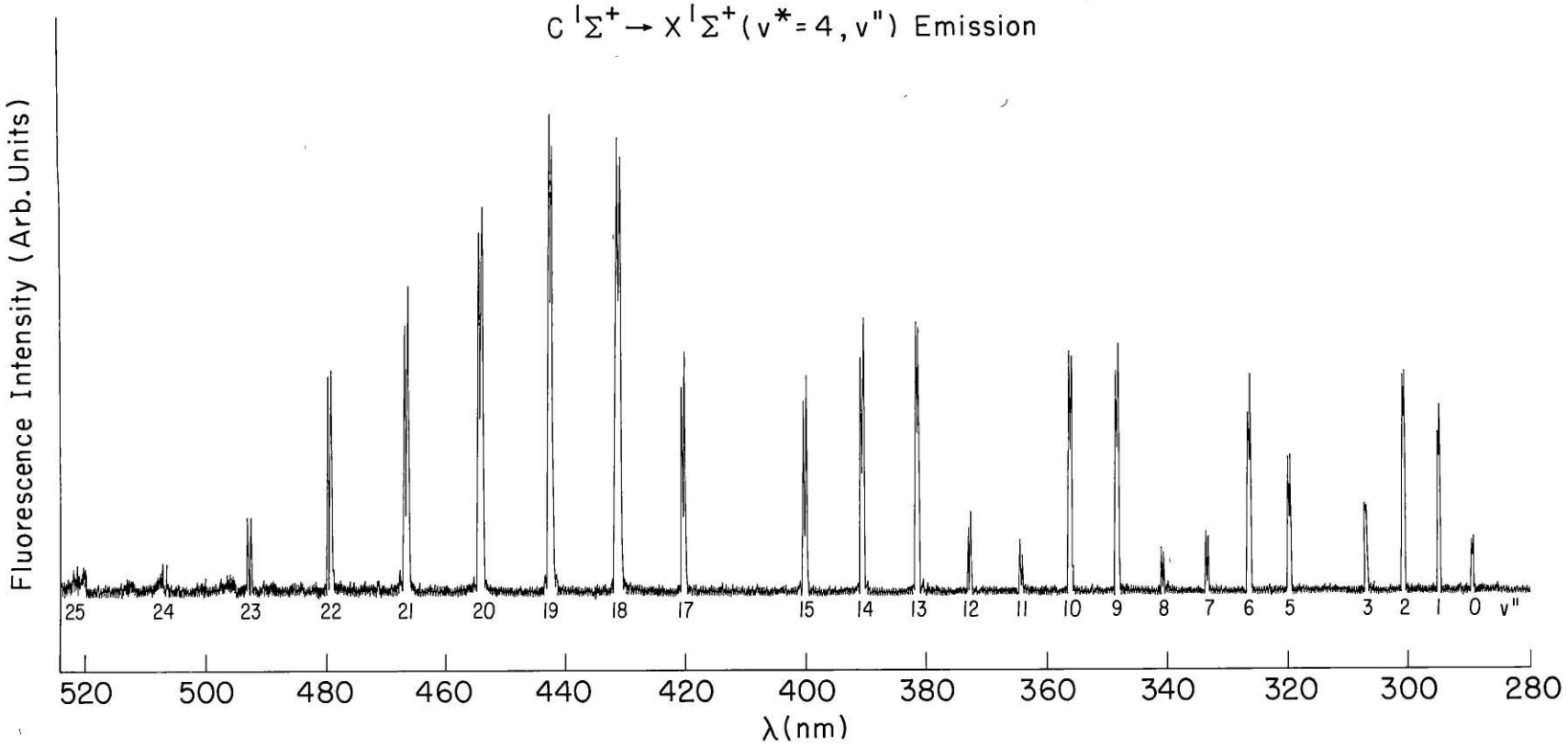
C $^1\Sigma^+ \rightarrow X\,^1\Sigma^+ (v^* = 4, v'')$ Emission
Fluorescence Intensity (Arb. Units)
25 24 23 22 21 20 19 18 17 15 14 13 12 11 10 9 8 7 6 5 3 2 1 0 v"
520 500 480 460 440 420 400 380 360 340 320 300 280
λ(nm)

Figure 3.4

Observation of only P($\Delta J = J^* - J' = -1$) and R($\Delta J = +1$) branches in $^* \leftarrow A^1\Sigma^+$ excitation is the basis for assigning the electronic symmetries as $^1\Sigma^+$. The $c \leftarrow A^1\Sigma^+$ (c+4,3) band does not exhibit simple P and R branch structure but is extensively perturbed; no rotational analysis of this band or of $C \leftarrow A$ (5,3) was attempted. The vibrational assignment, c+4, results from deperturbation of $C^1\Sigma^+$ and is discussed more fully below.

2. Rotational Structure

As mentioned above, the rotational structure for all of the bands in Table 3.1, except (c+4,3), consists of two branches, P and R; thus, only e parity levels (corresponding to reflection of electronic coordinates in a plane containing the internuclear axis)[36] are observed. In unperturbed spectral regions, the rotational assignments are straightforward owing to selection of at most two (when broad bandwidth pumping is employed) $A^1\Sigma^+$ rovibronic levels by the pump laser, and the fact that R(J') always lies to higher frequency from P(J'). Rotational relaxation in $A^1\Sigma^+$ resulting in many weaker transitions in the $^* \leftarrow A^1\Sigma^+$ excitation spectrum (Chapter 5) permits a rotational analysis of the entire band for one pump laser frequency: the collisional satellite rotational assignments are easily and quickly

made as a result of the unambiguous assignments made for the $*\leftarrow A^1\Sigma^+$ transitions from the pumped $A^1\Sigma^+$ rovibronic level (hereafter referred to as principal lines) (see Fig. 3.5). In practice, more than one $A^1\Sigma^+ \leftarrow X^1\Sigma^+$ pump frequency is used to facilitate rotational assignments in perturbed spectral regions.

When single mode pumping is employed, sub-Doppler excitation spectra are obtained not only for the principal lines but also for the collisional satellites (see Chapter 5 for a discussion of velocity randomization and line broadening observed as a function of the collisional change in J'). Fig. 3.6 illustrates the resolution obtained in the $C^1\Sigma^+ \leftarrow A^1\Sigma^+$ (3,1) band head.

Because of low resolution and low precision, perturbations are not readily detectable in broad bandwidth excitation spectra. However, the opposite is true for single mode OODR: perturbations are sensitively detected by the appearance of extra and shifted lines (Appendix 7). It is usually possible to analyze perturbed spectral regions from $A^1\Sigma^+$ combination differences[8] but it is sometimes necessary to verify assignments by selecting a different intermediate $A^1\Sigma^+$ rovibronic level: for example, for the $C^1\Sigma^+$ $v^* = 3$, $J^* = 50$ perturbed level both $A^1\Sigma^+$ $v' = 1$, $J' = 49$ and 51 are pumped, in turn, and the R(49) and P(51) principal transitions probed to reveal and verify the existence of

Figure 3.5: Low resolution $D^1\Sigma^+ \leftarrow A^1\Sigma^+$ (4,2) excitation spectrum (broad bandwidth excitation). $A^1\Sigma^+$ (v' = 2, J' = 22) is pumped. Note the strong R(22) and P(22) principal lines above the many weaker collisional satellite transitions; P(J') (lower numbers) and R(J' + 10) (upper numbers are unresolved at low J'.

Figure 3.6: High resolution excitation spectrum of $C^1\Sigma^+ \leftarrow A^1\Sigma^+$ (3,1) band head [R(6)]. $A^1\Sigma^+$ (v' = 1, J' = 15) is pumped; the principle R(15) and P(15) lines are at lower frequency and would be off scale. Note the resolution of $\approx$ 0.01 cm^{-1}.

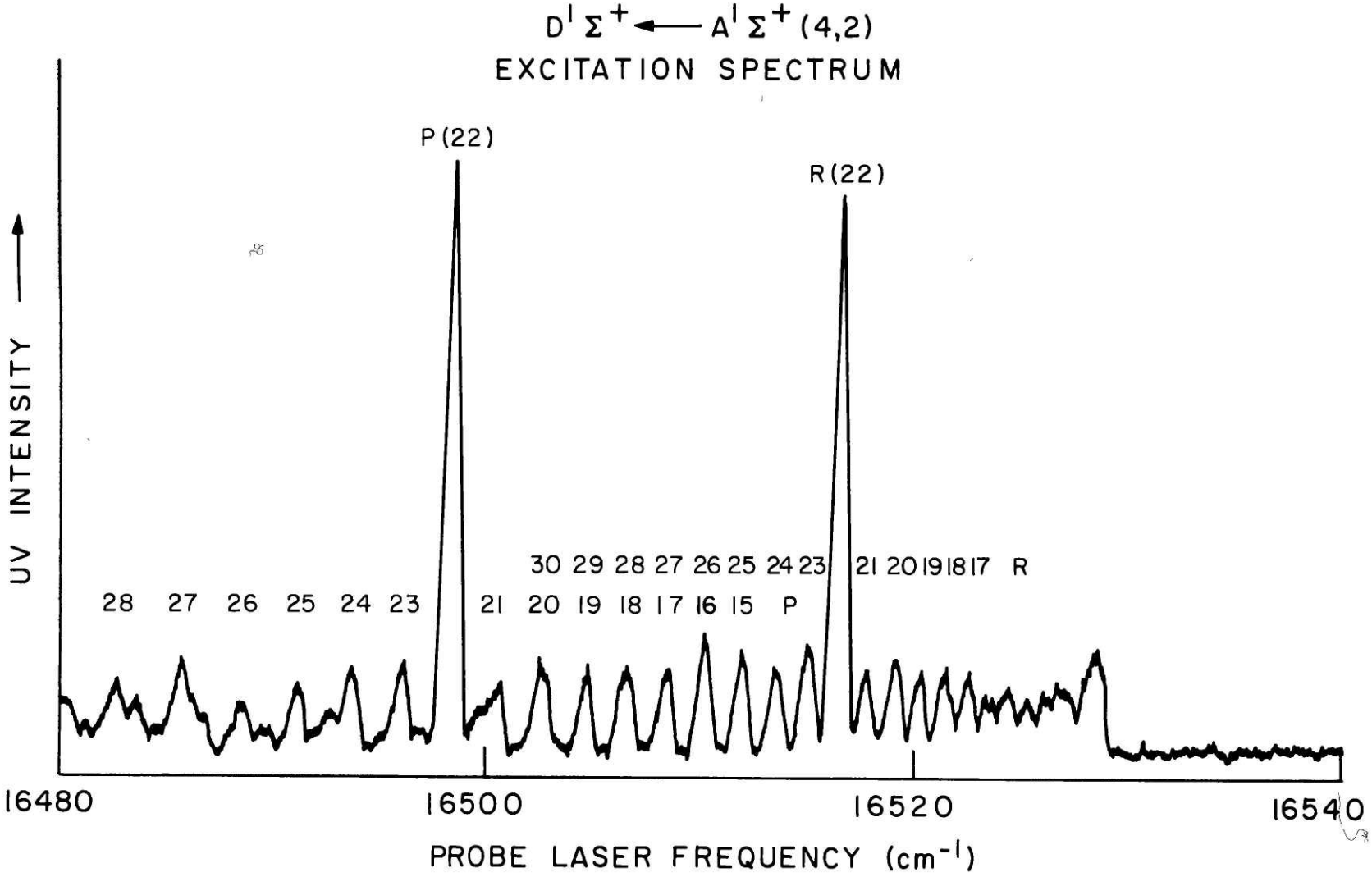
D¹Σ⁺ ← A¹Σ⁺ (4,2)
EXCITATION SPECTRUM
P(22)
R(22)
UV INTENSITY
28 27 26 25 24 23 21 20 19 18 17 16 15 P
30 29 28 27 26 25 24 23 21 20 19 18 17 R
16480
16500
16520
16540
PROBE LASER FREQUENCY (cm⁻¹)

FIGURE 3.5

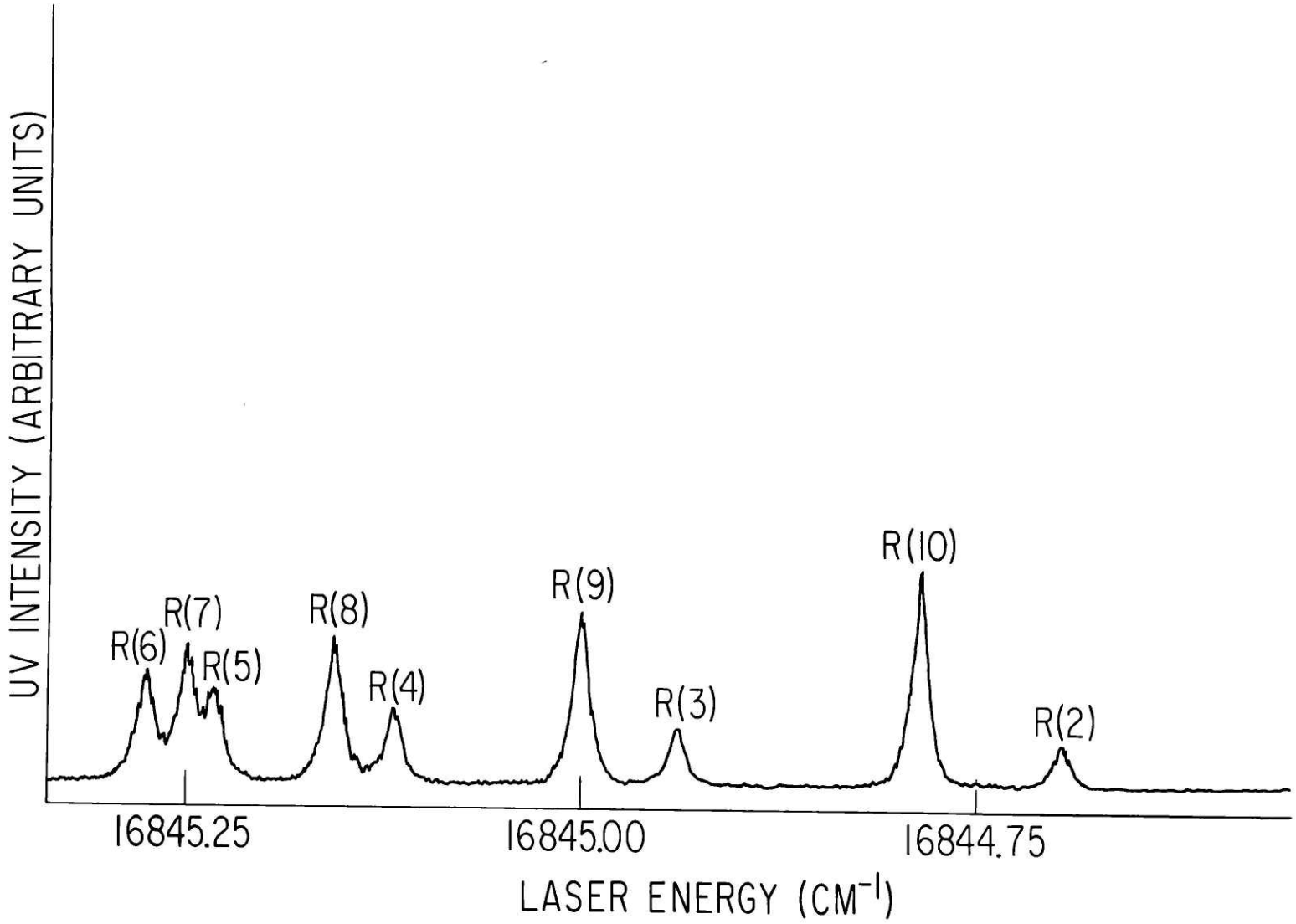
UV INTENSITY (ARBITRARY UNITS)
R(6)
R(7)
R(5)
R(8)
R(4)
R(9)
R(3)
R(10)
R(2)
16845.25
16845.00
16844.75
LASER ENERGY (CM⁻¹)

Figure 3.6

four J* = 50 extra lines (see Appendix 7)!

$C^1\Sigma^+ - A^1\Sigma^+$, $D^1\Sigma^+ - A^1\Sigma^+$, and $E^1\Sigma^+ - A^1\Sigma^+$ transition frequencies are given in Tables 3.2, 3.3, and 3.4, respectively. Only the $C^1\Sigma^+ - A^1\Sigma^+$ (1,0), (2,1), and (3,1) bands are measured by single mode OODR.

Rather than fit the bands in Tables 3.2-3.4 by varying $A^1\Sigma^+$ constants as well as * state constants, transition frequencies are converted to * term values by adding calculated $A^1\Sigma^+$ term values (precise to 0.01 cm^{-1}) determined below (Section III.B.). This greatly simplifies the deperturbation since the lower state need not be considered and, except for the single mode OODR data, results in an insignificant loss in precision. For the single mode OODR data the sub-Doppler precision is all but lost. The factor of three gain in precision obtainable by fitting transition frequencies rather than term values is sacrificed for faster and more economical fitting of term values. Term values for $C^1\Sigma^+$, $D^1\Sigma^+$, and $E^1\Sigma^+$ are given in Tables 3.5, 3.6, and 3.7.

3. $C^1\Sigma^+$ Deperturbation

A total of eleven peturbations in $C^1\Sigma^+ \sim A^1\Sigma^+$ excitation spectra have been detected and are summarized in Table 3.8 and Fig. 3.7.[†] Extra lines

[†]In addition to perturbations resulting from lower level interactions (Section III.B.)

Table 3.2: $C^1\Sigma^+ - A^1\Sigma^+$ Transition Wave Numbers

J^b	R(J)		P(J)	
		(0,0)		
17	16 029.6			
28			15 995.6	
33	16 016.8			
37	16 013.3	16 024.0[c]	15 978.2	15 990.1[c]
38	16 012.0	16 023.5	15 976.9	15 987.7
39				
40				
41	16 006.1	16 018.2	15 968.5	15 979.9
42	16 016.6	16 004.0	15 965.5	15 977.0
43				
44	16 013.0	15 999.9	15 971.5	15 959.0
45				
46	16 009.1	15 995.4	15 966.3	15 952.7
47				
48				
49			15 957.5	

Table 3.2: $C^1\Sigma^+ - A^1\Sigma^+$ Transition Wave Numbers (continued)

J	R(J)		(1,0)[d]	P(J)	
0		16 483.041[c]			
1		16 483.416			16 482.083
2		16 483.745			16 481.490
3	16 447.694	16 483.996			16 480.841
4	16 448.114	16 484.181*			16 480.132
5	16 448.476	16 484.301*			
6	16 448.772	16 484.352*			
7	16 449.017	16 484.344*			
8	16 449.194	16 484.268*			
9	16 449.309*	16 484.129*			
10	16 449.359*	16 483.926			
11	16 449.349*	16 483.660			
12	16 449.274*	16 483.330		16 437.519	16 472.065
13	16 449.139	16 482.946	16 428.900*	16 436.460	16 470.768
14	16 448.949	16 482.495	16 427.231	16 435.361	16 469.412
15	16 448.671	16 481.984	16 425.480	16 434.192	16 467.992
16	16 448.351	16 481.412	16 423.700	16 432.976	16 466.512
17	16 447.967	16 480.777	16 421.781		16 464.972*
18	16 447.514	16 480.097		16 430.324	16 463.378
19	16 446.995	16 479.353		16 428.906	16 461.719
20				16 427.431	16 460.007
21				16 425.882	16 458.237
22				16 424.275	16 456.406
23				16 422.599	16 454.533
24				16 420.855	
25					

Table 3.2: $C^1\Sigma^+ - A^1\Sigma^+$ Transition Wave Numbers (continued)

J	R(J)	P(J)
	(1,0) continued	
26	16 472.660	
27	16 471.498	
28	16 470.289	
29	16 469.034	
30	16 467.732	
31	16 466.383	16 437.634
32	16 464.980*	16 435.309
33	16 463.545	16 432.931
34	16 462.052	16 430.508*
35		16 428.054
36	16 458.921	16 425.543
37	16 457.232	16 422.973
38	16 455.544	16 420.361
39	16 453.682	
40	16 451.492	

Table 3.2: $C^1\Sigma^+ - A^1\Sigma^+$ Transition Wave Numbers (continued)

J	R(J)	(2,1)[d]	P(J)
0	16 406.662		
1	16 407.066		16 405.695
2	16 407.418		16 405.135
3	16 407.715		16 404.510
4	16 407.957		16 403.839
5	16 408.144*		16 403.106
6	16 408.276*		16 402.321
7	16 408.356*		16 401.488
8	16 408.380		16 400.593
9			16 399.645*
10			16 398.648
11	16 408.124*		16 397.591
12	16 407.930		16 396.481
13	16 407.678		16 395.313
14	16 407.370		16 394.095
15	16 407.004		16 392.817
16	16 406.578		16 391.487
17	16 406.094		16 390.096
18	16 405.552		16 388.643
19	16 404.939		16 387.137
20	16 404.251		16 385.560
21	16 403.451		
22	16 402.518	16 404.835[c]	
23	16 401.301	16 403.252	16 380.395

Table 3.2: $C^1\Sigma^+ - A^1\Sigma^+$ Transition Wave Numbers (continued)

J	R(J)		P(J)	
		(2,1) continued		
24	16 401.917	16 399.678	16 378.432	16 380.747
25	16 400.753	16 397.714	16 376.196	16 378.145
26	16 399.624*		16 375.786	
27	16 398.401	16 399.128	16 373.604	
28	16 397.398		16 371.453	
29	16 396.110		16 369.207	16 369.929[c]
30	16 394.766		16 367.183	
31	16 393.337		16 364.876	
32	16 391.795		16 362.518	
33			16 360.071	
34			16 357.510	
40	16 377.062[†]	16 377.508[†]		
42	16 372.108[†]			

Table 3.2: $C^1\Sigma^+ - A^1\Sigma^+$ Transition Wave Numbers (continued)

J	R(J)		P(J)	
		(3,1)[d]		
0	16 844.029*			
1	16 844.403			
2	16 844.711	16 828.602*		
3	16 844.952	16 828.784*	16 841.828	16 825.777
4	16 845.124*		16 841.113	
5	16 845.230*	16 828.894*	16 840.327	16 824.178
6	16 845.268*	16 828.822	16 838.476	16 823.248
7	16 845.244*	16 828.662	16 838.544	16 822.233
8	16 845.158*	16 828.415	16 837.568	
9	16 845.010	16 828.080	16 836.520	16 919.939
10	16 844.800	16 827.653	16 935.406	16 818.666
11	16 844.532	16 827.133	16 834.234*	16 817.307
12	16 844.206	16 826.521	16 832.998	16 815.849*
13	16 843.826	16 825.816	16 831.707	16 814.305
14	16 843.388	16 825.015	16 830.356	16 812.676*
15	16 842.897	16 824.122	16 828.943	16 810.941
16	16 842.352	16 823.123	16 827.486	16 809.114
17	16 841.744	16 822.027	16 825.971	16 807.194
18	16 841.139	16 820.832	16 824.412	16 805.349
19	16 840.426	16 819.526	16 822.783	
20	16 839.684	16 818.134*	16 821.152*	
21		16 816.632*	16 819.409	
22	16 838.053	16 815.029	16 817.644	
23	16 837.166	16 813.334*	16 815.825*	

Table 3.2: $C^1\Sigma^+ - A^1\Sigma^+$ Transition Wave Numbers (continued)

J	R(J)		P(J)	
		(3,1) continued		
24	16 836.232	16 811.529	16 813.967	
25	16 835.251	16 809.627	16 812.057	
26	16 834.244*	16 807.622	16 810.106	
27	16 833.146	16 805.478	16 808.114	
28	16 832.024		16 806.055	
29	16 830.850		16 803.956	
30	16 829.626		16 801.807	
31	16 828.350		16 799.616	
32	16 827.010		16 797.366	
33	16 825.803		16 795.083	
34	16 824.282		16 792.728	
35	16 822.722		16 790.497	16 790.104
36	16 821.134*		16 787.955	
37	16 819.781			
38	16 818.146*			
39	16 816.456			
40	16 814.710			
41	16 812.915*			
42	16 811.047			
43				
44	16 807.122			
45	16 805.294	16 804.425		
46	16 802.649		16 760.553	
47	16 800.303		16 757.463	

Table 3.2: $C^1\Sigma^+ - A^1\Sigma^+$ Transition Wave Numbers (continued)

J	R(J)		P(J)	
		(3,1) continued		
48	16 797.723		16 754.246	
49	16 794.898	16 804.947	16 750.866	
50	16 791.729	16 801.314	16 747.294	
51		16 788.175	16 743.448	16 753.500
52			16 739.283	16 748.871
53			16 734.735	

Table 3.2: $C^1\Sigma^+ - A^1\Sigma^+$ Transition Wave Numbers (continued)

J	R(J)	P(J)
	(3,2)[a]	
21		16 324.8
22		16 323.0
23		16 321.3
24		16 319.4
25		
26		
27		16 313.8
28		
29		
30	16 335.6	16 307.6
31	16 334.4	16 305.2
32	16 333.1	16 303.3
33		16 301.0
34		16 298.8
35		16 296.5
36		
37		16 291.7
38		16 289.3
39		16 286.8
40	16 321.4	16 284.2
41		16 281.9
42	16 317.8	16 279.0
43	16 316.0	16 276.1

Table 3.2: $C^1\Sigma^+ - A^1\Sigma^+$ Transition Wave Numbers (continued)

J	R(J)		P(J)	
		(3,2) continued		
44	16 313.9		16 273.7	
45	16 312.0		16 270.6	
46	16 310.0		16 267.6	
47	16 307.7		16 264.6	
48	16 305.3		16 261.2	
49			16 257.6	
50			16 254.5	
51			16 251.1	
52	16 302.0	16 291.4[c]	16 246.7	16 255.9[c]

Table 3.2: $C^1\Sigma^+ - A^1\Sigma^+$ Transition Wave Numbers (continued)

J	R(J)	P(J)
	(4,2)[a]	
16		16 748.8
17		16 747.3
18		16 745.6
19		16 744.0
20		16 742.2
21		16 740.2
22		16 738.3
23		16 736.3
24		16 734.1
25		16 731.6
26		16 729.5
27	16 750.7	16 727.0
28	16 748.8	16 724.2
29	16 747.3	16 721.7
30		16 718.6
31		16 715.6
32		16 712.4
33		16 709.0
34		16 705.3
35		16 701.7
36		16 697.6

Table 3.2: $C^1\Sigma^+ - A^1\Sigma^+$ Transition Wave Numbers (continued)

Footnotes:

[a]Absolute accuracy of 0.5 cm^{-1} and relative precision of 0.2 cm^{-1} from broadband ($\Delta\nu \approx 1$ cm^{-1}) laser spectra.

[b]J is $A^1\Sigma^+$ rotational quantum number.

[c]Underlined frequencies correspond to extra lines.

[d]Absolute accuracy of 0.005 cm^{-1} and relative precision of 0.003 cm^{-1} from single mode ($\Delta\nu \approx 3.3\times10^{-5}$ cm^{-1}) laser spectra.

*Blended line, accuracy and precision of 0.01 cm^{-1}.

†Not included in deperturbation analysis.

Table 3.3: $D^1\Sigma^+ - A^1\Sigma^+$ Transition Wave Numbers

J[b]	R(J)	P(J)
	(3,2)[a]	
17	16 149.2	16 134.3
18	16 148.1	16 132.6
19	16 147.1	
20	16 146.1	16 128.2
21	16 144.8	16 126.1
22	16 143.5	16 124.2
23	16 141.8	16 121.7
24	16 140.0	16 119.3
25	16 138.2	16 116.8
26	16 136.9	16 114.5
27	16 135.1	16 112.0
28	16 133.3	16 109.1
29	16 131.3	16 106.1
30	16 129.1	16 103.2
31	16 127.0	16 100.2
32		16 097.0
33	16 122.4	16 094.1
34	16 120.2	16 090.8
35	16 117.5	16 087.6
36	16 115.2	16 084.1
37		16 080.4

Table 3.3: (continued)

J	R(J)	P(J)
	(3,2) (cont.)	
38	16 076.8	
39	16 073.1	
40	16 069.2	
41	16 065.3	
	(4,2)[a]	
15		16 511.2
16	16 523.5	16 509.4
17	16 522.5	16 507.5
18	16 521.3	16 505.6
19	16 520.2	16 503.5
20	16 518.9	16 501.3
21	16 517.5	16 499.2
22	16 516.1	16 497.2
23	16 514.5	16 494.5
24	16 512.9	16 492.1
25	16 511.2	16 489.6
26	16 509.4	16 486.9
27	16 507.5	16 484.3
28	16 505.6	16 481.4
29	16 503.5	16 478.4
30	16 501.3	16 475.4
31		16 472.0

Table 3.3: (continued)

J	R(J)	P(J)
	(4,2) (cont.)	
32		
33		16 465.4
	(5,3)[a]	
18		16 382.8
19		16 380.4
20		16 378.0
21		16 375.8
22	16 392.8	16 373.7
23	16 391.4	16 371.3
24	16 389.8	16 368.8
25	16 387.8	16 366.3
26	16 386.1	16 364.0
27	16 384.1	16 361.3
28	16 382.7	16 358.6
29	16 380.4	16 355.6
30	16 378.0	16 352.5
31	16 375.8	16 349.3
32	16 373.7	16 346.5
33	16 371.3	16 343.0
34	16 368.8	16 339.9
35	16 366.3	16 336.3
36		

Table 3.3: (continued)

J	R(J)	P(J)
	(5,3) (cont.)	
37	16 361.3	
38	16 358.6	16 326.2
39	16 355.6	16 322.5
40	16 352.5	16 318.4
41	16 349.3	16 314.5
42	16 346.5	16 310.9
43	16 343.0	16 306.6
44	16 339.9	16 302.2
45	16 336.4	16 298.5
46	16 333.4	16 294.1
47	16 328.9	
48	16 325.9	
49	16 322.8	
50	16 318.4	
51	16 314.5	
52	16 310.3	
	(6,3)[a]	
19		16 756.7
20	16 772.4	16 754.7
21	16 770.8	16 752.5
22	16 769.7	16 750.6
23	16 768.1	16 748.2

Table 3.3: (continued)

J	R(J)	P(J)
	(6,3)[a] (cont.)	
24	16 766.5	16 745.4
25	16 764.6	16 743.1
26	16 763.0	16 740.4
27		
28		16 735.0
29	16 756.7	16 732.3
30	16 754.7	16 728.9
31	16 752.5	16 725.8
32	16 750.6	16 722.4
33	16 748.2	16 719.3
34	16 745.4	
35	16 743.1	
36	16 740.4	

[a]See footnote a in Table 3.2

[b]See footnote b in Table 3.2

Table 3.4: $E^1\Sigma^+ - A^1\Sigma^+$ Transition Wave Numbers

J[b]	R(J)	P(J)
	(e,2)[a]	
19		16 491.6
20		16 489.4
21	16 506.0	16 487.5
22	16 504.8	16 485.4
23	16 503.7	16 482.9
24	16 502.2	16 480.7

[a] See footnote a in Table 3.2.

[b] See footnote b in Table 3.2.

Table 3.5: $C^1\Sigma^+$ Term Values

J		T(cm^{-1}) v=0[a]	
18	32 830.5		
27	32 928.5		
34	33 029.9		
36	33 063.3	33 075.2[b]	
37	33 081.7	33 092.5	
38	33 098.4	33 109.1	
39	33 116.8	33 128.3	
40	33 135.3	33 146.8	
41	33 154.1	33 165.5	
42	33 185.0	33 172.9	
43	33 205.1	33 192.6	
44			
45	33 246.8	33 233.4	
46			
47	33 289.8	33 276.0	
48	33 312.3		

Table 3.5: $C^1\Sigma^+$ Term Values (continued)

J		$T(cm^{-1})$	
		v=1 ^{c}	
0		33 204.834	
1		33 205.274	
2		33 206.168	
3		33 207.524	
4	33 173.023	33 209.325	
5	33 175.505	33 211.572	
6	33 178.445	33 214.270	
7	33 181.835	33 217.415	
8	33 185.690	33 221.017	
9	33 189.991	33 225.065	
10	33 194.756*	33 229.566	
11	33 199.959*	33 234.518	
12	33 205.616	33 239.920	
13	33 211.724	33 245.778	33 205.266
14	33 218.289	33 252.092	33 211.328
15	33 225.317	33 258.858	33 217.822
16	33 232.765	33 266.078	33 224.803
17	33 240.698	33 273.755	33 232.159
18	33 249.073	33 281.884	
19	33 257.898	33 290.477	
20	33 267.169	33 299.524	
21	33 276.898	33 309.029	
22	33 287.068	33 319.002	
23	33 297.685		

Table 3.5: $C^1\Sigma^+$ Term Values (continued)

J		T(cm^{-1})
		v=1 (continued)
24		
25		
26		
27		33 375.751
28		33 388.490
29		33 401.695
30	33 415.363	33 415.363
31	33 429.501	
32	33 444.102	
33	33 459.166*	
34	33 474.710	
35	33 490.709	
36	33 507.163	
37	33 524.087	
38	33 541.422	
39	33 559.269	
40	33 577.452	
41	33 595.817	

Table 3.5: $C^1\Sigma^+$ Term Values (continued)

J	T(cm^{-1}) v=2 C
0	33 623.410
1	33 623.871
2	33 624.786
3	33 626.166
4	33 628.000
5	33 630.294
6	33 633.049
7	33 636.264*
8	33 639.928*
9	33 644.058*
10	33 648.650*
11	33 653.695*
12	33 659.189
13	33 665.150
14	33 671.564
15	33 678.437
16	33 685.762
17	33 693.541
18	33 701.771
19	33 710.448
20	33 719.579
21	33 729.142
22	33 739.106
23	33 749.443

33 751.760

Table 3.5: C^{1+} Term Values (continued)

J		$T(cm^{-1})$
		v=2 (continued)
24	33 760.013	33 761.963
25	33 772.923	33 770.685
26	33 784.567	33 781.526
27		
28	33 809.358	33 810.082
29	33 822.693	
30	33 836.253	
31	33 850.269	
32	33 864.707	
33	33 879.540	

Table 3.5: $C^1\Sigma^+$ Term Values (continued)

J	T(cm^{-1}) v=3 ^{C}	
0		
1	34 061.232	
2	34 062.119	34 046.058
3	34 063.453	34 047.344*
4	34 065.233	34 049.076*
5	34 067.458	34 051.224*
6	34 070.128	34 053.796
7	34 073.220	34 056.798*
8	34 076.810	34 060.228
9	34 080.830	34 064.085
10	34 085.298	34 068.367
11	34 090.217	34 073.067
12	34 095.591	34 078.189
13	34 101.420	34 083.736
14	34 107.707	34 089.695
15	34 114.449	34 096.073
16	34 121.650	34 102.870
17	34 129.308	
18	34 137.419	34 117.699
19	34 146.041	34 125.732
20	34 155.064	34 134.166
21	34 164.573	34 143.025*
22	34 174.538*	34 152.286*
23	34 184.978	34 161.957

Table 3.5: $C^1\Sigma^+$ Term Values (continued)

J		$T(cm^{-1})$
		v=3 (continued)
24	34 195.876	34 172.047*
25	34 207.240	34 182.538
26	34 219.071	34 193.443
27	34 231.353	34 204.755
28	34 244.105	34 216.439
29	34 257.317	
30	34 270.993	
31	34 285.122	
32	34 299.719	
33	34 314.756	
34	34 330.426	
35	34 346.294	
36	34 362.651	
37	34 379.473*	
38	34 397.038	
39	34 414.828*	
40	34 433.069	
41	34 451.761	
42	34 470.910*	
43	34 490.489	
44		
45	34 530.930	
46	34 551.778	
47	34 573.031	

Table 3.5: $C^1\Sigma^+$ Term Values (cont.)

J	T (cm^{-1}) v=3 (cont.)	
48	34 594.627	
49	34 616.513	
50	34 639.664	34 648.714
51	34 660.973	34 670.559
52		34 638.397

Table 3.5: $C^1\Sigma^+$ Term Values (continued)

J	T(cm^{-1}) v=4[a]
15	34 530.6
16	34 537.7
17	34 545.3
18	34 553.3
19	34 561.8
20	34 570.5
21	34 579.9
22	34 589.6
23	34 599.7
24	34 609.9
25	34 621.0
26	34 632.4
27	34 643.8
28	34 656.1
29	34 668.4
30	34 681.5
31	34 694.3
32	34 707.8
33	34 721.4
34	34 735.7
35	34 749.9

[a]Absolute accuracy of 0.5 cm^{-1} and relative precision of 0.2 cm^{-1}. Energies are relative to $X^1\Sigma^+$(v"=0, J"=0).

Table 3.5: (cont.) (footnotes)

---

[b] Underlined energies correspond to perturbing levels (derived from extra lines).

[c] Absolute accuracy of 0.02 cm^{-1} and relative precision of 0.01 cm^{-1}. Energies are relative to $X^1\Sigma^+$ (v"=0, J"=0).

* Blended or otherwise degraded line. Relative precision 0.02 cm^{-1}.

Table 3.6: $D^1\Sigma^+$ Term Values

J	$T(cm^{-1})$
	$v = 3^a$
16	33 924.8
17	33 932.3
18	33 940.7
19	33 947.8
20	33 956.4
21	33 965.7
22	33 975.0
23	33 984.9
24	33 995.1
25	33 005.9
26	34 016.9
27	34 028.7
28	34 040.5
29	34 053.0
30	34 065.7
31	34 079.0
32	34 092.7
33	34 107.0
34	34 121.3
35	34 136.4
36	34 151.6
37	34 167.4

Table 3.6: (continued)

J	T(cm^{-1}) v = 3[a] (cont.)
38	34 183.5
39	34 200.0
40	34 217.0

J	T(cm^{-1}) v = 4[a]
14	34 284.8
15	34 291.2
16	34 297.9
17	34 305.3
18	34 312.9
19	34 320.9
20	34 329.5
21	34 338.6
22	34 347.8
23	34 357.6
24	34 367.9
25	34 378.5
26	34 389.6
27	34 401.0
28	34 412.9
29	34 425.2
30	34 437.8

Table 3.6: (continued)

J	T(cm^{-1})
	v = 4[a] (cont.)
31	34 451.1
32	34.464.2

v = 5[a]

J	T(cm^{-1})	J	T(cm^{-1})
17	34 670.0	36	34 887.0
18	34 678.1	37	34 903.1
19	34 685.7	38	34 919.1
20	34 694.1	39	34 935.5
21	34 703.1	40	34 952.2
22	34 712.3	41	34 969.6
23	34 722.1	42	34 987.2
24	34 732.3	43	35 005.3
25	34 743.1	44	35 024.0
26	34 754.0	45	35 042.9
27	34 765.4	46	35 062.1
28	34 777.1	47	35 082.3
29	34 789.6	48	35 102.3
30	74 802.1	49	35 122.9
31	34 815.2	50	35 144.5
32	34 828.6	51	35 165.3
33	34 842.7	52	35 187.1
34	34 856.9	53	35 209.1
35	34 871.8		

Table 3.6: (continued)

J	T(cm^{-1})
v = 6[a]	
18	35 054.5
19	35 062.4
20	35 070.9
21	35 080.1
22	35 089.2
23	35 098.9
24	35 109.2
25	35 119.7
26	35 130.6
27	35 142.1
28	35 154.1
29	35 165.9
30	35 178.5
31	35 191.5
32	35 205.2
33	35 219.6
34	35 233.9
35	35 248.4
36	35 263.8
37	35 279.4

[a]See footnote a in Table 3.5

Table 3.7: $E^1\Sigma^+$ Term Values

J	$T(cm^{-1})$
	$v = e^a$
18	34 301.0
19	34 309.0
20	34 317.8
21	34 326.9
22	34 336.2
23	34 346.3
24	34 357.0
25	34 367.8

[a]See footnote a in Table 3.5.

Table 3.8: Summary of $C^1\Sigma^+$ Perturbations

	Perturbing State			
$C^1\Sigma^+(v^*)$	2	3	4	5
0	$J_2 = 41.5$ $\eta = 0.139(2)$ $B^1\Pi$ (v=b)	—	—	—
1[b]	$J_2 < 0$ $\eta = -0.09(3)$ $B^1\Pi$ (v=b+1)	$J_3 = 31.0$ $\xi = 17.64(25)$	$J_4 > 41$ $\xi = 1.09(11)$ c(v=c)	—
2	$J_2 = 24.0$ $\xi = 1.004(5)$	$J_3 = 28.5$ $\xi = 0.270(16)$ c(v=c+1)	$J_4 > 33$ $\eta_{14} = 0.24(4)$	—
3	$J_2 < 0$ $\xi = 7.689(12)$ c(v=c+2)	$J_3 = 33.6$ $\xi = 0.19(3)$	$J_4 = 37.4$ $\xi = 0.35(4)$	$J_5 = 51.5$ $\xi = 4.824(7)$

[a] Each perturbation is characterized by the J value where it culminates (J_2, J_3,...), a heterogeneous (η) or homogeneous (ξ) parameter in cm^{-1} (see Table 3.9), and a

Table 3.8: (Continued) (Footnotes)

perturbing state assignment (when possible). Uncertainties of 1σ in the last digit are given in parentheses. Values of η and ξ may also be found in Table 3.10 with extra digits necessary to reproduce the data precisely (see Footnote a to Table 3.10).

[b] A heterogeneous interaction matrix element between perturbing states 2 and 3 was also fitted (see Table 3.10).

Figure 3.7: $C^1\Sigma^+$ vibration-rotation energy vs. J(J+1) indicating presence of spectroscopic perturbations. ⊏⊐ s denote culminations of heterogeneous $B^1\Pi \sim C^1\Sigma^+$ interactions; ● s denotes homogeneous $c \sim C^1\Sigma^+$ interactions; o s and x s denote unassigned homogeneous and heterogeneous interactions, respectively.

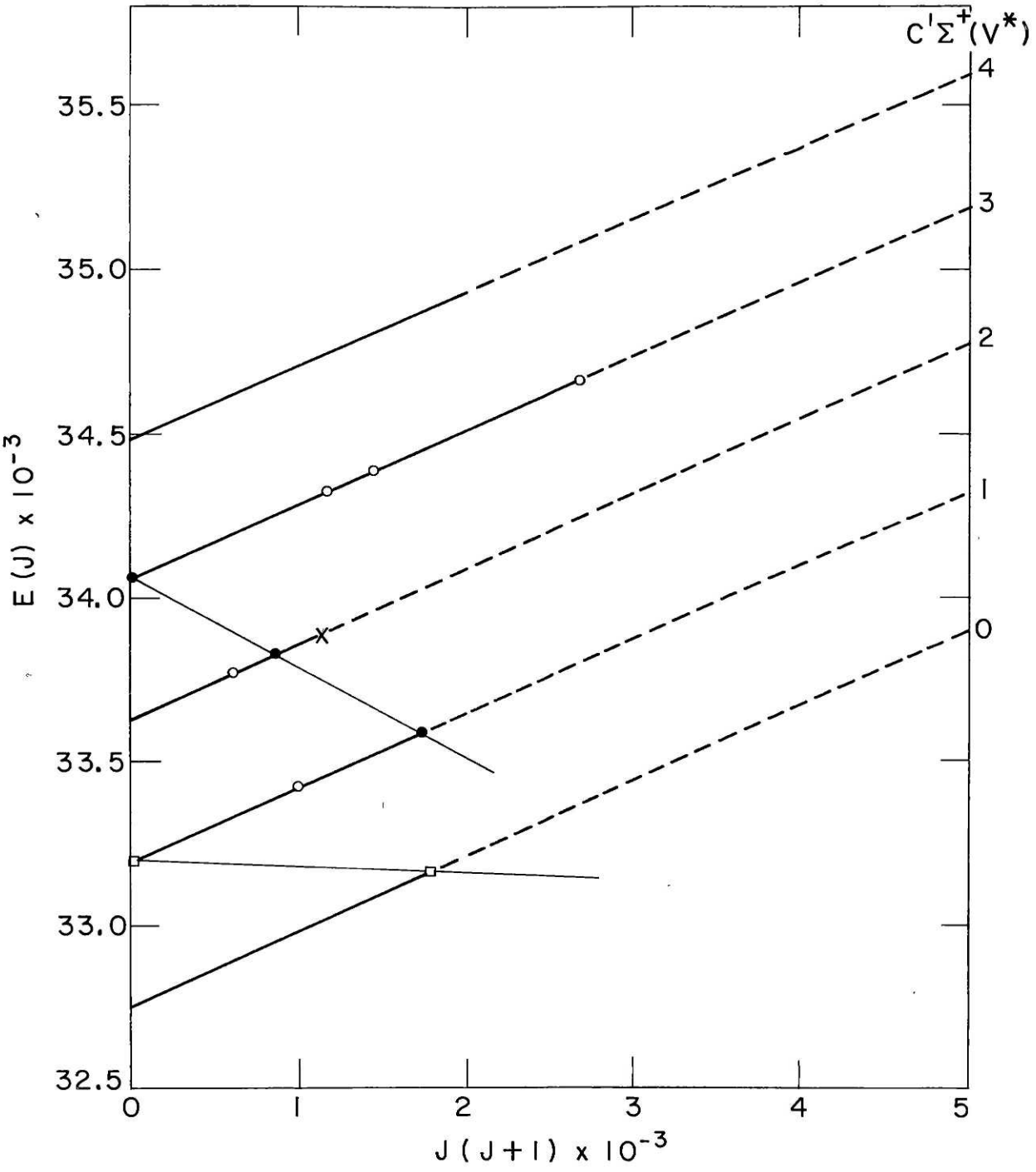

FIGURE 3.7

and corresponding term values may be found in Tables 3.2 and 3.5 respectively.

To deperturb $C^1\Sigma^+$, a simple, phenomenological Hamiltonian matrix (Table 3.9) is employed for reasons discussed below. Only e-parity levels are considered: a total of four perturbing states, numbered 2 through 5, (1 corresponds to $C^1\Sigma^+$), are included with two types of interactions: J-dependent, or heterogeneous, and J-independent, or homogeneous. The computer program is listed in Appendix 2.

In Hund's case 'a', homogeneous perturbations result from spin-orbit or configuration interactions; heterogeneous perturbations are a consequence of rotation-electronic interactions.[37] States which can perturb $^1\Sigma^+$ are $^1\Sigma^+$, $^1\Pi$, $^3\Pi_0$, and $^3\Sigma^-$ in the case 'a' limit; only the $^1\Sigma^+ \sim {}^1\Pi$ interaction is J-dependent. However, if the $^3\Pi$ state is intermediate between Hund's case 'a' and Hund's case 'b' (i.e. if spin is partially decoupled from the internuclear axis), nominal $^3\Pi_1$ and $^3\Pi_2$ may also perturb $^1\Sigma^+$; and since spin-uncoupling increases with J, $^3\Pi \sim {}^1\Sigma^+$ interactions may exhibit a J dependence.[37] Only one interaction matrix element - either homogeneous or heterogeneous - is fit for each perturbation; where the J-dependence of the interaction is not obvious, the homogeneous model is selected.

Diagonal matrix elments are represented by $^1\Sigma^+$ rotational energy expressions: $E+BJ(J+1)-DJ^2(J+1)^2$.

Deperturbed $C^1\Sigma^+$ and perturbing state energies, rotational constants, and interaction matrix elements are given in Table 3.10. Correlation matrices for each fitted level are given in Table 3.11. The results are discussed below for each $C^1\Sigma^+$ vibrational level.

$v^* = 0$

One perturbation culminating at J = 41.5 was previously reported and analyzed (Appendix 5). From interference between $\parallel$ and $\perp$ transition moments in $C^1\Sigma^+ \rightarrow X^1\Sigma^+$ UV fluorescence, it was concluded that the perturbation was heterogeneous and the perturbing state was assigned as $B^1\Pi(v = b)$ which lies higher and has a smaller rotational constant than $C^1\Sigma^+$ ($v^* = 0$).

$v^* = 1$

Three perturbations are observed. A strong, homogeneous perturbation culminating at J = 31.0 results in a doubling of the $C \leftarrow A$ (1,0) head (Table 3.1). The perturbing state (#3) lies higher and has a smaller rotational constant than $C^1\Sigma^+$ ($v^* = 1$).

In addition, several extra lines (Table 3.2) are observed corresponding to a level (#2) below $C^1\Sigma^+$ ($v^* = 1$) but with a smaller rotational constant so that no crossing

Table 3.9: e-Parity Hamiltonian Matrix for $C^1\Sigma^+$ Deperturbation

State

1	$E_1 + B_1x - D_1x^2$				
2	$\xi_{12} + \eta_{12}\, x^{\frac{1}{2}}$	$E_2 + B_2x - D_2x^2$		SYMMETRIC	
3	ξ_{13}	$\eta_{23}x^{\frac{1}{2}}$	$E_3 + B_3x - D_3x^2$		
4	$\xi_{14} + \eta_{14}\, x^{\frac{1}{2}}$	0	0	$E_4 + B_4x - D_4x^2$	
5	ξ_{15}	0	0	0	$E_5 + B_5x - D_5x^2$

where $x = J(J+1)$

E vibronic energy

$B = \frac{h}{8\pi^2 c\mu R^2}$ rotational constant

D centrifugal distortion constant

ξ homogeneous interaction parameter

η heterogeneous interaction parameter

Table 3.10: $C^1\Sigma^+$ Parameters[a]

	v = 0		
E_1	$= 3.27497_{000}$	$\pm$ 0.00005	x 10^4
B_1	$= 0.2383_{290}$	$\pm$ 0.0003	
D_1	= 2.8	fixed	x 10^{-7}
E_2	$= 3.27708_{000}$	$\pm$ 0.00010	x 10^4
B_2	$= 0.2264_{188}$	$\pm$ 0.0006	
D_2	= 2.8	fixed	x 10^{-7}
η_{12}	$= 0.139_{540}$	$\pm$ 0.002	

$\sigma^2 = 0.4$

Table 3.10: (cont.)

	$v = 1$
E_1	$= 3.31808_{874} \pm 0.00007 \times 10^4$
B_1	$= 0.2379_{111} \pm 0.0005$
D_1	$= 1.30_{106} \pm 0.18 \times 10^{-6}$
E_2	$= 3.316689_{918} \pm 0.000006 \times 10^4$
B_2	$= 0.2223_{938} \pm 0.0014$
D_2	$= 2.8$ fixed $\times 10^{-7}$
η_{12}	$= -0.09_{093} \pm 0.03$
E_3	$= 3.31918_{415} \pm 0.00008 \times 10^4$
B_3	$= 0.2167_{654} \pm 0.0010$
D_3	$= 2.8$ fixed $\times 10^{-7}$
ξ_{13}	$= 1.764_{284} \pm 0.025 \times 10^1$
E_4	$= 3.323611_{595} \pm 0.000016 \times 10^4$
B_4	$= 0.21$ fixed
D_4	$= 2.8$ fixed $\times 10^{-7}$
ξ_{14}	$= 1.09_{293} \pm 0.11$
η_{23}	$= 0.23_{938} \pm 0.04$

$\sigma^2 = 0.9$

Table 3.10: (cont.)

$\underline{v = 2}$

E_1	$= 3.3623484_{700}$	± 0.0000003	$\times 10^4$
B_1	$= 0.2314_{050}$	± 0.0004	
D_1	$= -5.8_{029}$	± 2.4	$\times 10^{-7}$
E_2	$= 3.363831_{560}$	± 0.000006	$\times 10^4$
B_2	$= 0.20469_{540}$	± 0.00009	
D_2	$= 2.8$	fixed	$\times 10^{-7}$
ξ_{12}	$= 1.004_{086}$	± 0.005	
E_3	$= 3.3639631_{100}$	± 0.0000011	$\times 10^4$
B_3	$= 0.21$	fixed	
D_3	$= 2.8$	fixed	$\times 10^{-7}$
ξ_{13}	$= 0.270_{146}$	± 0.016	
E_4	$= 3.36629_{340}$	± 0.000020	$\times 10^4$
B_4	$= 0.21$	fixed	
D_4	$= 2.8$	fixed	$\times 10^{-7}$
η_{14}	$= 0.27_{034}$	± 0.04	

$\sigma^2 = 0.5$

Table 3.10: (cont.)

$\nu = 3$

E_1	$= 3.405545_{520}$	± 0.000003	$\times 10^4$
B_1	$= 0.23027_{713}$	± 0.00003	
D_1	$= 2.11_{005}$	± 0.12	$\times 10^{-7}$
E_2	$= 3.405042_{181}$	± 0.000003	$\times 10^4$
B_2	$= 0.20753_{364}$	± 0.00003	
D	$= 2.8$	fixed	$\times 10^{-7}$
ξ_{12}	$= 7.689_{472}$	± 0.012	
E_3	$= 3.40843_{613}$	± 0.00003	$\times 10^4$
B_3	$= 0.2068_{682}$	± 0.0003	
D_3	$= 2.8$		$\times 10^{-7}$
ξ_{13}	$= 0.19_{134}$	± 0.03	
E_4	$= 3.40880_{230}$	± 0.00011	$\times 10^4$
B_4	$= 0.2080_{771}$	± 0.0008	
D_4	$= 2.8$		$\times 10^{-7}$
ξ_{14}	$= 0.35_{352}$	± 0.04	
E_5	$= 3.41226_{168}$	± 0.00004	$\times 10^4$
B_5	$= 0.20563_{445}$	± 0.00015	
D_5	$= 2.8$	fixed	$\times 10^{-7}$
ξ_{15}	$= 4.824_{352}$	± 0.007	

$\sigma^2 = 1.6$

Table 3.10: (cont.)

$v = 4$		
E_1	$= 3.447602_{018}$	$\pm 0.000017 \times 10^4$
B_1	$= 0.2291_{425}$	± 0.0005
D_1	$= 9.2_{277}$	$\pm 0.4 \times 10^{-7}$
σ^2	$= 0.5$	

[a]All units are cm^{-1}. Parameters are defined by Table 3.9. Uncertainties quoted are 1σ estimates. Three extra digits, statistically insignificant, are given in order to account for correlations among parameters when using these parameters to reproduce the data (Ref. 38); correlation coefficients can be found in Table 3.11. Variances quoted are a measure of the accuracy of the experimental errors quoted in Table 3.5: $\sigma^2 > 1$ means these errors were underestimated and vice versa for $\sigma^2 < 1$; $\sigma^2 = 1$ means the uncertainties quoted are comparable to the differences between observed and calculated term values. This variance is approximately related to the rms deviation by: $\sigma_{rms} \sim 0.2\sigma$ cm^{-1} for $v^*=1$ and 4 and $\sigma_{rms} \sim 0.01\sigma$ cm^{-1} for $v^*=2,3$, and 4. All parameters not listed were fixed at zero.

Table 3.11: $C^1\Sigma^+$ Correlation Matrices[a]

V=0

E_1	1.000				
B_1	-0.941	1.000			
E_2	-0.440	0.462	1.000		
B_2	0.432	-0.483	-0.986	1.000	
η_{12}	0.263	-0.308	-0.848	0.842	1.000

Table 3.11: (cont.)

V=1

E_1	1.000									
B_1	0.553	1.000								
D_1	0.589	0.998	1.000							
E_2	-0.648	-0.921	-0.934	1.000						
B_2	-0.650	-0.819	-0.836	0.973	1.000					
E_3	-0.614	-0.996	-0.999	0.938	0.841	1.000				
B_3	-0.552	-0.982	-0.975	0.843	0.720	0.973	1.000			
E_4	0.061	-0.215	-0.197	-0.022	-0.204	0.194	0.293	1.000		
ξ_{13}	0.641	0.992	0.997	-0.941	-0.847	-0.999	-0.968	-0.183	1.000	
η_{12}	0.563	0.980	0.971	-0.863	-0.758	-0.968	-0.992	-0.252	0.963	1.000
η_{23}	0.594	0.987	0.981	-0.886	-0.785	-0.979	-0.992	-0.234	0.976	0.998
ξ_{14}	0.288	0.081	0.105	-0.366	-0.546	-0.110	0.030	0.916	0.123	0.024

V=1 (CONT.)

η_{23}	1.000	
ξ_{14}	0.051	1.000

Table 3.11: (cont.)

V=2

E_1	1.000									
B_1	0.127	1.000								
D_1	-0.261	-0.950	1.000							
ξ_{12}	0.195	0.049	0.058	1.000						
E_2	-0.147	-0.122	-0.001	-0.786	1.000					
B_2	0.142	0.087	0.038	0.790	-0.995	1.000				
E_4	0.091	0.984	-0.891	0.064	-0.146	0.116	1.000			
E_3	-0.143	-0.212	0.227	-0.190	0.146	-0.137	-0.164	1.000		
ξ_{13}	-0.059	-0.828	0.779	0.053	0.048	-0.019	-0.841	-0.209	1.000	
η_{14}	0.155	0.999	-0.959	0.030	-0.102	0.068	0.983	-0.203	-0.833	1.000

Table 3.11 (cont.)

V=3

E_1	1.000									
B_1	-0.954	1.000								
D_1	-0.858	0.954	1.000							
ξ_{12}	-0.963	0.889	0.766	1.000						
E_2	-0.971	0.920	0.804	0.957	1.000					
B_2	0.880	-0.862	-0.765	-0.839	-0.936	1.000				
E_5	-0.179	0.152	0.314	0.067	0.092	-0.091	1.000			
B_5	0.156	-0.122	-0.278	-0.047	-0.070	0.070	-0.999	1.000		
ξ_{15}	0.398	-0.444	-0.536	-0.326	-0.347	0.335	-0.080	0.052	1.000	
E_3	0.015	0.087	0.174	-0.008	-0.013	0.007	0.068	-0.058	-0.110	1.000
B_3	-0.010	-0.093	-0.179	0.004	0.008	-0.002	-0.068	0.057	0.111	-0.998
ξ_{13}	0.115	-0.017	0.078	-0.100	-0.109	0.097	0.058	-0.051	-0.068	0.962
E_4	-0.069	0.208	0.306	0.068	0.069	-0.075	0.067	-0.052	-0.162	0.189
B_4	0.074	-0.216	-0.312	-0.072	-0.074	0.080	-0.062	0.047	0.162	-0.205
ξ_{14}	0.027	0.110	0.229	-0.020	-0.023	0.013	0.076	-0.062	-0.139	0.158

Table 3.11 (cont.)

V=3 (CONT.)

B_3	1.000				
ξ_{13}	-0.959	1.000			
E_4	-0.182	0.188	1.000		
B_4	0.198	-0.203	-0.998	1.000	
ξ_{14}	-0.149	0.170	0.923	-0.907	1.000

Table 3.11 (cont.)

V=4

E_1	1.000		
B_1	-0.960	1.000	
D_1	-0.903	0.983	1.000

[a]Parameters are defined by Table 3.9. Correlation matrices are symmetric and related to the covariance matrix by: $c_{ij}=\sigma^2_{ij}/(\sigma^2_i\sigma^2_j)^{1/2}$ where c_{ij} is the ij^{th} correlation coefficient, σ^2_{ij} the ij^{th} covariance matrix element, and σ^2_i the i^{th} variance

occurs. In order to fit the data, interactions between not only this state and v* = 1 (η_{12}) but also interaction between 2 and 3 (η_{23}) needs to be considered; both interactions are found to be heterogeneous. Comparing E_2 and B_2 values in the v* = 0 and v* = 1 fits (Table 3.10),

$$\begin{aligned} E_2(v^* = 1) - E_2(v^* = 0) &= 396.1 \text{ cm}^{-1} \\ B_2(v^* = 1) - B_2(v^* = 0) &= -0.004 \text{ cm}^{-1}. \end{aligned} \tag{3.1}$$

where E_2 and B_2 are the perturbing state energy and rotational constant, respectively. These differences are typical of vibrational and rotational intervals observed in this energy region (see below and Ref. 3) and it seems plausible, therefore, that these vibrational levels belong to the same electronic state (i.e. $B^1\Pi$); the heterogeneous nature of the 1 $\sim$ 2 and 2 $\sim$ 3 interactions in v* = 1 further supports this hypothesis.

A third perturbation is apparent at J > 40 and is assumed to be homogeneous.

v* = 2

Three perturbations are observed with crossings at $J_2 = 24.0$, $J_3 = 28.5$, and $J_4 > 33$. The first two (states 2 and 3) are well characterized by the appearance

of extra lines and appear to be J-independent although the interactions are two weak to be certain. At $J > 33$ a strong perturbation becomes apparent; it is not possible to extend the analysis with only the R branch data in hand. A J-dependent interaction is assumed but the term values could be equally well fit assuming a J-independent interaction. The former model is chosen because it results in a more reasonable value for the $C^1\Sigma^+$ rotational constant; the homogeneous interaction model gives a value of B_1 ($v^* = 2$) less than the value of B_1 ($v^* = 3$). It is apparent from the negative value of D_1 (Table 3.10) that $v^* = 2$ is incompletely deperturbed.

$v^* = 3$

Four interactions are observed with crossings $J_2 < 0$, $J_3 = 33.6$, $J_4 = 37.4$, and $J_5 = 51.5$. An extra head results from the $1 \sim 2$ perturbation (Table 3.1, Fig. 3.8); extra lines are also observed at the other crossings. All four perturbations are fit to homogeneous interaction models but only the $1 \sim 2$ interaction is definitely J-independent. This level is well fit despite the exclusion of at least three other weakly interacting perturbing states detected by the appearance of extra lines (Appendix 7). $v^* = 3$ perturbations

are illustrated in Fig. 3.8.

Comparing the energies of perturbing levels 4(v* = 1), 3(v* = 2), and 2(v* = 3),

$$E_2(v^* = 3) - E_3(v^* = 2) = 410.8 \text{ cm}^{-1}$$
$$E_3(v^* = 2) - E_4(v^* = 1) = 403.6 \text{ cm}^{-1} \qquad (3.2)$$

and considering that these interactions are all homogeneous, it is plausible that they belong to the same electronic state. Unfortunately, the data are insufficient to determine rotational constants except for level 2 (v* = 3). Extrapolating to higher energy, the next two levels of this state are predicted to lie at 34458 cm^{-1} and 34865 cm^{-1}. The latter is close to the c (v = c+4) level mentioned above, E(v=c+4) ≈ 34855 cm^{-1}†, which is in turn near $C^1\Sigma^+(v^*=5)$ from which it may borrow oscillator strength. On this basis the 4(v* = 1), 3(v* = 2), and 2(v* = 3) perturbing levels, and the level with head at 16 655.2 cm^{-1} in Table 3.1 are tentatively assigned as c(v = c), c(v=c+1), c(v=c+2), and c(v=c+4), respectively. The lower case c label for this state is chosen because oscillator strength to $A^1\Sigma^+$ and $X^1\Sigma^+$ appears to be borrowed from

†Calculated from the head position given in Table 3.1 and assuming the head-origin separation to be negligible

Figure 3.8: Perturbations in $C^1\Sigma^+$ ($v^* = 3$). Observed minus calculated term values are plotted against J.

a) Calculated term values with ξ_{12}, ξ_{13}, ξ_{14}, and ξ_{15} (see Table 3.9) set equal to zero. O s denote main levels (> 50% $C^1\Sigma^+$ character), □ s denote #2 perturbing state levels, ● denotes #3 extra level and x s denote #5 extra levels.

b) As in (a) except ξ_{12} included and equal to 7.689 cm^{-1}. Insert shows $1 \sim 3$ and $1 \sim 4$ interactions when ξ_{15} (4.824 cm^{-1}) is also included. Note that the center of gravity for the $1 \sim 3$ interaction is preserved despite appearances when $\xi_{12} = \xi_{15} = 0$. This illustrates the complicated level shifts associated with multiple perturbations.

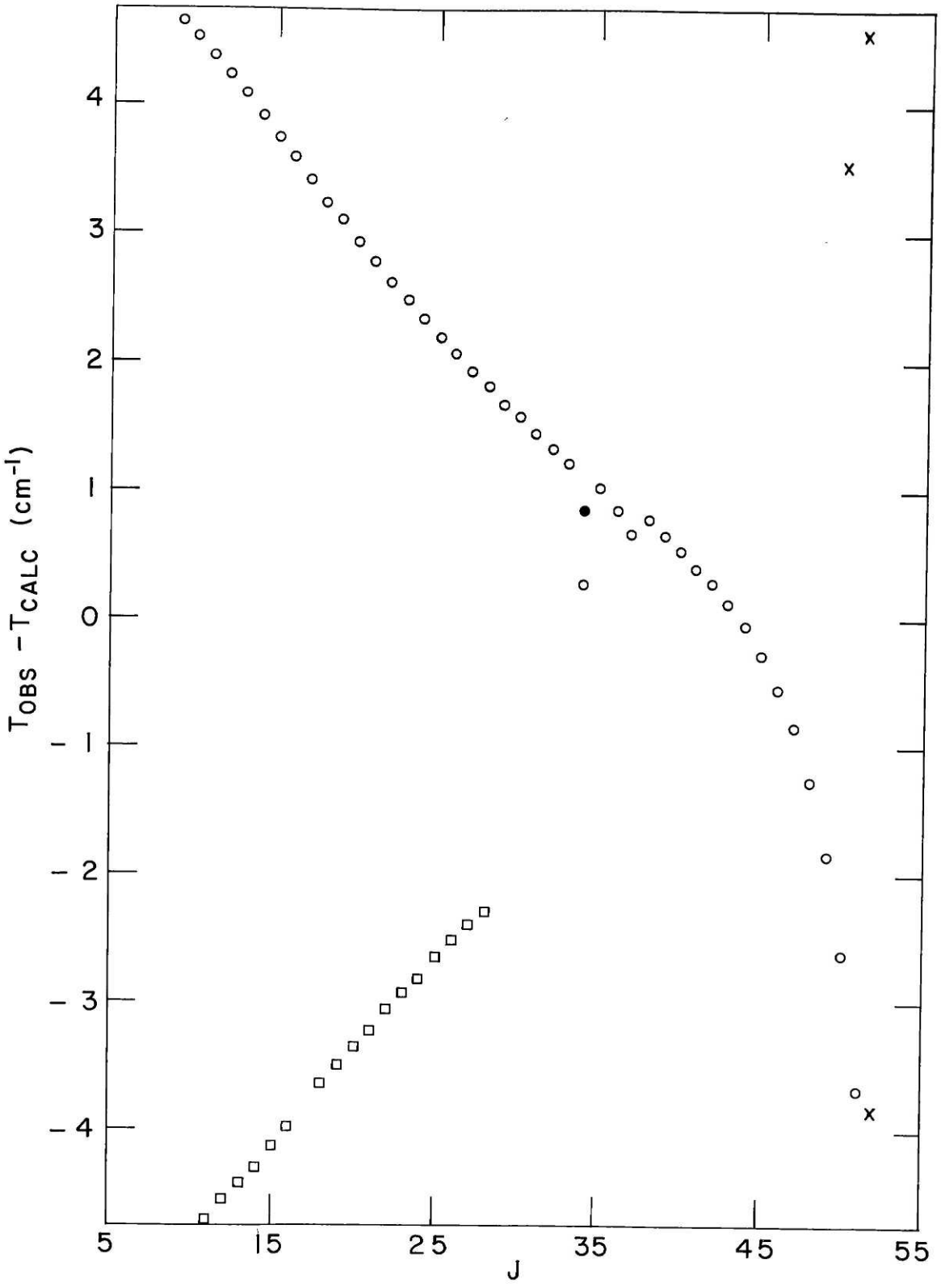

FIGURE 3.8a

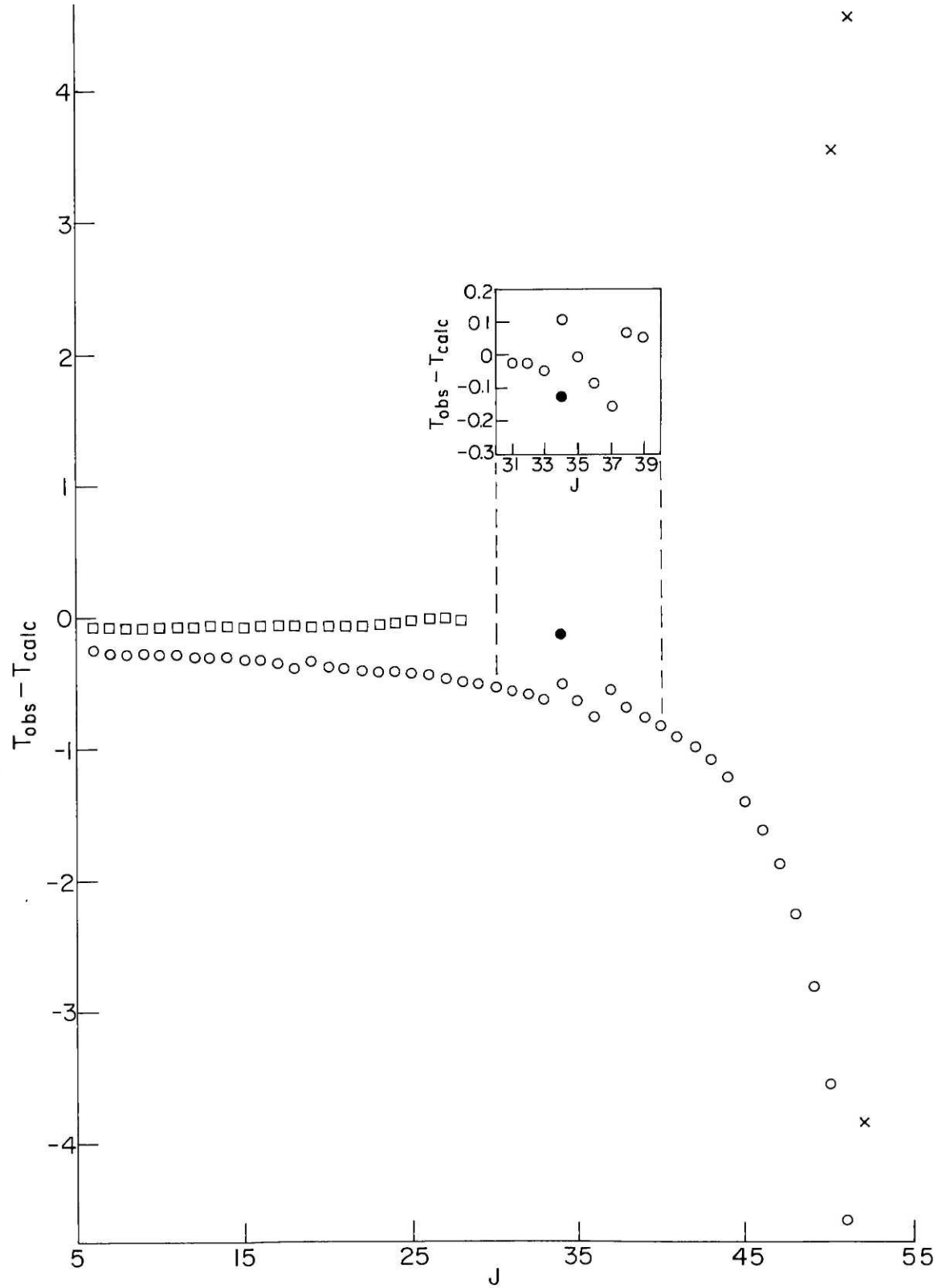
4
3
2
1
0
-1
-2
-3
-4
$T_{obs} - T_{calc}$
5
15
25
35
45
55
J
0.2
0.1
0
-0.1
-0.2
-0.3
31
33
35
37
39
J
$T_{obs} - T_{calc}$

Figure 3 8b

$C^1\Sigma^+$. This intensity borrowing, the homogeneous nature of c $\sim$ $C^1\Sigma^+$ interactions, and observation of $C^1\Sigma^+ \rightarrow a^3\Sigma^+$ and $b^3\Pi_0$ emission (Section III.B) suggest that this state has predominantly triplet character.†

$v^* = 4$

No perturbations are obvious within the precision of the broad bandwidth excitation spectrum.

It is seen From Table 3.10 that the deperturbed $C^1\Sigma^+$ energies and rotational intervals decrease

---

†Only three states may homogeneously perturb $C^1\Sigma^+$ in first order: $^1\Sigma^+$, $^3\Pi_0$, and $^3\Sigma^-$. It is conceivable that c could have $^1\Sigma^+$ character but somewhat surprising that it would have no oscillator strength to the $A^1\Sigma^+$ or $X^1\Sigma^+$ states; moreover, $^1\Sigma^+ \sim {}^1\Sigma^+$ mixing cannot explain $C^1\Sigma^+ \rightarrow a^3\Sigma^+$ and $b^3\Pi_0$ emission. Similarly, $^3\Sigma^- \sim {}^1\Sigma^+$ mixing cannot account for this emission intensity since $^3\Sigma^- \sim {}^3\Sigma^+$ electric dipole transitions are forbidden[32]. In addition $^3\Sigma^- \sim {}^1\Sigma^+$ perturbations should exhibit two crossings for each pair of interacting vibrational levels (for a near Hund's case 'b' $^3\Sigma^-$ state)[37] whereas the data do not provide conclusive evidence of multiple crossings: in $v^* = 2$, the $1 \sim 3$ and $1 \sim 4$ interactions could correspond to the two e parity[36] components of $^3\Sigma^-$ but the $1 \sim 3$ interaction is ~ 5 times stronger than the $1 \sim 4$ interaction, contrary to expectations.[37] Evidence for such a multiple crossing is not observed in $v^* = 1$ (Fig. 3.7). $^3\Pi_0 \sim {}^1\Sigma^+$ mixing accounts for all observations: $^3\Pi_0 \rightarrow b^3\Pi_0$ and $a^3\Sigma^+$ emission is allowed and only one homogeneous interaction is expected for a Hund's case 'a' $^3\Pi$ state. It is plausible, therefore, that the c state has $^3\Pi_0$ symmetry.

monotonically with increasing v as expected from anharmonicities in the potential but in contrast to the irregularities observed for perturbed values.[23] However, the variations are not regular even after deperturbation. This is not surprising considering (1) the phenomenological nature of the Hamiltonian matrix, (2) strong correlations between fitted parameters (Table 3.11), (3) neglect of second order energy and rotational constant corrections, and (4) neglect of additional perturbing states. The great density of electronic states in this energy region manifested by the large number of perturbing levels detected would make complete deperturbation difficult even with additional data; second order effects, in particular, are on the order of 1-10 cm^{-1} owing to strong spin-orbit interactions associated with the heavy Ba atom. Nonetheless, local deperturbation of individual vibrational levels has been achieved: the constants given in Table 3.10 reproduce the spectra to within experimental error and provide reliable mixing coefficients essential to population monitoring of lower energy states.

It is convenient to summarize spectroscopic data in the form of potential energy curves. To this purpose $C\,^1\Sigma^+$ energies and rotational constants from Table 3.10 are combined with data from Ref. 23 and least squares fitted to a polynomial in $(v + 1/2)$ (i.e. a Dunham

expansion[39]):

$$E(v,J) = \sum_{\ell,k} Y_{\ell k} (v+1/2)^{\ell} J^{k} (J+1)^{k} \qquad (3.3)$$

where E(v,J) is the vibration-rotation energy and the $Y_{\ell k}$ are spectroscopic constants (ω_e, B_e,...). Ref. 23 data are assigned uncertainties of 1 cm^{-1}, which is greater than the quoted error, since they are derived from band heads and not origins. Although the energies from Ref. 23 are perturbed, the unperturbed energies determined here are weighted according to their uncertainties in Table 3.10 and constrain the fitted parameters. In addition, first order perturbation energy shifts tend to average to zero if enough levels are considered; the results presented in Table 3.12 represent a potential not designed to precisely reproduce observed energies but rather provide estimates for properties such as bond strength, equilibrium internuclear distance, and Franck-Condon factors. Comparison with constants from Refs. 22 and 23 is also given; the latter rotational constants were determined by matching observed and calculated $C^1\Sigma^+ \rightarrow X^1\Sigma^+$ Franck-Condon intensity factors. Vibrational constants reported in Ref. 22 were obtained from less precise as well as perturbed data. Also given in Table 3.12, are spectroscopic constants for $B^1\Pi$ and c determined from the

Table 3.12: Spectroscopic Constants for High Lying States of BaO[a]

	$D^1\Sigma^+$	$C^1\Sigma^+$	$B^1\Pi$	$E^1\Sigma^+$	c
$\nu_{00} \times 10^{-4}$	3.2701 (6)	3.27562 (30)	$\leq$ 3.27708 (30)	3.4226 (6)	$\leq$ 3.32361 (30)
$T_e \times 10^{-4}$	3.2835 (6)	3.28727 (30)			
Y_{00}	-0.425	0.943			
$Y_{10}(\omega_e) \times 10^{-2}$	4.036 (28)	4.360 (8) [4.39][b]	$\geq$ 3.96 (5)		$\geq$ 4.08 (5)
$Y_{20}(-\omega_e x_e)$	-3.8 (3)	-0.90 (16)			-1.2 (5)
$Y_{30}(\omega_e y_e) \times 10^2$		4.1 (10)			
$Y_{01}(B_e)$	0.2197(20)	0.2397 (6) [0.23931][c]	$\geq$ 0.2284 (10)	$\geq$ 0.2174 (10)	$\geq$ 0.210 (10)
$Y_{11}(-\alpha_e) \times 10^3$	-1.5 (4)	-2.70 (18) [-0.17][c]	-4.1 (15)		
R_e(Å)	2.314 (10)	2.2151 (28)	$\leq$ 2.269 (5)	$\leq$ 2.326 (5)	$\leq$ 2.37 (6)

[a] All units are cm^{-1} except where noted. Uncertainties of 1σ in last digit are given in parentheses and are generously estimated to account for incomplete deperturbation. Previously reported values are given in brackets below the values determined here.

[b] Ref. 22

[c] Ref. 23

assignments made above and the fitted parameters in Table 3.10.

4. $D^1\Sigma^+$ and $E^1\Sigma^+$

Since no perturbations are obvious within the limited precision and resolution afforded by broad bandwidth OODR, $D^1\Sigma^+$ and $E^1\Sigma^+$ term values from Tables 3.6 and 3.7, respectively, are least squares fitted to $^1\Sigma^+$ energy expressions. The results are given in Tables 3.13 - 3.15. The $D^1\Sigma^+$ energies and rotational constants are subsequently fit to polynomials in $v + 1/2$. The results are given in Table 3.12; in the energy expansion, $D^1\Sigma^+(v^* = 6)$ is excluded because the energy is ≈ 20 cm^{-1} too high due to a perturbation near the band origin. Insufficient data preclude varying a perturbation matrix element and deperturbing the $D^1\Sigma^+ - A^1\Sigma^+$ (6,3) band origin.

B. $C^1\Sigma^+$ Fluorescence Spectra

1. Electronic and Vibrational Assignments

Emission from $C^1\Sigma^+$ to not only $X^1\Sigma^+$ and $A^1\Sigma^+$ but also $a^3\Sigma^+$, $b^3\Pi_0$, $b^3\Pi_1$, and $A'^1\Pi$ is observed (Appendices 5 and 6). $C^1\Sigma^+ \rightarrow b^3\Pi$ and $A'^1\Pi$ fluorescence assignments are based upon the constants for the lower states reported by Field[9] as well as the rotational

Table 3.13: $D^1\Sigma^+$ Parameters[a]

v = 3	v = 4
$E_1 = 3.386637_{768} \pm 0.000012 \times 10^4$	$E_1 = 3.423970_{344} \pm 0.000013 \times 10^4$
$B_1 = 0.2149_{985} \pm 0.0003$	$B_1 = 0.2147_{217} \pm 0.0005$
$D_1 = 6.2_{415} \pm 2.0 \times 10^{-7}$	$D_1 = 1.8_{237} \pm 0.4 \times 10^{-6}$
$\sigma^2 = 0.9$	$\sigma^2 = 0.24$
v = 5	**v = 6**
$E_1 = 3.460543_{743} \pm 0.000010 \times 10^4$	$E_1 = 3.498212_{789} \pm 0.000010 \times 10^4$
$B_1 = 0.21217_{615} \pm 0.00017$	$B_1 = 0.21167_{334} \pm 0.00013$
$D_1 = 3.4_{447} \pm 0.6 \times 10^{-7}$	$D_1 = 2.8$ fixed $\times 10^{-7}$
$\sigma^2 = 2.0$	$\sigma^2 = 0.5$

[a]See footnote a, Table 3.10

Table 3.14: $D^1\Sigma^+$ Correlation Matrices[a]

v = 3

E_1	1.000		
B_1	-0.959	1.000	
D_1	-0.904	0.984	1.000

v = 4

E_1	1.000		
B_1	-0.962	1.000	
D_1	-0.907	0.983	1.000

v = 5

E_1	1.000		
B_1	-0.934	1.000	
D_1	-0.844	0.970	1.000

v = 6

E_1	1.000	
B_1	-0.929	1.000

[a]See footnote a, Table 3.11.

Table 3.15a: $E^1\Sigma^+$ Parameters[a]

$E_1 = 3.422650_{281} \pm 0.000027 \times 10^4$

$B_1 = 0.2174_{172} \pm 0.0005$

$D_1 = 2.8$ fixed $\times 10^{-7}$

$\sigma^2 = 0.6$

---

[a]See footnote a, Table 3.10.

Table 3:15b: $E^1\Sigma^+$ Correlation Matrix[a]

E_1	1.000	
B_1	-0.979	1.000

---

[a]See footnote a, Table 3.11.

structure observed: P,R, doublets for $b^3\Pi_0$ and P,Q,R triplets for $b^3\Pi_1$ and $A'^1\Pi$ (Appendix 5). The former implies $\Delta\Omega = 0$ and the latter implies $\Delta\Omega = 1$, where Ω is the projection of J onto the internuclear axis.[32,40] $a^3\Sigma^+$ assignments are made from (1) the pattern of emission (^{P}P, ^{P}Q, ^{P}R, and ^{R}R branches, where the superscript denotes the change in N = J, J $\pm$ 1)[41] and (2) observation of $a^3\Sigma^+ \sim A'^1\Pi$ perturbations described below.[37] In addition, emission ascribed to $a^3\Sigma^+$ could not be accounted for by any other known lower state (Appendix 6). Typical emission spectra can be found in Appendices 5 and 6. The $^3\Sigma^+$ energy level structure is illustrated in Figure 1 of Appendix 6.

Vibrational assignments for $b^3\Pi$ and $A'^1\Pi$ are made from Field's analysis.[9] $a^3\Sigma^+$ vibrational assignments are made from the vibrational variation of $a^3\Sigma^+ \sim A'^1\Pi$ matrix elements (see Chapter 2 and Appendix 6).

Observed $C^1\Sigma^+$ emission bands are given in Table 3.16 along with calculated band head positions. Band heads are <u>not</u> observed since emission from a single $C^1\Sigma^+$ rovibronic level is monitored; evidence for $C^1\Sigma^+$ rotational relaxation, which could produce a band head, in the form of collisional satellite lines is not observed at pressures $\simeq$ 1 torr.

In order to provide estimates of band head positions useful to the experimentalist, <u>perturbed</u> $A'^1\Pi$ and $b^3\Pi_1$

energies[†], 17 577 cm^{-1} [10-12] and 17 322 cm^{-1} [9] respectively, are used. $C^1\Sigma^+$ perturbed energies are also used by correcting the deperturbed energies in Table 3.10 by the difference between observed (from Table 3.1) and calculated (from constants in Tables 3.10 and 3.31) $C^1\Sigma^+ - A^1\Sigma^+$ band heads observed in excitation. Differences between perturbed and deperturbed energies for the remaining states are neglected since large, low J interactions responsible for shifting the band head are not present (see below). The heads calculated in Table 3.16 are accurate to $\pm$ 5 cm^{-1}. Emission from $C^1\Sigma^+$ ($v^* = 4$), $D^1\Sigma^+$, and $E^1\Sigma^+$ to states other than $X^1\Sigma^+$ was not examined.

2. Rotational Analysis

32 of the bands listed in Table 3.16 are rotationally analyzed. Transition wave numbers and rotational assignments are given in Tables 3.17 through 3.20. The bands are only partially analyzed since emission from a single rovibronic level populates at most four (e.g. $C^1\Sigma^+ \rightarrow a^3\Sigma^+$ emission) and as few as two (e.g. $C^1\Sigma^+ \rightarrow A^1\Sigma^+$ or $b^3\Pi_0$) lower levels. Thus, to obtain complete rotational analyses it is necessary to painstakingly re-tune both pump and probe

---

[†] ν_{00}

Table 3.16: Observed $C^1\Sigma^+$ Emission Bands[a]

Band (v*,v)	σ_{Head} (cm^{-1})	λ^{Air}_{Head} (nm)
	$C^1\Sigma^+ \rightarrow a^3\Sigma^+$	
(3,6)	14 813	674.9
(3,7)	14 362	696.1
(3,8)	13 916	718.4
(2,11)	12 166	821.7
(2,12)	11 735	851.9
	$C^1\Sigma^+ \rightarrow A^1\Sigma^+$	
(3,0)	17 325	577.0
(2,0)	16 905	591.4
(3,1)	16 829	594.1
(1,0)	16 449	607.8
(2,1)	16 408	609.3
(3,2)	16 336	612.0
(0,0)	16 032	623.6
(1,1)	15 953	626.7
(2,2)	15 916	628.1
(3,3)	15 846	630.9
(0,1)	15 536	643.5
(1,2)	15 460	646.6
(2,3)	15 426	648.1
(3,4)	15 359	650.9
(0,2)	15 043	664.6

Table 3.16: (cont.)

Band (v*,v)	σ_{Head} (cm^{-1})	λ^{Air}_{Head} (nm)
	$C^1\Sigma^+ \rightarrow A^1\Sigma^+$ (cont.)	
(1,3)	14 971	667.8
(2,4)	14 939	669.2
(3,5)	14 875	672.1
(0,3)	14 553	686.9
(2,5)	14 455	691.6
(3,6)	14 394	694.5
(2,6)	13 974	715.4
(3,7)	13 915	718.4
(1,6)	13 519	739.5
(2,7)	13 495	740.8
(3,8)	13 439	743.9
(2,8)	13 019	767.9
(3,9)	12 966	771.1
(1,9)	12 092	826.8
(2,10)	12 074	828.0
(1,10)	11 621	860.3
	$C^1\Sigma^+ \rightarrow b^3\Pi_1$	
(3,1)	16 264	614.7
(2,1)	15 844	631.0
(1,0)	15 833	631.4
(3,2)	15 826	631.7
(0,0)	15 416	648.5

Table 3.16: (cont.)

Band (v*,v)	σ_{Head} (cm^{-1})	λ^{Air}_{Head} (nm)
	$C^1\Sigma^+ \rightarrow b^3\Pi_1$ (cont.)	
(1,1)	15 390	649.6
(0,1)	14 973	667.7
(2,3)	14 973	667.7
(3,4)	14 964	668.1
(1,2)	14 952	668.6
(3,5)	14 540	687.6
(0,2)	14 535	687.8
(3,6)	14 120	708.0
(3,7)	13 705	729.5
(2,6)	13 700	729.7
(3,8)	13 294	752.0
(2,7)	13 284	752.6
(3,9)	12 888	775.7
(1,7)	12 829	779.3
(2,9)	12 467	801.9
(1,8)	12 418	805.0
(3,11)	12 089	827.0
(1,9)	12 012	832.3

Table 3.16: (cont.)

Band (v*,v)	$\sigma_{Head}(cm^{-1})$	$\lambda^{Air}_{Head}(nm)$
	$C^1\Sigma^+ \rightarrow b^3\Pi_o$	
(3,0)	16 551	604.0
(2,1)	15 689	637.2
(3,3)	15 238	656.1
(2,3)	14 818	674.7
(3,4)	14 810	675.1
(3,5)	14 385	695.0
(1,3)	14 364	696.0
(3,6)	13 965	715.9
(3,7)	13 550	737.8
(2,6)	13 545	738.1
(3,8)	13 139	760.9
(3,9)	12 733	785.1
(2,8)	12 719	786.0
(3,10)	12 331	810.7
(1,8)	12 264	815.2
(3,11)	12 934	837.7
(1,9)	11 857	843.1
	$C^1\Sigma^+ \rightarrow A'^1\Pi$	
(3,1)	16 018	624.1
(2,1)	15 598	640.9
(1,0)	15 588	641.3

Table 3.16: (cont.)

Band (v*,v)	σ_{Head} (cm^{-1})	λ^{Air}_{Head} (nm)
	$C^1\Sigma^+ \rightarrow A'^1\Pi$ (cont.)	
(3,2)	15 580	641.7
(0,0)	15 171	659.0
(1,1)	15 144	660.1
(0,1)	14 727	678.8
(2,3)	14 725	678.9
(3,4)	14 714	679.4
(1,2)	14 705	679.8
(2,4)	14 294	699.4
(0,2)	14 288	699.7
(3,5)	14 287	699.7
(1,3)	14 270	700.6
(2,5)	13 867	720.9
(3,6)	13 864	721.1
(1,4)	13 839	722.4
(3,7)	13 445	743.6
(2,6)	13 444	743.6
(3,8)	13 029	767.3
(2,7)	13 024	767.6
(3,9)	12 618	792.3
(3,10)	12 210	818.8
(2,9)	12 197	819.6
(1,8)	12 154	822.6

Table 3.16: (cont.) (Footnote)

---

[a] Band head positions are calculated from $C^1\Sigma^+$ constants in Table 3.10; $a^3\Sigma^+$, $A^1\Sigma^+$, $b^3\Pi$, and $A'^1\Pi$ constants are taken from Table 3.31 except for the energies of $A'^1\Pi$ and $b^3\Pi_1$ for which the perturbed values, ν_{oo} = 17577 cm^{-1} [10-12] and 17 322[9] cm^{-1} respectively, were used. $C^1\Sigma^+$ energies from Table 3.10 were changed so that calculated C→A heads agreed with those observed in Table 3.1 (see Text). Heads are accurate to ± 5 cm^{-1} or ± 0.3 nm.

Table 3.17: $C^1\Sigma^+ - a^3\Sigma^+$ Transition Frequencies (cm^{-1})†

J'	$R_{R(J'-1)}$	$R_{Q(J')}$	$P_{Q(J')}$	$P_{P(J'+1)}$
		(3,6)		
9	14 818.1	14 815.9	14 804.3	14 808.5
13	14 818.0*	14 815.0*	14 800.6*	14 804.0*
20	14 815.5	14 812.3	14 792.8	14 795.2
30	14 810.0	14 806.3	14 779.0*	14 779.0*
40	14 804.4*	14 797.3	14 745.8	14 763.5
		(3,7)		
9	14 368.2	14 366.4	14 356.8	14 358.9
13	14 368.3*	14 366.5*	14 353.5*	14 355.4*
20	14 367.1	14 364.6	14 345.9	14 347.1
27	14 364.9	14 361.7	14 338.9*	14 338.9*
30	14 363.0	14 358.5	14 334.0	14 335.1
40	14 338.5	14 350.7	14 305.2	
		(3,8)		
20	13 920.6	13 918.7	13 892.4	
30	13 907.9	13 914.7		
		(2,11)≠		
16	12 166.8	12 165.8	12 150.1	12 151.1
22	12 165.4*	12 165.4*	12 143.8	12 144.8
32	12 163.6*	12 163.0*	12 131.3	12 132.5
43	12 153.2*	12 152.7*	12 110.6	12 112.0

Table 3.17: $C^1\Sigma^+ - a^3\Sigma^+$ Transition Frequencies (cm^{-1}) (cont.)

J'	$^R R(J'-1)$	$^R Q(J')$	$^P Q(J')$	$^P P(J'+1)$
		(2,12)≠		
16	11 735.4	11 734.4	11 718.5	11 719.5
22	11 734.3*	11 734.3*	11 712.5	11 713.6
32	11 733.1*	11 732.5*	11 701.0	11 702.1
43	11 723.5*	11 723.5*	11 681.2	11 682.3

≠Assignments chosen correspond to C_a ($a^3\Sigma^+$ spin-spin constant, See Table 3.25) greater than 0. See text for discussion of the branch assignments.

†J' is $C^1\Sigma^+$ rotational quantum nmuber.

*Blended or otherwise degraded line. See text for discussion.

Table 3.18: $C^1\Sigma^+ - A^1\Sigma^+$ Transition Frequencies (cm^{-1})†

J'	R(J'-1)	P(J'+1)
	(3,6)	
9	14 406.2	14 396.9
13	14 405.8	14 392.6
20	14 404.8	14 384.2
27	14 400.8	14 373.0
30	14 397.9	14 367.1
40	14 386.8	14 345.7
	(3,7)	
9	13 928.8	13 919.4
13	13 928.5	13 914.8
20	13 926.2	13 905.5
27		13 896.6
30	13 918.9	13 888.6
	(3,8)	
20	13 451.9	13 431.6
30	13 445.8	13 415.1
	(3,9)	
13	12 978.6	12 965.0
27	12 973.4	12 946.4

†J' is $C^1\Sigma^+$ rotational quantum number.

Table 3.19: $C^1\Sigma^+ - b^3\Pi$ Transition Frequencies (cm^{-1})†

J	Ω=0 R(J'-1)	Ω=0 P(J'+1)		Ω=1 R(J'-1)	Ω=1 Q(J')	Ω=1 P(J'+1)
			(0,0)			
18				15 430.1	15 422.3	15 413.2
27				15 437.7	15 425.6	15 412.8
34				15 444.8	15 429.5	15 413.8
48				15 471.3	15 449.9	15 427.7
			(0,1)			
18				14 987.7	14 979.6	14 970.9
27				14 997.0	14 984.5	14 972.4*
34				15 004.5	14 990.1	14 973.6
48				15 030.3	15 010.0	14 988.2*
			(0,2)			
18				14 551.3	14 543.5	14 534.9
			(3,2)			
9				15 852.6	15 849.1	15 844.5
			(3,4)			
9	14 841.9	14.833.8		14 987.6	14 983.5	14 979.2
13	14 844.5	14.832.4		14 990.2	14 984.7	14 978.3
20	14 848.7	14 830.8		14 995.0	14 986.4	14 976.9
30				15 002.2	14 989.2	14 975.2
40	14 870.3	14 834.2		15 013.0*	14 995.3	14 977.7*

†J' is $C^1\Sigma^+$ rotational quantum number.

*Blended or otherwise degraded line. See text for discussion of precision.

Table 3.19: $C^1\Sigma^+$-$b^3\Pi$ Transition Frequencies (cm^{-1}) (cont.)

	Ω=0		Ω=1		
J'	R(J'-1)	P(J'+1)	R(J'-1)	Q(J')	P(J'+1)
		(3,5)			
9	14 417.9	14 409.4	14 560.7	14 556.8	14 552.4
13	14 419.7	14 407.8*	14 563.2	14 557.3	14 551.4
20	14 424.4	14 406.4	14 568.1	14 559.3	14 550.1
27	14 430.7	14 406.6	14 574.7	14 563.0	14 550.7
30	14 432.6	14 406.4	14 576.5	14 563.3	14 549.7
40			14 588.0	14 570.4	14 552.3
		(3,6)			
9	13 993.8	13 985.7	14 137.3	14 133.4	14 129.1
13	13 996.2	13 984.0	14 139.7	14 134.2	14 128.1
20	14 002.5*	13 984.4	14 144.9	14 136.1	14 127.0
27			14 151.8	14 140.0	14 127.8
30			14 154.5	14 141.2	14 127.8
		(3,7)			
9	13 573.8	13 565.5	13 717.7	13 713.6	13 709.5
20	13 582.6	13 564.7	13 725.4	13 716.8	13 707.7
40	13 606.4	13 571.6	13 748.6	13 731.6	13 713.8

Table 3.19: $C^1\Sigma^+ - b^3\Pi$ Transition Frequencies (cm^{-1}) (cont.)

J'	Ω=0 R(J'-1)	Ω=0 P(J'+1)	Ω=1 R(J'-1)	Ω=1 Q(J')	Ω=1 P(J'+1)
		(3,8)			
9	13 157.2	13 149.0	13 301.1	13 297.2	13 292.9
13	13 158.7	13 147.0	13 301.7	13 296.0	13 290.2
20	13 166.9	13 149.4	13 310.2	13 301.6	13 292.7
27	13 172.2	13 148.6	13 314.2	13 302.8	13 291.0
30			13 320.6	13 307.8	13 294.6
40			13 334.3*	13 317.1	13 299.5*
		(3,9)			
9	12 744.7	12 736.5	12 888.2	12 884.4	12 880.1
13	12 746.9	12 735.6	12 890.0	12 884.3*	12 878.4
20	12 754.8	12 737.6	12 898.1	12 889.5	12 880.6
27	12 761.3	12 737.8	12 903.7	12 892.3	12 880.5
30	12 766.4*	12 740.6*	12 909.4	12 896.5	12 883.0
40	12 781.6	12 747.7*	12 923.9	12 906.8	12 889.3
		(3,10)			
20	12 345.4	12 328.6			
27	12 353.0	12 330.3			
30	12 357.8	12 332.0			
40	12 374.2*	12 339.8*			
		(3,11)			
27			12 090.8	12 079.4	12 067.8
30			12 095.4	12 082.8	12 069.8
40			12 112.2*	12 095.7*	12 078.1*

Table 3.20: $C^1\Sigma^+ - A'^1\Pi$ Transition Frequencies (cm^{-1})

J'	R(J'-1)	Q(J')	P(J'+1)
		(0,0)	
18	15 191.0	15 182.7	15 174.4
27	15 199.2	15 186.6	15 174.6
34	15 206.8	15 189.8	15 175.2
48	15 233.9	15 209.4	15 189.4
		(0,1)	
18	14 751.6	14 743.2	14 735.0
27	14 760.6	14 748.4	14 735.9
34	14 769.5	14 753.7	14 738.1*
48	14 798.7	14 776.2	14 755.3
		(0,2)	
18	14 314.4	14 306.4	14 298.1
27	14 324.6*	14 312.4*	14 300.0*
34	14 331.7	14 316.5	14 301.5
48	14 363.8	14 342.4	14 320.3
		(3,2)	
9	15 616.9	15 612.8	15 608.2
13	15 618.2	15 612.6	15 606.4
40	15 640.8	15 623.1	15 604.9

---

†J' is $C^1\Sigma^+$ rotational quantum number.

*Blended or otherwise degraded line. See text for discussion of precision.

Table 3.20: $C^1\Sigma^+ - A'^1\Pi$ Transition Frequencies (cm^{-1}) (cont.)

J'	R(J'-1)	Q(J')	P(J'+1)
		(3,4)	
9	14 748.1		14 739.7
13	14 750.6	14 744.6	14 738.6
20	14 754.6	14 745.4	14 736.5
30	14 762.2	14 747.6	14 735.2
40	14 770.7	14 768.2	
		(3,5)	
9	14 320.5	14 316.4	14 312.2
13	14 322.8	14 316.8	14 310.8
20	14 327.6	14 317.8	14 309.3
27	14 333.1	14 319.0	14 308.6
30	14 334.0	14 317.0	14 306.8
40	14 361.3	14 334.7	14 324.2
		(3,6)	
9	13 897.4	13 893.3	13 889.1
13	13 899.6	13 893.2	13 887.5
20	13 903.4	13 902.4	13 885.2
27	13 907.8	13 902.9	13 881.8
30	13 923.0	13 903.8	13 895.0
40	13 931.9	13 914.7	13 896.5

Table 3.20 : $C^1\Sigma^+ - A'^1\Pi$ Transition Frequencies (cm^{-1}) (cont.)

J'	R(J'-1)	Q(J')	P(J'+1)
		(3,7)	
9	13 478.7	13 474.6	13 470.6
20	13 488.6	13 479.6	13 470.2
30	13 497.9	13 485.2	13 472.3
40	13 511.7	13 494.2	13 476.9
		(3,8)	
9	13 062.2*	13 058.4	13 053.8*
13	13 063.8	13 058.3	13 052.2
20	13 071.7	13 063.4	13 054.7
27	13 077.2	13 065.6	13 053.7
30	13 082.8	13 069.9	13 056.5
40	13 096.9*	13 079.6	13 062.1
		(3,9)	
9	12 649.2	12 645.2*	12 641.0
13	12 650.8	12 645.7*	12 639.9
20	12 659.0		
27	12 665.2	12 653.7	12 641.8
30	12 670.3	12 657.6	12 644.3
40	12 685.7	12 668.5	12 651.1
		(3,10)	
9	12 239.5	12 235.6	12 231.4

lasers and then re-scan the monochromator from ≈ 600 nm to ≈ 850 nm. Instead, a grid of $C^1\Sigma^+$ levels spanning J* = 9 to 40 was used to provide bits of rotational data in the lower levels over the same J range without undue loss in spectroscopic characterization of the lower states.

Rotational assignments are straightforward from knowledge of J* determined by $C^1\Sigma^+ \leftarrow A^1\Sigma^+$ excitation spectra (Section III.A) and ΔJ selection rules.[32] However, in perturbed spectral regions where the relative positions of P, Q, and R branches are anomalous, assignments are more difficult but still possible. From predicted perturbation patterns[37] and random differences comparable to experimental error between calculated and observed term values, the rotational assignments made in these regions are verified.

In the case of $C^1\Sigma^+ \rightarrow a^3\Sigma^+$ emission where the lower levels are not perturbed (v_a = 11 and 12) it is not possible to distinguish between P and Q or R and Q in the P-form and R-form branches, respectively†. This corresponds to an ambiguity in the sign of the $a^3\Sigma^+$

---

†It is possible to determine this by examining emission from both J* and J* + 2 where the term values for all three of the $^3\Sigma^+$ sub-levels for N = J* + 1 can be unambiguously measured and assigned: P-form emission from J* populates the J=J* (f parity) and J=J*+1 (e parity) sub-levels of the N=J*+1 $^3\Sigma^+$ level; R-form emission from J*+2 populates the J =J*+1 (e parity) and J=J*+2 (f parity) sub-levels of the same N=J*+1 level.

spin-spin constant, C_a. In Table 3.17, $C_a > 0$ has been assumed. For perturbed $^3\Sigma^+$ levels, the sign of C_a is unambiguously determined, for $A'^1\Pi \sim a^3\Sigma^+$ interactions are diagonal in J and not N so that each spin sub-level with a different value of J is affected differently. In this case, only one sign for C_a (i.e. one set of line assignments), yields a calculated spectrum with random residuals comparable to experimental error.

Transition frequencies are converted to term values, relative to $X^1\Sigma^+$ (v" = 0, J" = 0), by subtracting the frequencies in Tables 3.17-3.20 from $C^1\Sigma^+$ term values in Table 3.5. This does not degrade the data precision since E(v*,J*) is precise to 0.01 cm^{-1} whereas the fluorescence transition frequencies are measured to an accuracy of only 0.5 cm^{-1} and a precision of $\sim$ 0.2 cm^{-1}. Term values are given in Table 3.21 through 3.24. In fitting these term values, differences between transitions belonging to different branches but the same band were fit, weighted according to their uncertainty of 0.2 cm^{-1}[†], as well as term values for each level, which were given uncertainties of 0.5 cm^{-1}. The discrepancy between

[†]The weights are $1/\delta_i^2$ where δ_i is the experimental error associated with the i^{th} datum.

Table 3.21: $a^3\Sigma^+$ Term Values[a]

J	$F_1(cm^{-1})$	$F_2(cm^{-1})$	$F_3(cm^{-1})$
	v = 6		
8		19 262.7	
9	19 265.3		19 276.5
10		19 272.3	
12		19 283.4	
13	19 286.4		19 300.8
14		19 297.4	
19		19 339.6	
20	19 342.7		19 362.3
21		19 359.9	
29		19 461.0	
30	19 464.7		19 492.0
31		19 492.0	
39		19 628.6*	
40	19 635.8		19 687.2
41		19 669.5	
	v = 7		
8		19 712.6	
9	19 714.5		19 724.0
10		19 721.9	
12		19 733.1*	
13	19 734.9*		19 747.9*
14		19 746.0*	
19		19 788.0	
20	19 790.5		19 809.2
21		19 808.0	
26		19 866.4	

Table 3.21: $a^3\Sigma^+$ Term Values (cont.)

J	$F_1(cm^{-1})$	$F_2(cm^{-1})$	$F_3(cm^{-1})$
27	19 869.6	v=7 (cont.)	19 892.5*
28		19 892.5*	
29		19 908.0	
30	19 912.5		19 935.9
31		19 936.9	
39		20 094.6	
40	20 082.4		20 127.8
41			
	v = 8		
19		20 234.5	
20	20 236.3		20 262.6
29		20 363.1	
30	20 356.3		
	v = 11		
15		21 519.0	
16	21 520.0		21 535.7
17		21 534.7	
21		21 573.7*	
22	21 573.7*		21 595.3
23		21 594.3	
31		21 701.1*	
32	21 701.8*		21 733.4
33		21 732.2	
42		21 898.4*	
43	21 898.9*		21 940.9
44		21 939.6	

Table 3.21: $a^3\Sigma^+$ Term Values (cont.)

J	$F_1(cm^{-1})$	$F_2(cm^{-1})$	$F_3(cm^{-1})$
	v = 12		
15		21 950.4	
16	21 951.4		21 967.2
17		21 966.2	
21		22 004.8*	
22	22 004.8*		22 026.6
23		22 025.5	
31		22 131.6*	
32	22 132.2*		22 163.7
33		22 162.6	
42		22 328.0*	
43	22 328.0*		22 369.2
44		22 370.4	

[a] F_1, F_2, and F_3 refer to levels with J = N + 1, N, and N-1, respectively.[32]

*Blended or otherwise degraded line. See text for discussion of precision.

Table 3.22: $A^1\Sigma^+$ Term Values†

J	T (cm^{-1})	J	T (cm^{-1})
	v = 6		v = 7
8	19 674.6	8	20 152.0
10	19 683.9	10	20 161.4
12	19 695.6	12	20 172.9
14	19 708.6	14	20 186.6
19	19 750.3	19	20 228.9
21	19 770.9	21	20 249.5
26	19 830.6	26	
28	19 858.3	28	20 334.7
29	19 873.1	29	20 352.1
31	19 903.9	31	20 382.4
39	20 046.2	39	20 524.2
41	20 087.4	41	20 564.7
	v = 8		v = 9
19	20 703.2	12	21 122.8
21	20 723.5	14	21 136.4
29	20 825.2	26	21 258.0
31	20 855.9	28	21 285.0

†See text for discussion of precision.

Table 3.23: $b^3\Pi$ Term Values

J	Ω = 0 $T_e(cm^{-1})$	Ω = 1 $T_e(cm^{-1})$	Ω = 1 $T_f(cm^{-1})$
		v = 0	
17		17 400.9	
18			17 408.6
19		17 417.8	
26		17 489.2	
27			17 501.4
28		17 514.2	
33		17 583.2	
34			17 598.5
35		17 614.2	
47		17 838.0	
48			17 859.4
49		17 881.6	
		v = 1	
17		17 843.3	
18			17 851.3
19		17 860.1	
26		17 929.9	
27			17 942.4
28		17 954.6*	
33		18 023.5	
34			18 037.9
35		18 054.4	
47		18 279.0	
48			18 299.3
49		18 321.1*	
		v = 2	
8		18 228.2	
9			18 231.8
10		18 236.3	
17		18 279.7	
18			18 287.5
19		18 296.1	

*Blended or otherwise degraded line. See text for discussion of precision.

Table 3.23: $b^3\Pi$ Term Values (cont.)

	Ω = 0		Ω = 1	
J	T_e(cm^{-1})		T_e(cm^{-1})	T_f(cm^{-1})
		v = 4		
8	19 238.9		19 093.3	
9				19 097.3
10	19 247.0		19 101.6	
12	19 256.9		19 111.2	
13				19 116.7
14	19 269.0		19 123.0	
19	19 306.3		19 160.0	
20				19 168.7
21	19 324.2		19 178.2	
29			19 268.8	
30				19 281.8
31			19 295.8	
39	19 562.8		19 420.0*	
40				19 437.8
41	19 598.9		19 455.4*	
		v = 5		
8	19 663.0		19 520.1	
9				19 524.0
10	19 671.4		19 528.4	
12	19 681.7		19 538.2	
13				19 544.1
14	19 693.8		19 550.0	
19	19 730.6		19 587.0	
20				19 595.7
21	19 748.7		19 605.0	
26	19 800.6		19 656.7	
27				19 668.4
28	19 824.8		19 680.7	
29	19 838.4		19 694.5	
30				19 707.7
31	19 864.6		19 721.3	
39			19 845.0	
40				19 862.6
41			19 880.8	

Table 3.23: $b^3\Pi$ Term Values (cont.)

	Ω = 0	Ω = 1	
J	T_e(cm^{-1})	T_e(cm^{-1})	T_f(cm^{-1})
		v = 6	
8	20 087.0	19 943.6	
9			19 947.4
10	20 095.1	19 951.8	
12	20 105.3	19 961.7	
13			19 967.2
14	20 117.4	19 973.3	
19		20 010.2	
20			20 019.0
21		20 028.1	
26		20 079.6	
27			20 091.3
28		20 103.6	
29		20 116.5	
30			20 129.8
31		20 143.2	
		v = 7	
8	20 507.0	20 363.2	
9			20 367.2
10	20 515.3	20 371.3	
19	20 572.5	20 429.7	
20			20 438.2
21	20 590.3	20 447.4	
39	20 826.6	20 684.4	
40			20 701.5
41	20 861.4	20 719.3	

Table 3.23: $b^3\Pi$ Term Values (cont.)

J	Ω = 0 $T_e(cm^{-1})$	Ω = 0 $T_e(cm^{-1})$	Ω = 0 $T_f(cm^{-1})$
		v = 8	
8	20 923.6	20 779.8	
9			20 783.7
10	20 931.8	20 787.9	
12	20 942.7	20 799.7	
13			20 805.4
14	20 954.4	20 811.2	
19	20 988.1	20 844.9	
20			20 853.4
21	21 005.6	20 862.4	
26	21 059.2	20 917.2	
27			20 928.7
28	21 082.8	20 940.3	
29		20 950.4	
30			20 963.2
31		20 976.4	
39		21 098.7*	
40			21 115.9
41		21 133.6*	
		v = 9	
8	21 336.1	21 192.6	
9			21 196.4
10	21 344.3	21 200.7	
12	21 354.5	21 211.4	
13			21 217.1*
14	21 365.8	21 223.0	
19	21 400.2	21 256.9	
20			21 265.6
21	21 417.4	21 274.5	
26	21 470.1	21 327.6	
27			21 399.0
28	21 493.5	21 350.9	
29	21 504.6*	21 361.6	
30			21 374.5
31	21 530.4*	21 388.0	
39	21 651.4	21 509.2	
40			21 526.3
41	21 685.4*	21 543.8	

Table 3.23: $b^3\Pi$ Term Values (cont.)

	Ω = 0	Ω = 1	
J	T_e (cm^{-1})	T_e (cm^{-1})	T_f (cm^{-1})
	v = 10		
19	21 809.6		
21	21 826.5		
26	21 878.3		
28	21 901.1		
29	21 913.2		
31	21 939.0		
39	22 058.9*		
41	22 093.2*		
	v = 11		
26		21 140.5	
27			21 151.9
28		21 163.5	
29		21 175.6	
30			21 188.1
31		21 301.1	
39		21 420.8*	
40			21 437.4*
41		21 455.0*	

Table 3.24: $A'^{1}\Pi$ Term Values

J	$T_e(cm^{-1})$	$T_f(cm^{-1})$
	v = 0	
17	17 640.0	
18		17 648.2
19	17 656.5	
26	17 727.7	
27		17 740.4
28	17 752.4	
33	17 821.2	
34		17 838.2
35	17 852.8	
47	18 057.4	
48		18 099.9
49	18 119.9	
	v = 1	
17	18 079.4	
18		18 087.7
19	18 096.0	
26	18 166.4	
27		18 178.5
28	18 191.0	
33	18 258.5	
34		18 274.3
35	18 289.9*	
47	18 510.6	
48		18 533.1
49	18 554.0	

*Blended or otherwise degraded line.
See text for discussion of precision.

Table 3.24: $A'^{1}\Pi$ Term Values (cont.)

J	$T_e(cm^{-1})$	$T_f(cm^{-1})$
	v = 2	
8	18 464.0	
9		18.468.0
10	18 472.6	
12	18 483.2	
13		18 488.8
14	18 495.0	
17	18 516.6	
18		18 524.6
19	18 532.9	
27	18 602.3*	
28		18 614.6*
29	18 627.0*	
33	18 696.3	
34		18 711.5
35	18 726.5	
39	18 792.3	
40		18 809.9
41	18 828.1	
47	18 945.5	
48		18 966.9
49	18 989.0	
	v = 4	
8	19 332.7	
9		
10	19 341.1	
12	19 350.9	
13		19 356.8
14	19 362.8	
19	19 400.5	
20		19 409.6
21	19 418.6	
29	19 508.8	
30		19 523.4
31	19 535.8	
39	19 662.4	
40		19 664.8

Table 3.24: $A'^{1}\Pi$ Term Values (cont.)

J	T_e (cm^{-1})	T_f (cm^{-1})
	v = 5	
8	19 760.4	
9		19 764.4
10	19 768.6	
12	19 778.6	
13		19 784.6
14	19 790.7	
19	19 827.5	
20		19 837.3
21	19 845.8	
26	19 898.3	
27		19 912.4
28	19 922.7	
29	19 936.9	
30		19 954.0
31	19 964.2	
39	20 071.8	
40		20 098.4
41	20 108.8	
	v = 6	
8	20 183.4	
9		20 187.6
10	20 191.7	
12	20 201.8	
13		20 208.2
14	20 213.9	
19	20 251.6	
20		20 252.6
21	20 269.9	
26	20 323.6	
27		20 328.5
28	20 349.5	
29	20 348.0	
30		20 367.2
31	20 376.0	
39	20 501.2	
40		20 518.4
41	20 536.6	

Table 3.24: $A'^{1}\Pi$ Term Values (cont.)

J	T_e (cm^{-1})	T_f (cm^{-1})
	v = 7	
8	20 602.1	
9		20 606.2
10	20 610.3	
19	20 666.4	
20		20 675.5
21	20 684.9	
29	20 773.1	
30		20 785.8
31	20 798.7	
39	20 921.3	
40		20 938.8
41	20 956.2	
	v = 8	
8	21 018.6*	
9		21 022.5
10	21 027.1*	
12	21 037.7	
13		21 043.1
14	21 049.3	
19	21 083.3	
20		21 091.7
21	21 100.4	
26	21 154.2	
27		21 165.7
28	21 177.7	
29	21 188.2	
30		21 201.1
31	21 214.5	
39	21 336.2*	
40		21 353.4
41	21 370.9	

Table 3.24 : $A'^{1}\Pi$ Term Values (cont.)

J	T_e (cm^{-1})	T_f (cm^{-1})
	v = 9	
8	21 431.6	
9		21 435.6*
10	21 439.8	
12	21 450.6	
13		21.455.8*
14	21 461.5	
19	21 496.1	
26	21 566.1	
27		21 577.7
28	21 589.5	
29	21 600.7	
30		21 613.4
31	21 626.7	
39	21 747.4	
40		21 764.6
41	21 782.0	
	v = 10	
8	21 841.3	
9		21 845.3
10	21 849.4	

precision and accuracy results from calibration of spectra against Ne and Ar reference lines:[31] absolute wavelength measurements made on different days varied by as much as 0.02 nm ($\approx$ 0.5 cm^{-1}) because of irreproducibility in alignment of the standard atomic pen lamp with respect to both OODR induced fluorescence and the monochromator slit. Interpolation between atomic lines separated by more than 5 nm is accurate to no better than 0.02 nm. On the other hand, separations between OODR fluorescence lines separated by less than 3 nm are precise to $\approx$ 0.01 nm ($\approx$ 0.2 cm^{-1}) from day to day. Thus, differences between emission line frequencies for given J* are weighted more heavily than absolute term values.

Blended line (indicated by an asterisk in Tables 3.17-3.24) uncertainties were estimated to be 1.0 cm^{-1} absolute accuracy and 0.5 cm^{-1} relative precision.

3. Deperturbation

In order to more precisely deperturb the low lying states of BaO, $A^1\Sigma^+ \rightarrow X^1\Sigma^+$ transition frequencies from Ref. 8[†] and MODR frequencies from Ref. 19

[†]Four lines from Ref. 8 could not be fit and were excluded: R(77) in $A^1\Sigma^+ - X^1\Sigma^+$ (1,1) was 0.7 cm^{-1} too low, $R_e(61)$ and $P_e(63)$ (extra lines) in (3,0) were both 0.4 cm^{-1} too low, and R(96) in (4,0) was 0.6 cm^{-1} too high.

are included. Ref. 8 data are first converted to term values by adding ground state term values calculated from Ref. 16 (rotational energies) and Ref. 3 (vibrational energies) to the transition frequencies in Ref. 8. Although, this is not statistically rigorous, the superior precision with which $X^1\Sigma^+$ rotational constants are known effectively breaks correlations between $A^1\Sigma^+$ and $X^1\Sigma^+$ term values. The term values so obtained are given uncertainties of 0.05 cm^{-1} and 0.25 cm^{-1} for unblended and blended lines, repspectively. MODR data from Ref. 19 are weighted according to the uncertainties quoted there.

The Hamiltonian matrix used for deperturbation is given in Table 3.25. In addition to one $a^3\Sigma^+$, one $b^3\Pi$, and one $A'^1\Pi$ vibrational level a second $A^1\Sigma^+$ level and a second $b^3\Pi_2$ level are included. These matrix elements have been derived previously but with a different phase convention[42]; the phase convention of Condon and Shortley[43] [i.e. $\langle S\ \Sigma\pm1|S_\pm|S\Sigma\rangle = +\sqrt{S(S+1)-\Sigma(\Sigma\pm1)}$] is employed here. The second $b^3\Pi_2$ (b2) diagonal matrix element (H_{99}) is taken from Ref. 32 and is accurate for any degree of spin uncoupling. The interaction of this state with $A^1\Sigma^+$ is expressed as a product of a J-dependent $b^3\Pi_0 \sim {}^3\Pi_2$ mixing coefficient and the $b^3\Pi_0 \sim A^1\Sigma^+$ spin-orbit matrix element since no first order interaction between $b^3\Pi_2$ and $A^1\Sigma^+$ exists.[37]

Table 3.25: Hamiltonian Matrix Used for Deperturbation of Low Lying States of BaO[a]

$$H^{e}_{11} = [E_a + B_A\, x - D_A\, x^2]$$

$$H_{22} = E_{A'} + B_{A'}(x-1) - D_{A'}(x-1)^2$$

$$H_{33} = E_b + B_b(x+1) - D_b(x^2 + 4x + 1) - A_b - C_b$$

$$H_{44} = E_b + B_b(x+1) - D_b(x^2 + 6x - 3) + 2C_b$$

$$H_{55} = E_b + B_b(x-3) - D_b(x^2 - 4x + 5) + A_b - C_b$$

$$H^{f}_{66} = [E_a + B_a(x+2) - D_a(x^2 + 8x + 4) + 2C_a - 2\gamma_a]$$

$$H_{77} = E_a + B_a x - D_a[x^2 + 2x(1 \mp 1)] - C_a - \gamma_a$$

$$H^{e}_{88} = [E_{A2} + B_{A2}x - D_{A2}x^2]$$

$$H_{99} = E_{b2} + B_{b2}(x - Z_1^{1/2} - 2Z_2) - D_{b2}[0.5(1+4x)^{1/2} - 1]^4$$

$$H^{e}_{12} = H^{e}_{21} = -2^{1/2}\,[\eta_{AA'} + \eta^{J}_{AA'}, x]\, x^{1/2}$$

$$H^{e}_{13} = H^{e}_{31} = 2^{1/2}\xi_{Ab}$$

$$H^{e}_{19} = H^{e}_{91} = [B_{b2}[(1+4x)^{1/2} - 1]/(2A_{b2})]^2\, \xi_{Ab2}$$

$$H_{24} = H_{42} = \xi_{A'b}$$

$$H_{27} = H_{72} = \xi_{A'a}$$

$$H_{28} = H_{82} = -2^{1/2}\eta_{A'A2}\, x^{1/2}$$

$$H_{34} = H_{43} = -(2x)^{1/2}\,[B_b - 2\,(x+1)D_b]^{1/2}$$

$$H_{35} = H_{53} = 2D_b[x(x-2)]^{1/2}$$

$$H^{f}_{36} = H^{f}_{63} = 2[\xi_{ba} - \eta_{ba}]$$

$$H_{37} = H_{73} = \mp\, x^{1/2}\eta_{ba}$$

$$H^{e}_{38} = H^{e}_{83} = 2^{1/2}\xi_{A2b}$$

$$H_{45} = H_{54} = -[2(x-2)]^{1/2}[B_b - 2(x-1)D_b]$$

$$H^{f}_{46} = H^{f}_{64} = (2x)^{1/2}\eta_{ba}$$

Table 3.25 (cont.):

$H_{47} = H_{74} = (2)^{\frac{1}{2}}[\xi_{ba} - \eta_{ba}]$

$H_{57} = H_{75} = -(x-2)^{\frac{1}{2}}\eta_{ba}$

$H^{f}_{67} = H^{f}_{76} = -2x^{\frac{1}{2}}[B_a - 2(x+1)D_a - \gamma_a/2]$

where $x = J(J+1)$

1,2,...,9 denotes $A^1\Sigma^+(v_A)$, $A'^1\Pi(v_{A'})$, $b^3\Pi_0(v_b)$, $b^3\Pi_1(v_b)$, $b^3\Pi_2(v_b)$, $a^3\Sigma^+_0(v_a)$, $a^3\Sigma^+_1(v_a)$, $A^1\Sigma^+(v_A + 1)$, and $b^3\Pi_2(v_b+1)$, respectively

A2 denotes $A^1\Sigma^+(v_a+1)$

b2 denotes $b^3\Pi_2(v_b + 1)$

E vibronic energy

$B = \frac{h}{8\pi^2 c\mu R^2}$ rotational constant

D centrifugal distortion constant

A_b $b^3\Pi$ spin-orbit constant

C spin-spin constant

γ_a $a^3\Sigma^+$ spin-rotation constant

$Z_1 = Y(Y-4) + 4/3 + 4x$

$Z_2 = (3Z_1)^{-1}[Y(Y-1)-4/9-2x]$

$Y = A_b/B_b$

$\eta_{ij} = \langle i||BL_{\pm}||j\rangle$ rotation-electronic interaction

$\xi_{ij} = \langle i||H^{SO}||j\rangle$ spin-orbit interaction

---

[a] All elements are for both e and f parity[36] except where parity labels are explicitly given. When two signs are given the upper (lower) refers to e(f).

Only those parameters which could be determined are given in Table 3.25; since no $A'^1\Pi$ or $b^3\Pi$ Λ-doubling is observed, these terms are not included. The computer program is given in Appendix 1.

Tables 3.26 and 3.27 and Figure 3.9 summarize the $A^1\Sigma^+ \sim b^3\Pi$ and $A^1\Sigma^+ \sim A'^1\Pi$ perturbations observed here as well as those observed and analyzed previously.[8,9] $a^3\Sigma^+ \sim A'^1\Pi$ perturbations are summarized in Table 3.28 and Fig. 3.10. The double perturbation between $a^3\Sigma^+$ ($v_a = 8$) and $A'^1\Pi$($v_{A'} = 6$) and $A^1\Sigma^+$ ($v_A = 7$) at $J \simeq 28.5$ is depicted in Fig. 3.11. Perturbations in each level and the corresponding deperturbation model are described below. The final set of parameters and the corresponding correlation matrices are given in Tables 3.29 and 3.30, respectively. $A^1\Sigma^+$ term values calculated by diagonalizing the matrix in Table 3.25 with the parameters in Table 3.29 were used in converting $* \leftarrow A^1\Sigma^+$ transition frequencies to * term values above (Section III.A.).

Not all parameters in Table 3.25 are determined but some are fixed at estimated values in order to obtain physically significant varied parameters (see Chapter 2). Centrifugal distortion constants were fixed at 2.8×10^{-7} cm^{-1}, the value reported for $A^1\Sigma^+$ in Ref. 8, except where noted. Fixed energies and rotational constants were calculated from Ref. 8 ($A^1\Sigma^+$), Ref. 9 ($A'^1\Pi$, and $b^3\Pi$), or Appendix 6

($a^3\Sigma^+$). When indeterminate, $b^3\Pi$ spin-orbit constants (A_b) and $b^3\Pi \sim A'^1\Pi$ spin-orbit interaction matrix elements ($\xi_{A',b}$) are fixed at -100 cm^{-1} which is approximately the final mean value for both A_b and $\xi_{A'b}$. $b^3\Pi$ and $a^3\Sigma^+$ spin-spin constants, C_b and C_a respectively, and $a^3\Sigma^+$ spin-rotation constants, γ_a, are fixed at zero except where noted. All other off-diagonal matrix elements which could not be varied are fixed at values calculated from the product of electronic (Ref. 9 for $A^1\Sigma^+ \sim A'^1\Pi$, $A^1\Sigma^+ \sim b^3\Pi$, and $a^3\Sigma^+ \sim b^3\Pi$ and Appendix 6 for $a^3\Sigma^+ \sim A'^1\Pi$) and vibrational factors. The latter are calculated by generating Rydberg Klein Rees (RKR) potential curves[44] from spectroscopic constants in Ref. 8 ($A^1\Sigma^+$), Ref. 9 ($A'^1\Pi$ and $b^3\Pi$), and Appendix 6 ($a^3\Sigma^+$) and then numerically solving the Schrodinger equation to obtain vibrational wavefunctions and matrix elements.

Figure 3.9: $A^1\Sigma^+$ vibration-rotation energy vs. J(J+1) illustrating perturbations by $b^3\Pi_2$(○), $b^3\Pi_1$(□), $b^3\Pi_0$(●), and $A^1\Sigma^+$(x). Data for v_A = 0 through 5 is primarily from Ref. 8.

Figure 3.10: $A'^1\Pi$ vibration-rotation energy vs. J(J+1) illustrating perturbations by $a^3\Sigma^+$ F_3(□), F_2(●), F_1(■), and $A^1\Sigma^+$(x). Note double crossing, $A'^1\Pi \sim a^3\Sigma^+ \sim A^1\Sigma^+$, at $J_o \sim 28.5$ in $v_{A'} = 6$.

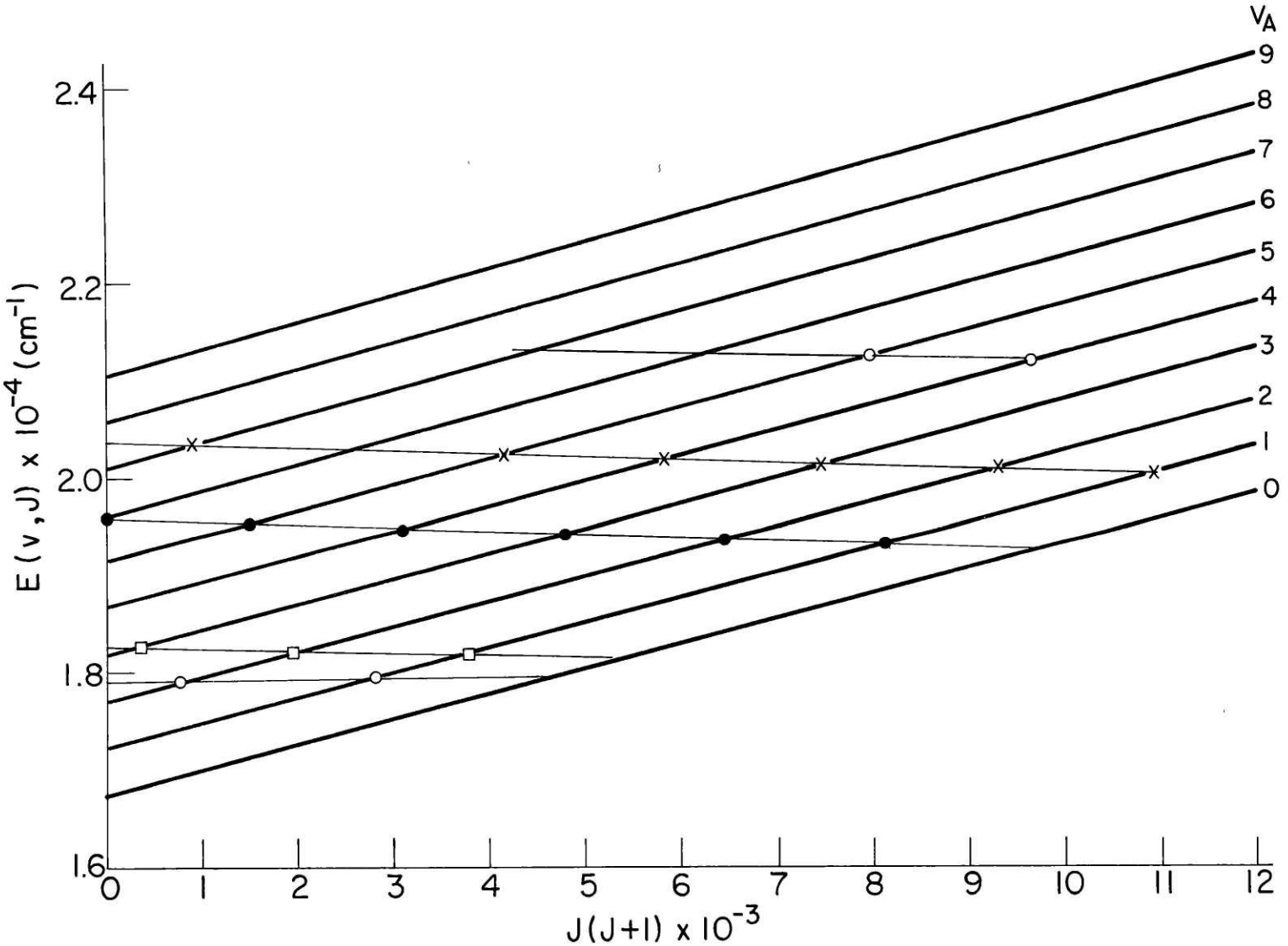
V_A
9
8
7
6
5
4
3
2
1
0
2.4
2.2
2.0
1.8
1.6
$E(v,J) \times 10^{-4}$ (cm^{-1})
0
1
2
3
4
5
6
7
8
9
10
11
12
$J(J+1) \times 10^{-3}$

Figure 3.9

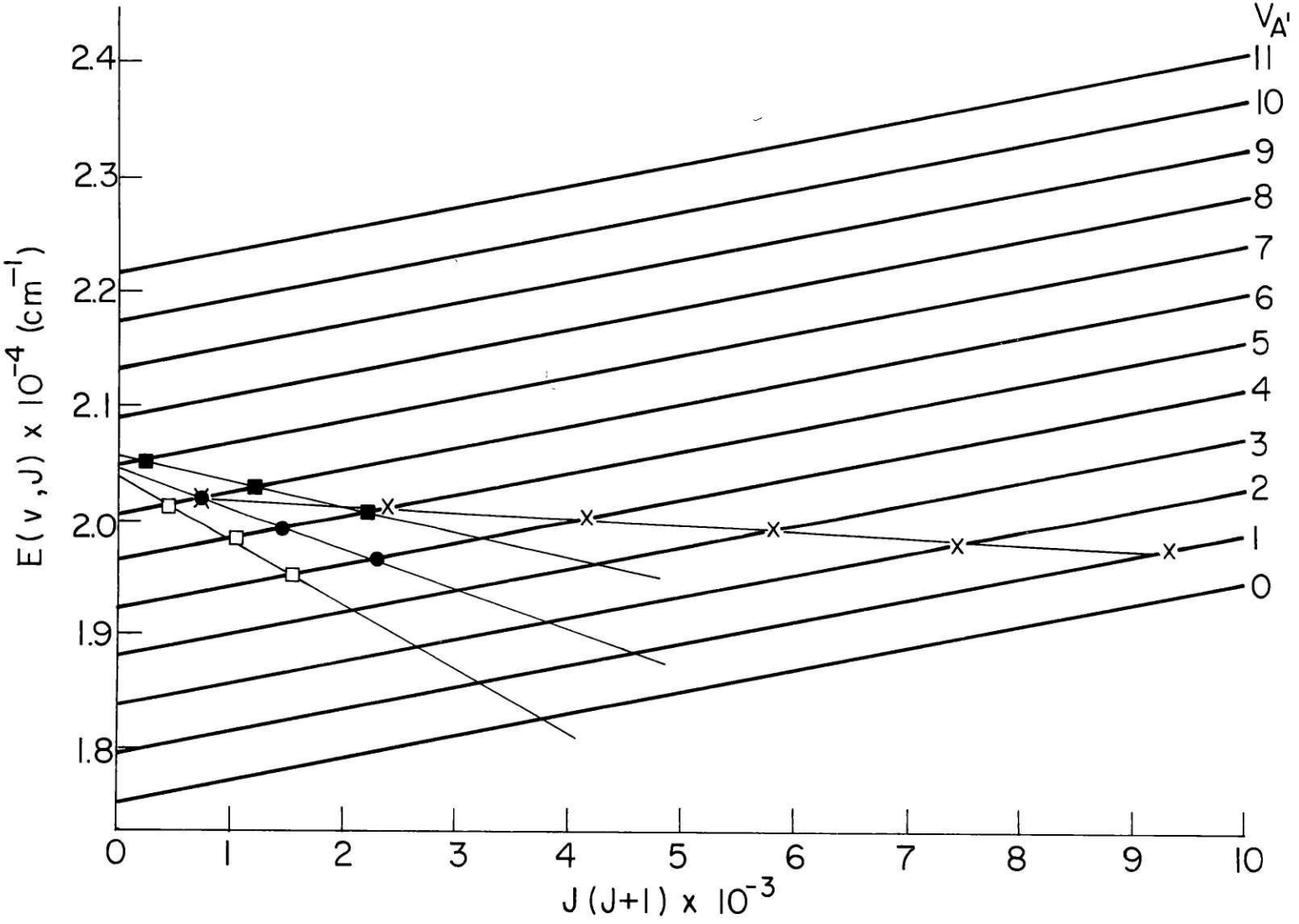
$V_{A'}$
11
10
9
8
7
6
5
4
3
2
1
0
2.4
2.3
2.2
2.1
2.0
1.9
1.8
$E(v,J) \times 10^{-4}$ (cm^{-1})
0
1
2
3
4
5
6
7
8
9
10
$J(J+1) \times 10^{-3}$

Figure 3.10

Figure 3.11: Double perturbation between $a^3\Sigma^+$ ($v_a = 8$), $A'^1\Pi$($v_{A'} = 6$), and $A^1\Sigma^+$ ($v_A = 7$). The $a^3\Sigma^+(F_3) \sim A'^1\Pi$ crossing is depicted here. The $A^1\Sigma^+ \sim A'^1\Pi$ interaction, which culminates at $J_o = 28.5$, is still weak. $C^1\Sigma^+$ ($v^* = 3$, $J^* = 20$) is prepared by OODR.

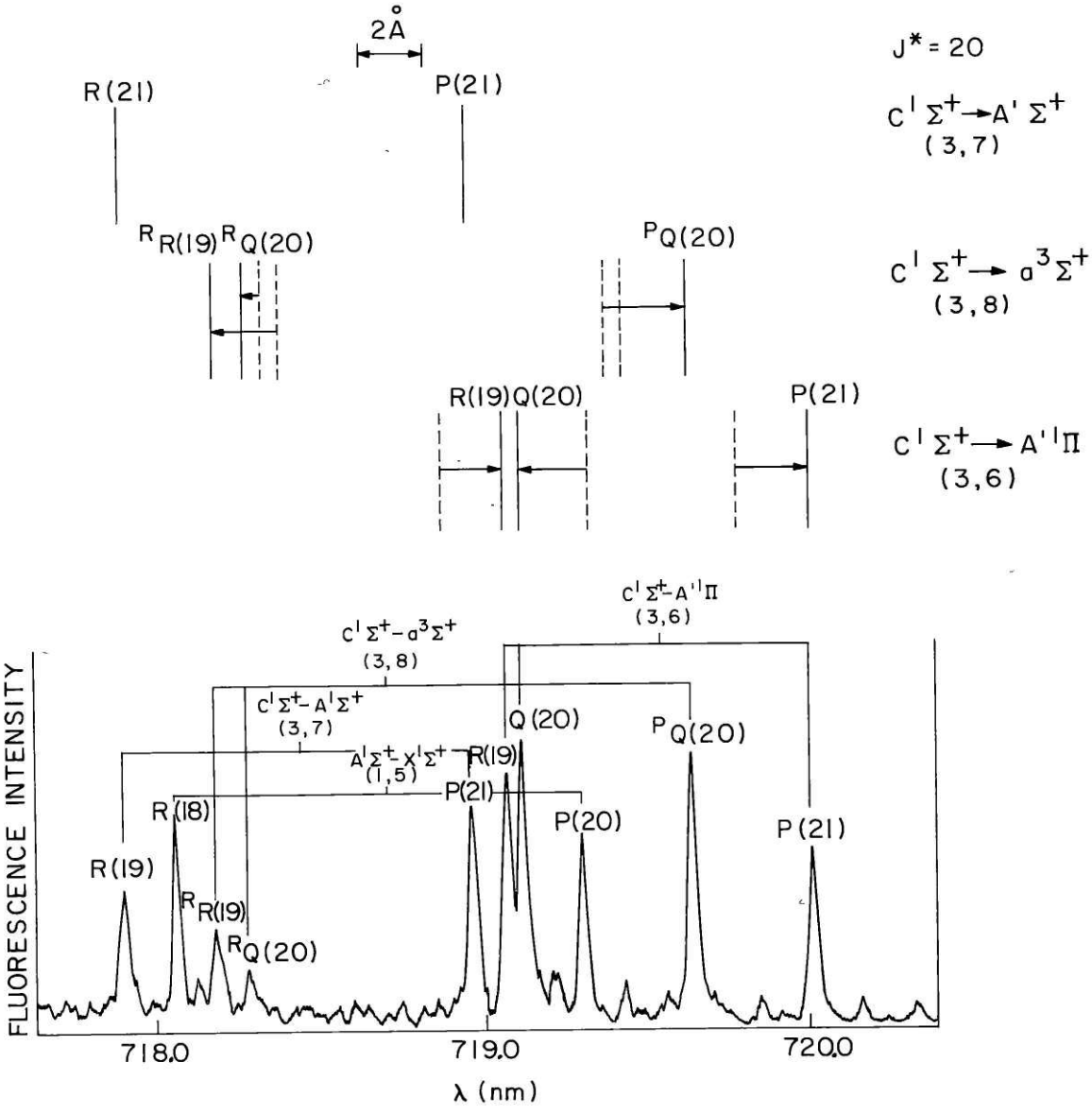
2Å
J* = 20
R(21)
P(21)
C¹Σ⁺→A'Σ⁺
(3,7)
R R(19) R Q(20)
P Q(20)
C¹Σ⁺→a³Σ⁺
(3,8)
R(19) Q(20)
P(21)
C¹Σ⁺→A'¹Π
(3,6)
C¹Σ⁺-A'¹Π
(3,6)
C¹Σ⁺-a³Σ⁺
(3,8)
C¹Σ⁺-A¹Σ⁺
(3,7)
A¹Σ⁺-X¹Σ⁺
(1,5)
Q (20)
P Q(20)
R(19)
P(21)
R(18)
P(20)
P(21)
R(19)
R R(19)
R Q(20)
FLUORESCENCE INTENSITY
718.0
719.0
720.0
λ (nm)

Figure 3.11

Table 3.26: Summary of $A^1\Sigma^+ \sim b^3\Pi$ Perturbations

$A^1\Sigma^+(v_A)$	$b^3\Pi(v_b)$	$\Omega = 2$	J_o^a = 1	0	$\xi_{Ab}(cm^{-1})^b$	$\xi_{Ab}/\langle v_A \mid v_b \rangle$ (cm^{-1})
1[c]	0	45.1	60.3	89.6	11.02(2)	22.79 (4)
2[c]	1	27.6	43.6	79.7	-2.78(4)	22.7 (3)
3[c]	2		18.8	68.7	-7.89(2)	21.92 (6)
4[c]	3			55.6	-6.485(12)	22.76 (4)
4[c]	4	97.7			7.08(fixed)	
5[c]	4			38.3	-1.52(3)	20.8 (4)
5[c]	5	88.9			11.(5)	38. (17)
6	5			<0	3.5(3)	26.3 (22)
7	6			<0	14.0(21)	54. (8)

$\langle b^3\Pi \| H^{SO} \| A^1\Sigma^+ \rangle = 22.6 \pm 0.4$ cm^{-1}

[a] J value at which unperturbed levels would be degenerate.

[b] Defined in Table 3.25. Uncertainties in parentheses are 1σ estimates.

[c] $A^1\Sigma^+ - X^1\Sigma^+$ transitions from Ref. 8 and MODR data from Ref. 19 were used.

Table 3.27: Summary of $A^1\Sigma^+ \sim A'^1\Pi$ Perturbations

$A^1\Sigma^+(v_A)$	$A'^1\Pi(v_{A'})$	J_o[a]	$\eta^b_{AA'}$ (cm^{-1})	$\eta_{AA'}/\langle v_A\|B\|v_{A'}\rangle$ (unitless)
1	0	104.0	0.11117(11)	1.0114 (10)
2[c]	1	96.0	-0.0212 (19)	0.64 (6)
3[c,d]	2	85.7	-0.0512 (21)	0.61 (3)
4[c]	3	75.7	-0.0700 (4)	1.128 (6)
5[c]	4	63.9	-0.0149 (9)	1.37 (8)
5[c]	5	—	0.063 (20)	0.9 (3)
7	6	28.5	0.088 (14)	1.44 (23)
8	7	< 0	0.086 (16)	1.4 (3)

$\langle A'^1\Pi||L_+||A^1\Sigma^+\rangle = 1.014 \pm 0.024$ unitless

[a] See footnote a in Table 3.26.

[b] See footnote b in Table 3.26.

[c] See footnote c in Table 3.26.

[d] An additional interaction parameter, which is multiplied by $x^{3/2}$ (see Table 3.25), was determined to be $-9.3 \pm 0.3 \times 10^{-6}$ cm^{-1}.

Table 3.28: Summary of $A'^1\Pi \sim a^3\Sigma^+$ Perturbations

$A'^1\Pi(v_{A'})$	$a^3\Sigma^+(v_a)$	$F_1(f)$	$\frac{J_o{}^a}{F_2(e)}$	$F_3(f)$	$\xi^b_{A'a}$	$\xi_{A'a}/\langle v_{A'}\|v_a$
0	2			(57.5)[c]	35.9 (13)	64.3 (23)
1	3			(55.5)	25. (8)	94. (30)
4	6			39.5	-19.5 (7)	58.1 (21)
5	7	(45.0)	37.5	31.2	-16.48 (29)	58.5 (10)
6	8	34.8	28.5	20.1	- 8.6 (7)	52. (4)
7	9	11.2			1.0 (6)	38. (23)

$\langle A'^1\Pi||H^{SO}||a^3\Sigma^+\rangle = 58.9 \pm 2.7\ cm^{-1}$

[a] See footnote a in Table 3.26.

[b] See footnote b in Table 3.26.

[c] J_o values in parentheses are extrapolated values.

Table 3.29: Deperturbed Constants for Low Lying States[a] of BaO

Fit 1

$v_A = 0,\ v_b = 0,\ v_{A'} = 0$			
$E_A = 1.6722373_{000}$	$\pm$ 0.0000003	x 10^4	
$B_A = 0.2578369_{200}$	$\pm$ 0.0000015		
$D_A = 2.7435_{127}$	$\pm$ 0.0016	x 10^{-7}	
$E_b = 1.7388$	fixed	x 10^4	
$B_b = 0.2237$	fixed		
$D_b = 2.8$	fixed	x 10^{-7}	
$A_b = -1.00$	fixed	x 10^2	
$\xi_{Ab} = 7.2886$	fixed		
$E_{A'} = 1.7515$	fixed	x 10^4	
$B_{A'} = 0.2237$	fixed		
$D_{A'} = 2.8$	fixed	x 10^{-7}	
$\eta_{AA'} = 0.05017$	fixed		
$\xi_{A'b} = -1.00$	fixed	x 10^2	
$\sigma^2 = 0.07$[b]			

[a] See Table 3.25 for definitions of parameters.

[b] See Footnote a in Table 3.10 for definition of σ^2.

Table 3.29: (cont.)

Fit 2

$v_A = 1,\ v_b = 0,\ v_{A'} = 0,\ v_a = 2$

$E_A = 1.721810_{0000}$	$\pm$ 0.0000009	$\times 10^4$
$B_A = 0.256734_{740}$	$\pm$ 0.000004	
$D_A = 2.775_{313}$	$\pm$ 0.010	$\times 10^{-7}$
$E_b = 1.738771_{200}$	$\pm$ 0.000004	$\times 10^4$
$B_b = 0.22243_{333}$	$\pm$ 0.00012	
$D_b = 1.36_{094}$	$\pm$ 0.09	$\times 10^{-7}$
$A_b = -9.65_{904}$	$\pm$ 0.012	$\times 10^1$
$C_b = -0.4_{408}$	$\pm$ 0.3	
$\xi_{Ab} = 1.1020_{567}$	$\pm$ 0.0018	$\times 10^1$
$E_{A'} = 1.75180_{650}$	$\pm$ 0.00008	$\times 10^4$
$B_{A'} = 0.22277_{100}$	$\pm$ 0.00018	
$D_{A'} = 1.2538652$	fixed	$\times 10^{-7}$
$\eta_{AA'} = 0.1116_{819}$	$\pm$ 0.0011	
$\xi_{A'b} = 9.14_{098}$	$\pm$ 0.07	$\times 10^1$
$E_a = 1.74335_{590}$	$\pm$ 0.00022	$\times 10^4$
$B_a = 0.256426$	fixed	
$D_a = 2.8$	fixed	$\times 10^{-7}$
$\xi_{A'a} = 3.59_{291}$	$\pm$ 0.22	$\times 10^1$
$\xi_{ba} = -9.85$	fixed	
$\eta_{A'a} = -0.0902$	fixed	

$\sigma^2 = 1.0$

Table 3.29 (cont.)

Fit 3

$v_A = 2,\ v_b = 1,\ v_{A'} = 1,\ v_a = 3$

$E_A = 1.7712318_{000}$	$\pm$ 0.0000010	x 10^4
$B_A = 0.255676_{960}$	$\pm$ 0.000004	
$D_A = 2.809_{186}$	$\pm$ 0.006	x 10^{-7}
$E_b = 1.783804_{700}$	$\pm$ 0.000003	x 10^4
$B_b = 0.22246_{869}$	$\pm$ 0.00019	
$D_b = 2.65_{489}$	$\pm$ 0.22	x 10^{-7}
$A_b = -9.18_{621}$	$\pm$ 0.06	x 10^1
$C_b = 4.8_{617}$	$\pm$ 0.7	
$\xi_{Ab} = -2.77_{951}$	$\pm$ 0.04	
$E_{A'} = 1.79398_{430}$	$\pm$ 0.00004	x 10^4
$B_{A'} = 0.2205_{635}$	$\pm$ 0.0016	
$D_{A'} = 2.3_{553}$	$\pm$ 1.9	x 10^{-7}
$\eta_{AA'} = -0.0212_{386}$	$\pm$ 0.0019	
$\xi_{A'b} = 1.0587_{442}$	$\pm$ 0.0016	x 10^2
$E_a = 1.7877_{063}$	$\pm$ 0.0011	x 10^4
$B_a = 0.254903$	fixed	
$D_a = 2.8$	fixed	x 10^{-7}
$\xi_{A'a} = 2.4_{611}$	$\pm$ 0.8	x 10^1
$\xi_{ba} = -8._{452}$	$\pm$ 3.	
$\eta_{ba} = -0.03855$		

$\sigma^2 = 0.7$

Table 3.29 (cont.)

Fit 4

$v_A = 3,\ v_b = 2,\ v_{A'} = 2,\ v_b = 4$ (fixed)

E_A	$= 1.8201474_{000}$	± 0.0000007	$\times 10^4$
B_A	$= 0.254555_{720}$	± 0.000004	
D_A	$= 2.811_{358}$	± 0.007	$\times 10^{-7}$
E_b	$= 1.826884_{100}$	± 0.000016	$\times 10^4$
B_b	$= 0.2226_{030}$	± 0.0004	
D_b	$= 3.1_{338}$	± 0.4	$\times 10^{-7}$
A_b	$= -1.108_{952}$	± 0.008	$\times 10^2$
C_b	$= 2.298_{514}$	± 0.013	$\times 10^1$
ξ_{Ab}	$= -7.891_{379}$	± 0.018	
$E_{A'}$	$= 1.834618_{900}$	± 0.000028	$\times 10^4$
$B_{A'}$	$= 0.2193_{150}$	± 0.0004	
$D_{A'}$	$= 1.6_{176}$	± 0.4	$\times 10^{-7}$
$\eta_{AA'}$	$= -0.0511_{855}$	± 0.0021	
$\eta^J_{AA'}$	$= -9.32_{408}$	± 0.27	$\times 10^{-6}$
$\xi_{A'b}$	$= 1.1636_{320}$	± 0.0010	$\times 10^2$
E_a	$= 1.833263$	fixed	$\times 10^4$
B_a	$= 0.25338$	fixed	
D_a	$= 2.8$	fixed	$\times 10^{-7}$
$\xi_{A'a}$	$= -7.307$	fixed	
ξ_{ba}	$= 1.853$	fixed	
η_{ba}	$= 0.0172$	fixed	

$\sigma^2 = 0.4$

Table 3.29 (cont.)

Fit 5

$v_A = 4$, $v_b = 3$, $v_{b2} = 4$, $v_{A'} = 3$, $v_a = 5$ (fixed)

E_A	$= 1.8688413_{000}$	± 0.0000005	$\times 10^4$
B_A	$= 0.253541_{330}$	± 0.0000023	
D_A	$= 2.795_{837}$	± 0.003	$\times 10^{-7}$
E_b	$= 1.869603_{100}$	± 0.000010	$\times 10^4$
B_b	$= 0.22032_{746}$	± 0.00004	
D_b	$= 2.8$	fixed	$\times 10^{-7}$
A_b	$=-9.607_{877}$	± 0.019	$\times 10^1$
ξ_{Ab}	$=-6.484_{644}$	± 0.012	
$E_{A'}$	$= 1.883477_{500}$	± 0.000013	$\times 10^4$
$B_{A'}$	$= 0.22011_{257}$	± 0.00012	
$D_{A'}$	$= 2.8$	fixed	$\times 10^{-7}$
$\eta_{AA'}$	$=-0.0700_{302}$	± 0.0004	
$\xi_{A'b}$	$= 9.64_{547}$	± 0.06	$\times 10^1$
E_a	$= 1.879089$	fixed	
B_a	$= 0.251858$	fixed	
D_a	$= 2.8$	fixed	$\times 10^{-7}$
$\xi_{A'a}$	$=-2.1017$	fixed	$\times 10^1$
ξ_{ba}	$= 5.329$	fixed	
η_{ba}	$= 0.0487$	fixed	
E_{b2}	$= 1.9136169_{000}$	± 0.022	$\times 10^4$
B_{b2}	$= 0.21882542$	fixed	
D_{b2}	$= 2.9752034$	fixed	$\times 10^{-7}$

Table 3.29 (cont.)

Fit 5 (cont.)

$A_{b2} = -1.0$	fixed	$\times 10^{2}$
$\xi_{Ab2} = -7.08$	fixed	

$\sigma^2 = 0.25$

Fit 6

$v_A = 5,\ v_b = 4,\ v_{A'} = 4,\ v_a = 6$

$E_A = 1.9172725_{000}$	$\pm$ 0.0000011	$\times 10^{4}$
$B_A = 0.252450_{720}$	$\pm$ 0.000006	
$D_A = 2.793_{857}$	$\pm$ 0.016	$\times 10^{-7}$
$E_b = 1.913455_{600}$	$\pm$ 0.000009	$\times 10^{4}$
$B_b = 0.21890_{975}$	$\pm$ 0.00009	
$D_b = 2.8$	fixed	$\times 10^{-7}$
$A_b = -8.844_{690}$	$\pm$ 0.013	$\times 10^{1}$
$\xi_{Ab} = -1.519_{492}$	$\pm$ 0.029	
$E_{A'} = 1.925747_{600}$	$\pm$ 0.000013	$\times 10^{4}$
$B_{A'} = 0.21874_{284}$	$\pm$ 0.00008	
$D_{A'} = 2.8$	fixed	$\times 10^{-7}$
$\eta_{AA'} = -0.0142_{142}$	$\pm$ 0.0009	
$\xi_{A'b} = 1.0088_{293}$	$\pm$ 0.0019	$\times 10^{2}$
$E_a = 1.92475_{570}$	$\pm$ 0.00003	$\times 10^{4}$
$B_a = 0.2495_{473}$	$\pm$ 0.0003	
$D_a = 2.8$	fixed	$\times 10^{-7}$

Table 3.29 (cont.)

Fit 6 (cont.)

$C_a = 0.83_{855}$	$\pm$ 0.15	
$\gamma_a = -0.012_{642}$	$\pm$ 0.004	
$\xi_{A'a} = -1.93_{913}$	$\pm$ 0.07	$\times 10^1$
$\xi_{ba} = 4.1_{267}$	$\pm$ 0.6	
$\eta_{ba} = 0.094_{683}$	$\pm$ 0.007	

$\sigma^2 = 1.5$

Fit 7

$\nu_A = 5$, $\nu_b = 5$, $\nu_{A'} = 5$, $\nu_a = 7$, $\nu_{A2} = 6$

$E_A = 1.91739_{311}$	$\pm$ 0.00011	$\times 10^4$
$B_A = 0.25227_{678}$	$\pm$ 0.00026	
$D_A = 2.54_{374}$	$\pm$ 0.27	$\times 10^{-7}$
$E_b = 1.9556_{846}$	$\pm$ 0.0004	$\times 10^4$
$B_b = 0.2175_{796}$	$\pm$ 0.0006	
$D_b = 2.8$	fixed	$\times 10^{-7}$
$A_b = -9.1_{965}$	$\pm$ 0.4	$\times 10^1$
$\xi_{Ab} = 1.0_{603}$	$\pm$ 0.5	$\times 10^1$
$E_{A'} = 1.9689_{342}$	$\pm$ 0.0004	$\times 10^4$
$B_{A'} = 0.2174_{055}$	$\pm$ 0.0003	
$D_{A'} = 2.8$	fixed	$\times 10^{-7}$
$\eta_{AA'} = 0.062_{952}$	$\pm$ 0.020	
$\xi_{A'b} = 9.80_{652}$	$\pm$ 0.25	$\times 10^1$

Table 3.29 (cont.)

Fit 7 (cont.)

$E_a = 1.969662_{318}$	$\pm$ 0.000026	x 10^4
$B_a = 0.24910_{899}$	$\pm$ 0.00027	
$D_a = 2.8$	fixed	x 10^{-7}
$C_a = -0.07_{477}$	$\pm$ 0.05	
$\xi_{A'a} = -1.648_{075}$	$\pm$ 0.029	x 10^1
$\xi_{ba} = 4.3$	fixed	
$\eta_{ba} = 0.0388$	fixed	
$E_{A2} = 1.96534_{646}$	$\pm$ 0.00005	x 10^4
$B_{A2} = 0.2521_{213}$	$\pm$ 0.00041	
$D_{A2} = 2.8$	fixed	x 10^{-7}
$\xi_{bA2} = -3.4_{891}$	$\pm$ 0.3	
$\eta_{A'A2} = -0.022$	fixed	

$\sigma^2 = 3.9$

Table 3.29 (cont.)

Fit 8

$v_A = 7,\ v_b = 6,\ v_{A'} = 6,\ v_a = 8$

$E_A = 2.01270_{264}$	$\pm$ 0.00023	x 10^4
$B_A = 0.2527_{363}$	$\pm$ 0.0008	
$D_A = 2.8$	fixed	x 10^{-7}
$E_b = 1.9981_{766}$	$\pm$ 0.0016	x 10^4
$B_b = 0.2163_{528}$	$\pm$ 0.0013	
$D_b = 2.8$	fixed	x 10^{-7}
$A_b = -9.5_{898}$	$\pm$ 1.5	x 10^1
$\xi_{Ab} = 1.40_{327}$	$\pm$ 2.1	x 10^1
$E_{A'} = 2.0111_{821}$	$\pm$ 0.0016	x 10^4
$B_{A'} = 0.2157_{984}$	$\pm$ 0.0004	
$D_{A'} = 2.8$	fixed	x 10^{-7}
$\eta_{AA'} = 0.088_{526}$	$\pm$ 0.014	
$\xi_{A'b} = 9.9_{856}$	$\pm$ 1.1	x 10^1
$E_a = 2.01433_{090}$	$\pm$ 0.00006	x 10^4
$B_a = 0.2478_{206}$	$\pm$ 0.0010	
$D_a = 2.8$	fixed	x 10^{-7}
$C_a = -0.57_{035}$	$\pm$ 0.26	
$\xi_{A'a} = -8.5_{520}$	$\pm$ 0.7	
$\xi_{ba} = 1.692$	fixed	
$\eta_{ba} = 0.01494$	fixed	

$\sigma^2 = 1.5$

Table 3.29 (cont.)

Fit 9

$v_A = 8,\ v_b = 7,\ v_{A'} = 7,\ v_a = 9$

E_A	$= 2.06072_{882}$	$\pm$ 0.00005	x 10^4
B_A	$= 0.2506_{302}$	$\pm$ 0.0007	
D_A	$= 2.8$	fixed	x 10^{-7}
E_b	$= 2.04034_{532}$	$\pm$ 0.00024	x 10^4
B_b	$= 0.21484_{028}$	$\pm$ 0.00028	
D_b	$= 2.8$	fixed	x 10^{-7}
A_b	$=-8.82_{193}$	$\pm$ 0.23	x 10^1
ξ_{Ab}	$= 6.6984$	fixed	
$E_{A'}$	$= 2.05301_{065}$	$\pm$ 0.00024	x 10^4
$B_{A'}$	$= 0.2151_{103}$	$\pm$ 0.0003	
$D_{A'}$	$= 2.8$	fixed	x 10^{-7}
$\eta_{AA'}$	$= 0.086_{365}$	$\pm$ 0.016	
$\xi_{A'b}$	$= 1.012_{132}$	$\pm$ 0.016	x 10^2
E_a	$= 2.058736966$	fixed	x 10^4
B_a	$= 0.245677$	fixed	
D_a	$= 2.8$	fixed	x 10^{-7}
$\xi_{A'a}$	$= 1.0_{360}$	$\pm$ 0.6	
ξ_{ba}	$=-1.0$	fixed	
η_{ba}	$=-0.00946$	fixed	

$\sigma^2 = 2.8$

Fit 10

v_A = 8 (fixed), v_b = 8, $v_{A'}$=8, v_a=10 (fixed), v_{A2}=9 (fixed)

E_A =	2.060136	fixed	$\times 10^4$
B_A =	0.249225	fixed	
D_A =	2.8	fixed	$\times 10^{-7}$
E_b =	2.0816_{613}	$\pm$ 0.0008	$\times 10^4$
B_b =	0.2138_{894}	$\pm$ 0.0006	
D_b =	2.8	fixed	$\times 10^{-7}$
A_b =	-9.1_{577}	$\pm$ 0.8	$\times 10^1$
ξ_{Ab} =	-4.4574	fixed	
$E_{A'}$ =	2.0954_{887}	$\pm$ 0.0008	$\times 10^4$
$B_{A'}$ =	0.2115_{919}	$\pm$ 0.0004	
$D_{A'}$ =	2.8	fixed	$\times 10^{-7}$
$\eta_{AA'}$ =	-0.02993	fixed	
$\xi_{A'b}$ =	9.8_{982}	$\pm$ 0.6	$\times 10^1$
E_a =	2.102578	fixed	$\times 10^4$
B_a =	0.244243	fixed	
D_a =	2.8	fixed	$\times 10^{-7}$
$\xi_{A'a}$ =	1.2368	fixed	$\times 10^1$
ξ_{ba} =	-3.136	fixed	
η_{ba} =	-0.0286	fixed	
E_{A2} =	2.107154	fixed	$\times 10^4$
B_{A2} =	0.248155	fixed	
D_{A2} =	2.8	fixed	$\times 10^{-7}$
$\eta_{A'A2}$ =	0.02803	fixed	
ξ_{bA2} =	-4.336	fixed	

σ^2 = 3.8

Table 3.29 (cont.)

Fit 11

$v_A = 9$, $v_b = 9$, $v_{A'} = 9$, $v_a = 10$ (fixed)

E_A	$= 2.10835_{194}$	$\pm$ 0.00006	$\times 10^4$
B_A	$= 0.2521_{374}$	$\pm$ 0.0023	
D_A	$= 2.8$	fixed	$\times 10^{-7}$
E_b	$= 2.1223_{958}$	$\pm$ 0.0004	$\times 10^4$
B_b	$= 0.21190_{686}$	$\pm$ 0.00021	
D_b	$= 2.8$		$\times 10^{-7}$
A_b	$=-9.6_{253}$	$\pm$ 0.4	$\times 10^1$
ξ_{Ab}	$=-6.17562$	fixed	
$E_{A'}$	$= 2.1368_{192}$	$\pm$ 0.0004	$\times 10^4$
$B_{A'}$	$= 0.21248_{284}$	$\pm$ 0.00021	
$D_{A'}$	$= 2.8$	fixed	$\times 10^{-7}$
$\eta_{AA'}$	$=-0.04118$	fixed	
$\xi_{A'b}$	$= 9.5_{968}$	$\pm$ 0.3	$\times 10^1$
E_a	$= 2.102578$	fixed	$\times 10^4$
B_a	$= 0.244243$	fixed	
D_a	$= 2.8$	fixed	$\times 10^{-7}$
$\xi_{A'a}$	$= 1.7259$	fixed	$\times 10^1$
ξ_{ba}	$=-4.376$	fixed	
η_{ba}	$=-0.0395$	fixed	

$\sigma^2 = 1.7$

Table 3.29 (cont.)

Fit 12

$v_A = 10$ (fixed), $v_b = 10$, $v_{A'} = 10$, $v_a = 11$

E_A	$= 2.1538850$	fixed	$\times 10^4$
B_A	$= 0.247085$	fixed	
D_A	$= 2.8$	fixed	$\times 10^{-7}$
E_b	$= 2.16294_{412}$	± 0.00005	$\times 10^4$
B_b	$= 0.2105_{862}$	± 0.0005	
D_b	$= 2.8$	fixed	$\times 10^{-7}$
A_b	$=-1.0$	fixed	$\times 10^2$
ξ_{Ab}	$=-5.7415$	fixed	
$E_{A'}$	$= 2.17752_{958}$	± 0.00009	$\times 10^4$
$B_{A'}$	$= 0.213_{602}$	± 0.007	
$D_{A'}$	$= 2.8$	fixed	$\times 10^{-7}$
$\eta_{AA'}$	$=-0.03804$	fixed	
$\Xi_{A'b}$	$= 1.0$	fixed	$\times 10^2$
E_a	$= 2.14614_{622}$	± 0.00003	$\times 10^4$
B_a	$= 0.2424_{673}$	± 0.0003	
D_a	$= 2.8$	fixed	$\times 10^{-7}$
$\lvert C_a \rvert$	$= 0.67_{874}$	± 0.04	
$\xi_{A'a}$	$=-0.4657$	fixed	
ξ_{ba}	$= 0.1181$	fixed	
η_{ba}	$= 0.001488$	fixed	

$\sigma^2 = 2.4$

Table 3.29 (cont.)

Fit 13

v_A = 11 (fixed), v_b = 11, $v_{A'}$ = 11 (fixed), v_a = 12

E_A =	2.200247	fixed	x 10^4
B_A =	0.246015	fixed	
D_A =	2.8	fixed	x 10^{-7}
E_b =	2.20443_{155}	$\pm$ 0.00007	x 10^4
B_b =	0.2101_{431}	$\pm$ 0.0006	
D_b =	2.8	fixed	x 10^{-7}
A_b =	-1.062_{406}	$\pm$ 0.020	x 10^2
ξ_{Ab} =	-3.606	fixed	
$E_{A'}$ =	2.218382	fixed	x 10^4
$B_{A'}$ =	0.2083	fixed	
$D_{A'}$ =	2.8	fixed	x 10^{-7}
$\eta_{AA'}$ =	-0.0237	fixed	
$\xi_{A'b}$ =	1.0	fixed	x 10^2
E_a =	2.189347_{785}	$\pm$ 0.000025	x 10^4
B_a =	0.24150_{537}	$\pm$ 0.00023	
D_a =	2.8	fixed	x 10^{-7}
$\lvert C_a \rvert$ =	0.43_{585}	$\pm$ 0.03	
$\xi_{A'a}$ =	-7.8326	fixed	
ξ_{ba} =	1.9861	fixed	
η_{ba} =	0.01871	fixed	

σ^2 = 1.3

Table 3.30: Low Lying State Correlation Matrices[a]

FIT 1

E_A	1.000		
B_A	-0.722	1.000	
D_A	-0.546	0.943	1.000

Table 3.30 :(cont.)

FIT 2

E_A	1.000									
$E_{A'}$	0.090	1.000								
E_b	-0.200	0.120	1.000							
B_A	-0.363	0.084	-0.125	1.000						
$B_{A'}$	-0.058	0.117	0.207	0.145	1.000					
B_b	0.000	-0.649	-0.344	-0.194	-0.725	1.000				
D_A	-0.024	-0.479	-0.225	0.373	-0.635	0.695	1.000			
D_b	-0.001	-0.537	-0.261	-0.275	-0.558	0.920	0.485	1.000		
A_b	-0.004	-0.401	-0.405	0.085	-0.632	0.566	0.624	0.240	1.000	
C_b	-0.014	-0.651	-0.260	-0.121	-0.806	0.932	0.783	0.735	0.712	1.000
$\eta_{AA'}$	-0.049	0.514	0.013	0.262	0.730	-0.824	-0.691	-0.743	-0.420	-0.815
ξ_{Ab}	-0.179	-0.692	-0.195	-0.125	-0.430	0.656	0.504	0.431	0.657	0.754
$\xi_{A'b}$	-0.023	0.397	0.291	0.116	0.924	-0.890	-0.733	-0.728	-0.687	-0.936
E_a	0.038	-0.055	-0.113	-0.022	-0.447	0.230	0.195	0.158	0.302	0.302
$\xi_{A'a}$	-0.095	-0.429	0.135	0.005	0.648	-0.143	-0.152	-0.098	-0.250	-0.206

Table 3.30:(cont.)

FIT 2 (CONT.)

$\eta_{AA'}$	1.000				
ξ_{Ab}	-0.459	1.000			
$\xi_{A'b}$	0.752	-0.610	1.000		
E_a	-0.164	0.123	-0.450	1.000	
$\xi_{A'a}$	0.100	0.097	0.509	-0.604	1.000

Table 3.30: (cont.)

FIT 3

E_A	1.000									
$E_{A'}$	0.273	1.000								
E_b	-0.351	-0.312	1.000							
B_A	-0.408	0.019	0.018	1.000						
$B_{A'}$	0.017	-0.268	0.002	0.134	1.000					
B_b	-0.123	-0.199	-0.133	-0.256	-0.407	1.000				
D_A	0.047	0.260	-0.086	0.811	0.024	-0.250	1.000			
$D_{A'}$	0.020	-0.278	0.014	0.126	0.982	-0.328	0.034	1.000		
D_b	-0.047	0.113	-0.103	-0.266	-0.275	0.621	-0.245	-0.310	1.000	
A_b	0.023	-0.011	-0.458	0.041	0.170	0.255	0.014	0.217	-0.208	1.000
C_b	-0.174	-0.572	0.326	-0.067	0.001	0.456	-0.127	0.125	-0.133	-0.124
$\eta_{AA'}$	0.337	0.631	-0.059	-0.063	-0.426	0.132	0.325	-0.393	0.257	-0.123
ξ_{Ab}	0.410	0.643	-0.117	0.171	0.087	-0.531	0.491	0.063	-0.176	-0.163
$\xi_{A'b}$	0.017	0.243	0.025	-0.107	-0.882	0.239	0.012	-0.930	0.229	-0.268
E_a	-0.012	-0.268	0.024	0.102	0.907	-0.213	0.000	0.956	-0.254	0.204
$\xi_{A'a}$	-0.017	0.178	0.048	-0.123	-0.936	0.341	-0.019	-0.958	0.240	-0.242
ξ_{ba}	0.064	0.397	-0.162	-0.045	-0.709	-0.051	0.032	-0.787	0.239	-0.077

Table 3.30: (cont.)

FIT 3 (CONT.)

C_b	1.000						
$\eta_{AA'}$	-0.213	1.000					
ξ_{Ab}	-0.488	0.678	1.000				
$\xi_{A'b}$	-0.097	0.440	0.038	1.000			
E_a	0.230	-0.406	-0.027	-0.940	1.000		
$\xi_{A'a}$	0.010	0.406	-0.063	0.980	-0.947	1.000	
ξ_{ba}	-0.638	0.334	0.181	0.680	-0.837	0.665	1.000

Table 3.30: (cont.)

FIT 4

E_A	1.000									
$E_{A'}$	0.614	1.000								
E_b	-0.337	-0.886	1.000							
B_A	0.179	0.441	-0.607	1.000						
$B_{A'}$	-0.224	-0.447	0.432	-0.038	1.000					
B_b	0.205	0.419	-0.391	-0.057	-0.927	1.000				
D_A	0.659	0.640	-0.617	0.782	-0.302	0.157	1.000			
$D_{A'}$	-0.251	-0.479	0.458	-0.052	0.991	-0.924	-0.315	1.000		
D_b	0.206	0.426	-0.396	-0.066	-0.919	0.997	0.142	-0.923	1.000	
A_b	0.224	0.341	-0.253	-0.149	-0.859	0.976	0.087	-0.860	0.969	1.000
C_b	-0.452	-0.455	0.205	-0.026	-0.077	-0.139	-0.129	0.003	-0.155	-0.261
$\eta_{AA'}$	0.937	0.460	-0.113	-0.122	-0.139	0.145	0.419	-0.161	0.149	0.201
ξ_{Ab}	0.651	0.652	-0.551	0.488	0.245	-0.295	0.627	0.206	-0.287	-0.338
$\xi_{A'b}$	0.088	0.116	-0.126	0.099	0.324	-0.103	-0.024	0.233	-0.088	-0.026
$\eta_{AA'}$ J	-0.921	-0.426	0.098	0.129	0.264	-0.233	-0.455	0.268	-0.227	-0.278

Table 3.30: (cont.)

FIT 4 (CONT.)

C_b	1.000				
$\eta_{AA'}$	-0.465	1.000			
ξ_{Ab}	-0.400	0.542	1.000		
$\xi_{A'b}$	-0.653	0.055	0.264	1.000	
$\eta^{J}_{AA'}$	0.327	-0.977	-0.447	0.083	1.000

Table 3.30: (cont.)

FIT 5

E_A	1.000									
$E_{A'}$	-0.184	1.000								
E_b	-0.553	0.291	1.000							
B_A	-0.289	-0.309	-0.206	1.000						
$B_{A'}$	0.074	-0.091	-0.001	0.064	1.000					
B_b	-0.028	-0.070	0.256	-0.084	-0.251	1.000				
D_A	0.083	-0.484	-0.456	0.880	0.057	-0.028	1.000			
A_b	-0.300	0.114	0.720	-0.160	-0.111	0.848	-0.254	1.000		
$\eta_{AA'}$	-0.098	0.637	0.253	-0.195	0.655	-0.311	-0.362	-0.032	1.000	
ξ_{Ab}	0.539	-0.183	-0.915	0.182	0.172	-0.421	0.406	-0.780	-0.035	1.000
$\xi_{A'b}$	0.015	0.095	0.128	-0.007	0.973	-0.135	-0.052	0.044	0.757	0.051
E_{b2}	0.078	-0.007	-0.039	-0.083	-0.003	0.036	0.035	0.003	-0.023	0.039

FIT 5 (CONT.)

$\xi_{A'b}$	1.000	
E_{b2}	-0.004	1.000

Table 3.30: (cont.)

FIT 6

E_A	1.000									
$E_{A'}$	0.089	1.000								
E_b	-0.351	-0.151	1.000							
B_A	-0.242	-0.045	-0.297	1.000						
$B_{A'}$	0.090	0.080	-0.157	0.008	1.000					
B_b	-0.023	-0.314	-0.083	0.062	-0.460	1.000				
D_A	0.142	0.093	-0.433	0.830	0.040	0.031	1.000			
A_b	-0.156	-0.417	0.428	-0.083	-0.341	0.778	-0.179	1.000		
$\eta_{AA'}$	0.103	0.763	0.018	-0.117	0.287	-0.380	-0.026	-0.326	1.000	
ξ_{Ab}	0.262	0.211	-0.837	0.316	0.155	0.012	0.443	-0.421	0.062	1.000
$\xi_{A'b}$	0.109	0.365	-0.189	-0.009	0.821	-0.148	0.058	-0.150	0.464	0.190
E_a	-0.019	-0.133	-0.019	0.036	-0.415	-0.207	0.020	-0.214	-0.213	0.012
B_a	0.032	-0.016	-0.050	-0.003	0.458	-0.052	0.000	0.046	0.123	0.045
C_a	-0.022	-0.169	-0.028	0.051	-0.609	-0.109	0.032	-0.191	-0.291	0.011
γ_a	0.022	-0.144	-0.095	0.041	0.045	-0.318	0.033	-0.236	-0.109	0.081
$\xi_{A'a}$	-0.027	-0.130	-0.016	0.046	-0.648	-0.119	0.030	-0.199	-0.268	0.004
ξ_{ba}	0.013	0.211	0.052	-0.057	0.489	0.202	-0.035	0.240	0.293	-0.032
η_{ba}	-0.046	0.020	0.078	0.003	-0.668	0.288	-0.003	0.042	-0.163	-0.078

Table 3.30: (cont.)

FIT 6 (CONT.)

$\xi_{A'b}$	1.000							
E_a	-0.691	1.000						
B_a	0.550	-0.642	1.000					
C_a	-0.789	0.844	-0.558	1.000				
γ_a	-0.284	0.603	-0.190	0.476	1.000			
$\xi_{A'a}$	-0.812	0.851	-0.600	0.971	0.454	1.000		
ξ_{ba}	0.749	-0.885	0.479	-0.949	-0.608	-0.959	1.000	
η_{ba}	-0.474	0.166	-0.484	0.426	-0.318	0.449	-0.248	1.000

Table 3.30: (cont.)

FIT 7

E_A	1.000									
$E_{A'}$	-0.555	1.000								
E_b	0.557	-0.996	1.000							
B_A	-0.945	0.526	-0.526	1.000						
$B_{A'}$	-0.073	-0.172	0.117	0.068	1.000					
B_b	-0.510	0.991	-0.994	0.457	-0.143	1.000				
D_A	-0.979	0.514	-0.516	0.879	0.061	0.483	1.000			
A_b	0.615	-0.985	0.989	-0.550	0.093	-0.989	-0.592	1.000		
$\eta_{AA'}$	0.773	-0.134	0.131	-0.585	0.006	-0.127	-0.866	0.240	1.000	
ξ_{Ab}	-0.592	0.321	-0.326	0.304	0.042	0.360	0.717	-0.440	-0.849	1.000
$\xi_{A'b}$	-0.563	0.997	-0.998	0.533	-0.117	0.992	0.522	-0.988	-0.135	0.327
E_a	-0.022	0.141	-0.115	0.027	-0.302	0.123	0.018	-0.112	0.005	-0.004
B_a	-0.083	0.019	-0.036	0.071	0.425	0.028	0.078	-0.053	-0.023	0.067
C_a	0.235	-0.367	0.375	-0.204	0.021	-0.378	-0.229	0.385	0.098	-0.183
$\xi_{A'a}$	-0.496	0.888	-0.879	0.475	-0.142	0.872	0.458	-0.866	-0.119	0.276
E_{A2}	-0.186	0.494	-0.470	0.176	-0.329	0.461	0.170	-0.418	-0.019	0.107
B_{A2}	0.104	-0.364	0.341	-0.101	0.456	-0.338	-0.095	0.292	0.010	-0.053
ξ_{bA2}	-0.200	0.476	-0.473	0.186	-0.165	0.456	0.184	-0.413	-0.020	0.124

Table 3.30: (cont.)

FIT 7 (CONT.)

$\xi_{A'b}$	1.000							
E_a	0.126	1.000						
B_a	0.030	-0.773	1.000					
C_a	-0.382	-0.036	0.009	1.000				
$\xi_{A'a}$	0.873	-0.015	0.183	-0.134	1.000			
E_{A2}	0.472	0.254	-0.248	-0.160	0.411	1.000		
B_{A2}	-0.341	-0.291	0.461	0.109	-0.292	-0.879	1.000	
ξ_{bA2}	0.472	0.116	-0.111	-0.148	0.419	0.827	-0.648	1.000

Table 3.30 (cont.)

FIT 8

E_A	1.000									
$E_{A'}$	0.631	1.000								
E_b	-0.632	-1.000	1.000							
B_A	-0.956	-0.639	0.639	1.000						
$B_{A'}$	-0.309	-0.604	0.598	0.374	1.000					
B_b	0.605	0.955	-0.958	-0.612	-0.644	1.000				
A_b	-0.541	-0.994	0.994	0.557	0.607	-0.950	1.000			
$\eta_{AA'}$	-0.766	-0.838	0.839	0.764	0.538	-0.820	0.799	1.000		
ξ_{Ab}	0.997	0.624	-0.626	-0.943	-0.292	0.603	-0.534	-0.764	1.000	
$\xi_{A'b}$	0.631	1.000	-1.000	-0.638	-0.598	0.956	-0.994	-0.839	0.625	1.000
E_a	0.018	0.003	-0.003	-0.021	0.116	-0.040	-0.003	0.277	0.009	0.004
B_a	-0.003	0.013	-0.012	-0.002	-0.180	0.069	-0.012	-0.318	0.005	0.011
C_a	-0.243	-0.333	0.333	0.274	0.196	-0.328	0.326	0.144	-0.242	-0.332
$\xi_{A'b}$	0.606	0.961	-0.961	-0.630	-0.583	0.917	-0.955	-0.735	0.601	0.960

Table 3.30:(cont.)

FIT 8 (CONT.)

E_a	1.000			
B_a	-0.950	1.000		
C_a	-0.472	0.477	1.000	
$\xi_{A'b}$	0.160	-0.121	-0.509	1.000

Table 3.30: (cont.)

FIT 9

E_A	1.000									
$E_{A'}$	-0.050	1.000								
E_b	0.089	-0.985	1.000							
B_A	-0.882	0.027	-0.048	1.000						
$B_{A'}$	-0.168	0.190	-0.288	0.186	1.000					
B_b	-0.109	0.405	-0.492	0.103	0.370	1.000				
A_b	0.072	-0.992	0.994	-0.042	-0.262	-0.433	1.000			
$\eta_{AA'}$	-0.062	0.035	-0.025	-0.071	0.110	-0.010	-0.027	1.000		
$\xi_{A'b}$	-0.078	0.993	-0.994	0.042	0.267	0.435	-0.994	0.020	1.000	
$\xi_{A'a}$	0.037	-0.848	0.838	-0.027	-0.177	-0.334	0.845	0.040	-0.847	1.000

Table 3.30: (cont.)

FIT 10

$E_{A'}$	1.000					
E_b	-0.998	1.000				
$B_{A'}$	-0.127	0.095	1.000			
B_b	0.757	-0.775	-0.082	1.000		
A_b	-0.999	0.999	0.102	-0.763	1.000	
$\xi_{A'b}$	0.999	-0.999	-0.096	0.757	-0.999	1.000

FIT 11

E_A	1.000							
$E_{A'}$	0.011	1.000						
E_b	-0.003	-0.997	1.000					
B_A	-0.835	-0.020	0.022	1.000				
$B_{A'}$	-0.078	0.041	-0.087	-0.009	1.000			
B_a	-0.026	0.482	-0.522	-0.035	0.448	1.000		
A_b	-0.007	-0.999	0.999	0.022	-0.072	-0.497	1.000	
$\xi_{A'b}$	0.006	0.999	-0.999	-0.021	0.073	0.497	-0.999	1.000

Table 3.30: (cont.)

FIT 12

$E_{A'}$	1.000						
E_b	-0.187	1.000					
$B_{A'}$	-0.744	0.052	1.000				
B_b	-0.209	-0.854	-0.121	1.000			
E_a	0.000	0.000	0.000	0.001	1.000		
B_a	-0.000	0.000	0.000	-0.001	-0.822	1.000	
C_a	-0.001	-0.003	0.002	0.005	0.057	-0.032	1.000

FIT 13

E_b	1.000					
B_b	-0.926	1.000				
A_b	0.123	-0.260	1.000			
E_a	-0.015	0.019	-0.042	1.000		
B_a	0.016	-0.019	-0.015	-0.818	1.000	
C_a	0.015	-0.019	0.065	0.028	-0.009	1.000

[a]See footnote a, Table 3.11.

Fit 1: $v_A = 0$, $v_b = 0$ (fixed), $v_{A'} = 0$ (fixed)
No perturbations in $A^1\Sigma^+(v_A = 0)$ are observed so this level is fit with $b^3\Pi(v_b = 0)$ and $A'^1\Pi(v_{A'} = 0)$ constants held fixed.

Fit 2: $v_A = 1$, $v_b = 0$, $v_{A'} = 0$, $v_a = 2$
In addition to $A^1\Sigma^+ \sim b^3\Pi$, and $A^1\Sigma^+ \sim A'^1\Pi$ perturbations reported in Ref. 8, $A'^1\Pi$ Λ-doubling resulting from interaction with $a^3\Sigma^+$ is detected although no $a^3\Sigma^+ \sim A'^1\Pi$ crossings are observed in the J range sampled. The $A'^1\Pi \sim A^1\Sigma^+$ perturbation at $J_o = 104.0$ is poorly characterized since the $A^1\Sigma^+ - X^1\Sigma^+$ (1,0) band analysis in Ref. 8 ends at this point. Although D_b could be determined, $D_{A'}$ could not be and is fixed at a preliminary value of D_b which is nearly equal to the final D_b fitted value. It was also necessary to vary C_b although it is only marginally determined.

Fit 3: $v_A = 2$, $v_b = 1$, $v_{A'} = 1$, $v_a = 3$
In addition to the perturbations reported in Ref. 8, $a^3\Sigma^+ \sim A'^1\Pi$ interactions are again observed in the form of Λ-doubling and level shifts of the $A'^1\Pi$ state at $J > 40$. No crossings are observed in the J range sampled.

Fit 4: $v_A = 3$, $v_b = 2$, $v_{A'} = 2$, $v_b = 4$ (fixed)
No new perturbations are observed, however these term values could not be fit without varying a centrifugal distortion $A^1\Sigma^+ \sim A'^1\Pi$ interaction parameter, $\eta_{AA'}$. Other problems are apparent when this fit is compared with others: (1) the $A'^1\Pi$ energy is anomalously low by $\approx$ 35 cm^{-1}; (2) both the $b^3\Pi$ spin-orbit constant, A_b, and the $b^3\Pi \sim A'^1\Pi$ spin-orbit interaction parameter, $\xi_{A'b}$, are anomalously large by $\approx$ 15 cm^{-1}; (3) the $b^3\Pi$ spin-spin constant, C_b, is also unusually large by $\approx$ 15 cm^{-1}; and (4) the $b^3\Pi$ rotational constant, B_b, is larger than expected by $\approx$ 0.003 cm^{-1}, which is ten times the 1σ error. Attempts to force the program to converge about the expected parameter values were utterly unsuccessful. Nor did varying the $b^3\Pi$ spin-rotation constant or the third order $A^1\Sigma^+$ centrifugal distortion constant, H, diminish the magnitude of these anomalies: neither parameter could be determined. Explanations for these problems, which are unique to this fit, are discussed below.

Fit 5: $v_A = 4$, $v_b = 3$, $v_{b2} = 4$, $v_{A'} = 3$, $v_a = 5$ (fixed)
No new perturbations are detected. As mentioned above, a second $b^3\Pi$ vibrational level is needed to simultaneously fit the $A^1\Sigma^+$ ($v_A = 4$) $\sim$ $b^3\Pi_2$ ($v_{b2} = 4$) perturbation at $J_o = 97.7$ and the $A^1\Sigma^+$ ($v_A = 4$) $\sim$ $b^3\Pi_o$($v_b = 3$) perturbation at $J_o = 55.6$. Only the energy for $b^3\Pi(v_b = 4)$ is varied; B_{b2} and D_{b2} are fixed at preliminary Fit 6 values.

The $b^3\Pi(v_{b2} = 4)$ energy so determined agrees well with the value determined in Fit 6.†

Fit 6: $v_A = 5$, $v_b = 4$, $v_{A'} = 4$, $v_a = 6$
Both $a^3\Sigma^+ \sim A'^1\Pi$ and $a^3\Sigma^+ \sim b^3\Pi$ perturbations are observed. No crossing for the latter is observed since the $b^3\Pi_o(v_b = 4)$ origin lies below $a^3\Sigma^+(v_a=6)$ and $B_a > B_b$; however, both $a^3\Sigma^+ \sim b^3\Pi$ perturbation parameters, ξ_{ba} and η_{ba}, are determined. One $a^3\Sigma^+ \sim A'^1\Pi$ crossing is observed at $J_o = 39.5$. A second $b^3\Pi$ vibrational level must be considered at $J > 74$ owing to the $b^3\Pi_2(v_b = 5)$

† Although the difference between the two values exceeds three times their combined standard errors, this is reasonable when one considers the effects of fixing parameters as discussed in Chapter 2 and Appendix 1.

$\sim A^1\Sigma^+$ ($v_A = 5$) crossing at $J_o = 88.9$; however, this is treated differently from Fit 5 since $b^3\Pi_o(v_b = 5) \sim A^1\Sigma^+$ ($v_A = 6$) interactions are observed (Fit 7). Instead of including $b^3\Pi_2(v_b = 5)$ in this fit, $A^1\Sigma^+(v_A = 5)$ data from Ref. 8 are truncated at $J = 74$ and included in Fit 7, where all three Ω components of $b^3\Pi(v_b = 5)$ are fit simultaneously. The two sets of $A^1\Sigma^+$ ($v_A = 5$) parameters determined from Fits 6 and 7 are in agreement to within 3 standard deviations. Both the $a^3\Sigma^+$ spin-spin and spin-rotation constants, C_a and γ_a respectively, are determined.

Fit 7: $v_A = 5$, $v_b = 5$, $v_{A'} = 5$, $v_a = 7$, $v_{A2} = 6$
As mentioned above, $A^1\Sigma^+$ ($v_A = 5$) J levels above $J = 74$ (from Ref. 8) are fit along with $v_{A2} = 6$ OODR data. Two $a^3\Sigma^+ \sim A'^1\Pi$ crossings are observed. Although no $A^1\Sigma^+(v_{A2} = 6) \sim b^3\Pi_o$ crossing is observed the two levels are nearly degenerate at $J = 0$ and ξ_{bA2} is determined.

Fit 8: $v_A = 7$, $v_b = 6$, $v_{A'} = 6$, $v_a = 8$

Two new perturbations are observed: $A^1\Sigma^+$ ($v_A = 7$) $\sim$ $A'^1\Pi(v_{A'} = 6)$ and $A'^1\Pi(v_{A'} = 6) \sim a^3\Sigma^+(v_a = 8)$. A double e-parity crossing occurs between $A^1\Sigma^+$, $A'^1\Pi$, and $a^3\Sigma^+$ (F_2) and is illustrated in Fig. 3.11. Although $b^3\Pi_o(v_b = 6)$ lies below the $v_A = 7$ origin, ξ_{Ab} could still be determined from the $A'^1\Pi \sim A^1\Sigma^+$ interaction owing to $A'^1\Pi \sim b^3\Pi_1$ mixing and $b^3\Pi$ spin-uncoupling which results in finite $b^3\Pi_o$ character in the nominal $A'^1\Pi$ $v_{A'}=6$ level. These perturbations were previously observed by Sakurai, Johnson, and Broida[45] but these authors made no attempt at analysis.

Fit 9: $v_A = 8$, $v_b = 7$, $v_{A'} = 7$, $v_a = 9$

A very small perturbation ($\xi_{A'a} = 1.0\ cm^{-1}$) between $A'^1\Pi(v_{A'}=7)$ and $a^3\Sigma^+$ ($v_a = 9$) is observed at $J_o = 11.2$. Although no $A^1\Sigma^+ \sim A'^1\Pi$ crossing is observed, $\eta_{AA'}$ is marginally determined.

Fit 10: $v_A = 8$ (fixed), $v_b=8$, $v_{A'}=8$, $v_a=10$(fixed), $v_{A2}=9$(fixed)

No perturbations are observed.

Fit 11: $v_A = 9$, $v_b = 9$, $v_{A'} = 9$, $v_a = 10$ (fixed)
No perturbations are observed.

Fit 12: $v_A = 10$ (fixed), $v_b = 10$, $v_{A'} = 10$, $v_a = 11$
No perturbations are observed. As mentioned above, $C^1\Sigma^+ \rightarrow a^3\Sigma^+$ P- and R-form branch emission is arbitrarily assigned such that $C_a > 0$; if the Q branch assignments are systematically interchanged with the P and R assignments in Table 3.17 the values in Table 3.29 change by less than the 1σ estimates quoted except for C_a which changes sign (but has the same magnitude). Thus, the absolute value of C_a is reported.

Fit 13: $v_A = 11$ (fixed), $v_b = 11$, $v_{A'} = 11$ (fixed), $v_a = 12$
No perturbations are observed. Again, only $|C_a|$ is determined.

From Table 3.29, it is seen that vibrational intervals and rotational constants, particularly those for $A'^1\Pi$ and $b^3\Pi$, do not vary in a regular fashion. The precision to which second order corrections to E and B[46-49] can be calculated ($\approx$ 40%) does not warrant making these adjustments. However, the magnitude of these corrections precludes their being responsible for the anomalies apparent from examination of Table 3.29: for example, the $A'^1\Pi(v_{A'} = 2)$ energy is low by $\approx$ 35 cm^{-1} with respect to $v_{A'} = 1$ and 3, whereas the second order energy correction (from interaction with $a^3\Sigma^+$) is estimated to be -1.0 ± 0.4 cm^{-1}. Similarly, second order $A^1\Sigma^+ \sim b^3\Pi$ and $a^3\Sigma^+ \sim b^3\Pi$ spin-orbit interactions which primarily determine C_b[42,48,50-53] cannot account for the anomalous value of 22.98 cm^{-1} determined for $v_b = 2$.† On the other hand, these interactions, as well as second order $A'^1\Pi \sim b^3\Sigma^+$ interactions, are of the right magnitude to explain observed C_a values. In fact, the $A^1\Sigma^+$ and $a^3\Sigma^+$ E and B values are not anomalous.

It is curious that in Fit 4 it is necessary to vary an additional $A'^1\Pi \sim A^1\Sigma^+$ interaction parameter,

---

†γ_a may similarly be explained by second order $b^3\Pi \sim a^3\Sigma^+$ rotation-electronic interactions.

$\eta^{J}_{AA'}$. Although this centrifugal distortion parameter can be explained as second order interactions with $A'^{1}\Pi$ and $A^{1}\Sigma^{+}$ vibrational levels not explicitly included in the Fit 4 Hamiltonian, it is peculiar that it is not required in any other fit. These problems are not unique to $v_{A'} = v_b = 2$: $B_{A'}(v_{A'} = 3)$ is certainly too large when contrasted with $B_{A''}$ for $v_{A'} = 2$ and 4. And the B_b values for $v_b = 0$, 1, and 2 are the same to within experimental error, contrary to the expected monotonic decrease of B with v.

The magnitude of these anomalies and the inability of second order effects to account for them is suggestive of incomplete deperturbation. The presence of an additional perturbing state (or states) is indicated. The fact that these anomalies are manifested only by $A'^{1}\Pi$ and $b^{3}\Pi$ leads to the conclusion that this state (or states) has Δ symmetry (see discussion below).[37]

The above observations illustrate the utility and sensitivity of deperturbation in detecting the presence of new electronic states. Experiments designed to test this hypothesis are described below.

4. Equilibrium Constants

Dunham coefficients (Eq. 3.1)[39] for the low lying states of BaO are given in Table 3.31. The E and B values from Table 3.29 were fit to polynomials

Table 3.31: Spectroscopic Constants for Low Lying States of BaO[a]

	$X^1\Sigma^+$[b]	$a^3\Sigma^+$	$A^1\Sigma^+$	$b^3\Pi$	$A'^1\Pi$
$\nu_{00}x10^{-4}$	0.0	1.6496(3)	1.6722373(10) [1.672225][c]	1.73915(10) [1.7372][e]	1.75088(12)
$T_e x10^{-4}$	0.0	1.6596(3)	1.6807345(10)	1.75026(10)	1.76197(12)
Y_{00}	0.0173	0.0928	-0.0611	-0.1468	-0.1230
$Y_{10}(\omega_e)x10^{-2}$	6.6976(6)	4.690(7)	4.99620(19) [4.997][c]	4.4762(8) [4.483][e]	4.4795(22) [4.4245][f]
$Y_{20}(-\omega_e x_e)$	2.028(17)	-1.48(4)	-1.716 (8) [-1.64][c]	-2.287(12) [-2.39][e]	-2.139(8) [-1.652][f]
$Y_{30}(\omega_e y_e)x10^{2}$	-0.35 (11)		2.14 (9)		1.02 (3)
$Y_{40}(\omega_e z_e)x10^{5}$	-6.3 (21)				
$Y_{01}(B_e)$	0.3126140(7)	0.2594(5)	0.2583908(26) [0.25832][d]	0.22426(16) [0.2244][e]	0.22385(16) [0.2244][e]
$Y_{11}(-\alpha_e)x10^{3}$	-1.3921(9)	-1.44 (5)	-1.111 (3) [-1.070][d]	-1.18 (4) [-1.4][e]	-1.15 (4) [-1.4][e]
$Y_{21}(\gamma_e)x10^{6}$	-4.33 (24)		7.0 (7)		-4.0 (21)
$A \quad x10^{1}$				-9.4[g](4)	
R_e(Å)	1.939677 (3)	2.1294(20)	2.133512(11)	2.2901(8)	2.2922(8)

[a] All units are cm^{-1} except where noted. All energies are deperturbed. Uncertainties of 1σ are given in parentheses. Previously reported values are given in parentheses.

Table 3.31: (cont.) Footnotes (cont.)

---

[b] $X^1\Sigma^+$ constants taken from Ref. 3.

[c] Ref. 8.

[d] Ref. 19.

[e] Ref. 9.

[f] Ref. 11.

[g] Weighted average of values in Table 3.29.

in (v+1/2) ignoring correlations between parameters but weighting according to the uncertainties ($1/\sigma^2$) in Table 3.29. For $A'^1\Pi$, $G(v_{A'})$ values up to $v_{A'} = 29$ from Ref. 11 and $B(v_{A'})$ values up to $v_{A'} = 18$ from Ref. 12 are fit along with these data.†

The constants for $a^3\Sigma^+$, $A^1\Sigma^+$, $b^3\Pi$, and $A'^1\Pi$ have been extended and improved over previous determinations. Discrepancies between $A'^1\Pi$ constants in Table 3.31 and those in Ref. 11 result from the use of band heads instead of origins as well as extrapolation from high v in the latter. It cannot be overemphasized that the energies in Table 3.31 are deperturbed and should not be used to reproduce spectra without diagonalizing the matrix in Table 3.25. In fact, the parameters in Table 3.29 reproduce the spectra to within experimental error but those in Table 3.31 will not owing to incomplete deperturbation (see above) and neglect of correlations

---

†$G(v_{A'})$ values from Ref. 11 are given uncertainties twice those quoted, for band heads, rather than origins, were measured. In addition it is necessary to adjust these energies to the deperturbed values by subtracting the difference between ν_{oo} from Ref. 11 and the deperturbed ν_{oo} determined here. The difference of 80 cm^{-1} results from repulsion of $A'^1\Pi$ by $b^3\Pi_1$.

between parameters. The constants in Table 3.31 are useful for calculating potential energy curves (Fig. 3.12) and vibrational matrix elements.

The A_b value in Table 3.31 is a weighted average of the values in Table 3.29. Values for C_a, C_b, and γ_a are not averaged as they are generally small and vary from level to level.

Figure 3.12: a) RKR potential energy curves for the vibrationally analyzed states of BaO. On this scale, the $a^3\Sigma^+$ and $A^1\Sigma^+$ as well as the $b^3\Pi$ and $A'^1\Pi$ states are indistinguishable.

b) Expanded view of the low energy region.

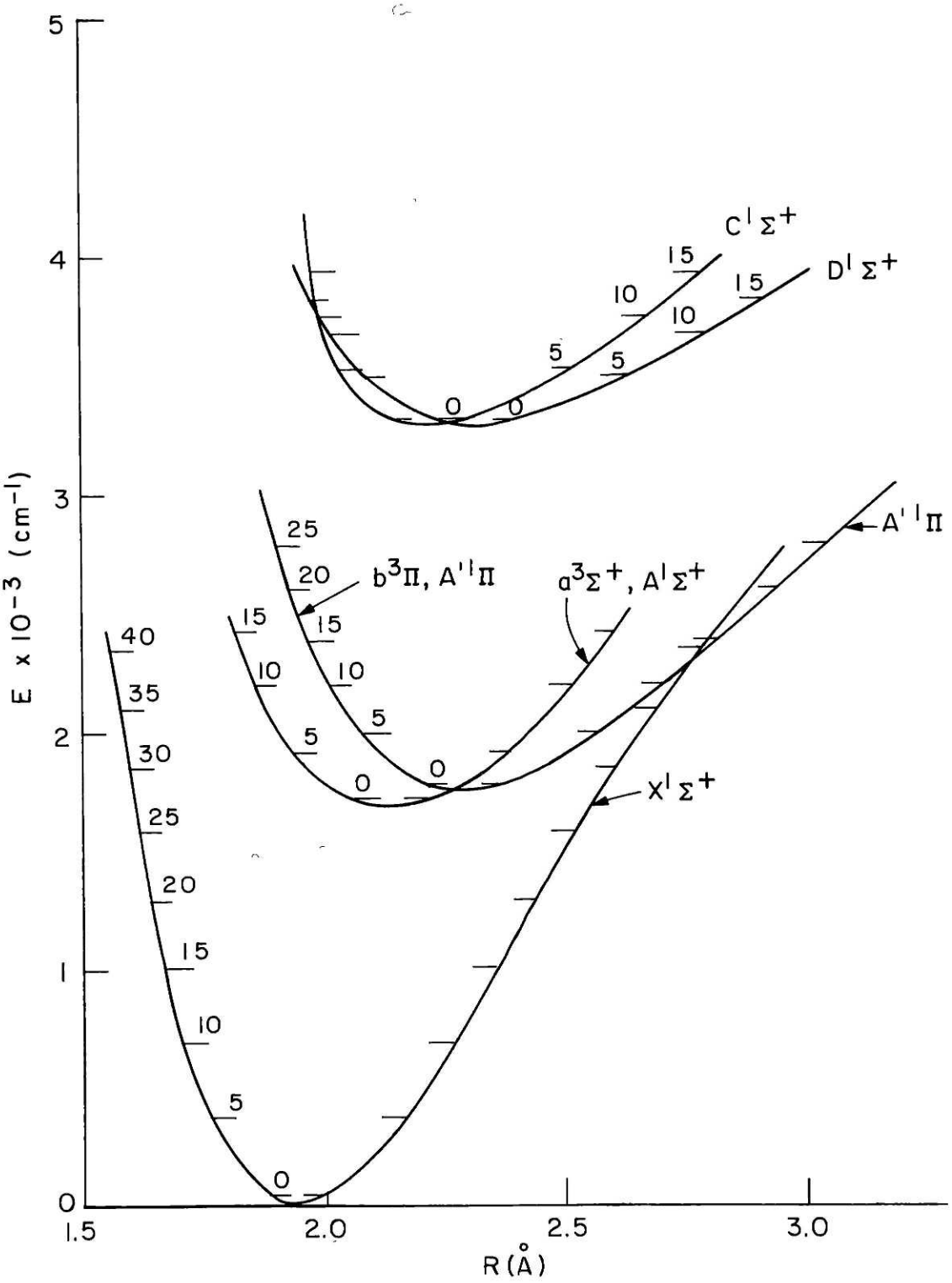

FIGURE 3.12a

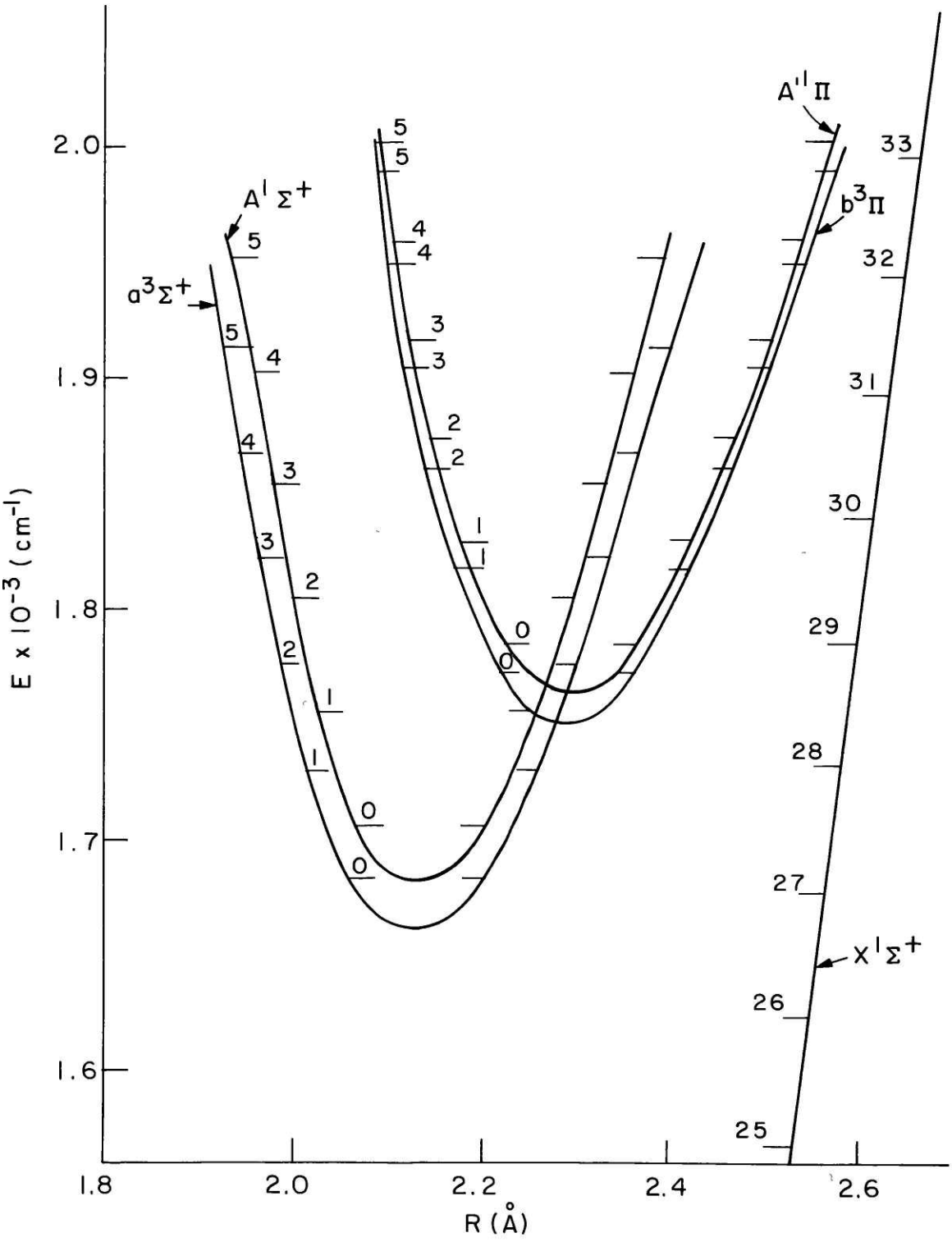

FIGURE 3.12b

IV. Discussion

A. Perturbation Matrix Elements

Spin-orbit and rotation-electronic interactions are responsible for perturbations among low-lying states of BaO:

$$H^{RE} = -B(J_+L_- + J_-L_+ - L_+S_- - L_-S_+) \qquad (3.2a)$$

$$H^{SO} = \sum_{e^-} \hat{a}\ell_i \cdot s_i \qquad (3.2b)$$

where H^{RE} and H^{SO} are the rotation-electronic and spin-orbit Hamiltonians, respectively;

$\hat{a} = \frac{Z_{Ba}}{r^3_{Ba}} + \frac{Z_O}{r^3_O}$ is the one-electron radial part of the spin-orbit operator, Z is an effective nuclear charge, r is the distance between nucleus and electron, and all other symbols have their usual meanings.[40,54]

Weighted averages of $A^1\Sigma^+ \sim b^3\Pi$, $A^1\Sigma^+ \sim A'^1\Pi$, and $a^3\Sigma^+ \sim A'^1\Pi$ electronic perturbation matrix elements are given in Tables 3.26, 3.27, and 3.28 respectively. These were obtained by dividing the vibronic matrix elements by the appropriate vibrational factors (see Chapter 2). The constancy of preliminary values for these electronic factors has been used to determine

vibrational numberings for $a^3\Sigma^+$ (Appendix 6), $b^3\Pi$,[9] and $A'^1\Pi$.[9]

That vibronic matrix elements can be factored into vibrational and electronic parts results from constant R-centroids for pairs of mutually interacting levels[55,56], where

$$\text{R-centroid} = \frac{\langle v|R|v'\rangle}{\langle v|v'\rangle} . \qquad (3.3)$$

For the above states with interacting v and v' levels, average R-centroids are:

$$\text{R-centroid } (A^1\Sigma^+ \sim b^3\Pi) = 2.26 \pm 0.04 \text{ Å} \quad (3.4a)$$

$$\text{R-centroid } (A^1\Sigma^+ \sim A'^1\Pi) = 2.26 \pm 0.04 \text{ Å} \quad (3.4b)$$

$$\text{R-centroid } (a^3\Sigma^+ \sim A'^1\Pi) = 2.34 \pm 0.15 \text{ Å} \quad (3.4c)$$

where the uncertainties quoted represent the <u>range</u> of R-centroid values sampled. As expected, these values correspond to the internuclear distances where the potential energy curves intersect (see Fig. 3.12b).[55]

In this single configuration limit, matrix elements of operators in Eq. 3.2 between pairs of electronic states are related by matrix elements of one-electron operators between molecular orbitals[55-58] (Appendices 3 and 4). The lowest lying states of BaO derive from the following electronic configurations:

$$X^1\Sigma^+ \quad z\sigma^2 \; y\sigma^2 \; w\pi^4 \qquad (3.5a)$$

$$a^3\Sigma^+,\ A^1\Sigma^+ \quad z\sigma^2\ y\sigma\ x\sigma w\pi^4 \tag{3.5b}$$

$$b^3\Pi,\ A'^1\Pi \quad z\sigma^2\ y\sigma^2\ x\sigma\ w\pi^3 \tag{3.5c}$$

Using these configurations and the methods outlined in Refs. 54, 57, 58 and in Appendix 3, matrix elments between lowest lying states of BaO are expressed in terms of one-electron integrals in Table 3.32. It is seen from this table that these one-electron integrals have different values when evaluated for different pairs of interacting states.

In addition to the relationships in Table 3.32, values of b, a_+, and a_z (defined in Table 3.32) can be related to atomic integrals by employing the LCAO method:

$$|w\pi> = |\pi O2p> \tag{3.6a}$$

$$|y\sigma> = \epsilon|\sigma O2p> + (1-\epsilon^2)^{\frac{1}{2}}\ |\sigma Ba>. \tag{3.6b}$$

In Eq. 3.6, the molecular orbital $w\pi$ is assumed to be localized on O and $y\sigma$ is localized on O but has some Ba atomic character. Field[9] has shown that Eq. 3.6a adequately accounts for the $b^3\Pi$ spin-orbit constant which is small ($-94\ cm^{-1}$) compared with atomic Ba ^3P spin-orbit splittings ($833\ cm^{-1}$).[59] If ϵ is unity in Eq. 3.6b (i.e. $y\sigma$ is comprised primarily of O2p), $a_+ = \sqrt{\ell(\ell+1)}\, a_z = \sqrt{2}\ a_z$. On the other hand, if $\epsilon \neq 0$, the Ba atomic character does not contribute significantly to the off-

Table 3.32: One-Electron Perturbation Matrix Elements

	b(unitless)	$a_+(cm^{-1})$	$a_z(cm^{-1})$
$A^1\Sigma^+ \sim A'^1\Pi$	1.014 ± 0.024[a]		
$A^1\Sigma^+ \sim b^3\Pi$		63.9 ± 1.1[b]	
$a^3\Sigma^+ \sim A'^1\Pi$		$167. \pm 8.$[c]	
$a^3\Sigma^+ \sim b^3\Pi$	1.26 ± 0.09[d]	$52. \pm 8.$[d]	
$b^3\Pi \sim A'^1\Pi$			222 ± 16[e]
$b^3\Pi$			188 ± 16[f]

where $b = \langle w\pi|\ell_+|y\sigma\rangle = \eta_{AA'}/\langle v_A|B|v_{A'}\rangle = -\eta_{ba}/\langle v_b|B|v_a\rangle$

$a_+ = \langle w\pi|\hat{a}\ell_+|y\sigma\rangle = (2)^{3/2}\xi_{Ab}/\langle v_A|v_b\rangle = (2)^{3/2}\xi_{A'a}/\langle v_{A'}|v_a\rangle = -4\xi_{ba}/\langle v_b|v_a\rangle$

$a_z = \langle w\pi|\hat{a}|w\pi\rangle = -2A_b = 2\xi_{A'b}$

[a] From Table 3.27.
[b] From Table 3.26.
[c] From Table 3.28.
[d] Obtained from Table 3.29, Fits 3 and 6, and calculated $\langle v_b|v_a\rangle$ and $\langle v_b|B|v_a\rangle$ factors.
[e] From weighted average of values in Table 3.29.
[f] From Table 3.31.

diagonal matrix elements, a_+, since two-center contributions to these integrals are small.[60] Thus, Ba atomic character in yσ merely dilutes the yσ ∿ wπ interaction and a_+ can be less than a_z:

$$a_+ = \langle w\pi \mid \hat{a}\ell_+ \mid y\sigma \rangle = \varepsilon\sqrt{2}\ a_z. \qquad (3.7)$$

Using the $a^3\Sigma^+$ ∿ $A'^1\Pi$ and $A^1\Sigma^+$ ∿ $b^3\Pi$ a_+ values and average a_z values from Table 3.32,

$$\varepsilon(a^3\Sigma^+) \approx 0.58 \qquad (3.8a)$$

$$\varepsilon(A^1\Sigma^+) \approx 0.22.^{\dagger} \qquad (3.8b)$$

These simple arguments indicate that the yσ orbital in $A^1\Sigma^+$ is different from the $a^3\Sigma^+$ yσ orbital. Alternatively, configuration interaction, which also dilutes the one-electron spin-orbit interaction, plays a greater role in determining the $A^1\Sigma^+$ electronic structure than it does for $a^3\Sigma^+$.

B. Singlet ∿ Triplet Energy Splittings

To the extent that the single configuration

---

†The $a^3\Sigma^+$ ∿ $b^3\Pi$ a_+ and b parameters are not considered since they are poorly determined for only two pairs of interacting levels.

approximation is valid, the $a^3\Sigma^+ - A^1\Sigma^+$ and $b^3\Pi - A'^1\Pi$ deperturbed (i.e. not considering spin-orbit interactions) energy splittings are a function of the exchange integrals:[61]

$$\Delta E_\Sigma = E(A^1\Sigma^+) - E(a^3\Sigma^+) = 2\langle y\sigma(1)x\sigma(1)|\frac{1}{r_{12}}|y\sigma(2)x\sigma(2)\rangle \quad (3.9a)$$

$$\Delta E_\Pi = E(A'^1\Pi) - E(b^3\Pi) = 2\langle w\pi(1)x\sigma(1)|\frac{1}{r_{12}}|w\pi(2)x\sigma(2)\rangle \quad (3.9b)$$

where 1 and 2 are electron indices. If the $w\pi$, $y\sigma$, and $x\sigma$ orbitals were identical for each electronic state, and $w\pi$ and $y\sigma$ were both comprised of only O2p ΔE_Σ would equal ΔE_Π. In fact ΔE_Σ (226 cm^{-1}) is remarkably close to ΔE_Π (117 cm^{-1}). The similarity between the pairs of Σ and Π potential energy curves (Figure 3.12) is a further manifestation of the validity of the single configuration approximation.

This apparent contradiction with the bonding picture drawn above from perturbation matrix elements results simply from the sampling of different properties of electronic wave functions by different operators ($\frac{Z_K}{r_{iK}^3}$ for spin-orbit, where K is a nuclear index, and $1/r_{ij}$ for exchange interactions).

C. Electronic Structure of BaO

Figures 3.12 and 3.13 summarize the known electronic structure of BaO. From measurements of $X^1\Sigma^+$ and $A^1\Sigma^+$

Figure 3.13: BaO energy level diagram illustrating the emission observed from a single $C^1\Sigma^+$ ($v^* = 3,J$) level. Rotational constants are given on the levels; shortest and longest wavelengths of band heads are given in nm along the transition arrows.

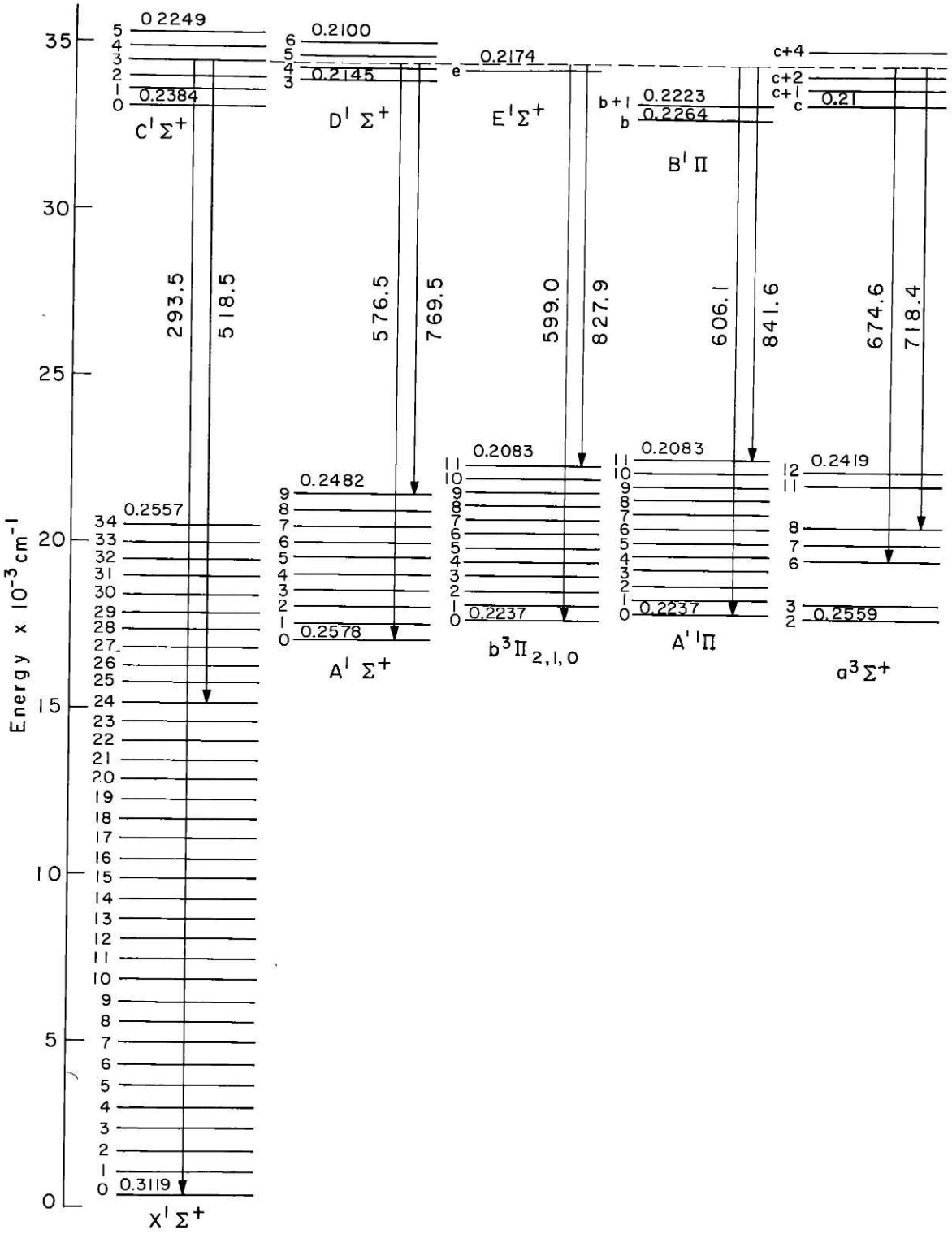
Energy x 10^{-3} cm^{-1}
35
30
25
20
15
10
5
0
$C^1\Sigma^+$
$D^1\Sigma^+$
$E^1\Sigma^+$
$B^1\Pi$
$A^1\Sigma^+$
$b^3\Pi_{2,1,0}$
$A'^1\Pi$
$a^3\Sigma^+$
$X^1\Sigma^+$
0.2249
0.2384
0.2100
0.2145
0.2174
e
0.2223
0.2264
b+1
b
c+4
c+2
c+1
c
0.21
0.2482
0.2578
0.2083
0.2237
0.2083
0.2237
0.2419
0.2559
0.2557
0.3119
293.5
518.5
576.5
769.5
599.0
827.9
606.1
841.6
674.6
718.4

FIGURE 3.13

dipole moments, 7.955D (v" = 0) and 2.20D (v' = 1) respectively, it has already been concluded that $X^1\Sigma^+$ is ionic, Ba^+O^-, while $A^1\Sigma^+$ is primarily covalent.[13,20] $A^1\Sigma^+ \leftarrow X^1\Sigma^+$ excitation entails charge transfer from O^- to Ba^+ with a concomittant decrease in bond strength ($\omega_e" > \omega_e'$) and increase in bond length ($B_e" > B_e'$). Similarly the $C^1\Sigma^+ \leftarrow A^1\Sigma^+$ and $D^1\Sigma^+ \leftarrow C^1\Sigma^+$ transitions result in further weakening of the bond ($\omega_e' > \omega_e*$) which is suggestive of additional charge transfer. The relatively long $A^1\Sigma^+$ lifetime, 356 nsec for v' = 0,[62] is further evidence that an electron is being promoted from O to Ba.

The most curious feature of these band systems is the observation of strong parallel($\Delta\Lambda = 0$) but weak perpendicular ($\Delta\Lambda = \pm 1$) transitions: the $A'^1\Pi$ lifetime, for example, is 9 μsec;[12] strong excitation from $A^1\Sigma^+$ into a $^1\Pi$ state is not observed. Zare and Herschbach have shown that the dominance of parallel over perpendicular transition intensity in alkali halide (isoelectronic with alkaline-earth oxides) results from (1) equally mixed covalent and ionic character in both the upper and lower states or (2) pure <u>covalent</u> character in both states.[63] Pure ionic to pure covalent charge transfer transitions on the other hand, result in strong perpendicular and weak parallel bands.

Again, there seems to be a paradox. The electronic states are both ionic and covalent and can appear to have different charge distributions depending on which observable, is sampled. No one, simple molecular orbital configuration accounts for all of the observations.

It is not surprising that many electronic states in the high energy (> 20,000 cm^{-1}) range are observed via a plethora of $C^1\Sigma^+$ perturbations. From the first excited state of Ba ($6s5d^3D$) and the ground state of $O(2s^22p^4\ ^3P)$, alone, twenty-seven molecular electronic states of singlet, triplet, and quintet multiplicity are derived.[32] To be sure, not all of these states will be bound but it is certain that many will be. In particular, molecular states correlating to these atomic states may be responsible for the anomalous $A'^1\Pi$ and $b^3\Pi$ deperturbation results obtained above.

D. Population Monitoring

The band systems described above can be used in population probes of low lying states of BaO[23] although several points warrant consideration before proceeding with such experiments. The perturbations responsible for the intercombination bands observed

also complicate population monitoring: line intensities will generally vary with both J and v in an irregular fashion. In principle, the J variations can be computed from the depeturbation results above: the unitary transformation matrices which diagonalize the Hamiltonians provide mixing coefficients which in turn permit the relative line intensities to be calculated. For example, percent Σ character in the $C^1\Sigma^+(v^* = 3)$ main levels near the vibrational origin varies from 64% at J = 0 to 83% at J = 20. Competing transition moments, owing to the multiplicity of perturbing states in both the upper and lower levels make reliable relative intensity calculations difficult at best.

It is recommended, instead, that careful fluorescence intensity measurements be made via OODR pumping of $C^1\Sigma^+$ prior to using these same transitions in excitation (e.g. $C^1\Sigma^+ \leftarrow b^3\Pi$ followed by $C^1\Sigma^+ \rightarrow X^1\Sigma^+$ UV fluorescence) to monitor populations. This is particularly necessary for comparisons of populations between different vibrational levels where the upper level perturbing state vibrational numberings remain undetermined: for example, $c \sim b^3\Pi$ Franck-Condon factors most likely determine the vibrational envelope of $C^1\Sigma^+ \rightarrow b^3\Pi$ emission intensity.

V. Conclusion

The technique of optical-optical double resonance has been shown to be a convenient and sensitive means by which low lying, long lived electronic states can be systematically detected and characterized. Although crucial intercombination bands result from ubiquitous perturbations in the highly excited electronic states of the heavy BaO molecule, the OODR technique assisted by perturbations is by no means unique to this molecule. Local perturbations exist in most molecules and with the selectivity afforded by OODR these isolated perturbed levels can be prepared at will.

A population monitoring scheme for the $a^3\Sigma^+$, $b^3\Pi$, and $A'^1\Pi$ reservoir states has been established. It is hoped that this work will stimulate such experiments in the future.

Additional spectroscopic OODR experiments on BaO are warranted in light of the evidence for metastable reservoir Δ states in the $\sim$ 16,000 cm^{-1} energy range.

References For Chapter 3

1. R.H. Barnes, C.E. Moeller, J.F. Kircher, and C.M. Verber, Appl. Phys. Lett. 24, 610 (1974).
2. D.L. Rousseau and P.F. Williams, Phys. Rev. Lett. 33, 1368 (1974).
3. R.W. Field, G.A. Capelle, and M.A. Revelli, J. Chem. Phys. 63, 3228 (1975).
4. M.D. Danyluk and G.W. King,
   a) Chem. Phys. Lett. 43, 1 (1976);
   b) Chem. Phys. Lett. 44, 440 (1976);
   c) Chem. Phys. Lett. 22, 59 (1977).
5. M.E. Kaminsky, R.T. Hawkins, F.V. Kowalski, and A.L. Schawlow, Phys. Rev. Lett. 36, 671 (1976).
6. J.I. Steinfeld and P.L. Houston, "Double Resonance Spectroscopy", in Laser and Coherence Spectroscopy, ed. J.I. Steinfeld, (Plenum, 1978), p. 1.
7. P.C. Mahanti, Proc. Phys. Soc. 46, 51 (1934).
8. A. Lagerqvist, E. Lind, and R.F. Barrow, Proc. Phys. Soc. A 63, 1132 (1950).
9. R.W. Field, J. Chem. Phys. 60, 2400 (1974).
10. C.J. Hsu, W.D. Krugh, H.B. Palmer, R.H. Obenauf, and C.F. Aten, J. Mol. Spectrosc. 53, 273 (1974).
11. J.C. Wyss and H.P. Broida, J. Mol. Spectrosc. 59, 235 (1976).
12. J.G. Pruett and R.N. Zare, J. Chem. Phys. 62, 2050 (1975).

13. L. Wharton, M. Kaufman, and W. Klemperer, J. Chem. Phys. 37, 621 (1962).

14. L. Wharton and W. Klemperer, J. Chem. Phys. 38, 2705 (1963).

15. E. Tiemann, M. Bojaschewsky, Ch. Sauter-Servaes, and T. Törring, Z. Naturforsch. 29a, 1692 (1974).

16. W.H. Hocking, E.F. Pearson, R.A. Creswell, and G. Winnewisser, J. Chem. Phys. 68, 1128 (1978).

17. R.W. Field, R.S. Bradford, D.O. Harris, and H.P. Broida, J. Chem. Phys. 56, 4712 (1972).

18. R.W. Field, R.S. Bradford, H.P. Broida, and D.O. Harris, J. Chem. Phys. 57, 2209 (1972).

19. R.W. Field, A.D. English, T. Tanaka, D.O. Harris, and D.A. Jennings, J. Chem. Phys. 59, 2191 (1973).

20. R. F. Wormsbecher, S.L. Lane, and D.O. Harris, J. Chem. Phys. 66, 2745 (1977).

21. W.H. Parkinson, Proc. Phys. Soc. 78, 705 (1961).

22. R.W. Parker, "BaO, the Parkinson System", unpublished report, Department of Physics, University of California, Santa Barbara (1971).

23. A. Torres-Filho and J.G. Pruett, J. Chem. Phys. (in press, 1979).

24. C.R. Jones and H.P. Broida, J. Chem. Phys. 60, 4369 (1974).

25. J.B. West, R.S. Bradford Jr., J.D. Eversole, and C.R. Jones, Rev. Sci. Instrum. 46, 164 (1975).

26. S. Gerstenkorn and P. Luc, Atlas du Spectra de la Molecule de L'iode, Laboratoire Aimé Cotton, CNRS II, Bât. 505, 91405-Orsay, France.

27. D. Jennings and R. Barger, National Bureau of Standards, Boulder, Co.

28. A.L. Bloom, J. Opt. Soc. 64, 447 (1974).

29. H.W. Kogelnik, E.P. Ippen, A. Dienes, and C.V. Shank, I.E.E.E. J. Quant. Electr. QE-8, 373 (1972).

30. J.B. Koffend, Ph.D. Thesis, Massachusetts Institute of Technology, 1978.

31. H.M. Crosswhite and G.H. Dieke, "Important Atomic Spectra", in Amer. Inst. Phys. Handbook, 2nd Ed., D.E. Gray, ed., (McGraw-Hill, 1963).

32. G. Herzberg, Molecular Spectra and Molecular Structure I. Spectra of Diatomic Molecules, (Van Nostrand Reinhold, New York, 1950).

33. R.W. Field, Coherent Focus on Science 1, 1 (1977).

34. E.U. Condon, Phys. Rev. 32, 858 (1928).

35. G. Gerber and H.P. Broida, J. Chem. Phys. 64, 3423 (1976).

36. J.M. Brown, J.T. Hougen, K.-P. Huber, J.W.C. Johns, I. Kopp., H. Lefebvre-Brion, A.J. Merer, D.A. Ramsay, J. Rostas, and R.N. Zare, J. Mol. Spectrosc. 55, 500 (1975).

37. I. Kovacs, Rotational Structure in the Spectra of Diatomic Molecules (American Elsevier, New York, 1969).

38. J.K.G. Watson, J. Mol. Spectrosc. 66, 500 (1977).

39. J.L. Dunham, Phys. Rev. 41, 721 (1932).

40. J.T. Hougen, Natl. Bureau Standards, U.S. Monogr. 115, (1970).

41. R. Schlapp, Phys. Rev. 39, 806 (1932).

42. K.F. Freed, J. Chem. Phys. 45, 4214 (1966).

43. E.U. Condon and G.H. Shortley, The Theory of Atomic Spectra, Cambridge University Press, Cambridge, 1951.

44. R. Rydberg, Z. Physik 73, 376 (1931); 80, 514 (1933); O. Klein, Z. Physik 76, 226 (1932); and A.L.G. Rees, Proc. Phys. Soc. 59, 998 (1947).

45. K. Sakurai, S.E. Johnson, and H.P. Broida, J. Chem. Phys. 52, 1625 (1970).

46. a) E.L. Hill and J.H. Van Vleck, Phys. Rev. 32, 250 (1928);

b) J.H. Van Vleck, Phys. Rev. 33, 467 (1929);

c) J.H. Van Vleck, Phys. Rev. 40, 544 (1932);

d) J.H. Van Vleck, Rev. Mod. Phys. 23, 213 (1951).

47. R.N. Zare, A.L. Schmeltekopf, W.J. Harrop, and D.L. Albritton, J. Mol. Spectrosc. 46, 37 (1973).

48. J. Rostas, D. Cossart, J.R. Bastien, Can. J. Phys. 52, 1274 (1974).

49. J.A. Coxon, J. Mol. Spectrosc. 58, 1 (1975).

50. M.H. Hebb, Phys. Rev. 49, 610 (1936).

51. K. Kayama and J.C. Baird, J. Chem. Phys. 46, 2604 (1967).

52. M. Horani, J. Rostas, and H. Lefebvre-Brion, Can. J. Phys. 45, 3319 (1967).

53. R.W. Field and H. Lefebvre-Brion, Acta. Phys. Acad. Scient. Hung. 35, 51 (1974).

54. H. Lefebvre-Brion, "Perturbations in the Spectra of Diatomic Molecules" in Atoms, Molecules, and Lasers, International Atomic Energy Agency (Vienna, 1974) pp. 411-448.

55. J.A. Hall, J. Schamps, J.M. Robbe, and H. Lefebvre-Brion, J. Chem. Phys. 59, 3271 (1973).

56. J. Schamps, J. Quant. Spectrosc. Radiat. Transfer 17, 685 (1977).

57. T.E.H. Walker, Mol. Phys. 23, 489 (1972).

58. R.W. Field, B.G. Wicke, J.D. Simmons, and S.G. Tilford, J. Mol. Spectrosc. 44, 383 (1972).

59. C.E. Moore, A Multiplet Table of Astrophysical Interest, Natl. Stand. Ref. Data Ser. 40, (1972).

60. T.E.H. Walker and W.G. Richards, J. Chem. Phys. 52, 1311 (1970).

61. J. Raftery, P.R. Scott, and W.G. Richards, J. Phys. B5, 1293 (1972).

62. S.E. Johnson, J. Chem. Phys. 56, 149 (1972).

63. R.N. Zare and D.R. Herschbach, J. Mol. Spectrosc. 15, 462 (1965).

Chapter 4: Laser Spectroscopy of CaO

I. Introduction

This chapter reports results of Ar^+ and dye laser excitation of CaO. Emission from five Ar^+ lines (501.717, 487.986, 476.486, 472.689, and 457.936 nm)[†] is observed and partially analyzed. Excitation spectra of the CaO green and orange band systems using a broad bandwidth, tunable dye laser have also been obtained. The results of these experiments indicate that: (1) the green and orange Ca arc bands are certainly comprised of diatomic CaO emission and (2) at least two of the lower electronic states of these systems correspond to the energy reservoir $a^3\Pi$ and $A'^1\Pi$ states.

The known spectrum of CaO consists of six band systems: ultraviolet ($C^1\Sigma^+ - X^1\Sigma^+$)[1], blue ($B^1\Pi - X^1\Sigma^+$)[1], green[2-9], orange[2-9], infra-red ($A^1\Sigma^+ - X^1\Sigma^+$)[10,11], and $A'^1\Pi - X^1\Sigma^+$.[12] The $A^1\Sigma^+ - X^1\Sigma^+$ system was first vibrationally and rotationally analyzed correctly by Hultin and Lagerqvist[10] who observed 30 perturbations in the $A^1\Sigma^+$ state of which all but 3 were subsequently assigned by Field[13] to the $a^3\Pi$ and $A'^1\Pi$ states. Brewer and Hauge[11] extended the analysis of this system and improved both the $X^1\Sigma^+$ and $A^1\Sigma^+$ constants. The blue and ultraviolet systems were first correctly analyzed by Lagerqvist.[1]

[†]All wavelengths quoted in this chapter are in air at room temperature.

The green and orange systems have been the subject of controversy ever since their discovery[2-4] and have yet to be analyzed. Only one band in the green system has been rotationally analyzed but the electronic symmetries were not unambiguously established.[6]

The controversy surrounding the green and orange systems stems from their extraordinary complexity leading several authors to conclude that they do not arise from diatomic CaO at all but rather from CaOH[5,11] or Ca_2O_2.[5] Isotopic substitution of deuterium for hydrogen provided further evidence that the bands resulted from CaOH.[11] In fact, both CaO and CaOH bands exist in the green and orange and confusion has resulted primarily from flame reactions with water as an impurity. Benard et al.[7,8] have recently distinguished emission from these two systems and by analogy with MgO bands have assigned the CaO green system as $^1\Delta$- A'$^1\Pi$ and the orange system as $d^3\Delta$ - $a^3\Pi$. These conclusions seem overly simple in light of theoretical predictions that not only $C^1\Sigma^+$, $B^1\Pi$, and $d^3\Delta$ but also $^3\Pi$, $^3\Sigma^+$, $^3\Sigma^-$, $^3\Delta$, $^1\Sigma^+$, $^1\Delta$ (2), and $^1\Sigma^-$ states lie in this energy range.[14]

Although the green and orange systems have not yet been analyzed they have already been used as measures of $a^3\Pi$ and A'$^1\Pi$ populations in reactions of metastable Ca atoms with O_2 and CO_2.[15]

Green and orange band intensities are a sensitive function of CO concentration in $Ca + 2N_2O + CO \rightarrow CaO + 2N_2 + CO_2$ flame reactions in the presence of a buffer gas).[7,8] The proposed mechanism for this reaction is:

$$Ca + N_2O \rightarrow CaO^* + N_2 \qquad (4.1a)$$

$$CaO^* + CO \rightarrow Ca(^3P) + CO_2 \qquad (4.1b)$$

$$Ca(^3P) + N_2O \rightarrow CaO(d^3\Delta) + N_2 \qquad (4.1c)$$

$$CaO(d^3\Delta) \xrightarrow{h\nu} CaO\ (a^3\Pi) \qquad (4.1d)$$

where CaO* denotes dark, metastable, vibrationally excited CaO $X\ ^1\Sigma^+$. The addition of CO converts the chemically stored energy in $X^1\Sigma^+$ to optical energy via $d^3\Delta \rightarrow a^3\Pi$ fluorescence in the orange and green systems.[7,16,17] The reaction sequence in Eqs. 4.1a and 4.1b has been proposed as an efficient means for the efficient production of metastable alkaline-earth atoms to be used in excimer lasers.[16,17]

The Ar^+ and dye laser experiments described below are intended as a beginning to the analysis of the green and orange band systems in order that the kinetic work described briefly above may be verified and further characterized. Although time has not permitted me to

finish these experiments, the preliminary analyses presented below prove unambiguously that $a^3\Pi$ and $A'^1\Pi$ are lower levels in both the green and orange systems. Upper level symmetries identified include $C^1\Sigma^+$, $^3\Delta$, and $^1\Pi$.

Besides spectroscopic investigations, the CO dependence of green and orange band dye laser excitation spectra is qualitatively characterized and found to be consistent with the reaction mechanism described by Eq. 4.1.

In Section II a brief description of experimental details is presented. Section III describes Ar^+ and dye laser fluorescence and excitation spectra and assignments. This work is summarized and future experiments are suggested in Section IV.

II. Experimental

CaO is prepared in the same fashion as BaO (Chapter 3) except that N_2O (Matheson, 99.0% purity) is used as an oxidant. CO (Matheson, 99.5% purity) is added by mixing with N_2O prior to injection into the reactor. Ca metal from Alfa, Inc. (99.5%) is used. Typical operating pressures are 1-4 torr Ar, 1×10^{-4} torr Ca, 1×10^{-2} torr CO, and 3×10^{-2} torr N_2O.

In order to eliminate overlapping from chemiluminescence, both Ar^+ and dye lasers are amplitude modulated by mechanical chopping and fluorescence is detected with a Keithley 840 Autotrac Lock-In detector.

For Ar^+ laser (Spectra Physics #171) experiments, fluorescence is resolved by a Spex 1802 monochromator. Absolute frequency calibration is provided by Ar^+ laser lines;[18] relative frequency calibration is obtained from marker pulses output by the Spex 1802 monochromator. For some Ar^+ laser experiments an intracavity etalon (Spectra Physics #589) is used to obtain single frequency operation and consequently simplify fluorescence spectra. The laser is operated at maximum power [Spectra Physics specifications: 4.0W, 0.5W, 3.2W, 1.0W, 0.2W, 0.3W, for 514.5nm, 501.7 nm, 488.0 nm, 476.5 nm, 472.7 nm, and 457.9 nm, respectively].

For dye laser excitation spectra (home made dye

laser described in Chapter 3), total fluorescence is collected through the monochromator in 0^{th} order. Absolute frequency calibration is provided by excitation of Ca and Na (an impurity in the Ca) atomic lines.[19] For single mode dye laser excitation, a 60% reflecting, solid quartz etalon is inserted into the laser cavity.

A Hamamatsu R212 photomultiplier tube operated at -600 VDC is mounted on the monochromator exit slit.

III. Results

A. Ar^+ laser excitation

Table 4.1 summarizes the observations. Two types of fluorescence - relaxed and unrelaxed (or resonant) - are usually resolved. The upper level rotational quantum number, J', is assigned from P and R branch splittings when B" and D" are known:

$$\Delta PR = (4B"-6D")(J'+0.5)-8D"(J'+0.5)^3 \qquad (4.2)$$

where B" and D" are the lower level rotational and centrifugal distortion constants, respectively, and ΔPR is the splitting between $P(\Delta J = J'=J" = -1)$ and $R(\Delta J = +1)$ branch emission.

Fluorescence from each analyzed excitation line is described and discussed in detail below.

501.717 nm (19 926.014 cm^{-1}) line

Two progressions of P,R doublets extending from 345 nm to 400 nm are observed. P,R splittings as well as spacings between successive PR doublets indicate that: (1) J' = 28 and J' = 51 are simultaneously excited and (2) the lower levels of the progression are $X^1\Sigma^+$ v" = 1 to 6. A single maximum at v" = 3 and no nodes are observed. P to R branch intensity ratios

Table 4.1: Ar^+ Laser Induced Fluorescence of CaO

Laser Line (nm)[a]	Excitation	Fluorescence
514.532	? Multi-mode.	a) Weak, relaxed fluorescence from 410-470nm. b) Strong, resonant and relaxed emission in green, 545-555 nm. c) Strong, resonant and relaxed emission in orange, 590-615nm.
501.717	$?\leftarrow a^3\Pi_2$(v=2) R(27) $?\leftarrow a^3\Pi_2$(v=2) P(52) Multi-mode.	a) Progressions into $X^1\Sigma^+$ from 345 to 400nm with no nodes. PR intensity anomalies. b) Strong, resonant green and orange band emission.
487.986[b]	$^1\Pi\leftarrow X^1\Sigma^+$(1,10)Q(16) At least two other transitions. Multi-mode and single mode.	a) Two progressions into $X^1\Sigma^+$: Q branch emission into v" = 0 to 12 with node at v" = 6 and PR emission into v" = 0 to 6. b) $^1\Pi\rightarrow A'^1\Pi$(1,2), (1,1), and (1,0) in green. c) Weak fluorescence in orange.
476.486	$?\leftarrow X^1\Sigma^+$(v"=6) P(36) At least two other transitions. Multi-mode.	a) Resonant and relaxed fluorescence from 390 to 630 nm. Progression of PR doublets into $X^1\Sigma^+$ v" = 2 through 6. b) Progression of three PR doublets into either $a^3\Pi$ or $A'^1\Pi$ in green. c) Two PQR triplets into either $a^3\Pi_2$ and $a^3\Pi_1$ or $a^3\Pi_1$ and $a^3\Pi_0$ in orange

Table 4.1 (cont.)

Laser Line (nm)[a]	Excitation	Fluorescence
472.689	$C^1\Sigma^+ \leftarrow X^1\Sigma^+$(2,13) P(28) and R(48) At least two additional transitions. Multi-mode and single mode.	a) Resonant and relaxed structure from 350 to 480 nm. Two PR progressions into $X^1\Sigma^+$ v" = 0 to 13 with two nodes in each. b) Relaxed and resonant structure in orange and green.
457.936[b]	$^1\Pi \leftarrow X^1\Sigma^+$ (1,7) P(32) and Q(37) Multi-mode.	a) Two progressions (P,Rand Q) into $X^1\Sigma^+$ v" = 0 to 8 with one node between v" = 2 and 3. b) $^1\Pi \rightarrow A'^1\Pi$ (1,0) and (1,1) in green. c) Relaxed and resonant structure in orange.
335.849[c]	$C^1\Sigma^+ \leftarrow X^1\Sigma^+$ (2,0) R(41) At least two additional transitions. Multi-mode.	a) $C^1\Sigma^+ \rightarrow A'^1\Pi$ (2,0) and (2,1) R(41), Q(42), and P(43) at 468.55, 469.30, 469.80, 481.41, and 482.08 respectively.

[a] Ref. 18. Air wavelengths.

[b] The electronic and vibrational assignments of $^1\Pi$ and v' = 1 respectively are tentative, see text.

[c] Ref. 20.

deviate markedly from the expected value[21] of 1 and vary dramatically with v". This is indicative of heterogeneous (i.e. J-dependent, $\Delta\Omega = \pm 1$) perturbations in the upper level and resultant interference between parallel ($\Delta\Omega = 0$) and perpendicular ($\Delta\Omega = \pm 1$) transition moments (see Appendix 5 and references therein).

From the laser frequency, fluorescence frequencies, and $X^1\Sigma^+$ term values,[10,11] energies for lower levels of the laser excited transitions are 9795 $\pm$ 5 cm^{-1} (J' = 28 excited) and 10 465 $\pm$ 5 cm^{-1} (J' = 51 excited)†. Known levels nearest in energy and capable of undergoing an electric dipole transition into J' = 28 and 51 are $a^3\Pi_2$(v = 2, J = 27), 9793 $\pm$ 25 cm^{-1} and $a^3\Pi_2$(v = 2, J = 52), 10 451 $\pm$ 25 cm^{-1}.[13]

Fluorescence in the laser band was not resolved but resonant structure was apparent.

It seems likely that the upper level of this transition is $^3\Sigma^-$ since transitions from $a^3\Pi_2$ to $^3\Sigma^-$ are electric dipole allowed[23] and spin-orbit perturbations with both $\Omega = 0$ and $\Omega = 1$ states, particularly $^1\Sigma^+$ and $^1\Pi$, are non-zero[22] and could account for emission into $X^1\Sigma^+$ with anomalous P and R branch intensity ratios. Both singlet $\Omega = 0^+$ and $\Omega = 1$ character is required for the X intensity anomalies; such is not possible for $^3\Sigma^+$.

---

†All energies in this chapter are referenced to $X^1\Sigma^+$ v" = J" = 0.

Strong laser dependent, resonant emission in both the green and orange systems is observed but could not be linked to either of the laser excited transitions assigned above.

487.986 nm (20 486.69 cm^{-1})

A Q branch progression into $X^1\Sigma^+$ from v" = 0 to 12 with one node at v" = 6 is observed. Excitation is from a rotational level in $X^1\Sigma^+$ v" = 10.

From single mode experiments[23], a progression of three P,R doublets in the green system is linked to the Q branch progression into $X^1\Sigma^+$. The wavelengths for these transitions are: λ_1 = 534.63 λ_2 = 535.00, λ_3 = 550.26, λ_4 = 550.90, λ_5 = 567.15, and λ_6 = 567.82 nm ($\pm$ 0.02 nm). The 3,4 doublet is $\approx$ 10 times more intense than the 1,2 and 5,6 doublets. Green band P,R splittings and vibrational intervals suggest that (1) the lower levels of this progression are either $a^3\Pi$ or $A'^1\Pi$ v = 0, 1, and 2 and (2) J' = 16.[12,13] Thus the laser pumps Q(16) from $X^1\Sigma^+$ v" = 10.

Since J" = 16 and v" = 10 are known, the energy of the upper level of the laser excited transition is calculated from $X^1\Sigma^+$ term values[10,11] and the laser frequency: E' = 27 402 cm^{-1}. This corresponds to neither $C^1\Sigma^+$ nor $B^1\Pi$.[1] The vibrational numbering of the upper level

is inferred to be v' = 1 from observation of only a single node in the $X^1\Sigma^+$ Q branch progression (Chapter 3).[24,25] Q branch emission to $X^1\Sigma^+$ and P and R branch emission to $A'^1\Pi$ or $a^3\Pi$ indicates that the upper level is an f-parity $\Omega = 1$ state.[21]

From E' and λ_1 through λ_6, term values for lower levels of the green band progression are: $E_1 = 8703$, $E_2 = 8716$, $E_3 = 9234$, $E_4 = 9255$, $E_5 = 9775$, and $E_6 = 9796$ cm^{-1} ($\pm$ 5 cm^{-1}). Calculated $A'^1\Pi$ energies are[12]:

v = 0	J = 15	8693 $\pm$ 15 cm^{-1}
	J = 17	8715
v = 1	J = 15	9233
	J = 17	9255
v = 2	J = 15	9768
	J = 17	9790.

Since emission occurs from the upper level of the laser excited transition into both $X^1\Sigma^+$ and $A'^1\Pi$ it seems likely that this $\Omega = 1$ level is in fact $^1\Pi$; however, only one $^1\Pi$ state is predicted in this energy region and this is presumably $B^1\Pi$.[14]

In addition to the Q branch progression into $X^1\Sigma^+$, a progression of P,R doublets into $X^1\Sigma^+$ v" = 0 to 6 with no nodes is observed. The PR spacings were not measured with sufficient precision to determine J' to better than 40 $\pm$ 4. This large uncertainty in J' precludes

assignment of the lower level from which excitation occurs. The most probable states are $A'^{1}\Pi(v=0)$ and $a^{3}\Pi_{o}(v=0)$.

Several other progressions in the green system are observed as well as relaxed structure in the green and orange. These have not yet been linked to emission into $X^{1}\Sigma^{+}$.

476.486 nm (20 981.13 cm^{-1})

Strong emission extending from 390 to 630 nm is observed. The anti-Stokes emission exhibits both resonant and relaxed structure but only one progression is assigned: P,R doublets into $X^{1}\Sigma^{+}$ v" = 2 to 6 with the laser exciting from v" = 5. From P,R splittings, J' = 35 $\pm$ 1 is excited by P(36). The upper level term value is 25064 $\pm$ 5 cm^{-1}.

At least three other transitions, resulting in anti-Stokes emission, are excited but complicated structure and overlapping prohibits assignment with multi-mode excitation. Single mode excitation is required.

In the green system a progression of three P,R, doublets, in addition to relaxed structure, is observed: λ_1 = 539.33, λ_2 = 540,18, λ_3 = 554.54, λ_4 = 555.42, λ_5 = 570.55, and λ_6 = 571.47 nm ($\pm$ 0.02 nm). The 3,4

doublet is ≈ 3 times stronger than the 1,2 and 5,6 doublets. Spacings between successive doublets and P,R splittings indicate that the lower levels are either $a^3\Pi$ or $A'^1\Pi$ v = 6,7, and 8 (J = 21 and 23)[12,13] and, therefore, J' = 22. Single mode excitation should allow this progression to be linked with emission into $X^1\Sigma^+$.

In the orange system, two sets of P,Q,R, triplets separated by 51 cm^{-1} and with P,R spacings of 49 cm^{-1} and 52 cm^{-1} are observed in addition to complicated relaxed and resonant structure. The triplet wavelengths are: λ_1 = 622.55, λ_2 =623.51, λ_3 = 624.47 nm ($\pm$ 0.02 nm) and λ_4 = 624.8, λ_5 = 625.8, λ_6 = 626.8 nm ($\pm$ 0.1 nm). The 1,2,3, triplet is ≈ 17 times more intense than the 4,5,6 triplet. The separation between triplets of 51 cm^{-1}, comparable to the $a^3\Pi$ spin-orbit constant (A_Π = -58 cm^{-1})[13], and the lack of an asymmetry in the PQ and QR splittings suggest that the 1,2,3 and 4,5,6 levels belong to $a^3\Pi_2$ and $a^3\Pi_1$, respectively. Assuming that the lower vibrational level is v = 0, the P,R splittings give J' = 37 $\pm$ 1.[13] Although this value of J' is the same to within experimental error as the value determined from the analyzed progression into $X^1\Sigma^+$ (J' = 35 $\pm$ 1, see above), making this assignment yields energies for the lower levels of these orange band transitions which are ≈ 100 cm^{-1} from calculated

$a^3\Pi$ (v = 1) energies. Therefore, the upper levels of these two progressions appear to be different. From the emission complexity, it is not unreasonable that two upper levels with nearly equal J' are excited. Single mode excitation will unambiguously determine whether or not the transitions are linked.

472.689 nm (21 149.66 cm^{-1})

When multi-mode excitation is employed several progressions are observed to the blue of the laser line. Some of these do not include the laser line and one progression, in particular, appears to be composed of band heads only (i.e. no resonance structure). When single mode excitation is employed two strong progressions are isolated and assigned as emission into $X^1\Sigma^+$ v" = 0 to v" = 13 with nodes at v" = 2 and v" = 5 indicating that v' = 2. From PR separations, the transitions excited are P(28) and R(48). $C^1\Sigma^+ - X^1\Sigma^+$ (2,13) P(28) and R(48) transitions are calculated to be: 21140.3 and 21145.9 cm^{-1},[1] respectively. Lagerqvist reports perturbations in $C^1\Sigma^+$ (v' = 2) which culminate at J_o = 27.5 and 48.5;[1] these perturbations may be responsible for the discrepancies between calculated and laser frequencies as well as error in B''_{13} which is extrapolated from lower vibrational B values.[10,11] Alternatively, the laser may be exciting extra lines associated with the perturbing state.

Emission in the green and orange bands is by and large relaxed, although some resonance structure is apparent in the green system.

457.936 nm (21 931.01 cm^{-1})

A progression of P,R doublets from 370 to 475 nm corresponding to emission into $X^1\Sigma^+$ v" = 0 to 8 with one node between v" = 2 and 3 is observed. The laser line fits into this progression at $X^1\Sigma^+$ v" = 7 and from P,R splittings it is determined that P(32 $\pm$ 2) (J' = 31 $\pm$ 2) is excited. The P branch lines are always $\approx$ 2.5 times more intense than the R branch lines and in some bands the P branch appears to be an unresolved doublet. This implies that a Q branch transition is simultaneously excited from $X^1\Sigma^+$ v"= 7. This overlapping is responsible for the uncertainty in J' quoted above: P,R splittings from different bands give a range of J' values from 30 to 34. Assuming J' = 31, the upper level energy is E' = 27 130 $\pm$ 5 cm^{-1} which corresponds to neither $C^1\Sigma^+$ nor $B^1\Pi$.

Emission in the green and orange systems is observed again. Although the orange band emission is a complicated mixture of resonance and relaxed structure, emission in the green consists of a simple quartet: λ_1 = 549.18, λ_2 = 549.26, λ_3 = 550.56, and λ_4 = 550.69 nm

($\pm$ 0.02 nm). The λ_1, λ_3 splitting corresponds to $J' = 31$, assuming λ_1 and λ_3 terminate in $A'^1\Pi$ $v = 0$. Thus λ_1 and λ_3 appear to be connected to the P,R doublet progression into $X^1\Sigma^+$. From λ_1, λ_3, and E' the lower level energies are: $E_1 = 8926 \pm 5$ cm^{-1} and $E_2 = 8972 \pm 5$ cm^{-1}. $A'^1\Pi$ $v = 0$ energies are $E(J=30) = 8924 \pm 15$ cm^{-1} and $E(J = 32) = 8966 \pm 15$ cm^{-1}.[12] This validates the assumption made above: λ_1 and λ_3 do terminate in $A'^1\Pi$ $v = 0, J = 30$ and 32, respectively. This excellent agreement suggests that λ_2 and λ_4 share the same upper level as the $X^1\Sigma^+$ Q branch progression; the λ_2, λ_4 splitting yields $J' = 37$ and from $X^1\Sigma^+$ term values[10,11] and the laser frequency $E'(J'=37) = 27\,276 \pm 5$ cm^{-1}. From this energy and λ_2 and λ_4, $E_2 = 9074 \pm 5$ cm^{-1} and $E_v = 9122 \pm 5$ cm^{-1}. Calculated $A'^1\Pi$ $v = 0$ energies are: $E(J = 36) = 9058 \pm 15$ cm^{-1} and $E(J = 38) = 9109 \pm 15$ cm^{-1}. Again, agreement is excellent and it is concluded that the laser excites both P(32) and Q(37).

Note that the excited $J' = 32$ and 37 levels have e and f parity, respectively.[26] P,R emission into $A'^1\Pi$ and P,R and Q branch emission into $X^1\Sigma^+$ implies that the upper level of the laser excited transition has $\Omega = 1$ symmetry[21] and is likely $^1\Pi$. The single node in $X^1\Sigma^+$ emission implies $v' = 1$.[24,25]

From E'(J' = 31) and E'(J' = 37), B' and E'(J'=0) are

determined to be 0.353 ± 0.005 cm^{-1} and 26780 ± 20 cm^{-1}, respectively.

Resonant structure is also observed with low resolution between 560 and 570 nm where emission into $A'^1\Pi$ (v=1) is expected. However, the intensity of this band is ≈ 10 times weaker than emission into $A'^1\Pi$, v=0. However, from the similarity between B values for the upper and lower, $A'^1\Pi$, levels the $\Delta v = 0$ sequence is expected to be more intense than the $\Delta v = \pm 1$ sequences. It is also curious that this value of E' is approximately one vibrational quantum lower than the $^1\Pi$ state excited by the 488.0 nm line, hinting that these levels belong to the same electronic state. However, progressions into $X^1\Sigma^+$ indicate that v' = 1 for both laser excitation lines! If both upper levels belong to different $^1\Pi$ states, then <u>three</u> $^1\Pi$ states (including $B^1\Pi$) lie in the same energy region. This is, again, inconsistent with theoretical expectations.[14]

It seems plausible that these two previously unseen $^1\Pi$ levels belong to the same electronic state and that they borrow radiative character from $B^1\Pi$ thus invalidating node counting in $X^1\Sigma^+$ progressions as a means of determining the v' numbering. By analogy with $A'^1\Pi \sim a^3\Pi_1$ spin-orbit mixing,[13] the most likely state to mix with $B^1\Pi$ would be the $^3\Pi$ state from the same

$1\sigma^2$ ...$7\sigma^2$ 8σ $1\pi^4$ ... $3\pi^4$ 4π configuration.[14] However, this assignment suffers from the lack of observed emission into $a^3\Pi$.

B. Dye Laser Excitation Spectra

1. Band Structure

Dye laser excitation spectra of the green and orange band systems are shown in Figs. 4.1 and 4.2, respectively. Band head positions are given in Tables 4.3 and 4.4. The resolution in these spectra is determined primarily by the $\approx$ 1 cm^{-1} FWHM of the dye laser.

While the green system appears to be comprised of only violet degraded bands, the orange system consists of both violet and red degraded features. No assignments are obvious.

2. Single mode laser induced fluorescence in 609.8 band

Fluorescence in the 609.8 orange band induced by single mode dye laser excitation exhibits very simple structure: only two P,Q,R, triplets separated by 55 $\pm$ 2 cm^{-1} (Fig. 4.3) are observed. The longer wavelength triplet includes the laser, which

Figure 4.1: Green band system of CaO. Total fluorescence intensity is plotted against laser frequency.

Figure 4.2: Orange band system of CaO. Total fluorescence intensity is plotted against laser frequency.

CaO Green Band
EXCITATION SPECTRUM

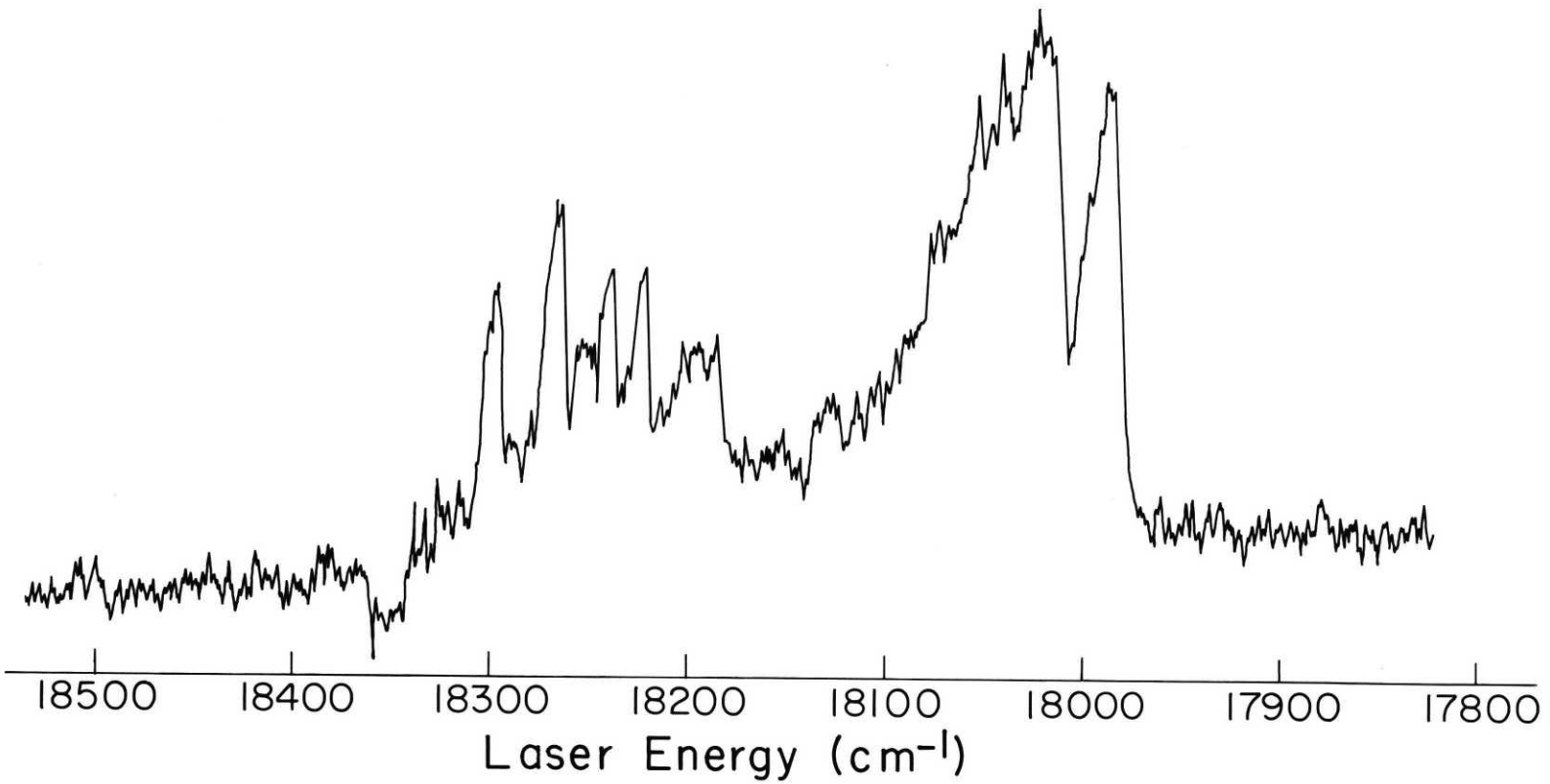

FIGURE 4.1

CaO
EXCITATION SPECTRUM

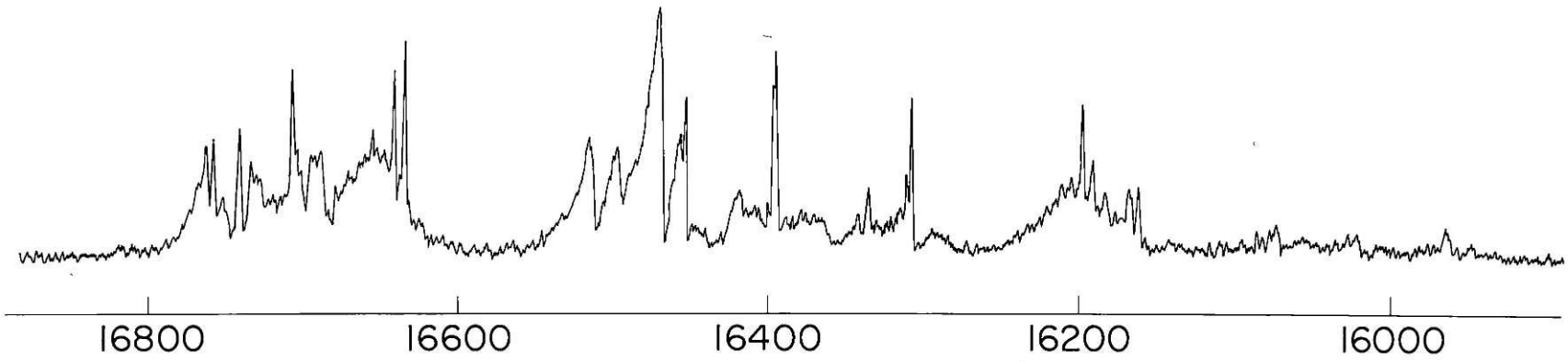

FIGURE 4.2

Table 4.2: CaO Green System Band Heads

$\sigma_{Head}(cm^{-1})$	$\lambda^{Air}_{Head}(nm)$	Relative Intensity
17 980 ± 3	556.0 ± 0.1	4.5
18 008	555.2	5.0
18 026	554.6	4.8
18 036	554.3	4.5
18 053	553.8	3.0
18 153	550.7	2.1
18 177	550.0	3.0
18 192	549.5	3.0
18 214	548.9	3.7
18 240	548.1	2.8

Table 4.3: CaO Orange System Band Heads

$\sigma_{Head}(cm^{-1})$	$\lambda^{Air}_{Head}(nm)$	Relative Intensity	$\sigma_{Head}(cm^{-1})$	$\lambda^{Air}_{Head}(nm)$	Relative Intensity
15 928 ± 3	627.7 ± 0.1	0.2	16 183	617.8	0.6
15 937	627.3	0.2	16 190	617.5	2.3
15 947	626.9	0.8	16 197	617.2	4.0
15 950	626.8	0.7	16 204	617.0	1.6
15 958	626.5	1.4	16 210	616.7	0.5
15 961	626.4	5.7	16 224	616.2	0.8
15 968	626.1	2.6	16 305	613.1	5.4
15 974	625.8	2.7	16 309	613.0	2.3
15 976	625.8	1.0	16 313	612.8	0.6
15 980	625.6	0.5	16 315	612.8	0.1
16 028	623.7	4.5	16 329	612.2	0.8
16 035	623.5	2.9	16 334	612.1	1.5
16 041	623.2	1.4	16 340	611.8	0.6
16 045	623.1	1.4	16 363	611.0	0.5
16 057	622.6	0.9	16 395	609.8	5.3

Table 4.3: (cont.)

$\sigma_{Head}(cm^{-1})$	Air $\lambda_{Head}(nm)$	Relative Intensity	$\sigma_{Head}(cm^{-1})$	Air $\lambda_{Head}(nm)$	Relative Intensity
16 071	622.1	1.0	16 396	609.7	4.6
16 077	621.8	1.0	16 401	609.6	1.0
16 082	621.6	0.5	16 411	609.2	0.4
16 087	621.4	0.5	16 418	608.9	1.0
16 132	619.7	0.2	16 422	608.8	1.0
16 140	619.4	0.2	16 453	607.6	4.3
16 158	618.7	0.2	16 457	607.5	3.0
16 163	618.5	2.7	16 459	607.4	2.0
16 168	618.3	1.5	14 463	607.3	1.0
16 169	618.3	1.9	16 470	607.0	4.0
16 177	618.0	0.4	16 472	606.9	5.5
			16 499	605.9	2.0
			16 516	605.3	2.3
			16 571	603.3	0.2
			16 579	603.0	0.3

Table 4.3: (cont.)

$\sigma_{Head}(cm^{-1})$	$\lambda^{Air}_{Head}(nm)$	Relative Intensity
16 644 ± 3	600.7 ± 0.1	4.0
16 653	600.3	2.2
16 667	599.8	0.6
16 703	598.5	1.7
16 709	598.3	1.5
16 720	597.9	1.0
16 723	597.8	2.7
16 738	597.3	0.2
16 752	596.8	1.5
16 759	596.5	1.8
16 769	596.2	0.7
16 772	596.1	0.2
16 778	595.9	1.1
16 783	595.7	1.7

Figure 4.3: Orange band fluorescence into $a^3\Pi_0$ and $a^3\Pi_1$ when the 609.8 nm band is pumped with a single mode dye laser: The laser (off scale) pumps a Q branch transition out of $a^3\Pi_0$.

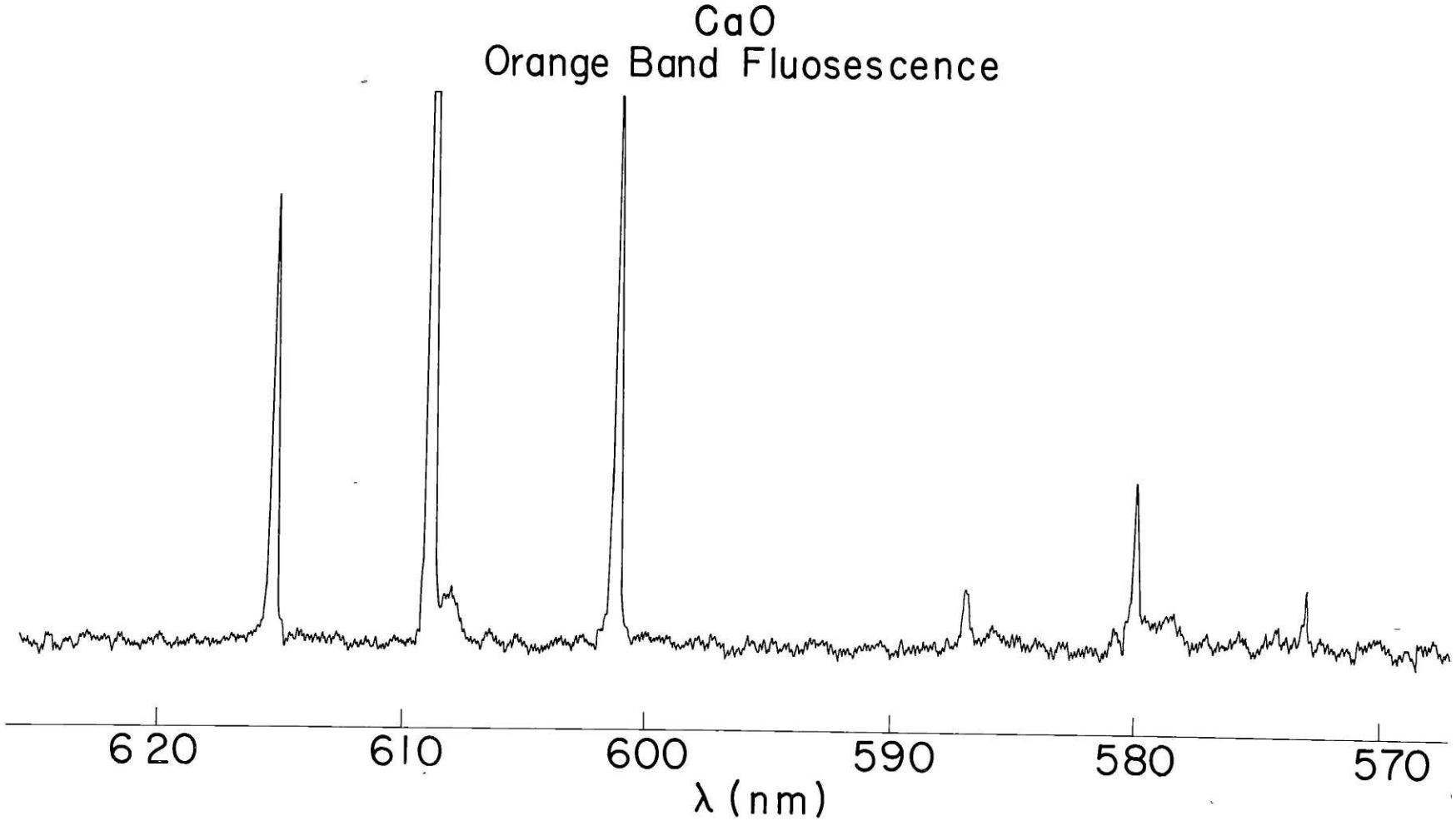

FIGURE 4.3

excites a Q branch line, and is ≈ 10 times more intense than the shorter wavelength triplet. The splitting between triplets suggests that the lower level is $a^3\Pi$ ($A_\Pi = -58\ cm^{-1}$)[13] and that the short and long wavelength components are either $a^3\Pi_1$ and $a^3\Pi_0$ or $a^3\Pi_2$ and $a^3\Pi_1$, respectively. Asymmetries in the long wavelength P,Q,R, splittings (i.e. $\Delta PQ \neq \Delta QR$) which persist even at low J indicate that the lower level is Λ-doubled. Only $a^3\Pi_0$ can be Λ-doubled as J approaches zero[21] so that the short and long wavelength triplets are assigned as $a^3\Pi_1$ and $a^3\Pi_0$ respectively. Since strong Q branches are observed, the upper state must have $\Omega = 1$ symmetry. Lack of emission into $a^3\Pi_2$ and the greater intensity of emission into $a^3\Pi_0$ relative to $a^3\Pi_1$ indicates that the upper state must be $^3\Delta_1$: emission from $^3\Sigma^-$ or $^3\Sigma^+$ into each Ω component of $^3\Pi$ should exhibit comparable intensity.[21]

These assignments have recently been verified by Mr. Ronald Marks who is at present rotationally analyzing this band system using the technique of intermodulation fluorescence spectroscopy.[23,27] No vibrational assignment has yet been made.

C. Effects of CO addition to the flame

The addition of CO to CaO flames has been observed to increase chemiluminescence and absorption intensity in the orange and green systems.[7,8,16,17] This is observed here as well: addition of $\approx$ 1 x 10^{-2} torr of CO increases the entire orange and green system laser induced fluorescence intensity by a factor of 2 to 3. However, excess CO (> 0.1 torr) quenches CaO laser induced fluorescence but enhances the Ca $5^3S_1 \leftarrow 4^3P_2^o$, $5^3S_1 \leftarrow 4^3P_1^o$, and $5^3S_1 \leftarrow 4^3P_0^o$ atomic resonance lines. These observations are consistent with the reaction mechanism in Eq. 4.1: an excess of CO quenches not only high $X^1\Sigma^+$ vibrational levels but also the lower levels of the green and orange systems, $a^3\Pi$ and $A'^1\Pi$, and produces metastable Ca 4^3P^o.

IV. Conclusion

The experiments described above demonstrate that: (1) much of the green and orange band systems of CaO can be explained in terms of transitions involving $A'^1\Pi$ and $a^3\Pi$ and (2) the $A'^1\Pi$ vibrational assignments made by Field[13] are correct.

Clearly, much work remains. The most difficult problem is linking the energies of the upper and lower levels of the green and orange systems to the ground state, since strong progressions into $X^1\Sigma^+$ have not been observed when the orange and green systems are pumped with a dye laser. Ar^+ laser excitation, on the other hand, generally yields anti-Stokes emission into $X^1\Sigma^+$ and permits levels of the green system to be vibrationally assigned. Additional, single mode Ar^+ laser experiments can provide more information of this sort in both the green and orange systems.

Determining the upper state symmetries and rotational constants is best done by systematic, high resolution tunable dye laser spectroscopy of the sort that Marks[23] has already begun. The combination of dye laser and Ar^+ laser excitation in an optical-optical double resonance experiment (Chapter 3) is an attractive approach to the understanding of these systems: decreases in Ar^+ laser induced fluorescence as the dye laser is

tuned will indicate which transitions are linked via a common upper or lower level.

References for Chapter 4

1. A. Lagerqvist, Ark. Fys. 8, 83 (1954).
2. B. Rosen, Nature 156, 570 (1945).
3. J.M. Lejeune, Bull. Soc. Roy. Sci. Liége 14, 318 (1945).
4. J.M. Lejeune and B. Rosen, Bull. Soc. Roy. Sci. Liége 14, 322 (1945).
5. A.G. Gaydon, Proc. Roy. Soc. A231, 437 (1955).
6. G.A. Volnyets, G.V. Kovalenok, and V.A. Sokolov, Opt. Spectrosc. 36, 609 (1974).
7. a) D.J. Benard, W.D. Slafer, and J. Hecht, J. Chem. Phys. 66, 1012 (1977).
   b) D.J. Benard and W.D. Slafer, J. Chem. Phys. 66, 1017 (1977).
8. D.J. Benard, W.D. Slafer, P.J. Love, and P.H. Lee, Appl. Opt. 16, 2108 (1977).
9. P. Frank and L. Krauss, to be published.
10. M. Hultin and A. Lagerqvist, Ark. Fys. 2, 471 (1951).
11. a) L. Brewer and R. Hauge, J. Mol. Spectrosc. 25, 330 (1968).
    b) R.H. Hauge, Ph.D. thesis, University of California, Berkeley (1965).
12. R.W. Field, G.A. Capelle, and C.R. Jones, J. Mol. Spectrosc. 54, 156 (1975).

13. R.W. Field, J. Chem. Phys. 60, 2400 (1974).

14. C.W. Bauschlicher, Jr. and D.R. Yarkony, J. Chem. Phys. 68, 3990 (1978).

15. L. Pasternack and P.J. Dagdigian, Chem. Phys. (in press).

16. D.J. Benard, W.D. Slafer, and P.H. Lee, Chem. Phys. Lett. 43, 69 (1976).

17. a) W.D. Slafer, D.J. Benard, and P.H. Lee, Electronic Transition Lasers II, eds. L.E. Wilson, S.N. Suchard, and J.I. Steinfeld, MIT Press, Cambridge, Mass., Chapter II-8 (1977);
    b) D.J. Benard, W.D. Slafer, J. Hecht, and P.H. Lee, ibid, Chapter II-7.

18. W.B. Bridges and A.N. Chester, IEEE J. Quant. Electron. QE1,66 (1965).

19. G.R. Harrison, MIT Wavelength Tables, MIT Press (1969).

20. I. Renhorn and P.G. Cummins, unpublished results.

21. G. Herzberg, Molecular Spectra and Molecular Structure I. Spectra of Diatomic Molecules, (Van Nostrand Reinhold, New York, 1950).

22. I. Kovács, Rotational Structure in the Spectra of Diatomic Molecules (American Elsevier, New York, 1969).

23. R.F. Marks, unpublished results.

24. E.U. Condon, Phys. Rev. 32, 858 (1928).

25. G. Gerber and H.P. Broida, J. Chem. Phys. 64, 3423 (1976).

26. J.M. Brown, J.T. Hougen, K.-P. Huber, J.W.C. Johns, I. Kopp, H. Lefebvre-Brion, A.J. Merer, D.A. Ramsay, J. Rostas, and R.N. Zare, J. Mol. Spectrosc. 55, 500 (1975).

27. M.S. Sorem and A.L. Schawlow, Opt. Comm. 5, 148 (1972).

Volume II. Laser Spectroscopy of Alkaline Earth Oxide Flames and Deperturbation of Diatomic Molecular Spectra

by

Richard Alan Gottscho

Submitted to the Department of Chemistry February 8, 1979, in partial fulfillment of the requirements for the degree of Doctor of Philosophy.

CHAPTER 5: Optical-Optical Double Resonance Monitoring of BaO $A^1\Sigma^+$ Rotational and Translational Relaxation

I. Introduction

Optical-optical double resonance (OODR) (Chapter 3) is a unique means by which the dynamics of gaseous molecular interactions in bulk can be extensively characterized. A pump laser with spectral width less than the Doppler width prepares,via the Doppler shift, a specific rovibronic level with a narrow distribution (dictated by the laser and homogeneous line widths) of speeds along the laser propagation direction, v_x[†]. A narrow bandwidth probe laser subsequently samples the populations of both initially pumped and collisionally populated levels while simultaneously determining the final v_x distributions from the excitation line shape (Fig. 5.1). If these populations and line shapes are studied as a function of pressure, state to state rate constants can, in principle, be obtained:

$$|J,M,\ n,v_x\rangle \xrightarrow{kP} |J',M',\ n',v_x'\rangle \qquad (5.1)$$

where J, M, n, and v_x denote initial rotational quantum number, projection of J onto the pump laser polarization direction (laboratory fixed z axis), vibrational and electronic quantum number(s), and speed along the laser propagation direction, respectively. A prime denotes final

---

[†]This unconventional choice of $+\hat{x}$ for the laser propagation direction results from the choice of $\hat{z}$ for pump laser polarization which simplifies subsequent calculations in this chapter and in Chapter 6.

Figure 5.1: OODR excitation scheme for probing BaO $A^1\Sigma^+$ rotational and translational relaxation. The $A^1\Sigma^+ \leftarrow X^1\Sigma^+$ (1,0) P(16) pump line prepares J' = 15; collisions subsequently transfer population to J' = 12, which is probed by exciting $C^1\Sigma^+ \leftarrow A^1\Sigma^+$ (3,1) R(12).

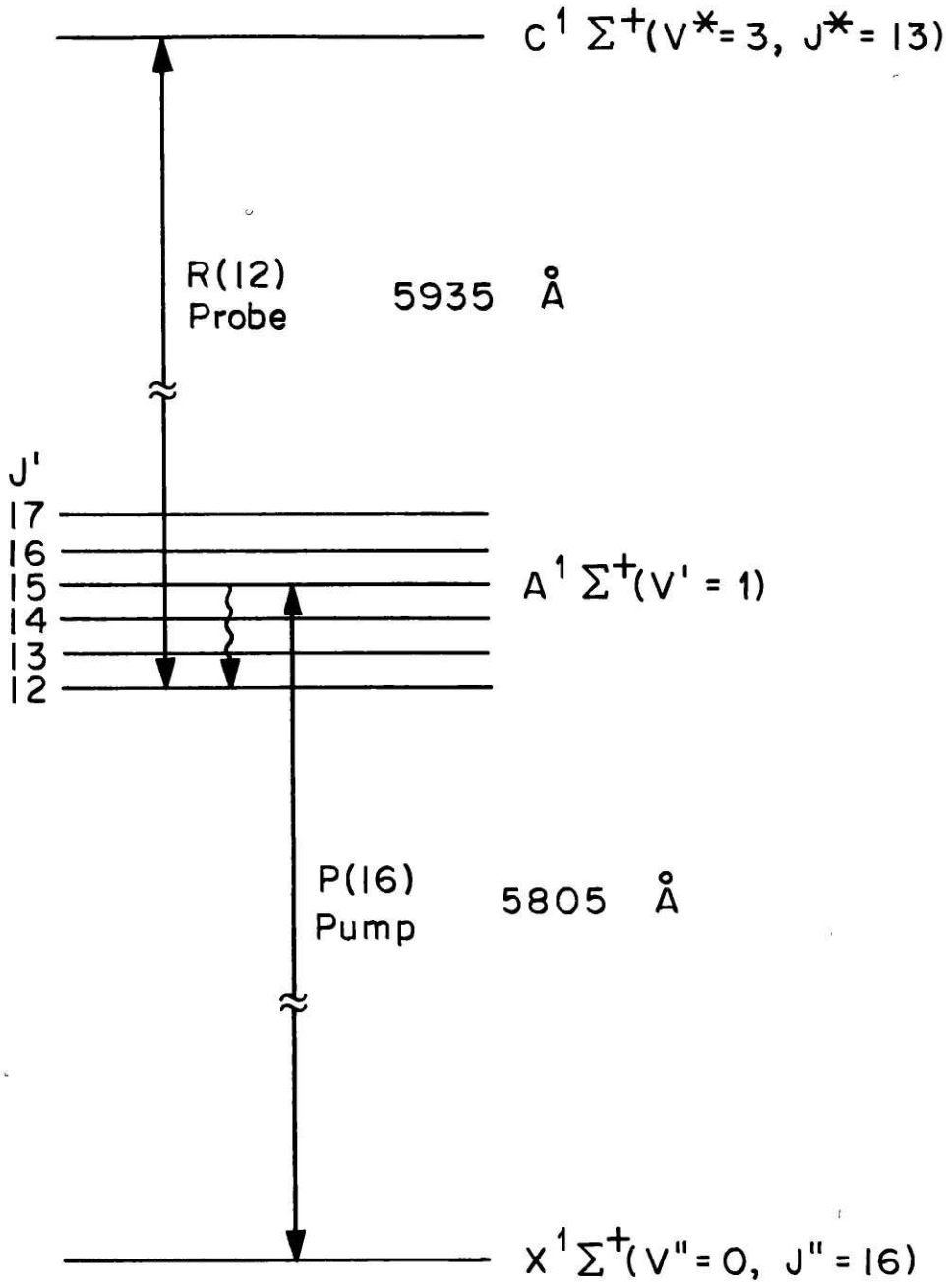
C 1 Σ+(V*= 3, J*= 13)
R(12)
Probe
5935 Å
J'
17
16
15
14
13
12
A 1 Σ+(V' = 1)
P(16)
Pump
5805 Å
X 1 Σ+(V"= 0, J"= 16)

FIGURE 5.1

quantum numbers; k is the state to state rate constant in units of $torr^{-1}$ sec^{-1} and P is the pressure in torr.

This chapter reports the results of OODR experimental studies of the dynamics of BaO ($A^1\Sigma^+$) ∿ Ar and CO_2 interactions in a Ba + CO_2 + Ar → BaO + CO + Ar flame reaction. Reaction (5.1) averaged over initial and final M states is considered here; discussion of collision induced changes in M are deferred to Chapter 6. Although precise, quantitative determinations of state to state rate constants were not obtained (owing to multiple collision complications), <u>propensities</u> for small changes in J were observed for both Ar and CO_2: $k(|\Delta J| = 1) > k(|\Delta J| = 2) > k(|\Delta J| = 3)$, where $\Delta J = J'-J$.

For both Ar and CO_2, velocity randomization, or translational relaxation, was found to proceed via forward scattering in the center of mass (COM) coordinate system ($\psi < 60°$ where ψ is the COM scattering angle) at rates comparable to $\Delta J = \pm 1$ transfer. Two differences between BaO($A^1\Sigma^+$) ∿ Ar and BaO($A^1\Sigma^+$) ∿ CO_2 collisions were apparent: 1) CO_2 pressure broadening (k_T ∿ 19 ± 3 MHz $torr^{-1}$) for a specific BaO ($A^1\Sigma^+$) rovibronic level is ≳ 1.5 times that for Ar and 2) CO_2 translational relaxation proceeds via smaller angle scattering than does Ar relaxation. These observations are qualitatively consistent with a longer range interaction for BaO ∿ CO_2 than for BaO ∿ Ar collisions owing to the CO_2 quadrupolar moment (-4.3×10^{26} esu cm^2)[1]

and internal degrees of freedom (facilitating long range exchange resonances).

In Section II.A. theoretical relationships between moments of the v_x distribution and moments of cos ψ are derived. These relationships are applicable when the collisional change in relative translational energy can be neglected with respect to the initial relative energy: in other words, the rotational energy change is small compared to kT. Section II.B. presents theoretical representations for observed principal (probe excitation from pumped level) and collisional satellite line shapes in terms of convolution integrals of the homogeneous line shape function with the v_x distribution; a deconvolution procedure to obain the v_x distribution is described. In Section II.C. the method by which line intensities are transformed into state to state rate constants is outlined.

Experimental details pertinent to this kinetic work are given in Sec. III. The OODR experiment is described generally and in more detail in Chapter 3.

In Section IV the experimental results are presented and analyzed.

Section V summarizes the observations, and theoretical interpretations, and suggests future experiments.

The remainder of this introduction is devoted to a summary of previous work and its relationship to these experiments.

State to state reaction cross sections have been measured by laser induced fluorescence (LIF) detection of molecular beam reaction† products.[2] Molecular beams allow specification of a well defined initial relative translational energy. In conjunction with LIF probes of internal state distributions and angular resolution of scattered products this yields differential cross sections for production of a specific final state as a function of initial relative velocity. If the reactant states are selectively prepared as well, state to state cross sections can be obtained.[2,3] Dagdigian and coworkers have recently measured state to state cross sections for LiF ∿ rare gas collisions in a beam-gas arrangement[2] by initial quadrupolar state selection of an LiF beam followed by LIF probes of the final state distributions.[4]

Kinsey[5] has shown that the three dimensional COM scattering angle distribution may be simultaneously obtained with product internal energy distributions employing the LIF technique of Fourier Transform Doppler Spectroscopy (FTDS) with an increase in data acquisition rate for a given signal to noise ratio of $\approx 10^4$ over traditional molecular beam detection methods.[5] Experimentally, this technique has already been demonstrated

---

†Reaction is used here in a general sense and need not imply chemical rearrangement.

by obtaining state-resolved differential cross sections in a $Na(3^2P_{1/2}) + Ar \rightarrow Na(3^2P_{3/2}) + Ar$ crossed beam reaction.[6]

In the bulk phase, monochromatic excitation is a long proven technique for obtaining state to state rate constants.[7,8] The most systematic and precise determinations of state to state rate constants have been done by Steinfeld et al.[7] and more recently by Brunner, et al.[9] The dependence of $J \rightarrow J'$ rate constants on initial J and the inequality of $\Delta J > 0$ and $\Delta J < 0$ (for equal $|\Delta J|$) rate constants has led to the conclusion that M tends to be conserved in these collisions.[9] (See Chapter 6 for a more complete discussion.) However, no attempts were made in Refs. 7 and 9 to measure either the initial velocity dependence of the rate constants or the final v_x distribution.

Advantage has been taken of the Doppler shift in determining the velocity dependence of state to state rate constants in both molecular[10,11] and atomic[12] systems. Phillips and Pritchard[13] have derived an expression for the energy, or velocity, resolution resulting from velocity selection by Doppler shift (VSDS).

A variety of double resonance experiments on both atomic and molecular systems, in bulk, have already been employed in the characterization of velocity changing collisions[14-31] (VCC). Beginning in 1969,[16]

the pressure dependence of Lamb dip line shapes and widths in He-Ne,[16,17] CO_2[18], and CO[19] lasers have been interpreted in terms of VCC.

Infrared-infrared double resonance experiments have been used to study velocity randomization in collisions of various inert molecules and atoms with NH_3[20,25], CO_2[22,26], H_2CO[24] and CH_3F.[23,24] The technique of coherent optical transients has also been used to study the time dependence of velocity randomizing collisions in $CH_3F \sim CH_3F$ interactions.[21,25] In atomic systems,optical double resonance (either saturation spectroscopy involving two levels or OODR involving three levels) has been the technique of choice in measuring quasi-elastic (i.e. no change in the internal electronic degrees of freedom) VCC.[14,18,30,31] The theoretical interpretation of double resonance line shapes influenced by VCC has been developed largely by Berman[14,27] using the density matrix formalism. Quantitative analyses have proceeded by fitting the observed line shape to a theoretical line shape function involving a phenomenological collision kernel; an average speed change, δv_x, is obtained.[14,24-26] The magnitude of δv_x has been interpreted in terms of collision strength: large (small) velocity jumps are associated with strong (weak) interactions. Values of v_x ranging from $\sim$ 85 cm sec^{-1} in $CH_3F \sim CH_3F$ collisions[25]

to $\sim 10^3$ cm sec^{-1} in Xe $\sim$ Xe collisions[30] have been observed

Energy transfer studies of BaO $A^1\Sigma^+$ have emphasized the elucidation of $A^1\Sigma^+ \sim b^3\Pi$ intersystem crossing mechanisms and rates (see Chapter 1).[32-37] Sakurai, et al.,[32] have measured total cross sections (summed over final states) for electronic quenching (with He), vibrational relaxation (with He, Ar, and N_2) and rotational relaxation (with He) from a single $A^1\Sigma^+$ rovibronic level prepared by Ar^+ laser excitation. Johnson[33] has measured radiative lifetimes and He quenching rates as a function of $A^1\Sigma^+$ vibration by excitation with a pulsed tunable dye laser.

The experiments described below differ in several respects from the works referenced above. Because of the disparity in BaO $C^1\Sigma^+$ and $A^1\Sigma^+$ radiative lifetimes (25 ± 10 nsec[37] and 363 nsec[33,†] respectively). OODR line shapes are determined primarily by $A^1\Sigma^+$ relaxation. All previous VCC studies on molecular systems measured both upper and lower state dynamics simultaneously making analysis more difficult. VCC are understood here in terms of the COM scattering angle distribution rather than δv_x; deconvolution of the observed line shape to obtain moments of cos ψ is completely model independent.

[†] $A^1\Sigma^+$ (v = 1).

Previous molecular VCC experiments utilized CO, CO_2 or N_2O infrared lasers of limited tunability.[16-26] Visible dye lasers yield not only greater velocity resolution (the Doppler shift is proportional to frequency) but also tunability over hundreds of nanometers permitting systematic studies of state to state cross sections. The combined tunability and high resolution of OODR allows investigation of rotational and translational relaxation out of rotationless levels (J = 0) whose transitions are usually weak and unresolvable by small monochromators. In general, any initial level may be chosen and examined for unique dynamical properties.

II. Theory

A. Velocity Selection and Analysis

Because of the Doppler shift, molecules travelling with different velocity components along the laser propagation direction (specified by $\hat{x}$) are resonant with the field at different frequencies:

$$\nu = \nu_o \, (1 + v_x/c), \tag{5.2}$$

where ν is the resonant frequency for molecules with velocity component along the laser propagation direction v_x, ν_o is the rest frequency (when $v_x = 0$), and c is the speed of light. Note that v_x is a signed quantity (+ (-) for travel with (against) $\hat{x}$). Thus, molecules with different speeds may be <u>selected</u> by tuning the pump laser across the Doppler line profile. Similarly, the probe laser may be used to <u>analyze</u> the final, v_x', velocity distribution.

The relationship between $\delta v_x = v_x' - v_x$ and moments of the scattering angle distribution is derived below for molecules with well defined v_x but thermal (Maxwellian) distributions of v_y and v_z velocity components colliding with particles characterized by a completely thermal velocity distribution.

In the laboratory coordinate system,

$$\vec{v}_i = v_{ix}\hat{x} + v_{iy}\hat{y} + v_{iz}\hat{z} \qquad (5.3)$$

where v_i is the i^{th} molecular velocity with magnitude $v_i = \sqrt{v_{ix}^2 + v_{iy}^2 + v_{iz}^2}$. $i = 1$ is chosen for the v_x selected molecule and $i = 2$ denotes the collision partner.

It is most convenient to picture the collision in the COM coordinate system where the COM kinetic energy (a constant of the motion) is zero. Since the OODR experiment samples only v_{ix}, it is sufficient and simpler to work only with x velocity components:

$$w_{ix} = v_{ix} - \frac{1}{M}(m_i v_{ix} + m_j v_{jx}) = w_i \cos\eta_i \qquad (5.4)$$

where w_{ix} is the laboratory x component of the i^{th} molecular COM velocity, $\vec{w}_i$ (with magnitude w_i); $M = (m_1 + m_2)$ is the total mass of the collision system; η_i is the polar angle of $\vec{w}_i$ with respect to x (Fig. 5.2); and $i = 1(2)$ when $j = 2(1)$. The collision between i and j is simply represented by pivoting the relative velocity vector $\vec{w} = \vec{w}_i - \vec{w}_j$ about the COM by an angle ψ (COM scattering angle) in the plane specified by $\vec{v}_i$ and $\vec{v}_j$ and by an angle γ out of the plane and by changing the length of $\vec{w}$ consonantly with the change in internal energy (Fig. 5.3). All values of γ from 0 to 2π are equally probable so that a cone of equal scattering intensity is obtained.[38]

Changes in the magnitude of $\vec{w}$, δw, can be

Figure 5.2: Collision of molecule 1 with molecule 2 and transformation to COM. For simplicity $\vec{v}_1$ is chosen equal to $v_{1x}\hat{x}$ ($v_{1y} = v_{1z} = 0$) and the collision takes place in the xz plane ($v_{2y} = 0$).

Figure 5.3: Elastic scattering ($w' = w$) in the COM. $\vec{w}'$ is rotated in the plane about COM by ψ and out of the plane by γ. All values of γ from 0 to 2π are equally probable resulting in a cone of equal scattering intensity for given ψ. Two w's on the same cone are shown, corresponding to the same value of ψ but different γs.

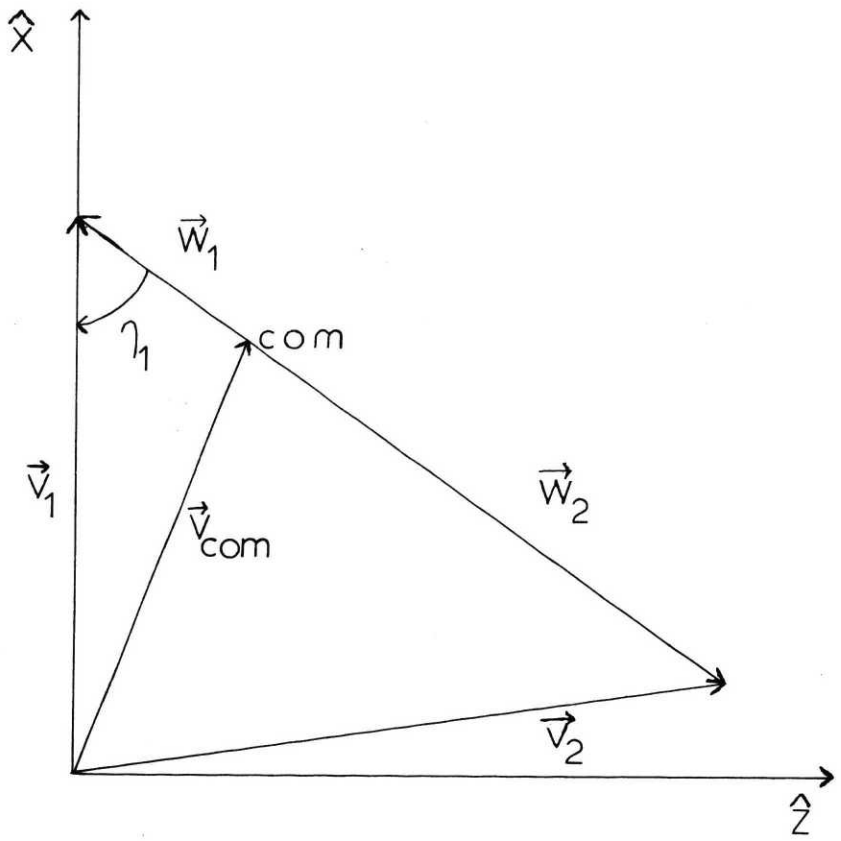

FIGURE 5.2

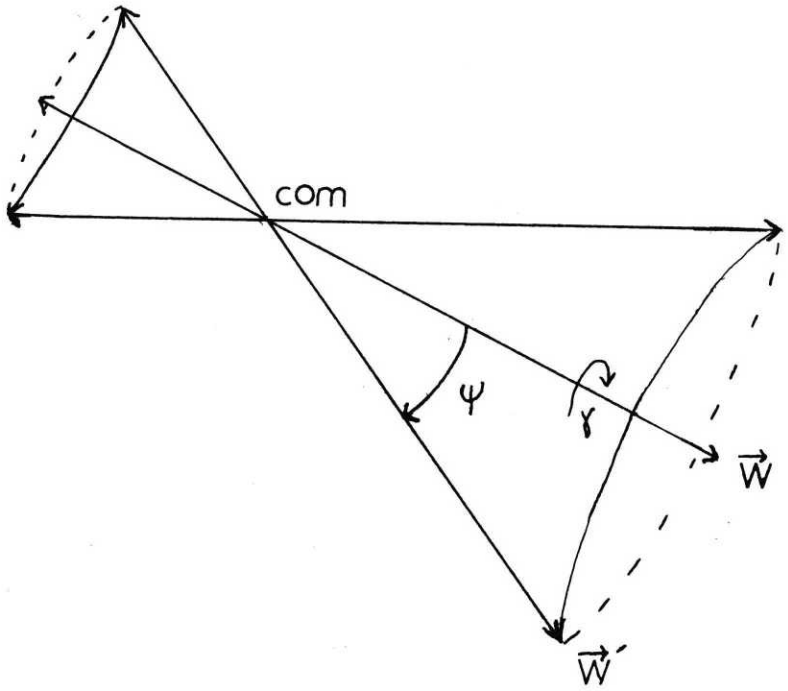

FIGURE 5.3

neglected when the internal energy change, ΔE_{int}, is much less than kT. This is the situation in BaO $A^1\Sigma^+$ rotational relaxation considered below; hereafter, $w' = w$ is assumed.†

From geometrical considerations, the projection of w_i' on x is derived[39]

$$w'_{ix} = w_i[\cos\psi\cos\eta_i - \cos\gamma\sin\psi\sin\eta_i], \qquad (5.5)$$

where the quasi-elastic condition, $w_i' = w_i$, is assumed. It is convenient to examine only the change in v_{ix}, $\delta v_{ix} = v'_{ix} - v_{ix} = \delta w_{ix} = w'_{ix} - w_{ix}$, induced by the collision; in the frequency domain, this corresponds to $\delta\nu = \nu' - \nu = \delta v_{ix}(\nu_o/c)$ (not to be confused with the line width $\Delta\nu_{FWHM}$):

$$\delta\nu_i = \frac{\nu_o}{c} w_i[\cos\eta_i(\cos\psi-1)-\cos\gamma\sin\psi\sin\eta_i]. \qquad (5.6)$$

1. Average frequency shift

Equation (5.6) relates a frequency shift to the COM scattering angles ψ and γ for given initial trajectories of molecules 1 and 2 (specified by η_1 and w_1). It is necessary to average over the y and z velocity components of molecule 1 and all three velocity components

---

†The maximum rotational energy change observed, J = 15 → J = 30, is ∿ 0.5kT.

of molecule 2 since these are not selected. Averaging γ from 0 to 2π and ψ over the scattering angle distribution $P(\psi)$ results in an average frequency shift which may be obtained from the observed line shape (see Section IIB). First averaging γ from 0 to 2π,

$$<\delta\nu_1> = \frac{\nu_o}{c} \int_o^{2\pi} \delta v_{1x}\, d\gamma = \frac{\nu_o}{c} w_1 \cos\eta_1(\cos\psi - 1). \qquad (5.7)$$

Substituting for $\cos\eta_i$ from Eq. (5.4),

$$<\delta\nu_1> = \frac{\nu_o}{c}\left[v_{1x} - \frac{1}{M}(m_1 v_{1x} + m_2 v_{2x})\right](\cos\psi - 1), \qquad (5.8)$$

averaging v_{2x} over the Maxwellian distribution from $-\infty$ to $+\infty$,

$$<<\delta\nu_1>> = \frac{\nu_o}{c} v_{1x} \frac{m_2}{M} \left[<\cos\psi> - 1\right] \qquad (5.9)$$

where $<\cos\psi> = \int_o^{\pi} \cos P(\psi)\sin\psi d\psi$ and $<v_{2x}> = 0$. The great simplicity of Eq. 5.9 results from neglect of changes in the relative translational energy and the energy dependence of ψ. Note that v_y and v_z for both molecules 1 and 2 need not be considered. Several predictions are immediately obvious from Eq. 5.9: 1) $<<\delta\nu_1>>$ scales as $v_{1x}\left[<\cos\psi> - 1\right]$ so that asymmetric lines skewed towards ν_o ($v_{1x} = 0$) are expected for $v_{1x} \neq 0$ and $\psi > 0$; 2) large asymmetries imply large scattering angles or backward scattering; 3) when $v_{1x} = 0$ ($\nu = \nu_o$) is

selected, the probe laser excitation line shapes should be symmetrical with an average shift of zero so that $\langle\cos\psi\rangle$ cannot be determined from $\langle\langle\delta\nu_1\rangle\rangle$; and 4) the relative masses of the two collision partners affects the precision with which $\langle\cos\psi\rangle$ can be determined from $\langle\langle\delta\nu_1\rangle\rangle$ (if $m_1 \simeq M >> M_2$, $\langle\langle\delta\nu_1\rangle\rangle \simeq 0$ and $\cos\psi$ is indeterminate.

$\langle\langle\delta\nu_1\rangle\rangle$ is zero when $v_{1x} = 0$ because collision partners with $v_{2x} > 0$ and $v_{2x} < 0$ for given $|v_{2x}|$ produce average frequency shifts of equal magnitude but opposite sign: from conservation of linear momentum and energy $v_{2x} > 0$ produces blue shifts (i.e. $v'_{1x} \geq 0$) and $v_{2x} < 0$ produces red shifts (i.e. $v_{1x} \leq 0$). Thus, if Eq. 5.8 is averaged over v_{2x} from 0 to ∞ (or $-\infty$ to 0) rather than from $-\infty$ to ∞, the average blue (red) shift is given by

$$\langle\langle\delta\nu_1\rangle\rangle_0 \equiv \langle\langle\delta\nu_1\rangle\rangle_0^{\text{Blue}} = -\langle\langle\delta\nu\rangle\rangle_0^{\text{Red}} = -\frac{\nu_o}{C}\frac{m_2}{M}\left(\frac{kT}{2\pi m_2}\right)[1-\langle\cos\psi\rangle] \tag{5.10}$$

and $\langle\cos\psi\rangle$ can be determined when $v_{1x} = 0$.[†]

2. Second Moment of the Frequency Shift

Higher moments of $\cos\psi$ can be determined from higher moments of $\delta\nu_1$. The second moment of $\delta\nu_1$ as a function of $\langle\cos^2\psi\rangle$ and $\langle\cos\psi\rangle$ is derived below.

[†]If the energy dependence of ψ is neglected, selecting molecules with $v_{1x} \neq 0$ provides the same information as $v_{1x}=0$ selection.

Squaring Eq. 5.6,

$$(\delta\nu_1)^2 = \frac{\nu_o^2}{c^2} w_1^2 \{[\cos\psi\cos\eta_1 - \cos\gamma\sin\psi\sin\eta_1]^2$$

$$-2\cos\eta_1 [\cos\psi\cos\eta_1 - \cos\gamma\sin\psi\sin\eta_1]$$

$$+ \cos^2\eta_1\}, \qquad (5.11)$$

and averaging γ from 0 to 2π,

$$\langle\delta\nu_1^2\rangle = \frac{\nu_o^2}{c^2} w_1^2 \{[\cos^2\psi\cos^2\eta_1 + \frac{1}{2}\sin^2\psi\sin^2\eta_1]$$

$$-2\cos^2\eta_1\cos\psi + \cos^2\eta_1\}. \qquad (5.12)$$

From Eq. 5.4

$$w_1^2\cos^2\eta_1 = v_{1x}^2 - \frac{2v_{1x}}{M}(m_1v_{1x} + m_2v_{2x})$$

$$+ \frac{1}{M^2}(m_1^2v_{1x}^2 + 2m_1m_2v_{1x}v_{2x} + m_1^2v_{2x}^2). \qquad (5.13a)$$

Averaging v_{2x} from $-\infty$ to $+\infty$,

$$\langle w_1^2\cos^2\eta_1\rangle = [v_{1x} + \frac{1}{3}\langle v_2^2\rangle]\frac{m_2^2}{M^2} \qquad (5.13b)$$

where $\langle v_2^2\rangle = \langle v_{2x}^2\rangle + \langle v_{2y}^2\rangle + \langle v_{2z}^2\rangle = 3\langle v_{2x}^2\rangle$ for collision partner 2 with a thermal velocity distribution. Similarly,

$$\langle w_1^2\rangle = \frac{m_2^2}{M^2}[2\langle v_1^2\rangle + v_{1x}^2 + \langle v_2^2\rangle] \qquad (5.14)$$

where $\langle v_{1\perp}^2\rangle = \langle v_{1y}^2\rangle = \langle v_{1z}^2\rangle$ is the average square speed perpendicular to x for molecule 1. Providing the

temperature, T, is known, $\langle v_{1\perp}^2 \rangle$ and $\langle v_2^2 \rangle$ are readily calculated:

$$\langle v_{1\perp}^2 \rangle = kT/m_1 \tag{5.15a}$$

$$\langle v_2^2 \rangle = 3kT/m_2. \tag{5.15b}$$

Combining Eqs. 5.12, 5.13b, 5.14, and 5.15,

$$\langle\langle \delta\nu_1^2 \rangle\rangle \frac{\nu_o^2}{c^2} \frac{m_2^2}{M^2} \{[v_1^2 - \frac{kT}{m_1}]\langle\cos^2\psi\rangle - 2[v_{1x}^2 + \frac{kT}{m_2}]\langle\cos\psi\rangle + [v_{1x}^2 + kT(\frac{1}{m_1} + \frac{2}{m_2})]\} \tag{5.16}$$

where ψ has been averaged over the distribution $P(\psi)$. Eq. 5.16 relates the second moment of the frequency shift to first and second moments of $\cos\psi$. Again if $m_1 \simeq M >> m_2$ little information is obtained since $\langle\langle \delta\nu_1^2 \rangle\rangle \simeq 0$. If $v_{1x} \simeq kT/m_1$ is selected $\langle\cos^2\psi\rangle$ is undetermined. When $v_{1x} = 0$,

$$\langle\langle \delta\nu_1^2 \rangle\rangle_o \frac{\nu_o^2}{c^2} \frac{m_2^2}{M^2} kT\{\frac{1}{m_1}[1-\langle\cos^2\psi\rangle] + \frac{2}{m_2}[1-\langle\cos\psi\rangle]\}. \tag{5.17}$$

Qualitatively, Eq. 5.17 states that the frequency shift increases monotonically with scattering angle. For narrow scattering angle distributions, $\langle\cos^2\psi\rangle \sim \langle\cos\psi\rangle^2$ and Eq. 5.17 can be solved for $\langle\cos\psi\rangle$ given an experimental value of $\langle\langle \delta\nu_1^2 \rangle\rangle$.

B. Line Shapes

1. General expression

The observed excitation line shape is proportional to a convolution integral of a pressure and power dependent homogeneous line shape function with a sum of v_x distributions. Each v_x distribution corresponds to molecules with different trajectories between time of excitation and emission:[40]

$$I(\nu) \sim \int_{-\infty}^{\infty} G(\nu-\nu') \left[\sum_{i=0}^{N} n_i V_i(\nu')\right] d\nu' \qquad (5.18a)$$

or

$$I(\nu) \sim \int_{-\infty}^{\infty} G(\nu-\nu') V(\nu') d\nu' \qquad (5.18b)$$

where $G(\nu-\nu')$ is the homogeneous line shape, n_i is the number density of molecules which have traversed trajectory i, $V_i(\nu')$ is the velocity distribution resulting from trajectory i, N is the pressure dependent number of trajectories, and $V(\nu')$ is the resultant, total velocity distribution. For low pressures, the single collision limit is applicable and only one class of trajectories for satellite lines corresponding to $J \rightarrow J'$ transfer and two classes of trajectories for the principal line corresponding to stationary state oscillation and elastic (i.e. $\Delta J = 0$) velocity randomization need be included in Eq. 5.18.

$G(\nu-\nu')$ is generally not a simple Lorentzian but rather a sum of three functions resulting from (1) step-wise excitation ($C^1\Sigma^+ \leftarrow A^1\Sigma^+ \leftarrow X^1\Sigma^+$) and population of $A^1\Sigma^+$, (2) two-photon excitation ($C^1\Sigma^+ \leftarrow\!\!\leftarrow X^1\Sigma^+$) involving only virtual intermediate levels, and (3) interference between (1) and (2).[41-43] $G(\nu-\nu')$ is a function of pump and probe laser power and detuning from ν_o as well as pressure.[42]

2. Deconvolution procedure

If $G(\nu-\nu')$ is known, $I(\nu)$ can, in principle, be deconvoluted to obtain $V(\nu')$, which may then be used to obtained moments of $\cos\psi$ via Eqs. 5.9, 5.10 and 5.16:[44]

$$I^*(t) = G^*(t)\cdot V^*(t) \tag{5.19a}$$

and

$$V(\nu) = (2\pi)^{-1/2}\int_{-\infty}^{\infty} \frac{I^*(t)}{G^*(t)}\, e^{i\nu t}\, dt \tag{5.19b}$$

where starred functions are one-dimensional Fourier transforms.

C. Determination of State to State Rate Constants

1. Fluorescence intensity

Populations in a $|J,M,v_x,n\rangle$ state, with

speed distribution V, are sampled by OODR or $A^1\Sigma^+ \rightarrow X^1\Sigma^+$ fluorescence. The integrated fluourescence intensity is proportional to the number density in $|J,M,n\rangle$, but is also a function of probe laser polarization and probe laser frequency (for OODR population monitoring), fluorescence detection geometry, and fluorescence frequency:[2,45-47]

$$I_{JM}^{\mu\mu'} \propto n_J f(M) E^{\mu}(a,b,\nu_E) F^{\mu'}(b,c,\nu_F) D^{\mu\mu'}(\nu_F) \qquad (5.20)$$

where $I_{JM}^{\mu\mu'}$ is the LIF signal from the $|JM\rangle$ level in the $|n\rangle$ state; a, b, and c are shorthand for initial, intermediate, and final state quantum numbers; n_J is the total number density in the J^{th} level; f(M) is the fraction of n_J in the M^{th} sub-level; E is an excitation factor, related to the Einstein B coefficient, for probe laser polarization μ; F is defined analogously to E; D is a polarization and frequency dependent fluorescence detection factor; and ν_E and ν_F are probe laser excitation and fluorescence frequencies, respectively.

Obtaining $I_{JM}^{\mu\mu'}$ experimentally is non-trivial (see Chapter 6). Instead, $I_J^{\mu\mu'}$ is measured; where:

$$I_J^{\mu\mu'} = \sum_{M=-J}^{J} I_{JM}^{\mu\mu'} \qquad (5.21)$$

If $D^{\mu\mu'}$ and $I_J^{\mu\mu'}$ are experimentally determined, E^{μ} and $F^{\mu'}$ can be calculated[47] to yield n_J provided f(M) is known. In practice f(M) has been assumed to be a constant and equal to $(2J+1)^{-1}$, implying equal M sublevel populations. This assumption is justified when the variation in intensity ratios, used to determine $k(J \rightarrow J')$ as μ and μ' are varied is comparable to the experimental error in $I_{J'}/I_J$ (for example, see Ref. 9). A recent review by Kinsey[2] gives a more complete discussion of LIF measurements of internal energy state distributions.

2. Rate constants

In steady state, the number densities in each rovibronic level are interrelated (the following discussion closely follows Ref. 9b):

$$\frac{dn_J}{dt} = 0 = \sum_{J'}^{*} n_{J'} K_{JJ'} - n_J \Gamma - \sum_{J'}^{*} n_J K_{JJ'} \qquad (5.22)$$

where $K_{JJ'}$ is the pressure dependent rate for $J \rightarrow J'$ collisions, starred summations denote exclusion of J=J' terms (elastic $J \rightarrow J$ rates are not determined), and Γ is a pressure dependent decay constant given by,

$$\Gamma = k_{rad} + \sum_{\ell} k_{\ell}^{c} n_{\ell} \qquad (5.23)$$

where k_{rad} is a radiative decay rate and k_{ℓ}^{c} is a quenching rate (removal from the vibrational level considered by vibrational or electronic transfer or by chemical reaction) for collision species ℓ with number density n_{ℓ}. Eq. 5.22 is not valid when $J = J_o$, where J_o denotes the pumped level, since no pump source term is included. The effects of probe laser saturation are neglected (valid when the probe excitation rate is much less than the collision rate which is the situation for this work). The first term in Eq. 5.22 represents collisional transfer into J from J'; the third term represents transfer from J to J'.

If $K_{JJ'}$, is assumed to be a function only of $\Delta J = J'-J$, Brunner, et al.[96] have shown that:

$$1 = \sum_{J'=-J_{min}}^{J_{max}} (R_{J'J} - 1)\ T(\Delta J) \qquad (5.24)$$

where $R_{J'J} = n_{J'}/n_J$ is the ratio of number densities in levels J' and J and $T(\Delta J) = K(\Delta J)\Gamma^{-1}$. Eq. 5.24 leads to a set of equations for each value of J which is conveniently expressed in matrix form:

$$\underset{\sim}{1} = \underset{\sim}{X}\ \underset{\sim}{T} \qquad (5.25a)$$

and

$$\underset{\sim}{X}^{-1}\ \underset{\sim}{1} = \underset{\sim}{T} \qquad (5.25b)$$

where $\underset{\sim}{X}$ is the matrix of $(R_{J'J}-1)$ values, $\underset{\sim}{T}$ is the vector

of $T(\Delta J)$ values, and $\underset{\sim}{1}$ is the identity vector. Providing $K_{JJ'}$ is only a function of ΔJ, Eq. 5.25b yields $T(\Delta J)$ corrected for the effects of multiple collisions. In using Eqs.5.24 and 5.25, it should be noted that if J ranges from J_1 to J_2, $J_{min} = J_1 - J_0$ and $J_{max} = J_2 + J_0$.[9b]

III. Experimental

The OODR experiment was described in Chapter 3. Details relevant to kinetic measurements only are presented here.

A. Pressure measurements

Pressure measurements were made using both a Wallace and Tiernan (model #FA 160) 0 to 20 torr mechanical gauge and an MKS baratron (model #220-2A6-1) 0 to 1 torr capacitance manometer gauge. The position of the baratron gauge was varied with respect to the flame and pump; identical readings were obtained when the end of the gas collection tube (≈ 6 in. from capacitance manometer) was placed in the flame and when placed ≈ 2 ft. downstream toward the pump (Welch #1397B). All experiments were carried out under flow conditions (pumping speed ≈ 300 ℓmin^{-1}). A constant discrepancy of 0.22 torr between the W&T and MKS gauges was observed. By checking against a second MKS gauge, the W&T readings were corrected accordingly by adding 0.22 torr to the observed readings. Partial pressures of Ar and CO_2 were determined, under flow conditions, by first adjusting the Ar pressure and then adding CO_2; ideality (Dalton's law) is assumed.

Pressures are precise to 0.02 torr; 0.01 torr was the smallest detectable pressure change.

B. Line intensities

For $J \lesssim 20$, populations were probed via OODR - $C^1\Sigma^+ \leftarrow A^1\Sigma^+$ (3,1) excitation and $C^1\Sigma^+ \rightarrow X^1\Sigma^+$ UV fluorescence detection. For $J > 20$, the probe laser was blocked and $A^1\Sigma^+ \rightarrow X^1\Sigma^+$ (1,1) fluorescence was resolved through a Spex 1802 spectrometer (See Chapter 3 for details); spectral resolution was $\simeq 0.3\mathring{A}$.

Pump and probe lasers were polarized along $\hat{z}$ and propagated along $\hat{x}$. $\hat{x} + \hat{y}$ polarized $C^1\Sigma^+ \rightarrow X^1\Sigma^+$ OODR induced fluorescence and $\hat{y} + \hat{z}$ polarized $A^1\Sigma^+ \rightarrow X^1\Sigma^+$ fluorescence were detected. Integrated intensities were approximated from probe laser excitation spectra by multiplying peak heights by widths (FWHM) to account for variations in velocity randomization with J (see below). For spectrometer data, peak heights alone were used as intensity measures since all line widths were equal and determined by the $0.3\mathring{A}$ spectral slit width.

The lasers were sometimes focussed with a 12 in. focal length lens into the flame center in order to obtain optimal signal to noise ratios. However, intensity ratios were insensitive to laser focussing.

Line intensities were corrected for pump and probe

laser power fluctuations by monitoring $A^1\Sigma^+ \rightarrow X^1\Sigma^+$ 91,2) fluorescence (Chapter 3) and the transmission intensities of a 300 MHz Fabry-Perot, respectively:†

$$\left[I_{J'}/I_{J_o}\right]_{true} = \left[I_{J'}/I_{J_o}\right]_{obs} \frac{P_{pump}(J_o)P_{probe}(J_o)}{P_{pump}(J')P_{probe}(J')} \qquad (5.26)$$

where the Ps are monitor signals proportional to laser intensities (P_{probe} was not used for spectrometer data). The difference between true and observed intensity ratios were less than 10%. Note that A→X (1,2) fluorescence monitoring corrects for not only pump laser power fluctuations but also BaO concentration fluctuations.

Line widths and intensity ratios were measured as a function of oven current over a range of 40 to 70 amps (corresponding to estimated oven temperatures from ∿ 600 to 1000K) for various CO_2 and Ar pressures. No dependence of widths or intensity ratios on oven current was observed.

---

†If laser frequency is tuned smoothly, the Fabry-Perot transmission intensity is proportional to laser power.

IV. Results

A. Line shapes and widths

1. Principal line

The observed excitation line shape for the $C\,^1\Sigma^+ \leftarrow A\,^1\Sigma^+$ (3,1), R(15) principal line at 0.32 torr Ar and 0.05 torr CO_2 and no focussing lens is shown in Fig. 5.4; $A\,^1\Sigma^+ \leftarrow X\,^1\Sigma^+$ (1,0), R(14), $v_x = 0$ is pumped. Also shown is a least squares fit[†] of the observed line shape to a Lorentzian with FWHM=34.24±0.14 MHz. Figs. 5.5 and 5.6 illustrate the R(15) principal line width dependence upon Ar and CO_2 partial pressure, respectively. Over the pressure range sampled, the principal excitation line shape is well characterized by a Lorentzian function. Without the focussing lens, the line widths remain unchanged when the power of both pump and probe lasers are attenuated (using neutral density filters) by a factor of ten each. These observations imply that velocity randomization and two-photon transitions (TPT) make smaller contributions to the line shape than do dephasing and decay processes. If VCC and TPT are neglected, then

---

[†] Using M.I.T. Information Processing Center library routines LSMARQ and LSMERR.

the principal line shape function may be used to deconvolute satellite line shapes according to Eq. 5.19. Further evidence that VCC make only small contributions, relative to Lorentz broadening, to the principal line shape is provided by comparing the satellite and principal line width dependences on CO_2 pressure for fixed Ar pressure: increasing P_{CO_2} merely broadens the principal line width but narrows the satellite line widths via VCC (see below); if VCC collisions were important, the principal line should also narrow as P_{CO_2} is increased.

There remain four contributions to the line shape: collisions and radiative decay in the upper $C^1\Sigma^+$ and lower $A^1\Sigma^+$ levels. The laser line width is ≈ 1MHz and is neglected. Because $C^1\Sigma^+$ radiatively decays ten times more rapidly than $A^1\Sigma^+$[33,37], $A^1\Sigma^+$ radiative decay and $C^1\Sigma^+$ collisional broadening are neglected. No evidence of $C^1\Sigma^+$ relaxation is apparent at total pressures below 1 torr. If tertiary and higher order collisions are unimportant, principal line widths vary linearly with Ar and CO_2 partial pressures:

$$\Delta\nu_{FWHM} = (2\pi)^{-1}[k_{rad} + k^T_{Ar}P_{Ar} + k^T_{CO_2}P_{CO_2}] \qquad (5.27)$$

where k_{rad} is the $C^1\Sigma^+$ radiative decay rate and k^T represents a total collision rate for a single $A^1\Sigma^+$ rovibronic level. Linear least squares fits to the data are shown in Figs. 5.4

Figure 5.4: Experimental (Δ) excitation line shape for the principal line $C^1\Sigma^+ \leftarrow A^1\Sigma^+$ (3,1), R(15) as a function of detuning frequency, $\Delta\nu = \nu - \nu_o$; the solid line is a least squares fit of the data to a Lorentzian with FWHM = 34.24 $\pm$ 0.14 MHz. Ar pressure, 0.32 torr. CO_2 pressure, 0.05 torr. $A^1\Sigma^+ \leftarrow X^1\Sigma^+$ (1,0), R(14), $v_x = 0$ is pumped.

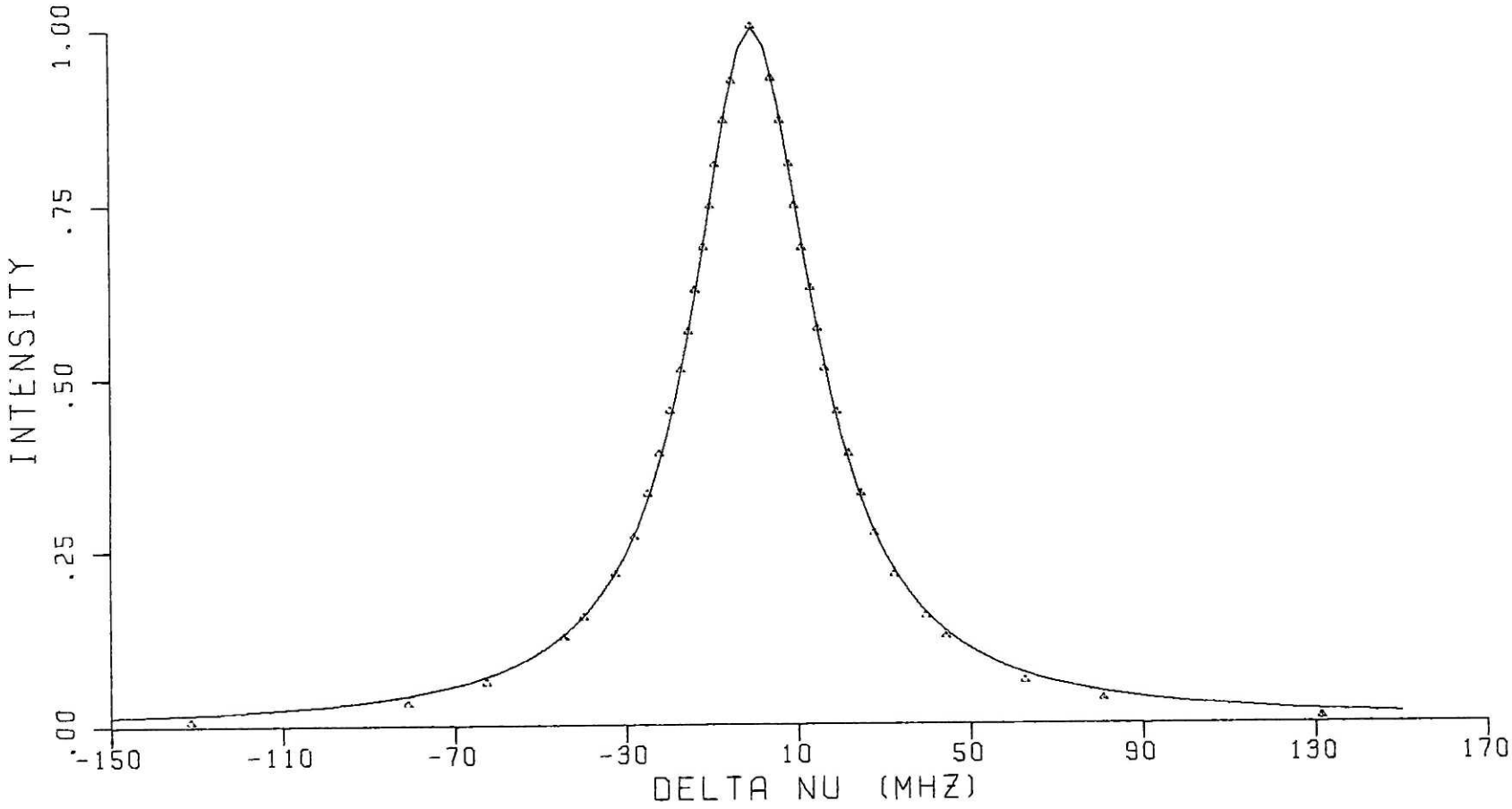
INTENSITY
.00
.25
.50
.75
1.00
-150
-110
-70
-30
10
50
90
130
170
DELTA NU (MHZ)

FIGURE 5.4

Figure 5.5: Plot of line width $\Delta\nu_{FWHM}$ vs. total pressure P_t (P_{CO_2} < 0.01 torr.) for $C^1\Sigma^+ \leftarrow A^1\Sigma^+$ (3,1) R(15) principal line. Circles are experimental measurements; line is a linear least squares fit to data with slope of 14 $\pm$ 2 MHz $torr^{-1}$ and intercept of 28 $\pm$ 2 MHz.

Figure 5.6: Same as Fig. 5.4 except P_{AR} = 0.32 torr is held fixed. Slope is 19 $\pm$ 3 MHz $torr^{-1}$ and intercept is 30 $\pm$ 3 MHz. Error bars are 1σ estimates.

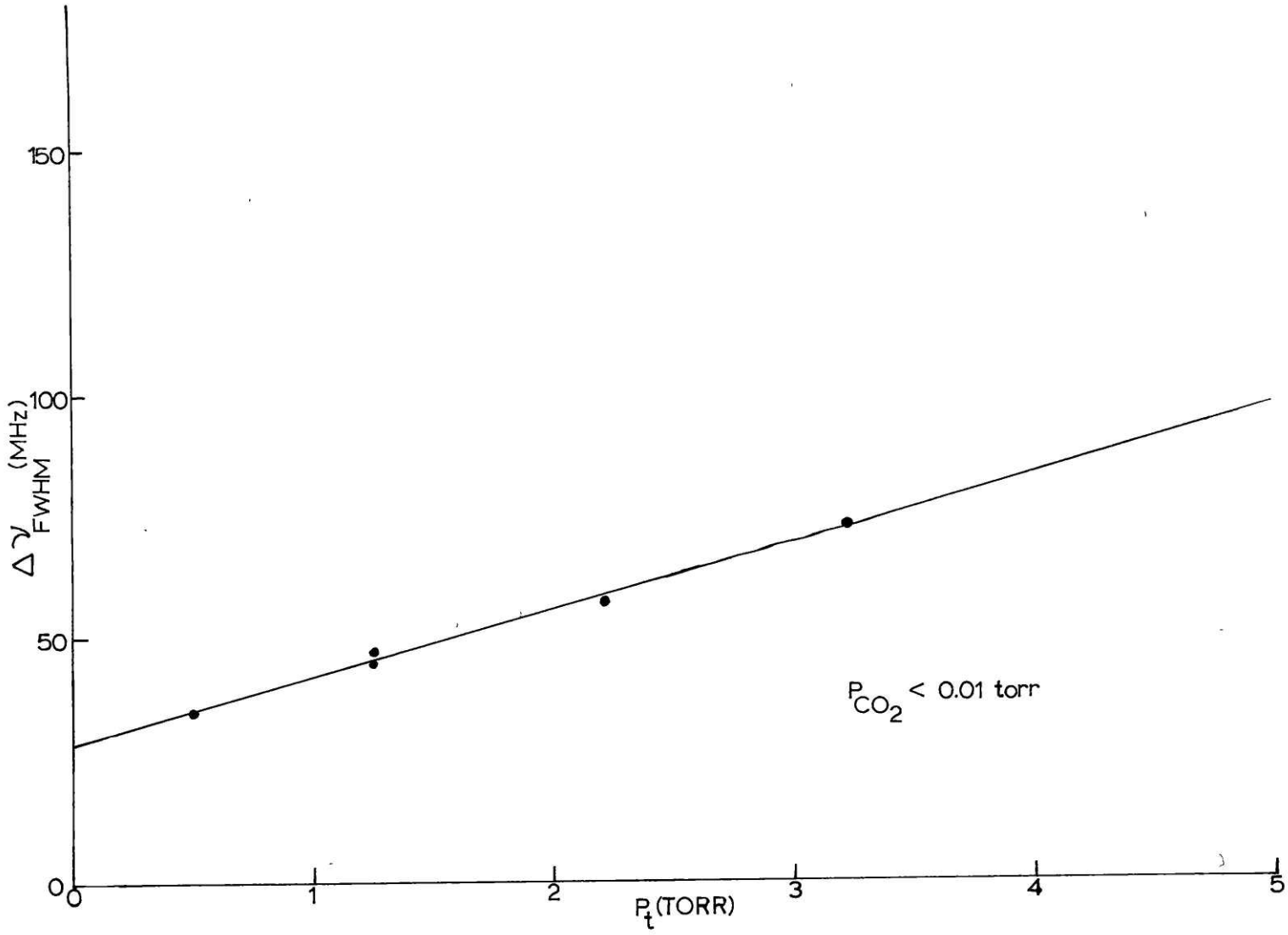

FIGURE 5.5

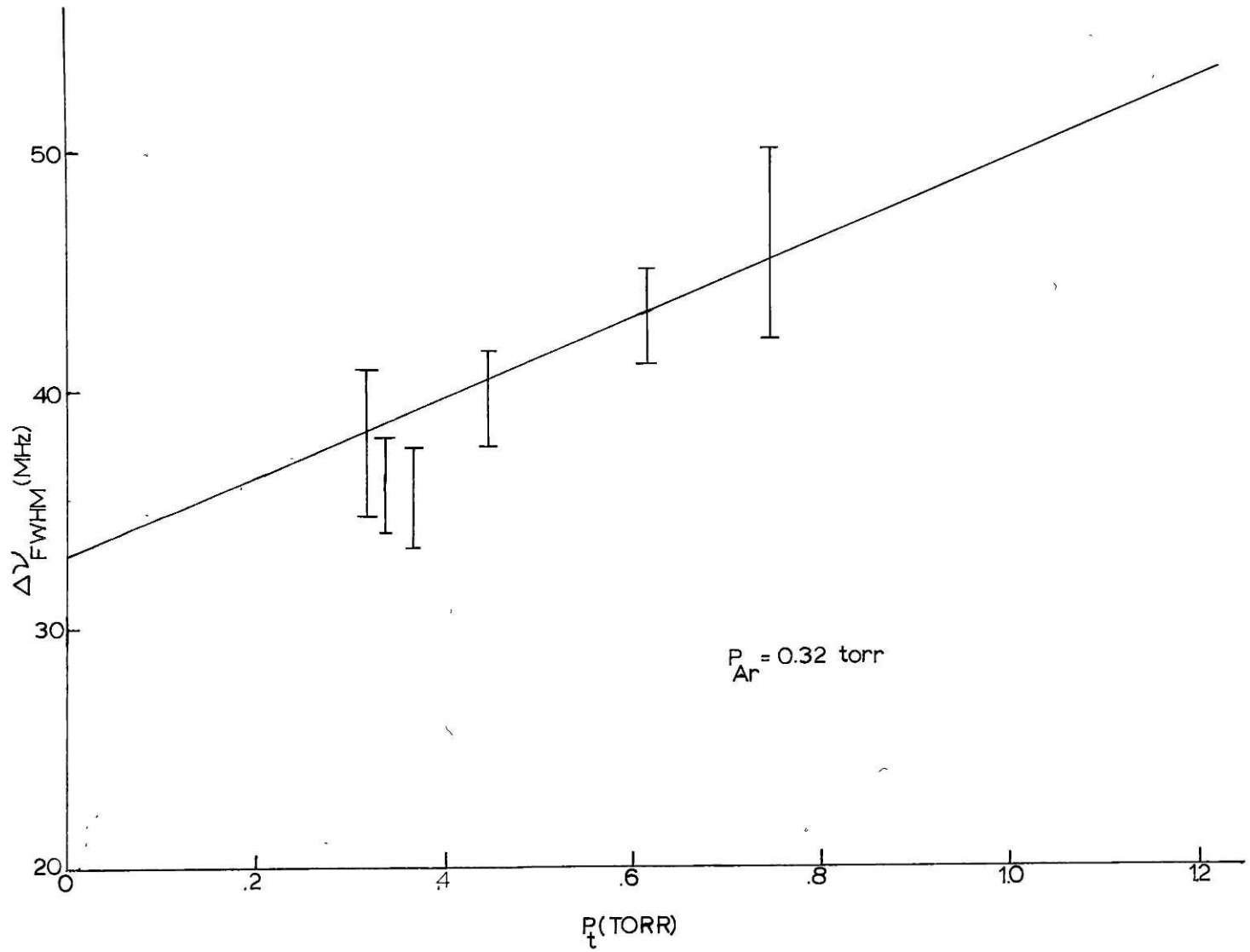

FIGURE 5.6

and 5.5 and yield[†]:

$$k_{Ar}^{T} = 8.8 \pm 1.3 \times 10^{7} sec^{-1} torr^{-1} = 4.3 \pm 0.6 \times 10^{-9} cm^{3} sec^{-1} \quad (5.28a)$$

$$k_{CO_2}^{T} = 1.19 \pm 0.19 \times 10^{8} sec^{-1} torr^{-1} = 5.9 \pm 0.9 \times 10^{-9} cm^{3} sec^{-1} \quad (5.28b)$$

$$k_{rad} = 1.68 \pm 0.13 \times 10^{8} sec^{-1} \text{ or } \tau_{rad} = 6.0 \pm 0.5 \times 10^{-9} sec \quad (5.28c)$$

In terms of cross sections,

$$\sigma_{Ar}^{T} = \langle w_{Ar} \rangle^{-1} k_{Ar}^{T} = 870 \pm 120 \text{ A}^2 \quad (5.29a)$$

$$\sigma_{CO_2}^{T} = \langle w_{CO_2} \rangle^{-1} k_{CO_2}^{T} = 1\,230 \pm 190 \text{ A}^2 \quad (5.29b)$$

where $\langle w_2 \rangle = \frac{(kT)^{\frac{1}{2}}}{2} \left[\left(\frac{\pi}{m_1} \right)^{\frac{1}{2}} + \frac{4}{(\pi m_2)^{\frac{1}{2}}} \right]$ is the mean square relative speed for particle 1 (BaO) colliding with particle 2 (Ar or CO_2) when $v_{1x} = 0$ has been selected.[48] The collision rates in Eq. 5.28 are total rates including all quenching and relaxation mechanisms as well as phase changing collisions and are upper bounds to $A^1\Sigma^+$ relaxation

---

[†]In converting from $sec^{-1}torr^{-1}$ to cm^3sec^{-1} in Eqs. 5.28a and 5.28b the ideal gas equation, P = nkT, has been used with $T=[\Delta\nu_D c^2 M/8\nu_o R \ln 2] = 475K$ where $\Delta\nu_D = 790MHz$ is the observed $A^1\Sigma^+ - X^1\Sigma^+$ Doppler width, M is the BaO molecular mass and R is the gas constant.[40]

processes since line width contributions from TPT, $C^1\Sigma^+$ relaxation, and VCC are neglected. Identical line width vs. pressure curves (Fig. 5.5 and 5.6) are obtained for $J_o = 0$ through 15.

The value of τ_{rad} in Eq. 5.28c is significantly different from the vibrationaly and rotationally averaged $C^1\Sigma^+$ radiative lifetime of 25 $\pm$ 10 nsec reported by Torres-Filho and Pruett (TP) by pulsed dye laser excitation of $C^1\Sigma^+ \leftarrow X^1\Sigma^+$ and subsequent temporal monitoring of $C^1\Sigma^+ \rightarrow X^1\Sigma^+$ fluorescence[37a]. Because of $C^1\Sigma^+$ perturbations (Chapter 3), τ_{rad} is expected to vary with both vibration and rotation; in fact Pruett recently measured $C^1\Sigma^+$ lifetimes for individual rotational levels near the v= 3 vibrational origin and found τ = 14 $\pm$ 1 nsec[37b]. Nonetheless, a discrepancy still exists between this value and that of Eq. 5.28c. As mentioned above, power broadening is not detectable without the focussing lens. Transit time broadening resulting from molecules leaving the field of interaction can also be neglected since the beam waist, u, without the focussing lens (1/e distance from maximum intensity) is $\simeq$ 0.8 cm and the average BaO speed transverse to $\hat{x}$ is 1.47 x 10^4 cm sec^{-1} so that:

$$\tau_{trans} \simeq \frac{u}{\langle v_1 \rangle} \simeq 5 \times 10^{-5} \text{ sec}$$

$$\Delta\nu_{trans} = \frac{1}{2\pi\tau_{trans}} \approx 3 \times 10^3 \text{ Hz.} \qquad (5.30a)$$

Residual Doppler broadening owing to beam misalignment is small:

$$\Delta\nu_D = \frac{\nu_o \langle v^2 \rangle^{\frac{1}{2}}}{C}\theta \lesssim 5 \times 10^6 \text{ Hz} \qquad (5.30b)$$

where $\Delta\nu_D$ is the residual Doppler width, $\langle v^2 \rangle^{\frac{1}{2}}$ the BaO rms speed, and θ is the angle between the pump and probe estimated to be less than 0.01 rad; this correction results in only a 1 nsec increase in the lifetime. It seems likely, therefore, that $\Delta\nu_{FWHM}$ varies in a non-linear fashion at low pressures (< 0.3 torr) where VCC can no longer be neglected with respect to Lorentz broadening. This non-linear behavior has been observed in other systems[11,29,30]. It follows that extrapolation of the lines in Figs. 5.5 and 5.6 to zero pressure leads to a lower bound for the $C^1\Sigma^+$ radiative lifetime not inconsistent with the values measured by Pruett et al.[37]

2. Satellite lines

As expected (Section II.B.), satellite line shapes cannot be represented as simple Lorentzians or Gaussians: velocity randomization results in broadening comparable to the homogeneous linewidth.

Fig. 5.7 illustrates the dependence of the R(14) collisional satellite ($\Delta J = -1$) line width, $\Delta\nu_{FWHM}$, upon Ar pressure for a CO_2 pressure less than 0.01 torr (without the focussing lens). $\Delta\nu_{FWHM}$ is seen to vary linearly with Ar pressure with a slope of 27 ± 2 MHz $torr^{-1}$ and an intercept of 66 ± 3 MHz. Because of velocity randomization, the satellite-width pressure slope and intercept are greater than the corresponding principal-line-width slope and intercept.

Fig. 5.8 illustrates the R(14) ($\Delta J = -1$) satellite line width dependence upon CO_2 pressure for an Ar pressure of 0.31 torr. A dramatic decrease of 30% in line width is observed upon addition of only 0.06 torr CO_2. This should be contrasted with the principal line width dependence on CO_2 pressure (Fig. 5.6) where a monotonic, linear increase in line width is observed. This line narrowing may be understood by examination of Eqs. 5.9, 5.10, and 5.17: the mass change from Ar to CO_2 (40 amu as opposed to 44 amu) would be expected to result in slightly larger frequency shifts for CO_2 (i.e. broader lines); however, if ψ is smaller ($\cos\psi$ larger) for CO_2 than for Ar, smaller frequency shifts,or narrower lines,are predicted. Thus, Fig. 5.7 implies smaller angle scattering for CO_2 than for Ar. This effect is not apparent in Fig. 5.6, $\Delta J = 0$, because velocity

Figure 5.7: $C^1\Sigma^+ \leftarrow A^1\Sigma^+$ (3,1) R(14) collisional satellite line width ($\Delta J = -1$) vs. total pressure, P_t, for fixed $P_{CO_2} < 0.01$ torr. Line is linear least squares fit with slope = 27 ± 2 MHz $torr^{-1}$ and intercept = 66 ± 3 MHz. Error bars are 1σ estimates.

Figure 5.8: Same as Fig. 5.6 except for fixed $P_{Ar} = 0.31$ torr.

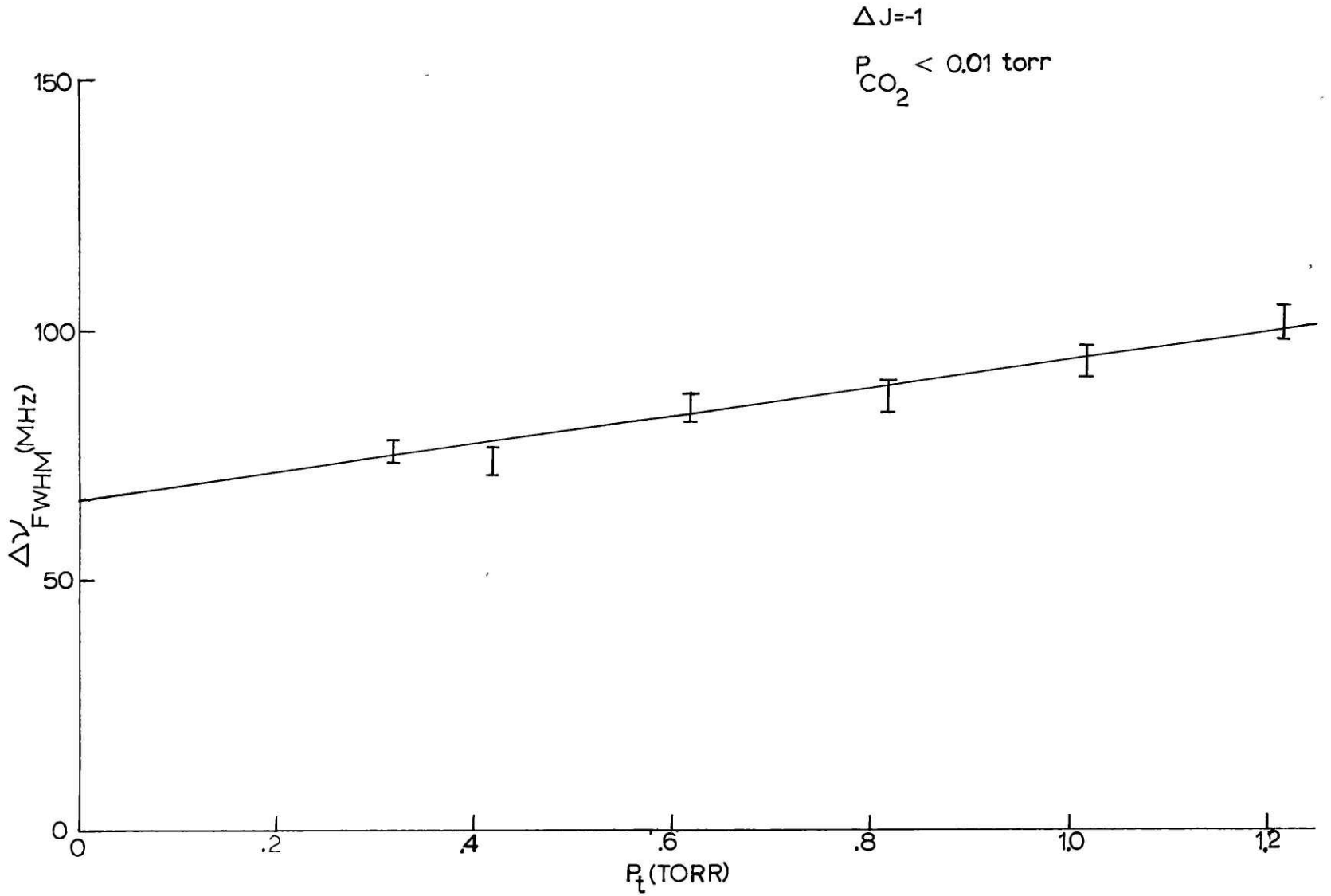
ΔJ=-1
P_{CO_2} < 0.01 torr
150
100
50
0
$\Delta\nu_{FWHM}$ (MHz)
0
.2
.4
.6
.8
1.0
1.2
P_t (TORR)

FIGURE 5.7

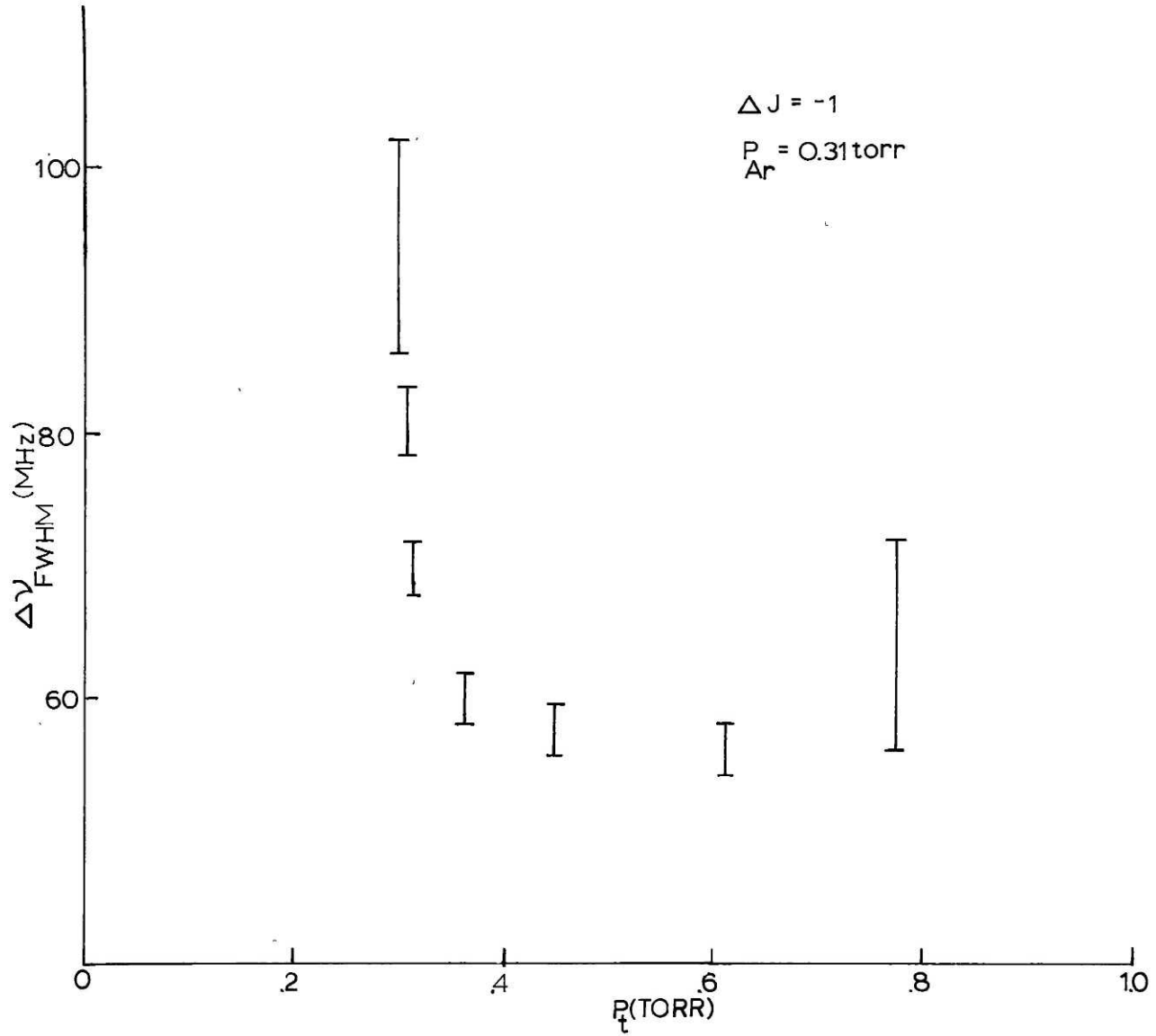

FIGURE 5.8

randomization for Ar as well as CO_2 is minimal when J is not changed; increases in pressure merely increase the collisional deactivation and dephasing rates.

Fig. 5.9 illustrates the variation in line width with ΔJ for $J_o = 15$ at an Ar pressure of 0.31 torr and a CO_2 pressure of 0.01 torr; the monotonic increase of $\Delta\nu_{FWHM}$ with $|\Delta J|$ exhibited in Fig. 5.8 is observed for all pressures and for different J_o. Two mechanisms for this phenomenon are possible: (1) ψ increases, $\cos\psi$ decreases, monotonically with ΔJ under single collision conditions; and, (2) large changes in ΔJ result from a series of small ΔJ collisions,each of which randomizes v_x. It is certain that the latter mechanism is important (see discussion below of multiple collision effects). When satellite line widths are linearly extrapolated to zero pressure,the monotonic increase of $\Delta\nu_{FWHM}$ with J seems to persist but the non-linear dependence of $\Delta\nu_{FWHM}$ on pressure (see discussion above) precludes drawing a definite conclusion concerning the importance of the former mechanism.

Eqs. 5.9, 5.10, and 5.16 predict that VCC frequency shifts should scale with initial v_{1x} selected. Thus if $|v_{1x}| > 0$ is selected, satellite line profiles are expected to be asymmetric and shaded towards ν_o ($v_{1x} = 0$) for $\psi \neq 0$. Principal and satellite excitation line shapes

Figure 5.9: $C^1\Sigma^+ \leftarrow A^1\Sigma^+$ (3,1) excitation line widths as a function of J for $J_o = 15$. Δ data denote <u>without</u> focussing lens. All other data are <u>with</u> focussing lens and are power broadened. Error bars are 1σ estimates.

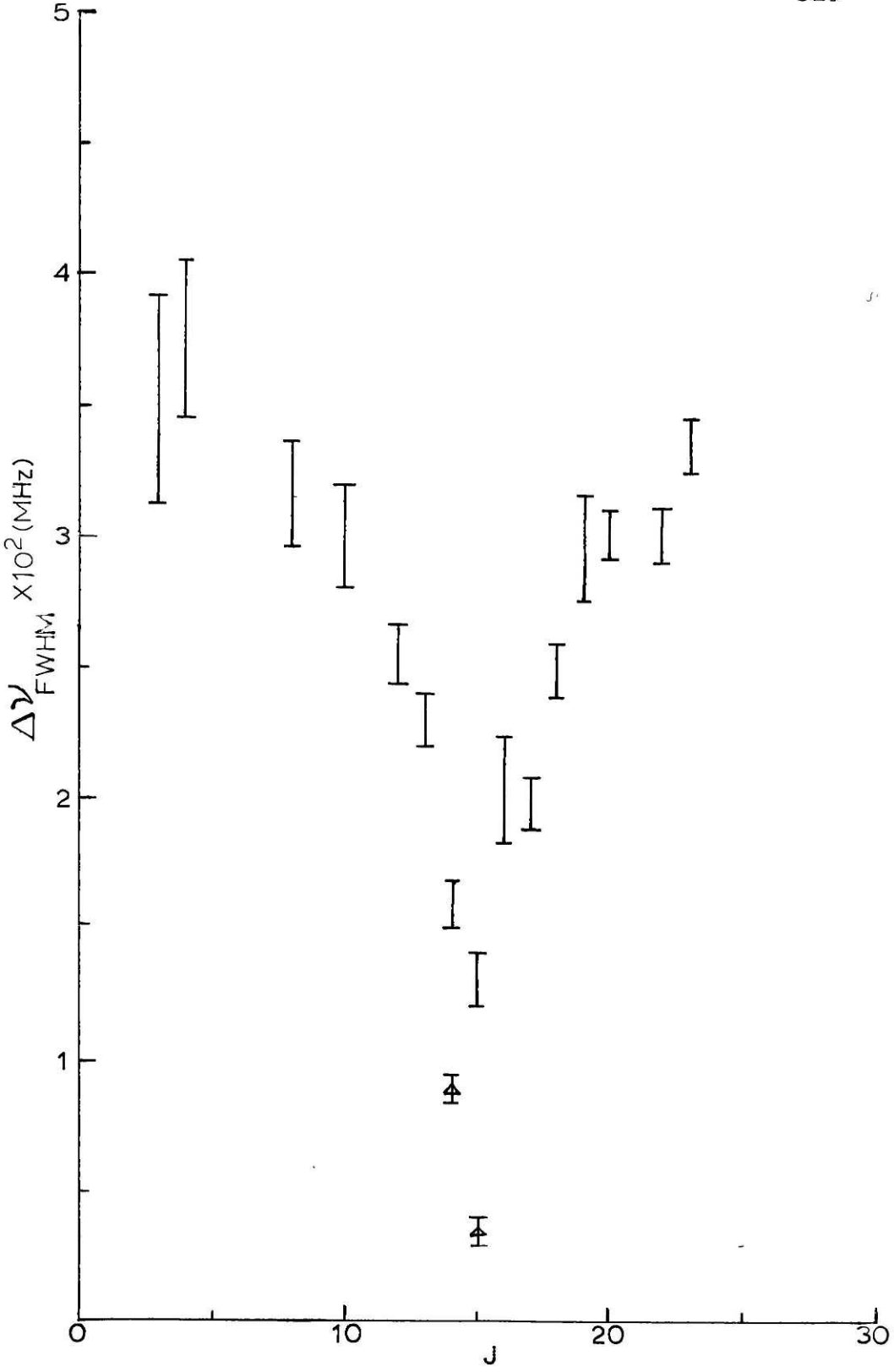

FIGURE 5.9

for $J_o = 11$ and $v_{1x} = + 4.27 \times 10^4$ cm sec^{-1} ($\nu-\nu_o = + 720$ MHz), taken with the focussing lens for optimal signal to noise, are shown in Fig. 5.10. Focussing both lasers not only power broadens these lines but also increases the TPT probability resulting in a slight asymmetry for the principal, R(11), line[42,43]: without the focussing lens, the principal is symmetric whereas satellite lines remain asymmetric. The line asymmetry clearly increases with $|\Delta J|$ (see Fig. 5.10) consistent with the $v_{1x} = 0$ results displayed in Fig. 5.9.

As described above (Section II.B.), excitation line shapes can be deconvoluted when the homogeneous line shape function is known. Neglecting $\Delta J=0$ velocity randomization and TPT, permits deconvolution of satellite line profiles, assuming that the homogeneous line shape is only a function of Ar and CO_2 pressure and not of J. This assumption appears to be valid since the same width vs. pressure curves (Figs. 5.5 and 5.6) are obtained for different values of J_o. Thus G in Eq. 5.18 is a simple Lorentzian with pressure dependent FWHM given by Figs. 5.4 and 5.5. Since the spectra were recorded onto graph paper (see Chapter 3), it was necessary to first digitize the data by hand before using the Fast Fourier Transform (FFT) algorithmn[49,†] to deconvolute $I(\nu)$

[†]MIT IPC library routine FOURT.

Figure 5.10: $C^1\Sigma^+ \leftarrow A^1\Sigma^+$ (3,1) OODR excitation spectrum with focussing lens for $J_o = 11$ and $v_{lx} = 4.27 \times 10^4$ cm sec^{-1}. Note asymmetry in line shapes with shading towards ν_o ($v_{lx} = 0$). Slight asymmetry in R(11) (off scale) principal line results from two-photon transitions and not velocity randomization (see text).

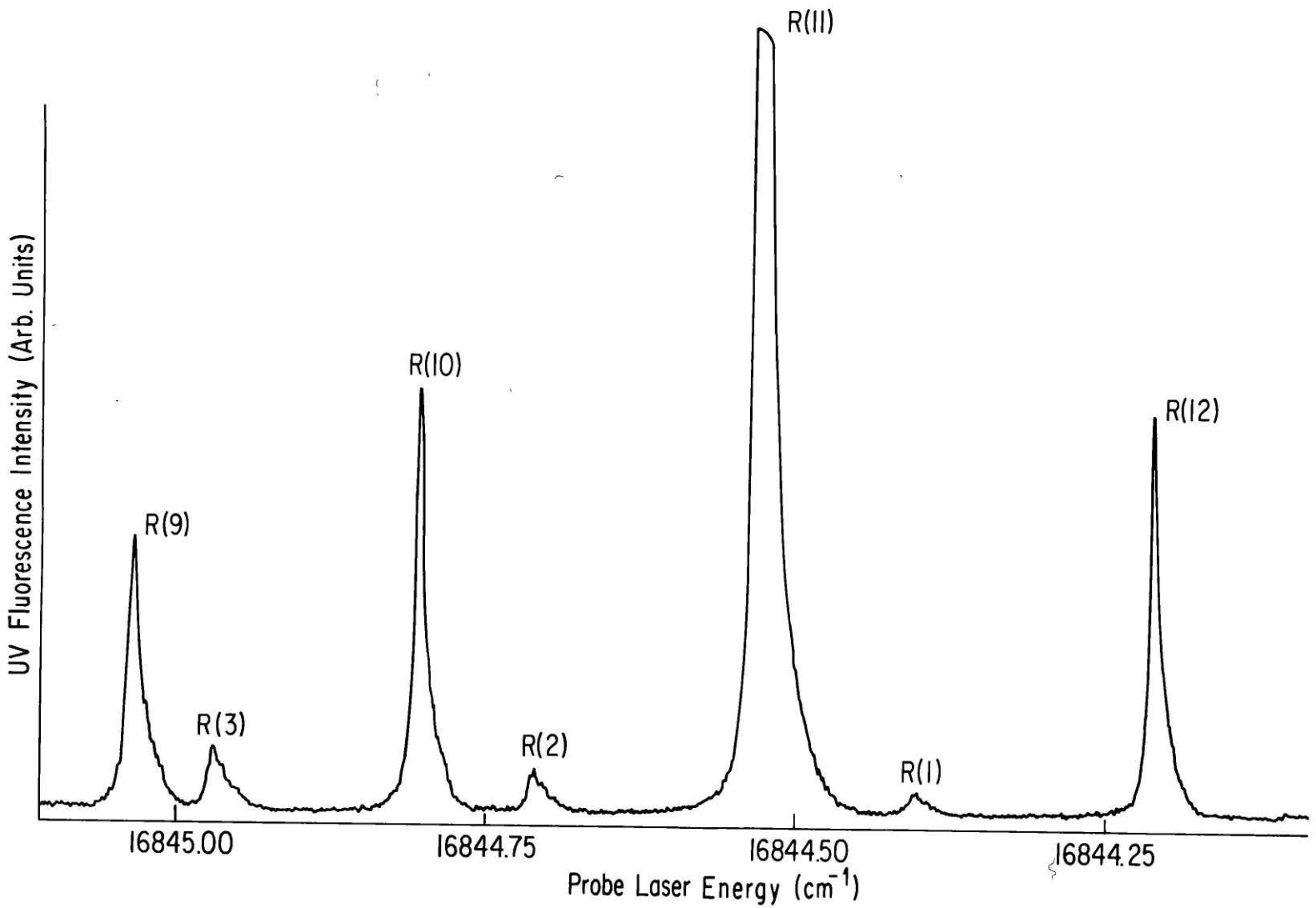
R(11)
R(10)
R(12)
R(9)
R(3)
R(2)
R(1)
UV Fluorescence Intensity (Arb. Units)
16845.00
16844.75
16844.50
16844.25
Probe Laser Energy (cm⁻¹)

FIGURE 5.10

according to Eq. 5.19 and obtain the v_x distribution, V. Unfortunately, hand digitization reduced the signal to noise ratio (S/N) from ≈ 200 to ≈ 30. Poor S/N complicates deconvolution because high frequency noise in $I(\nu)$ is amplified when I* is divided by G* (Eq. 5.19). Since I is a slowly varying function, high frequency components of I* result largely from noise; setting these frequency components to zero acts as a filter on I and reduces the noise in V. However, as more and more frequency components of I* are zeroed, information on V is lost. Figures 5.11 and 5.12 illustrate the results of this procedure for the R(14) satellite line ($\Delta J = -1$) at $P_{Ar} = 0.32$ torr and $P_{CO_2} = 0.05$ torr ($G(\nu-\nu_o)$ is illustrated in Fig. 5.3). The line shape was digitized into 128 bits over the frequency range $\Delta\nu = -138$ to + 136 MHz (triangles); the lines in Figs.5.10 and 5.11 are the $V(\nu)$ distributions obtained when I* components 24 to 128 and 14 to 128 were zeroed, respectively (0 and 128 correspond to lowest and highest frequency components respectively). In order to test for distortion, I* was inversely transformed after zeroing to obtain I. Fig. 5.13 shows the maximum distortion resulting from zeroing components 14 to 128. It is apparent from Figs. 5.11 and 5.12 that V is poorly determined (the oscillations are spurious) even when 114 components are discarded; however, first and second

Figure 5.11: R(14) satellite line ($\Delta J = -1$) (triangles) at $P_{AR} = 0.32$ torr and $P_{CO_2} = 0.05$ torr with deconvoluted $V(\nu)$ distribution (line) obtained when $I^*(t)$ components 24 through 128 were zeroed. Noise in experimental line profile results from hand digitization of data.

Figure 5.12: Same as Fig. 5.10 except $I^*(t)$ components 14 through 128 were zeroed. Note broadening of $V(\nu)$ relative to Fig. 5.11.

Figure 5.13: Same as Fig. 5.11 except line is $I(\nu)$, R(14) satellite line shape, obtained by zeroing $I^*(t)$ components 14 through 128 and then inverse Fourier transforming.

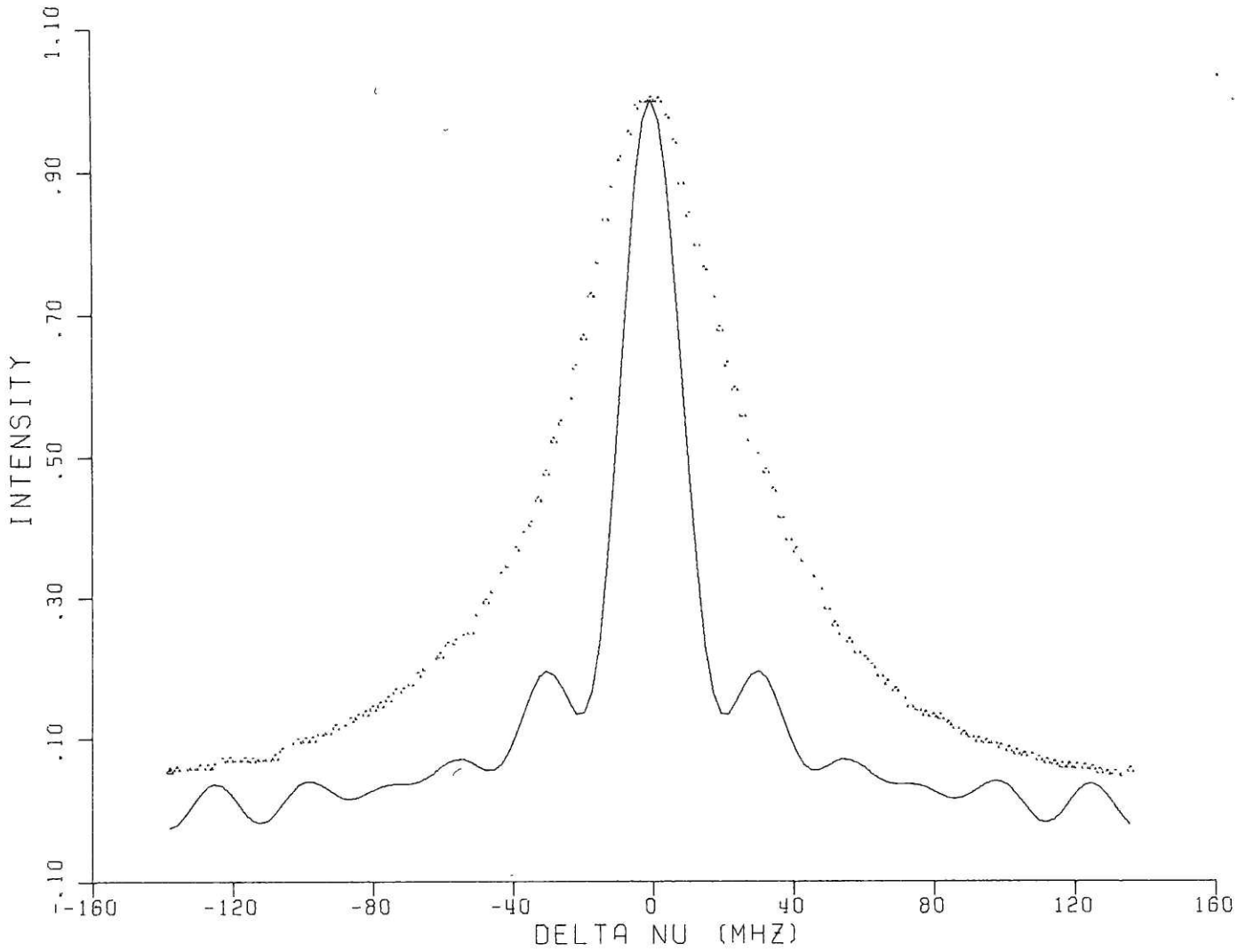
INTENSITY
1.10
.90
.70
.50
.30
.10
-.10
-160
-120
-80
-40
0
40
80
120
160
DELTA NU (MHZ)

FIGURE 5.11

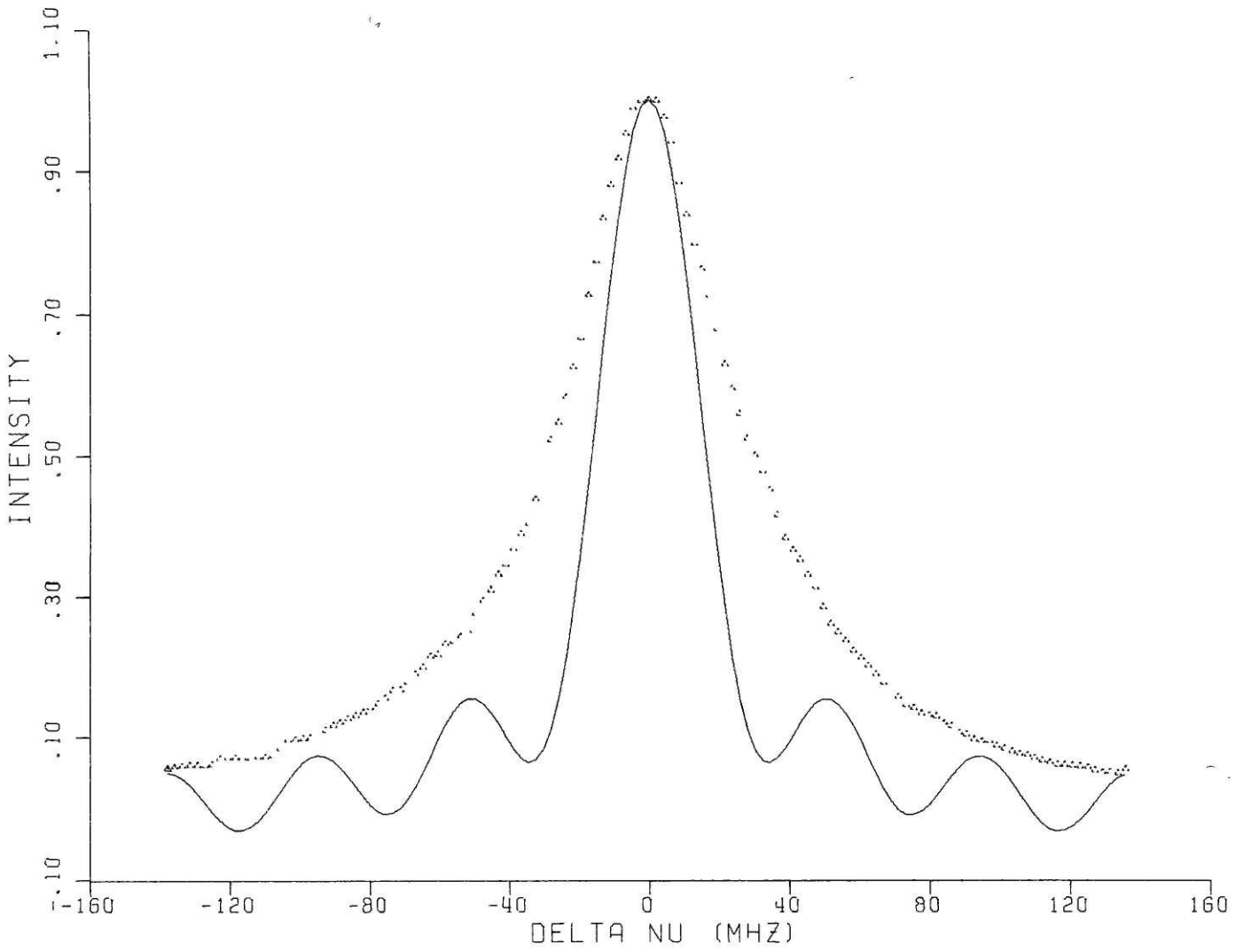
INTENSITY
1.10
.90
.70
.50
.30
.10
-.10
-160
-120
-80
-40
0
40
80
120
160
DELTA NU (MHZ)

FIGURE 5.12

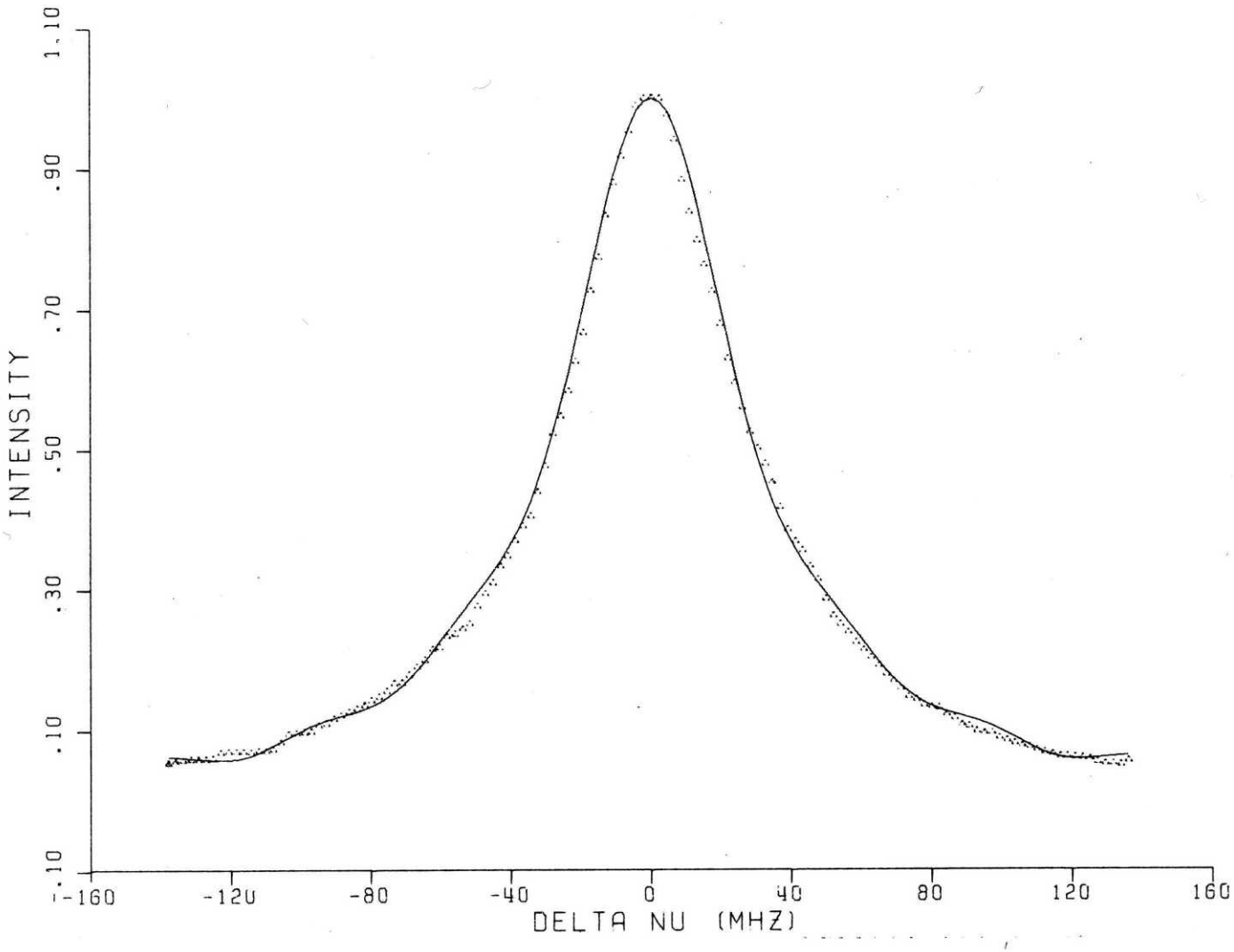
INTENSITY
1.10
.90
.70
.50
.30
.10
-.10
-160
-120
-80
-40
0
40
80
120
160
DELTA NU (MHZ)

FIGURE 5.13

moments of V are found to be relatively insensitive to component zeroing and $\langle\cos\psi\rangle$ is estimated in Table 5.1. $\langle\cos^2\psi\rangle$ obtained by simultaneously solving Eqs. 5.10 and 5.17 is negative which results from underestimating $\langle\langle\delta\nu_1^2\rangle\rangle_o$ by numerical computation over only a finite range of ν. $\langle\langle\delta\nu_1\rangle\rangle_o$ is less sensitive to truncation of V and yields[†]:

$$\begin{aligned} \langle\cos\psi\rangle &= 0.5 \pm 0.1 \\ \langle\psi\rangle &\equiv \arccos\langle\cos\psi\rangle = 60 \pm 6^o \\ \langle\langle\delta v_{1x}\rangle\rangle &= c/\nu_o \langle\langle\delta\nu_1\rangle\rangle_o = 1.3 \pm 0.2 \times 10^3 \text{cm sec}^{-1} \end{aligned} \tag{5.31}$$

Note that the values quoted in Eq. 5.31 represent averages over multiple collisions with both Ar and CO_2.

B. Rotational State to State Rate Constants

As mentioned above (Section II.C.), $A^1\Sigma^+$ rotational populations are measured by monitoring $A^1\Sigma^+ \rightarrow X^1\Sigma^+$ resolved fluorescence or probing $C^1\Sigma^+ \leftarrow A^1\Sigma^+$ and detecting $C^1\Sigma^+ \rightarrow X^1\Sigma^+$ fluorescence. The former method is used for J levels greater than 20 where P and R branches (J'-J" = -1 and +1, respectively, where J' denotes upper

---

[†]A 1σ error of 3 MHz in $\langle\langle\delta\nu_1\rangle\rangle_o$ is estimated from the spread of red and blue average shifts in Table 5.1 and gives the uncertainties quoted in Eq. 5.31.

Table 5.1: Deconvolution of $I(\nu)$[a] and Moments of $\cos\psi$

Components Zeroed	$\langle\langle\delta\nu_1\rangle\rangle^{Red}$ (MHz)	$\langle\langle\delta\nu_1\rangle\rangle^{Blue}$ (MHz)	$\langle\langle\delta\nu_1^2\rangle\rangle$ (MHz^2)	$\langle\cos\psi\rangle$[b]	$\langle\cos^2\psi\rangle$[c]
34 to 128	-26	18	2367	0.50	-4
24 to 128	-23	21	2245	0.50	-4
14 to 128	-24	21	2312	0.50	-4

[a] R(14) satellite ($\Delta J = -1$) with $P_{AR} = 0.32$ torr, $P_{CO_2} = 0.05$ torr, and $G(\nu-\nu')$ equal to a Lorentzian with FWHM = 34.24 MHz.

[b] Average of values obtained from using red and blue average shifts in Eq. 5.10 with $\nu_o = 5.0530166 \times 10^{14}$ Hz and $m_2 = 42$ amu (average of m_{AR} and m_{CO_2}).

[c] From simlutaneous solution of Eqs. 5.10 and 5.17.

and J" denotes lower level of transition) are resolvable; OODR is used for population probes at low J near the bandhead and origin. In order to convert line intensities to populations, a form for the M sub-level distribution, f(M), (see Eq. 5.20) must be assumed. Two models are considered: (1) M is conserved upon collision so that f(M) is determined by the pump transition and (2) M is completely randomized upon collision so that $f(M) = (2J+1)^{-1}$. It is <u>always</u> assumed that f(M) for J_o is determined by the A ← X pump transition. (This assumption is justified in Chapter 6.) Table 5.2 presents intensity factors (corresponding to terms in Eq. 5.20) for both f(M) models and for both A → X fluorescence and C ← A OODR, monitoring. Table 5.3 presents intensity expressions divided by n_J, I_J/n_J, for the detection geometries described in Section III for both f(M) models. The frequency dependence of excitation and fluorescence factors is neglected since the maximum variation is $\sim$ 2% (ν^3 factor) over the range of J levels sampled compared with an experimental uncertainty in intensity ratios of 20%. The detection factor of 0.5 for resolved $\hat{Z}$ polarized fluorescence results from the polarization dependence of grating reflection; note that this factor conveniently (and coincidentally) makes the A → X (1,1) probe insensitive to the form of f(M).

Table 5.2: Rotational Intensity Factors[a]

Monitor	f(m)	E^{μ} (R branch)	$F^{\mu'}$ (R branch)	$F^{\mu'}$ (P branch)	$D^{\mu'}$ [c]
OODR $\mu = \hat{Z}$ $\mu' = \hat{X} = \hat{Y}$	$[2J+1]^{-1}$	$\frac{(J+1)^2 - M^2}{(2J+1)(2J+3)}$	$\frac{J(J+1)+M^2}{2(2J+3)(2J+1)}$	$\frac{(J+3)(J+2)+M^2}{2(2J+3)(2J+5)}$	1
OODR $\mu = \hat{Z}$ $\mu' = \hat{X} = \hat{Y}$ R pump	$\frac{J_o^2 - M^2}{J_o(2J_<+1) - \frac{1}{3}J_<(J_<+1)(2J_<+1)}$ [b]	$\frac{(J+1)^2 - M^2}{(2J+1)(2J+3)}$	$\frac{J(J+1)+M^2}{2(2J+3)(2J+1)}$	$\frac{(J+3)(J+2)+M^2}{2(2J+3)(2J+5)}$	1
$A \rightarrow X(1,1)$ $\mu' = \hat{Y}$	$[2J+1]^{-1}$	1	$\frac{J(J-1)+M^2}{2(4J^2-1)}$	$\frac{(J+1)(J+2)+M^2}{2(2J+1)(2J+3)}$	1
$A \rightarrow X(1,1)$ $\mu' = \hat{Z}$	$[2J+1]^{-1}$	1	$\frac{J^2 - M^2}{4J^2-1}$	$\frac{(J+1)^2 - M^2}{(2J+1)(2J+3)}$	0.5
$A \rightarrow X(1,1)$ $\mu' = \hat{Y}$ R pump	$\frac{J_o^2 - M^2}{J_o^2(2J_<+1) - \frac{1}{3}J_<(J_<+1)(2J_<+1)}$ [b]	1	$\frac{J(J-1)+M^2}{2(4J^2-1)}$	$\frac{(J+1)(J+2)+M^2}{2(2J+1)(2J+3)}$	1
$A \rightarrow X(1,1)$ $\mu' = \hat{Z}$ R pump	$\frac{J_o^2 - M^2}{J_o^2(2J_<+1) - \frac{1}{3}J_<(J_<+1)(2J_<+1)}$ [b]	1	$\frac{J^2 - M^2}{4J^2-1}$	$\frac{(J+1)^2 - M^2}{(2J+1)(2J+3)}$	0.5

[a] J_o and J denote initial and final (collisionally populated) $A^1\Sigma^+$ levels, respectively. $J_<$ denotes the lesser of J_o and J. R and P branch mean J'-J" = +1 and -1 respectively, where J' is upper and J" is lower level rotational quantum number. f, E, F, and D are defined by Eq. 5.20; only those polarizations relevant to this work

Table 5.2 (continued) (Footnotes)

are considered.

[b] For R branch $\hat{Z}$ polarized pumping only. When J_o was prepared by pumping $A^1\Sigma^+ \leftarrow X^1\Sigma^+$ (1,0) P(1) with $\hat{Z}$ polarization, f(M) = 1 always when M is conserved since only M = 0 exists for $J_o = 0$.

[c] Determined from grating reflection efficiency vs. polarization curve at λ = 600 nm corresponding to $A^1\Sigma^+ \rightarrow X^1\Sigma^+$ (1,1) emission.

Table 5.3: Summed Line Intensities[a]

Monitor	Model	I_J/n_J
OODR $\mu=\hat{Z}$ $\mu'=\hat{X}+\hat{Y}$	M randomized[c]	$(2J+1)^{-2}(2J+3)^{-2}\{A[\alpha'(J+1)^2-\beta']+B[\beta'(J+1)^2-\gamma']\}$
	M conserved R pump	$(\alpha J_o^2-\beta)^{-1}(2J+1)^{-1}(2J+3)^{-2}\{A[\alpha J_o^2(J+1)^2-[\beta[J_o^2+(J+1)^2]+\gamma]+$ $+B[\beta J_o^2(J+1)^2-\gamma[J_o^2+(J+1)^2+\delta]\}$
P+R branch[b] fluorescence	M conserved P(1) pump	$(2J+1)^{-1}(2J+3)^{-2}(J+1)^2\ A$
A→X(1,1) $\mu'=\hat{X}+\hat{Z}$ R branch	M randomized[c] or M conserved	$\frac{J}{2(2J+1)}$
A→X(1,1) $\mu'=\hat{X}+\hat{Z}$ P branch	M randomized[c] or M conserved	$\frac{J+1}{2(2J+1)}$

where

$$A = (2J+5)^{-1}(J+3)(J+2)+(2J+1)^{-1}\ J(J+1)$$

$$B = (2J+5)^{-1}+(2J+1)^{-1}$$

$$\alpha = (2J_<+1)$$

$$\beta = \sum_{M=-J_<}^{J_<}(M^2) = \frac{1}{3}\ J_<(J_<+1)(2J_<+1)$$

$$\gamma = \sum_{M=-J_<}^{J_<}(M^4) = \frac{1}{15}\ J_<(J_<+1)(2J_<+1)(3J_<^2+3J_<-1)$$

Table 5.3: (continued)

$$\delta = \sum_{M=-J}^{J_<} M^6 = \frac{1}{21} J_<(J_<+1)(2J_<+1)(3J_<^4 + 6J_<^3 - 3J_<+1)$$

α', β', and γ' are defined analogously to α, β, and γ with J substituted for $J_<$.

[a] See Table 5.2 footnote a.

[b] $C\,^1\Sigma^+ \rightarrow X\,^1\Sigma^+$ P and R branch fluorescence was not resolved.

[c] Valid for P or R branch pumping.

Using the factors in Table 5.3, it is found for OODR probing that the maximum discrepancy between ratios of n_J's calculated with the two f(M) models is $\sim$ 20%; since this is comparable to experimental error, the M conserved distribution is assumed in what follows below.

Intensities as a function of J were measured for $J_o = 0$ and $J_o = 15$ over a range of Ar and CO_2 partial pressures and then converted to relative populations using the M conserved model factors in Table 5.3. The results are given in Tables 5.4 and 5.5. Fig. 5.13 illustrates the results for $J_o = 0$, $P_{AR} = 0.33$ and 0.82 torr, and $P_{CO_2} = 0.01$ torr. Propensities for small ΔJ changes are observed: $k(\Delta J = 1) > k(\Delta J = 2) > k(\Delta J = 3)$. For $\Delta J > 3$, level populations do not vary significantly even at the lowest pressures attained. ($P_{AR} = 0.33$ torr, $P_{CO_2} = 0.01$ torr).

Fig. 5.14 compares population ratios, n_J/n_{J_o}, for $J_o = 0$ and 15 as a function of ΔJ.

To obtain pressure dependent, single collision $J_o \rightarrow J$ rates, the data of Tables 5.4 and 5.5 are inverted according to Eq. 5.25b; the results are given in Tables 5.6 and 5.7 for $|\Delta J| = 1$ to 4 and compared to the corresponding population ratios[†].

[†]Because of blending in the bandhead, populations for J = 5,6, and 7, necessary to determine the $T(\Delta J)$ in Table 5.6 for J_o=0 (see Sec. II.C.2), were interpolated.

Table 5.4: Population Ratios for $J_o = o$[a]

P_{Ar} = 0.33 torr, P_{CO_2} = 0.01 torr	
J	n_J/n_{J_o}
0	1.000
1	0.132
2	0.077
3	0.057
4	0.047
5	(0.041)
6	(0.036)
7	(0.030)
8	0.024
9	0.032
10	0.032
11	0.035
12	0.024
13	0.021
14	0.022
15	0.021
16	0.024
17	(0.02)
18	(0.02)
19	(0.015)
20	(0.015)

[a]Population ratios obtained from intensity ratios based on M conserved model (see Text and Table 5.3). 1σ uncertainties are estimated to be 20%. Numbers in parenthesis are interpolated or extrapolated values (see text).

Table 5.4: (cont.)

P_{Ar} = 0.33 torr, J	P_{CO_2} = 0.12 torr n_J/n_{J_o}
0	1.000
1	0.168
2	0.094
3	0.071
4	0.061
5	(0.054)
6	(0.046)
7	(0.039)
8	0.032
9	0.020
10	0.040
11	0.030
12	0.029
13	(0.030)
14	0.031
15	0.021
16	0.033
17	0.027
18	(0.02)
19	(0.015)
20	(0.015)

Table 5.4: (cont.)

P_{Ar} = 0.33 torr, P_{CO_2} = 0.27 torr

J	n_J/n_{J_o}
0	1.000
1	0.165
2	0.128
3	0.079
4	0.060
5	0.055
6	0.040
7	0.053
8	0.030
9	0.040
10	0.030
11	(0.02)
12	(0.02)
13	(0.015)
14	(0.01)
15	(0.01)
16	(0.01)
17	(0.005)
18	(0.005)
19	(0.005)
20	(0.005)

Table 5.4: (cont.)

P_{Ar} = 0.50 torr, P_{CO_2} = 0.01 torr

J	n_J/n_{J_O}
0	1.000
1	0.135
2	0.086
3	0.047
4	0.051
5	(0.046)
6	(0.041)
7	(0.036)
8	(0.032)
9	0.027
10	0.021
11	0.022
12	(0.025)
13	(0.028)
14	0.031
15	0.032
16	0.030
17	0.032
18	0.024
19	(0.02)
20	(0.02)

Table 5.4: (cont.)

P_{Ar} = 0.82 torr, P_{CO_2} = 0.01 torr

J	n_J/n_{J_o}
0	1.000
1	0.182
2	0.127
3	0.091
4	0.088
5	(0.082)
6	(0.076)
7	(0.070)
8	0.064
9	0.066
10	0.074
11	0.062
12	0.067
13	0.073
14	0.072
15	0.067
16	0.067
17	0.072
18	0.064
19	0.056
20	0.053
21	0.078
22	0.065

Table 5.4: (cont.)

P_{Ar} = 0.82 torr, P_{CO_2} = 0.01 torr (cont.)

J	n_J/n_{J_O}
23	0.062
24	0.054
25	0.063
26	0.054
27	0.056
28	0.044
29	0.052
30	0.040
31	0.043
32	0.047
33	0.026
34	0.051
35	0.043
36	0.043
37	0.043
38	0.038
39	0.034
40	0.016
41	0.026

Table 5.4: (cont.)

P_{Ar} = 2.33 torr, P_{CO_2} = 0.01 torr

J	n_J/n_{J_o}
0	1.000
1	0.164
2	0.118
3	0.097
4	0.090
5	(0.088)
6	(0.087)
7	(0.086)
8	0.084
9	0.104
10	0.105
11	0.116
12	0.107
13	0.118
14	0.112
15	0.114
16	0.133
17	0.126
18	0.116
19	0.116
20	0.096
21	0.124
22	0.121
23	0.118

Table 5.4: (cont.)

P_{Ar} = 2.33 torr, P_{CO_2} = 0.01 torr (cont.)

J	n_J/n_{Jo}
24	0.114
25	0.114
26	0.098
27	0.115
28	0.090
29	0.078
30	0.088
31	0.084
32	0.086
33	0.069
34	0.080
35	0.080
36	0.079
37	0.064
38	0.066
39	0.060
40	0.054
41	0.044
42	0.058
43	0.038
44	0.056
45	(0.042)
46	0.028
47	0.026

Table 5.4: (cont.)

P_{Ar} = 2.33 torr, P_{CO_2} = 0.01 torr (cont.)

J	n_J/n_{J_o}
48	0.034
49	0.055
50	0.038

Table 5.5: Population Ratios for $J_o = 15$[a]

P_{Ar} = 0.35 torr, P_{CO_2} = 0.02 torr	
J	n_J/n_{J_o}
0	(0.0005)
1	(0.0023)
2	0.0035
3	0.0062
4	0.0083
5	(0.011)
6	0.014
7	(0.013)
8	0.012
9	0.032
10	0.028
11	0.034
12	0.035
13	0.064
14	0.093
15	1.000
16	0.093
17	0.079
18	0.030
19	0.012

[a]See footnote a in Table 5.4.

Table 5.5: (cont.)

P_{Ar} = 0.35 torr, P_{CO_2} = 0.02 torr (cont.)

J	n_J/n_{J_o}
20	0.050
21	0.039
22	0.027
23	0.037
24	0.036
25	0.038
26	(0.036)
27	(0.033)
28	(0.031)
29	(0.028)
30	0.026
31	0.026
32	0.019
33	0.031
34	0.026
35	0.028
36	0.028
37	(0.026)
38	(0.024)
39	(0.022)
40	(0.019)
41	(0.017)
42	(0.014)

Table 5.5: (cont.)

P_{Ar} = 0.35 torr, P_{CO_2} = 0.02 torr (cont.)

J	n_J/n_{J_o}
43	(0.012)
44	(0.010)
45	(0.01)

Table 5.5: (cont.)

P_{Ar} = 0.35 torr, P_{CO_2} = 0.08 torr

J	n_J/n_{J_o}
0	(0.001)
1	0.003
2	0.0043
3	0.0065
4	0.012
5	(0.014)
6	0.017
7	(0.023)
8	0.029
9	0.043
10	0.047
11	0.047
12	0.059
13	0.080
14	0.144
15	1.000
16	0.141
17	0.098
18	0.068
19	0.079
20	0.042
21	0.041
22	0.041

Table 5.5: (cont.)

P_{Ar} = 0.35 torr, P_{CO_2} = 0.08 torr (cont.)

J	n_J/n_{J_o}
23	0.039
24	0.035
25	0.033
26	0.049
27	0.046
28	0.036
29	0.024
30	0.043
31	0.016
32	0.028
33	0.043
34	0.020
35	(0.022)
36	0.024
37	0.016
38	0.016
39	(0.015)
40	(0.014)
41	(0.013)
42	(0.012)
43	(0.012)
44	(0.011)
45	(0.010)

Table 5.5: (cont.)

P_{Ar} = 0.50 torr, P_{CO_2} = 0.04 torr

J	n_J/n_{J_o}
0	(0.0012)
1	(0.0051)
2	0.0070
3	0.010
4	0.012
5	(0.017)
6	0.022
7	(0.025)
8	0.029
9	0.033
10	0.038
11	0.045
12	0.056
13	0.073
14	0.115
15	1.000
16	0.114
17	0.073
18	0.047
19	0.057
20	0.062
21	0.041
22	0.043
23	0.045

Table 5.5 (cont.)

P_{Ar} = 0.50 torr, P_{CO_2} = 0.04 torr (cont.)

J	n_J/n_{J_o}
24	0.039
25	0.031
26	0.033
27	0.028
28	0.029
29	0.026
30	0.023
31	0.030
32	0.021
33	0.021
34	0.025
35	0.013
36	0.019
37	0.026
38	0.018
39	0.020
40	0.016
41	0.011
42	0.011
43	(0.01)
44	(0.01)
45	(0.01)

Table 5.5: (cont.)

P_{Ar} = 0.77 torr, P_{CO_2} = 0.04 torr

J	n_J/n_{J_o}
0	0.0017
1	0.0071
2	0.010
3	0.013
4	0.015
5	(0.021)
6	0.028
7	(0.034)
8	0.040
9	0.042
10	0.040
11	0.053
12	0.065
13	0.078
14	0.137
15	1.000
16	0.129
17	0.106
18	0.082
19	0.074
20	0.070
21	0.063
22	0.057
23	0.054

Table 5.5: (cont.)

P_{Ar} = 0.77 torr, P_{CO_2} = 0.04 torr (cont.)

J	n_J/n_{J_o}
24	0.053
25	0.044
26	0.044
27	0.043
28	0.041
29	0.034
30	0.038
31	0.033
32	0.034
33	0.028
34	0.025
35	0.028
36	0.028
37	0.022
38	0.021
39	0.021
40	0.020
41	0.018
42	0.016
43	0.016
44	0.014
45	0.013
46	0.016

Table 5.5: (cont.)

P_{Ar} = 0.77 torr, P_{CO_2} = 0.04 torr (cont.)	
J	n_J/n_{J_o}
47	0.013
48	0.010
49	0.0088
50	0.0098

Table 5.6: Single Collision Rates for $J_o = 0$

		$T(\Delta J)$[a]			
P_{Ar}(torr)	P_{CO_2}(torr)	ΔJ = 1	2	3	4
0.33	0.01	0.242 (0.132)[b]	0.110 (0.077)	0.072 (0.057)	0.054 (0.047)
0.33	0.12	0.337 (0.168)	0.133 (0.094)	0.089 (0.071)	0.070 (0.061)
0.33	0.27	0.298 (0.165)	0.182 (0.128)	0.075 (0.079)	0.048 (0.060)
0.50	0.01	0.263 (0.136)	0.131 (0.086)	0.050 (0.047)	0.069 (0.051)
0.82	0.01	0.848 (0.182)	0.440 (0.127)	0.238 (0.091	0.236 (0.088)
2.33	0.01	0.786 (0.164)	0.436 (0.118)	0.300 (0.097)	0.253 (0.090)

[a]Defined by Eq. 5.24. See text for discussion of error estimates.

[b]Population ratios from Table 5.4 are given in parentheses.

Table 5.7: Single Collision Rates for $J_o = 15$

		$T(\Delta J)$[a]							
P_{Ar}(torr)	P_{CO_2}(torr)	$\Delta J = -4$	-3	-2	-1	+1	+2	+3	+4
0.35	0.02	0.037 (0.034)[b]	0.033 (0.035)	0.098 (0.064)	0.159 (0.093)	0.154 (0.093)	0.131 (0.079)	0.017 (0.030)	-0.024 (0.012)
0.35	0.08	0.044 (0.047)	0.067 (0.059)	0.107 (0.080)	0.301 (0.144)	0.281 (0.141)	0.151 (0.098)	0.063 (0.068)	0.126 (0.079)
0.50	0.04	0.050 (0.045)	0.070 (0.056)	0.102 (0.073)	0.213 (0.115)	0.208 (0.114)	0.100 (0.073)	0.033 (0.047)	0.065 (0.057)
0.77	0.04	0.062 (0.053)	0.089 (0.066)	0.107 (0.078)	0.298 (0.137)	0.252 (0.129)	0.179 (0.106)	0.103 (0.082)	0.083 (0.074)

[a] See footnote a in Table 5.6.

[b] Population ratios from Table 5.5 are given in parentheses.

Figure 5.14: Population ratios, n_J/n_{J_o} as a function of J for $J_o = 0$, $P_{AR} = 0.33$ torr (closed circles), $P_{AR} = 0.82$ torr (open circles), and $P_{CO_2} = 0.01$ torr. Typical error bars of 20% are shown.

Figure 5.15: Population ratios $n_{\Delta J}/n_{J_o}$ as a function of $|\Delta J|$ for $J_o = 15$ (closed circles for $\Delta J < 0$, open circles for $\Delta J > 0$) at $P_{AR} = 0.33$ torr, $P_{CO_2} = 0.01$ torr, and $J_o = 0$ (triangles) at $P_{Ar} = 0.35$ torr, $P_{CO_2} = 0.02$ torr. Typical error bars of 20% are shown.

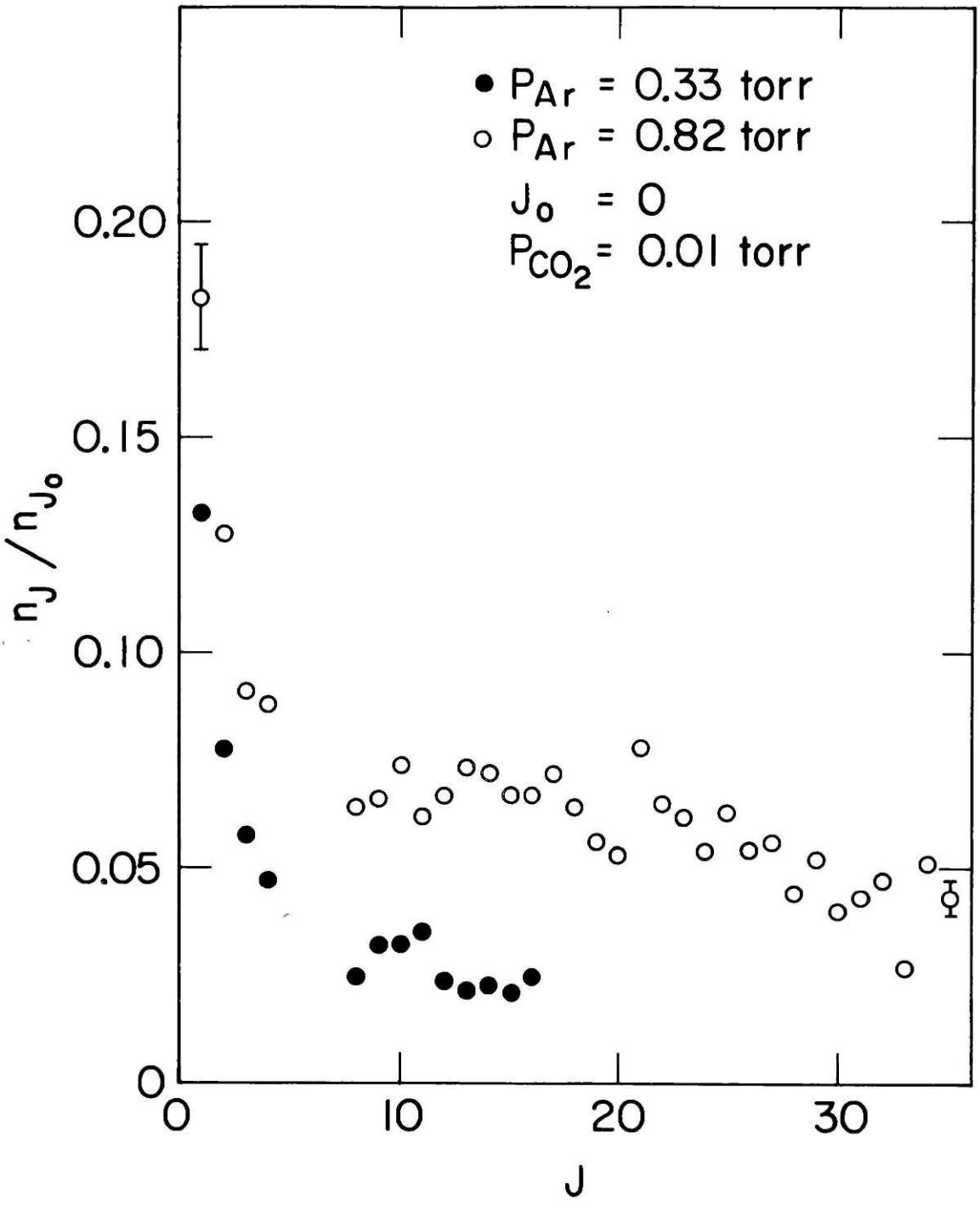
● P_{Ar} = 0.33 torr
○ P_{Ar} = 0.82 torr
J_o = 0
P_{CO_2} = 0.01 torr
0.20
0.15
0.10
0.05
0
n_J / n_{J_o}
0
10
20
30
J

FIGURE 5.14

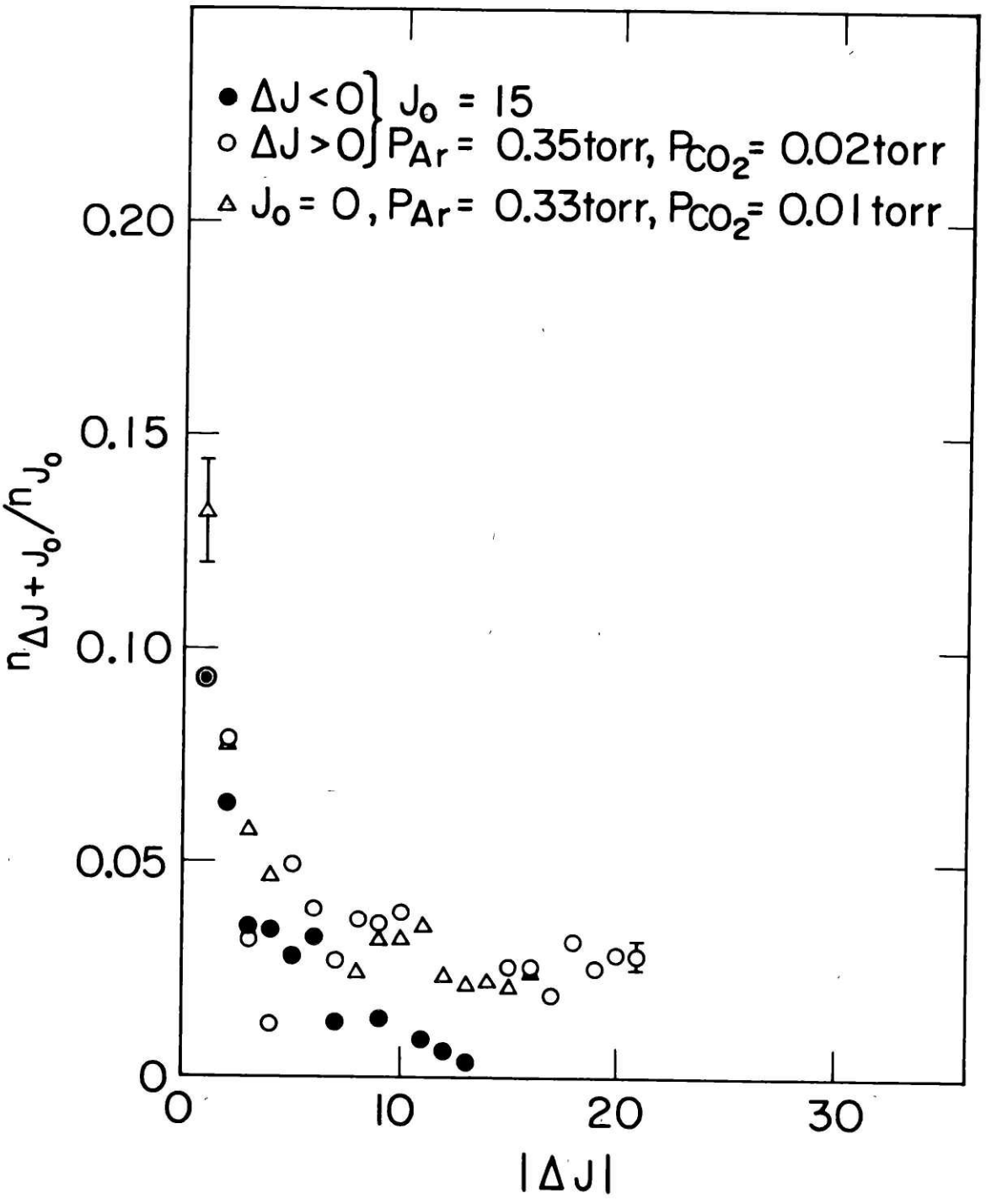
● ΔJ<0 } J₀ = 15
○ ΔJ>0 } P_Ar = 0.35torr, P_CO2 = 0.02torr
△ J₀ = 0, P_Ar = 0.33torr, P_CO2 = 0.01torr
0.20
0.15
0.10
0.05
0
0
10
20
30
n_ΔJ+J₀/n_J₀
|ΔJ|

FIGURE 5.15

Even at the lowest pressures attained, the $T(\Delta J)$ are significantly different from observed population ratios (e.g. $\sim$ 100% for $|\Delta J| = 1$) indicating the importance of multiple collisions: in the single collision limit, $T(\Delta J) = n_{J+\Delta J}/n_J$.

From Eq. 5.23, four rate constants determine $T(\Delta J)$ at given P_{Ar} and P_{CO_2}[†]:

$$T(\Delta J) = K(\Delta J)\Gamma^{-1} = \frac{k_{Ar}(\Delta J)P_{Ar} + k_{CO_2}(\Delta J)P_{CO_2}}{k_{rad}+k^c_{Ar}P_{Ar}+k^c_{CO_2}P_{CO_2}} \qquad (5.32)$$

Attempts to least squares fit the $T(\Delta J)$ as a function of P_{Ar} and P_{CO_2} to obtain the pressure independent rate constants, k s, were unsuccessful. This problem is attributed to (1) neglect of the J_o dependence of $T(\Delta J)$ (the assumption used in obtaining Eq. 5.24 from 5.22[9]) and (2) experimental error in n_J/n_{J_o}; both types of errors are amplified under multiple collision conditions. Consider, for example, the two collision process $J_o \rightarrow J_1 \rightarrow J_2$ such that $J = J_1-J_o = J_2-J_1$. Strictly, there are two rates, $T(J_1-J_o)$ and $T(J_2-J_1)$, but in Eq. 5.24 they are treated is one, $T(\Delta J)$; the error associated with the approximation that $T(\Delta J) \neq f(J_o)$

[†] BaO $\sim$ BaO and BaO $\sim$ Ba collisions are neglected since no variation in intensity ratios was observed with oven current.

clearly increases with collision frequency. In the single collision limit, only $T(\Delta J) = T(J_1-J_o)$ is measured. Similarly, errors in n_J/n_{J_o} propagate further with increasing collision frequency: both n_{J_1}/n_{J_o} and n_{J_2}/n_{J_o} are used to determine $T(\Delta J)$ instead of n_{J_1}/n_{J_o} in the single collision limit. Thus, when the multiple collision corrections are comparable to or greater than n_J/n_{J_o}, the $T(\Delta J)$ obtained from Eq. 5.25b must be used with caution. Quantitative comparisons between single collision rates would provide detailed dynamical information (see Ref. 9 for example) but are unwarranted here.

However, it is possible to make some qualitative statements and factor of two estimates of rate constants for BaO ∿ Ar and BaO ∿ CO_2 rotational relaxation. From low pressure data in Tables 5.6 and 5.7 and neglecting quenching rates in Eq. 5.32,

$$k_{Ar}(|\Delta J|=1) \approx k_{CO_2}(|\Delta J|=1) \approx 10^6 \text{torr}^{-1}\text{sec}^{-1} \approx 5 \times 10^{-11} \text{cm}^3\text{sec}^{-1} \quad (5.34)$$

or $\sigma(|\Delta J = 1|) \approx 10\text{Å}^2$.

A lower bound to the total rotational inelastic collision rate is estimated by summing the n_J/n_{J_o} at low pressures and multiplying by the total pressure and

radiative rate:

$$2k^{rot}(J_o=0) \approx k^{rot}(J_o=15) \approx 10^7 torr^{-1} sec^{-1}$$
$$\approx 5 \times 10^{-10} cm^3 sec^{-1} \qquad (5.34)$$

or $2\sigma^{rot}(J_o=0) \approx \sigma^{rot}(J_o=15) \approx 100A^2$.

The difference between $J_o = 0$ and 15 results from the different number of final channels available: from Table 5.7 and Fig. 5.15 it is apparent that for small $|\Delta J|$, $\Delta J < 0$ transfer occurs at rates comparable to $\Delta J > 0$ transfer; but $\Delta J < 0$ transfer is not possible for $J_o = 0$. The rate constant in Eq. 5.34 implies a rotation changing collision frequency of ≈ 4 per radiative lifetime at the lowest total pressure attained of 0.34 torr.

From Fig. 5.15, two additional qualitative conclusions are drawn: (1) $\Delta J = 1$ transfer is slightly more efficient for $J_o = 0$ ($n_1/n_o = 0.13$) than for $J_o = 15$ ($n_{16}/n_{15} = 0.09$) (also see Tables 5.6 and 5.7) and (2) an asymmetry between $\Delta J < 0$ and $\Delta J > 0$ transfer from $J_o = 15$ is observed for $|\Delta J| \gtrsim 9$ ($n_J/n_{J_o} = 0.02$ as opposed to 0.01). The first observation is <u>qualitatively</u> consistent with both information theory which states that $k(J_o \rightarrow J)$ should be proportional to $\exp(-\theta|\Delta E_r|)$, where ΔE_r is the collision induced change

in rotational energy and θ is the surprisal parameter[50], and the empirical scaling law found for $Na_2 \sim Xe$ collisions[9] where $k(J_o \rightarrow J)$ varies as $(\Delta E_r)^{-1}$. The second observation is merely a manifestation of statistical factors: fewer M sub-levels are available for $\Delta J < 0$ than for $\Delta J > 0$ transfer.

Finally, by comparing δv_{lx} to the thermal root mean square speed, $\langle v_{lx}^2 \rangle^{\frac{1}{2}}$, and $n(J_o+1)/n(J_o)$ to the thermal population ratio, $(2J_o+2)(2J_o+1)^{-1} \exp(-\Delta E_r/kT)$, a ratio of translational to rotational relaxation rates of approximately 1 is obtained.

V. Discussion

The results presented above are readily interpreted, albeit qualitatively, by considering the long range form of the intermolecular potential.[51-54] Propensities for small $|\Delta J|$ transfer result from the symmetry of the anisotropic part of the potential[54]. For BaO ∿ Ar collisions, the leading terms in the multipole expansion of the potential correspond to dipole (BaO) ∿ induced dipole (Ar) and quadrupole (BaO) ∿ induced dipole (Ar) interactions with BaO rotational selection rules: $\Delta J = 0, \pm 1, \pm 2$, $\Delta M = 0, \pm 1, \pm 2$, $+ \rightarrow +$, $- \rightarrow -$ and $\Delta J = 0, \pm 1, \pm 2, \pm 3$, $\Delta M = 0, \pm 1, \pm 2, \pm 3$, $+ \rightarrow -$, respectively[54,55]. + and - refer to total parity corresponding to space inversion. For BaO ∿ CO_2 collisions, dipole (BaO) ∿ quadrupole (CO_2) interaction is dominant with selection rules: $\Delta J = 0, \pm 1$, $\Delta M = 0, \pm 1$, and $+ \rightarrow -$[54,58]. These selection rules are by no means rigorous; the extent to which they are obeyed depends on the collision strength so that weak, long-range interactions exhibit propensities for transfer in accordance with the above selection rules whereas strong, short-range collisions exhibit no propensity rules and the ΔJ dependence of transfer rates is dictated by statistical factors alone. The observation of forward peaked scattering is consistent with a weak

collision picture.

As mentioned in Sec. IV.A.2, a monotonic increase in $\Delta\nu_{FWHM}$, or $\langle\langle \delta v_{1x} \rangle\rangle_o$ with $|\Delta J|$ is observed. It seems likely, in light of the discussion above, that this results partly from the impact parameter dependence of $k(\Delta J)$: large impact parameters resulting in weak interactions produce only small changes in J and v_{1x} whereas small impact parameters yield broad final J and v_{1x} distributions dictated by statistical factors. In order to verify this hypothesis, OODR experiments need to be performed in a single collision regime.

The radial dependences of the long range interaction described above are: R^{-6}, R^{-7}, and R^{-4} for dipole ∿ induced diple, quadrupole ∿ induced dipole, and dipole ∿ quadrupole interactions, respectively, where R is the intermolecular distance.[55] Thus BaO ∿ CO_2 interactions. are weaker, longer ranged than are BaO ∿ Ar interactions. Although this prediction cannot be verified from state to state cross section data, it is clearly manifested by satellite line narrowing, smaller angle scattering, induced by excess CO_2 (Fig. 5.8) and by the greater (relative to Ar) total pressure broadening rate of the principal line for CO_2 (Eqs. 5.28 and 5.29).

In summary, OODR has been used to simultaneously monitor rotational and translational relaxation in a low pressure flame. Double resonance intensities are

used to measure rovibronic populations while line shapes are inverted in a model-independent fashion to yield moments of the COM scattering angle distribution. Although precise, quantitative results are not obtained, a complete, qualitative picture of BaO ∿ Ar and BaO ∿ CO_2 scattering is realized. It is the relatively high operating pressure of the metal oxide oven (Chapter 3) and long lifetime of $A^1\Sigma^+$ which prohibits quantitative analysis and not the OODR technique. It is hoped that these experiments and the methods of analysis employed will inspire and aid future investigations.

References for Chapter 5

1. D.E. Stogyrn and A.P. Stogyrn, Mol. Phys. 11, 371 (1966).
2. For review see J.L. Kinsey, Ann. Rev. Phys. Chem. 28, 349 (1977) and references therein.
3. J.G. Pruett and R.N. Zare, J. Chem. Phys. 64, 1774(1976).
4. P.J. Dagdigian, MIT Physical Chemistry Seminar, Fall 1978.
5. J.L. Kinsey, J. Chem. Phys. 66, 2560 (1977).
6. W.D. Phillips, J.A. Serri, D.J. Ely, D.E. Pritchard, K.R.Way, and J.L.Kinsey,Phys. Rev. Lett. 41,937 (1978).
7a. J.I. Steinfeld and W. Klemperer, J. Chem. Phys. 42, 3475 (1965);
7b. R.B.Kurzel, J.I. Steinfeld, D.A. Hatzenbuhler, and G.E. Leroi, J. Chem. Phys. 55, 4822 (1971).
7c. R.B.Kurzel and J.I. Steinfeld, J. Chem. Phys. 53, 3293 (1970).
8. C.B. Moore and P.F. Zittel, Science 182, 541 (1973) and references therein.
9a. T. Brunner, R. Driver, N. Smith, and D.E. Pritchard, Phys. Rev. Lett. 41, 856 (1978).
9b. T. Brunner, R. Driver, N. Smith, and D.E. Pritchard, (submitted to J. Chem. Phys.).
10. A.T. Mattick, A. Sanchez, N.A. Kurnit, and A. Javan; Appl. Phys. Lett. 23, 675 (1973).
11. A.T. Mattick, N.A. Kurnit, and A. Javan, Chem. Phys. Lett. 38, 176 (1976).

12. J. Apt and D.E.Pritchard, Phys. Rev. Lett. 37, 91 (1976).

13. W.D. Phillips and D. Pritchard, Phys. Rev. Lett. 33, 1254 (1974).

14. P.R. Berman, Adv. Atom. Mol. Phys. 13, 57 (1978), D.R. Bates and B. Bederson, Ed., Academic Press, N.Y., and references therein.

15. W.K. Bischel and C.K. Rhodes, The Physics of Electronic and Atomic Collisions, p. 820, J.S. Risley and R. Meballe, ed., University of Washington, (Seattle, 1976).

16. T.W. Hänsch and P.E. Toschek,I.E.E.E. J. Quant. Electron. QE-5, 61 (1969).

17. P.W. Smith and T. Hänsch, Phys. Rev. Lett. 26, 740 (1971).

18. T. Kan and G.J. Wolga, I.E.E.E. J. Quant. Electron. QE-7, 141 (1971).

19. C. Freed and H.A. Haus, I.E.E.E. J. Quant. Electron. QE-9, 219 (1973).

20. S.M. Freund, J.W.C. Johns, A.R.W. McKellar, and T. Oka, J. Chem. Phys. 59, 3445 (1973).

21. J. Schmidt, P.R. Berman, and R.G. Brewer, Phys. Rev. Lett. 31, 1103 (1973).

22. T.W. Meyer and C.K. Rhodes, Phys. Rev. Lett. 32, 637 (1974).

23. R.L. Shoemaker, S. Stenholm, and R.G. Brewer, Phys. Rev. A10, 2037 (1974).

24. J.W.C. Johns, A.R.W. McKellar, T. Oka, and M. Römheld, J. Chem. Phys. 62, 1488 (1975).

25. P.R. Berman, J.M. Levy, and R.G. Brewer, Phys. Rev. A11, 1668 (1975).

26. W.K. Bischel and C.K. Rhodes, Phys. Rev. A14, 176 (1976).

27. P.R. Berman, Phys. Rev. A13, 2191 (1976).

28. C. Bréchignac, R. Vetter, P.R. Berman, J. Phys. B10, 3443 (1977).

29. L.S. Vasilenko, V.P. Kochanov, and V.P. Chebotayev, Opt. Comm. 20, 409 (1977).

30. P. Cahuzac, E. Marié, O. Robaux, R. Vetter, and P.R. Berman, J. Phys. B11, 645 (1978).

31. C. Brechign, R. Vetter, and P.R. Berman, Phys. Rev. A17, 1609 (1978).

32. K. Sakurai, S.E. Johnson, and H.P. Broida, J. Chem. Phys. 52, 1625 (1970).

33. S.E. Johnson, J. Chem. Phys. 56, 149 (1972).

34. H.B. Palmer, W.D. Krugh, and C.J. Hsu, Fifteenth Symposium (International) on Combustion (The Combustion Institute, Pittsburgh, 1975), p. 951.

35. C.J. Hsu, W.D. Krugh, and H.B. Palmer, J. Chem. Phys. 60, 5118 (1974).

36. W. Felder, R.K. Gould, and A. Fontijn, J. Chem. Phys. 66, 3256 (1977).

37a. A. Torres-Filho and J.G. Pruett, J. Chem. Phys. (in press).

37b. J.G. Pruett, private communication, 1/5/79.

38. See for example, R.D. Levine and R.B. Bernstein, Molecular Reaction Dynamics, Oxford University Press, New York (1974).

39. H. Goldstein, Classical Mechanics, Addison-Wesley (Mass. 1950), Chapter 4.

40. See for example, A.C.G. Mitchell and M.W. Zemansky, Resonance Radiation and Excited Atoms, Cambridge University, (Cambridge, England, 1971).

41. M.S. Feld, Fundamental and Applied Laser Physics: Proceedings of the Esfahan Symposium August 29 - September 5, 1971, M.S. Feld, A. Javan, and N. Kurnit, eds., (Wiley, 1973), p. 369.

42. I.M. Beterov, Y.A. Matyugin, V.P. Chebotayev,Zh. Eksp. Teor. Fiz. 64, 1495 (1973), Sov. Phys. JETP 37, 756 (1973).

43. V.S. Letokhov and V.P. Chebotayev, Nonlinear Laser Spectroscopy, Springer-Verlag (Berlin, 1977), particularly Chapter 5.

44. See for example, R. Bracewell, The Fourier Transform and Its Applications, McGraw-Hill Book Co., New York, 1965.

45. G. Breit, Rev. Mod. Phys. 5, 91 (1933).

46. P.A. Franken, Phys. Rev. 121, 508 (1961).

47. J.T. Hougen, Natl. Bur. Stand. U.S. Monogr. 115 (1970).

48. See for example, G.W. Castellan, Physical Chemistry, Addison-Wesley, Reading, Ma., 1971.

49. J.W. Cooley and J.W. Tukey, Math. Comp. 19, 297 (1965).

50. R.D. Levine and R.B. Bernstein, Acc. Chem. Res. 7, 393 (1974).

51. P.W. Anderson, Phys. Rev. 76, 647 (1949).

52. R.J. Cross and R.G. Gordon, J. Chem. Phys. 45, 3571 (1966).

53a. H.A. Rabitz and R.G. Gordon, J. Chem. Phys. 53, 1815 (1970);

53b. H.A. Rabitz and R.G. Gordon, J. Chem. Phys. 53, 1831 (1970).

54. For a review see, T. Oka, Adv. At. Mol. Phys. 9, 127 (1973).

55. J.O. Hirschfelder, C.F. Curtiss, and R.B. Bird, Molecular Theory of Gases and Liquids, John Wiley & Sons, Inc., (New York, 1954).

Chapter 6: Optical-Optical Resonance Monitoring of Depolarizing Collisions

I. Introduction

Optical-optical double resonance (OODR) spectroscopy has already been shown to be a powerful means of monitoring rotational and translational relaxation in the Ba + CO_2 + Ar → BaO + CO + Ar flame (Chapter 5). This chapter illustrates how the combined selectivity afforded by OODR and the variation of laser polarization can yield definitive measures of angular momentum reorientation processes (i.e. M changing collisions).

The results presented below indicate that M is not conserved when low J BaO $A^1\Sigma^+$ levels undergo collisions with CO_2. Specifically, the $A^1\Sigma^+$ J = 1, M = 0 level is pumped; J = 1, M = $\pm$ 1 and J = 2, M = 0, $\pm$ 1, $\pm$ 2 levels are probed as a function of probe laser polarization.

Besides being essential for the conversion of laser induced fluorescence intensities to level population densities (Chapter 5), collisional M sub-level distributions are a manifestation of the intermolecular forces at play in a collision.

There has been considerable theoretical[1-4] and experimental work on the depolarization of molecular fluorescence.[5-15] Additional references can be found in the review articles by Oka[15] and Baylis[17], which also provide excellent summaries of both the theoretical and experimental work.

A wide range of experimental results have been obtained. Generally, M seems to be conserved in collisions between non-polar molecules such as I_2 or Na_2 with themselves or with rare gases.[9,12-15] However, Kurzel and Steinfeld[7] have measured I_2 ∿ rare gas depolarization cross sections as large as 23 $\AA^2$ and average reorientation angles of 50^o.[2,7] In polar systems, conflicting results have also been obtained. Unland and Flygare did not observe reorientation in OCS J = 1 → J = 1 collisions with OCS and O_2[6]. Cox and Flynn also report negligible reorientation in OCS ∿ OCS collisions[5]. Experiments on CH_3OH ∿ CH_3OH collisions indicate that only small changes in M consonant with long range dipole ∿ dipole interactions occur.[11] On the other hand, Shoemaker et al.[8] report a cross section of 100 $\AA^2$ for $\Delta J = 0$, $\Delta M = \pm 1$ transfer in CH_3F ∿ CH_3F collisions and Leite et al.[10] report reorientation cross sections for NH_3 ∿ NH_3 collisions that are 50% larger than $\Delta J \neq 0$ collisional cross sections.

One reason for the wide range of experimental results is the selection of different initial J levels: classically, a rapidly rotating molecule is more difficult to reorient than is a rotationless molecule. Shoemaker et al.,[8] for example, do not observe reorientation in CH_3F ∿ CH_3F J = 12 → J' = 12 but do observe the 100 $\AA^2$ reorientation cross section mentioned above for

$J = 4 \rightarrow J' = 4$ transfer. Jeyes et al.[14] attempted to excite low J values in I_2 $B^3\Pi_{o_u^+}$ but could not precisely determine the extent of reorientation relative to higher J selection owing to overlapping of $B^3\Pi_{o_u^+} \rightarrow X^1\Sigma^+$ transitions at low J.

The experiments described below involve selection of a single $A^1\Sigma^+$ J,M level. Sub-Doppler resolution afforded by OODR eliminates problems associated with overlapping transitions near the band origin. By pumping $A^1\Sigma^+ \leftarrow X^1\Sigma^+$ (1,0) R(0) with $\hat{z}$ polarization, $A^1\Sigma^+$ $J' = 1$, $M' = 0$ is prepared. Probing $C^1\Sigma^+ \leftarrow A^1\Sigma^+$ (3,1) P(1) with first $\hat{z}$ polarization and then $\hat{y}$ polarization yields an unambiguous value for the BaO $\sim$ CO_2 $\Delta J = 0$, $\Delta|M| = 1$ reorientation cross section of 4.2 ± 1.2 $\mathring{A}^2$. When $C^1\Sigma^+ \leftarrow A^1\Sigma^+$ (3,1) P(2) is probed as a function of probe laser polarization a measure of the relative probabilities for $\Delta J = 1$, $\Delta|M| = 0$, 1, and 2 transfer is obtained and indicates that J is significantly reoriented.

II. Experimental

Only those details pertinent to these experiments and not presented in Chapters 3 and 5 will be described here.

The pump laser is $\hat{z}$ polarized and propagates in the $\hat{x}$ direction. In order to vary the polarization of the probe laser, which also propagates in the $\hat{x}$ direction, it is first circularly polarized by a Fresnel rhomb[18] (Carl Lambrecht Co:) and then linearly polarized in either the $\hat{z}$ or $\hat{y}$ directions by a calcite polarizer (Inrad). The dye lasers (Coherent Radiation Model CR599-21) are single mode and frequency stabilized with line widths (FWHM) equal to 1 MHz.

By the time the lasers have been combined, are propagating collinearly, and are reflected into the flame reactor, the beams have acquired a small ellipticity of polarization.† The extent of this depolarization is measured with an analyzer placed directly before the input window. The polarization dependent intensity ratios, I_y/I_z, used in determining M' sub-level populations are corrected accordingly.

---

†The Brewster angle window[18] ordinarily used to permit entry into the reactor with minimal reflection losses is replaced in these experiments by a flat, normal incidence, window in order to minimize depolarization of the lasers at this point.

In addition, because the Fresnel rhomb produces slightly elliptically polarized light instead of pure circular polarization, the probe laser power varies slightly as the calcite polarizer is rotated to select $\hat{z}$ or $\hat{y}$ polarization. Corrections for this power variation are also made.

Typical dye laser powers after polarizers, beam splitters, and mirrors are 50 mW for the pump and 10-20 mW for the probe. The lasers are not focussed.

1. Elastic ($\Delta J = 0$) Depolarization

The pump laser excites $A^1\Sigma^+ \leftarrow X^1\Sigma^+$ (1,0) R(0) and prepares the $J' = 0$, $M' = 0$ sub-level; the state is said to be aligned. The probe laser is tuned to the $C^1\Sigma^+ \leftarrow A^1\Sigma^+$ (3,1) P(1) transition and samples the $J' = 0$, $M' = 0$ population when $\hat{z}$ polarized and the $J' = 0, |M'| = 1$ sub-levels when $\hat{y}$ polarized since the electric dipole selection rules are $\Delta M = 0, \pm 1$. Thus a signal for $\hat{y}$ probe laser polarization results only when collisional transfer from $M' = 0$ to $|M'| = 1$ has occurred (Figure 6.1). $C^1\Sigma^+ \rightarrow X^1\Sigma^+$ P(1) $\hat{z}$ and $\hat{y}$ polarized fluorescence is detected through UV passing, visible absorbing filters (see Chapter 3).

Figure 6.1: Schematic energy level diagram for OODR probing of $J=1 \rightarrow J=1$, $\Delta M = \pm 1$ depolarizing collisions. $A^1\Sigma^+ \leftarrow X^1\Sigma^+$ (1,0) R(0) is pumped while $C^1\Sigma^+ \leftarrow A^1\Sigma^+$ (3,1) P(1) is probed. The pump laser is $\hat{z}$ polarized. The probe laser polarization is $\hat{z}$ for sampling $J' = 1$, $M' = 0$ and $\hat{y}$ for sampling $J' = 1$ $M' = \pm 1$. The splitting of the degenerate M' sub-levels is merely schematic.

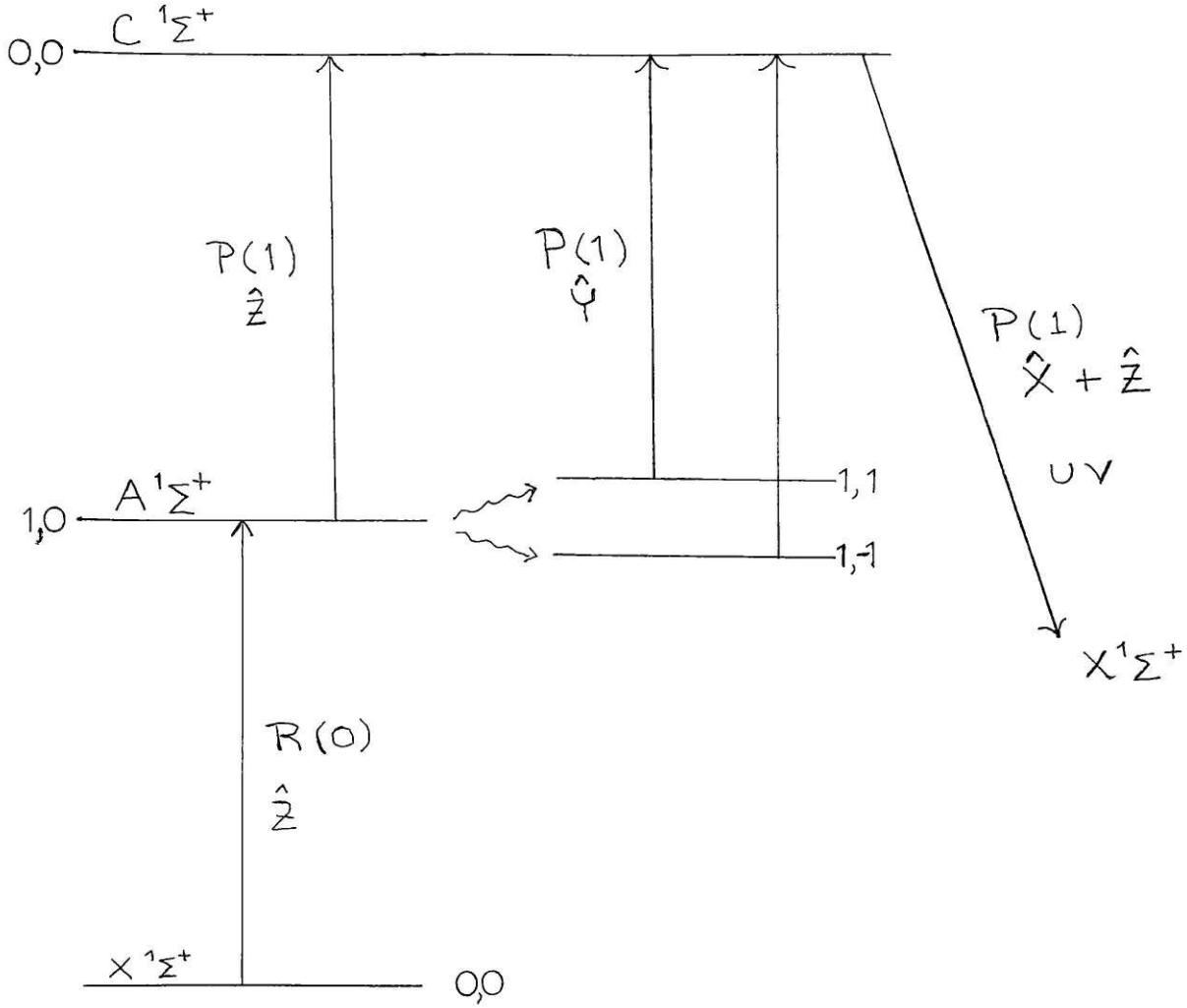
0,0
C $^1\Sigma^+$
P(1)
$\hat{Z}$
P(1)
$\hat{Y}$
P(1)
$\hat{X} + \hat{Z}$
UV
1,0
A $^1\Sigma^+$
1,1
1,-1
X $^1\Sigma^+$
R(0)
$\hat{Z}$
X $^1\Sigma^+$
0,0

FIGURE 6.1

2. Inelastic ($\Delta J \neq 0$) Depolarization

The pump laser again prepares $A^1\Sigma^+$ v' = 1, J' = 1, M' = 0. The probe laser, however, is now tuned to the $C^1\Sigma^+ \leftarrow A^1\Sigma^+$ P(2) resonance line so that J' = 2, M' sub-level populations resulting from J changing collisions are monitored by varying the probe laser polarization.

III. Theory

A. Line intensities

The relationship between OODR laser induced fluorescence intensity and f(M'), the M' sub-level population distribution, is given in Chapter 5.

Averaging over M' sub-levels is not performed here. For J' = 1,

$$\frac{I_y}{I_z} = \frac{n_1}{n_0} , \qquad (6.1)$$

and for J' = 2,

$$\frac{I_y}{I_z} = \frac{n_0 + 6n_1 + 9n_2}{8n_0 + 9n_1} \qquad (6.2)$$

where n_i (i = 0, 1, 2) is the $|M| = i$ sub-level population density, I_y and I_z are corrected $C^1\Sigma^+ \rightarrow X^1\Sigma^+$ fluorescence intensities when the probe is $\hat{y}$ and $\hat{z}$ polarized, respectively. Eqs. 6.1 and 6.2 are dependent upon excitation and detection geometry as desribed in Chapter 5.

The n_i s can be viewed as diagonal density matrix elements; off-diagonal density matrix elements representing coherence terms are rigorously zero since z polarized pumping is employed.[17] Similarly, $n_M = n_{-M}$ always, since collisions in the absence of an external field cannot produce an oriented

state (where $n_M \neq n_{-M}$) nor did the laser prepare an oriented state.[17]

B. Pressure Dependence

In the single collision and steady state regimes, the number density of molecules in the final, collisionally populated J,M level is given by:

$$n_f = \sum_{\ell} n_i n_{\ell} k_{\ell}(i \rightarrow f)/k_{rad} \qquad (6.3)$$

where n_i and n_f are the initial and final BaO $A^1\Sigma^+$ rovibronic level population densities, respectively, n_{ℓ} is the ℓ^{th} collision partner number density, $k_{\ell}(i \rightarrow f)$ and k_{rad} are state to state and radiative rate constants, respectively. Eq. 6.3 is not valid for $\Delta J = 0$, $\Delta M = 0$ collisions since a pump source term is not included. The probe laser transition rate is estimated to be at least an order of magnitude smaller than k_{rad} and is therefore neglected.

IV. Results and Analysis

A. Elastic Depolarization

The intensity ratio, $I_y/I_z = n_1/n_0$, is measured as a function of both Ar and CO_2 pressures. At CO_2 pressures $\lesssim$ 0.01 torr the ratio is less than 0.03 and does not vary signficantly with Ar pressure. Thus $\sigma_{Ar}(J=1\rightarrow J=1, \Delta|M|=1) < 1$ Å^2. The finite value of I_y observed under these conditions is due to either the residual CO_2 presssure being higher than indicated or failure to completely correct for laser beam depolarization.

I_y/I_z does vary significantly with CO_2 pressure (Figure 6.2). Measurements at a fixed Ar pressure of 0.3 torr are shown by open circles and I_y/I_z values averaged over different Ar pressures but constant CO_2 pressure are shown by crosses. The errors are such that only a linear least squares fit to the data are warranted. The effects of multiple collisions are ignored and Eq. 6.3 is employed:

$$\frac{I_y}{I_z} = \frac{n_1}{n_0} = k_{CO_2}(J = 1, M = 0, \rightarrow J = 1, |M| = 1) n_{CO_2} k_{rad}^{-1}. \tag{6.4}$$

The observed linear variation of I_y/I_z with n_{CO_2} suggests that, to within experimental error, multiple collisions

Figure 6.2: Ratio of $C^1\Sigma^+ \div A^1\Sigma^+$ (3,1) P(1) OODR excitation signals for $\hat{y}$ and $\hat{z}$ polarized probes vs. CO_2 partial pressure. Ar pressure is fixed at 0.3 torr (open circles). x s denote averages over all Ar pressures from 0.3 to 1.00 torr.

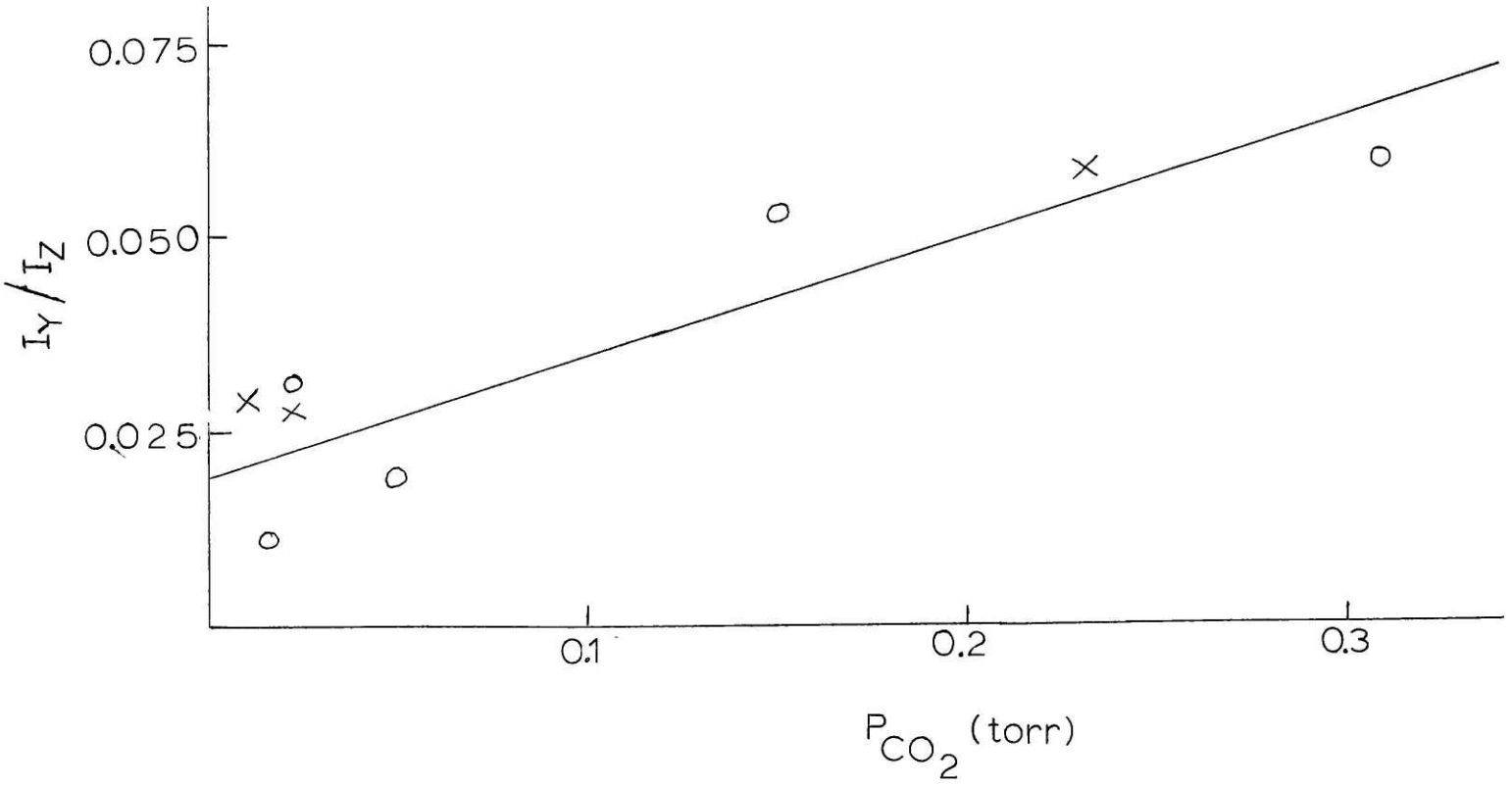

FIGURE 6.2

affect I_y and I_z equally.

Using a value of $k_{rad} = 2.75 \times 10^6$ sec^{-1}, the slope of the line in Fig. 6.2 yields k_{CO_2} ($J = 1 \rightarrow 1$, $|\Delta M| = 1$) $= 4.2 \pm 1.2 \times 10^5$ torr^{-1}sec^{-1} $= 2.0 \pm 0.6 \times 10^{-11}$ cm^{3}sec^{-1} and the corresponding cross section is 4.2 ± 1.2 Å^2.† Since the cross section for $\Delta M = -1$ equals that for $\Delta M = +1$, the total depolarization cross section is 8.4 ± 2.4 Å^2. These cross sections are comparable to state to state J changing cross sections (Chapter 5).

One other observation is noted: the line widths and shapes for $\hat{z}$ and $\hat{y}$ polarized probes are identical indicating that velocity randomization is insignificant for $\Delta M = 0$, $\Delta J = 0$ collisions; the line shape is determined solely from homogeneous pressure and radiative broadening mechanisms.

B. Inelastic depolarization

The experimental intensity ratio I_y/I_z shows no significant systematic variation with either CO_2 or Ar pressure. When the ratio is averaged over thirteen pressure combinations, a value of $I_y/I_z = 0.54 \pm 0.10$

---

†See Chapter 5 for conversion of rate constants from torr^{-1} sec^{-1} to cm^3 sec^{-1} to cross sections in Å^2.

is obtained.

From Eq. 6.2 it is seen that this one number is insufficient to determine all three M sub-level population densities.

Two conclusions can be drawn, however: (1) M changing collision cross sections are determined by dynamical rather than statistical factors, for the latter implies equal M sub-level populations in J = 2 and an intensity ratio of 0.941; and (2) M is not conserved, for this implies $I_y/I_z = 0.125$.

The fact that no pressure dependence to I_y/I_z is observed suggests that Ar and CO_2 yield similar M branching ratios for J = 1 → 2 collisions.

V. Conclusion

The results presented above provide conclusive evidence that M is conserved in neither BaO ∿ CO_2 J = 1 → 1 nor BaO ∿ CO_2 and BaO ∿ Ar J = 1 → 2 collisions. The data are not inconsistent with the long range, weak collision picture established in Chapter 5.

If the long range multipole moment interactions are the dominant mechanisms by which changes in angular momentum orientation are effected, then flourescence is not expected to be readily depolaried when higher initial J levels are selected: although changes in M of $\pm$ 1 and $\pm$ 2 may be efficient, they do not result in substantial depolarization ratios at higher J values where ΔM is small compared with 2J + 1, the number of M sub-levels.

Future experiments of the type suggested by Case *et al.*[4] are warranted to definitively determine M sub-level populations in collisionally populated J = 2.

The OODR experiment seems ideally suited for a systematic investigation of depolarization phenomena as a function of initial J, from low to moderate J values.

References for Chapter 6

1. P.W. Anderson, Phys. Rev. 76, 647 (1949).
2. R.G. Gordon, J. Chem. Phys. 45, 1643 (1966).
3. J.L. Kinsey, J.W. Riehl, and J.S. Waugh, J. Chem. Phys. 49, 5269 (1968).
4. D.A. Case, G.M. McClelland, and D.R. Herschbach, Mol. Phys. 35, 541 (1978).
5. A.P. Cox, G.W. Flynn, and E.B. Wilson, Jr., J. Chem. Phys. 42, 3094 (1965).
6. M.L. Unland and W.H. Flygare, J. Chem. Phys. 45, 2421 (1966).
7. J.I. Steinfeld and R.B. Kurzel, J. Chem. Phys. 56, 5188 (1972).
8. R.L. Shoemaker, S. Stenholm, and R.G. Brewer, Phys. Rev. A10, 2037 (1974).
9. H. Katô, R. Clark, and A.J. McCaffery, Mol. Phys. 31, 943 (1976).
10. J.R.R. Leite, M. Ducloy, A. Sanchez, D. Seligson, and M.S. Feld, Phys. Rev. Lett. 39, 1465 (1977).
11. R.M. Lees, Can. J. Phys. 56, 1417 (1978).
12. M.D. Rowe and A.J. McCaffery, Chem. Phys. 34, 81 (1978).
13. R. Clark and A.J. McCaffery, Mol. Phys. 35, 617 (1978).

14. S.R. Jeyes, A.J. McCaffery, and M.D. Rowe, Mol. Phys. 36. 845 (1978).

15. a) T. Brunner, R. Driver, N. Smith, and D.E. Pritchard, Phys. Rev. Lett. 41, 856 (1978).

b) T. Brunner, R. Driver, N. Smith, and D.E. Pritchard (submitted to J. Chem. Phys.).

16. T. Oka, Adv. At. Mol. Phys. 9, 127 (1973).

17. W.E. Bayliss, Progress in Atomic Spectroscopy, W. Hanle and H. Kleinpopper, eds., Plenum, (London, 1978).

18. G.R. Fowles; Introduction to Modern Optics; Holt, Reinhart, and Winston; (New York, 1968).

19. S.E. Johnson, J. Chem. Phys. 56, 149 (1972).

Appendix 1:

Deperturbation of the N_2^+ First Negative Group. $B^2\Sigma_u^+ - X^2\Sigma_g^+$

Richard A. Gottscho and Robert W. Field
Massachusetts Institute of Technology
Department of Chemistry
Cambridge, Massachusetts 02139

and

K.A. Dick and W. Benesch
University of Maryland
Institute for Physical Science and Technology
College Park, Maryland 20742

J. Mol. Spectrosc. (in press).

Abstract

Twelve bands of the N_2^+ $B^2\Sigma_u^+ - X^2\Sigma_g^+$ system, including v_B = 0-6 and v_X = 0-8, are reanalyzed. All effects of $B^2\Sigma_u^+ \sim A^2\Pi_u$ perturbations are explicitly considered. A major motivation for this work was the hope of utilizing recent high precision line measurements to detect small level shifts due to new perturbing states, particularly $a^4\Sigma_u^+$. No evidence for a perturber other than $A^2\Pi_u$ is obtained.

Deperturbed constants for the $B^2\Sigma_u^+$ and $X^2\Sigma_g^+$ states are derived. The deperturbation is shown to be self-consistent and complete (excluding effects of the $C^2\Sigma_u^+$ state) by examining semi-empirical relationships of the perturbation matrix elements with the spin-rotation constants of the B and X states and atomic spin-orbit parameters.

A number of previous analyses of transitions involving the v_B = 3 and 5 levels are found to be incorrect.

I. Introduction

Recently, highly precise and accurate spectral measurements of the first negative group of N_2^+ (N_2^+ 1NG: $B^2\Sigma_u^+ - X^2\Sigma_g^+$) were obtained (1). We have used these data to deperturb the $B^2\Sigma_u^+$ state and obtain constants for $B^2\Sigma_u^+$, the perturbing $A^2\Pi_u$ state, and $X^2\Sigma_g^+$.

Two criteria are used to define complete deperturbation: (1) the residuals must result solely from random measurement errors; and (2), perturbation matrix elements and second order constants such as centrifugal distortion and spin-rotation must be internally consistent. If these criteria are not met, either the data are systematically in error or the model Hamiltonian is incomplete. We show below that these criteria are met for N_2^+ 1NG(1) and that this system may be completely understood in terms of only the three states above. Several previous analyses are shown to be in error.

The high resolution data of (1) were least squares fitted band by band and the derived constants were merged (2,3). This analysis has led to the discovery of extra lines arising from levels with predominant $A^2\Pi_u$ character ($\geq$ 50%) but with a substantial admixture of $B^2\Sigma_u^+$. In addition, several transitions reported in (1) have been reassigned and several bands have been extended.

Several pitfalls have made analysis of the N_2^+ 1NG hazardous: overlapping by the ubiquitous N_2 second positive system, the complex nature (four crossings, two competing perturbation mechanisms) of the $B^2\Sigma_u^+ \sim A^2\Pi_u$ perturbations, and F_1 vs. F_2 assignment ambiguity. Four analyses of $B^2\Sigma_u^+$ ($v' = 3$) alone exist in the literature (4-7). This paper verifies the assignment by Crawford and Tsai (6) of the (3,5) band.

For v' = 5, the analyses of Refs. (5, 6, and 8) are shown to be incorrect.

It had been hoped that a rigorous deperturbation of N_2^+ 1NG combined with more precise line positions would supply evidence for small $a^4\Sigma_u^+ \sim B^2\Sigma_u^+$ perturbations. However, no such evidence has been obtained; therefore we can neither verify nor contest earlier reports concerning the metastable $a^4\Sigma_u^+$ state (9-13).

II. Experimental

The spectral data which form the basis of the present analysis were obtained using a 5-m vacuum spectrograph at Johns Hopkins University under conditions detailed in Ref. (1). The spectra were generated in a specially designed hollow cathode source and were photographed from 380.0 to 475.0 nm in high (12^{th} through 15^{th}) orders with a reciprocal dispersion of $\sim$ 0.018nm/mm. A total of over twenty sets of two 10 in. plates were used, each with several exposures, in order to provide complete coverage with various and complementary intensities. Calibration against standard iron lines led to an accuracy of approximately 0.01 cm^{-1} for N_2^+ isolated lines and a relative precision over band segments on a single plate of approximately 0.005 cm^{-1}.

III. Theory

$^2\Sigma^+ - {}^2\Sigma^+$ Transitions

Herzberg (14) has adequately detailed the nature of $^2\Sigma^+ - {}^2\Sigma^+$ transitions. Only one point needs to be reiterated here. In the absence of perturbations and without observation of a Q branch transition which connects levels of different Kronig symmetry [e and f (15) or F_1 and F_2, respectively], it is difficult to distinguish between P_1 and P_2 (or R_1 and R_2) branches and therefore to determine the signs of γ' and γ'' (upper and lower state spin-rotation constants, respectively) (14). In the past, these assignments have been made for N_2^+ lNG on the basis of intensity considerations (4, 6, 8, 16, 18): the unperturbed P_1 to P_2 (or R_1 to R_2) intensity ratio is $(N + 1)/N$ (14). However, for large N this ratio approaches one; moreover, in the presence of perturbations which affect e and f levels differently this ratio may vary significantly from the expected value. This problem was clearly realized by Childs in 1932 (17) but has nevertheless contributed to erroneous analyses (see below). Because $^2\Sigma \sim {}^2\Pi$ interactions are parity dependent (see Table I) they can provide an unambiguous determination of the signs of γ' and γ'' and a correct labelling of the branches.[1]

$^2\Sigma^+ \sim {}^2\Pi$ Perturbations

$^2\Sigma^+$ and $^2\Pi$ Born-Oppenheimer basis functions mix via rotation-electronic [$H^{RE} = -B(J_+L_- + J_-L_+) + \bar{B}(L_+S_- + L_-S_+)$] and spin-orbit [$H^{SO} = \Sigma_i \; a_i \ell_i \cdot s_i$] interactions (18). Both operators are diagonal in J and parity. Additional selection rules for H^{RE} are $\Delta S = 0$, $\Delta\Sigma = 0$, $\Delta\Omega = \Delta\Lambda \pm 1$ (first term) or $\Delta S = 0$, $\Delta\Sigma = -\Delta\Lambda = \pm 1$, $\Delta\Omega = 0$ (second term). For H^{SO}: $\Delta S = 0, \pm 1$,

$\Delta\Sigma = -\Delta\Lambda = \pm 1$, and $\Delta\Omega = 0$, where S,Σ,Λ, and Ω have their usual meanings (19). Matrix elements of these operators are given in Table I along with the remaining Hamiltonian matrix used in deperturbing $N\frac{1}{2}$ 1NG. The parity dependence of $^2\Sigma^+ \sim {}^1\Pi_{1/2}$ interactions should be noted. In fact, the effects of a perturbation may be unobservable for one set of parity levels and yet large in the other set due to interference between H^{SO} and H^{RE}.

Derivation of the matrix elements in Table I has been described elsewhere (18-21). We have used throughout this paper the phase convention detailed by Hougen (19) and the Kronig symmetry definition of Brown et al. (15). Only those parameters which could be fitted or calculated are included.

IV. Method

The least squares fitting of spectroscopic data has been well treated in the literature (2, 3, 21, 22) and need not be considered in detail here. The methods of deperturbation are also not new (23-26).

The data of (1) were compared with the calculated differences of upper and lower state eigenvalues of the Hamiltonian matrix given in Table I. The molecular parameters of Table I were then varied band by band using a weighted,non-linear,least squares routine (27) to obtain the best fit to the data.[2] The band by band constants obtained from these fits (Table II) were then combined along with band origins from Ref. (28) using the program MERGE (2) to yield molecular constants for $B^2\Sigma_u^+$, $A^2\Pi_u$, and $X^2\Sigma_g^+$ (see Tables III-VI).

The final fitted parameter values depend on the deperturbation model employed. For each band, at least two $A^2\Pi_u$ perturbing vibrational levels were included even when the parameters for only one (or perhaps none) could be determined from the data. Structural and perturbation parameters which could not be varied but could be calculated were held fixed at these calculated values (See Table II).
For $A^2\Pi_u$, the results of Ref. (29) were used to calculate vibronic energies, rotational constants, and spin-orbit constants.

When it was impossible to determine D and H centrifugal distortion constants for $X^2\Sigma_g^+$ and $B^2\Sigma_u^+$, they were held fixed at values calculated from RKR potential curves (30). For $A^2\Pi_u$,D and H were always fixed at calculated values. In Table V these calculated centrifugal distortion constants are compared with fitted values.

V. Results

Band by band and merged constants and uncertainties of one standard deviation are presented in Tables II-VI. Constants are reported with more significant figures than their uncertainties warrant in order to compensate for correlation among parameters (31).[3]

Although ill-determined, the values of H_o' and H_o'' were of necessity varied in the (0,0) band fit in order to eliminate systematic deviations between observed and calculated values for $N' > 45$. Bands not extending to $N > 50$ (1) were fit with H' and H" fixed at the values given in Table V.

In Tables III, IV, and V the constants derived here are compared with those obtained by earlier workers. Although the values and precision of the present $X^2\Sigma_g^+$ constants are comparable to previous results, a substantial improvement in precision for the $B^2\Sigma_u^+$ constants should be noted. Both $\omega_e y_e$ and $\omega_e z_e$ for $B^2\Sigma_u^+$, which are unusually large (compare $\omega_e' y_e'$ with $\omega_e'' y_e''$ for example), had to be considered in accounting for observed spacings.

Table IV gives Dunham coefficients for $X^2\Sigma_g^+$ and $B^2\Sigma_u^+$ based on the merged fits.[4] The $A^2\Pi_u$ constants in Table IV were obtained by combining merged T_Π's and B_Π's and data from (29) and (32) in (v + 1/2)polynomial fits; correlations with other parameters were ignored so that the uncertainties quoted for $A^2\Pi_u$ constants in Table IV are underestimated.

The standard deviation of the merged fit, σ_m, is 11.56 (66 degrees of freedom) indicating the existence of systematic errors between different band segments: ideally, σ_m should be unity (2). Comparison of constants from band to band in Table II further illustrates this problem: the

$E_{\Pi}-E_{\Sigma}$ values in (0,0) and (0,1), for example, differ by more than three times their combined standard deviations. It should be noted, however, that no systematic errors are observed within a particular band; σ for each band fit is nearly unity. Systematic errors between band segments are most likely a result of experimental measurement errors (in the wavelength dispersion curve) as well as the inability to vary all constants associated with a perturbing level. Fixing constants presumes that they are precisely known and completely uncorrelated with other parameters. To the extent that these presumptions are false, discrepancies between constants from two bands sharing a common level will be larger than the statistical uncertainties would suggest. As a result, σ_m is much larger than one; uncertainties quoted in Tables II, III, and IV are lower bounds to true one standard deviation limits; and merged constants cannot be expected to reproduce observed spectra as well as band by band constants.

Table III is a summary of the perturbations observed in (1) with the fitted spin-orbit and rotation-electronic vibronic interaction parameters, ξ and 2η. ξ and 2η were divided by $\langle v_A | v_B \rangle$ and $\langle v_A | B | v_B \rangle$, respectively, to obtain the constant electronic factors H_{el}^{SO} and H_{el}^{RE} (23, 24, 33, 34). The weighted average values are

$H_{el}^{SO} = \frac{\xi}{\langle v_B | v_A \rangle} = -33.2 \pm 0.6 \text{ cm}^{-1}$ and

$H_{el}^{RE} = \frac{2\eta}{\langle v_B | B | v_A \rangle} = 1.069 \pm 0.027$ unitless. These factors were in turn multiplied by the appropriate vibrational matrix elements to obtain fixed ξ and η values for those $v_B \sim v_A$ interactions for which these values could not be obtained by fitting.

Analysis of v' = 3

In fitting the data of (1), we found it necessary to change some previous assignments, particularly in the (3,5) band. As stated above, four distinct analyses of $B^2\Sigma_u^+$ (v' = 3) exist in the literature (4-7); the assignments for (3,5) made in (1) were based on the work of Ref. (5). However, these assignments were found to be inconsistent with the Hamiltonian matrix given in Table I. We have been able to reassign a large portion of the (3,5) band near the origin and achieve a fit comparable in quality to that of other bands (see Table VII).

$B^2\Sigma_u^+$ (v' = 3) is perturbed by $A^2\Pi_{u1/2}$(v=14) with crossings at the hypothetical J values 6.0 and 10.0 for the f and e levels, respectively. The signs and magnitudes of ξ and η for this perturbation are such that the f level interaction is weak (maximum level shift of $\sim$ 1 cm^{-1}) while the e level perturbation is strong (maximum level shift of $\sim$ 12 cm^{-1}) (see Fig. 1). This perturbation causes deviations from the expected (N + 1)/N P_1 to P_2 (or R_1 to R_2) intensity ratio (14). Moreover, the perturbation causes a change in the relative positions of the P_1 and P_2 (R_1 and R_2) lines: below the e level crossing for example, the P_1 lines, which would normally lie at higher frequency than the P_2 lines, are shifted to lower frequency than the P_2 lines; after the perturbation culminates, the branches usually recross. Incorrect analyses (4, 5, and 7) resulted from either confusing the F_1 and F_2 transitions (4 and 7) or from inclusion of spurious lines probably due to the second positive group of N_2 (5).[5] Crawford and Tsai (6) very carefully considered the effects of perturbations on line positions and intensities in making their assignments. Our analysis confirms theirs.

These reassignments and the subsequent deperturbation of the (3,5) band have also led to the prediction and discovery of several extra

lines (see Table VIII) which arise from the sharing of $B^2\Sigma_u^+$ and $A^2\Pi_u$ character. Ordinarily $A^2\Pi_u \rightarrow X^2\Sigma_g^+$ emission is not observed in this spectral region due to small Franck-Condon factors (however, see Ref. (35)).

Similarly, other bands were extended to higher J and extra lines were found at perturbations in $B^2\Sigma_u^+$ (v' = 1 and 5). Extra lines, reassignments, and extensions are given in Table VIII.

Analysis of v' = 5

$B^2\Sigma_u^+$ (v' = 5) also warrants special attention. Janin et al. (36) first deperturbed this level and obtained an energy for $A^2\Pi_u$(v=17) equal to 36805 cm^{-1} (relative to $X^2\Sigma_g^+$, v" = 0, J" = 0). This value is $\sim$ 20 cm^{-1} higher than the energy calculated from Table IV. However, Maier and Holland (35) observed emission from an ion beam, with low resolution, in the Meinel $A^2\Pi_u \rightarrow X^2\Sigma_g^+$ system from levels up to v' = 19. They did not observe an anomaly near v' = 17. On the contrary, emission was observed exactly where expected for v' = 17 but they felt that their data were inconclusive and that another perturbing state (e.g. $a^4\Sigma_u^+$) might be responsible for the anomalies observed in $B^2\Sigma_u^+$ (v = 5).

Our analysis of the (5,7) band from (1) is consistent with an $A^2\Pi_u \sim B^2\Sigma_u^+$ perturbation (see Table III); T_{17}^{Π} is in agreement with the calculated value (Table IV) and also with that calculated with the constants of (28). Since the (5,7) band of (1) is incomplete near the region of interest (See (1) and Table III), we decided to further test the assignments made in (6 and 8).[The assignments of the (5,8) band in (5)and (8) are essentially identical so that data from (5) were not examined]. Neither the (5,7) band from (6) nor the (5,8) band from (8) could be fitted with a $^2\Sigma^+ \sim {}^2\Pi$ model: even excluding the lines with lowest N-values,

the bands were poorly fit ($\sigma_{rms} \sim 0.3$ cm^{-1}) and under no circumstances were the perturbation matrix elements found to be consistent with the results of Table III. We then proceeded to fit the (5,8) band recently reported by Klynning and Pages (7) who have stated (37) that the previous determination of T^{Π}_{17} (36) was indeed in error. Holding the $A^2\Pi_u$ energy and perturbation parameters fixed at values calculated from Tables III and IV, but varying B', D', γ', B", and D" we obtained a good fit ($\sigma_{rms} \sim .05$ cm^{-1}) and values of the varied parameters consistent with those determined in our fits to the (5,7) and (6,8) bands from Ref. (1). The above tests suggest that the analyses (5,6, and 8) are in error and if a perturbing state other than $A^2\Pi_u$ is present, its effect on the energy levels of $B\,^2\Sigma^+_u(v' = 5)$ is a level shift smaller than 0.03 cm^{-1}.

VI. Discussion

$B^2\Sigma_u^+$ and $X^2\Sigma_g^+$ Spin-Rotation Interactions

Spin-rotation interaction in a $^2\Sigma$ state has been shown by Van Vleck (38) to arise from true spin-rotation interaction and second order spin-orbit and rotation-electronic effects (20, 21):

$$\gamma_\Sigma = \gamma_\Sigma^{true} - p_\Sigma$$

$$\text{or} \quad \gamma_\Sigma = \gamma_\Sigma^{true} - 2 \sum_{v,\Pi} \frac{\langle {}^2\Sigma, v|A(R)L_+|v', {}^2\Pi\rangle\langle {}^2\Pi, v'|BL_+|v, {}^2\Sigma\rangle}{E_\Sigma(v) - E_\Pi(v')} \qquad (1)$$

where $\langle {}^2\Sigma, v|A(R)L_+|v', {}^2\Pi\rangle \doteq 2H_{el}^{SO}\langle v|v'\rangle$

and $\langle {}^2\Pi, v'|BL_+|v, {}^2\Sigma\rangle \doteq H_{el}^{RE}\langle v'|B|v\rangle$.

Using the method of Green and Zare (39)[6], $\gamma_\Sigma{}^{"\,true} = 3.5 \times 10^{-5}$ cm^{-1}. This is negligible compared with the experimental values of γ" given in Table VI and the γ_Σ determined here is really $-p_\Sigma$.

The spin-orbit and rotation-electronic operators in Eq. (1) are composed primarily of one-electron operators so that only Π states arising from configurations differing by one spin-orbital from the $^2\Sigma$ configuration interact strongly and make a significant contribution to p_Σ.

The dominant configurations for the lowest states of N_2^+ are (40):

$$X^2\Sigma_g^+ \quad 1\sigma_g{}^2 1\sigma_u{}^2 2\sigma_g{}^2 2\sigma_u{}^2 1\pi_u{}^4 3\sigma_g \qquad (2a)$$

$$A^2\Pi_{u_i} \quad 1\sigma_g{}^2 1\sigma_u{}^2 2\sigma_g{}^2 2\sigma_u{}^2 1\pi_u{}^3 3\sigma_g{}^2 \qquad (2b)$$

$$B^2\Sigma_u^+ \quad 1\sigma_g{}^2 1\sigma_u{}^2 2\sigma_g{}^2 2\sigma_u{}^1 1\pi_u{}^4 3\sigma_g{}^2 \qquad (2c)$$

Because H^{SO} and H^{RE} are diagonal with respect to g-u inversion symmetry, $X^2\Sigma_g^+$ and $A^2\Pi_u$ cannot perturb one another. Two configurations which give rise to $^2\Pi_g$ states and can interact with $X^2\Sigma_g^+$ are:

$$\text{I} \quad 1\sigma_g^2 1\sigma_u^2 2\sigma_g^2 2\sigma_u^2 1\pi_u^4 1\pi_g \tag{3a}$$

$$\text{II} \quad 1\sigma_g^2 1\sigma_u^2 2\sigma_g^2 2\sigma_u^2 1\pi_u^3 3\sigma_g 3\sigma_u \tag{3b}$$

Configurations other than I and II are unimportant because they have the wrong g-u symmetry, differ by more than one spin-orbital, or are composed of atomic orbitals with n ℓ character different from those comprising the $X^2\Sigma_g^+$ molecular orbitals. Using the techniques outlined in Refs.(18, 23, 24, and 41) we obtain[7]:

$$\langle X^2\Sigma_g^+, v|H^{SO}|v', {}^2\Pi_{g1/2}\ (I)\rangle = \frac{1}{2}\langle 1\pi_g|\hat{a}\ \ell_+|3\sigma_g\rangle\langle v|v'\rangle \tag{4a}$$

$$\langle X^2\Sigma_g^+, v|H^{RE}|v', {}^2\Pi_{g1/2}(I)\rangle = \langle 1\pi_g|\ell_+|3\sigma_g\rangle\langle v|B|v'\rangle\ [1 \mp x], \tag{4b}$$

where $x = J + 1/2$ and the upper (lower) sign refers to e(f) parity. First, it should be noted that the vibronic parts of H^{SO} and H^{RE} in Eq. (4) have the same sign[8] so that for the $^2\Pi_g(I)$ state, which lies above $X^2\Sigma_g^+$, p_Σ is negative (see Eq. (1)) in accord with the experimental values of Table VI. Assuming pure precession,

$$|3\sigma_g\rangle = \frac{1}{\sqrt{2}}\{|\sigma 2p_{N_1}\rangle - |\sigma 2p_{N_2}\rangle\} \tag{5a}$$

$$|1\pi_g\rangle \quad \frac{1}{\sqrt{2}}\{|\pi 2p_{N_1}\rangle - |\pi 2p_{N_2}\rangle\} \tag{5b}$$

and ignoring the overlap between orbitals localized on different centers, we can rewrite Eq. (4) in terms of $\zeta(n\ell)$ atomic spin-orbit parameters (18, 42, 43):

$$< {}^2\Sigma_g^+, v|H^{SO}|v', {}^2\Pi_{g1/2}(I)> = \frac{\sqrt{2}}{4}[\zeta(2p_{N^+}) + \zeta(2p_N)] <v|v'> = 57 <v|v'>$$

$$<X^2\Sigma_g^+, v|H^{RE}|v', {}^2\Pi_{g1/2}(I)> = \sqrt{2} <v|B|v'>[1 \mp x] \quad (6)$$

using $\zeta(2p_N) = 73.3$ and $\zeta(2p_{N^+}) = 87.5$ cm^{-1} (43).

To the extent that Eq. (5) is valid, one may also assume

$$<v|v'> = \delta_{vv'} \quad (7)$$

and $$<v|B|v> = B_v^{\Pi} = B_v^{\Sigma} \sim B_e^{\Sigma} = 1.9316 \text{ cm}^{-1}.$$

A similar analysis of the interactions between configuration II of Eq. (5) and $X^2\Sigma_g^+$ shows H^{RE} to be zero in this case, so in fact configuration I and Eq. (6) are sufficient to estimate p_Σ".

The lowest known $^2\Pi_g$ state of N_2^+ is $D^2\Pi_g$ which bears little resemblance to $X^2\Sigma_g^+$ at values of R near R_e (i.e. $D^2\Pi_g$ and $X^2\Sigma_g^+$ spectroscopic constants are very different) (29). By analogy with isoelectronic CN (44), $D^2\Pi_g$ can be represented as a mixture of configurations I and

$$\text{III} \qquad 1\sigma_g{}^2 1\sigma_u{}^2 2\sigma_g{}^2 2\sigma_u{}^2\ 3\sigma_g{}^2\ 1\pi_u{}^2\ 1\pi_g \quad (8)$$

In CN, configuration III is dominant at values of R near R_e but at values of R near the inner $D^2\Pi$ wall, where overlap with low $X^2\Sigma^+$ vibrational levels is important, configuration I prevails. Thus,

$E_\Sigma(v) - E_\Pi(v') \sim T_e(D^2\Pi_g) = 52815.2$ (29) is assumed, placing an upper bound on γ_Σ'' of .012 cm^{-1} which is in accord with the results in Table VI.

In calculating p_Σ' (for $B^2\Sigma_u^+$) the effect of the $A^2\Pi_u$ state is considered. Using the values of H_{el}^{SO} and H_{el}^{RE} in Table III and vibrational matrix elements

calculated from RKR curves generated from the constants in Table IV we compute p, being careful to exclude from the summation in Eq. (1) $A^2\Pi_u(v_A)$ levels which are explicitly included in the v_B matrix (see Table II). The results of these computations are tabulated in Table VI and are illustrated in Fig. 2.

Second Order Corrections to B and ν_o

B and ν_o are completely correlated with second order perturbation parameters (20, 21):

$$\tilde{B}_v = B_v + q_\Sigma$$
$$\tilde{\nu}_o = E' + o_\Sigma' - E'' - o_\Sigma'' \qquad (9)$$

where

$$q_\Sigma \equiv 2 \sum_{v',\Pi} \frac{|\langle {}^2\Pi, v'|BL_+|v, {}^2\Sigma\rangle|^2}{E_\Sigma(v) - E_\Pi(v')}$$

$$o_\Sigma \equiv \frac{1}{4} \sum_{v',\Pi} \frac{|\langle {}^2\Pi, v'|A(R)L_+|v, {}^2\Sigma\rangle|^2}{E_\Sigma(v) - E_\Pi(v')}$$

As for p_Σ, these summations were evaluated explicitly for $B^2\Sigma_u^+$. $\tilde{B}'$ and $\tilde{\nu}_o$ were converted to B' and ν_o before merging (see Table II). q_Σ'' and o_Σ'' were ignored since they do not vary significantly with v" and they can not be reliably estimated.

Semi-Empirical Estimates of H_{el}^{SO} and H_{el}^{RE}

The $2\sigma_u$ orbital in Eq. (2b) and (2c) must have some 2p atomic character in order to be strongly perturbed by $A^2\Pi_u$:

$$|2\sigma_u> = \left[\frac{1-\varepsilon^2}{2}\right]^{1/2} [|\sigma 2s_{N_1}> - |\sigma 2s_{N_2}>] + \frac{\varepsilon}{\sqrt{2}}[|\sigma 2p_{N_1}> + |\sigma 2p_{N_2}>] \quad (10a)$$

$$|1\pi_u> = \frac{1}{\sqrt{2}}[|\pi 2p_{N_1}> + |\pi 2p_{N_2}>] \quad (10b)$$

where ε^2 represents the 2p character in $2\sigma_u$. Employing the same assumptions used in deriving Eq. (6), and assuming Eq.(10) to be valid:

$$H_{el}^{RE} = \varepsilon<\pi 2p|\ell_+|\sigma 2p> = 1.414\varepsilon \quad (11a)$$

$$H_{el}^{SO} = -\frac{\varepsilon\sqrt{2}}{4}[\zeta(2p_N) + \zeta(2p_{N^+})] = -56.85\varepsilon. \quad (11b)$$

Using the Hartree Fock value for $\varepsilon = .573$ determined for $X^2\Sigma_g^+(45)$ and assuming the $B^2\Sigma_u^+$ and $X^2\Sigma_g^+$ $2\sigma_u$ orbitals to be identical,

$$H_{el}^{RE} \sim 0.810$$

$$H_{el}^{SO} \sim -32.6 \text{ cm}^{-1}.$$

These values are in surprisingly good agreement with the results of Table III.

The Determination and Interpretation of γ_J'

Table VI reports values of γ_J' for $B^2\Sigma_u^+$ (v' = 0-3). Although these parameters were only marginally determined, their inclusion in the fits for v' = 0-3 were essential to eliminate small systematic deviations between observed and calculated transition frequencies. An attempt was

also made to vary γ_J'' but it was found that γ_J' and γ_J'' were almost completely correlated (correlation coefficient $\sim$ 0.95) so that only $\gamma_J' - \gamma_J''$ could be determined (all other γ_J' and γ_J'' correlation coefficient magnitudes were <0.1).

Veseth (46) has derived an expression for γ_J in terms of higher order (>2) $^2\Pi \sim {}^2\Sigma$ interactions which for the case of pure precession reduces to:

$$\gamma_J \sim -2\gamma \frac{D_V}{B_V} \qquad (12)$$

As shown above, $X^2\Sigma_g^+$ may be considered to be in pure precession with $^2\Pi_g(I)$, so that Eq. (12) should be a reasonable approximation for γ_J'':

$$\gamma_J'' \sim -6 \times 10^{-8}\ cm^{-1}.$$

This is approximately an order of magnitude smaller than the values of γ_J' in Table VI and indicates that we are primarily determining γ_J' and not $\gamma_J' - \gamma_J''$. Eq. (12) is not expected to be valid for $B^2\Sigma_u^+$ because of interaction with the significantly different $A^2\Pi_u$ state. An additional term to Eq. (12) may be considered in the case where pure precession is invalid but interaction with only one $^2\Pi$ level is important (46):

$$\gamma_J \sim -2\gamma \frac{D_V}{B_V} - \gamma \frac{B_\Pi - B_\Sigma}{\gamma_e(\Pi\Sigma)} \qquad (13)$$

Although this equation is of dubious value here, it provides an order of magnitude estimate of $\gamma_J' \sim -6 \times 10^{-7} cm^{-1}$, which is comparable to the values given in Table VI.

Anharmonicity of the $B^2\Sigma_u^+$ Potential Well

From Table IV we note the large negative values of Y_{30} and Y_{40}. If these values are used to extrapolate $B^2\Sigma_u^+$ to the dissociation limit, dissociation is predicted between v' = 17 and 18; however, v' = 29 has been observed (28). Thus, these constants are valid only for interpolation through v' = 6 and extrapolation to v' $\sim$ 8. Higher order terms Y_{50}, Y_{60}, etc. are important for higher v'. This anharmonicity is caused by the J independent $B^2\Sigma_u^+ \sim C^2\Sigma_u^+$ interaction (47), which may also be responsible for $C^2\Sigma_u^+$ predissociation (48). Douglas (47) has already discussed the "peculiar manner in which $B^2\Sigma_u^+$" dissociates.

VII. Conclusion

Described above is the deperturbation of N_2^+ 1NG using a model Hamiltonian including only $^2\Pi_u$ perturbing states. It should be emphasized that the numbers given in Tables II-VI are not minimum-variance-linear-unbiased (MVLU) estimates (22). On the contrary, we have exercised a bias by holding fixed many constants at calculated values to insure an internally consistent, complete deperturbation. To the extent that our calculated values are in error, our quoted uncertainties are underestimates. We believe this method to be a practical deperturbation procedure if not statistically rigorous.

Our analysis has been shown to be self-consistent using the following critera:[9] 1) centrifugal distortion constants calculated from RKR potential energy curves agree with the experimental, fitted values; 2) the fitted values of γ_Σ" are less than semi-empirically predicted upper bounds; 3) γ_Σ' may be calculated from fitted matrix elements and vibrational factors calculated from RKR potential energy curves; 4) the magnitude of the spin-orbit and rotation-electronic matrix elements are explained in terms of simple LCAO-MO theory; and 5) the deperturbed band by band constants reproduce the observed spectra to within the estimated experimental uncertainty without systematic deviations.

Acknowledgements

We are indebted to Dr. Daniel Albritton for generously giving us copies of and helpful advice on the computer programs MERGE and DHL.

We also thank Dr. H. Lefebvre-Brion for kindly providing us with results from *ab initio* calculations on $X\,^2\Sigma_g^+$ and Mr. Anthony Kotlar for his modifications of the least squares fitting program. Discussions with Dr. R. Bacis, Dr. I. Renhorn, and Professor J. d'Incan were both stimulating and informative. We thank Dr. L. Klynning for graciously supplying us with results of his studies on N_2^+ 1NG prior to publication.

Critical readings of the original manuscript by Dr. J. Coxon, Dr. M. Horani, and Dr. J. Rostas, and Dr. H. Lefebvre-Brion are most appreciated.

This work was supported, in part, by grants from the National Science Foundation. Computer time for this project was partly provided by the Computer Science Center of the University of Maryland, the M.I.T. Chemistry Department, and by a contract from IBM to the M.I.T. Laboratory for Computer Science.

Footnotes:

1. If the $^2\Sigma$ state is not known to be either $^2\Sigma^+$ or $^2\Sigma^-$, it is never possible to unambiguously determine the signs of γ' and γ''. It should be noted that the sign of γ'' could be determined from $A^2\Pi_u - X^2\Sigma_g^+$ band spectra but to date this has not been accomplished owing to insufficient resolution.

2. Lines from Ref. (1) are divided into five categories for the weighting procedure:

Line Type	Uncertainty
δ	0.1
)	0.03
intensity 0	0.02
intensity 1	0.01
all others	0.007

The weight associated with each line is equal to the reciprocal of the uncertainty squared. δ denotes a doubly assigned line;) denotes an incompletely resolved line.

3. The covariance and correlation matrices are available from the authors upon request. If for some reason the authors cannot be reached, a limited number of copies have been deposited at the Editorial Office.

4. We have combined the (2,5), (4,7), (5,3), (5,8), and (6,9) band origins of Ref. (28) with our data [using uncertainties of 0.5 cm^{-1}].

5. The authors of (7) have indicated to us that the branches as given are indeed mislabelled.

6. Although Green and Zare(36) give a formula for γ^{true} [Eqn. (5) in (36)] applicable to a $^2\Pi$ state, it is also valid for a $^2\Sigma^+$ state arising from a σ orbital outside a closed shell, as in the case of N_2^+ $X^2\Sigma_g^+$. These ab initio calculations were performed for us by Dr. H. Lefebvre-Brion.

7. Only matrix elements between $X^2\Sigma_g^+$ and $^2\Pi_{g1/2}$ are considered because the second order $X^2\Sigma_g^+ \sim {}^2\Pi_{g3/2}$ interaction contributes nothing to γ_Σ in Eqn. (1).

8. $\langle 1\pi_g|\hat{a}\ell_+|3\sigma_g\rangle$ and $\langle 1\pi_g|\ell_+|3\sigma_g\rangle$ are positive definite (18); $\langle v|v'\rangle$ and $\langle v|B|v'\rangle$ have the same sign except for small overlap when their signs might be different.

9. Except for criterion number five, these conditions are met for both band by band and merged constants.

References

1. K.A. Dick, W. Benesch, H.M. Crosswhite, S.G. Tilford, R.A. Gottscho, and R.W. Field; J. Mol. Spectrosc. 69, 95-108 (1978).
2. D.L. Albritton, A.L. Schmeltekopf, and R.N. Zare; J. Mol. Spectrosc. 67, 132-156 (1977).
3. D.L. Albritton, A.L. Schmeltekopf, W.J. Harrop, and R.N. Zare; J. Mol. Spectrosc. 67, 157-184 (1977).
4. D. Coster and H.H. Brons, Z. Physik 73, 747-774 (1932).
5. H.H. Brons, K. Akad. Wet. Amst. (Sci.) 38, 271-280 (1935).
6. F.H. Crawford and P.M. Tsai, Proc. Am. Acad. Arts Sci. 69, 407-437 (1935).
7. L. Klynning and P. Pagés, Physica Scripta 6, 195-199 (1972).
8. A.E. Parker, Phys. Rev. 44, 914-918 (1933).
9. J. d'Incan and A. Topouzkhanian, J. Chem. Phys. 63, 2683-2689 (1975).
10. K. Dressler, J. Chem. Phys. 64, 3493-3494 (1976).
11. J. d'Incan and A. Topouzkhanian, J. Chem. Phys. 64, 3494 (1976).
12. V. Cermak and Z. Herman, Coll. Czech. Chem. Commun. 27, 1493-1495 (1962).
13. J.Dufayard and O. Nedelec, Comp. Rend. Ac. Sc. B 285, 173-174 (1977).
14. G. Herzberg, Molecular Spectra and Molecular Structure. I. Spectra of Diatomic Molecules (Van Nostrand Reinhold Co., New York, 1950).
15. J.M. Brown, J.T. Hougen, K.-P. Huber, J.W.C. Johns, I. Kopp, H. Lefebvre-Brion, A. J. Merer, D.A. Ramsay, J. Rostas, and R.N. Zare, J. Mol. Spectrosc. 55, 500-503 (1975).
16. A.E. Parker, Phys. Rev. 44, 90-91 (1933).

17. W.H.J. Childs, Proc. Roy. Soc. A 137, 641-661 (1932).

18. H. Lefebvre-Brion, "Perturbations in the Spectra of Diatomic Molecules" in Atoms, Molecules, and Lasers, International Atomic Energy Agency (Vienna, 1974) pp. 411-448.

19. J.T. Hougen, "The Calculation of Rotational Energy Levels and Rotational Line Intensities in Diatomic Molecules", Nat. Bur. Std. Mono. 115 (1970).

20. J.A. Coxon, J. Mol. Spectrosc. 58, 1-28 (1975).

21. R.N. Zare, A.L. Schmeltekopf, W.J.Harrop, and D.L. Albritton; J. Mol. Spectrosc. 46, 37-66 (1973).

22. D.L. Albritton, A.L. Schmeltekopf, and R.N. Zare, "An introduction to the least-squares fitting of spectroscopic data" in Modern Spectroscopy, Modern Research II (K. Narahari Rao, Ed.), pp. 1-67, Academic Press, New York, 1976.

23. R.W. Field, S.G. Tilford, R.A. Howard, and J.D. Simmons; J. Mol. Spectrosc. 44, 347-382 (1972).

24. R.W. Field, B.G. Wicke, J.D. Simmons, and S.G. Tilford; J. Mol. Spectrosc. 44, 383-399 (1972).

25. A. Lagerqvist and E. Miescher, Can. J. Phys. 44, 1525-1539 (1966).

26. E. Bartholdi, M. Leoni, and K. Dressler, J. Appl. Math. Phys. (ZAMP) 22, 797-799 (1971).

27. a) W.E. Wentworth, J. Chem. Ed. 42, 96-103 (1965).

b) D.W. Marquardt, J. Soc. Indust. Appl. Math. 11, 431-441 (1963). This program was originally written by R. Stern and has since been modified by T. Bergeman and A. Kotlar.

28. A. Lofthus and P. Krupenie, J. Phys. Chem. Ref. Data 6, 113-307 (1977).

29. J. Janin, J. d'Incan, R. Stringat, and J. Magnaval; Rev. d'Opt. 42, 120-128 (1963).

30. D.L. Albritton, W.J. Harrop, A.L. Schmeltekopf, and R.N. Zare, J. Mol. Spectrosc. 25-36 (1973).

31. J.K.G. Watson, J. Mol. Spectrosc. 66, 500-502 (1977).

32. A.E. Douglas, Astrophys. J. 117 , 380-386 (1953).

33. J.A. Hall, J. Schamps, J.M. Robbe, and H. Lefebvre-Brion; J. Chem. Phys. 59, 3271-3283 (1973).

34. R.W. Field, J. Chem. Phys. 60, 2400-2413 (1974).

35. W.B. Maier and R.F. Holland, J. Chem. Phys. 59, 4501-4534 (1973).

36. J. Janin, J. d'Incan, and J. Marchand; Annales, Sec. B; Univ. Lyon, Sci. Phys. Chim. 12, 29-42 (1959).

37. P. Pagès, "The N_2^+ Molecule", pp. 17-18 in Annual Report 1976/77, Molecular Physics, Institute of Physics, University of Stockholm.

38. J.H. Van Vleck, Phys. Rev. 33, 467-506 (1929).

39. S. Green and R.N. Zare, J. Mol. Spectrosc. 64, 217-222 (1977).

40. R.C. Sahni and B.C. Sawhney. Int. J. Quant. Chem. 1, 251-270 (1967).

41. T.E.H. Walker, Mol. Phys. 23, 489-498 (1972).

42. H. Lefebvre-Brion and C.M. Moser, J. Chem. Phys. 44, 2951-2954 (1966).

43. E. Ishiguro and M. Kobori, J. Phys. Soc. Japan 22, 263-270 (1967).

44. H.F. Schaeffer and T.G. Heil, J. Chem. Phys. 54, 2573-2580 (1971).

45. H. Lefebvre-Brion (private communication).

46. L. Veseth, J. Phys. B. Atom. Molec. Phys. 3, 1677-1690 (1970).

47. A.E. Douglas, Can. J. Phys. 30, 302-313 (1952).

48. J. Tellinghuisen and D.L. Albritton, Chem. Phys. Lett., 31, 91-96 (1975).

Figure Captions

Figure 1. Perturbations in the N_2^+ $B^2\Sigma_u^+ - X^2\Sigma_g^+$ (3,5) band illustrating the different interaction strengths for e and f parity levels. Plotted against N" is $R(N")_{calc} - R(N")_{obs}$ where $R_{1,2}(N")_{calc} = \nu_o + F'_{1,2}(N" + 1) - F"_{1,2}(N")$, $F_1(N) = BN(N+1) - DN^2(N+1)^2 + HN^3(N+1)^3 + 1/2\gamma N$ and $F_2(N) = F_1(N) - \gamma(N + 1/2)$. Open circles o represent $R_{1,calc} - R_{1,obs}$ and closed circles • represent $R_{2,calc} - R_{2,obs}$.

Figure 2. $B^2\Sigma_u^+$ spin rotation constant, γ, as a function of v. Error bars represent one standard deviation. Closed circles • are calculated $-p_\Sigma$'s (see text).

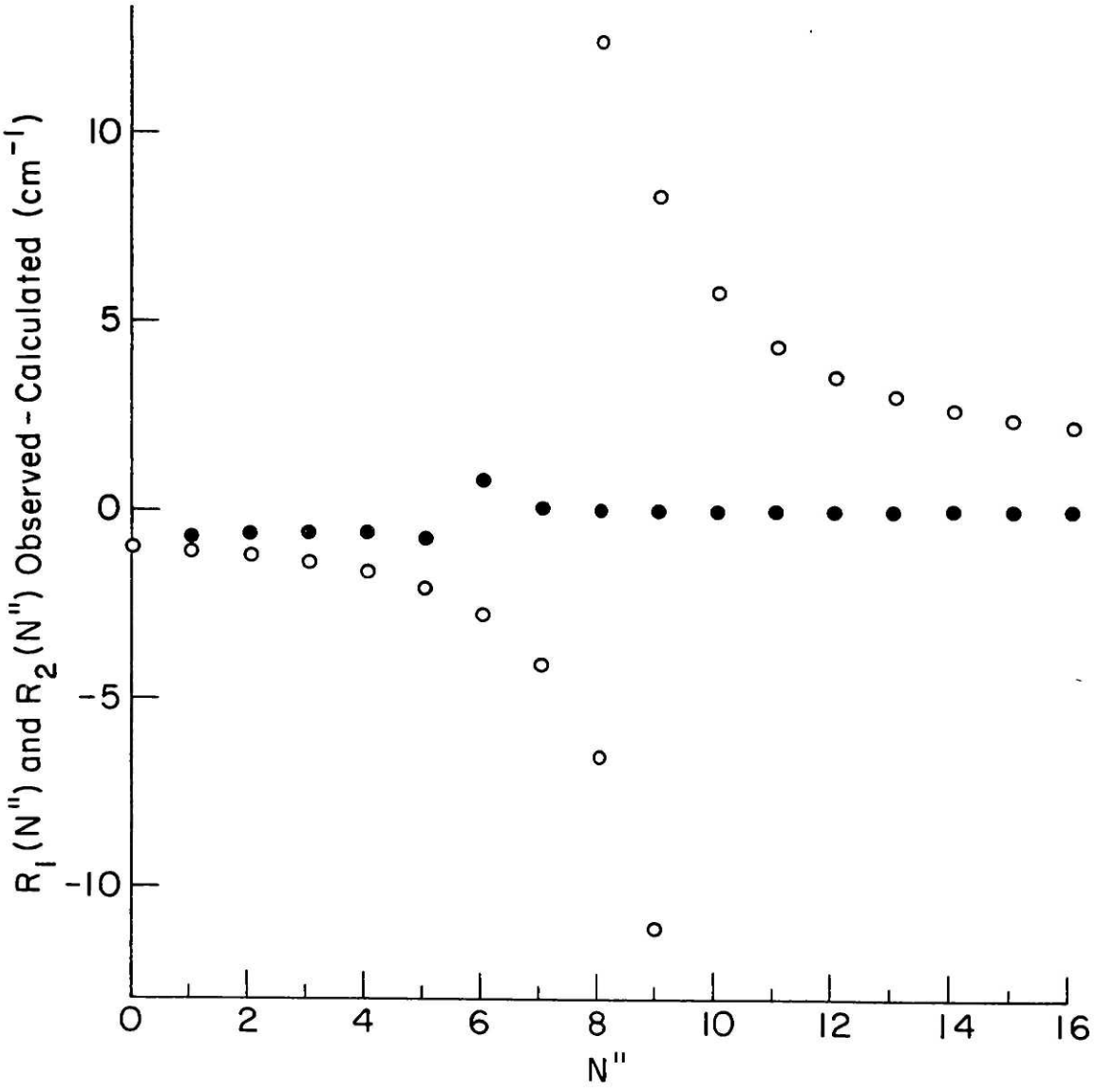
$R_1(N'')$ and $R_2(N'')$ Observed - Calculated (cm^{-1})
10
5
0
-5
-10
0
2
4
6
8
10
12
14
16
N''

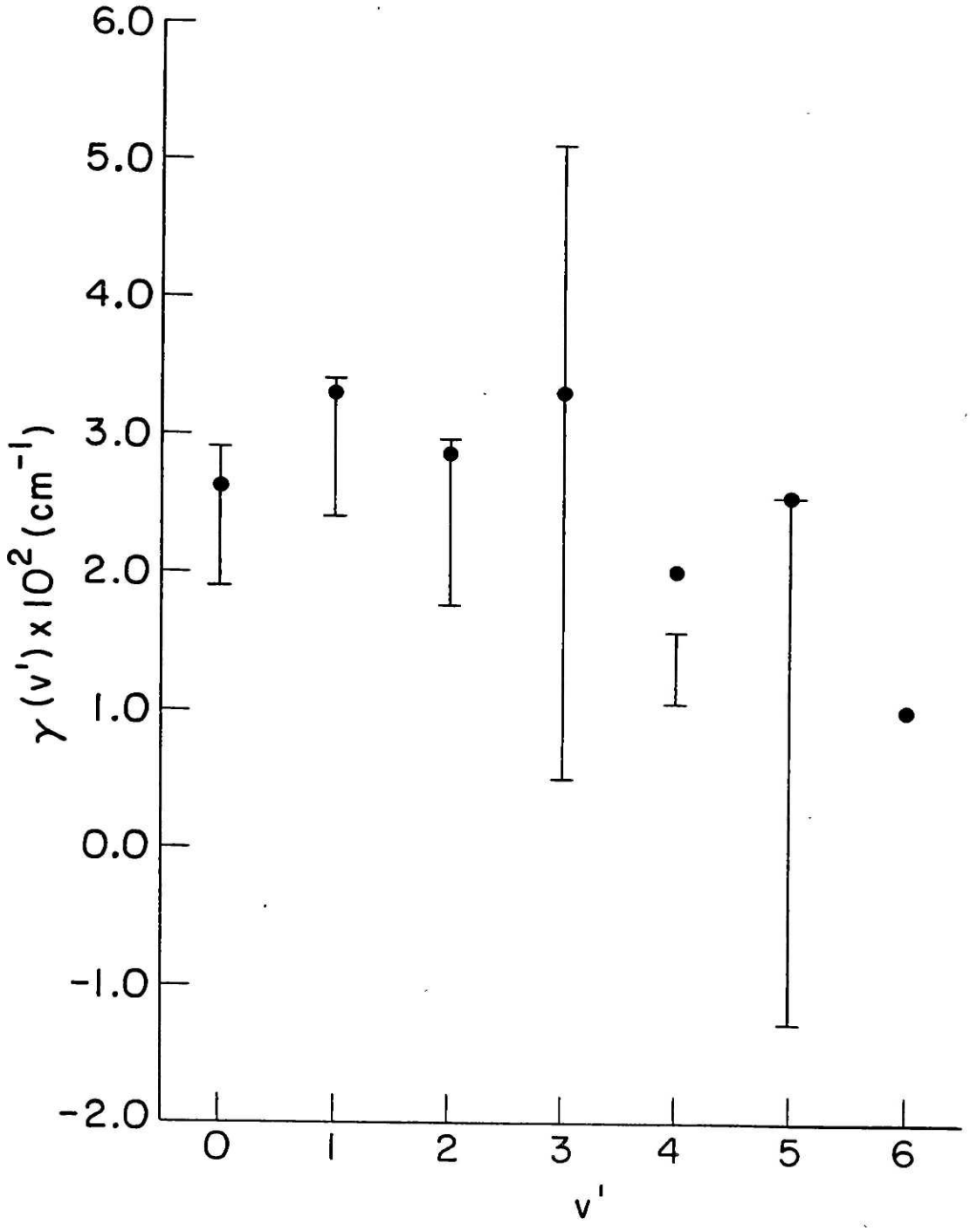
6.0
5.0
4.0
3.0
2.0
1.0
0.0
-1.0
-2.0
$\gamma(v') \times 10^2 (cm^{-1})$
0
1
2
3
4
5
6
v'

Table Headings

	$^2\Sigma^+$	$^2\Pi_{1/2}$	$^2\Pi_{3/2}$
$^2\Sigma^+$	$T^\Sigma + o^\Sigma + (B^\Sigma + q^\Sigma)x(x \mp 1) - D^\Sigma x^2 (x \mp 1)^2 + H^\Sigma x^3 (x \mp 1)^3$ $- \frac{1}{2}(1 \mp x)[\gamma^\Sigma + \gamma_J^\Sigma (x^2 - 1/4)]$	symmetric	symmetric
$^2\Pi_{1/2}$	$\xi + 2\eta (1 \mp x)$	$T^\Pi + B^\Pi x^2 - D^\Pi [x^4 + x^2 - 1]$ $+ H^\Pi [x^6 + 3x^4 - 5x^2 + 2] - \frac{1}{2} A^\Pi$	symmetric
$^2\Pi_{3/2}$	$- 2\eta (x^2 - 1)^{1/2}$	$-B^\Pi (x^2-1)^{1/2} + 2D^\Pi (x^2 - 1)^{3/2}$ $-H^\Pi [(x^2 - 1)^{1/2}(3x^4 - 5x^2 + 3)]$	$T_v^\Pi + B^\Pi (x^2 - 2) - D^\Pi [x^4 - 3x^2 + 3]$ $+H^\Pi [(x^2 - 2)^3 + 3x^4 - 7x^2 + 4] + \frac{1}{2} A^\Pi$

where T = vibronic energy

B = $h/8\pi^2 c\mu R^2$ = rotational constant

D = 2nd order centrifugal distortion constant

H = 3rd order centrifugal distortion constant

γ = spin-rotation constant

γ_J = centrifual distortion of γ

A = spin-orbit constant

$\xi = \langle v', {}^2\Pi | \Sigma \hat{a}_i \ell_i \cdot s_i | {}^2\Sigma^+, v \rangle$ = vibronic spin-orbit matrix element.

$2\eta = \langle v', {}^2\Pi | BL_+ | {}^2\Sigma^-, v \rangle$ = vibronic rotation-electronic matrix element.

x = J + 1/2

[a] Only parameters which were either fitted or fixed at non-zero values are included here.

[b] Upper(lower) signs are for e(f) parity levels [J. M. Brown et al., J. Mol. Spectrosc. 55, 500-503 (1975)].

	(0,0)[b]	(0,1)	(0,2)
$\tilde{\nu}_o$	25566.051 ± 0.022	23391.307 ± 0.0010	21249.081 ± 0.022
o_v'	0.025	0.025	0.025
ν_o	25566.026	23391.282	21249.056
B"	1.9220488 ± 0.00004	1.9033125 ± 0.000024	1.8842765 ± 0.00004
D" x 10^6	5.89767 ± 0.027	5.933945 ± 0.011	6.002490 ± 0.03
γ"	0.008228 ± 0.0016	0.0085318 ± 0.0010	0.0068812 ± 0.0014
$\tilde{B}'$	2.0743336 ± 0.00004	2.0745547 ± 0.000024	2.0746170 ± 0.00004
q' x 10^3	0.903	0.903	0.903
B'	2.0734306	2.0736517	2.0737140
D' x 10^6	6.27900 ± 0.029	6.29159 ± 0.011	6.31464 ± 0.04
γ'	0.023011 ± 0.0016	0.023111 ± 0.0010	0.021494 ± 0.0014
γ_J' x 10^6	-1.3748 ± 0.05	-1.3230 ± 0.09	-1.3842 ± 0.27
v_Π[c]	9, 10, 11[d]	9, 10, 11	9, 10, 11
$E_\Pi - E_\Sigma$	837.337 ± 0.14	836.371 ± 0.10	834.886 ± 1.1
B_Π	1.541078 ± 0.00015	1.5418722 ± 0.00011	1.5421220 (fixed)
A_Π	-74.6 (fixed)	-74.6 (fixed)	-73.602583 (fixed)
ξ	-1.77700 ± 0.015 v_Π = 10 1.7504 ± 0.5 v_Π = 11[d]	-1.74660 ± 0.012	-1.7836639 (fixed)
2η	0.1394485 ± 0.00023 v_Π = 10 -0.107334 ± 0.0004 v_Π = 11[d]	0.1391175 ± 0.00026	0.134519 ± 0.0017

[a] See text and Table I for definitions of parameters. Uncertainties quoted represent one standard deviation.

[b] For (0,0) it was necessary to vary the third order centrifugal distortion constants: $H_0' = 4.918 \pm 5 \times 10^{-12}$ and $H_0'' = 7.431 \pm 5 \times 10^{-12}$ cm^{-1}. For all other bands the values of H' and H" were held fixed (see Table V).

	(1,1)	(1,2)	(1,3)
$\tilde{\nu}_o$	25762.9405 ± 0.0025	23620.7310 ± 0.0024	21511.2695 ± 0.006
σ'_v	0.028	0.028	0.028
ν_o	25762.9125	23620.703	21511.2415
B"	1.9034268 ± 0.00004	1.8842233 ± 0.000024	1.8651016 ± 0.00004
D" x 10^6	6.03681 ± 0.029	5.96975 ± 0.017	6.12577 ± 0.029
γ"	0.010630 ± 0.0012	0.008187 ± 0.0008	0.010021 ± 0.0017
$\tilde{B}'$	2.0518113 ± 0.00004	2.0517413 ± 0.000024	2.0519134 ± 0.00005
q' x 10^3	1.09	1.09	1.09
B'	2.0507213	2.0506513	2.0508234
D' x 10^6	6.60360 ± 0.029	6.51156 ± 0.016	6.62873 ± 0.028
γ'	0.030147 ± 0.0012	0.027826 ± 0.0008	0.029781 ± 0.0017
γ'_J x 10^6	-2.8463 ± 0.25	-3.0620 ± 0.14	-2.7845 ± 0.22
v_Π[c]	11, 12	11, 12	11, 12
$E_\Pi - E_\Sigma$	36.3159 ± 0.012	36.0589 ± 0.008	35.8311 ± 0.023
B_Π	1.524082 ± 0.0004	1.5262590 ± 0.00029	1.527876 ± 0.0008
A_Π	-74.7061 ± 0.16	-74.1101 ± 0.11	-73.8283 ± 0.38
ξ	-3.64284 ± 0.012	-3.66083 ± 0.012	-3.68234 ± 0.036
2η	0.295327 ± 0.0012	0.292143 ± 0.0013	0.288508 ± 0.0036

[c]Values of v_Π given are those levels included in the band fit. The underlined v_Π corresponds to the level or levels for which constants were varied. Constants for these levels only are given in the entries below v_Π.

[d]For (0,0), only the matrix elements ξ and η for the $v_\Pi = 11 \sim v' = 0$ interaction were varied. The $v_\Pi = 11$ energy and rotational constant were held fixed at the values determined by fits to $v'_\Sigma = 1$. The energy and rotational constant given under (0,0) for the Π state are those for $v_\Pi = 10$.

	(2,3)	(2,4)	(3,5)
$\tilde{\nu}_o$	23830.163 ± 0.04	21753.674 ± 0.002	21971.475 ± 0.003
o'_v	0.024	0.024	0.027
ν_o	23830.139	21753.650	21971.448
B"	1.8613181 ± 0.00022	1.8452253 ± 0.00004	1.8259291 ±0.00007
D" x 10^6	5.5238 ± 0.27	5.9444 ± 0.04	6.1429 ± 0.06
γ"	0.01717 ± 0.004	0.008127 ± 0.0014	0.010202 ± 0.0021
$\tilde{B}'$	2.0236871 ± 0.00021	2.0268155 ± 0.00005	2.0010520 ± 0.00007
q' x 10^3	0.906	0.906	1.03
B'	2.0227811	2.0259095	2.000022
D' x 10^6	6.6493 ± 0.23	6.7702 ± 0.05	7.1534 ± 0.07
γ'	0.030980 ± 0.0034	0.022374 ± 0.0014	0.030862 ± 0.0020
γ'_J x 10^6	-6.808 ± 0.8	-3.906 ± 0.4	-5.694 ± 0.5
v_Π [c]	12, 13	12, 13	14, 15
$E_\Pi - E_\Sigma$	754.46 ± 5.0	774.317 ±	-2.251 ± 0.04
B_Π	1.478 (fixed)	1.478 (fixed)	1.466822 ± 0.0007
A_Π	-74.6 (fixed)	-74.6 (fixed)	-76.4256 ± 0.27
ξ	4.551 (fixed)	4.551 (fixed)	5.96180 ± 0.010
2η	-0.284447 ± 0.013	-0.32797 ± 0.008	-0.474730 ± 0.0008

	(4,6)	(5,7)	(6,8)
$\tilde{\nu}_o$	22158.357 ± 0.006	2306.675 ± 0.10	22406.410 ± 0.025
o'_v	0.014	0.015	0.0027
ν_o	22158.343	22306.660	22406.407
B"	1.8057790 ± 0.0003	1.785443 ± 0.0010	1.765478 ±0.0010
D" x 10^6	5.9833 ± 0.28	5.3818 ± 2.8	6.4489 ± 2.3
γ"	0.008 (fixed)	0.008 (fixed)	0.0 (fixed)
$\tilde{B}'$	1.9712615 ± 0.0003	1.939226 ± 0.0021	1.903477 ±0.0010
q' x 10^3	0.425	0.472	-0.152
B'	1.9708365	1.938754	1.903629
D' x 10^6	6.8209 ± 0.26	6.9952 ± 5.0	7.662 ± 2.1
γ'	0.0135066 ± 0.00023	0.026795 ± 0.0028	0.0 (fixed)
γ'_J x 10^6	0.0 (fixed)	0.0 (fixed)	0.0 (fixed)
v_Π^c	15, 16	17, 18	18, 19
$E_\Pi - E_\Sigma$	——	-45.059 ± 0.25	——
B_Π	——	1.41068 ± 0.013	——
A_Π	——	-74.6 (fixed)	——
ξ	——	-6.1285 ± 0.20	——
2η	——	0.52239 ± 0.032	——

v_B	v_A	$J^e_{1/2}$	$J^f_{1/2}$	$J^e_{3/2}$	$J^f_{3/2}$	$\xi(cm^{-1})$	$\xi/\langle v_A\|v_B\rangle(cm^{-1})$	$2\eta(cm^{-1})$	$2\eta/\langle v_B\|B\|v_A\rangle$
0	10	43.0	39.0	39.2	35.9	-1.77192 ± 0.09	-34.1± 1.7	0.1387880 ± 0.0018	1.067 ± 0.014
0	11	69.0	65.1	66.0	62.7	1.8051 ± 0.5	-50 ± 14	-0.107340 ± 0.004	1.17 ± 0.04
1	11	13.8	10.0	—	—	-3.68494 ± 0.09 [-3][b]	-33.2 ± 0.8	0.289337 ± 0.009 [0.24]	1.05 ± 0.03
2	13	—	—	—	33.8	4.551 (fixed)	—	-0.30115 ± 0.06	0.90 ± 0.18
3	14	10.0	6.0	—	—	5.95605 ± 0.09 [-5.51 ± 0.27][c]	-33.1 ± 0.5	-0.475710 ± 0.007 [0.206 ± 0.020]	1.064 ± 0.016
5	17	<0.5	<0.5	—	—	-6.6993 ± 0.7	-32 ± 3	0.47716 ± 0.13	0.92 ± 0.25

Weighted average of $\xi/\langle v_B|v_A\rangle = H^{so}_{el} = -33.2 \pm 0.6(cm^{-1})$

Weighted average of $2\eta/\langle v_B|B|v_A\rangle = H^{RE}_{el} = 1.069 \pm 0.027$(unitless)

[a]Only perturbations observed in this work are summarized here. The J_Ω(e and f) entries are the J values for which the $B^2\Sigma^+_u$ and $A^2\Pi_{u\Omega}$(e and f) levels would be degenerate in the absence of any interaction. Uncertainties quoted represent one standard deviation. The uncertainties in $\langle v_B|v_A\rangle$ and $\langle v_B|B|v_A\rangle$ were neglected so that our uncertainties of H^{so}_{el} and H^{RE}_{el} are slightly underestimated.

[b]A.M. Bouchoux and J.P. Goure, Can. J. Phys. 55, 1492 (1977).

[c]L. Kynning and P. Pagès Physica Scripta 6, 195-199 (1972).

TABLE IV

	$X^2\Sigma_g^+$	$A^2\Pi_u$ [b]	$B^2\Sigma_u^+$
T_e	0.0	9167.4668 ± 0.20 [9167.4]	25461.1267 ± 0.06 [25462.8]
Y_{00}	-0.0936	0.9822	-1.3354
$Y_{10}(\omega_e)$	2207.0366 ± 0.05 [2207.00]	1903.5111 ±0.10 [1903.53]	2420.8255 ± 0.15 [2419.84]
$Y_{20}(-\omega_e x_e)$	-16.07860 ± 0.019 [-16.10]	-15.02904 ± 0.017 [-15.011]	-23.8506 ± 0.10 [-23.19]
$Y_{30}(\omega_e y_e)$	-0.039756 ± 0.0023 [-0.040]	0.002027 ± 0.0010	-0.35865 ± 0.026
$Y_{40}(\omega_e z_e)$	———	———	-0.061924 ± 0.0020
$Y_{01}(B_e)$	1.9316578 ± 0.00015 [1.9319]	1.75302 ± 0.007 [1.748]	2.0844684 ± 0.00015 [2.073]
$Y_{11}(-\alpha_e)x10^2$	-1.87791 ± 0.009 [-1.9]	-2.2168 ± 0.20 [-2.0]	-2.13210 ± 0.013 [-2.0]
$Y_{21}(\gamma_e)x10^4$	-0.9572 ± 0.21	1.948 ± 1.3	-8.510 ± 0.5
r_e(Å)	1.116454 [1.116384]	1.17196 [1.17364]	1.074752 [1.07772]

[a] Numbers in brackets are values from: A. Lofthus and P. Krupenie, J. Phys. Chem. Ref. Data 6, 113-307 (1977). Uncertainties quoted represent one standard deviation. All units are cm^{-1} except where noted.

[b] Determined from merged constants and data from A.E. Douglas, Astrophys. J. 117, 380-386 (1953) and J. Janin, J. d'Incan, R. Stringat, and J. Magnaval, Rev. d'Opt. 42, 120-128 (1963).

				$X^2\Sigma_g^+$		
		$DX10^6(cm^{-1})$			$HX10^{12}(cm^{-1})$	
v	Exp.	Calc. I	Calc. II	Exp.	Calc. I	Calc. II
0	5.9099 ± 0.08	5.9330	5.9342	-0.0649 ± 1.5	2.37	2.39
1	5.9223 ± 0.08	5.9676	5.9667		2.53	1.78
2	5.9350 ± 0.08	6.0099	6.0013		2.82	1.16
3	5.9354 ± 0.09	6.0607	6.0383		3.26	0.53
4	5.8864 ± 0.16	6.1200	6.0778		3.88	-0.10
5	5.7508 ± 0.37	6.1894	6.1202		4.70	-0.79
6	5.352 ± 0.7	6.2690	6.1652		5.12	-2.29
7	5.763 ± 10.	6.3542	6.2062		-6.34[b]	-17.40[b]
8	0.560 ± 11.	6.3347	6.1243		-216.[b]	-273.[b]

				$A^2\Pi_u$		
		$DX10^6(cm^{-1})$			$HX10^{12}(cm^{-1})$	
v	Exp.	Calc. I	Calc. II	Exp.	Calc. I	Calc. II
9		6.0258			-3.77	
10		6.0613			-3.45	
11		6.1025			-2.94	
12		6.1498			-2.20	
13		6.2041			-1.18	
14		6.2658			0.17	
15		6.3360			1.88	
16		6.4152			3.90	
17		6.5047			5.44[b]	
18		6.6050			2.12[b]	
19		6.7156			-28.6[b]	

				$B^2\Sigma_u^+$		
		$DX10^6(cm^{-1})$			$HX10^{12}(cm^{-1})$	
v	Exp.	Calc. I	Calc. II	Exp.	Calc. I	Calc. II
0	6.2691 ± 0.08	6.2534	6.2522	-7.05 ± 18.	4.18	-1.96
1	6.5002 ± 0.08	6.4252	6.4200		5.81	-6.37
2	6.7354 ± 0.29	6.6115	6.6478		7.80	-9.78
3	6.608 ± 0.4	6.8140	6.9835		10.02	-10.97
4	7.156 ± 0.7	7.0336	7.4874		13.10	-8.41[b]
5	10.823 ± 13.	7.2728	8.2347		16.62	-8.78[b]
6	19.977 ± 11.	7.5334	9.2143[b]		20.47	-213.[b]

---

[a]Calculated I values were used as fixed parameters in cases where D or H could not be varied. They were generated using the method of D.L. Albritton et al., J. Mol. Spectrosc. 46, 25-36 (1973) and constants from A. Lofthus and P. Krupenie (see footnotes to Table IV). Calculated II values were generated from the constants in Table IV. Experimental values are merged constants (2). Uncertainties quoted are one standard deviation.

[b]Summation is incomplete. See Albritton et al. (30).

TABLE VI

	$X^2\Sigma_g^+$	$B^2\Sigma_u^+$		
v	$\gamma_v \times 10^2(cm^{-1})^a$	$\gamma_v \times 10^2(cm^{-1})^a$	$-p_v^{\Sigma} \times 10^2(cm^{-1})^c$	$\gamma_J \times 10^6(cm^{-1})^a$
0	0.929 ± 0.5^d	2.401 ± 0.5^d	2.63	-1.323 ± 0.5
1	0.938 ± 0.5^d	2.902 ± 0.5^d	3.30	-2.900 ± 1.2
2	0.949 ± 0.5	2.351 ± 0.5	2.87	-5.689 ± 4.0
3	0.935 ± 0.5	2.810 ± 2.3	3.32	-6.00 ± 6.0
4	0.913 ± 0.5	1.333 ± 0.3	2.03	——
5	0.749 ± 2.4	0.537 ± 1.9	2.56	——

[a]Merged values. Uncertainties quoted are one standard deviation.

[b]See Fig. 2.

[c]See text for definition.

[d]A.M. Bouchoux et al., J. Quant. Spectrosc. Radiat. Transfer 66, 451-456 (1976) report: $\gamma_0'' = 0.010 \pm 0.008$ and $\gamma_0' - \gamma_0'' = 0.015 \pm 0.002$ cm^{-1}. A.M. Bouchoux and J.P. Goure, Can. J. Phys. 55, 1492-1498 (1977) report $\gamma_1' = 0.025$ cm^{-1}. E.A. Colbourn and A.E. Douglas, J. Mol. Spectrosc. 65, 332-333 (1977) report: $\gamma_0'' = \gamma_1'' = 0.0083$ and $\gamma_0' = 0.0229$ cm^{-1}.

TRANSITION	OBSERVED FREQUENCY (CM^{-1})	EXPT-CALC (CM^{-1})	UNCERTAINTY (CM^{-1})
R_1 (0)	21 974.439	-0.003	0.100
R_1 (1)	21 978.688	0.000	0.020
R_1 (2)	21 983.242	-0.011	0.007
R_1 (3)	21 988.111	-0.007	0.020
R_1 (4)	21 993.243	0.002	0.007
R_1 (5)	21 998.562	0.009	0.020
R_1 (6)	22 003.965	0.042	0.100
R_1 (7)	22 009.072	0.001	0.100
R_1 (8)	22 013.416	0.010	0.007
$^{S}R_{21}$(8)	22 032.395	-0.002	0.020
R_1 (9)	22 035.442	0.003	0.020
$^{S}R_{21}$(9)	22 015.989	-0.018	0.030
R_1 (10)	22 040.351	-0.005	0.010
R_1 (11)	22 046.753	0.002	0.020
R_1 (12)	22 054.102	0.003	0.007
R_1 (13)	22 062.113	0.007	0.020
R_1 (14)	22 070.630	0.000	0.007
R_1 (15)	22 079.600	0.001	0.020
R_1 (16)	22 088.978	0.002	0.007
R_1 (17)	22 098.745	0.007	0.030
R_1 (18)	22 108.868	-0.002	0.007
R_1 (19)	22 119.368	0.002	0.020
R_1 (20)	22 130.212	-0.004	0.007
R_1 (21)	22 141.428	0.008	0.010
R_1 (22)	22 152.968	-0.001	0.010
R_1 (23)	22 164.870	0.004	0.020
R_1 (24)	22 177.090	-0.013	0.010
R_1 (25)	22 189.685	0.003	0.020
R_1 (26)	22 202.589	-0.009	0.010
R_1 (27)	22 215.851	-0.001	0.020
R_1 (28)	22 229.434	-0.006	0.020
R_1 (29)	22 243.377	0.014	0.020
P_1 (1)	21 966.832	-0.041	0.100
P_1 (2)	21 963.472	-0.005	0.100
P_1 (3)	21 960.418	-0.000	0.020
P_1 (4)	21 957.648	-0.035	0.100
P_1 (5)	21 955.247	0.000	0.100
P_1 (6)	21 953.055	-0.013	0.030
P_1 (7)	21 951.084	0.002	0.020
P_1 (8)	21 949.160	0.004	0.007
P_1 (9)	21 947.014	0.004	0.020
P_1 (10)	21 944.033	-0.019	0.010
$^{Q}P_{21}$(10)	21 963.012	-0.032	0.100
$^{Q}P_{21}$(11)	21 939.357	-0.008	0.020
P_1 (11)	21 958.794	-0.002	0.020
P_1 (12)	21 956.407	-0.021	0.100
P_1 (13)	21 955.592	0.051	0.100
P_1 (14)	21 955.592	-0.017	0.100
P_1 (15)	21 956.407	0.065	0.100
P_1 (16)	21 957.648	0.052	0.100
P_1 (17)	21 959.287	-0.011	0.030
P_1 (18)	21 961.418	0.003	0.007
P_1 (19)	21 963.914	-0.006	0.020
P_1 (20)	21 966.832	0.029	0.100
P_1 (21)	21 970.045	-0.008	0.020
P_1 (22)	21 973.676	0.010	0.030
P_1 (23)	21 977.642	0.006	0.100
P_1 (24)	21 981.959	-0.001	0.010
P_1 (25)	21 986.648	0.010	0.100
P_1 (26)	21 991.667	0.003	0.007
P_1 (27)	21 997.002	-0.035	0.020
P_1 (28)	22 002.763	0.004	0.020
P_1 (30)	22 015.238	0.005	0.030
P_1 (31)	22 021.989	0.006	0.020
P_1 (32)	22 029.082	0.008	0.020
P_1 (34)	22 044.280	0.012	0.020
R_2 (1)	21 979.130	-0.007	0.020
R_2 (2)	21 983.911	0.002	0.010
R_2 (3)	21 989.003	-0.005	0.010
R_2 (4)	21 994.412	0.006	0.010
R_2 (5)	21 999.999	0.054	0.050

TRANSITION	OBSERVED FREQUENCY (CM^{-1})	EXPT-CALC (CM^{-1})	UNCERTAINTY (CM^{-1})	TRANSITION	OBSERVED FREQUENCY (CM^{-1})	EXPT-CALC (CM^{-1})	UNCERTAINTY (CM^{-1})
R_2 (6)	22 007.683	-0.003	0.010	P_2 (12)	21 950.841	-0.032	0.100
R_2 (7)	22 013.416	-0.025	0.020	P_2 (13)	21 951.423	-0.018	0.007
R_2 (8)	22 020.146	-0.005	0.007	P_2 (14)	21 952.361	-0.000	0.100
R_2 (9)	22 027.276	-0.006	0.010	P_2 (15)	21 953.635	0.004	0.100
R_2 (10)	22 034.781	0.000	0.007	P_2 (16)	21 955.247	-0.000	0.100
R_2 (11)	22 042.633	0.001	0.030	P_2 (17)	21 957.215	0.003	0.020
R_2 (12)	22 050.834	0.004	0.007	P_2 (18)	21 959.515	-0.009	0.100
R_2 (13)	22 059.365	-0.008	0.030	P_2 (19)	21 962.188	0.004	0.020
R_2 (14)	22 068.259	-0.002	0.007	P_2 (20)	21 965.187	-0.002	0.100
R_2 (15)	22 077.491	-0.000	0.030	P_2 (21)	21 968.539	-0.003	0.007
R_2 (16)	22 087.063	-0.002	0.007	P_2 (22)	21 972.242	0.000	0.010
R_2 (17)	22 096.990	0.009	0.020	P_2 (23)	21 976.259	-0.027	0.100
R_2 (18)	22 107.256	0.019	0.030	P_2 (24)	21 980.680	0.002	0.010
R_2 (19)	22 117.856	0.021	0.020	P_2 (25)	21 985.423	0.010	0.020
R_2 (20)	22 128.772	-0.000	0.007	P_2 (26)	21 990.487	-0.006	0.100
R_2 (21)	22 140.043	-0.006	0.100	P_2 (27)	21 995.943	0.024	0.020
R_2 (22)	22 151.670	0.003	0.100	P_2 (28)	22 001.693	0.006	0.020
R_2 (23)	22 163.625	0.004	0.020	P_2 (30)	22 014.258	0.007	0.100
R_2 (24)	22 175.904	-0.008	0.010	P_2 (31)	22 021.046	0.000	0.020
R_2 (25)	22 188.519	-0.022	0.020	P_2 (32)	22 028.125	-0.054	0.020
R_2 (26)	22 201.599	0.092	0.030				
R_2 (27)	22 214.815	0.009	0.020				
R_2 (28)	22 228.448	0.009	0.030				
R_2 (29)	22 242.422	0.017	0.020				
$^{P}Q_{12}$(1)	21 966.832	-0.056	0.030				
P_2 (2)	21 963.692	-0.066	0.100				
P_2 (3)	21 960.883	-0.005	0.020				
P_2 (4)	21 958.361	0.002	0.020				
P_2 (5)	21 956.159	0.002	0.010				
P_2 (6)	21 954.258	0.003	0.007				
P_2 (7)	21 952.484	-0.010	0.030				
P_2 (8)	21 952.921	-0.018	0.030				
P_2 (9)	21 951.423	0.022	0.007				
P_2 (10)	21 950.841	0.022	0.100				
P_2 (11)	21 950.650	-0.011	0.100				

[a]Extra lines may be recognized by left superscripts denoting change in N.

Line	Energy[a] (cm^{-1})		Intensity[b]	Comments[c]
		(0,0)		
$P_1(50)$	25748.156_2		0	N
$P_2(53)$	25782.419_2)		0	A
$P_1(56)$	————		-	D
$P_1(66)$	25963.180_2)		1	A
$P_2(66)$	25963.950_2		1	A
$P_1(68)$	25999.196_2)		2	A
$P_2(68)$	25998.441_2		3	A
$P_1(72)$	26067.071_2)		3	A
$P_2(72)$	26066.342_2		2	A
		(1,1)		
No changes.				
		(0,1)		
No changes.				
		(1,2)		
$^{S}R_{21}(12)$	23708.994_1		2	E[$R_1(12)$]
$^{Q}P_{21}(14)$	23607.354_1		2	E[$P_1(14)$]
		(2,3)		
$R_1(3)$	23848.351_1)		10	N
$R_2(3)$	23848.260_1)		10	N
$R_1(29)$ $R_2(29)$	24090.919_3		2	A
$R_1(30)$ $R_2(30)$	24104.297_3		2	A
$R_1(31)$	24117.929_3		0	A
$R_2(31)$	24118.048_3		0	A
$R_1(32)$	24131.633_3		1	A
$R_1(33)$	24145.319_3		1	A

Line	Energy[a] (cm^{-1})		Intensity[b]	Comments[c]
		(2,3) Cont.		
$P_1(24)$	23830.550_1		0	N
$P_2(24)$	23830.256_1		0	N
		(0,2)		
$R_2(31)$	21569.242_1		0	N
		(1,3)		
No changes.				
		(2,4)		
No changes.				
		(3,5)		
$R_1(0)$	21974.439_2		0	N
$R_2(1)$	21979.130_2		0	N
$R_2(2)$	21983.911_2		1	N
$R_2(3)$	21989.003_2		1	N
$R_2(4)$	21994.412_2		1	N
$R_2(5)$	21999.999_2)		1	N
$R_2(6)$	22007.683_2		1	N
$R_2(7)$	22013.416_2		3	N
$^{S}R_{21}(8)$	22032.395_2		0	E[$R_1(8)$]
$^{S}R_{21}(9)$	22015.989_2		0	E[$R_1(9)$]
$R_1(21)$	22141.428_2		1	N
$P_1(2)$	21963.472_2		0	N
$P_2(2)$	21963.692_2)		3	N
$P_2(3)$	21960.883_2		0	N
$P_2(4)$	21958.361_2		0	N
$P_2(5)$	21956.159_2		1	N
$P_1(6)$	21953.055_2)		3	N
$P_2(6)$	21954.258_2		1	N
$P_2(7)$	21952.484_2)		1	N
$P_2(8)$	21952.921_2		5	N
$P_2(9)$	21951.423_2		3	N
$^{Q}P_{21}(10)$	21963.012_2		5	E[$P_1(10)$]
$^{Q}P_{21}(11)$	21939.357_2		0	E[$P_1(11)$]

Line	Energy[a] (cm^{-1})		Intensity[b]	Comments[c]
		(3,5) Cont.		
$P_2(29)$	———		-	D
$^{P}Q_{12}(1)$	21966.832_2		2	A
$^{R}Q_{21}(0)$	———			D
		(4,6)		
$R_1(17)$ / $R_2(17)$	22279.571_3		0	N
$R_2(22)$	22331.823_3		0	N
$R_1(24)$	22354.485_3		0	N
$R_2(24)$	22354.873_3		0	N
$R_1(26)$	22378.462_3		0	N
$R_2(26)$	22379.027_3		0	N
$P_1(23)$	22158.626_3		0	N
$P_2(23)$	22158.782_3		0	N
$P_1(24)$	22162.465_3		0	N
$P_2(24)$	22162.708_3		0	N
$P_1(25)$	22166.599_3		0	N
$P_2(26)$	22171.478_3		0	N
		(5,7)		
$^{S}R_{21}(3)$	22309.139_3		1	E[$R_1(3)$]
$P_1(18)$	22291.057_3		0	A
		(6,8)		
$R_1(12)$ / $R_2(12)$	22477.242_3		0	N
$R_1(13)$ / $R_2(13)$	———		-	D
$R_1(14)$ / $R_2(14)$	22492.186_3		0	N
$R_1(15)$ / $R_2(15)$	———		-	D
$R_1(16)$ / $R_2(16)$	22508.205_3		0	N
$R_1(17)$ / $R_2(17)$	———		-	D

Line	Energy[a] (cm^{-1})	Intensity[b]	Comments[c]
	(6,8) Cont.		
$R_1(18)$ / $R_2(18)$	22525.211_3	0	N
$R_1(19)$ / $R_2(19)$	————	-	D
$P_1(11)$ / $P_2(11)$	22382.656	0	N
$P_1(12)$ / $P_2(12)$	22382.212_3	1	N
$P_1(13)$ / $P_2(13)$	————	-	D
$P_1(14)$ / $P_2(14)$	22382.009_3	0	N
$P_1(15)$ / $P_2(15)$	————	-	D
$P_1(16)$ / $P_2(16)$	$22382.934_3\delta$	0	N
$P_1(17)$ / $P_2(17)$	————	-	D
$P_1(18)$ / $P_2(18)$	22384.869_3	0	N
$P_1(19)$ / $P_2(19)$	————	-	D
$P_1(20)$ / $P_2(20)$	————	-	D

[a] For explanation of subscripts, parenthesis, and δ see Ref. 1.

[b] See Ref. 1.

[c] A ≡ additional value not reported in Ref. 1 determined from an extended analysis.
D ≡ value reported in Ref. 1 is in error and should be deleted.
E ≡ extra line. Main line is given in brackets.
N ≡ value reported in Ref. 1 is in error and should be replaced by value given here.

Appendix 2:

Computer Programs

```
C   THIS PROGRAM CALCULATES 2SIG+-2SIG+ AND 2PI-2SIG+ TRANSITIONS                CALC0001
C                                                                                CALC0002
C   GROUND STATE IS 2SIG+                                                        CALC0003
C                                                                                CALC0004
C                                                                                CALC0005
C   ACCEPTS OUTPUT FROM LSQ DOUBLET FITTER                                       CALC0006
C                                                                                CALC0007
C   INPUT SHOULD BE AS FOLLOWS:                                                  CALC0008
C                                                                                CALC0009
C        FIRST CARD IS PROBLEM NAME IN COLUMNS 10 THROUGH 80                     CALC0010
C                                                                                CALC0011
C        SECOND CARD CONTAINS NMAX, MAXRK, AND NERGY.                            CALC0012
C          NMAX IS MAX J FOR UPPER STATE +0.5.  NMAX MUST BE AN INTEGER.         CALC0013
C         MAXRK IS MAXIMUM DIMENSION OF HAMILTONIAN USED.                        CALC0014
C         MAXRK CANNOT BE GREATER THAN 9.                                        CALC0015
C         NERGY IS AN INTEGER ADDED TO UPPER STATE ENERGIES.                     CALC0016
C         FORMAT IS (3I5)                                                        CALC0017
C                                                                                CALC0018
C         THE NEXT CARD CONTAINS THE NUMBER OF GROUND STATE                      CALC0019
C         CONSTANTS WHICH WERE VARIED                                            CALC0020
C         IN I5 FORMAT.                                                          CALC0021
C                                                                                CALC0022
C        THE NEXT CARD CONTAINS THE CODE NUMBERS FOR THE VARIED PARAMETERS       CALC0023
C         FOR THE GROUND STATE IN 15I5 FORMAT.                                   CALC0024
C                                                                                CALC0025
C         THE NEXT CARDS GIVE THE VALUES OF THE GROUND STATE CONSTANTS           CALC0026
C         ALONG WITH THE PARAMETER NUMBER AND CODE FOR UNITS.                    CALC0027
C         UNIT CODE IS 1 FOR CM-1 AND 0 FOR MC                                   CALC0028
C         AFTER LAST CARD THERE MUST BE A CARD WITH A -99 TYPED IN I5 FORMAT.    CALC0029
C                                                                                CALC0030
C        THE NEXT CARD CONTAINS THE NUMBER OF UPPER STATE CONSTANTS VARIED (I5)  CALC0031
C                                                                                CALC0032
C        THE NEXT CARD CONTAINS THE CODE NUMBERS FOR THE PARAMETERS VARIED.      CALC0033
C         USE 15I5 FORMAT.                                                       CALC0034
C                                                                                CALC0035
C        THE NEXT CARDS GIVE THE VALUES FOR THE UPPER STATE PARAMETERS ALONG     CALC0036
```

```
C        WITH PARAMETER NUMBER, AND CODE FOR UNITS.                          CALC0037
C        THESE CARDS ARE TAKEN FROM OUTPUT OF FITTER.                        CALC0038
C                                                                            CALC0039
C       AFTER LAST PARAMETER CARD THERE MUST BE A CARD WITH A -99 TYPED      CALC0040
C        IN I5 FORMAT                                                        CALC0041
C                                                                            CALC0042
C       THE NUMBER OF PARAMETERS IS LIMITED TO 75.                           CALC0043
C                                                                            CALC0044
C       IREG IS INPUT IN I1 FORMAT. IF IREG=1 PI STATES ARE REGULAR          CALC0045
C        OTHERWISE IREG=0 AND PI STATE IS INVERTED.                          CALC0046
C                                                                            CALC0047
C      SLIM AND ICODE INPUT IN F4.1, I1 FORMAT                               CALC0048
C         IF ICODE=1 PI STATES ARE PRINTED OUT                               CALC0049
C     IF ICODE=2 ALL LINES ARE PRINTED OUT                                   CALC0050
C        OTHERWISE SIGMA STATES ARE PRINTED OUT                              CALC0051
C      SLIM IS FRACTION   OF SIGMA CHATACTER USED TO JUDGE WHETHER A LEVEL IS CALC0052
C      SIGMA OR PI.  FOR EXAMPLE, IF SIGMA IS .01 AND ICODE IS 0             CALC0053
C         ALL LEVELS WITH GREATER THAN 1 PERCENT SIGMA CHARACTER ARE PRINTED OUT CALC0054
C     IF ICODE=1 AND SLIM=0.01 ALL STATES WITH LESS THAN 99% SIGMA CHARACTER CALC0055
C      ARE OUTPUT                                                            CALC0056
C                                                                            CALC0057
C        IF NO FURTHER DECKS ARE TO BE INPUT PUT TWO BLANK CARDS AT END      CALC0058
C         OF DECK.                                                           CALC0059
C                                                                            CALC0060
      INTEGER FLAG,UNITS                                                     CALC0061
      INTEGER GAMAX,GVAR                                                     CALC0062
      INTEGER GFLAG                                                          CALC0063
      DIMENSION GVAR(30)                                                     CALC0064
      DIMENSION GFLAG(75)                                                    CALC0065
      DOUBLE PRECISION D(9),E(9),GP(75),GS(26),GT(26),BOT(2,101)             CALC0066
      DOUBLE PRECISION SAVE                                                  CALC0067
      DIMENSION TS(9,2,101),TP(9,2,101),PP(4300),PS(4300)                    CALC0068
      DOUBLE PRECISION P(75),S(26),T(26),DFLOAT,                             CALC0069
     1X,H(9,9),U(9,9),                          TE(9,2,101),VU(             CALC0070
     14300),TERM(4300),                      SHIFT                          CALC0071
      DIMENSION FLAG(75),IRANK(4300),PTY(4300),DJ(4300),NCVAR(               CALC0072
```

```
     130),DIM(2)
      DOUBLE PRECISION  X1,X2,X3,X4,X5,DN,VLAM(4300)
      REAL*8  NAMES(75)
      REAL*4 PAR(2)/1HE,1HF/
      REAL*8 BCH(4300)
      REAL*8 B(12)  /4H-R1(,5H-R21(,4H-R2(,5H-R12(,4H-P1(,5H-P21(,4H-P2(,
     15H-P12(,5H-Q12(,4H-Q2(,5H-Q21(,4H-Q1(/
      DATA  DIM(1)/2HMC/,DIM(2)/2HCM/
      REAL*8 FIT(2)/6HFITTED,5HFIXED/
    1 DO 820 I=1,4300
      VLAM(I)=0.0
      DJ(I)=0.0
      PTY(I)=0.0
      TERM(I)=0.0
      PP(I)=0.0
      PS(I)=0.0
      BCH(I)=0.0
      VU(I)=0.0
  820 IRANK(I)=0
      DO 821 I=1,75
      GFLAG(I)=0
      GP(I)=0.0
      FLAG(I)=0
  821 P(I)=0.0
      READ9
    9 FORMAT(10X,70H
     1                                         )
      READ19,NMAX,MAXRK,NERGY
   19 FORMAT(3I5)
      IF(NMAX.EQ.0) GO TO 999
      READ29,GAMAX
      READ29,(GVAR(I),I=1,GAMAX)
   17 WAVE=1.0
      READ39,I,GP(I),GFLAG(I)
      IF(I.EQ.-99) GO TO 22
      IF(GFLAG(I).EQ.1) WAVE=29979.25D0
```

```
      GP(I)=GP(I)*WAVE                                                  CALC0109
      GO TO 17                                                          CALC0110
   22 CONTINUE                                                          CALC0111
      READ29,IAMAX                                                      CALC0112
   29 FORMAT(15I5)                                                      CALC0113
      READ29,(NCVAR(I),I=1,IAMAX)                                       CALC0114
    7 WAVE=1.0                                                          CALC0115
      READ39,I,P(I),FLAG(I)                                             CALC0116
      IF(I.EQ.-99) GO TO 2                                              CALC0117
   39 FORMAT(I5,D15.8,I5)                                               CALC0118
      IF(FLAG(I).EQ.1) WAVE=29979.25D0                                  CALC0119
      P(I)=P(I)*WAVE                                                    CALC0120
      GO TO 7                                                           CALC0121
    2 CONTINUE                                                          CALC0122
      READ59,IREG                                                       CALC0123
   59 FORMAT(I1)                                                        CALC0124
      READ69,SLIM,ICODE                                                 CALC0125
   69 FORMAT(F4.1,I1)                                                   CALC0126
    4 SHIFT=DFLOAT(NERGY)                                               CALC0127
      NCALC=NMAX+1                                                      CALC0128
      CALL NAMEIT (NAMES,75)                                            CALC0129
      CALL SETUP(GP,GS,1.0)                                             CALC0130
      CALL SETUP(GP,GT,-1.0)                                            CALC0131
      M=MAXRK                                                           CALC0132
      DO 1010 J=1,NCALC                                                 CALC0133
      X=DFLOAT(J)                                                       CALC0134
      CALL MATRIX(GS,GP,X,H)                                            CALC0135
      BOT(1,J)=H(1,1)/29979.25D0                                        CALC0136
      CALL MATRIX(GT,GP,X,H)                                            CALC0137
1010  BOT(2,J)=H(1,1)/29979.25D0                                        CALC0138
      CALL SETUP (P,S,1.0)                                              CALC0139
      CALL SETUP(P,T,-1.0)                                              CALC0140
      DO 10 J=1,NCALC                                                   CALC0141
      X=DFLOAT(J)                                                       CALC0142
      CALL MATRIX(S,P,X,H)                                              CALC0143
      DO 832 KK=1,9                                                     CALC0144
```

```
      DO 822 II=1,9                                                      CALC0145
  822 U(KK,II)=0.0D0                                                     CALC0146
  832 U(KK,KK)=1.0D0                                                     CALC0147
      CALL TRED2(M,9,H,D,E,U)                                            CALC0148
      CALL TQL2(M,9,D,E,U,IERR)                                          CALC0149
      IF (IERR.NE.0) GO TO 824                                           CALC0150
      GO TO 825                                                          CALC0151
  824 WRITE(6,829) IERR                                                  CALC0152
  829 FORMAT (' ERROR IN HAMILTONIAN DIAGONALIZATION, IERR=',I2)         CALC0153
  825 CONTINUE                                                           CALC0154
      DO 20 L=1,MAXRK                                                    CALC0155
      TS(MAXRK-L+1,1,J)=SNGL(U(1,L)**2+U(4,L)**2)                        CALC0156
      TP(MAXRK-L+1,1,J)=SNGL(U(2+IREG,L)**2+U(7+IREG,L)**2+U(5+IREG,L)** CALC0157
     12)                                                                 CALC0158
   20 TE(MAXRK-L+1,1,J)=D(L)/29979.25D0                                  CALC0159
      CALL MATRIX(T,P,X,H)                                               CALC0160
      DO 833 KK=1,9                                                      CALC0161
      DO 823 II=1,9                                                      CALC0162
  823 U(KK,II)=0.0D0                                                     CALC0163
  833 U(KK,KK)=1.0D0                                                     CALC0164
      CALL TRED2(M,9,H,D,E,U)                                            CALC0165
      CALL TQL2(M,9,D,E,U,IERR)                                          CALC0166
      IF (IERR.NE.0) GO TO 826                                           CALC0167
      GO TO 827                                                          CALC0168
  826 WRITE(6,829) IERR                                                  CALC0169
  827 CONTINUE                                                           CALC0170
      DO 30 L=1,MAXRK                                                    CALC0171
      TS(MAXRK-L+1,2,J)=SNGL(U(1,L)**2+U(4,L)**2)                        CALC0172
      TP(MAXRK-L+1,2,J)=SNGL(U(2+IREG,L)**2+U(7+IREG,L)**2+U(5+IREG,L)** CALC0173
     12)                                                                 CALC0174
   30 TE(MAXRK-L+1,2,J)=D(L)/29979.25D0                                  CALC0175
   10 CONTINUE                                                           CALC0176
      MAX1=MAXRK                                                         CALC0177
      DO 200 J=1,NMAX                                                    CALC0178
      DO 200 L=1,MAX1                                                    CALC0179
      DO 200 I=1,2                                                       CALC0180
```

```
      IF(TE(L,I,J).LE.0.1) GO TO 200                                    CALC0181
      TE(L,I,J)=TE(L,I,J)+SHIFT                                         CALC0182
  200 CONTINUE                                                          CALC0183
      ICODE=ICODE+1                                                     CALC0184
      N=1                                                               CALC0185
      DO 50 J=3,NMAX                                                    CALC0186
      DO 50 L=1,MAX1                                                    CALC0187
      DO 50 I=1,2                                                       CALC0188
      IF(TE(L,I,J).LT..01) GO TO 50                                     CALC0189
      GO TO (51,52,53),ICODE                                            CALC0190
   51 IF(TS(L,I,J).LE.SLIM) GO TO 50                                    CALC0191
      GO TO 53                                                          CALC0192
   52 SLIM=1.0D0-SLIM                                                   CALC0193
      IF (TS(L,I,J).GE.SLIM) GO TO 50                                   CALC0194
   53 CONTINUE                                                          CALC0195
      VU(N)=TE(L,I,J)-BOT(I,J-1)                                        CALC0196
      TERM(N)=TE(L,I,J)                                                 CALC0197
      IRANK(N)=L                                                        CALC0198
      PP(N)=TP(L,I,J)                                                   CALC0199
      PS(N)=TS(L,I,J)                                                   CALC0200
      PRP=1.0-PP(N)-PS(N)                                               CALC0201
      PMAX=AMAX1(PS(N),PP(N),PRP)                                       CALC0202
      IF(I.EQ.2) GO TO 701                                              CALC0203
      BCH(N)=B(1)                                                       CALC0204
      IF(PMAX.EQ.PS(N)) GO TO 702                                       CALC0205
      IF(PMAX.EQ.PRP) BCH(N)=B(2)                                       CALC0206
      GO TO 702                                                         CALC0207
  701 BCH(N)=B(3)                                                       CALC0208
      IF(PMAX.EQ.PS(N)) GO TO 702                                       CALC0209
      IF(PMAX.EQ.PP(N)) BCH(N)=B(4)                                     CALC0210
  702 PTY(N)=PAR(I)                                                     CALC0211
      DJ(N)=FLOAT(J-1)-0.5                                              CALC0212
      N=N+1                                                             CALC0213
   50 CONTINUE                                                          CALC0214
      DO 70 J=2,NMAX                                                    CALC0215
      DO 70 L=1,MAX1                                                    CALC0216
```

```
      DO 70 I=1,2                                                       CALC0217
      IF(TE(L,I,J).LT..01) GO TO 70                                     CALC0218
      GO TO (71,72,73),ICODE                                            CALC0219
   71 IF(TS(L,I,J).LE.SLIM) GO TO 70                                    CALC0220
      GO TO 73                                                          CALC0221
   72 SLIM=1.0D0-SLIM                                                   CALC0222
      IF (TS(L,I,J).GE.SLIM) GO TO 70                                   CALC0223
   73 CONTINUE                                                          CALC0224
      VU(N)=TE(L,I,J)-BOT(I,J+1)                                        CALC0225
      IRANK(N)=L                                                        CALC0226
      PP(N)=TP(L,I,J)                                                   CALC0227
      PS(N)=TS(L,I,J)                                                   CALC0228
      PRP=1.0-PP(N)-PS(N)                                               CALC0229
      PMAX=AMAX1(PS(N),PP(N),PRP)                                       CALC0230
      IF(I.EQ.2) GO TO 703                                              CALC0231
      BCH(N)=B(5)                                                       CALC0232
      IF(PMAX.EQ.PS(N)) GO TO 704                                       CALC0233
      IF(PMAX.EQ.PRP) BCH(N)=B(6)                                       CALC0234
      GO TO 704                                                         CALC0235
  703 BCH(N)=B(7)                                                       CALC0236
      IF(PMAX.EQ.PS(N)) GO TO 704                                       CALC0237
      IF(PMAX.EQ.PP(N)) BCH(N)=B(8)                                     CALC0238
  704 DJ(N)=FLOAT(J+1)-0.5                                              CALC0239
      PTY(N)=PAR(I)                                                     CALC0240
      TERM(N)=TE(L,I,J)                                                 CALC0241
      N=N+1                                                             CALC0242
   70 CONTINUE                                                          CALC0243
      DO 90 J=2,NMAX                                                    CALC0244
      DO 90 L=1,MAX1                                                    CALC0245
      DO 90 I=1,2                                                       CALC0246
      IF(TE(L,I,J).LT..01) GO TO 90                                     CALC0247
      GO TO (91,92,93),ICODE                                            CALC0248
   91 IF(TS(L,I,J).LE.SLIM) GO TO 90                                    CALC0249
      GO TO 93                                                          CALC0250
   92 SLIM=1.0D0-SLIM                                                   CALC0251
      IF (TS(L,I,J).GE.SLIM) GO TO 90                                   CALC0252
```

```
 93 CONTINUE                                                        CALC0253
    MR=2                                                            CALC0254
    IF (I.EQ.2) MR=1                                                CALC0255
    VU(N)=TE(L,I,J)-BOT(MR,J)                                       CALC0256
    IRANK(N)=L                                                      CALC0257
    PP(N)=TP(L,I,J)                                                 CALC0258
    PS(N)=TS(L,I,J)                                                 CALC0259
    PRP=1.0-PP(N)-PS(N)                                             CALC0260
    PMAX=AMAX1(PS(N),PP(N),PRP)                                     CALC0261
    IF(I.EQ.2) GO TO 705                                            CALC0262
    BCH(N)=B(9)                                                     CALC0263
    IF(PMAX.EQ.PS(N)) GO TO 706                                     CALC0264
    IF (PMAX.EQ.PRP) BCH(N)=B(10)                                   CALC0265
    GO TO 706                                                       CALC0266
705 BCH(N)=B(11)                                                    CALC0267
    IF(PMAX.EQ.PS(N)) GO TO 706                                     CALC0268
    IF(PMAX.EQ.PP(N)) BCH(N)=B(12)                                  CALC0269
706 DJ(N)=FLOAT(J)-0.5                                              CALC0270
    PTY(N)=PAR(I)                                                   CALC0271
    TERM(N)=TE(L,I,J)                                               CALC0272
    N=N+1                                                           CALC0273
 90 CONTINUE                                                        CALC0274
    DO 120 L=1,MAX1                                                 CALC0275
    DO 120 I=1,2                                                    CALC0276
    IF(TE(L,I,1).LT..01) GO TO 120                                  CALC0277
    GO TO (121,122,123),ICODE                                       CALC0278
121 IF(TS(L,I,1).LE.SLIM) GO TO 120                                 CALC0279
    GO TO 123                                                       CALC0280
122 SLIM=1.0D0-SLIM                                                 CALC0281
    IF (TS(L,I,1).GE.SLIM) GO TO 120                                CALC0282
123 CONTINUE                                                        CALC0283
    VU(N)=TE(L,I,1)-BOT(I,2)                                        CALC0284
    IRANK(N)=L                                                      CALC0285
    PP(N)=TP(L,I,1)                                                 CALC0286
    PS(N)=TS(L,I,1)                                                 CALC0287
    PRP=1.0-PP(N)-PS(N)                                             CALC0288
```

```
      PMAX=AMAX1(PS(N),PP(N),PRP)                                       CALC0289
      IF(I.EQ.2) GO TO 707                                              CALC0290
      BCH(N)=B(5)                                                       CALC0291
      IF(PMAX.EQ.PS(N)) GO TO 708                                       CALC0292
      IF(PMAX.EQ.PRP) BCH(N)=B(6)                                       CALC0293
      GO TO 708                                                         CALC0294
  707 BCH(N)=B(7)                                                       CALC0295
      IF(PMAX.EQ.PS(N)) GO TO 708                                       CALC0296
      IF(PMAX.EQ.PP(N)) BCH(N)=B(8)                                     CALC0297
  708 DJ(N)=1.5                                                         CALC0298
      PTY(N)=PAR(I)                                                     CALC0299
      TERM(N)=TE(L,I,1)                                                 CALC0300
      N=N+1                                                             CALC0301
  120 CONTINUE                                                          CALC0302
      DO 140 L=1,MAX1                                                   CALC0303
      DO 140 I=1,2                                                      CALC0304
      IF(TE(L,I,1).LT..01) GO TO 140                                    CALC0305
      GO TO (143,144,145),ICODE                                         CALC0306
  143 IF(TS(L,I,1).LE.SLIM) GO TO 140                                   CALC0307
      GO TO 145                                                         CALC0308
  144 SLIM=1.0D0-SLIM                                                   CALC0309
      IF (TS(L,I,1).GE.SLIM) GO TO 140                                  CALC0310
  145 CONTINUE                                                          CALC0311
      IF(I.EQ.2) GO TO 141                                              CALC0312
      VU(N)=TE(L,I,1)-BOT(2,1)                                          CALC0313
      GO TO 142                                                         CALC0314
  141 VU(N)=TE(L,I,1)-BOT(1,1)                                          CALC0315
  142 IRANK(N)=L                                                        CALC0316
      PP(N)=TP(L,I,1)                                                   CALC0317
      PS(N)=TS(L,I,1)                                                   CALC0318
      PRP=1.0-PP(N)-PS(N)                                               CALC0319
      PMAX=AMAX1(PS(N),PP(N),PRP)                                       CALC0320
      IF(I.EQ.2) GO TO 709                                              CALC0321
      BCH(N)=B(9)                                                       CALC0322
      IF(PMAX.EQ.PS(N)) GO TO 710                                       CALC0323
      IF(PMAX.EQ.PRP) BCH(N)=B(10)                                      CALC0324
```

```
      GO TO 710                                                         CALC0325
709   BCH(N)=B(11)                                                      CALC0326
      IF(PMAX.EQ.PS(N)) GO TO 710                                       CALC0327
      IF(PMAX.EQ.PP(N)) BCH(N)=B(12)                                    CALC0328
710   DJ(N)=0.5                                                         CALC0329
      PTY(N)=PAR(I)                                                     CALC0330
      TERM(N)=TE(L,I,1)                                                 CALC0331
      N=N+1                                                             CALC0332
140   CONTINUE                                                          CALC0333
      DO 150 L=1,MAX1                                                   CALC0334
      DO 150 I=1,2                                                      CALC0335
      IF(TE(L,I,2).LT..01) GO TO 150                                    CALC0336
      GO TO (151,152,153),ICODE                                         CALC0337
151   IF(TS(L,I,2).LE.SLIM) GO TO 150                                   CALC0338
      GO TO 153                                                         CALC0339
152   SLIM=1.0D0-SLIM                                                   CALC0340
      IF (TS(L,I,2).GE.SLIM) GO TO 150                                  CALC0341
153   CONTINUE                                                          CALC0342
      VU(N)=TE(L,I,2)-BOT(I,1)                                          CALC0343
      IRANK(N)=L                                                        CALC0344
      TERM(N)=TE(L,I,2)                                                 CALC0345
      PP(N)=TP(L,I,2)                                                   CALC0346
      PS(N)=TS(L,I,2)                                                   CALC0347
      PRP=1.0-PP(N)-PS(N)                                               CALC0348
      PMAX=AMAX1(PS(N),PP(N),PRP)                                       CALC0349
      IF(I.EQ.2) GO TO 711                                              CALC0350
      BCH(N)=B(1)                                                       CALC0351
      IF(PMAX.EQ.PS(N)) GO TO 712                                       CALC0352
      IF(PMAX.EQ.PRP) BCH(N)=B(2)                                       CALC0353
      GO TO 712                                                         CALC0354
711   BCH(N)=B(3)                                                       CALC0355
      IF(PMAX.EQ.PS(N)) GO TO 712                                       CALC0356
      IF(PMAX.EQ.PP(N)) BCH(N)=B(4)                                     CALC0357
712   PTY(N)=PAR(I)                                                     CALC0358
      DJ(N)=0.5                                                         CALC0359
      N=N+1                                                             CALC0360
```

```
150  CONTINUE                                                    CALC0361
     MCALC=N-1                                                   CALC0362
     DO 211 N=1,MCALC                                            CALC0363
     PS(N)=100.0*PS(N)                                           CALC0364
211  PP(N)=100.0*PP(N)                                           CALC0365
210  NF=0                                                        CALC0366
     DO 230 N=2,MCALC                                            CALC0367
     K=N-1                                                       CALC0368
     IF(VU(N).LE.VU(K)) GO TO 230                                CALC0369
     SAVE=VU(K)                                                  CALC0370
     VU(K)=VU(N)                                                 CALC0371
     VU(N)=SAVE                                                  CALC0372
     ISAVE=IRANK(K)                                              CALC0373
     IRANK(K)=IRANK(N)                                           CALC0374
     IRANK(N)=ISAVE                                              CALC0375
     SAVE=BCH(K)                                                 CALC0376
     BCH(K)=BCH(N)                                               CALC0377
     BCH(N)=SAVE                                                 CALC0378
     SAVE1=DJ(K)                                                 CALC0379
     DJ(K)=DJ(N)                                                 CALC0380
     DJ(N)=SAVE1                                                 CALC0381
     SAVE1=PTY(K)                                                CALC0382
     PTY(K)=PTY(N)                                               CALC0383
     PTY(N)=SAVE1                                                CALC0384
     SAVE=TERM(K)                                                CALC0385
     TERM(K)=TERM(N)                                             CALC0386
     TERM(N)=SAVE                                                CALC0387
     SAVE1=PP(K)                                                 CALC0388
     PP(K)=PP(N)                                                 CALC0389
     PP(N)=SAVE1                                                 CALC0390
     SAVE1=PS(K)                                                 CALC0391
     PS(K)=PS(N)                                                 CALC0392
     PS(N)=SAVE1                                                 CALC0393
     NF=1                                                        CALC0394
230  CONTINUE                                                    CALC0395
     IF(NF.GT.0) GO TO 210                                       CALC0396
```

```
      X1=1.0D0+6.4328D-05                                                    CALC0397
      X2=2.949810D+06                                                        CALC0398
      X3=2.5540D+04                                                          CALC0399
      X4=1.46D+10                                                            CALC0400
      X5=4.1D+09                                                             CALC0401
      DO 240 L=1,MCALC                                                       CALC0402
      DN=X1+X2/(X4-VU(L)**2)+X3/(X5-VU(L)**2)                                CALC0403
      VLAM(L)=1.0D+08/VU(L)                                                  CALC0404
      VLAM(L)=VLAM(L)/DN                                                     CALC0405
  240 CONTINUE                                                               CALC0406
      PRINT219                                                               CALC0407
  219 FORMAT(1H1,///,20X,25H2-SIGMA+&-,2-PI ESTIMATOR,//)                    CALC0408
      PRINT9                                                                 CALC0409
      PRINT419                                                               CALC0410
  419 FORMAT(///20X,28HGROUND STATE PARAMETERS USED)                         CALC0411
      DO 425 I=1,75                                                          CALC0412
      IF(GFLAG(I).EQ.1) GO TO 451                                            CALC0413
      GO TO 452                                                              CALC0414
  451 GP(I)=GP(I)/29979.25D0                                                 CALC0415
  452 CONTINUE                                                               CALC0416
      L=2                                                                    CALC0417
      DO 450 J=1,GAMAX                                                       CALC0418
  450 IF(I.EQ.GVAR(J)) L=1                                                   CALC0419
      K=GFLAG(I)+1                                                           CALC0420
      PRINT239,NAMES(I),GP(I),DIM(K),FIT(L)                                  CALC0421
  425 CONTINUE                                                               CALC0422
      PRINT229                                                               CALC0423
  229 FORMAT ('1',///,20X,29HEXCITED STATE PARAMETERS USED)                  CALC0424
      DO 225 I=1,75                                                          CALC0425
      IF (FLAG(I).EQ.1) GO TO 251                                            CALC0426
      GO TO 252                                                              CALC0427
  251 P(I)=P(I)/29979.25D0                                                   CALC0428
  252 CONTINUE                                                               CALC0429
      L=2                                                                    CALC0430
      DO 250 J=1,JAMAX                                                       CALC0431
  250 IF(I.EQ.NCVAR(J)) L=1                                                  CALC0432
```

```
      K=FLAG(I)+1                                                        CALC0433
      PRINT239,NAMES(I),P(I),DIM(K),FIT(L)                               CALC0434
  239 FORMAT(10X,A8,5X,D15.8,2X,A6,2X,A10)                               CALC0435
  225 CONTINUE                                                           CALC0436
      PRINT779,NERGY                                                     CALC0437
  779 FORMAT(' ',5X,I5,' CM-1 SHOULD BE ADDED TO UPPER STATE ENERGIES')  CALC0438
      PRINT259                                                           CALC0439
  259 FORMAT('1',5X,32HENERGY ORDERED TRANSISITION LIST//)               CALC0440
      PRINT897                                                           CALC0441
  897 FORMAT(3X,11HRANK-BRANCH,13X,6HENERGY,9X,7HPERCENT,10X,7HPERCENT,2 CALC0442
     13X,13HEXCITED STATE,9X,3HAIR)                                      CALC0443
      IF(IREG.EQ.1) GO TO 920                                            CALC0444
      PRINT898                                                           CALC0445
  898 FORMAT(28X,6H(CM-1),9X,5HPI3/2,13X,5HSIGMA,23X,11HTERM ENERGY,3X,6 CALC0446
     1HPARITY,1X,9HLAMBDA(A)//)                                          CALC0447
      GO TO 922                                                          CALC0448
  920 PRINT899                                                           CALC0449
  899 FORMAT(28X,6H(CM-1),9X,5HPI1/2,13X,5HSIGMA,23X,11HTERM ENERGY,3X,6 CALC0450
     1HPARITY,1X,9HLAMBDA(A)//)                                          CALC0451
  922 DO 910 N=1,MCALC                                                   CALC0452
  910 PRINT900,IRANK(N),BCH(N),DJ(N),VU(N),PP(N),PS(N),TERM(N),PTY(N)    CALC0453
     1,VLAM(N)                                                           CALC0454
  900 FORMAT(2X,I2,A5,F4.1,1H),10X,F12.4,3X,F10.4,7X,F10.4,8X,13X,F13.6, CALC0455
     15X,A1,3X,F9.3)                                                     CALC0456
  998 GO TO 1                                                            CALC0457
  999 STOP                                                               CALC0458
      END                                                                CALC0459
```

2-SIGMA+&-,2-PI ESTIMATOR

N2+ B2SIG+-X2SIG+ (3,5) CALCULATED SPECTRUM

GROUND STATE PARAMETERS USED

E1S	0.10552040D+05	CM	FIXED
B1S	0.18259093D+01	CM	FITTED
D1S	0.18081905D+00	MC	FITTED
GAM1S	0.52306955D-02	CM	FITTED
BETA12	0.0	MC	FIXED
A13	0.0	MC	FIXED
C14	0.0	MC	FIXED
BETA15	0.0	MC	FIXED
A16	0.0	MC	FIXED
E1P	0.0	MC	FIXED
B1P	0.0	MC	FIXED
A1P	0.0	MC	FIXED
GAM1P	0.0	MC	FIXED
Q1P+	0.0	MC	FIXED
D1P	0.0	MC	FIXED
AJV1P	0.0	MC	FIXED
AVO1P	0.0	MC	FIXED
P1P+	0.0	MC	FIXED
BETA24	0.0	MC	FIXED
H1P	0.0	MC	FIXED
H2P	0.0	MC	FIXED
O1P	0.0	MC	FIXED
A34	0.0	MC	FIXED
H1S	0.69100000D-07	MC	FIXED
H2S	0.0	MC	FIXED
E2S	0.0	MC	FIXED
B2S	0.0	MC	FIXED
D2S	0.0	MC	FIXED
GAM2S	0.0	MC	FIXED
BETA45	0.0	MC	FIXED
A46	0.0	MC	FIXED
A2P	0.0	MC	FIXED
GAM2P	0.0	MC	FIXED
Q2P+	0.0	MC	FIXED
D2P	0.0	MC	FIXED
AJV2P	0.0	MC	FIXED
AVO2P	0.0	MC	FIXED
P2P+	0.0	MC	FIXED
O2P	0.0	MC	FIXED
E2P	0.0	MC	FIXED
B2P	0.0	MC	FIXED
Q1P-	0.0	MC	FIXED
P1P-	0.0	MC	FIXED
Q2P-	0.0	MC	FIXED
P2P-	0.0	MC	FIXED
Q1S	0.0	MC	FIXED
P1S	0.0	MC	FIXED
O1S	0.0	MC	FIXED
Q2S	0.0	MC	FIXED
P2S	0.0	MC	FIXED
O2S	0.0	MC	FIXED
GAMJ1S	0.0	MC	FIXED

GAMJ2S	0.0	MC	FIXED
BETA17	0.0	MC	FIXED
A18	0.0	MC	FIXED
E3P	0.0	MC	FIXED
B3P	0.0	MC	FIXED
A3P	0.0	MC	FIXED
GAM3P	0.0	MC	FIXED
Q3P+	0.0	MC	FIXED
D3P	0.0	MC	FIXED
AJV3P	0.0	MC	FIXED
AV03P	0.0	MC	FIXED
Q3P-	0.0	MC	FIXED
H3P	0.0	MC	FIXED
P3P+	0.0	MC	FIXED
P3P-	0.0	MC	FIXED
BETA47	0.0	MC	FIXED
O3P	0.0	MC	FIXED
A48	0.0	MC	FIXED
	0.0	MC	FIXED
	0.0	MC	FIXED
	0.0	MC	FIXED
	0.0	MC	FIXED
	0.0	MC	FIXED

EXCITED STATE PARAMETERS USED

B1S	0.0	MC	FIXED
B1S	0.0	MC	FIXED
D1S	0.0	MC	FIXED
GAM1S	0.0	MC	FIXED
BETA12	0.0	MC	FIXED
A13	0.0	MC	FIXED
C14	0.0	MC	FIXED
BETA15	0.0	MC	FIXED
A16	0.0	MC	FIXED
E1P	0.12522270D+05	CM	FITTED
B1P	0.14652300D+01	CM	FITTED
A1P	-0.74600000D+02	CM	FIXED
GAM1P	0.0	MC	FIXED
Q1P+	0.0	MC	FIXED
D1P	0.12290000D+00	MC	FIXED
AJV1P	0.0	MC	FIXED
AVO1P	0.0	MC	FIXED
P1P+	0.0	MC	FIXED
BETA24	0.49504233D+00	CM	FITTED
H1P	-0.45900000D-07	MC	FIXED
H2P	-0.45900000D-07	MC	FIXED
O1P	0.0	MC	FIXED
A34	-0.58444630D+01	CM	FITTED
H1S	0.0	MC	FIXED
H2S	0.10300000D-06	MC	FIXED
E2S	0.12523469D+05	CM	FITTED
B2S	0.20007736D+01	CM	FITTED
D2S	0.21507079D+00	MC	FITTED
GAM2S	0.17551033D-01	CM	FITTED
BETA45	-0.16375000D+00	CM	FIXED
A46	0.52931100D+01	CM	FIXED
A2P	-0.74600000D+02	CM	FIXED
GAM2P	0.0	MC	FIXED
Q2P+	0.0	MC	FIXED
D2P	0.12290000D+00	MC	FIXED
AJV2P	0.0	MC	FIXED
AVO2P	0.0	MC	FIXED
P2P+	0.0	MC	FIXED
O2P	0.0	MC	FIXED
E2P	0.13966800D+05	CM	FIXED
B2P	0.14380000D+01	CM	FIXED
Q1P-	0.0	MC	FIXED
P1P-	0.0	MC	FIXED
Q2P-	0.0	MC	FIXED
P2P-	0.0	MC	FIXED
Q1S	0.0	MC	FIXED
P1S	0.0	MC	FIXED
O1S	0.0	MC	FIXED
Q2S	0.0	MC	FIXED
P2S	0.0	MC	FIXED
O2S	0.0	MC	FIXED
GAMJ1S	0.0	MC	FIXED
GAMJ2S	0.0	MC	FIXED
BETA17	0.0	MC	FIXED
A18	0.0	MC	FIXED
E3P	0.0	MC	FIXED
B3P	0.0	MC	FIXED
A3P	0.0	MC	FIXED
GAM3P	0.0	MC	FIXED

Q3P+	0.0	MC	FIXED
D3P	0.0	MC	FIXED
AJV3P	0.0	MC	FIXED
AVO3P	0.0	MC	FIXED
Q3P-	0.0	MC	FIXED
H3P	0.0	MC	FIXED
P3P+	0.0	MC	FIXED
P3P-	0.0	MC	FIXED
BETA47	0.0	MC	FIXED
O3P	0.0	MC	FIXED
A48	0.0	MC	FIXED
	0.0	MC	FIXED
	0.0	MC	FIXED
	0.0	MC	FIXED
	0.0	MC	FIXED
	0.0	MC	FIXED

20000 CM-1 SHOULD BE ADDED TO UPPER STATE ENERGIES

ENERGY ORDERED TRANSISITION LIST

RANK-BRANCH	ENERGY (CM-1)	PERCENT PI3/2	PERCENT SIGMA	EXCITED STATE TERM ENERGY	PARITY	AIR LAMBDA(A)
6-R2(81.5)	23425.2039	0.0159	99.9724	46125.504446	F	4267.705
6-Q21(82.5)	23424.7723	0.0159	99.9724	46125.504446	F	4267.784
6-R1(81.5)	23397.0324	0.0166	99.9579	45811.563765	E	4272.844
6-R2(80.5)	23395.6052	0.0163	99.9717	45809.710256	F	4273.104
6-Q21(81.5)	23395.1789	0.0163	99.9717	45809.710256	F	4273.182
6-R1(80.5)	23367.6746	0.0171	99.9565	45499.179310	E	4278.212
6-R2(79.5)	23366.2529	0.0168	99.9710	45497.336505	F	4278.472
6-Q21(80.5)	23365.8318	0.0168	99.9710	45497.336505	F	4278.549
6-R1(79.5)	23338.5658	0.0176	99.9549	45190.229527	E	4283.548
6-R2(78.5)	23337.1492	0.0173	99.9703	45188.397090	F	4283.808
6-Q21(79.5)	23336.7334	0.0173	99.9703	45188.397090	F	4283.884
6-R1(78.5)	23309.7083	0.0181	99.9533	44884.728183	E	4288.851
6-R2(77.5)	23308.2965	0.0178	99.9695	44882.905747	F	4289.111
6-Q21(78.5)	23307.8859	0.0178	99.9695	44882.905747	F	4289.187
6-R1(77.5)	23281.1044	0.0186	99.9516	44582.688883	E	4294.121
6-R2(76.5)	23279.6970	0.0183	99.9686	44580.876047	F	4294.380
6-Q21(77.5)	23279.2916	0.0183	99.9686	44580.876047	F	4294.455
6-R1(76.5)	23252.7564	0.0192	99.9497	44284.125078	E	4299.356
6-R2(75.5)	23251.3529	0.0189	99.9677	44282.321401	F	4299.615
6-Q21(76.5)	23250.9527	0.0189	99.9677	44282.321401	F	4299.689
6-R1(75.5)	23224.6666	0.0198	99.9476	43989.050059	E	4304.556
6-R2(74.5)	23223.2665	0.0195	99.9668	43987.255053	F	4304.816
6-Q21(75.5)	23222.8716	0.0195	99.9668	43987.255053	F	4304.889
6-R1(74.5)	23196.8372	0.0205	99.9454	43697.476965	E	4309.720
6-R2(73.5)	23195.4401	0.0202	99.9657	43695.690090	F	4309.980
6-Q21(74.5)	23195.0504	0.0202	99.9657	43695.690090	F	4310.052
6-R1(73.5)	23169.2705	0.0212	99.9430	43409.418779	E	4314.848
6-R2(72.5)	23167.8757	0.0209	99.9647	43407.639431	F	4315.108
6-Q21(73.5)	23167.4912	0.0209	99.9647	43407.639431	F	4315.179
6-R1(72.5)	23141.9688	0.0220	99.9403	43124.888335	E	4319.939
6-R2(71.5)	23140.5755	0.0217	99.9635	43123.115837	F	4320.199
6-Q21(72.5)	23140.1963	0.0217	99.9635	43123.115837	F	4320.270
6-R1(71.5)	23114.9341	0.0228	99.9374	42843.898319	E	4324.991
6-R2(70.5)	23113.5417	0.0225	99.9622	42842.131907	F	4325.252
6-Q21(71.5)	23113.1677	0.0225	99.9622	42842.131907	F	4325.322
6-R1(70.5)	23088.1688	0.0236	99.9342	42566.461274	E	4330.005
6-R2(69.5)	23086.7764	0.0234	99.9609	42564.700077	F	4330.266
6-Q21(70.5)	23086.4076	0.0234	99.9609	42564.700077	F	4330.335
6-R1(69.5)	23061.6752	0.0246	99.9305	42292.589605	E	4334.980
6-R2(68.5)	23060.2817	0.0244	99.9594	42290.832627	F	4335.242
6-Q21(69.5)	23059.9182	0.0244	99.9594	42290.832627	F	4335.310
6-R1(68.5)	23035.4553	0.0256	99.9264	42022.295589	E	4339.914
6-R2(67.5)	23034.0597	0.0255	99.9578	42020.541676	F	4340.177
6-Q21(68.5)	23033.7014	0.0255	99.9578	42020.541676	F	4340.244
6-R1(67.5)	23009.5115	0.0268	99.9218	41755.591381	E	4344.807
6-R2(66.5)	23008.1124	0.0267	99.9560	41753.839188	F	4345.072
6-Q21(67.5)	23007.7593	0.0267	99.9560	41753.839188	F	4345.138
6-R1(66.5)	22983.8461	0.0280	99.9164	41492.489037	E	4349.659
6-R2(65.5)	22982.4419	0.0280	99.9541	41490.736975	F	4349.925
6-Q21(66.5)	22982.0941	0.0280	99.9541	41490.736975	F	4349.991
6-R1(65.5)	22958.4615	0.0294	99.9101	41233.000526	E	4354.469
6-R2(64.5)	22957.0503	0.0295	99.9518	41231.246699	F	4354.736
6-Q21(65.5)	22956.7077	0.0295	99.9518	41231.246699	F	4354.801
6-R1(64.5)	22933.3600	0.0310	99.9027	40977.137770	E	4359.235
6-R2(63.5)	22931.9395	0.0312	99.9493	40975.379876	F	4359.505
6-Q21(64.5)	22931.6021	0.0312	99.9493	40975.379876	F	4359.569

6-R1(63.5)	22908.5443	0.0327	99.8939	40724.912684	E	4363.957
6-R2(62.5)	22907.1117	0.0332	99.9464	40723.147890	F	4364.230
6-Q21(63.5)	22906.7795	0.0332	99.9464	40723.147890	F	4364.293
6-R1(62.5)	22884.0172	0.0347	99.8830	40476.337252	E	4368.634
6-R2(61.5)	22882.5689	0.0355	99.9431	40474.561999	F	4368.911
6-Q21(62.5)	22882.2420	0.0355	99.9431	40474.561999	F	4368.973
6-R1(61.5)	22859.7818	0.0369	99.8693	40231.423638	E	4373.266
6-R2(60.5)	22858.3132	0.0382	99.9391	40229.633356	F	4373.547
6-Q21(61.5)	22857.9915	0.0382	99.9391	40229.633356	F	4373.609
6-P2(83.5)	22843.3375	0.0159	99.9724	46125.504446	F	4376.414
6-R1(60.5)	22835.8416	0.0394	99.8516	39990.184385	E	4377.851
6-R2(59.5)	22834.3467	0.0416	99.9342	39988.373038	F	4378.137
6-Q21(60.5)	22834.0303	0.0416	99.9342	39988.373038	F	4378.198
6-Q12(82.5)	22821.9053	0.0166	99.9579	45811.563765	E	4380.524
6-P1(83.5)	22821.4685	0.0166	99.9579	45811.563765	E	4380.608
6-P2(82.5)	22820.0518	0.0163	99.9717	45809.710256	F	4380.880
6-R1(59.5)	22812.2013	0.0422	99.8279	39752.632747	E	4382.388
6-R2(58.5)	22810.6718	0.0457	99.9282	39750.792089	F	4382.682
6-Q21(59.5)	22810.3606	0.0457	99.9282	39750.792089	F	4382.741
6-Q12(81.5)	22798.8787	0.0171	99.9565	45499.179310	E	4384.949
6-P1(82.5)	22798.4472	0.0171	99.9565	45499.179310	E	4385.032
6-P2(81.5)	22797.0359	0.0168	99.9710	45497.336505	F	4385.303
6-R1(58.5)	22788.8667	0.0452	99.7944	39518.783343	E	4386.875
6-R2(57.5)	22787.2910	0.0509	99.9204	39516.901603	F	4387.178
6-Q21(58.5)	22786.9850	0.0509	99.9204	39516.901603	F	4387.237
6-Q12(80.5)	22776.1245	0.0176	99.9549	45190.229527	E	4389.329
6-P1(81.5)	22775.6982	0.0176	99.9549	45190.229527	E	4389.412
6-P2(80.5)	22774.2921	0.0173	99.9703	45188.397090	F	4389.683
6-R1(57.5)	22765.8468	0.0481	99.7442	39288.653509	E	4391.311
6-R2(56.5)	22764.2069	0.0579	99.9100	39286.712858	F	4391.627
6-Q21(57.5)	22763.9062	0.0579	99.9100	39286.712858	F	4391.685
6-Q12(79.5)	22753.6446	0.0181	99.9533	44884.728183	E	4393.666
6-P1(80.5)	22753.2235	0.0181	99.9533	44884.728183	E	4393.747
6-P2(79.5)	22751.8221	0.0178	99.9695	44882.905747	F	4394.018
6-R1(56.5)	22743.1565	0.0498	99.6610	39062.266522	E	4395.692
6-R2(55.5)	22741.4231	0.0675	99.8953	39060.237588	F	4396.027
6-Q21(56.5)	22741.1275	0.0675	99.8953	39060.237588	F	4396.084
6-Q12(78.5)	22731.4410	0.0186	99.9516	44582.688883	E	4397.958
6-P1(79.5)	22731.0252	0.0186	99.9516	44582.688883	E	4398.038
6-P2(78.5)	22729.6282	0.0183	99.9686	44580.876047	F	4398.309
6-R1(55.5)	22720.8261	0.0474	99.4998	38839.660991	E	4400.012
6-R2(54.5)	22718.9440	0.0815	99.8733	38837.488534	F	4400.377
6-Q21(55.5)	22718.6537	0.0815	99.8733	38837.488534	F	4400.433
6-Q12(77.5)	22709.5158	0.0192	99.9497	44284.125078	E	4402.204
6-P1(78.5)	22709.1052	0.0192	99.9497	44284.125078	E	4402.283
6-P2(77.5)	22707.7121	0.0189	99.9677	44282.321401	F	4402.554
6-R21(51.5)	22705.3520	26.0147	1.0270	38057.459836	E	4403.011
6-R1(54.5)	22698.9397	0.0335	99.0761	38620.928907	E	4404.255
6-R2(53.5)	22696.7766	0.1037	99.8370	38618.480740	F	4404.675
6-Q21(54.5)	22696.4915	0.1037	99.8370	38618.480740	F	4404.730
6-Q12(76.5)	22687.8710	0.0198	99.9476	43989.050059	E	4406.404
6-P1(77.5)	22687.4656	0.0198	99.9476	43989.050059	E	4406.483
6-P2(76.5)	22686.0760	0.0195	99.9668	43987.255053	F	4406.752
6-R1(53.5)	22677.9445	0.1246	96.5460	38406.525483	E	4408.333
5-R1(47.5)	22675.5406	73.9077	1.1577	37316.283955	E	4408.800
6-R2(52.5)	22674.9339	0.1431	99.7685	38403.235079	F	4408.918
6-Q21(53.5)	22674.6541	0.1431	99.7685	38403.235079	F	4408.972
6-R21(52.5)	22673.5636	21.0881	13.6415	38212.181559	E	4409.184
6-Q12(75.5)	22666.5085	0.0205	99.9454	43697.476965	E	4410.557
6-P1(76.5)	22666.1083	0.0205	99.9454	43697.476965	E	4410.635
6-P2(75.5)	22664.7216	0.0202	99.9657	43695.690090	F	4410.904
6-R2(51.5)	22653.4471	0.2271	99.6072	38191.790452	F	4413.100
6-Q21(52.5)	22653.1724	0.2271	99.6072	38191.790452	F	4413.153
5-R1(52.5)	22652.5293	7.3373	85.3811	38191.147298	E	4413.279
6-Q12(74.5)	22645.4303	0.0212	99.9430	43409.418779	E	4414.662
6-P1(75.5)	22645.0353	0.0212	99.9430	43409.418779	E	4414.739

6-P2(74.5)	22643.6509	0.0209	99.9647	43407.639431	F	4415.009
5-R1(48.5)	22643.2307	72.1427	3.4635	37456.599381	E	4415.091
5-R21(53.5)	22634.7533	28.2277	2.8854	38363.334275	E	4416.745
5-R1(51.5)	22634.1112	3.1826	96.7567	37986.219092	E	4416.870
6-R2(50.5)	22632.4293	0.4897	99.0180	37984.267760	F	4417.198
6-Q21(51.5)	22632.1599	0.4897	99.0180	37984.267760	F	4417.251
6-R2(48.5)	22627.4951	25.7147	3.2028	37616.712127	F	4418.161
6-Q21(49.5)	22627.2362	25.7147	3.2028	37616.712127	F	4418.212
6-Q12(73.5)	22624.6383	0.0220	99.9403	43124.888335	E	4418.719
6-P1(74.5)	22624.2486	0.0220	99.9403	43124.888335	E	4418.795
6-P2(73.5)	22622.8658	0.0217	99.9635	43123.115837	F	4419.065
5-R1(50.5)	22615.8841	8.5505	90.1898	37784.942149	E	4420.430
5-R1(49.5)	22614.6714	56.5819	25.5363	37604.147280	E	4420.667
6-R2(49.5)	22613.0324	3.2950	90.5806	37781.826278	F	4420.987
6-Q21(50.5)	22612.7682	3.2950	90.5806	37781.826278	F	4421.039
6-Q12(72.5)	22604.1345	0.0228	99.9374	42843.898319	E	4422.727
6-P1(73.5)	22603.7501	0.0228	99.9374	42843.898319	E	4422.803
6-P2(72.5)	22602.3681	0.0225	99.9622	42842.131907	F	4423.073
5-R2(48.5)	22588.9153	0.3226	96.5522	37578.132316	F	4425.707
5-R2(49.5)	22588.7571	23.0678	9.2774	37757.551007	F	4425.738
5-Q21(49.5)	22588.6564	0.3226	96.5522	37578.132316	F	4425.758
5-Q21(50.5)	22588.4930	23.0678	9.2774	37757.551007	F	4425.790
6-Q12(71.5)	22583.9209	0.0236	99.9342	42566.461274	E	4426.686
6-P1(72.5)	22583.5417	0.0236	99.9342	42566.461274	E	4426.760
4-R1(49.5)	22582.4368	17.4210	74.2099	37571.912709	E	4426.977
6-P2(71.5)	22582.1597	0.0234	99.9609	42564.700077	F	4427.031
5-R12(45.5)	22574.0383	73.6113	1.4359	37045.402038	F	4428.624
5-Q1(46.5)	22573.7951	73.6113	1.4359	37045.402038	F	4428.672
5-R2(47.5)	22569.4902	0.1391	98.7965	37382.605173	F	4429.517
5-Q21(48.5)	22569.2365	0.1391	98.7965	37382.605173	F	4429.566
4-R1(48.5)	22567.7445	2.1268	96.3453	37381.113200	E	4429.859
4-R1(50.5)	22566.8763	65.2844	9.3905	37735.934383	E	4430.030
6-Q12(70.5)	22563.9994	0.0246	99.9305	42292.589605	E	4430.594
6-P1(71.5)	22563.6254	0.0246	99.9305	42292.589605	E	4430.668
6-P2(70.5)	22562.2424	0.0244	99.9594	42290.832627	F	4430.939
5-R2(46.5)	22551.3482	9.1719	85.8283	37191.843125	F	4433.080
5-Q21(47.5)	22551.0998	9.1719	85.8283	37191.843125	F	4433.129
4-R1(47.5)	22548.8535	0.6740	98.6796	37189.596832	E	4433.570
6-Q12(69.5)	22544.3719	0.0256	99.9264	42022.295589	E	4434.452
6-P1(70.5)	22544.0032	0.0256	99.9264	42022.295589	E	4434.524
6-P2(69.5)	22542.6180	0.0255	99.9578	42020.541676	F	4434.797
4-R12(46.5)	22535.7287	65.4915	13.9260	37176.223605	F	4436.153
4-Q1(47.5)	22535.4802	65.4915	13.9260	37176.223605	F	4436.202
4-R1(51.5)	22533.6870	70.8325	2.1357	37885.794817	E	4436.555
4-R1(46.5)	22529.5791	0.3252	99.2913	37001.186000	E	4437.364
4-R2(45.5)	22528.8359	1.4516	98.4111	37000.199602	F	4437.510
4-Q21(46.5)	22528.5927	1.4516	98.4111	37000.199602	F	4437.558
6-Q12(68.5)	22525.0405	0.0268	99.9218	41755.591381	E	4438.258
6-P1(69.5)	22524.6769	0.0268	99.9218	41755.591381	E	4438.329
6-P2(68.5)	22523.2883	0.0267	99.9560	41753.839188	F	4438.603
4-R1(45.5)	22510.3931	0.1968	99.5328	36816.359260	E	4441.146
4-R2(44.5)	22509.7870	0.3805	99.5898	36815.515105	F	4441.265
4-Q21(45.5)	22509.5490	0.3805	99.5898	36815.515105	F	4441.312
6-Q12(67.5)	22506.0070	0.0280	99.9164	41492.489037	E	4442.011
6-P1(68.5)	22505.6487	0.0280	99.9164	41492.489037	E	4442.082
6-P2(67.5)	22504.2550	0.0280	99.9541	41490.736975	F	4442.357
4-R1(44.5)	22491.4210	0.1376	99.6501	36635.248602	E	4444.892
4-R2(43.5)	22490.7786	0.1948	99.7789	36634.373440	F	4445.019
4-Q21(44.5)	22490.5458	0.1948	99.7789	36634.373440	F	4445.065
6-Q12(66.5)	22487.2737	0.0294	99.9101	41233.000526	E	4445.712
6-P1(67.5)	22486.9207	0.0294	99.9101	41233.000526	E	4445.781
6-P2(66.5)	22485.5199	0.0295	99.9518	41231.246699	F	4446.058
4-R1(43.5)	22472.7108	0.1065	99.7141	36457.908585	E	4448.593
4-R2(42.5)	22472.0205	0.1294	99.8436	36456.990737	F	4448.729
4-Q21(43.5)	22471.7929	0.1294	99.8436	36456.990737	F	4448.774
6-Q12(65.5)	22468.8427	0.0310	99.9027	40977.137770	E	4449.359

6-P1(66.5)	22468.4949	0.0310	99.9027	40977.137770	F	4449.427
6-P2(65.5)	22467.0848	0.0312	99.9493	40975.379876	F	4449.707
4-R1(42.5)	22454.2853	0.0887	99.7513	36284.368462	E	4452.243
4-R2(41.5)	22453.5519	0.0991	99.8728	36283.412699	F	4452.389
4-Q21(42.5)	22453.3296	0.0991	99.8728	36283.412699	F	4452.433
6-Q12(64.5)	22450.7163	0.0327	99.8939	40724.912684	E	4452.951
6-P1(65.5)	22450.3736	0.0327	99.8939	40724.912684	E	4453.019
6-P2(64.5)	22448.9515	0.0332	99.9464	40723.147890	F	4453.301
4-R1(41.5)	22436.1573	0.0780	99.7733	36114.647126	E	4455.841
4-R2(40.5)	22435.3869	0.0830	99.8879	36113.659581	F	4455.994
4-Q21(41.5)	22435.1698	0.0830	99.8879	36113.659581	F	4456.037
6-Q12(63.5)	22432.8969	0.0347	99.8830	40476.337252	E	4456.488
6-P1(64.5)	22432.5595	0.0347	99.8830	40476.337252	E	4456.555
6-P2(63.5)	22431.1216	0.0355	99.9431	40474.561999	F	4456.841
4-R1(40.5)	22418.3347	0.0714	99.7861	35948.758520	E	4459.383
4-R2(39.5)	22417.5324	0.0739	99.8961	35947.744349	F	4459.543
4-Q21(40.5)	22417.3206	0.0739	99.8961	35947.744349	F	4459.585
6-Q12(62.5)	22415.3874	0.0369	99.8693	40231.423638	E	4459.969
6-P1(63.5)	22415.0553	0.0369	99.8693	40231.423638	E	4460.035
6-P2(62.5)	22413.5972	0.0382	99.9391	40229.633356	F	4460.326
4-R1(39.5)	22400.8229	0.0674	99.7927	35786.713928	E	4462.869
4-R2(38.5)	22399.9926	0.0686	99.9003	35785.677092	F	4463.035
4-Q21(39.5)	22399.7860	0.0686	99.9003	35785.677092	F	4463.076
6-Q12(61.5)	22398.1913	0.0394	99.8516	39990.184385	E	4463.394
6-P1(62.5)	22397.8644	0.0394	99.8516	39990.184385	E	4463.459
6-P2(61.5)	22396.3799	0.0416	99.9342	39988.373038	F	4463.755
4-R1(38.5)	22383.6257	0.0652	99.7949	35628.523069	E	4466.298
4-R2(37.5)	22382.7705	0.0657	99.9022	35627.466493	F	4466.469
4-Q21(38.5)	22382.5691	0.0657	99.9022	35627.466493	F	4466.509
6-Q12(60.5)	22381.3126	0.0422	99.8279	39752.632747	E	4466.760
6-P1(61.5)	22380.9909	0.0422	99.8279	39752.632747	E	4466.824
6-P2(60.5)	22379.4719	0.0457	99.9282	39750.792089	F	4467.127
4-R1(37.5)	22366.7462	0.0641	99.7936	35474.194659	E	4469.669
4-R2(36.5)	22365.8682	0.0642	99.9025	35473.120427	F	4469.844
4-Q21(37.5)	22365.6720	0.0642	99.9025	35473.120427	F	4469.883
6-Q12(59.5)	22364.7570	0.0452	99.7944	39518.783343	E	4470.066
6-P1(60.5)	22364.4406	0.0452	99.7944	39518.783343	E	4470.129
6-P2(59.5)	22362.8753	0.0509	99.9204	39516.901603	F	4470.442
4-R1(36.5)	22350.1871	0.0638	99.7896	35323.736721	E	4472.980
4-R2(35.5)	22349.2876	0.0639	99.9017	35322.646243	F	4473.160
4-Q21(36.5)	22349.0966	0.0639	99.9017	35322.646243	F	4473.199
6-Q12(58.5)	22348.5333	0.0481	99.7442	39288.653509	E	4473.311
6-P1(59.5)	22348.2220	0.0481	99.7442	39288.653509	E	4473.374
6-P2(58.5)	22346.5926	0.0579	99.9100	39286.712858	F	4473.700
4-R1(35.5)	22333.9505	0.0643	99.7832	35177.156775	E	4476.232
4-R2(34.5)	22333.0303	0.0643	99.9000	35176.050904	F	4476.417
4-Q21(35.5)	22332.8446	0.0643	99.9000	35176.050904	F	4476.454
6-Q12(57.5)	22332.6559	0.0498	99.6610	39062.266522	E	4476.492
6-P1(58.5)	22332.3499	0.0498	99.6610	39062.266522	E	4476.553
6-P2(57.5)	22330.6270	0.0675	99.8953	39060.237588	F	4476.898
6-Q2(52.5)	22329.1587	26.0147	1.0270	38057.459836	E	4477.193
6-P21(53.5)	22328.8788	26.0147	1.0270	38057.459836	E	4477.249
5-Q12(48.5)	22327.0670	73.9077	1.1577	37316.283955	E	4477.612
5-P1(49.5)	22326.8080	73.9077	1.1577	37316.283955	E	4477.664
4-R1(34.5)	22318.0382	0.0652	99.7745	35034.461949	E	4479.424
6-Q12(56.5)	22317.1551	0.0474	99.4998	38839.660991	E	4479.601
4-R2(33.5)	22317.0978	0.0653	99.8976	35033.341062	F	4479.612
4-Q21(34.5)	22316.9174	0.0653	99.8976	35033.341062	F	4479.649
6-P1(57.5)	22316.8543	0.0474	99.4998	38839.660991	F	4479.661
6-P2(56.5)	22314.9826	0.0815	99.8733	38837.488534	F	4480.037
4-R1(33.5)	22302.4522	0.0666	99.7635	34895.659050	E	4482.554
6-Q12(55.5)	22302.1144	0.0335	99.0761	38620.928907	E	4482.622
6-P1(56.5)	22301.8169	0.0335	99.0761	38620.928907	E	4482.681
4-R2(32.5)	22301.4915	0.0668	99.8946	34894.523112	F	4482.747
4-Q21(33.5)	22301.3162	0.0668	99.8946	34894.523112	F	4482.782
6-P2(55.5)	22299.6662	0.1037	99.8370	38618.480740	F	4483.114

6-Q2(53.5)	22290.4774	21.0881	13.6415	38212.181559	E	4484.962
6-P21(54.5)	22290.1923	21.0881	13.6415	38212.181559	E	4485.020
6-Q12(54.5)	22287.9809	0.1246	96.5460	38406.525483	E	4485.465
5-Q12(49.5)	22287.8055	72.1427	3.4635	37456.599381	E	4485.500
6-P1(55.5)	22287.6906	0.1246	96.5460	38406.525483	E	4485.523
5-P1(50.5)	22287.5413	72.1427	3.4635	37456.599381	E	4485.553
4-R1(32.5)	22287.1939	0.0683	99.7503	34760.754620	E	4485.623
4-R2(31.5)	22286.2125	0.0688	99.8911	34759.603211	F	4485.821
4-Q21(32.5)	22286.0425	0.0688	99.8911	34759.603211	F	4485.855
6-P2(54.5)	22284.6905	0.1431	99.7685	38403.235079	F	4486.127
4-R1(31.5)	22272.2650	0.0704	99.7346	34629.754968	E	4488.630
4-R2(30.5)	22271.2621	0.0712	99.8872	34628.587303	F	4488.832
4-Q21(31.5)	22271.0973	0.0712	99.8872	34628.587303	F	4488.865
6-P2(53.5)	22270.0863	0.2271	99.6072	38191.790452	F	4489.069
5-Q12(53.5)	22269.4432	7.3373	85.3811	38191.147298	E	4489.199
5-P1(54.5)	22269.1581	7.3373	85.3811	38191.147298	E	4489.256
6-P2(50.5)	22264.8737	25.7147	3.2028	37616.712127	F	4490.120
5-Q12(52.5)	22257.9179	3.1826	96.7567	37986.219092	E	4491.523
4-R1(30.5)	22257.6669	0.0727	99.7163	34502.666198	E	4491.574
5-P1(53.5)	22257.6381	3.1826	96.7567	37986.219092	E	4491.580
4-R2(29.5)	22256.6413	0.0740	99.8827	34501.481125	F	4491.781
4-Q21(30.5)	22256.4818	0.0740	99.8827	34501.481125	F	4491.813
6-P2(52.5)	22255.9666	0.4897	99.0180	37984.267760	F	4491.917
5-Q12(50.5)	22252.3088	56.5819	25.5363	37604.147280	E	4492.655
5-P1(51.5)	22252.0394	56.5819	25.5363	37604.147280	E	4492.710
5-Q12(51.5)	22246.5988	8.5505	90.1898	37784.942149	E	4493.808
5-P1(52.5)	22246.3241	8.5505	90.1898	37784.942149	E	4493.864
5-Q2(54.5)	22244.7897	28.2277	2.8854	38363.334275	E	4494.174
5-P21(55.5)	22244.4994	28.2277	2.8854	38363.334275	E	4494.233
6-P2(51.5)	22243.4829	3.2950	90.5806	37781.826278	F	4494.438
4-R1(29.5)	22243.4010	0.0752	99.6948	34379.494232	E	4494.455
4-R2(28.5)	22242.3513	0.0771	99.8778	34378.290217	F	4494.667
4-Q21(29.5)	22242.1970	0.0771	99.8778	34378.290217	F	4494.698
5-P12(47.5)	22232.2871	73.6113	1.4359	37045.402038	F	4496.701
4-R1(28.5)	22229.4688	0.0780	99.6697	34260.244833	E	4497.271
4-R2(27.5)	22228.3930	0.0806	99.8725	34259.019928	F	4497.489
4-Q21(28.5)	22228.2439	0.0806	99.8725	34259.019928	F	4497.519
5-P2(50.5)	22226.2938	0.3226	96.5522	37578.132316	F	4497.914
4-Q12(50.5)	22220.0742	17.4210	74.2099	37571.912709	E	4499.173
4-P1(51.5)	22219.8049	17.4210	74.2099	37571.912709	E	4499.227
5-P2(51.5)	22219.2076	23.0678	9.2774	37757.551007	F	4499.348
4-R1(27.5)	22215.8718	0.0809	99.6404	34144.923624	E	4500.024
4-R2(26.5)	22214.7674	0.0844	99.8667	34143.675418	F	4500.248
4-Q21(27.5)	22214.6236	0.0844	99.8667	34143.675418	F	4500.277
5-P2(49.5)	22213.8113	0.1391	98.7965	37382.605173	F	4500.441
4-Q12(49.5)	22212.3193	2.1268	96.3453	37381.113200	E	4500.744
4-P1(50.5)	22212.0552	2.1268	96.3453	37381.113200	E	4500.797
5-P2(48.5)	22202.6261	9.1719	85.8283	37191.843125	F	4502.709
4-R1(26.5)	22202.6113	0.0840	99.6060	34033.536110	E	4502.712
4-R2(25.5)	22201.4755	0.0887	99.8604	34032.261659	F	4502.942
4-Q21(26.5)	22201.3369	0.0887	99.8604	34032.261659	F	4502.970
4-Q12(48.5)	22200.3798	0.6740	98.6796	37189.596832	E	4503.164
4-P1(49.5)	22200.1209	0.6740	98.6796	37189.596832	E	4503.217
4-Q12(51.5)	22197.5910	65.2844	9.3905	37735.934383	E	4503.730
4-P1(52.5)	22197.3164	65.2844	9.3905	37735.934383	E	4503.786
4-R1(25.5)	22189.6889	0.0872	99.5653	33926.087709	E	4505.334
4-R2(24.5)	22188.5181	0.0933	99.8537	33924.783438	F	4505.572
4-Q21(25.5)	22188.3847	0.0933	99.8537	33924.783438	F	4505.599
4-Q12(47.5)	22188.0710	0.3252	99.2913	37001.186000	E	4505.662
4-P1(48.5)	22187.8173	0.3252	99.2913	37001.186000	E	4505.714
4-P2(47.5)	22187.0846	1.4516	98.4111	37000.199602	F	4505.863
4-P12(48.5)	22187.0066	65.4915	13.9260	37176.223605	F	4505.879
4-R1(24.5)	22177.1053	0.0904	99.5166	33822.583791	E	4507.890
4-R2(23.5)	22175.8960	0.0983	99.8465	33821.245359	F	4508.136
4-Q12(46.5)	22175.8644	0.1968	99.5328	36816.359260	E	4508.143
4-Q21(24.5)	22175.7678	0.0983	99.8465	33821.245359	F	4508.162

4-P1(47.5)	22175.6159	0.1968	99.5328	36816.359260	b	4508.193
4-P2(46.5)	22175.0202	0.3805	99.5898	36815.515105	F	4508.314
4-R1(23.5)	22164.8651	0.0935	99.4563	33723.029719	b	4510.380
4-Q12(45.5)	22163.8849	0.1376	99.6501	36635.248602	E	4510.579
4-P1(46.5)	22163.6417	0.1376	99.6501	36635.248602	E	4510.629
4-R2(22.5)	22163.6101	0.1038	99.8387	33721.651839	F	4510.635
4-Q21(23.5)	22163.4872	0.1038	99.8387	33721.651839	F	4510.660
4-P2(45.5)	22163.0097	0.1948	99.7789	36634.373440	F	4510.757
4-Q12(52.5)	22157.4937	70.8325	2.1357	37885.794817	E	4511.880
4-P1(53.5)	22157.2138	70.8325	2.1357	37885.794817	e	4511.937
4-R1(22.5)	22152.9673	0.0964	99.3871	33627.430930	E	4512.802
4-Q12(44.5)	22152.1805	0.1065	99.7141	36457.908585	b	4512.963
4-P1(45.5)	22151.9425	0.1065	99.7141	36457.908585	E	4513.011
4-R2(21.5)	22151.6611	0.1097	99.8305	33626.007113	F	4513.068
4-Q21(22.5)	22151.5434	0.1097	99.8305	33626.007113	F	4513.092
4-P2(44.5)	22151.2626	0.1294	99.8436	36456.990737	F	4513.150
4-R1(21.5)	22141.4152	0.0988	99.2989	33535.793024	E	4515.157
4-Q12(43.5)	22140.7736	0.0887	99.7513	36284.368462	E	4515.288
4-P1(44.5)	22140.5409	0.0887	99.7513	36284.368462	E	4515.335
4-R2(20.5)	22140.0498	0.1161	99.8219	33534.315229	F	4515.435
4-Q21(21.5)	22139.9374	0.1161	99.8219	33534.315229	F	4515.458
4-P2(43.5)	22139.8179	0.0991	99.8728	36283.412699	F	4515.483
4-R1(20.5)	22130.2115	0.1006	99.1877	33448.121924	E	4517.443
4-Q12(42.5)	22129.6768	0.0780	99.7733	36114.647126	e	4517.552
4-P1(43.5)	22129.4493	0.0780	99.7733	36114.647126	E	4517.598
4-R2(19.5)	22128.7768	0.1230	99.8128	33446.580051	F	4517.736
4-P2(42.5)	22128.6893	0.0830	99.8879	36113.659581	F	4517.753
4-Q21(20.5)	22128.6696	0.1230	99.8128	33446.580051	F	4517.757
4-R1(19.5)	22119.3597	0.1013	99.0447	33364.424106	E	4519.659
4-Q12(41.5)	22118.8977	0.0714	99.7861	35948.758520	e	4519.753
4-P1(42.5)	22118.6754	0.0714	99.7861	35948.758520	e	4519.799
4-P2(41.5)	22117.8835	0.0739	99.8961	35947.744349	F	4519.961
4-R2(18.5)	22117.8428	0.1304	99.8033	33362.805257	F	4519.969
4-Q21(19.5)	22117.7408	0.1304	99.8033	33362.805257	F	4519.990
4-R1(18.5)	22108.8643	0.1004	98.8562	33284.706971	E	4521.805
4-Q12(40.5)	22108.4412	0.0674	99.7927	35786.713928	e	4521.891
4-P1(41.5)	22108.2241	0.0674	99.7927	35786.713928	E	4521.936
4-P2(40.5)	22107.4044	0.0686	99.9003	35785.677092	F	4522.103
4-R2(17.5)	22107.2484	0.1382	99.7936	33282.994340	F	4522.135
4-Q21(18.5)	22107.1517	0.1382	99.7936	33282.994340	F	4522.155
4-R1(17.5)	22098.7315	0.0971	98.6000	33208.979466	e	4523.878
4-Q12(39.5)	22098.3111	0.0652	99.7949	35628.523069	E	4523.964
4-P1(40.5)	22098.0993	0.0652	99.7949	35628.523069	E	4524.007
4-P2(39.5)	22097.2546	0.0657	99.9022	35627.466493	F	4524.180
4-R2(16.5)	22096.9941	0.1465	99.7839	33207.150607	F	4524.234
4-Q21(17.5)	22096.9026	0.1465	99.7839	33207.150607	F	4524.252
4-R1(16.5)	22088.9702	0.0905	98.2393	33137.253155	E	4525.877
4-Q12(38.5)	22088.5102	0.0641	99.7936	35474.194659	E	4525.971
4-P1(39.5)	22088.3036	0.0641	99.7936	35474.194659	E	4526.014
4-P2(38.5)	22087.4360	0.0642	99.9025	35473.120427	F	4526.192
4-R2(15.5)	22087.0805	0.1552	99.7744	33135.277189	F	4526.264
4-Q21(16.5)	22086.9942	0.1552	99.7744	33135.277189	F	4526.282
4-R1(15.5)	22079.5941	0.0793	97.7086	33069.544173	E	4527.799
4-Q12(37.5)	22079.0407	0.0638	99.7896	35323.736721	E	4527.913
4-P1(38.5)	22078.8393	0.0638	99.7896	35323.736721	e	4527.954
4-P2(37.5)	22077.9502	0.0639	99.9017	35322.646243	F	4528.136
4-R2(14.5)	22077.5080	0.1640	99.7658	33067.377040	F	4528.227
4-Q21(15.5)	22077.4270	0.1640	99.7658	33067.377040	F	4528.244
4-R1(14.5)	22070.6254	0.0621	96.8855	33005.876980	E	4529.639
4-Q12(36.5)	22069.9045	0.0643	99.7832	35177.156775	E	4529.787
4-P1(37.5)	22069.7084	0.0643	99.7832	35177.156775	E	4529.827
4-P2(36.5)	22068.7986	0.0643	99.9000	35176.050904	F	4530.014
4-R2(13.5)	22068.2772	0.1729	99.7587	33003.452963	F	4530.121
4-Q21(14.5)	22068.2014	0.1729	99.7587	33003.452963	F	4530.137
4-R1(13.5)	22062.1024	0.0384	95.5227	32946.292072	E	4531.389
4-Q12(35.5)	22061.1043	0.0652	99.7745	35034.461949	e	4531.594

4-P1(36.5)	22060.9123	0.0652	99.7745	35034.461949	E	4531.633
4-P2(35.5)	22059.9824	0.0653	99.8976	35033.341062	F	4531.824
4-R2(12.5)	22059.3885	0.1813	99.7544	32943.507644	F	4531.946
4-Q21(13.5)	22059.3179	0.1813	99.7544	32943.507644	F	4531.961
4-R1(12.5)	22054.0964	0.0117	93.0834	32890.862825	E	4533.034
4-Q12(34.5)	22052.6384	0.0666	99.7635	34895.659050	E	4533.334
4-P1(35.5)	22052.4528	0.0666	99.7635	34895.659050	E	4533.372
4-P2(34.5)	22051.5025	0.0668	99.8946	34894.523112	F	4533.567
4-R2(11.5)	22050.8426	0.1887	99.7545	32887.543727	F	4533.703
4-Q21(12.5)	22050.7773	0.1887	99.7545	32887.543727	F	4533.716
4-R1(11.5)	22046.7502	0.0019	88.3317	32839.733898	E	4534.544
4-Q12(33.5)	22044.5114	0.0683	99.7503	34760.754620	E	4535.005
4-P1(34.5)	22044.3309	0.0683	99.7503	34760.754620	E	4535.042
4-P2(33.5)	22043.3600	0.0688	99.8911	34759.603211	F	4535.242
4-R2(10.5)	22042.6404	0.1941	99.7616	32835.563995	F	4535.390
4-Q21(11.5)	22042.5803	0.1941	99.7616	32835.563995	F	4535.402
4-R1(10.5)	22040.3588	0.0807	78.5545	32793.202031	E	4535.859
4-Q12(32.5)	22036.7233	0.0704	99.7346	34629.754968	E	4536.608
4-P1(33.5)	22036.5481	0.0704	99.7346	34629.754968	E	4536.644
4-P2(32.5)	22035.5557	0.0712	99.8872	34628.587303	F	4536.848
4-R1(9.5)	22035.4450	0.3990	60.3051	32751.791497	E	4536.871
4-R2(9.5)	22034.7835	0.1956	99.7787	32787.571799	F	4537.007
4-Q21(10.5)	22034.7286	0.1956	99.7787	32787.571799	F	4537.018
4-R21(8.5)	22032.4099	0.9230	37.6692	32715.905007	E	4537.496
4-R21(7.5)	22030.7734	1.2588	21.4521	32685.063708	E	4537.833
4-R21(6.5)	22029.6179	1.2870	12.8419	32658.351146	E	4538.071
4-Q12(31.5)	22029.2755	0.0727	99.7163	34502.666198	E	4538.142
4-P1(32.5)	22029.1055	0.0727	99.7163	34502.666198	E	4538.177
4-R21(5.5)	22028.3532	1.1328	8.4017	32635.178177	E	4538.332
4-P2(31.5)	22028.0904	0.0740	99.8827	34501.481125	F	4538.386
4-R2(8.5)	22027.2755	0.1900	99.8054	32743.572289	F	4538.554
4-Q21(9.5)	22027.2258	0.1900	99.8054	32743.572289	F	4538.564
4-R21(4.5)	22026.7035	0.9033	5.9535	32615.269694	E	4538.671
4-R21(3.5)	22024.5417	0.6580	4.4967	32598.499607	E	4539.117
4-Q12(30.5)	22022.1690	0.0752	99.6948	34379.494232	E	4539.606
4-P1(31.5)	22022.0042	0.0752	99.6948	34379.494232	E	4539.640
4-R21(2.5)	22021.8057	0.4293	3.5733	32584.806125	E	4539.681
4-P2(30.5)	22020.9650	0.0771	99.8778	34378.290217	F	4539.854
4-R2(7.5)	22020.1262	0.1701	99.8098	32703.576828	F	4540.027
4-Q21(8.5)	22020.0817	0.1701	99.8098	32703.576828	F	4540.036
4-R21(1.5)	22018.4622	0.2362	2.9602	32574.156597	E	4540.370
3-R21(10.5)	22016.3876	5.4090	20.7521	32769.230803	E	4540.798
3-R21(9.5)	22016.0042	4.4691	38.9696	32732.350683	E	4540.877
4-Q12(29.5)	22015.4050	0.0780	99.6697	34260.244833	E	4541.001
4-P1(30.5)	22015.2455	0.0780	99.6697	34260.244833	E	4541.034
3-R21(11.5)	22014.9547	6.1252	11.0123	32807.938442	E	4541.094
4-R21(0.5)	22014.4926	0.0907	2.5419	32566.532577	E	4541.189
4-P2(29.5)	22014.1801	0.0806	99.8725	34259.019928	F	4541.253
3-R1(8.5)	22013.4045	3.3393	61.5837	32696.899604	E	4541.413
4-R2(6.5)	22013.3760	0.1149	99.4041	32667.627115	F	4541.419
4-Q21(7.5)	22013.3368	0.1149	99.4041	32667.627115	F	4541.427
3-R21(12.5)	22012.2269	6.7674	6.3004	32848.993401	E	4541.656
4-R2(1.5)	22010.5396	0.2474	2.0641	32573.526969	F	4542.005
4-Q21(2.5)	22010.5265	0.2474	2.0641	32573.526969	F	4542.007
4-R2(0.5)	22010.4381	0.0935	1.9520	32566.124632	F	4542.026
4-Q21(1.5)	22010.4302	0.0935	1.9520	32566.124632	F	4542.027
4-R2(2.5)	22009.9934	0.4554	2.4208	32583.933026	F	4542.117
4-Q21(3.5)	22009.9751	0.4554	2.4208	32583.933026	F	4542.121
5-Q21(0.5)	22009.6825	0.0	1.9652	32561.722520	F	4542.181
3-R1(7.5)	22009.0702	2.4126	77.7951	32663.360530	E	4542.308
4-Q12(28.5)	22008.9847	0.0809	99.6404	34144.923624	E	4542.325
4-P1(29.5)	22008.8304	0.0809	99.6404	34144.923624	E	4542.357
4-R2(3.5)	22008.8176	0.6972	3.5070	32597.360301	F	4542.360
4-Q21(4.5)	22008.7941	0.6972	3.5070	32597.360301	F	4542.365
3-R21(13.5)	22008.4979	7.4053	3.9011	32892.687653	E	4542.426
4-P2(28.5)	22007.7365	0.0844	99.8667	34143.675418	F	4542.583

4-R2(5.5)	22007.4535	0.0072	85.4722
4-Q21(6.5)	22007.4195	0.0072	85.4722
4-R2(4.5)	22007.1277	0.8561	9.2926
4-Q21(5.5)	22007.0990	0.8561	9.2926
5-Q2(0.5)	22006.2365	0.0	2.2556
5-P21(1.5)	22006.2286	0.0	2.2556
3-R1(6.5)	22003.9209	1.8063	86.4230
3-R21(14.5)	22003.9092	8.0564	2.5773
4-Q2(1.5)	22003.5452	0.0907	2.5419
4-P21(2.5)	22003.5321	0.0907	2.5419
3-R2(5.5)	22003.3780	1.8318	14.3349
3-Q21(6.5)	22003.3440	1.8318	14.3349
4-Q12(27.5)	22002.9092	0.0840	99.6060
4-P1(28.5)	22002.7601	0.0840	99.6060
4-P2(27.5)	22001.6347	0.0887	99.8604
4-Q2(2.5)	22000.2170	0.2362	2.9602
4-P21(3.5)	22000.1987	0.2362	2.9602
3-R2(4.5)	22000.1012	0.5556	90.5214
3-Q21(5.5)	22000.0724	0.5556	90.5214
5-P2(1.5)	21998.7351	0.0	1.9652
3-R1(5.5)	21998.5492	1.3936	90.9115
3-R21(15.5)	21998.5306	8.7216	1.7911
4-Q12(26.5)	21997.1797	0.0872	99.5653
4-P1(27.5)	21997.0359	0.0872	99.5653
4-Q2(3.5)	21996.2634	0.4293	3.5733
4-P21(4.5)	21996.2399	0.4293	3.5733
4-P2(26.5)	21995.8754	0.0933	99.8537
3-R2(3.5)	21994.4833	0.3293	96.3249
3-Q21(4.5)	21994.4598	0.3293	96.3249
3-R1(4.5)	21993.2348	1.0689	93.4438
3-R21(16.5)	21992.3993	9.3976	1.2952
4-P2(2.5)	21992.1851	0.0935	1.9520
4-Q12(25.5)	21991.7976	0.0904	99.5168
4-Q2(4.5)	21991.7034	0.6580	4.4967
4-P21(5.5)	21991.6747	0.6580	4.4967
4-P1(26.5)	21991.6590	0.0904	99.5168
4-P2(25.5)	21990.4592	0.0983	99.8465
3-R2(2.5)	21989.0566	0.2300	97.4415
3-Q21(3.5)	21989.0383	0.2300	97.4415
3-R1(3.5)	21988.1095	0.7807	95.0196
4-Q12(24.5)	21986.7643	0.0935	99.4583
4-P1(25.5)	21986.6310	0.0935	99.4583
4-Q2(5.5)	21986.5705	0.9033	5.9535
4-P21(6.5)	21986.5365	0.9033	5.9535
4-P2(24.5)	21985.3865	0.1038	99.8387
4-P2(3.5)	21984.9843	0.2474	2.0641
3-R2(1.5)	21983.9398	0.1456	97.8409
3-Q21(2.5)	21983.9267	0.1456	97.8409
3-R1(2.5)	21983.2423	0.5151	96.0860
4-Q12(23.5)	21982.0816	0.0964	99.3871
4-P1(24.5)	21981.9534	0.0964	99.3871
4-Q2(6.5)	21980.9271	1.1328	8.4017
4-P21(7.5)	21980.8879	1.1328	8.4017
4-P2(23.5)	21980.6577	0.1097	99.8305
3-R2(0.5)	21979.1551	0.0655	98.0025
3-Q21(1.5)	21979.1472	0.0655	98.0025
3-R1(1.5)	21978.6737	0.2825	96.8442
4-Q12(22.5)	21977.7513	0.0988	99.2989
4-P1(23.5)	21977.6284	0.0988	99.2989
4-P2(4.5)	21977.1369	0.4554	2.4208
4-P2(22.5)	21976.2735	0.1161	99.8219
4-Q2(7.5)	21974.9005	1.2870	12.8419
4-P21(8.5)	21974.8560	1.2870	12.8419
4-Q21(0.5)	21974.7090	0.0	98.0337
3-R1(0.5)	21974.4293	0.1048	97.3829
4-Q12(21.5)	21973.7759	0.1006	99.1877

32636.152790	F	4542.641
32636.152790	F	4542.648
32613.923898	F	4542.709
32613.923898	F	4542.715
32561.923052	E	4542.893
32561.923052	E	4542.894
32632.654117	E	4543.371
32939.160771	E	4543.373
32566.532577	E	4543.448
32566.532577	E	4543.451
32632.077287	F	4543.483
32632.077287	F	4543.490
34033.536110	E	4543.580
34033.536110	E	4543.610
34032.261659	F	4543.843
32574.156597	E	4544.136
32574.156597	E	4544.139
32606.897325	F	4544.160
32606.897325	F	4544.166
32561.722520	F	4544.442
32605.374110	E	4544.480
32988.480729	E	4544.484
33926.087709	E	4544.763
33926.087709	E	4544.793
32584.806125	E	4544.952
32584.806125	E	4544.957
33924.783438	F	4545.033
32583.026037	F	4545.320
32583.026037	F	4545.325
32581.801002	E	4545.578
33040.682312	E	4545.751
32566.124632	F	4545.795
33822.583791	E	4545.875
32598.499607	E	4545.895
32598.499607	E	4545.901
33822.583791	E	4545.904
33821.245359	F	4546.152
32562.996172	F	4546.442
32562.996172	F	4546.446
32562.067405	E	4546.638
33723.029719	E	4546.916
33723.029719	E	4546.944
32615.269694	E	4546.956
32615.269694	E	4546.963
33721.651839	F	4547.201
32573.526969	F	4547.284
32546.927160	F	4547.500
32546.927160	F	4547.503
32546.242804	E	4547.645
33627.430930	E	4547.885
33627.430930	E	4547.911
32635.178177	E	4548.124
32635.178177	E	4548.132
33626.007113	F	4548.179
32534.841625	F	4548.490
32534.841625	F	4548.492
32534.368130	E	4548.590
33535.793024	E	4548.781
33535.793024	E	4548.806
32583.933026	F	4548.908
33534.315229	F	4549.087
32658.351146	E	4549.371
32658.351146	E	4549.380
32526.748992	F	4549.411
32526.469311	E	4549.468
33448.121924	E	4549.604

4-P1(22.5)	21973.6583	0.1006	99.1877	33448.121924	E	4549.628
4-P2(21.5)	21972.2341	0.1230	99.8128	33446.580051	F	4549.923
4-Q12(20.5)	21970.1587	0.1013	99.0447	33364.424106	E	4550.353
4-P1(21.5)	21970.0462	0.1013	99.0447	33364.424106	E	4550.376
4-Q2(8.5)	21968.7669	1.2588	21.4521	32685.063708	E	4550.641
4-P21(9.5)	21968.7172	1.2588	21.4521	32685.063708	E	4550.651
4-P2(5.5)	21968.6611	0.6972	3.5070	32597.360301	F	4550.663
4-P2(20.5)	21968.5399	0.1304	99.8033	33362.805257	F	4550.688
4-Q12(19.5)	21966.9038	0.1004	98.8562	33284.706971	E	4551.027
4-Q12(0.5)	21966.8757	0.0	97.7431	32522.562270	E	4551.033
4-P1(1.5)	21966.8679	0.0	97.7431	32522.562270	E	4551.035
4-P1(20.5)	21966.7965	0.1004	98.8562	33284.706971	E	4551.049
4-P2(19.5)	21965.1911	0.1382	99.7936	33282.994340	F	4551.382
4-Q12(18.5)	21964.0171	0.0971	98.6000	33208.979466	E	4551.625
4-P1(19.5)	21963.9151	0.0971	98.6000	33208.979466	E	4551.646
4-P2(1.5)	21963.7616	0.0	98.0337	32526.748992	F	4551.678
3-Q12(1.5)	21963.4819	0.1048	97.3829	32526.469311	E	4551.736
3-P1(2.5)	21963.4688	0.1048	97.3829	32526.469311	E	4551.739
4-Q2(9.5)	21963.1167	0.9230	37.6692	32715.905007	E	4551.812
4-P21(10.5)	21963.0618	0.9230	37.6692	32715.905007	E	4551.823
4-P2(18.5)	21962.1882	0.1465	99.7839	33207.150607	F	4552.004
4-Q12(17.5)	21961.5072	0.0905	98.2393	33137.253155	E	4552.145
4-P1(18.5)	21961.4105	0.0905	98.2393	33137.253155	E	4552.165
3-P2(2.5)	21960.9020	0.0655	98.0025	32534.841625	F	4552.271
3-Q12(2.5)	21960.4285	0.2825	96.8442	32534.368130	E	4552.369
3-P1(3.5)	21960.4102	0.2825	96.8442	32534.368130	E	4552.373
4-P2(6.5)	21959.6728	0.8561	9.2926	32613.923898	F	4552.526
4-P2(17.5)	21959.5313	0.1552	99.7744	33135.277189	F	4552.555
4-Q12(16.5)	21959.3877	0.0793	97.7086	33069.544173	E	4552.585
4-P1(17.5)	21959.2962	0.0793	97.7086	33069.544173	E	4552.604
4-Q12(10.5)	21958.8679	0.3990	60.3051	32751.791497	E	4552.693
4-P1(11.5)	21958.8078	0.3990	60.3051	32751.791497	E	4552.705
3-P2(3.5)	21958.3845	0.1456	97.8409	32546.927160	F	4552.793
3-Q12(3.5)	21957.7001	0.5151	96.0860	32546.242804	E	4552.935
4-Q12(15.5)	21957.6803	0.0621	96.8855	33005.876980	E	4552.939
3-P1(4.5)	21957.6766	0.5151	96.0860	32546.242804	E	4552.940
4-P1(16.5)	21957.5940	0.0621	96.8855	33005.876980	E	4552.957
4-P2(16.5)	21957.2206	0.1640	99.7658	33067.377040	F	4553.034
4-Q12(11.5)	21956.5010	0.0807	78.5545	32793.202031	E	4553.183
4-P1(12.5)	21956.4356	0.0807	78.5545	32793.202031	E	4553.197
4-Q12(14.5)	21956.4231	0.0384	95.5227	32946.292072	E	4553.200
4-P1(15.5)	21956.3420	0.0384	95.5227	32946.292072	E	4553.216
3-P2(4.5)	21956.2000	0.2300	97.4415	32562.996172	F	4553.246
4-Q12(13.5)	21955.6871	0.0117	93.0834	32890.862825	E	4553.352
4-Q12(12.5)	21955.6148	0.0019	88.3317	32839.733898	E	4553.367
4-P1(14.5)	21955.6112	0.0117	93.0834	32890.862825	E	4553.368
4-P1(13.5)	21955.5442	0.0019	88.3317	32839.733898	E	4553.382
3-Q12(4.5)	21955.2712	0.7807	95.0196	32562.067405	E	4553.438
4-P2(15.5)	21955.2563	0.1729	99.7587	33003.452963	F	4553.442
3-P1(5.5)	21955.2425	0.7807	95.0196	32562.067405	E	4553.444
3-P2(5.5)	21954.3268	0.3293	96.3249	32583.026037	F	4553.634
4-P2(14.5)	21953.6386	0.1813	99.7544	32943.507644	F	4553.777
3-Q12(5.5)	21953.1018	1.0689	93.4438	32581.801002	E	4553.888
3-P1(6.5)	21953.0678	1.0689	93.4438	32581.801002	E	4553.895
4-P2(7.5)	21952.7021	0.0072	85.4722	32636.152790	F	4553.971
3-P2(6.5)	21952.6462	0.5556	90.5214	32606.897325	F	4553.983
4-P2(13.5)	21952.3680	0.1887	99.7545	32887.543727	F	4554.041
4-P2(12.5)	21951.4449	0.1941	99.7616	32835.563995	F	4554.232
4-P2(8.5)	21951.3303	0.1149	99.4041	32667.627115	F	4554.256
3-Q12(6.5)	21951.1230	1.3936	90.9115	32605.374110	E	4554.299
3-P1(7.5)	21951.0838	1.3936	90.9115	32605.374110	E	4554.307
4-P2(11.5)	21950.8707	0.1956	99.7787	32787.571799	F	4554.351
4-P2(9.5)	21950.7886	0.1701	99.8098	32703.576826	F	4554.368
4-P2(10.5)	21950.6487	0.1900	99.8054	32743.572289	F	4554.397
3-Q12(7.5)	21949.2035	1.8063	86.4230	32632.654117	E	4554.697
3-P1(8.5)	21949.1590	1.8063	86.4230	32632.654117	E	4554.706

3-P2(7.5)	21948.6266	1.8318	14.3349	32632.077287	F	4554.817
3-Q12(8.5)	21947.0637	2.4126	77.7951	32663.360530	E	4555.141
3-P1(9.5)	21947.0140	2.4126	77.7951	32663.360530	E	4555.152
3-Q12(9.5)	21944.1113	3.3393	61.5837	32696.899604	E	4555.754
3-P1(10.5)	21944.0564	3.3393	61.5837	32696.899604	E	4555.766
3-Q2(10.5)	21939.4271	4.4691	38.9696	32732.350683	E	4556.727
3-P21(11.5)	21939.3670	4.4691	38.9696	32732.350683	E	4556.739
3-Q2(11.5)	21932.5297	5.4090	20.7521	32769.230803	E	4558.160
3-P21(12.5)	21932.4643	5.4090	20.7521	32769.230803	E	4558.173
3-Q2(12.5)	21923.8193	6.1252	11.0123	32807.938442	E	4559.971
3-P21(13.5)	21923.7487	6.1252	11.0123	32807.938442	E	4559.986
3-Q2(13.5)	21913.8176	6.7674	6.3004	32848.993401	E	4562.052
3-P21(14.5)	21913.7418	6.7674	6.3004	32848.993401	E	4562.068
3-Q2(14.5)	21902.8186	7.4053	3.9011	32892.687653	E	4564.343
3-P21(15.5)	21902.7376	7.4053	3.9011	32892.687653	E	4564.360
3-Q2(15.5)	21890.9641	8.0564	2.5773	32939.160771	E	4566.815
3-P21(16.5)	21890.8778	8.0564	2.5773	32939.160771	E	4566.833
3-Q2(16.5)	21878.3243	8.7216	1.7911	32988.480729	E	4569.453
3-P21(17.5)	21878.2327	8.7216	1.7911	32988.480729	E	4569.472
3-Q2(17.5)	21864.9364	9.3976	1.2952	33040.682312	E	4572.251
3-P21(18.5)	21864.8396	9.3976	1.2952	33040.682312	E	4572.271

```
C THIS IS LSQ9. IT CAN HANDLE A 9X9 HAMILTONIAN, ODD AND EVEN MULTIPLICITIES.     LSQ 0001
C     LSQ SIMULATOR PACKAGE.  COMPARES EIGENVALUES OF HAMILTONIAN TO              LSQ 0002
C     TRANSITIONS OR TERM ENERGIES.                                               LSQ 0003
C     THIS IS MAIN FOR ANY PROBLEM INVOLVING A HAMILTONIAN WITH MAXIMUM           LSQ 0004
C     DIMENSION OF 9 BY 9.                                                        LSQ 0005
C     MODIFIED SO THAT ALL ENERGIES, TRANSITIONS, AND PARAMETERS ARE              LSQ 0006
C     DOUBLE PRECISION.                                                           LSQ 0007
C     MODIFIED TO USE DISC (SYSQUE) UNIT 2 FOR INTERMEDIATE STORAGE.              LSQ 0008
C     JCL FOR DISC IS AS FOLLOWS:                                                 LSQ 0009
C/GO.FT02F001  DD  UNIT=SYSQUE,SPACE=(TRK,(50,50)),DSN=&FIELD,                    LSQ 0010
C/   DISP=(NEW,PASS),DCB=(RECFM=VSB,BLKSIZE=7294,BUFNO=1)                         LSQ 0011
C                                                                                LSQ 0012
C     REQUIRES SUBROUTINES: LEVEL, MATRIX, SETUP, NEWFIT, NAMEIT,                LSQ 0013
C     PUNCH, PRINT, PRINTA, TRED2, TQL2, DSINV, DMFSD, AND PLOT.                  LSQ 0014
C                                                                                LSQ 0015
C                                                                                LSQ 0016
C     INPUT                                                                      LSQ 0017
C                                                                                LSQ 0018
C     FIRST CARD IS A 70 SPACE HOLLERITH STATEMENT STARTING IN LINE 11           LSQ 0019
C     THIS CARD MUST BE INCLUDED                                                 LSQ 0020
C                                                                                LSQ 0021
C     ITEST AND IPLOT IN 2I5 FORMAT. IF ITEST=0 PROGRAM STOPS, ITEST=1           LSQ 0022
C     AND ITEST=2 ARE FOR ODD AND EVEN MULTIPLICITIES RESPECTIVELY.              LSQ 0023
C    IF IPLOT=1 OBS-CALC ARE PLOTTED OTHERWISE NOT                               LSQ 0024
C  YMIN AND YMAX (2F5.2) ARE THE MIN AND MAX POINTS ON ORDINATE OF GRAPH OF      LSQ 0025
C   OBSERVED-CALCULATED VERSUS J                                                 LSQ 0026
C                                                                                LSQ 0027
C     NUM(1,N),NUM(2,N),...NUM(6,N),Y(N),DEV(N),WAVE(N)   (6I5,2F10.5,I5)        LSQ 0028
C     THESE GIVE THE IDENTIFICATION AND VALUE OF THE EXPTL POINT                 LSQ 0029
C     NUM = THE QUANTUM NUMBERS OF A TRANSITION FROM NUM(1 THRU 3,N) TO          LSQ 0030
C     NUM(4 THRU 6,N).  NUM 1 AND 4 ARE J, NUM 2 AND 5 ARE THE RANK             LSQ 0031
C     THE RANK IS A NUMBER FROM 1 TO 9 WHICH DESCRIBES THE LOCATION OF           LSQ 0032
C     THIS LEVEL WITH RESPECT TO OTHERS WITH SAME J AND PARITY.                  LSQ 0033
C     RANK=1 CORRESPONDS TO HIGHEST ENERGY.                                      LSQ 0034
C     PARITY IS INDICATED BY NUM 3 AND 6 WHERE 1 IS E AND 2 IS F                 LSQ 0035
C     Y IS THE LINE FREQUENCY OR TERM ENERGY.                                    LSQ 0036
```

```
C      DEV IS ITS STANDARD DEVIATION.  THE UNITS ON THE LAST TWO NUMBERS          LSQ 0037
C      ARE SPECIFIED BY WAVE, WAVE = 0 IS MC, WAVE = 1 IS WAVENUMBERS.           LSQ 0038
C      THE LAST DATUM SHOULD BE FOLLOWED BY A BLANK CARD.                        LSQ 0039
C                                                                                LSQ 0040
C*****************************************************************************  LSQ 0041
C*****************************************************************************  LSQ 0042
C NUM1 AND NUM4 SHOULD BE J+0.5 (INTEGER) FOR EVEN MULTIPLICITY PROBLEMS.        LSQ 0043
C                                                                                LSQ 0044
C*****************************************************************************  LSQ 0045
C*****************************************************************************  LSQ 0046
C                                                                                LSQ 0047
C      IAMAX (I5) IS THE NUMBER OF PARAMETERS FITTED                             LSQ 0048
C      MAXIMUM IS 30.                                                            LSQ 0049
C                                                                                LSQ 0050
C      (NCVAR(I),I=1,IAMAX)  (15I5) GIVES THE PARAMETERS FITTED BY               LSQ 0051
C      SPECIFYING THEIR NUMBERS ON THE STANDARD CONSTANT LIST ENCLOSED           LSQ 0052
C      IF MORE THAN 15 PARAMETERS ARE VARIED, PUT UP TO 15 PARAMETER             LSQ 0053
C      NUMBERS ON ONE CARD AND THE REMAINDER ON THE NEXT.                        LSQ 0054
C                                                                                LSQ 0055
C      JMAX1 IS MAXIMUM J OF DESIRED TERM ENERGIES (USE J+0.5 FOR EVEN MULT.)    LSQ 0056
C      M101 IS THE DIMENSION OF                                                  LSQ 0057
C      THE HAMILTONIAN, MAXP1 IS MAX  E DIM OF INPUT, MAXM1 IS MAX               LSQ 0058
C      F DIMENSION OF INPUT. 4I5                                                 LSQ 0059
C       CURRENTLY JMAX1 IS LIMITED TO 150                                        LSQ 0060
C                                                                                LSQ 0061
C                                                                                LSQ 0062
C      I(PS(I),FLAG(I)  (I5,D15.8,I5)  GIVE THE INITIAL PARAMETERS,             LSQ 0063
C         ONE PER CARD.  I IS THE CODE NUMBER OF THE PARAMETER (SEE NAMEIT       LSQ 0064
C         LISTING), FLAG=0 IF ITS UNITS ARE MC, =1 IF THEY ARE CM-1.             LSQ 0065
C      ONLY NON-ZERO CONSTANTS NEED BE SPECIFIED, THE OTHERS ARE TAKEN AS        LSQ 0066
C      ZERO.                                                                     LSQ 0067
C                                                                                LSQ 0068
C      THE LAST PARAMETER MUST BE FOLLOWED BY A BLANK CARD                       LSQ 0069
C                                                                                LSQ 0070
C                                                                                LSQ 0071
C      NENUF,FITS  (I5,F10.5)  GIVE THE CONVERGENCE IN THE FIT.  THE LSQ         LSQ 0072
```

```
C     PROGRAM STOPS AFTER NENUF PASSES OR IF THE CHANGE IN THE VARIANCE          LSQ 0073
C     FROM THE PREVIOUS PASS IS LESS THAN FITS                                   LSQ 0074
C                                                                                LSQ 0075
C                                                                                LSQ 0076
C      NPRINT, NPUNCH, LPUNCH ARE INPUT IN 3I5 FORMAT                            LSQ 0077
C      NPUNCH=0 NOTHING IS PUNCHED                                               LSQ 0078
C      NPUNCH=1 AND LPUNCH=0 ONLY NEW PARAMETERS ARE PUNCHED NOT                 LSQ 0079
C      COVARIANCE MATRIX UNLESS CONVERGENCE IS ACHIEVED                          LSQ 0080
C      NPUNCH=1 AND LPUNCH=1 BOTH PARAMETERS AND COV MATRIX                      LSQ 0081
C         ARE PUNCHED NO MATTER WHAT                                             LSQ 0082
C                                                                                LSQ 0083
C                                                                                LSQ 0084
C      DEL, LAMBDA, NU, TAU, EPS, AND TRACE ARE INPUT                            LSQ 0085
C         FORMAT(5E10.3,I5)                                                      LSQ 0086
C        SUGGESTED VALUES:                                                       LSQ 0087
C        DEL=0.001  INCREMENT FOR DERIVATIVES                                    LSQ 0088
C         LAMBDA=0.1          NU*VALUE OF LAMBDA YOU WANT                       LSQ 0089
C         NU=10.0           RESULTS IN INITIAL LAMBDA OF .01                    LSQ 0090
C         TAU=5.4E-79           EFFECTIVELY ZERO                                LSQ 0091
C         EPS=1.0E-06            DEFINES CONVERGENCE (SEE MARQUARDT PAPER)     LSQ 0092
C         TRACE=0 OR 1       1 WILL PRINT OUT COSINE, LAMBDA, VARB, AND STEP   LSQ 0093
C                0  THE ABOVE ARE NOT PRINTED                                    LSQ 0094
C                                                                                LSQ 0095
C                                                                                LSQ 0096
C                                                                                LSQ 0097
C     REFCOS IS INPUT IN E10.3 FORMAT.                                           LSQ 0098
C          MARQUARDT SUGGESTS REFCOS=0.707;  IPC SUGGESTS REFCOS=.866            LSQ 0099
C                                                                                LSQ 0100
C                                                                                LSQ 0101
C                                                                                LSQ 0102
C                                                                                LSQ 0103
C                                                                                LSQ 0104
      INTEGER FLAG, FLAGA, WAVE, CFLAG                                           LSQ 0105
      REAL*8  NAMES(75)                                                          LSQ 0106
      DOUBLE PRECISION CINV, SCR1, VAREX, VRLD, P, GE, A, Y, CSQT                LSQ 0107
      DOUBLE PRECISION  UNITS, PS, UN, TERM, PSA, COR(30,30)                     LSQ 0108
```

```
      DIMENSION DNUM(2,600)                                                    LSQ 0109
      DIMENSION NUM(6,600),Y(600),DEV(600),WAVE(600),NCVAR(30),FLAG(75),       LSQ 0110
     1UNITS(75),PS(75),PSA(76),FLAGA(76),          DIM(2),A(30),P(75),GE      LSQ 0111
     2(600,3)        ,DELA(30),CHGE(30)    ,AERR(30),CINV(30,30),UNCRT(30     LSQ 0112
     3),SCR1(30,30),UGH(600)                        ,PART(2)                  LSQ 0113
      DIMENSION TERM(150,9,2),FZERO(600)                                       LSQ 0114
      DIMENSION TP(9,2,150),TS(9,2,150)                                        LSQ 0115
      DIMENSION YY(600),CSQT(30)                                               LSQ 0116
      DIMENSION YNUM(600)                                                      LSQ 0117
      COMMON P,GE,NUM                                                          LSQ 0118
      COMMON/BLK1/ CINV,SCR1,VAREX,CSQT,A,Y,DELA,DEV      ,FZERO,AERR,         LSQ 0119
     1UNCRT,CHGE,NCVAR ,IXMAX,IAMAX,NDATA,CFLAG                               LSQ 0120
      COMMON/BLK2/ TERM,JMAX1,M101,MAXP1,MAXM1                                 LSQ 0121
      COMMON/BLK3/TP,TS                                                        LSQ 0122
      EQUIVALENCE (PSA(2),PS(1)),(FLAGA(2),FLAG(1))                            LSQ 0123
      DATA       DIM(1)/2HMC/,DIM(2)/2HCM/,PART(1)/1HE/,PART(2)/1HF/           LSQ 0124
      CALL NAMEIT(NAMES,75)                                                    LSQ 0125
C     READ INPUT                                                               LSQ 0126
4     READ (5,5)                                                               LSQ 0127
    5 FORMAT (10X,70H                                                          LSQ 0128
     1                    )                                                   LSQ 0129
      CFLAG=0                                                                  LSQ 0130
      READ (5,10) ITEST,IPLOT                                                  LSQ 0131
   10 FORMAT (2I5)                                                             LSQ 0132
      IF (ITEST.EQ.0) GO TO 999                                                LSQ 0133
      READ 11,YMIN,YMAX                                                        LSQ 0134
   11 FORMAT(2F5.2)                                                            LSQ 0135
      N=1                                                                      LSQ 0136
   12 CONTINUE                                                                 LSQ 0137
      READ (5,20) ((NUM(L,N),L=1,6),Y(N),DEV(N),WAVE(N))                       LSQ 0138
      IF (NUM(2,N).EQ.0) GO TO 13                                              LSQ 0139
      N=N+1                                                                    LSQ 0140
      GO TO 12                                                                 LSQ 0141
   13 NDATA=N-1                                                                LSQ 0142
   20 FORMAT (6I5,2F10.3,I5)                                                   LSQ 0143
C     ADJUST EXPTL VALUES TO MC                                                LSQ 0144
```

```
      DO 25 N=1,NDATA                                                    LSQ 0145
      IF(WAVE(N).EQ.0) GO TO 25                                          LSQ 0146
      Y(N)=Y(N)*29979.25D0                                               LSQ 0147
      DEV(N)=DEV(N)*29979.25                                             LSQ 0148
   25 CONTINUE                                                           LSQ 0149
      READ (5,30) IAMAX                                                  LSQ 0150
   30 FORMAT (I5)                                                        LSQ 0151
      READ (5,32) (NCVAR(I),I=1,IAMAX)                                  LSQ 0152
   32 FORMAT (15I5)                                                      LSQ 0153
      READ (5,35)  JMAX1,M101,MAXP1,MAXM1                               LSQ 0154
35    FORMAT (4I5)                                                       LSQ 0155
C     READ PARAMETERS SO THAT NUMBER NEED NOT BE SPECIFIED               LSQ 0156
      DO 40 I=1,75                                                       LSQ 0157
      FLAG(I)=0                                                          LSQ 0158
C     FILL UNITS ARRAY FOR PARAMETERS                                    LSQ 0159
      UNITS(I)=1.0D0                                                     LSQ 0160
   40 PS(I)=0.0D0                                                        LSQ 0161
   45 READ(5,50) I,PSA(I+1),FLAGA(I+1)                                   LSQ 0162
   50 FORMAT (I5,D15.8,I5)                                               LSQ 0163
      IF (I.EQ.0) GO TO 51                                               LSQ 0164
      IF (FLAG(I).EQ.1) UNITS(I)=29979.25D0                              LSQ 0165
      GO TO 45                                                           LSQ 0166
   51 CONTINUE                                                           LSQ 0167
      READ (5,70) NENUF,FITS                                             LSQ 0168
   70 FORMAT (I5,F10.5)                                                  LSQ 0169
      READ (5,75) NPRINT, NPUNCH , LPUNCH                                LSQ 0170
   75 FORMAT (3I5)                                                       LSQ 0171
      IXMAX=0                                                            LSQ 0172
C     INITIAL HEADING                                                    LSQ 0173
      WRITE (6,4545)                                                     LSQ 0174
4545   FORMAT (1H1)                                                      LSQ 0175
      WRITE (6,5)                                                        LSQ 0176
      WRITE (6,85)                                                       LSQ 0177
   85 FORMAT (///20X,18HINITIAL PARAMETERS//)                            LSQ 0178
      DO 100 I=1,75                                                      LSQ 0179
      K=FLAG(I)+1                                                        LSQ 0180
```

```
      WRITE (6,95) NAMES(I),PS(I),DIM(K)                                LSQ 0181
   95 FORMAT (10X,A8,5X,D15.8,2X,A6)                                    LSQ 0182
  100 CONTINUE                                                          LSQ 0183
C     SET FINAL OUTPUT AND LSQ PASS INDICATORS                          LSQ 0184
      NTRY=0                                                            LSQ 0185
      WRITE (6,110)                                                     LSQ 0186
  110 FORMAT (1H1///20X,11HTHE LSQ FIT//)                               LSQ 0187
C     SET INITIAL PARAMETERS IN LSQ                                     LSQ 0188
      DO 120 I=1,IAMAX                                                  LSQ 0189
      NBR=NCVAR(I)                                                      LSQ 0190
  120 A(I)=PS(NBR)*UNITS(NBR)                                           LSQ 0191
  170 DO 172 I=1,75                                                     LSQ 0192
172   P(I)=PS(I)*UNITS(I)                                               LSQ 0193
      CALL LEVEL(1,NDATA)                                               LSQ 0194
C     INPUT TRANSITIONS TO LSQ                                          LSQ 0195
C     SET UP DIFFERENCES                                                LSQ 0196
  210 DO 215 N=1,NDATA                                                  LSQ 0197
215   FZERO(N)=GE(N,1)-Y(N)                                             LSQ 0198
      CALL NEWFIT (1,NPRINT)                                            LSQ 0199
      VRLD=VAREX                                                        LSQ 0200
      GO TO 8165                                                        LSQ 0201
C     OUTPUT AFTER EACH LSQ PASS                                        LSQ 0202
  130 NTRY=NTRY+1                                                       LSQ 0203
      WRITE (6,140) NTRY                                                LSQ 0204
  140 FORMAT (///10X,15HAFTER LSQ PASS ,I5,22H THE FITTED VALUES ARE//) LSQ 0205
C     RESET PARAMETERS TO NEW VALUES                                    LSQ 0206
      DO 160 I=1,IAMAX                                                  LSQ 0207
      NBR=NCVAR(I)                                                      LSQ 0208
      PS(NBR)=A(I)/UNITS(NBR)                                           LSQ 0209
      K=FLAG(NBR)+1                                                     LSQ 0210
C     PRINT NEW VALUES OF PARAMETERS                                    LSQ 0211
      WRITE (6,155) I,NAMES(NBR),PS(NBR),DIM(K)                         LSQ 0212
155   FORMAT (11X,I4,5X,A8,2X,D15.8,3X,  11X ,4X,A4)                    LSQ 0213
  160 CONTINUE                                                          LSQ 0214
C     SET DP PARAMETERS FOR ENERGY CALCULATION                          LSQ 0215
 8165 WRITE (6,165) VAREX                                               LSQ 0216
```

```
  165 FORMAT (/10X,19HVARIANCE OF THE FIT,D15.7////)                    LSQ 0217
C     TEST FOR COMPLETION OF FIT                                       LSQ 0218
      IF (NTRY.GE.NENUF) GO TO 275                                     LSQ 0219
      IXMAX=0                                                          LSQ 0220
C     CALL LSQ ROUTINE                                                 LSQ 0221
      CALL NEWFIT(2,NPRINT)                                            LSQ 0222
      IF (CFLAG.EQ.1) GO TO 275                                        LSQ 0223
      IF(DABS(VAREX-VRLD).LT.DBLE(FITS)) GO TO 276                     LSQ 0224
      VRLD=VAREX                                                       LSQ 0225
C     LOOP ON LSQ                                                      LSQ 0226
      GO TO 130                                                        LSQ 0227
C     FINAL DIAGNOSTIC LSQ PASS                                        LSQ 0228
  276 WRITE(6,279)                                                     LSQ 0229
  279 FORMAT(/,' CONVERGENCE/VARIANCE',/)                              LSQ 0230
      CFLAG=1                                                          LSQ 0231
  275 IF (NENUF.EQ.0) GO TO 3912                                       LSQ 0232
      CALL NEWFIT(3,NPRINT)                                            LSQ 0233
C     FINAL OUTPUT FROM LSQ ROUTINE                                    LSQ 0234
      WRITE (6,300)                                                    LSQ 0235
  300 FORMAT (1H1,///,20X,25HOUTPUT FROM LAST LSQ PASS)                LSQ 0236
      WRITE (6,305)                                                    LSQ 0237
  305 FORMAT (///,34X,5HFINAL,12X,8HSTANDARD)                          LSQ 0238
      WRITE (6,306)                                                    LSQ 0239
  306 FORMAT (10X,6HNUMBER,4X,4HNAME,10X,5HVALUE,12X,9HDEVIATION,/)    LSQ 0240
      DO 308 I=1,75                                                    LSQ 0241
      K=FLAG(I)+1                                                      LSQ 0242
      DO 311 IB=1,IAMAX                                                LSQ 0243
      NBR=NCVAR(IB)                                                    LSQ 0244
  310 IF (NBR.EQ.I) GO TO 320                                          LSQ 0245
  311 CONTINUE                                                         LSQ 0246
  315 WRITE (6,3151) NAMES(I),PS(I),DIM(K)                             LSQ 0247
 3151 FORMAT (20X,A8,2X,D15.8,21X,A4)                                  LSQ 0248
      GO TO 308                                                        LSQ 0249
  320 AERR(IB)=AERR(IB)/SNGL(UNITS(I))                                 LSQ 0250
      WRITE (6,3201) IB,NAMES(I),PS(I),AERR(IB),DIM(K)                 LSQ 0251
 3201 FORMAT (11X,I4,5X,A8,2X,D15.8,5X,D11.4,4X,A4)                    LSQ 0252
```

```
  308 CONTINUE                                                          LSQ 0253
      WRITE (6,340)                                                     LSQ 0254
  340 FORMAT (///,20X,17HCOVARIANCE MATRIX,/,10X,42HELEMENTS ARE ARRANGE LSQ 0255
     1D BY PARAMETER NUMBERS,/)                                         LSQ 0256
      CALL PRINT(CINV,30,IAMAX,IAMAX)                                   LSQ 0257
      IF(NPUNCH.EQ.1) CALL PUNCH(IAMAX,NCVAR,PS,FLAG,CINV,CFLAG,LPUNCH) LSQ 0258
C  COMPUTE AND PRINT CORRELATION MATRIX                                 LSQ 0259
      L=IAMAX-1                                                         LSQ 0260
      DO 3000 I=1,L                                                     LSQ 0261
      K=I+1                                                             LSQ 0262
      DO 3000 J=K,IAMAX                                                 LSQ 0263
      COR(I,J)=CINV(I,J)/DSQRT(CINV(I,I)*CINV(J,J))                     LSQ 0264
 3000 COR(J,I)=COR(I,J)                                                 LSQ 0265
      DO 3010 I=1,IAMAX                                                 LSQ 0266
 3010 COR(I,I)=1.0D0                                                    LSQ 0267
      WRITE(6,3009)                                                     LSQ 0268
 3009 FORMAT(///,20X,'CORRELATION MATRIX',/,10X,'ELEMENTS ARE ARRANGED B LSQ 0269
     1Y PARAMETER NUMBERS',/)                                           LSQ 0270
      CALL PRINT(COR,30,IAMAX,IAMAX)                                    LSQ 0271
C     PRINT OUT STD DEVS OF LINEARLY INDEPENDENT PARAMETER COMBINATIONS. LSQ 0272
      WRITE (6,380)                                                     LSQ 0273
  380 FORMAT(//,20X,'EIGENVALUES OF SCALED CURVATURE MATRIX',/10X,      LSQ 0274
     1'PARAMETER          EIGENVALUE',13X,'SQRT',21X,'SCALE FACTOR',//) LSQ 0275
      DO 390 I=1,IAMAX                                                  LSQ 0276
      SD=SQRT(UNCRT(I))                                                 LSQ 0277
      WRITE (6,3905)  I,UNCRT(I),SD,CSQT(I)                            LSQ 0278
3905  FORMAT (15X,I2,8X,E15.7,5X,E15.7,15X,D15.7)                       LSQ 0279
390   CONTINUE                                                          LSQ 0280
      WRITE (6,385)                                                     LSQ 0281
  385 FORMAT(///10X,'EIGENVECTORS OF SCALED CURVATURE MATRIX',/,10X,'COL LSQ 0282
     1UMNS ARE IND COMBINATIONS IN THE ORDER OF EIGENVALUES ABOVE',/)   LSQ 0283
      DO 391 I=1,IAMAX                                                  LSQ 0284
      NBR=NCVAR(I)                                                      LSQ 0285
  391 WRITE (6,3911) NAMES(NBR), (SCR1(I,J),J=1,IAMAX)                  LSQ 0286
 3911 FORMAT (1X,A8,15(1X,F7.4))                                        LSQ 0287
 3912 CONTINUE                                                          LSQ 0288
```

```
      WRITE (6,395) NTRY                                                LSQ 0289
  395 FORMAT (///,10X,22HNUMBER OF LSQ PASSES =,I5)                     LSQ 0290
  400 WRITE (6,410)                                                     LSQ 0291
  410 FORMAT (////20X,26HFIT TO EXPERIMENTAL POINTS,//20X,33HTRANSITION LSQ 0292
     1BETWEEN LEVELS 1 AND 2,//)                                        LSQ 0293
      WRITE (6,420)                                                     LSQ 0294
  420 FORMAT (11X,2HJ1,5X,6HSTATE1,4X,7HPARITY1,5X,2HJ2,4X,6HSTATE2,4X,7H LSQ 0295
     1PARITY2,9X,4HEXPT,8X,4HCALC,5X,9HEXPT-CALC,2X,13HEXPTL STD DEV,3X, LSQ 0296
     25HUNITS,//)                                                       LSQ 0297
      DO 430 N=1,NDATA                                                  LSQ 0298
C     ADJUST OUTPUT TO INPUT UNITS                                      LSQ 0299
      UN=1.0D0                                                          LSQ 0300
      IF (WAVE(N).EQ.1) UN=29979.25D0                                   LSQ 0301
      GE(N,1)=GE(N,1)/UN                                                LSQ 0302
      Y(N)=Y(N)/UN                                                      LSQ 0303
      UGH(N)=SNGL(Y(N)-GE(N,1))                                         LSQ 0304
      DEV(N)=DEV(N)/SNGL(UN)                                            LSQ 0305
      K=WAVE(N)+1                                                       LSQ 0306
      L=NUM(3,N)                                                        LSQ 0307
      M=NUM(6,N)                                                        LSQ 0308
      GO TO (421,422),ITEST                                             LSQ 0309
  421 DNUM(1,N)=FLOAT(NUM(1,N))                                         LSQ 0310
      DNUM(2,N)=FLOAT(NUM(4,N))                                         LSQ 0311
      GO TO 423                                                         LSQ 0312
  422 DNUM(1,N)=FLOAT(NUM(1,N))-0.5                                     LSQ 0313
      DNUM(2,N)=FLOAT(NUM(4,N))-0.5                                     LSQ 0314
  423 IF (M.EQ.0) GO TO 426                                             LSQ 0315
      WRITE (6,425) DNUM(1,N),NUM(2,N),PART(L),DNUM(2,N),NUM(5,N),PART(M LSQ 0316
     1),Y(N),GE(N,1),UGH(N),DEV(N),DIM(K)                               LSQ 0317
  425 FORMAT(4X,2(5X,F5.1,5X,I3,8X,A1),2X,4(1X,F12.5),4X,A6)            LSQ 0318
      GO TO 430                                                         LSQ 0319
  426 WRITE(6,427) DNUM(1,N),NUM(2,N),PART(L),Y(N),GE(N,1),UGH(N),DEV(N) LSQ 0320
     1,DIM(K)                                                           LSQ 0321
  427 FORMAT(4X,5X,F5.1,5X,I3,8X,A1,29X,4(1X,F12.5),4X,A6)              LSQ 0322
  430 CONTINUE                                                          LSQ 0323
      IF(IPLOT.NE.1) GO TO 433                                          LSQ 0324
```

```
      PRINT431                                                          LSQ 0325
  431 FORMAT (' 1',2X,' OBSERVED-CALCULATED',2X,//)                     LSQ 0326
      DO 432 N=1,NDATA                                                  LSQ 0327
      YNUM(N)=DNUM(1,N)                                                 LSQ 0328
  432 YY(N)=UGH(N)                                                      LSQ 0329
      CALL PLOT (YY,NDATA,YMIN,YMAX,6,1,YNUM)                           LSQ 0330
  433 CONTINUE                                                          LSQ 0331
C     PRINT OUT TERM ENERGIES IN CM-1.                                  LSQ 0332
      DO 4430 I=1,JMAX1                                                 LSQ 0333
      DO 4435 II=1,MAXP1                                                LSQ 0334
 4435 TERM(I,II,1)=TERM(I,II,1)/29979.25D0                              LSQ 0335
      DO 4436 II=1,MAXM1                                                LSQ 0336
 4436 TERM(I,II,2)=TERM(I,II,2)/29979.25D0                              LSQ 0337
 4430 CONTINUE                                                          LSQ 0338
      WRITE(6,4442)                                                     LSQ 0339
 4442 FORMAT (1H1)                                                      LSQ 0340
      WRITE(6,4445)                                                     LSQ 0341
 4445 FORMAT(9X,25HTERM ENERGIES PLUS PARITY,//)                        LSQ 0342
      DO 4444 I=1,JMAX1                                                 LSQ 0343
      GO TO (4447,4448),ITEST                                           LSQ 0344
 4447 XI=FLOAT(I)-1.0                                                   LSQ 0345
      GO TO 4449                                                        LSQ 0346
 4448 XI=FLOAT(I)-0.5                                                   LSQ 0347
 4449 WRITE(6,4446) XI,(TERM(I,J,1),J=1,MAXP1)                          LSQ 0348
 4446 FORMAT (1X,F5.1,9(2X,F12.5))                                      LSQ 0349
      WRITE (6,5446) (TP(J,1,I),TS(J,1,I),J=1,MAXP1)                    LSQ 0350
 5446 FORMAT(7X,9(1X,2HPI,F4.3,3HSIG,F4.3))                             LSQ 0351
 4444 CONTINUE                                                          LSQ 0352
      WRITE(6,4450)                                                     LSQ 0353
 4450 FORMAT (//,9X,26HTERM ENERGIES MINUS PARITY,//)                   LSQ 0354
      DO 4452 I=1,JMAX1                                                 LSQ 0355
      GO TO (4453,4454),ITEST                                           LSQ 0356
 4453 XI=FLOAT(I)-1.0                                                   LSQ 0357
      GO TO 4455                                                        LSQ 0358
 4454 XI=FLOAT(I)-0.5                                                   LSQ 0359
 4455 WRITE(6,4446) XI,(TERM(I,J,2),J=1,MAXM1)                          LSQ 0360
```

```
      WPITE (6,5446)  (TP(J,2,I),TS(J,2,I),J=1,MAXM1)                    LSQ 0361
 4452 CONTINUE                                                           LSQ 0362
      GO TO 4                                                            LSQ 0363
  999 STOP                                                               LSQ 0364
      END                                                                LSQ 0365
```

```
      SUBROUTINE NEWFIT(NHELP,NPRINT)                                   NEWF0001
      REAL NU,LAMBDA                                                    NEWF0002
      INTEGER CFLAG                                                     NEWF0003
      INTEGER TRACE, EFLAG                                              NEWF0004
      DOUBLE PRECISION D(30),    L,TP,CNORM,ERNORM,CINV,DDELA,SREM,DDENM NEWF0005
     1,VAREX,SCR1,SCR3,CSQT,Y,A,QNORM,SUM1,SUM2,PSAVE,VARB              NEWF0006
      DOUBLE PRECISION P,GE,DP,SCR2                                     NEWF0007
      DOUBLE PRECISION DBLE,DSQRT,DABS                                  NEWF0008
      DIMENSION A(30),DEV(600),NCVAR(30),SCR2(600),                     NEWF0009
     1   Y(600),FZERO(600),L(600),CNORM(30,30),ERNORM(30),CINV(30,30),DE NEWF0010
     2LA(30),AERR(30),UNCRT(30),DDELA(30),SCR1(30,30)              ,SCR3(4 NEWF0011
     365)   ,CSQT(30)                                                  NEWF0012
      DIMENSION P(75),GE(600,3),NUM(6,600),CHGE(30)                     NEWF0013
      COMMON P,GE,NUM                                                   NEWF0014
      COMMON/BLK1/ CINV,SCR1,VAREX,CSQT,A,Y,DELA,DEV      ,FZERO,AERR,  NEWF0015
     1UNCRT,CHGE,NCVAR ,IXMAX,IAMAX,NDATA,CFLAG                         NEWF0016
      GO TO (205,236,8000),NHELP                                        NEWF0017
  205 EFLAG=0                                                           NEWF0018
      DO 220 N=1,NDATA                                                  NEWF0019
      L(N)=DBLE(DEV(N))**2                                              NEWF0020
  220 CONTINUE                                                          NEWF0021
       READ(5,8010) DEL, LAMBDA, NU, TAU, EPS, TRACE                    NEWF0022
 8010 FORMAT(5E10.3,I5)                                                 NEWF0023
      READ (5,8050) REFCOS                                              NEWF0024
 8050 FORMAT(1E10.3)                                                    NEWF0025
      SREM=0.0D+00                                                      NEWF0026
      DO 235 N=1,NDATA                                                  NEWF0027
  235 SREM=SREM+(DBLE(FZERO(N))**2)/L(N)                                NEWF0028
      DENM=NDATA-IAMAX                                                  NEWF0029
      DDENM=DBLE(DENM)                                                  NEWF0030
      VAREX=SREM/DDENM                                                  NEWF0031
      IF (NHELP.EQ.1) GO TO 500                                         NEWF0032
  236 CONTINUE                                                          NEWF0033
      LAMBDA=LAMBDA/NU                                                  NEWF0034
 8500 DO 245 I=1,IAMAX                                                  NEWF0035
      ERNORM(I)=0.0D+00                                                 NEWF0036
```

```
      DO 245 J=1,IAMAX                                                  NEWF0037
  245 CNORM(I,J)=0.0D+00                                                NEWF0038
      REWIND 2                                                          NEWF0039
      DO 260 I=1,IAMAX                                                  NEWF0040
      NBR=NCVAR(I)                                                      NEWF0041
      PSAVE=P(NBR)                                                      NEWF0042
       DP=DABS(PSAVE*DBLE(DEL))                                         NEWF0043
      P(NBR)=PSAVE+DP                                                   NEWF0044
      IF(PSAVE.EQ.0.0D0)  P(NBR)=DEL                                    NEWF0045
      IF(PSAVE.EQ.0.0D0)  DP=DEL                                        NEWF0046
      CALL LEVEL(3,NDATA)                                               NEWF0047
      P(NBR)=PSAVE                                                      NEWF0048
      DO 258 N=1,NDATA                                                  NEWF0049
      GE(N,2)=(GE(N,3)-GE(N,1))/DP                                      NEWF0050
  258 ERNORM(I)=ERNORM(I)+DBLE(FZERO(N))*GE(N,2)/L(N)                   NEWF0051
  260 WRITE(2)  (GE(N,2),N=1,NDATA)                                     NEWF0052
      REWIND 2                                                          NEWF0053
      DO 262 I=1,IAMAX                                                  NEWF0054
      READ(2)  (GE(N,2),N=1,NDATA)                                      NEWF0055
      DO 263 N=1,NDATA                                                  NEWF0056
  263 CNORM(I,I)=CNORM(I,I)+GE(N,2)*GE(N,2)/L(N)                        NEWF0057
      IF (I.EQ.IAMAX)  GO TO 262                                        NEWF0058
      JJ=I+1                                                            NEWF0059
      DO 261 J=JJ,IAMAX                                                 NEWF0060
      READ (2)  (SCR2(N),N=1,NDATA)                                     NEWF0061
      DO 261 N=1,NDATA                                                  NEWF0062
  261 CNORM(I,J)=CNORM(I,J)+GE(N,2)*SCR2(N)/L(N)                        NEWF0063
      REWIND 2                                                          NEWF0064
      DO 2622 K=1,I                                                     NEWF0065
 2622 READ  (2)  (GE(N,2),N=1,NDATA)                                    NEWF0066
  262 CONTINUE                                                          NEWF0067
      DO 264 I=1,IAMAX                                                  NEWF0068
      DO 264 J=I,IAMAX                                                  NEWF0069
  264 CNORM(J,I)=CNORM(I,J)                                             NEWF0070
      IF (NPRINT.EQ.0)  GO TO 256                                       NEWF0071
      WRITE (6,250)                                                     NEWF0072
```

```
250 FORMAT (///,20X,16HNORMAL EQ MATRIX,//)                          NEWF0073
    CALL PRINT(CNORM,30,IAMAX,IAMAX)                                NEWF0074
256 CONTINUE                                                        NEWF0075
    IF (NPRINT.EQ.0) GO TO 2691                                     NEWF0076
    WRITE (6,265)                                                   NEWF0077
265 FORMAT (///,10X,24HN, EXPT POINT, CALC-EXPT,//)                 NEWF0078
    DO 267 N=1,NDATA                                                NEWF0079
    WRITE (6,266) N,Y(N),FZERO(N)                                   NEWF0080
266 FORMAT (10X,I5,2F15.7)                                          NEWF0081
267 CONTINUE                                                        NEWF0082
    WRITE (6,268)                                                   NEWF0083
268 FORMAT (///,20X,9HERNORM(I),//)                                 NEWF0084
    CALL PRINTA(ERNORM,30,IAMAX)                                    NEWF0085
2691 CONTINUE                                                       NEWF0086
    QNORM=0.0D0                                                     NEWF0087
    DO 2681 I=1,IAMAX                                               NEWF0088
    CSQT(I)=DSQRT(CNORM(I,I))                                       NEWF0089
2681 QNORM=QNORM+(ERNORM(I)/CSQT(I))**2                             NEWF0090
    REWIND 2                                                        NEWF0091
    DO 2692 I=1,IAMAX                                               NEWF0092
    DO 2692 J=1,I                                                   NEWF0093
    II=J+I*(I-1)/2                                                  NEWF0094
    SCR3(II)=CNORM(J,I)/CSQT(I)/CSQT(J)                             NEWF0095
2692 WRITE(2) SCR3(II)                                              NEWF0096
    GO TO 7130                                                      NEWF0097
7778 DO 7779 I=1,IAMAX                                              NEWF0098
    DO 7779 J=1,I                                                   NEWF0099
     II=J+I*(I-1)/2                                                 NEWF0100
7779 READ(2) SCR3(II)                                               NEWF0101
7130 REWIND 2                                                       NEWF0102
    IF (EFLAG.EQ.1) GO TO 2796                                      NEWF0103
7777 DO 2795 I=1,IAMAX                                              NEWF0104
    II=I+I*(I-1)/2                                                  NEWF0105
2795 SCR3(II)=SCR3(II)+DBLE(LAMBDA)                                 NEWF0106
2796 CALL DSINV (SCR3,IAMAX,1.0E-13,IER)                            NEWF0107
    IF (IER.NE.0) WRITE (6,2693) IER                                NEWF0108
```

```
2693 FORMAT(5X,'ERROR PARAMETER IN INVERSION ROUTINE, IER=',I3,/)          NEWF0109
     DO 2694 I=1,IAMAX                                                    NEWF0110
     DO 2694 J=1,I                                                        NEWF0111
     II=J+I*(I-1)/2                                                       NEWF0112
     CINV(J,I)=SCR3(II)/CSQT(I)/CSQT(J)                                   NEWF0113
2694 CINV(I,J)=CINV(J,I)                                                  NEWF0114
     IF (EFLAG.EQ.1) GO TO 8600                                           NEWF0115
     DO 270 I=1,IAMAX                                                     NEWF0116
     DELA(I)=0.0                                                          NEWF0117
     DDELA(I)=0.0D+00                                                     NEWF0118
     DO 270 J=1,IAMAX                                                     NEWF0119
     DDELA(I)=DDELA(I)+CINV(I,J)*ERNORM(J)                                NEWF0120
 270 DELA(I)=SNGL(DDELA(I))                                               NEWF0121
     IF (NPRINT.EQ.0) GO TO 297                                           NEWF0122
     WRITE (6,275)                                                        NEWF0123
 275 FORMAT (///,10X,27HINVERSE OF NORMAL EQ MATRIX,//)                   NEWF0124
     CALL PRINT(CINV,30,IAMAX,IAMAX)                                      NEWF0125
     WRITE (6,291)                                                        NEWF0126
 291 FORMAT (//,10X,25HTEST PRODUCT CINV X CNORM,//)                      NEWF0127
     DO 292 I=1,IAMAX                                                     NEWF0128
     DO 292 J=1,IAMAX                                                     NEWF0129
     SCR1(I,J)=0.0D0                                                      NEWF0130
     DO 292 K=1,IAMAX                                                     NEWF0131
 292 SCR1(I,J)=SCR1(I,J)+CINV(I,K)*CNORM(K,J)                             NEWF0132
     CALL PRINT(SCR1,30,IAMAX,IAMAX)                                      NEWF0133
     WRITE (6,295)                                                        NEWF0134
 295 FORMAT (///,20X,7HDELA(I),//)                                        NEWF0135
     CALL PRINTA(DDELA,15,IAMAX)                                          NEWF0136
 297 SUM1=0.0D0                                                           NEWF0137
     SUM2=0.0D0                                                           NEWF0138
     DO 7000 I=1,IAMAX                                                    NEWF0139
     SUM1=SUM1+DDELA(I)*ERNORM(I)                                         NEWF0140
7000 SUM2=SUM2+(DDELA(I)*CSQT(I))**2                                      NEWF0141
     COSINE=SNGL(SUM1/DSQRT(SUM2*QNORM))                                  NEWF0142
     IF (TRACE.EQ.0) GO TO 7171                                           NEWF0143
     WRITE(6,8200) COSINE,LAMBDA                                          NEWF0144
```

```
8200 FORMAT (5X,'COSINE:',E15.7,'     LAMBDA:',E11.3)                          NEWF0145
7171 STEP=1.0                                                                 NEWF0146
7170 DO 7180 I=1,IAMAX                                                        NEWF0147
     NBR=NCVAR(I)                                                             NEWF0148
     P(NBR)=A(I)                                                              NEWF0149
     IF (ABS(STEP*DELA(I)).GT.TAU+EPS*ABS(SNGL(A(I)))) GO TO 7190             NEWF0150
7180 CONTINUE                                                                 NEWF0151
     CFLAG=1                                                                  NEWF0152
      WRITE(6,7182)                                                           NEWF0153
7182 FORMAT (5X,'CONVERGENCE',///)                                            NEWF0154
     CALL LEVEL (1,NDATA)                                                     NEWF0155
     DO 7185 N=1,NDATA                                                        NEWF0156
7185 FZERO(N)=GE(N,1)-Y(N)                                                    NEWF0157
     RETURN                                                                   NEWF0158
7190 DO 7200 I=1,IAMAX                                                        NEWF0159
     NBR=NCVAR(I)                                                             NEWF0160
7200 P(NBR)=A(I)-DBLE(STEP)*DDELA(I)                                          NEWF0161
     SREM=0.0D0                                                               NEWF0162
     CALL LEVEL(1,NDATA)                                                      NEWF0163
     DO 7220 N=1,NDATA                                                        NEWF0164
     FZERO(N)=GE(N,1)-Y(N)                                                    NEWF0165
7220 SREM=SREM+((GE(N,1)-Y(N))**2)/L(N)                                       NEWF0166
     VARB=SREM/DDENM                                                          NEWF0167
     IF (TRACE.EQ.0) GO TO 7221                                               NEWF0168
     WRITE(6,8300) VARB,STEP                                                  NEWF0169
8300 FORMAT(5X,'VARB:',D 15.7,'     STEP:',E15.7)                            NEWF0170
7221 IF (VARB.LE.VAREX) GO TO 7240                                            NEWF0171
     IF (COSINE.LT.REFCOS) GO TO 7230                                         NEWF0172
     STEP=.5*STEP                                                             NEWF0173
     GO TO 7170                                                               NEWF0174
7230 LAMBDA=LAMBDA*NU                                                         NEWF0175
     GO TO 7778                                                               NEWF0176
7240 VAREX=VARB                                                               NEWF0177
     DO 9000 I=1,IAMAX                                                        NEWF0178
     NBR=NCVAR(I)                                                             NEWF0179
9000 A(I)=P(NBR)                                                              NEWF0180
```

```
      RETURN                                                                NEWF0181
 8000 EFLAG=1                                                               NEWF0182
      REWIND 2                                                              NEWF0183
      NPLUS1=EFLAG+1                                                        NEWF0184
      GO TO (8500,7778), NPLUS1                                             NEWF0185
 8600 DO 410 I=1,IAMAX                                                      NEWF0186
      DO 410 J=1,IAMAX                                                      NEWF0187
  410 CNORM(I,J)=CNORM(I,J)/CSQT(I)/CSQT(J)                                 NEWF0188
      DO 420 J=1,IAMAX                                                      NEWF0189
      DO 420 I=1,IAMAX                                                      NEWF0190
  420 CINV(I,J)=CINV(I,J)*VAREX                                             NEWF0191
      DO 425 I=1,IAMAX                                                      NEWF0192
  425 AERR(I)=SNGL(DSQRT(CINV(I,I)))                                        NEWF0193
C       ERNORM USED AS DUMMY TO CONSERVE CORE FOR TRIDIAGONAL ELEMENTS      NEWF0194
      DO 450 I=1,30                                                         NEWF0195
      DO 451 II=1,30                                                        NEWF0196
  451 SCR1(I,II)=0.0D0                                                      NEWF0197
      ERNORM(I)=0.0D0                                                       NEWF0198
      D(I)=1.0D0                                                            NEWF0199
  450 SCR1(I,I)=1.0D0                                                       NEWF0200
      CALL TRED2(IAMAX,30,CNORM,D,ERNORM,SCR1)                              NEWF0201
      CALL TQL2(IAMAX,30,D,ERNORM,SCR1,IERR3)                               NEWF0202
      DO 460 I=1,IAMAX                                                      NEWF0203
  460 UNCRT(I)=SNGL(D(I))                                                   NEWF0204
      IF (IERR3.NE.0) GO TO 426                                             NEWF0205
      GO TO 427                                                             NEWF0206
  426 WRITE(6,429) IERR3                                                    NEWF0207
  429 FORMAT(' ERROR IN COVARIANCE MATRIX DIAGONALIZATION, IERR=',I2)       NEWF0208
  427 CONTINUE                                                              NEWF0209
  500 CONTINUE                                                              NEWF0210
      RETURN                                                                NEWF0211
      END                                                                   NEWF0212
```

```
C                                                                       DSIN   10 DSIN0001
C     ...................................................................DSIN   20 DSIN0002
C                                                                       DSIN   30 DSIN0003
C        SUBROUTINE DSINV                                               DSIN   40 DSIN0004
C                                                                       DSIN   50 DSIN0005
C        PURPOSE                                                        DSIN   60 DSIN0006
C           INVERT A GIVEN SYMMETRIC POSITIVE DEFINITE MATRIX           DSIN   70 DSIN0007
C                                                                       DSIN   80 DSIN0008
C        USAGE                                                          DSIN   90 DSIN0009
C           CALL DSINV(A,N,EPS,IER)                                     DSIN  100 DSIN0010
C                                                                       DSIN  110 DSIN0011
C        DESCRIPTION OF PARAMETERS                                      DSIN  120 DSIN0012
C           A      - DOUBLE PRECISION UPPER TRIANGULAR PART OF GIVEN    DSIN  130 DSIN0013
C                    SYMMETRIC POSITIVE DEFINITE N BY N COEFFICIENT     DSIN  140 DSIN0014
C                    MATRIX.                                            DSIN  150 DSIN0015
C                    ON RETUEN A CONTAINS THE RESULTANT UPPER           DSIN  160 DSIN0016
C                    TRIANGULAR MATRIX IN DOUBLE PRECISION.             DSIN  170 DSIN0017
C           N      - THE NUMBER OF ROWS (COLUMNS) IN GIVEN MATRIX.      DSIN  180 DSIN0018
C           EPS    - SINGLE PRECISION INPUT CONSTANT WHICH IS USED      DSIN  190 DSIN0019
C                    AS RELATIVE TOLERANCE FOR TEST ON LOSS OF          DSIN  200 DSIN0020
C                    SIGNIFICANCE.                                      DSIN  210 DSIN0021
C           IER    - RESULTING ERROR PARAMETER CODED AS FOLLOWS         DSIN  220 DSIN0022
C                    IER=0  - NO ERROR                                  DSIN  230 DSIN0023
C                    IER=-1 - NO RESULT BECAUSE OF WRONG INPUT PARAME-  DSIN  240 DSIN0024
C                             TER N OR BECAUSE SOME RADICAND IS NON-    DSIN  250 DSIN0025
C                             POSITIVE (MATRIX A IS NOT POSITIVE        DSIN  260 DSIN0026
C                             DEFINITE, POSSIBLY DUE TO LOSS OF SIGNI-  DSIN  270 DSIN0027
C                             FICANCE)                                  DSIN  280 DSIN0028
C                    IER=K  - WARNING WHICH INDICATES LOSS OF SIGNIFI-  DSIN  290 DSIN0029
C                             CANCE. THE RADICAND FORMED AT FACTORIZA-  DSIN  300 DSIN0030
C                             TION STEP K+1 WAS STILL POSITIVE BUT NO   DSIN  310 DSIN0031
C                             LONGER GREATER THAN ABS(EPS*A(K+1,K+1)).  DSIN  320 DSIN0032
C                                                                       DSIN  330 DSIN0033
C        REMARKS                                                        DSIN  340 DSIN0034
C           THE UPPER TRIANGULAR PART OF GIVEN MATRIX IS ASSUMED TO BE  DSIN  350 DSIN0035
C           STORED COLUMNWISE IN N*(N+1)/2 SUCCESSIVE STORAGE LOCATIONS.DSIN  360 DSIN0036
```

```
C           IN THE SAME STORAGE LOCATIONS THE RESULTING UPPER TRIANGU-   DSIN 370 DSIN0037
C           LAR MATRIX IS STORED COLUMNWISE TOO.                        DSIN 380 DSIN0038
C           THE PROCEDURE GIVES RESULTS IF N IS GREATER THAN 0 AND ALL  DSIN 390 DSIN0039
C           CALCULATED RADICANDS ARE POSITIVE.                          DSIN 400 DSIN0040
C                                                                       DSIN 410 DSIN0041
C        SUBROUTINES AND FUNCTION SUBPROGRAMS REQUIRED                  DSIN 420 DSIN0042
C           DMFSD                                                       DSIN 430 DSIN0043
C                                                                       DSIN 440 DSIN0044
C        METHOD                                                         DSIN 450 DSIN0045
C           SOLUTION IS DONE USING FACTORIZATION BY SUBROUTINE DMFSD.   DSIN 460 DSIN0046
C                                                                       DSIN 470 DSIN0047
C     ..................................................................DSIN 480 DSIN0048
C                                                                       DSIN 490 DSIN0049
      SUBROUTINE DSINV (A,N,EPS,IER)                                    DSIN 500 DSIN0050
C                                                                       DSIN 510 DSIN0051
C                                                                       DSIN 520 DSIN0052
      DIMENSION A(1)                                                    DSIN 530 DSIN0053
      DOUBLE PRECISION A,DIN,WORK                                       DSIN 540 DSIN0054
C                                                                       DSIN 550 DSIN0055
C        FACTORIZE GIVEN MATRIX BY MEANS OF SUBROUTINE DMFSD            DSIN 560 DSIN0056
C        A = TRANSPOSE(T) * T                                           DSIN 570 DSIN0057
      CALL DMFSD(A,N,EPS,IER)                                           DSIN 580 DSIN0058
      IF(IER) 9,1,1                                                     DSIN 590 DSIN0059
C                                                                       DSIN 600 DSIN0060
C        INVERT UPPER TRIANGULAR MATRIX T                               DSIN 610 DSIN0061
C        PREPARE INVERSION-LOOP                                         DSIN 620 DSIN0062
    1 IPIV=N*(N+1)/2                                                    DSIN 630 DSIN0063
      IND=IPIV                                                          DSIN 640 DSIN0064
C                                                                       DSIN 650 DSIN0065
C        INITIALIZE INVERSION-LOOP                                      DSIN 660 DSIN0066
      DO 6 I=1,N                                                        DSIN 670 DSIN0067
      DIN=1.D0/A(IPIV)                                                  DSIN 680 DSIN0068
      A(IPIV)=DIN                                                       DSIN 690 DSIN0069
      MIN=N                                                             DSIN 700 DSIN0070
      KEND=I-1                                                          DSIN 710 DSIN0071
      LANF=N-KEND                                                       DSIN 720 DSIN0072
```

```
      IF (KEND) 5,5,2                                                    DSIN 730 DSIN0073
    2 J=IND                                                              DSIN 740 DSIN0074
C                                                                        DSIN 750 DSIN0075
C        INITIALIZE ROW-LOOP                                             DSIN 760 DSIN0076
      DO 4 K=1,KEND                                                      DSIN 770 DSIN0077
      WORK=0.D0                                                          DSIN 780 DSIN0078
      MIN=MIN-1                                                          DSIN 790 DSIN0079
      LHOR=IPIV                                                          DSIN 800 DSIN0080
      LVER=J                                                             DSIN 810 DSIN0081
C                                                                        DSIN 820 DSIN0082
C        START INNER LOOP                                                DSIN 830 DSIN0083
      DO 3 L=LANF,MIN                                                    DSIN 840 DSIN0084
      LVER=LVER+1                                                        DSIN 850 DSIN0085
      LHOR=LHOR+L                                                        DSIN 860 DSIN0086
    3 WORK=WORK+A(LVER)*A(LHOR)                                          DSIN 870 DSIN0087
C        END OF INNER LOOP                                               DSIN 880 DSIN0088
C                                                                        DSIN 890 DSIN0089
      A(J)=-WORK*DIN                                                     DSIN 900 DSIN0090
    4 J=J-MIN                                                            DSIN 910 DSIN0091
C        END OF ROW-LOOP                                                 DSIN 920 DSIN0092
C                                                                        DSIN 930 DSIN0093
    5 IPIV=IPIV-MIN                                                      DSIN 940 DSIN0094
    6 IND=IND-1                                                          DSIN 950 DSIN0095
C        END OF INVERSION-LOOP                                           DSIN 960 DSIN0096
C                                                                        DSIN 970 DSIN0097
C        CALCULATE INVERSE(A) BY MEANS OF INVERSE(T)                     DSIN 980 DSIN0098
C        INVERSE(A) = INVERSE(T) * TRANSPOSE(INVERSE(T))                 DSIN 990 DSIN0099
C        INITIALIZE MULTIPLICATION-LOOP                                  DSIN1000 DSIN0100
      DO 8 I=1,N                                                         DSIN1010 DSIN0101
      IPIV=IPIV+I                                                        DSIN1020 DSIN0102
      J=IPIV                                                             DSIN1030 DSIN0103
C                                                                        DSIN1040 DSIN0104
C        INITIALIZE ROW-LOOP                                             DSIN1050 DSIN0105
      DO 8 K=I,N                                                         DSIN1060 DSIN0106
      WORK=0.D0                                                          DSIN1070 DSIN0107
      LHOR=J                                                             DSIN1080 DSIN0108
```

```
C                                                                       DSIN1090 DSIN0109
C        START INNER LOOP                                               DSIN1100 DSIN0110
      DO 7 L=K,N                                                        DSIN1110 DSIN0111
      LVER=LHOR+K-I                                                     DSIN1120 DSIN0112
      WORK=WORK+A(LHOR)*A(LVER)                                         DSIN1130 DSIN0113
    7 LHOR=LHOR+L                                                       DSIN1140 DSIN0114
C        END OF INNER LOOP                                              DSIN1150 DSIN0115
C                                                                       DSIN1160 DSIN0116
      A(J)=WORK                                                         DSIN1170 DSIN0117
    8 J=J+K                                                             DSIN1180 DSIN0118
C        END OF ROW- AND MULTIPLICATION-LOOP                            DSIN1190 DSIN0119
C                                                                       DSIN1200 DSIN0120
    9 RETURN                                                            DSIN1210 DSIN0121
      END                                                               DSIN1220 DSIN0122
```

```
C        SUBROUTINE DMFSD                                                DMSD  40 DMFS0001
C                                                                        DMSD  50 DMFS0002
C        PURPOSE                                                         DMSD  60 DMFS0003
C           FACTOR A GIVEN SYMMETRIC POSITIVE DEFINITE MATRIX            DMSD  70 DMFS0004
C                                                                        DMSD  80 DMFS0005
C        USAGE                                                           DMSD  90 DMFS0006
C           CALL DMFSD(A,N,EPS,IER)                                      DMSD 100 DMFS0007
C                                                                        DMSD 110 DMFS0008
C        DESCRIPTION OF PARAMETERS                                       DMSD 120 DMFS0009
C           A      - DOUBLE PRECISION UPPER TRIANGULAR PART OF GIVEN     DMSD 130 DMFS0010
C                    SYMMETRIC POSITIVE DEFINITE N BY N COEFFICIENT      DMSD 140 DMFS0011
C                    MATRIX.                                             DMSD 150 DMFS0012
C                    ON RETURN A CONTAINS THE RESULTANT UPPER            DMSD 160 DMFS0013
C                    TRIANGULAR MATRIX IN DOUBLE PRECISION.              DMSD 170 DMFS0014
C           N      - THE NUMBER OF ROWS (COLUMNS) IN GIVEN MATRIX.       DMSD 180 DMFS0015
C           EPS    - SINGLE PRECISION INPUT CONSTANT WHICH IS USED       DMSD 190 DMFS0016
C                    AS RELATIVE TOLERANCE FOR TEST ON LOSS OF           DMSD 200 DMFS0017
C                    SIGNIFICANCE.                                       DMSD 210 DMFS0018
C           IER    - RESULTING ERROR PARAMETER CODED AS FOLLOWS          DMSD 220 DMFS0019
C                    IER=0  - NO ERROR                                   DMSD 230 DMFS0020
C                    IER=-1 - NO RESULT BECAUSE OF WRONG INPUT PARAME-   DMSD 240 DMFS0021
C                             TER N OR BECAUSE SOME RADICAND IS NON-     DMSD 250 DMFS0022
C                             POSITIVE (MATRIX A IS NOT POSITIVE         DMSD 260 DMFS0023
C                             DEFINITE, POSSIBLY DUE TO LOSS OF SIGNI-   DMSD 270 DMFS0024
C                             FICANCE)                                   DMSD 280 DMFS0025
C                    IER=K  - WARNING WHICH INDICATES LOSS OF SIGNIFI-   DMSD 290 DMFS0026
C                             CANCE. THE RADICAND FORMED AT FACTORIZA-   DMSD 300 DMFS0027
C                             TION STEP K+1 WAS STILL POSITIVE BUT NO    DMSD 310 DMFS0028
C                             LONGER GREATER THAN ABS(EPS*A(K+1,K+1)).   DMSD 320 DMFS0029
C                                                                        DMSD 330 DMFS0030
C        REMARKS                                                         DMSD 340 DMFS0031
C           THE UPPER TRIANGULAR PART OF GIVEN MATRIX IS ASSUMED TO BE   DMSD 350 DMFS0032
C           STORED COLUMNWISE IN N*(N+1)/2 SUCCESSIVE STORAGE LOCATIONS. DMSD 360 DMFS0033
C           IN THE SAME STORAGE LOCATIONS THE RESULTING UPPER TRIANGU-    DMSD 370 DMFS0034
C           LAR MATRIX IS STORED COLUMNWISE TOO.                         DMSD 380 DMFS0035
C           THE PROCEDURE GIVES RESULTS IF N IS GREATER THAN 0 AND ALL   DMSD 390 DMFS0036
```

```
C            CALCULATED RADICANDS ARE POSITIVE.                                DMSD 400 DMFS0037
C            THE PRODUCT OF RETURNED DIAGONAL TERMS IS EQUAL TO THE            DMSD 410 DMFS0038
C            SQUARE-ROOT OF THE DETERMINANT OF THE GIVEN MATRIX.               DMSD 420 DMFS0039
C                                                                              DMSD 430 DMFS0040
C         SUBROUTINES AND FUNCTION SUBPROGRAMS REQUIRED                        DMSD 440 DMFS0041
C            NONE                                                              DMSD 450 DMFS0042
C                                                                              DMSD 460 DMFS0043
C         METHOD                                                               DMSD 470 DMFS0044
C            SOLUTION IS DONE USING THE SQUARE-ROOT METHOD OF CHOLESKY.        DMSD 480 DMFS0045
C            THE GIVEN MATRIX IS REPRESENTED AS PRODUCT OF TWO TRIANGULAR      DMSD 490 DMFS0046
C            MATRICES, WHERE THE LEFT HAND FACTOR IS THE TRANSPOSE OF          DMSD 500 DMFS0047
C            THE RETURNED RIGHT HAND FACTOR.                                   DMSD 510 DMFS0048
C                                                                              DMSD 520 DMFS0049
C     ..........................................................................DMSD 530 DMFS0050
C                                                                              DMSD 540 DMFS0051
      SUBROUTINE DMFSD(A,N,EPS,IER)                                            DMSD 550 DMFS0052
C                                                                              DMSD 560 DMFS0053
C                                                                              DMSD 570 DMFS0054
      DIMENSION A(1)                                                           DMSD 580 DMFS0055
      DOUBLE PRECISION DPIV,DSUM,A                                             DMSD 590 DMFS0056
      DOUBLE PRECISION DSQRT                                                         DMFS0057
C                                                                              DMSD 600 DMFS0058
C        TEST ON WRONG INPUT PARAMETER N                                       DMSD 610 DMFS0059
      IF(N-1) 12,1,1                                                           DMSD 620 DMFS0060
    1 IER=0                                                                    DMSD 630 DMFS0061
C                                                                              DMSD 640 DMFS0062
C        INITIALIZE DIAGONAL-LOOP                                              DMSD 650 DMFS0063
      KPIV=0                                                                   DMSD 660 DMFS0064
      DO 11 K=1,N                                                              DMSD 670 DMFS0065
      KPIV=KPIV+K                                                              DMSD 680 DMFS0066
      IND=KPIV                                                                 DMSD 690 DMFS0067
      LEND=K-1                                                                 DMSD 700 DMFS0068
C                                                                              DMSD 710 DMFS0069
C        CALCULATE TOLERANCE                                                   DMSD 720 DMFS0070
      TOL=ABS(EPS*SNGL(A(KPIV)))                                               DMSD 730 DMFS0071
C                                                                              DMSD 740 DMFS0072
```

```
C         START FACTORIZATION-LOOP OVER K-TH ROW                                DMSD 750 DMFS0073
      DO 11 I=K,N                                                               DMSD 760 DMFS0074
      DSUM=0.D0                                                                 DMSD 770 DMFS0075
      IF(LEND) 2,4,2                                                            DMSD 780 DMFS0076
C                                                                               DMSD 790 DMFS0077
C         START INNER LOOP                                                      DMSD 800 DMFS0078
    2 DO 3 L=1,LEND                                                             DMSD 810 DMFS0079
      LANF=KPIV-L                                                               DMSD 820 DMFS0080
      LIND=IND-L                                                                DMSD 830 DMFS0081
    3 DSUM=DSUM+A(LANF)*A(LIND)                                                 DMSD 840 DMFS0082
C         END OF INNER LOOP                                                     DMSD 850 DMFS0083
C                                                                               DMSD 860 DMFS0084
C         TRANSFORM ELEMENT A(IND)                                              DMSD 870 DMFS0085
    4 DSUM=A(IND)-DSUM                                                          DMSD 880 DMFS0086
      IF(I-K) 10,5,10                                                           DMSD 890 DMFS0087
C                                                                               DMSD 900 DMFS0088
C         TEST FOR NEGATIVE PIVOT ELEMENT AND FOR LOSS OF SIGNIFICANCE          DMSD 910 DMFS0089
    5 IF(SNGL(DSUM)-TOL) 6,6,9                                                  DMSD 920 DMFS0090
    6 IF(DSUM) 12,12,7                                                          DMSD 930 DMFS0091
    7 IF(IER) 8,8,9                                                             DMSD 940 DMFS0092
    8 IER=K-1                                                                   DMSD 950 DMFS0093
C                                                                               DMSD 960 DMFS0094
C         COMPUTE PIVOT ELEMENT                                                 DMSD 970 DMFS0095
    9 DPIV=DSQRT(DSUM)                                                          DMSD 980 DMFS0096
      A(KPIV)=DPIV                                                              DMSD 990 DMFS0097
      DPIV=1.D0/DPIV                                                            DMSD1000 DMFS0098
      GO TO 11                                                                  DMSD1010 DMFS0099
C                                                                               DMSD1020 DMFS0100
C         CALCULATE TERMS IN ROW                                                DMSD1030 DMFS0101
   10 A(IND)=DSUM*DPIV                                                          DMSD1040 DMFS0102
   11 IND=IND+I                                                                 DMSD1050 DMFS0103
C         END OF DIAGONAL-LOOP                                                  DMSD1060 DMFS0104
C                                                                               DMSD1070 DMFS0105
      RETURN                                                                    DMSD1080 DMFS0106
   12 IER=-1                                                                    DMSD1090 DMFS0107
      RETURN                                                                    DMSD1100 DMFS0108
```

END

DMSD1110 DMFS0109

```
C                                                                       78440001 TRED0001
CC     ---------------------------------------------------------------78440002 TRED0002
C                                                                       78440003 TRED0003
      SUBROUTINE TRED2(NM,NN,A,D,E,Z)                                            TRED0004
C                                                                       78440005 TRED0005
      INTEGER I,J,K,L,N,II,NM,JP1,NN                                             TRED0006
      REAL*8 A(NN,NN),D(NN),E(NN),Z(NN,NN)                                       TRED0007
      REAL*8 F,G,H,HH,SCALE                                             78440008 TRED0008
      REAL*8 DSQRT,DABS,DSIGN                                           78440009 TRED0009
C                                                                       78440010 TRED0010
C     THIS SUBROUTINE IS A TRANSLATION OF THE ALGOL PROCEDURE TRED2,    78440011 TRED0011
C     NUM. MATH. 11, 181-195(1968) BY MARTIN, REINSCH, AND WILKINSON.   78440012 TRED0012
C     HANDBOOK FOR AUTO. COMP., VOL.II-LINEAR ALGEBRA, 212-226(1971).   78440013 TRED0013
C                                                                       78440014 TRED0014
C     THIS SUBROUTINE REDUCES A REAL SYMMETRIC MATRIX TO A              78440015 TRED0015
C     SYMMETRIC TRIDIAGONAL MATRIX USING AND ACCUMULATING               78440016 TRED0016
C     ORTHOGONAL SIMILARITY TRANSFORMATIONS.                            78440017 TRED0017
C                                                                       78440018 TRED0018
C     ON INPUT:                                                         78440019 TRED0019
C                                                                       78440020 TRED0020
C        NM IS DIMENSION OF MATRIX ACTUALLY TRANSFORMED.                         TRED0021
C                                                                       78440024 TRED0022
C        NN IS THE DIMENSION OF THE WHOLE MATRIX INCLUDING PARTS                 TRED0023
C        WHICH WILL NOT BE TRANSFORMED.                                          TRED0024
C                                                                       78440026 TRED0025
C        A CONTAINS THE REAL SYMMETRIC INPUT MATRIX.  ONLY THE          78440027 TRED0026
C          LOWER TRIANGLE OF THE MATRIX NEED BE SUPPLIED.               78440028 TRED0027
C                                                                       78440029 TRED0028
C     ON OUTPUT:                                                        78440030 TRED0029
C                                                                       78440031 TRED0030
C        D CONTAINS THE DIAGONAL ELEMENTS OF THE TRIDIAGONAL MATRIX;    78440032 TRED0031
C                                                                       78440033 TRED0032
C        E CONTAINS THE SUBDIAGONAL ELEMENTS OF THE TRIDIAGONAL         78440034 TRED0033
C          MATRIX IN ITS LAST N-1 POSITIONS.  E(1) IS SET TO ZERO;      78440035 TRED0034
C                                                                       78440036 TRED0035
C        Z CONTAINS THE ORTHOGONAL TRANSFORMATION MATRIX                78440037 TRED0036
```

```
C           PRODUCED IN THE REDUCTION;                                      78440038 TRED0037
C                                                                           78440039 TRED0038
C        A AND Z MAY COINCIDE.  IF DISTINCT, A IS UNALTERED.                78440040 TRED0039
C                                                                           78440041 TRED0040
C     QUESTIONS AND COMMENTS SHOULD BE DIRECTED TO B. S. GARBOW,            78440042 TRED0041
C     APPLIED MATHEMATICS DIVISION, ARGONNE NATIONAL LABORATORY             78440043 TRED0042
C                                                                           78440044 TRED0043
C     ------------------------------------------------------------------78440045 TRED0044
C                                                                           78440046 TRED0045
      N=NM                                                                         TRED0046
      DO 100 I = 1, N                                                       78440047 TRED0047
C                                                                           78440048 TRED0048
         DO 100 J = 1, I                                                    78440049 TRED0049
            Z(I,J) = A(I,J)                                                 78440050 TRED0050
  100 CONTINUE                                                              78440051 TRED0051
C                                                                           78440052 TRED0052
      IF (N .EQ. 1) GO TO 320                                               78440053 TRED0053
C     :::::::::: FOR I=N STEP -1 UNTIL 2 DO -- ::::::::::                  78440054 TRED0054
      DO 300 II = 2, N                                                      78440055 TRED0055
         I = N + 2 - II                                                     78440056 TRED0056
         L = I - 1                                                          78440057 TRED0057
         H = 0.0D0                                                          78440058 TRED0058
         SCALE = 0.0D0                                                      78440059 TRED0059
         IF (L .LT. 2) GO TO 130                                            78440060 TRED0060
C     :::::::::: SCALE ROW (ALGOL TOL THEN NOT NEEDED) ::::::::::          78440061 TRED0061
         DO 120 K = 1, L                                                    78440062 TRED0062
  120    SCALE = SCALE + DABS(Z(I,K))                                       78440063 TRED0063
C                                                                           78440064 TRED0064
         IF (SCALE .NE. 0.0D0) GO TO 140                                    73440065 TRED0065
  130    E(I) = Z(I,L)                                                      78440066 TRED0066
         GO TO 290                                                          78440067 TRED0067
C                                                                           78440068 TRED0068
  140    DO 150 K = 1, L                                                    78440069 TRED0069
            Z(I,K) = Z(I,K) / SCALE                                         78440070 TRED0070
            H = H + Z(I,K) * Z(I,K)                                         78440071 TRED0071
  150    CONTINUE                                                           78440072 TRED0072
```

```
C                                                                       78440073 TRED0073
      F = Z(I,L)                                                        78440074 TRED0074
      G = -DSIGN(DSQRT(H),F)                                            78440075 TRED0075
      E(I) = SCALE * G                                                  78440076 TRED0076
      H = H - F * G                                                     78440077 TRED0077
      Z(I,L) = F - G                                                    78440078 TRED0078
      F = 0.0D0                                                         78440079 TRED0079
C                                                                       78440080 TRED0080
      DO 240 J = 1, L                                                   78440081 TRED0081
         Z(J,I) = Z(I,J) / H                                            78440082 TRED0082
         G = 0.0D0                                                      78440083 TRED0083
C     :::::::::: FORM ELEMENT OF A*U ::::::::::                         78440084 TRED0084
         DO 180 K = 1, J                                                78440085 TRED0085
  180    G = G + Z(J,K) * Z(I,K)                                        78440086 TRED0086
C                                                                       78440087 TRED0087
         JP1 = J + 1                                                    78440088 TRED0088
         IF (L .LT. JP1) GO TO 220                                      78440089 TRED0089
C                                                                       78440090 TRED0090
         DO 200 K = JP1, L                                              78440091 TRED0091
  200    G = G + Z(K,J) * Z(I,K)                                        78440092 TRED0092
C     :::::::::: FORM ELEMENT OF P ::::::::::                           78440093 TRED0093
  220    E(J) = G / H                                                   78440094 TRED0094
         F = F + E(J) * Z(I,J)                                          78440095 TRED0095
  240 CONTINUE                                                          78440096 TRED0096
C                                                                       78440097 TRED0097
      HH = F / (H + H)                                                  78440098 TRED0098
C     :::::::::: FORM REDUCED A ::::::::::                              78440099 TRED0099
      DO 260 J = 1, L                                                   78440100 TRED0100
         F = Z(I,J)                                                     78440101 TRED0101
         G = E(J) - HH * F                                              78440102 TRED0102
         E(J) = G                                                       78440103 TRED0103
C                                                                       78440104 TRED0104
         DO 260 K = 1, J                                                78440105 TRED0105
            Z(J,K) = Z(J,K) - F * E(K) - G * Z(I,K)                     78440106 TRED0106
  260 CONTINUE                                                          78440107 TRED0107
C                                                                       78440108 TRED0108
```

```
  290     D(I) = H                                                          78440109 TRED0109
  300 CONTINUE                                                              78440110 TRED0110
C                                                                           78440111 TRED0111
  320 D(1) = 0.0D0                                                          78440112 TRED0112
      E(1) = 0.0D0                                                          78440113 TRED0113
C     :::::::::: ACCUMULATION OF TRANSFORMATION MATRICES ::::::::::       78440114 TRED0114
      DO 500 I = 1, N                                                       78440115 TRED0115
         I = I - 1                                                          78440116 TRED0116
         IF (D(I) .EQ. 0.0D0) GO TO 380                                     78440117 TRED0117
C                                                                           78440118 TRED0118
         DO 360 J = 1, L                                                    78440119 TRED0119
            G = 0.0D0                                                       78440120 TRED0120
C                                                                           78440121 TRED0121
            DO 340 K = 1, L                                                 78440122 TRED0122
  340       G = G + Z(I,K) * Z(K,J)                                         78440123 TRED0123
C                                                                           78440124 TRED0124
            DO 360 K = 1, L                                                 78440125 TRED0125
               Z(K,J) = Z(K,J) - G * Z(K,I)                                 78440126 TRED0126
  360    CONTINUE                                                          78440127 TRED0127
C                                                                           78440128 TRED0128
  380    D(I) = Z(I,I)                                                     78440129 TRED0129
         Z(I,I) = 1.0D0                                                     78440130 TRED0130
         IF (L .LT. 1) GO TO 500                                            78440131 TRED0131
C                                                                           78440132 TRED0132
         DO 400 J = 1, L                                                    78440133 TRED0133
            Z(I,J) = 0.0D0                                                  78440134 TRED0134
            Z(J,I) = 0.0D0                                                  78440135 TRED0135
  400    CONTINUE                                                          78440136 TRED0136
C                                                                           78440137 TRED0137
  500 CONTINUE                                                              78440138 TRED0138
C                                                                           78440139 TRED0139
      RETURN                                                                78440140 TRED0140
C     :::::::::: LAST CARD OF TRED2 ::::::::::                            78440141 TRED0141
      END                                                                   78440142 TRED0142
```

```
      SUBROUTINE TQL2(NM,NN,D,E,Z,IERR)                                  TQL20001
C                                                                 90220005 TQL20002
      INTEGER I,J,K,L,M,N,II,L1,NM,MML,IERR,NN                           TQL20003
      REAL*8 D(NN),E(NN),Z(NN,NN)                                        TQL20004
      REAL*8 B,C,F,G,H,P,R,S,MACHEP                               90220008 TQL20005
      REAL*8 DSQRT,DABS,DSIGN                                     90220009 TQL20006
C                                                                 90220010 TQL20007
C     THIS SUBROUTINE IS A TRANSLATION OF THE ALGOL PROCEDURE TQL2, 90220011 TQL20008
C     NUM. MATH. 11, 293-306(1968) BY BOWDLER, MARTIN, REINSCH, AND 90220012 TQL20009
C     WILKINSON.                                                  90220013 TQL20010
C     HANDBOOK FOR AUTO. COMP., VOL.II-LINEAR ALGEBRA, 227-240(1971). 90220014 TQL20011
C                                                                 90220015 TQL20012
C     THIS SUBROUTINE FINDS THE EIGENVALUES AND EIGENVECTORS      90220016 TQL20013
C     OF A SYMMETRIC TRIDIAGONAL MATRIX BY THE QL METHOD.         90220017 TQL20014
C     THE EIGENVECTORS OF A FULL SYMMETRIC MATRIX CAN ALSO        90220018 TQL20015
C     BE FOUND IF  TRED2  HAS BEEN USED TO REDUCE THIS            90220019 TQL20016
C     FULL MATRIX TO TRIDIAGONAL FORM.                            90220020 TQL20017
C                                                                 90220021 TQL20018
C     ON INPUT:                                                   90220022 TQL20019
C                                                                 90220023 TQL20020
C        NM IS DIMENSION OF MATRIX ACTUALLY TRANSFORMED.                   TQL20021
C                                                                 90220027 TQL20022
C        NN IS THE DIMENSION OF THE WHOLE MATRIX INCLUDING PARTS           TQL20023
C        WHICH WILL NOT BE TRANSFORMED.                                    TQL20024
C                                                                 90220029 TQL20025
C        D CONTAINS THE DIAGONAL ELEMENTS OF THE INPUT MATRIX;    90220030 TQL20026
C                                                                 90220031 TQL20027
C        E CONTAINS THE SUBDIAGONAL ELEMENTS OF THE INPUT MATRIX  90220032 TQL20028
C          IN ITS LAST N-1 POSITIONS.  E(1) IS ARBITRARY;         90220033 TQL20029
C                                                                 90220034 TQL20030
C        Z CONTAINS THE TRANSFORMATION MATRIX PRODUCED IN THE     90220035 TQL20031
C          REDUCTION BY  TRED2, IF PERFORMED.  IF THE EIGENVECTORS 90220036 TQL20032
C          OF THE TRIDIAGONAL MATRIX ARE DESIRED, Z MUST CONTAIN  90220037 TQL20033
C          THE IDENTITY MATRIX.                                   90220038 TQL20034
C                                                                 90220039 TQL20035
C     ON OUTPUT:                                                  90220040 TQL20036
```

```
C                                                                       90220041 TQL20037
C        D CONTAINS THE EIGENVALUES IN ASCENDING ORDER.  IF AN          90220042 TQL20038
C          ERROR EXIT IS MADE, THE EIGENVALUES ARE CORRECT BUT          90220043 TQL20039
C          UNORDERED FOR INDICES 1,2,...,IERR-1;                        90220044 TQL20040
C                                                                       90220045 TQL20041
C        E HAS BEEN DESTROYED;                                          90220046 TQL20042
C                                                                       90220047 TQL20043
C        Z CONTAINS ORTHONORMAL EIGENVECTORS OF THE SYMMETRIC           90220048 TQL20044
C          TRIDIAGONAL (OR FULL) MATRIX.  IF AN ERROR EXIT IS MADE,     90220049 TQL20045
C          Z CONTAINS THE EIGENVECTORS ASSOCIATED WITH THE STORED       90220050 TQL20046
C          EIGENVALUES;                                                 90220051 TQL20047
C                                                                       90220052 TQL20048
C        IERR IS SET TO                                                 90220053 TQL20049
C          ZERO       FOR NORMAL RETURN,                               90220054 TQL20050
C          J          IF THE J-TH EIGENVALUE HAS NOT BEEN              90220055 TQL20051
C                     DETERMINED AFTER 30 ITERATIONS.                  90220056 TQL20052
C                                                                       90220057 TQL20053
C     QUESTIONS AND COMMENTS SHOULD BE DIRECTED TO B. S. GARBOW,        90220058 TQL20054
C     APPLIED MATHEMATICS DIVISION, ARGONNE NATIONAL LABORATORY         90220059 TQL20055
C                                                                       90220060 TQL20056
C     ------------------------------------------------------------------90220061 TQL20057
C                                                                       90220062 TQL20058
C     :::::::::: MACHEP IS A MACHINE DEPENDENT PARAMETER SPECIFYING     90220063 TQL20059
C                THE RELATIVE PRECISION OF FLOATING POINT ARITHMETIC.   90220064 TQL20060
C                MACHEP = 16.0D0**(-13) FOR LONG FORM ARITHMETIC        90220065 TQL20061
C                ON S360 ::::::::::                                     90220066 TQL20062
      DATA MACHEP/Z3410000000000000/                                    90220067 TQL20063
C                                                                       90220068 TQL20064
                                                                                TQL20065
      N=NM                                                                      
      IERR = 0                                                          90220069 TQL20066
      IF (N .EQ. 1) GO TO 1001                                          90220070 TQL20067
C                                                                       90220071 TQL20068
      DO 100 I = 2, N                                                   90220072 TQL20069
  100 E(I-1) = E(I)                                                     90220073 TQL20070
C                                                                       90220074 TQL20071
      F = 0.0D0                                                         90220075 TQL20072
```

```
      B = 0.0D0                                                          90220076 TQL20073
      E(N) = 0.0D0                                                       90220077 TQL20074
C                                                                        90220078 TQL20075
      DO 240 L = 1, N                                                    90220079 TQL20076
         J = 0                                                           90220080 TQL20077
         H = MACHEP * (DABS(D(L)) + DABS(E(L)))                          90220081 TQL20078
         IF (B .LT. H) B = H                                             90220082 TQL20079
C     :::::::::: LOOK FOR SMALL SUB-DIAGONAL ELEMENT ::::::::::         90220083 TQL20080
         DO 110 M = L, N                                                 90220084 TQL20081
            IF (DABS(E(M)) .LE. B) GO TO 120                             90220085 TQL20082
C     :::::::::: E(N) IS ALWAYS ZERO, SO THERE IS NO EXIT                90220086 TQL20083
C                THROUGH THE BOTTOM OF THE LOOP ::::::::::               90220087 TQL20084
  110    CONTINUE                                                        90220088 TQL20085
C                                                                        90220089 TQL20086
  120    IF (M .EQ. L) GO TO 220                                         90220090 TQL20087
  130    IF (J .EQ. 30) GO TO 1000                                       90220091 TQL20088
         J = J + 1                                                       90220092 TQL20089
C     :::::::::: FORM SHIFT ::::::::::                                   90220093 TQL20090
         L1 = L + 1                                                      90220094 TQL20091
         G = D(L)                                                        90220095 TQL20092
         P = (D(L1) - G) / (2.0D0 * E(L))                                90220096 TQL20093
         R = DSQRT(P*P+1.0D0)                                            90220097 TQL20094
         D(L) = E(L) / (P + DSIGN(R,P))                                  90220098 TQL20095
         H = G - D(L)                                                    90220099 TQL20096
C                                                                        90220100 TQL20097
         DO 140 I = L1, N                                                90220101 TQL20098
  140    D(I) = D(I) - H                                                 90220102 TQL20099
C                                                                        90220103 TQL20100
         F = F + H                                                       90220104 TQL20101
C     :::::::::: QL TRANSFORMATION ::::::::::                            90220105 TQL20102
         P = D(M)                                                        90220106 TQL20103
         C = 1.0D0                                                       90220107 TQL20104
         S = 0.0D0                                                       90220108 TQL20105
         MML = M - L                                                     90220109 TQL20106
C     :::::::::: FOR I=M-1 STEP -1 UNTIL L DO -- ::::::::::             90220110 TQL20107
         DO 200 II = 1, MML                                              90220111 TQL20108
```

```
                I = M - II                                                      90220112 TQL20109
                G = C * E(I)                                                    90220113 TQL20110
                H = C * P                                                       90220114 TQL20111
                IF (DABS(P) .LT. DABS(E(I))) GO TO 150                          90220115 TQL20112
                C = E(I) / P                                                    90220116 TQL20113
                R = DSQRT(C*C+1.0D0)                                            90220117 TQL20114
                E(I+1) = S * P * R                                              90220118 TQL20115
                S = C / R                                                       90220119 TQL20116
                C = 1.0D0 / R                                                   90220120 TQL20117
                GO TO 160                                                       90220121 TQL20118
  150           C = P / E(I)                                                    90220122 TQL20119
                R = DSQRT(C*C+1.0D0)                                            90220123 TQL20120
                E(I+1) = S * E(I) * R                                           90220124 TQL20121
                S = 1.0D0 / R                                                   90220125 TQL20122
                C = C * S                                                       90220126 TQL20123
  160           P = C * D(I) - S * G                                            90220127 TQL20124
                D(I+1) = H + S * (C * G + S * D(I))                             90220128 TQL20125
C     :::::::::: FORM VECTOR ::::::::::                                         90220129 TQL20126
                DO 180 K = 1, N                                                 90220130 TQL20127
                   H = Z(K,I+1)                                                 90220131 TQL20128
                   Z(K,I+1) = S * Z(K,I) + C * H                                90220132 TQL20129
                   Z(K,I) = C * Z(K,I) - S * H                                  90220133 TQL20130
  180           CONTINUE                                                        90220134 TQL20131
C                                                                               90220135 TQL20132
  200     CONTINUE                                                              90220136 TQL20133
C                                                                               90220137 TQL20134
          E(L) = S * P                                                          90220138 TQL20135
          D(L) = C * P                                                          90220139 TQL20136
          IF (DABS(E(L)) .GT. B) GO TO 130                                      90220140 TQL20137
  220     D(L) = D(L) + F                                                       90220141 TQL20138
  240   CONTINUE                                                                90220142 TQL20139
C     :::::::::: ORDER EIGENVALUES AND EIGENVECTORS ::::::::::                  90220143 TQL20140
      DO 300 II = 2, N                                                          90220144 TQL20141
         I = II - 1                                                             90220145 TQL20142
         K = I                                                                  90220146 TQL20143
         P = D(I)                                                               90220147 TQL20144
```

```
C
      DO 260 J = II, N
         IF (D(J) .GE. P) GO TO 260
         K = J
         P = D(J)
  260 CONTINUE
C
      IF (K .EQ. I) GO TO 300
      D(K) = D(I)
      D(I) = P
C
      DO 280 J = 1, N
         P = Z(J,I)
         Z(J,I) = Z(J,K)
         Z(J,K) = P
  280 CONTINUE
C
  300 CONTINUE
C
      GO TO 1001
C     :::::::::: SET ERROR -- NO CONVERGENCE TO AN
C                EIGENVALUE AFTER 30 ITERATIONS ::::::::::
 1000 IERR = L
 1001 RETURN
C     :::::::::: LAST CARD OF TQL2 ::::::::::
      END
```

```
90220148 TQL20145
90220149 TQL20146
90220150 TQL20147
90220151 TQL20148
90220152 TQL20149
90220153 TQL20150
90220154 TQL20151
90220155 TQL20152
90220156 TQL20153
90220157 TQL20154
90220158 TQL20155
90220159 TQL20156
90220160 TQL20157
90220161 TQL20158
90220162 TQL20159
90220163 TQL20160
90220164 TQL20161
90220165 TQL20162
90220166 TQL20163
90220167 TQL20164
90220168 TQL20165
90220169 TQL20166
90220170 TQL20167
90220171 TQL20168
90220172 TQL20169
90220173 TQL20170
```

```
      SUBROUTINE PRINT(A,NA,NROW,NCOL)                                  PRIN0001
C     PRINTS DP ARRAY OF AN UNKNOWN NUMBER OF COLUMNS                   PRIN0002
C     NA=DIMENSION OF SQUARE MATRIX A IN CALLING PROGRAM                PRIN0003
C     NROW,NCOL=DIMENSION OF NROW BY NCOL UPPER LEFT HAND BLOCK OF A    PRIN0004
C     ACTUALLY PRINTED                                                  PRIN0005
      DOUBLE PRECISION A                                                PRIN0006
      DIMENSION A(NA,NA)                                                PRIN0007
      DO 100 I=1,NROW                                                   PRIN0008
      DO 100 NBOT=1,NCOL,7                                              PRIN0009
      NTOP=MIN0(NCOL,NBOT+6)                                            PRIN0010
      WRITE (6,120) (A(I,J),J=NBOT,NTOP)                                PRIN0011
  120 FORMAT (4X,7D18.10)                                               PRIN0012
  100 CONTINUE                                                          PRIN0013
      RETURN                                                            PRIN0014
      END                                                               PRIN0015
```

```
      SUBROUTINE PRINTA(A,NA,NCOL)                                      PRNA0001
C     PRINTS A DP ROW VECTOR OF AN UNKNOWN NUMBER OF COLUMNS            PRNA0002
C     NA=DIMENSION OF A IN CALLING PROGRAM                              PRNA0003
C     NCOL=NUMBER OF COLUMNS ACTUALLY PRINTED                           PRNA0004
      DOUBLE PRECISION A                                                PRNA0005
      DIMENSION A(NA)                                                   PRNA0006
      DO 100 NBOT=1,NCOL,7                                              PRNA0007
      NTOP=MIN0(NCOL,NBOT+6)                                            PRNA0008
      WRITE (6,120) (A(I),I=NBOT,NTOP)                                  PRNA0009
  120 FORMAT (4X,7D18.10)                                               PRNA0010
  100 CONTINUE                                                          PRNA0011
      RETURN                                                            PRNA0012
      END                                                               PRNA0013
```

```
      SUBROUTINE PUNCH (IAMAX,NCVAR,PS,FLAG,CINV,CFLAG,LPUNCH)          PUNC0001
      INTEGER FLAG                                                      PUNC0002
      DOUBLE PRECISION CINV,PS                                          PUNC0003
      DIMENSION CINV(30,30),UNITS(75),PS(75),NCVAR(30),FLAG(75)         PUNC0004
      WRITE (7,100) IAMAX                                               PUNC0005
      WRITE (7,100) (NCVAR(I), I=1,IAMAX)                               PUNC0006
      DO 10 I=1,75                                                      PUNC0007
      IF(DABS(PS(I)).LT.1.0D-70) GO TO 10                               PUNC0008
      WRITE (7,105) I, PS(I), FLAG(I)                                   PUNC0009
   10 CONTINUE                                                          PUNC0010
      IF (LPUNCH.EQ.0.AND.CFLAG.EQ.0) GO TO 25                          PUNC0011
      DO 15 I=1,IAMAX                                                   PUNC0012
      DO 15 J=1,I                                                       PUNC0013
      WRITE (7,110) I, J, CINV(I,J)                                     PUNC0014
   15 CONTINUE                                                          PUNC0015
   25 CONTINUE                                                          PUNC0016
  100 FORMAT (15I5)                                                     PUNC0017
  105 FORMAT (I5, D15.8, I5)                                            PUNC0018
  110 FORMAT (2I5, D25.16)                                              PUNC0019
      RETURN                                                            PUNC0020
      END                                                               PUNC0021
```

```
      SUBROUTINE PLOT (Y,NDIM,YMIN,YMAX,NWRITE,NGR,YNUM)                PLOT0001
      DIMENSION YNUM(600)                                               PLOT0002
      DIMENSION Y(NDIM),A(119),NZ(10),CHAR(10)                          PLOT0003
      DATA BLANK,PLUS,CHAR(1),CHAR(2),CHAR(3),CHAR(4),CHAR(5),CHAR(6),  PLOT0004
     1CHAR(7),CHAR(8),CHAR(9),CHAR(10)                                  PLOT0005
     1/1H ,1H+,1H*,1HB,1HC,1HD,1HE,1HF,1HG,1HI,1HJ,1HK/                 PLOT0006
      NPTS=NDIM/NGR                                                     PLOT0007
      YMNT=YMIN                                                         PLOT0008
      YMXT=YMAX                                                         PLOT0009
      DELTA=(YMAX-YMIN)/100.                                            PLOT0010
      YMN=YMIN-9.*DELTA                                                 PLOT0011
      DO 10 I=1,119                                                     PLOT0012
   10 A(I)=BLANK                                                        PLOT0013
      IF(YMAX-YMIN) 11,11,15                                            PLOT0014
   11 WRITE(NWRITE,29)                                                  PLOT0015
      RETURN                                                            PLOT0016
   15 WRITE(NWRITE,9) NPTS,DELTA                                        PLOT0017
      WRITE(NWRITE,19) YMNT,YMXT                                        PLOT0018
      DO 60 I=1,NPTS                                                    PLOT0019
      IF (MOD(I,6)-1) 24,17,24                                          PLOT0020
   17 DO 20 J=10,119,50                                                 PLOT0021
   20 A(J)=PLUS                                                         PLOT0022
   24 DO 30 J=1,NGR                                                     PLOT0023
      N=(Y(I+(J-1)*NPTS)-YMN)/DELTA+1.5                                 PLOT0024
      IF (N.LT.1) N=1                                                   PLOT0025
      IF(N.GT.119) N=119                                                PLOT0026
      NZ(J)=N                                                           PLOT0027
   30 A(N)=CHAR(J)                                                      PLOT0028
      WRITE(NWRITE,39) (A(J),J=1,119),YNUM(I)                           PLOT0029
      DO 40 J=1,NGR                                                     PLOT0030
      N=NZ(J)                                                           PLOT0031
   40 A(N)=BLANK                                                        PLOT0032
      IF (MOD(I,6)-1) 60,38,60                                          PLOT0033
   38 DO 50 J=10,119,50                                                 PLOT0034
   50 A(J)=BLANK                                                        PLOT0035
   60 CONTINUE                                                          PLOT0036
```

```
 9 FORMAT(' '31X,'NO. OF POINTS ON ABSCISSA = 'I5/32X,'NO. OF INTERVA      PLOT0037
  1LS ON ORDINATE = 118,  INCREMENT = 'E10.3)                             PLOT0038
19 FORMAT(' 'E16.6,E101.6/10X,'I'99X,'I'/' I',8X,'I',2(49X,'I'),8X,'I     PLOT0039
  1')                                                                     PLOT0040
29 FORMAT (' YMAX AND YMIN SPECIFIED INCORRECTLY')                        PLOT0041
39 FORMAT(' '119A1,F5.1)                                                  PLOT0042
   RETURN                                                                 PLOT0043
   END                                                                    PLOT0044
```

Parameter List for $^1\Sigma^+(2)$, $^3\Sigma^+$, $^1\Sigma^-$, $^{1,3}\Pi$, and $^3\Pi_2$ Hamiltonian

(Low Lying States of BaO)

No.	Name	Physical Origin
1	E1S	$^1\Sigma^+(1)$ energy
2	E1P	$^1\Pi$ energy
3	E3P	$^3\Pi$ energy
4	BR1S	$^1\Sigma^+(1)$ rotational constant
5	BR1P	$^1\Pi$ rotational constant
6	BR3P	$^3\Pi$ rotational constant
7	DR1S	$^1\Sigma^+(1)$ centrifugal distortion
8	DR1P	$^1\Pi$ centrifugal distortion
9	DR3P	$^3\Pi$ centrifugal distortion
10	A3P	$^3\Pi$ spin-orbit
11	AJ3P	$^3\Pi$ spin-orbit centrifugal distortion
12	C3P	$^3\Pi$ spin-spin
13	GAM3P	$^3\Pi$ spin-rotation
14	C3PD	$^3\Pi$ parity dependent spin-spin
15	QVP	$^3\Pi$ Λ-doubling
16	PVP	$^3\Pi$ Λ-doubling
17	B1O+	$^1\Pi \sim {}^1\Sigma^+(1)$ rotation electronic interaction
18	AO1+	$^3\Pi \sim {}^1\Sigma^+(1)$ spin-orbit interaction
19	A11	$^1\Pi \sim {}^3\Pi$ spin-orbit interaction
20	E1S-	$^1\Sigma^-$ energy
21	BR1S-	$^1\Sigma^-$ rotational constant

Parameter List for $^1\Sigma^+(2)$, $^3\Sigma^+$, $^1\Sigma^-$, $^{1,3}\Pi$, and $^3\Pi_2$ Hamiltonian (Low Lying States of BaO) (cont.)

No.	Name	Physical Origin
22	DR1S-	$^1\Sigma^-$ centrifugal distortion
23	H1S	$^1\Sigma^+(1)$ third order centrifugal distortion
24	H1P	$^1\Pi$ third order centrifugal distortion
25	H1S-	$^1\Sigma^-$ third order centrifugal distortion
26	QV1P	$^1\Pi$ Λ-doubling
27	E3SGM+	$^3\Sigma^+$ energy
28	B3SGM+	$^3\Sigma^+$ rotational constant
29	D3SGM+	$^3\Sigma^+$ centrifugal distortion
30	C3SGM+	$^3\Sigma^+$ spin-spin
31	G3SGM+	$^3\Sigma^+$ spin-rotation
32	A27	$^3\Pi \sim {}^3\Sigma^+$ spin-orbit interaction
33	ALPHAO	$^3\Pi \sim {}^3\Sigma^+$ spin-orbit interaction
34	BETAO	$^3\Pi \sim {}^3\Sigma^+$ rotation-electronic interaction
35	E2S	$^1\Sigma^+$ energy (2)
36	BR2S	$^1\Sigma^+$ rotational constant (2)
37	DR2S	$^1\Sigma^+$ centrifugal distortion (2)
38	2B1O+	$^1\Pi \sim {}^1\Sigma^+(2)$ rotational-electronic interaction
39	2AO1+	$^1\Pi \sim {}^1\Sigma^+(2)$ spin-orbit interaction
40	B1O+J	$^1\Pi \sim {}^1\Sigma^+(1)$ rotation-electronic centrifugal distortion

Parameter List for $^1\Sigma^+(2)$, $^3\Sigma^+$, $^1\Sigma^-$, $^1,^3\Pi$, and $^3\Pi_2$ Hamiltonian (Low Lying States of BaO) (cont.)

No.	Name	Physical Origin
41	E3P2	$^3\Pi_2$ energy
42	B3P2	$^3\Pi_2$ rotational constant
43	D3P2	$^3\Pi_2$ centrifugal distortion
44	A3P2	$^3\Pi_2$ spin-orbit constant
45	AO1+2	$^1\Sigma^+$ (1) $\sim$ $^3\Pi_2$ spin-orbit interaction

```
      SUBROUTINE NAMEIT(NAM,M)                                          NAME0001
C        NAMEIT FOR 8 STATE HAMILTONIAN.  1,3 SIGMA+, 1SIGMA-, 1,3 PI   NAME0002
C        3PI (OMEGA=2)                                                  NAME0003
C  ASSIGNS NAMES TO PARAMETERS  M IS MAX. NO. OF NAMES                  NAME0004
      REAL*8 NAM(M)                                                     NAME0005
C THESE PARAMETERS ARE FOR TRIPLETS PI, SINGLETS PI, AND SIGMA          NAME0006
      REAL*8 NAMES(75) /3HE1S,3HE1P,3HE3P,4HBR1S,4HBR1P,4HBR3P,4HDR1S,  NAME0007
     14HDR1P,4HDR3P,3HA3P,4HAJ3P,3HC3P,5HGAM3P,4HC3PD,3HQVP,3HPVP,      NAME0008
     14HB10+,4HA01+,3HA11,4HE1S-,5HBR1S-,5HDR1S-,                       NAME0009
     13HH1S,3HH1P,4HH1S-,4HQV1P,6HE3SGM+,6HB3SGM+,6HD3SGM+,6HC3SGM+,    NAME0010
     26HG3SGM+,3HA27,6HALPHA0,5HBETA0,3HE2S,4HBR2S,4HDR2S,5H2B10+,5H2A01 NAME0011
     1+,5HB10+J,4HE3P2,4HB3P2,4HD3P2,4HA3P2,5HA01+2,                    NAME0012
     1         1HO,1HO,1HO,1HO,1HO,1HO,1HO,1HO,1HO,1HO,1HO,1HO,1HO,     NAME0013
     11HO,1HO,1HO,1HO,1HO,1HO,1HO,1HO,1HO,1HO,1HO,1HO,1HO,1HO,1HO /    NAME0014
      DO 10 I=1,M                                                       NAME0015
   10 NAM(I)=NAMES(I)                                                   NAME0016
      RETURN                                                            NAME0017
      END                                                               NAME0018
```

```
      SUBROUTINE LEVEL(IE,NDATA)                                        LEVE0001
C        LEVEL FOR 1,3 SIGMA+, 1 SIGMA-, 1,3 PI AND 3 PI (OMEGA=2)      LEVE0002
      IMPLICIT REAL*8 (A-H,O-Z)                                         LEVE0003
      REAL*4       TP,TS,SNGL,FLOAT                                     LEVE0004
      DOUBLE PRECISION DBLE                                             LEVE0005
      DIMENSION TP(9,2,150),TS(9,2,150)                                 LEVE0006
      DIMENSION TE(9,2,150),GE(600,3),P(75),S(26),T(26),H(9,9)          LEVE0007
      DIMENSION NQ(6),NUM(6,600),U(9,9)                                 LEVE0008
      DIMENSION D(9),E(9)                                               LEVE0009
      DIMENSION TERM(150,9,2)                                           LEVE0010
      COMMON P,GE,NUM                                                   LEVE0011
      COMMON/BLK2/ TERM,JMAX,M,MAXP,MAXM                                LEVE0012
      COMMON/BLK3/TP,TS                                                 LEVE0013
      MMM=M                                                             LEVE0014
C     LEVEL FOR MAIN. M IS DIMENSION OF HAMILTONIAN.                    LEVE0015
C     MAXP IS MAXIMUM PLUS PARITY RANK, MAXM IS MAXIMUM MINUS RANK.     LEVE0016
      M1=JMAX                                                           LEVE0017
      M5=M1+1                                                           LEVE0018
C     TE(RANK,PARITY,J) ARE TERM ENERGIES.. 1ST DIM OF TE AGREES WITH M,LEVE0019
C     3ND WITH M1. 2ND INDEX, 1 IS PLUS AND 2 IS MINUS PARITY.          LEVE0020
C     DEFINE S AND T FOR TWO PARITIES TO BE USED AS R IN MATRIX.        LEVE0021
      CALL SETUP(P,S,1.0D0)                                             LEVE0022
      CALL SETUP(P,T,-1.0D0)                                            LEVE0023
C     CALCULATE ENERGY FOR AIL RANKS OF EACH J.                         LEVE0024
      DO 10 I=1,M5                                                      LEVE0025
      CJ=DBLE(FLOAT(I-1))                                               LEVE0026
C     PLUS PARITY                                                       LEVE0027
      X=CJ*(CJ+1.0D0)                                                   LEVE0028
      CALL MATRIX(S,P,X,H)                                              LEVE0029
      DO 55 K=1,9                                                       LEVE0030
      DO 5 L=1,9                                                        LEVE0031
    5 U(K,L)=0.0D0                                                      LEVE0032
   55 U(K,K)=1.0D0                                                      LEVE0033
C     DIAGONALIZE ONLY NONZERO PART OF H FOR PLUS PARITY.               LEVE0034
      M2=MAXP                                                           LEVE0035
      CALL TRED2(M2,9,H,D,E,U)                                          LEVE0036
```

```
      CALL TQL2(M2,9,D,E,U,IERR2)                                       LEVE0037
      IF (IERR2.NE.0) GO TO 11                                          LEVE0038
      GO TO 12                                                          LEVE0039
   11 WRITE(6,9) IERR2                                                  LEVE0040
    9 FORMAT(' ERROR IN HAMILTONIAN DIAGONALIZATION, IERR=',I2)         LEVE0041
   12 CONTINUE                                                          LEVE0042
      M=M2                                                              LEVE0043
      DO 6 L=1,M                                                        LEVE0044
      IF(IE.NE.1) GO TO 6                                               LEVE0045
      TP(M-L+1,1,I)=SNGL(U(2,L)**2)                                     LEVE0046
      TS(M-L+1,1,I)=SNGL(U(1,L)**2+U(6,L)**2+U(7,L)**2)                 LEVE0047
    6 TE(M-L+1,1,I)=D(L)                                                LEVE0048
C     MINUS PARITY                                                      LEVE0049
      CALL MATRIX(T,P,X,H)                                              LEVE0050
      DO 77 L=1,9                                                       LEVE0051
      DO 7 K=1,9                                                        LEVE0052
    7 U(L,K)=0.0D0                                                      LEVE0053
   77 U(L,L)=1.0D0                                                      LEVE0054
      M3=MAXM                                                           LEVE0055
      CALL TRED2(M3,9,H,D,E,U)                                          LEVE0056
      CALL TQL2(M3,9,D,E,U,IERR2)                                       LEVE0057
      IF (IERR2.NE.0) GO TO 13                                          LEVE0058
      GO TO 14                                                          LEVE0059
   13 WRITE(6,9) IERR2                                                  LEVE0060
   14 CONTINUE                                                          LEVE0061
      M=M3                                                              LEVE0062
      DO 8 L=1,M                                                        LEVE0063
      IF(IE.NE.1) GO TO 8                                               LEVE0064
      TP(M-L+1,2,I)=SNGL(U(2,L)**2)                                     LEVE0065
      TS(M-L+1,2,I)=SNGL(U(1,L)**2+U(6,L)**2+U(7,L)**2)                 LEVE0066
8     TE(M-L+1,2,I)=D(L)                                                LEVE0067
10    CONTINUE                                                          LEVE0068
C     SET UP TERM VALUES AND DIFFERENCES TO COMPARE WITH INPUT DATA.    LEVE0069
C     ON LAST PASS, LEVEL IS CALLED ONLY WITH IE=1.                     LEVE0070
      IF (IE.NE.1) GO TO 1001                                           LEVE0071
      DO 1000 N=1,M5                                                    LEVE0072
```

```
      DO 1010 L=1,M2                                                    LEVE0073
 1010 TERM(N,L,1)=TE(L,1,N)                                             LEVE0074
      DO 1020 L=1,M3                                                    LEVE0075
 1020 TERM(N,L,2)=TE(L,2,N)                                             LEVE0076
 1000 CONTINUE                                                          LEVE0077
 1001 CONTINUE                                                          LEVE0078
      M=MMM                                                             LEVE0079
      DO 50 N=1,NDATA                                                   LEVE0080
      DO 40 L=1,6                                                       LEVE0081
40    NQ(L)=NUM(L,N)                                                    LEVE0082
C     SECOND STATE TERM VALUE SUBTRACTED FROM FIRST.                    LEVE0083
      IF (NQ(2).EQ.0) TOP=0.0D0                                         LEVE0084
      IF (NQ(5).EQ.0) BOT=0.0D0                                         LEVE0085
      IF (NQ(2).NE.0) TOP=TE(NQ(2),NQ(3),NQ(1)+1)                       LEVE0086
      IF (NQ(5).NE.0) BOT=TE(NQ(5),NQ(6),NQ(4)+1)                       LEVE0087
50    GE(N,IE)=TOP-BOT                                                  LEVE0088
      RETURN                                                            LEVE0089
      END                                                               LEVE0090
```

```
      SUBROUTINE SETUP(P,R,PARITY)                                      SETU0001
C        SETUP FOR 1,3 SIGMA+, 1SIGMA-, 1,3 PI, AND 3 PI(OMEGA=2)       SETU0002
C  THIS CALCULATES MATRIX ELEMENT FACTORS THAT ARE J INDEPENDANT         SETU0003
      DOUBLE PRECISION P,R,PARITY,DSQRT                                 SETU0004
      DIMENSION P(75),R(26)                                             SETU0005
      IF(PARITY.LT.0)  PAR=-1.0D0                                       SETU0006
      IF(PARITY.GT.0)  PAR=1.0D0                                        SETU0007
      R(1)=DSQRT(2.0D0)                                                 SETU0008
      R(2)=1.0D0-PAR                                                    SETU0009
      R(3)=1.0D0+PAR                                                    SETU0010
      R(4)=1.0D0-2.0D0*PAR                                              SETU0011
      R(5)=1.0D0+2.0D0*PAR                                              SETU0012
      R(6)=P(3)-P(10)-P(12)-P(13)                                       SETU0013
      R(7)=P(3)+2.0D0*P(12)-2.0D0*P(13)                                 SETU0014
      R(8)=P(3)+P(10)-P(12)-P(13)                                       SETU0015
      R(9)=P(6)+P(11)-0.5D0*(P(13)-P(15)-0.5D0*P(16))                   SETU0016
      R(10)=P(6)+P(11)-0.5D0*(P(13)-P(15)-0.5D0*P(16))                  SETU0017
      R(11)=PAR                                                         SETU0018
      R(12)=P(27)-P(30)-P(31)                                           SETU0019
      R(13)=P(27)+2.0*P(30)-2.0*P(31)                                   SETU0020
      R(14)=P(28)-P(31)/2.0                                             SETU0021
      R(15)=P(33)-P(34)                                                 SETU0022
      RETURN                                                            SETU0023
      END                                                               SETU0024
```

```
      SUBROUTINE MATRIX(R,P,X,H)                                                MATR0001
C  CALCULATES MATRIX ELEMENTS FOR 8 STATE HAMILTONIAN                           MATR0002
C 1SIGMA+, 1SIGMA-, 1PI, 3PI, 3SIGMA+, 1SIGMA+, 3PI(OMEGA=2)                    MATR0003
      DOUBLE PRECISION R,P,X,XA,XB,DSQRT,H,Z1,Z2,Y,XJJ                          MATR0004
      DIMENSION R(26),P(75),H(9,9)                                              MATR0005
      DO 10 I=1,9                                                               MATR0006
      DO 10 J=1,9                                                               MATR0007
   10 H(I,J)=0.0D0                                                              MATR0008
      H(1,1)=0.1D0                                                              MATR0009
      H(2,2)=0.2D0                                                              MATR0010
      H(3,3)=0.3D0                                                              MATR0011
      H(4,4)=0.4D0                                                              MATR0012
      H(5,5)=0.5D0                                                              MATR0013
      H(6,6)=0.6D0                                                              MATR0014
      H(7,7)=0.7D0                                                              MATR0015
      H(8,8)=0.8D0                                                              MATR0016
      H(9,9)=0.9D0                                                              MATR0017
      XA=DSQRT(X)                                                               MATR0018
      IF(X.LT.1.0D0) GO TO 49                                                   MATR0019
      IF(X.LT.2.5D0) GO TO 44                                                   MATR0020
      XB=DSQRT(X-2.0D0)                                                         MATR0021
      H(5,7)=DSQRT(X-2.0)*P(34)                                                 MATR0022
      H(7,5)=H(5,7)                                                             MATR0023
      H(5,5)=R(8)+P(6)*(X-3.0D0)-P(9)*(X*X-4.0D0*X+5.0D0)+2.0D0*(X-3.0D0        MATR0024
     1)*P(11)+0.5D0*(X-2.0D0)*P(15)                                             MATR0025
      H(3,5)=XA*XB*(2.0D0*P(9)-R(11)*0.5D0*P(15))                               MATR0026
      H(4,5)=-R(1)*XB*(R(10)-2.0D0*(X-1.0D0)*P(9))                              MATR0027
      H(5,4)=H(4,5)                                                             MATR0028
      H(5,3)=H(3,5)                                                             MATR0029
      IF(DABS(P(42)).LT.1.D-60) GO TO 44                                        MATR0030
      XJJ=(-1.+DSQRT(1.+4*X))/2.                                                MATR0031
      Y=P(44)/P(42)                                                             MATR0032
      Z1=Y*(Y-4.)+4./3.+4.*X                                                    MATR0033
      Z2=(1./(3.*Z1))*(Y*(Y-1.)-4./9.-2.*X)                                     MATR0034
      IF(P(44).LT.0.0) GO TO 45                                                 MATR0035
      H(8,8)=P(41)+P(42)*(X+DSQRT(Z1)-2.*Z2)-P(43)*(XJJ+3./4.)**4               MATR0036
```

```
      GO TO 46                                                                  MATR0037
   45 H(3,8)=P(41)+P(42)*(X-DSQRT(Z1)-2.*Z2)-P(43)*(XJJ-0.5)**4                 MATR0038
   46 H(1,8)=R(3)*(P(42)*XJJ/P(44))**2*P(45)/2.                                 MATR0039
      H(8,1)=H(1,8)                                                             MATR0040
   44 H(2,2)=P(2)+P(5)*(X-1.0D0)-P(8)*(X-1.0D0)**2+X*(R(3)*P(26))               MATR0041
      H(2,2)=H(2,2)+P(24)*(X-1.0D0)**3                                          MATR0042
      H(4,4)=R(7)+P(6)*(X+1.0D0)-P(9)*(X*X+6.0D0*X-3.0D0)+.5D0*R(2)*            MATR0043
     1P(15)                                                                     MATR0044
      H(1,2)=-R(3)*(XA*P(17)+XA*X*P(40))/R(1)                                   MATR0045
      H(2,4)=-P(19)                                                             MATR0046
      H(3,4)=-(R(9)-2.0D0*(X+1.0D0)*P(9)+R(4)*(.25D0*P(16)+.5D0*P(15)))*        MATR0047
     1XA*R(1)                                                                   MATR0048
      H(2,1)=H(1,2)                                                             MATR0049
      H(4,2)=H(2,4)                                                             MATR0050
      H(4,3)=H(3,4)                                                             MATR0051
      H(4,6)=R(2)*DSQRT(X/2.0)*P(34)                                            MATR0052
      H(6,4)=H(4,6)                                                             MATR0053
      H(6,7)=-R(2)*(R(14)-2.0*(X+1.0)*P(29))*DSQRT(X)                           MATR0054
      H(7,6)=H(6,7)                                                             MATR0055
      H(7,7)=R(12)+P(28)*X-P(29)*X**2-2.0*R(2)*P(29)*X                          MATR0056
      H(2,7)=P(32)                                                              MATR0057
      H(7,2)=H(2,7)                                                             MATR0058
      H(3,7)=0.0-R(11)*DSQRT(X)*P(34)                                           MATR0059
      H(7,3)=H(3,7)                                                             MATR0060
      H(4,7)=DSQRT(2.0D0)*P(15)                                                 MATR0061
      H(7,4)=H(4,7)                                                             MATR0062
      H(2,6)=-R(3)*XA*P(38)/R(1)                                                MATR0063
      H(6,2)=H(2,6)                                                             MATR0064
   49 H(1,1)=(P(1)+P(4)*X-P(7)*X*X)*R(3)/2.0D0+(P(20)+P(21)*X-P(22)*X*X)        MATR0065
     1*R(2)/2.0D0                                                               MATR0066
      H(1,1)=H(1,1)+((P(23)*X**3)*R(3)/2.0D0)+((P(25)*X**3)*R(2)/2.0D0)         MATR0067
      H(3,3)=R(6)+P(6)*(X+1.0D0)-P(9)*(X*X+4.0D0*X+1.0D0)-2.0D0*                MATR0068
     1(X+1.0D0)*P(11)+.5D0*X*P(15)-R(11)*P(14)                                  MATR0069
      H(1,3)=R(3)*R(1)*P(18)/2.0D0                                              MATR0070
      H(3,1)=H(1,3)                                                             MATR0071
      H(6,6)=(R(2)/2.0)*(R(13)+P(28)*(X+2.0)-(X**2+8.0*X+4.0)*P(29))            MATR0072
```

```
H(6,6)=H(6,6)+(R(3)/2.0)*(P(35)+P(36)*X-P(37)*X*X)                    MATR0073
H(3,6)=R(2)*R(15)+R(3)*R(1)*P(39)/2.0                                 MATR0074
H(6,3)=H(3,6)                                                         MATR0075
RETURN                                                                MATR0076
END                                                                   MATR0077
```

Parameter List for BaO High Lying States

No.	Name	Physical Origin
1	E	$^1\Sigma^+(1)$ energy
2	B	$^1\Sigma^+(1)$ rotational constant
3	D	$^1\Sigma^+(1)$ centrifugal distortion
4	H	$^1\Sigma^+(1)$ third order centrifugal distortion
5	XI	$1\sim2$ homogeneous interaction
6	EP	$^1\Sigma^+(2)$ energy
7	BP	$^1\Sigma^+(2)$ rotational constant
8	DP	$^1\Sigma^+(2)$ centrifugal distortion
9	EP2	$^1\Sigma^+(3)$ energy
10	BP2	$^1\Sigma^+(3)$ rotational constant
11	DP2	$^1\Sigma^+(3)$ centrifugal distortion
12	XI2	$1\sim3$ homogeneous interaction
13	EP3	$^1\Sigma^+(4)$ energy
14	BP3	$^1\Sigma^+(4)$ rotational constant
15	DP3	$^1\Sigma^+(4)$ centrifugal distortion
16	XI3	$1\sim3$ homogeneous interaction
17	EP4	$^1\Sigma^+(5)$ energy
18	BP4	$^1\Sigma^+(5)$ rotational constant
19	DP4	$^1\Sigma^+(5)$ centrifugal distortion
20	XI4	$1\sim5$ homogeneous interaction
21	EP5	$^1\Sigma^+(6)$ energy
22	BP5	$^1\Sigma^+(6)$ rotational constant

Parameters List for BaO High Lying States (cont.)

No.	Name	Physical Origin
23	DP5	$^1\Sigma^+(6)$ centrifugal distortion
24	XI5	$1\sim6$ homogeneous interaction
25	XI23	$2\sim3$ homogeneous interaction
26	ETA1	$1\sim2$ heterogeneous interaction
27	ETA2	$1\sim3$ heterogeneous interaction
28	XI24	$2\sim4$ homogeneous interaction

```
      SUBROUTINE NAMEIT(NAM,M)                                                  NAME0001
C        NAMEIT FOR BAO * STATES                                                NAME0002
      REAL*8 NAM(M)                                                             NAME0003
      REAL*8  NAMES(28)/1HE,1HB,1HD,1HH,2HXI,2HEP,2HBP,2HDP,3HEP2,3HBP2,3      NAME0004
     1HDP2,3HXI2,3HEP3,3HBP3,3HDP3,3HXI3,3HEP4,3HBP4,3HDP4,3HXI4,3HEP5,        NAME0005
     23HBP5,3HDP5,3HXI5,4HXI23,4HETA1,4HETA2,4HXI24/                           NAME0006
      DO 10 I=29,M                                                              NAME0007
   10 NAM(I)=0.0D0                                                              NAME0008
      DO 20 J=1,28                                                              NAME0009
   20 NAM(J)=NAMES(J)                                                           NAME0010
      RETURN                                                                    NAME0011
      END                                                                       NAME0012
```

```
      SUBROUTINE LEVEL(IE,NDATA)                                        LEVE0001
C        LEVEL FOR BAO * STATES.                                        LEVE0002
      IMPLICIT REAL*8 (A-H,O-Z)                                         LEVE0003
      REAL*4       TP,TS,SNGL,FLOAT                                     LEVE0004
      DOUBLE PRECISION DBLE                                             LEVE0005
      DIMENSION TP(9,2,150),TS(9,2,150)                                 LEVE0006
      DIMENSION TE(9,2,150),GE(600,3),P(75),S(26),T(26),       H(9,9)   LEVE0007
      DIMENSION D(9),E(9)                                               LEVE0008
      DIMENSION NQ(6),NUM(6,600),U(9,9)                                 LEVE0009
      DIMENSION TERM(150,9,2)                                           LEVE0010
      COMMON P,GE,NUM                                                   LEVE0011
      COMMON/BLK2/ TERM,JMAX,M,MAXP,MAXM                                LEVE0012
      COMMON/BLK3/TP,TS                                                 LEVE0013
      MMM=M                                                             LEVE0014
C     LEVEL FOR MAIN. M IS DIMENSION OF HAMILTONIAN.                    LEVE0015
C     MAXP IS MAXIMUM PLUS PARITY RANK, MAXM IS MAXIMUM MINUS RANK.     LEVE0016
      M1=JMAX                                                           LEVE0017
      M5=M1+1                                                           LEVE0018
C     TE(RANK,PARITY,J) ARE TERM ENERGIES.. 1ST DIM OF TE AGREES WITH M,LEVE0019
C     3ND WITH M1. 2ND INDEX, 1 IS PLUS AND 2 IS MINUS PARITY.          LEVE0020
C     DEFINE S AND T FOR TWO PARITIES TO BE USED AS R IN MATRIX.        LEVE0021
      CALL SETUP(P,S,1.0)                                               LEVE0022
      CALL SETUP(P,T,-1.0)                                              LEVE0023
C     CALCULATE ENERGY FOR ALL RANKS OF EACH J.                         LEVE0024
      DO 10 I=1,M5                                                      LEVE0025
      CJ=DBLE(FLOAT(I-1))                                               LEVE0026
C     PLUS PARITY                                                       LEVE0027
      X=CJ*(CJ+1.0D0)                                                   LEVE0028
      CALL MATRIX(S,P,X,H)                                              LEVE0029
      DO 55 L=1,9                                                       LEVE0030
      DO 5 K=1,9                                                        LEVE0031
    5 U(L,K)=0.0D0                                                      LEVE0032
   55 U(L,L)=1.0D0                                                      LEVE0033
C     DIAGONALIZE ONLY NONZERO PART OF H FOR PLUS PARITY.               LEVE0034
      M2=MAXP                                                           LEVE0035
      CALL TRED2(M2,9,H,D,E,U)                                          LEVE0036
```

```
      CALL TQL2(M2,9,D,E,U,IERR2)                                          LEVE0037
      IF (IERR2.NE.0) GO TO 11                                             LEVE0038
      GO TO 12                                                             LEVE0039
   11 WRITE(6,9) IERR2                                                     LEVE0040
    9 FORMAT(' ERROR IN HAMILTONIAN DIAGONALIZATION, IERR=',I2)            LEVE0041
   12 CONTINUE                                                             LEVE0042
      M=M2                                                                 LEVE0043
      DO 6 L=1,M                                                           LEVE0044
      IF(IE.NE.1) GO TO 6                                                  LEVE0045
      TP(M-L+1,1,I)=SNGL(U(3,L)**2)                                        LEVE0046
      TS(M-L+1,1,I)=SNGL(U(1,L)**2)                                        LEVE0047
    6 TE(M-L+1,1,I)=D(L)                                                   LEVE0048
C     MINUS PARITY                                                         LEVE0049
      CALL MATRIX(T,P,X,H)                                                 LEVE0050
      DO 77 L=1,9                                                          LEVE0051
      DO 7 K=1,9                                                           LEVE0052
    7 U(L,K)=0.0D0                                                         LEVE0053
   77 U(L,L)=1.0D0                                                         LEVE0054
      M3=MAXM                                                              LEVE0055
      CALL TRED2(M3,9,H,D,E,U)                                             LEVE0056
      CALL TQL2(M3,9,D,E,U,IERR2)                                          LEVE0057
      IF (IERR2.NE.0) GO TO 13                                             LEVE0058
      GO TO 14                                                             LEVE0059
   13 WRITE(6,9) IERR2                                                     LEVE0060
   14 CONTINUE                                                             LEVE0061
      M=M3                                                                 LEVE0062
      DO 8 L=1,M                                                           LEVE0063
      IF (IE.NE.1) GO TO 8                                                 LEVE0064
      TP(M-L+1,2,I)=SNGL(U(4,L)**2)                                        LEVE0065
      TS(M-L+1,2,I)=SNGL(U(1,L)**2+U(2,L)**2+U(3,L)**2+U(6,L)**2)          LEVE0066
    8 TE(M-L+1,2,I)=D(L)                                                   LEVE0067
10    CONTINUE                                                             LEVE0068
C     SET UP TERM VALUES AND DIFFERENCES TO COMPARE WITH INPUT DATA.       LEVE0069
C     ON LAST PASS, LEVEL IS CALLED ONLY WITH IE=1.                        LEVE0070
      IF (IE.NE.1) GO TO 1001                                              LEVE0071
      DO 1000 N=1,M5                                                       LEVE0072
```

```
      DO 1010 L=1,M2                                                    LEVE0073
 1010 TERM(N,L,1)=TE(L,1,N)                                             LEVE0074
      DO 1020 L=1,M3                                                    LEVE0075
 1020 TERM(N,L,2)=TE(L,2,N)                                             LEVE0076
 1000 CONTINUE                                                          LEVE0077
 1001 CONTINUE                                                          LEVE0078
      M=MMM                                                             LEVE0079
      DO 50 N=1,NDATA                                                   LEVE0080
      DO 40 I=1,6                                                       LEVE0081
40    NQ(I)=NUM(I,N)                                                    LEVE0082
C     SECOND STATE TERM VALUE SUBTRACTED FROM FIRST.                    LEVE0083
      IF (NQ(2).EQ.0) TOP=0.0D0                                         LEVE0084
      IF (NQ(5).EQ.0) BOT=0.0D0                                         LEVE0085
      IF (NQ(2).NE.0) TOP=TE(NQ(2),NQ(3),NQ(1)+1)                       LEVE0086
      IF (NQ(5).NE.0) BOT=TE(NQ(5),NQ(6),NQ(4)+1)                       LEVE0087
50    GE(N,IE)=TOP-BOT                                                  LEVE0088
      RETURN                                                            LEVE0089
      END                                                               LEVE0090
```

```
      SUBROUTINE SETUP (P,R,PARITY)                                    SETU0001
C        SETUP FOR BAO * STATES                                        SETU0002
      DOUBLE PRECISION P(75),R(26)                                     SETU0003
      R(1)=(1.0D0+PARITY)/2.0D0                                        SETU0004
      RETURN                                                           SETU0005
      END                                                              SETU0006
```

```
      SUBROUTINE MATRIX (R,P,X,H)                                       MATR0001
C        MATRIX FOR BAO * STATES                                        MATR0002
      DOUBLE PRECISION R(26),P(75),H(9,9),XI,X                          MATR0003
      DO 10 I=1,9                                                       MATR0004
      DO 10 J=1,9                                                       MATR0005
   10 H(I,J)=0.0D0                                                      MATR0006
      XI=.1D0                                                           MATR0007
      DO 20 I=1,9                                                       MATR0008
      H(I,I)=XI                                                         MATR0009
   20 XI=XI+.1D0                                                        MATR0010
    1 H(1,1)=P(1)+X*(P(2)+X*(P(4)*X-P(3)))                              MATR0011
      H(1,2)=P(5)+P(26)*DSQRT(X)                                        MATR0012
      H(2,1)=H(1,2)                                                     MATR0013
      H(2,2)=P(6)+X*(P(7)-P(8)*X)                                       MATR0014
      H(3,3)=P(9)+X*(P(10)-P(11)*X)                                     MATR0015
      H(4,4)=P(13)+X*(P(14)-P(15)*X)                                    MATR0016
      H(1,3)=P(12)+P(27)*DSQRT(X)                                       MATR0017
      H(3,1)=H(1,3)                                                     MATR0018
      H(1,4)=P(16)                                                      MATR0019
      H(4,1)=H(1,4)                                                     MATR0020
      H(5,5)=P(17)+X*(P(18)-P(19)*X)                                    MATR0021
      H(1,5)=P(20)                                                      MATR0022
      H(5,1)=H(1,5)                                                     MATR0023
      H(6,6)=P(21)+X*(P(22)-P(23)*X)                                    MATR0024
      H(1,6)=P(24)                                                      MATR0025
      H(6,1)=H(1,6)                                                     MATR0026
      H(2,3)=P(25)                                                      MATR0027
      H(3,2)=H(2,3)                                                     MATR0028
      H(2,4)=P(28)                                                      MATR0029
      H(4,2)=H(2,4)                                                     MATR0030
      RETURN                                                            MATR0031
      END                                                               MATR0032
```

Parameter List for Doublet Fitter

No.	Name	Physical Origin
1	E1S	$^2\Sigma^+(1)$ energy
2	B1S	$^2\Sigma^+(1)$ rotational constant
3	D1S	$^2\Sigma^+(1)$ centrifugal distortion
4	GAM1S	$^2\Sigma^+(1)$ spin-rotation
5	ETA12	$^2\Sigma^+(1)\sim^2\Pi(1)$ rotation-electronic interaction
6	XI13	$^2\Sigma^+(1)\sim^2\Pi(1)$ spin-orbit interaction
7	C14	$^2\Sigma^+(1)\sim^2\Sigma^+(2)$ homogeneous interaction
8	ETA15	$^2\Sigma^+(1)\sim^2\Pi(2)$ rotation-electronic interaction
9	XI16	$^2\Sigma^+(1)\sim^2\Pi(2)$ spin-orbit interaction
10	E1P	$^2\Pi(1)$ energy
11	B1P	$^2\Pi(1)$ rotational constant
12	A1P	$^2\Pi(1)$ spin-orbit constant
13	GAM1P	$^2\Pi(1)$ spin-rotation
14	Q1P+	$^2\Pi(1)$ Λ-doubling (Σ^+)
15	D1P	$^2\Pi(1)$ centrifugal distortion
16	AJV1P	$^2\Pi(1)$ spin-orbit centrifugal distortion
17	AVO1P	$^2\Pi(1)$ second order spin-orbit
18	P1P+	$^2\Pi(1)$ Λ-doubling (Σ^+)
19	ETA24	$^2\Sigma^+(2)\sim^2\Pi(1)$ rotation-electronic interaction
20	H1P	$^2\Pi(1)$ third order centrifugal distortion

Parameter List for Doublet Fitter (cont.)

No.	Name	Physical Origin
21	H2P	$^2\Pi(2)$ third order centrifugal distortion
22	O1P	$^2\Pi(1)$ second order energy correction
23	XI34	$^2\Sigma^+(2) \sim ^2\Pi(1)$ spin-orbit interaction
24	H1S	$^2\Sigma^+(1)$ third order centrifugal distortion
25	H2S	$^2\Sigma^+(2)$ third order centrifugal distortion
26	E2S	$^2\Sigma^+(2)$ energy
27	B2S	$^2\Sigma^+(2)$ rotational constant
28	D2S	$^2\Sigma^+(2)$ centrifugal distortion
29	GAM2S	$^2\Sigma^+(2)$ spin-rotation
30	ETA45	$^2\Sigma^+(2) \sim ^2\Pi(2)$ rotation-electronic interaction
31	XI46	$^2\Sigma^+(2) \sim ^2\Pi(2)$ spin-orbit interaction
3]	A2P	$^2\Pi(2)$ spin-orbit constant
33	GAM2P	$^2\Pi(2)$ spin-rotation
34	Q2P+	$^2\Pi(2)$ Λ-doubling (Σ^+)
35	D2P	$^2\Pi(2)$ centrifugal distortion
36	AJV2P	$^2\Pi(2)$ spin-orbit centrifugal distortion
37	AVO2P	$^2\Pi(2)$ second order spin-orbit
38	P2P+	$^2\Pi(2)$ Λ-doubling (Σ^+)
39	O2P	$^2\Pi(2)$ second order energy correction

Parameter List for Doublet Fitter (cont.)

No.	Name	Physical Origin
40	E2P	$^2\Pi(2)$ energy
41	B2P	$^2\Pi(2)$ rotational constant
42	Q1P-	$^2\Pi(1)\Lambda$-doubling (Σ^-)
43	P1P-	$^2\Pi(1)\Lambda$-doubling (Σ^-)
44	Q2P-	$^2\Pi(2)\Lambda$-doubling (Σ^-)
45	P2P	$^2\Pi(2)\Lambda$-doubling (Σ^-)
46	Q1S	$^2\Sigma^+(1)$ second-order rotational constant correction
47	P1S	$^2\Sigma^+(1)$ second-order spin-rotation correction
48	O1S	$^2\Sigma^+(1)$ second-order energy correction
49	Q2S	$^2\Sigma^+(2)$ second-order rotational constant correction
50	P2S	$^2\Sigma^+(2)$ second-order spin-rotation correction
51	O2S	$^2\Sigma^+(2)$ second-order energy correction
52	GAMJ1S	$^2\Sigma^+(1)$ spin-rotation centrifugal distortion
53	GAMJ2S	$^2\Sigma^+(2)$ spin-rotation centrifugal distortion
54	ETA17	$^2\Sigma^+(1)\sim^2\Pi(3)$ rotation-electronic interaction
55	XI18	$^2\Sigma^+(1)\sim^2\Pi(3)$ spin-orbit interaction
56	E3P	$^2\Pi(3)$ energy
57	B3P	$^2\Pi(3)$ rotational constant
58	A3P	$^2\Pi(3)$ spin-orbit constant

Parameter List for Doublet Fitter (cont.)

No.	Name	Physical Origin
59	GAM3P	$^2\Pi(3)$ spin-rotation constant
60	Q3P+	$^2\Pi(3)$ Λ-doubling (Σ^+)
61	D3P	$^2\Pi(3)$ centrifugal distortion
62	AJV3P	$^2\Pi(3)$ spin-orbit centrifugal distortion
63	AVO3P	$^2\Pi(3)$ second-order spin-orbit
64	Q3P-	$^2\Pi(3)$ Λ-doubling (Σ^-)
65	H3P	$^2\Pi(3)$ third order centrifugal distortion
66	P3P+	$^2\Pi(3)$ Λ-doubling (Σ^+)
67	P3P-	$^2\Pi(3)$ Λ-doubling (Σ^-)
68	ETA48	$^2\Sigma^+(2)\sim^2\Pi(3)$ rotation-electronic interaction
69	O3P	$^2\Pi(3)$ second-order energy correction
70	XI48	$^2\Sigma^+(2)\sim^2\Pi(3)$ spin-orbit interaction

```
      SUBROUTINE NAMEIT (NAM,M)                                          NAME0001
C  THIS SUBROUTINE GOES WITH DOUBLET FITTER                              NAME0002
      REAL*8 NAM(M)                                                      NAME0003
      REAL*8 NAMES(70)/3HF1S,3HB1S,3HD1S,5HGAM1S,5HETA12,4HXI13,3HC14,5H NAME0004
     1ETA15,4HXI16,3HE1P,3HB1P,3HA1P,5HGAM1P,4HQ1P+,3HD1P,5HAJV1P,5HAVO1 NAME0005
     2P,4HP1P+,5HETA24,3HH1P,3HH2P,3HO1P,4HXI34,3HH1S,3HH2S,3HE2S,3HB2S, NAME0006
     33HD2S,5HGAM2S,5HETA45,4HXI46,3HA2P,5HGAM2P,4HQ2P+,3HD2P,5HAJV2P,5H NAME0007
     4AVO2P,4HP2P+,3HO2P,3HE2P,3HB2P,4HQ1P-,4HP1P-,4HQ2P-,4HP2P-,3HQ1S,3 NAME0008
     5HP1S,3HO1S,3HQ2S,3HP2S,3HO2S,6HGAMJ1S,6HGAMJ2S,5HETA17,4HXI18,3HE3 NAME0009
     6P,3HB3P,3HA3P,5HGAM3P,4HQ3P+,3HD3P,5HAJV3P,5HAVO3P,4HQ3P-,3HH3P,4H NAME0010
     7P3P+,4HP3P-,5HETA48,3HO3P,4HXI48/                                  NAME0011
      DO 10 I=71,M                                                       NAME0012
   10 NAM(I)=0.0D0                                                       NAME0013
      DO 20 J=1,70                                                       NAME0014
   20 NAM(J)=NAMES(J)                                                    NAME0015
      RETURN                                                             NAME0016
      END                                                                NAME0017
```

```
      SUBROUTINE LEVEL(IE,NDATA)                                        LEVE0001
      IMPLICIT REAL*8 (A-H,O-Z)                                         LEVE0002
      REAL*4 SIZE,TP,TS,SNGL,FLOAT                                      LEVE0003
      DOUBLE PRECISION DBLE                                             LEVE0004
      DIMENSION TP(9,2,150),TS(9,2,150)                                 LEVE0005
      DIMENSION TE(9,2,150),GE(600,3),P(75),S(26),T(26),      H(9,9)    LEVE0006
      DIMENSION D(9),E(9)                                               LEVE0007
      DIMENSION NQ(6),NUM(6,600),U(9,9)                                 LEVE0008
      DIMENSION TERM(150,9,2)                                           LEVE0009
      COMMON P,GE,NUM                                                   LEVE0010
      COMMON/BLK2/ TERM,JMAX,M1,MAXP,MAXM                               LEVE0011
      COMMON/BLK3/TP,TS                                                 LEVE0012
C  THIS SUBROUTINE GOES WITH DOUBLET FITTER                             LEVE0013
C     LEVEL FOR MAIN. M IS DIMENSION OF HAMILTONIAN.                    LEVE0014
C     MAXP IS MAXIMUM PLUS PARITY RANK, MAXM IS MAXIMUM MINUS RANK.     LEVE0015
C     TE(RANK,PARITY,J) ARE TERM ENERGIES.. 1ST DIM OF TE AGREES WITH M,LEVE0016
C     3ND WITH M1. 2ND INDEX, 1 IS PLUS AND 2 IS MINUS PARITY.          LEVE0017
C     DEFINE S AND T FOR TWO PARITIES TO BE USED AS R IN MATRIX.        LEVE0018
      MMM=M                                                             LEVE0019
      CALL SETUP(P,S,1.0)                                               LEVE0020
      CALL SETUP(P,T,-1.0)                                              LEVE0021
C     CALCULATE ENERGY FOR ALL RANKS OF EACH J.                         LEVE0022
      DO 10 I=1,JMAX                                                    LEVE0023
      X=FLOAT(I)                                                        LEVE0024
C E PARITY                                                              LEVE0025
      CALL MATRIX(S,P,X,H)                                              LEVE0026
      DO 55 L=1,9                                                       LEVE0027
      DO 5 K=1,9                                                        LEVE0028
    5 U(L,K)=0.0D0                                                      LEVE0029
   55 U(L,L)=1.0D0                                                      LEVE0030
C     DIAGONALIZE ONLY NONZERO PART OF H FOR PLUS PARITY.               LEVE0031
      M2=MAXP                                                           LEVE0032
      CALL TRED2(M2,9,H,D,E,U)                                          LEVE0033
      CALL TQL2(M2,9,D,E,U,IERR2)                                       LEVE0034
      IF (IERR2.NE.0) GO TO 11                                          LEVE0035
      GO TO 12                                                          LEVE0036
```

```
   11 WRITE(6,9) IERR2                                                                  LEVE0037
    9 FORMAT(' ERROR IN HAMILTONIAN DIAGONALIZATION, IERR=',I2)                         LEVE0038
   12 CONTINUE                                                                          LEVE0039
      M=M2                                                                              LEVE0040
      DO 6 L=1,M                                                                        LEVE0041
      IF(IE.NE.1) GO TO 6                                                               LEVE0042
      TP(M-L+1,1,I)=SNGL(U(2,L)**2+U(7,L)**2+U(5,L)**2)                                 LEVE0043
      TS(M-L+1,1,I)=SNGL(U(1,L)**2+U(4,L)**2)                                           LEVE0044
6     TE(M-L+1,1,I)=D(L)                                                                LEVE0045
C F PARITY                                                                              LEVE0046
      CALL MATRIX(T,P,X,H)                                                              LEVE0047
      DO 77 L=1,9                                                                       LEVE0048
      DO 7 K=1,9                                                                        LEVE0049
    7 U(L,K)=0.0D0                                                                      LEVE0050
   77 U(L,L)=1.0D0                                                                      LEVE0051
      M3=MAXM                                                                           LEVE0052
      CALL TRED2(M3,9,H,D,E,U)                                                          LEVE0053
      CALL TQL2(M3,9,D,E,U,IERR2)                                                       LEVE0054
      IF (IERR2.NE.0) GO TO 13                                                          LEVE0055
      GO TO 14                                                                          LEVE0056
   13 WRITE(6,9) IERR2                                                                  LEVE0057
   14 CONTINUE                                                                          LEVE0058
      M=M3                                                                              LEVE0059
      DO 8 L=1,M                                                                        LEVE0060
      IF(IE.NE.1) GO TO 8                                                               LEVE0061
      TP(M-L+1,2,I)=SNGL(U(2,L)**2+U(7,L)**2+U(5,L)**2)                                 LEVE0062
      TS(M-L+1,2,I)=SNGL(U(1,L)**2+U(4,L)**2)                                           LEVE0063
8     TE(M-L+1,2,I)=D(L)                                                                LEVE0064
10    CONTINUE                                                                          LEVE0065
C     SET UP TERM VALUES AND DIFFERENCES TO COMPARE WITH INPUT DATA.                    LEVE0066
C     ON LAST PASS, LEVEL IS CALLED ONLY WITH IE=1.                                     LEVE0067
      IF (IE.NE.1) GO TO 1001                                                           LEVE0068
      DO 1000 N=1,JMAX                                                                  LEVE0069
      DO 1010 L=1,M2                                                                    LEVE0070
 1010 TERM(N,L,1)=TE(L,1,N)                                                             LEVE0071
      DO 1020 L=1,M3                                                                    LEVE0072
```

```
 1020 TERM(N,L,2)=TE(L,2,N)                                              LEVE0073
 1000 CONTINUE                                                           LEVE0074
 1001 CONTINUE                                                           LEVE0075
      M=MMM                                                              LEVE0076
      DO 50 N=1,NDATA                                                    LEVE0077
      DO 40 L=1,6                                                        LEVE0078
40    NQ(L)=NUM(L,N)                                                     LEVE0079
C     SECOND STATE TERM VALUE SUBTRACTED FROM FIRST.                     LEVE0080
      IF (NQ(2).EQ.0) TOP=0.0D0                                          LEVE0081
      IF (NQ(5).EQ.0) BOT=0.0D0                                          LEVE0082
      IF (NQ(2).NE.0) TOP=TE(NQ(2),NQ(3),NQ(1))                          LEVE0083
      IF (NQ(5).NE.0) BOT=TE(NQ(5),NQ(6),NQ(4))                          LEVE0084
50    GE(N,IE)=TOP-BOT                                                   LEVE0085
      RETURN                                                             LEVE0086
      END                                                                LEVE0087
```

```
C  THIS SUBROUTINE GOES WITH DOUBLET FITTER                                    SETU0001
      DOUBLE PRECISION R,P,PAR                                                 SETU0002
      DIMENSION P(75),R(26)                                                    SETU0003
      IF (PARITY.LT.0) PAR=-1.0D0                                              SETU0004
      IF (PARITY.GT.0) PAR=1.0D0                                               SETU0005
C MINUS PARITY IS F                                                            SETU0006
C PLUS PARITY IS E                                                             SETU0007
      R(1)=P(1)-0.5D0*P(4)                                                     SETU0008
      R(2)=P(6)+P(5)                                                           SETU0009
      R(3)=P(9)+P(8)                                                           SETU0010
      R(4)=P(10)-2.0D0*P(11)+0.5D0*(P(12)-P(13))-0.5D0*P(14)+P(15)-2.0D0       SETU0011
     1*P(16)+0.25D0*P(17)                                                      SETU0012
      R(5)=0.5D0*P(13)-P(11)-0.25D0*P(18)-2.0D0*P(15)-0.5D0*P(14)              SETU0013
      R(6)=P(10)-0.5D0*P(12)-0.5D0*P(13)+P(22)+0.5D0*P(18)+0.25D0*P(17)+       SETU0014
     1P(15)                                                                    SETU0015
      R(7)=P(11)-P(16)-P(15)                                                   SETU0016
      R(8)=P(23)+P(19)                                                         SETU0017
      R(9)=P(26)-0.5D0*P(29)                                                   SETU0018
      P(10)=P(31)+P(30)                                                        SETU0019
      R(11)=P(40)-2.0D0*P(41)+0.5D0*(P(32)-P(33)-P(34))+P(35)-2.0D0*P(36       SETU0020
     1)+0.25D0*P(37)                                                           SETU0021
      R(12)=P(41)+0.5D0*P(34)-P(35)+P(36)                                      SETU0022
      R(13)=0.5D0*P(33)-P(41)-0.25D0*P(38)-0.5D0*P(34)-2.0D0*P(35)             SETU0023
      R(14)=P(40)-0.5D0*P(32)-0.5D0*P(33)+P(39)+0.5D0*P(38)+P(35)+0.25*P       SETU0024
     1(37)                                                                     SETU0025
      R(15)=P(11)+0.5D0*P(14)-P(15)+P(16)                                      SETU0026
      R(16)=P(41)-P(35)-P(36)                                                  SETU0027
      R(17)=1.0D0+PAR                                                          SETU0028
      R(18)=P(56)-2.0D0*P(57)+0.5D0*(P(58)-P(59))-0.5D0*P(60)+P(61)-2.0D       SETU0029
     10*P(62)+0.25D0*P(63)                                                     SETU0030
      R(19)=P(57)+0.5D0*P(60)-P(61)+P(62)                                      SETU0031
      P(20)=0.5D0*P(59)-P(57)-0.25D0*P(66)-2.0D0*P(61)-0.5D0*P(60)             SETU0032
      R(21)=P(56)-0.5D0*P(58)-0.5D0*P(59)+P(69)+0.5D0*P(66)+P(61)+0.25D0       SETU0033
     1*P(63)                                                                   SETU0034
      R(22)=P(57)-P(62)-P(61)                                                  SETU0035
      RETURN                                                                   SETU0036
```

END

SETU0037

```
      SUBROUTINE MATRIX(R,P,X,H)                                          MATR0001
C   THIS SUBROUTINE GOES WITH DOUBLET FITTER                              MATR0002
C THIS ROUTINE TREATS TWO 2SIG+ STATES AND TWO 2PI STATES                 MATR0003
C 1 IS INDEX FOR FIRST 2SIG+                                              MATR0004
C 2 IS INDEX FOR FIRST 2PI 3/2                                            MATR0005
C 3 IS INDEX FOR FIRST 2PI1/2                                             MATR0006
C 4 IS INDEX FOR SECOND 2SIG+                                             MATR0007
C 5 IS INDEX FOR SECOND 2PI3/2                                            MATR0008
C 6 IS INDEX FOR SECOND 2PI1/2                                            MATR0009
      DOUBLE PRECISION R(26),P(75),X,H(9,9),XA,XB,XC,DSQRT,XD,XE,XF       MATR0010
      PAR=R(17)-1.0D0                                                     MATR0011
      XA=X*(X-1.0D0)                                                      MATR0012
      XB=(X-(PAR*1.0D0))*X                                                MATR0013
      XB=XB**2                                                            MATR0014
      XC=(X**2-2.0D0)                                                     MATR0015
      XD=(X**2-1.0D0)                                                     MATR0016
      XE=1.0D0-PAR*X                                                      MATR0017
      XF=1.0D0+PAR*X                                                      MATR0018
      DO 10 I=1,9                                                         MATR0019
      DO 10 J=1,9                                                         MATR0020
   10 H(I,J)=0.0D0                                                        MATR0021
      H(1,1)=0.1D0                                                        MATR0022
      H(2,2)=0.2D0                                                        MATR0023
      H(3,3)=0.3D0                                                        MATR0024
      H(4,4)=0.4D0                                                        MATR0025
      H(5,5)=0.5D0                                                        MATR0026
      H(6,6)=0.6D0                                                        MATR0027
      H(7,7)=0.7D0                                                        MATR0028
      H(8,8)=0.8D0                                                        MATR0029
      H(9,9)=0.9D0                                                        MATR0030
      IF (X.LT.1.5D0) GO TO 49                                            MATR0031
      H(1,2)=0.0-P(5)*DSQRT(XD)                                           MATR0032
      H(2,1)=H(1,2)                                                       MATR0033
      H(1,5)=0.0-P(8)*DSQRT(XD)                                           MATR0034
      H(5,1)=H(1,5)                                                       MATR0035
      H(2,2)=R(4)+R(15)*(X**2)-P(15)*(XC**2)                              MATR0036
```

```
      H(2,2)=H(2,2)+0.5D0*P(42)*XD                                                    MATR0037
      H(2,2)=H(2,2)+P(20)*(XC**3+3.*X**4-7.*X**2+4.)                                  MATR0038
      H(2,3)=DSQRT(XD)*(R(5)+(0.5D0*PAR*P(14)*X)+2.0D0*P(15)*(X**2))                  MATR0039
      H(2,3)=H(2,3)-P(20)*(DSQRT(XD)*(3.0*X**4-5.0*X**2+3.0))                         MATR0040
      H(2,3)=H(2,3)-0.25D0*P(43)*DSQRT(XD)-0.5D0*P(42)*XF*DSQRT(XD)                   MATR0041
      H(3,2)=H(2,3)                                                                   MATR0042
      H(2,4)=0.0-P(19)*DSQRT(XD)                                                      MATR0043
      H(4,2)=H(2,4)                                                                   MATR0044
      H(4,5)=0.0-P(30)*DSQRT(XD)                                                      MATR0045
      H(5,4)=H(4,5)                                                                   MATR0046
      H(5,5)=R(11)+R(12)*(X**2)-P(35)*(XC**2)                                         MATR0047
      H(5,5)=H(5,5)+0.5D0*P(44)*XD                                                    MATR0048
      H(5,5)=H(5,5)+P(21)*(XC**3+3.*X**4-7.*X**2+4.)                                  MATR0049
      H(5,6)=DSQRT(XD)*(R(13)+(0.5D0*PAR*P(34)*X)+2.0D0*P(35)*(X**2))                 MATR0050
      H(5,6)=H(5,6)-((0.25D0*P(45)+0.5D0*P(44)*XF)*DSQRT(XD))                         MATR0051
      H(5,6)=H(5,6)-P(21)*(DSQRT(XD)*(3.0*X**4-5.0*X**2+3.0))                         MATR0052
      H(6,5)=H(5,6)                                                                   MATR0053
      H(1,7)=0.0-P(54)*DSQRT(XD)                                                      MATR0054
      H(7,1)=H(1,7)                                                                   MATR0055
      H(7,7)=R(18)+R(19)*X**2-P(61)*XC**2                                             MATR0056
      H(7,7)=H(7,7)+0.5D0*P(64)*XD                                                    MATR0057
      H(7,7)=H(7,7)+P(65)*(XC**3+3.*X**4-7.*X**2+4.)                                  MATR0058
      H(7,8)=DSQRT(XD)*(R(20)+PAR*P(60)*X+2.0D0*P(61)*X**2)                           MATR0059
      H(7,8)=H(7,8)-0.25D0*P(67)*DSQRT(XD)-0.5D0*P(64)*XF*DSQRT(XD)                   MATR0060
      H(7,8)=H(7,8)-P(65)*(DSQRT(XD)*(3.0D0*X**4-5.0D0*X**2+3.0D0))                   MATR0061
      H(8,7)=H(7,8)                                                                   MATR0062
      H(4,7)=0.0-P(68)*DSQRT(XD)                                                      MATR0063
      H(7,4)=H(4,7)                                                                   MATR0064
49    H(1,1)=R(1)+P(2)*DSQRT(XB)-P(3)*XB+(PAR*0.5D0*P(4)*X)                           MATR0065
      H(1,1)=H(1,1)+0.5D0*P(46)*(XD+XE**2)+0.5D0*P(47)*XE+P(48)                       MATR0066
      H(1,1)=H(1,1)+P(24)*(DSQRT(XB))**3                                              MATR0067
      H(1,1)=H(1,1)-0.5D0*P(52)*(X-0.5D0)*(X+0.5D0)*XE                                MATR0068
      H(1,3)=R(2)-PAR*P(5)*X                                                          MATR0069
      H(3,1)=H(1,3)                                                                   MATR0070
      H(1,4)=P(7)                                                                     MATR0071
      H(4,1)=P(7)                                                                     MATR0072
```

```
 H(1,6)=R(3)-PAR*P(8)*X                                                  MATR0073
 H(6,1)=H(1,6)                                                           MATR0074
 H(3,3)=R(6)+R(7)*(X**2)-(PAR*0.5D0*P(18)*X)+0.5D0*P(14)*(XE**2)-P(      MATR0075
1115)*(X**4)                                                             MATR0076
 H(3,3)=H(3,3)+0.5D0*P(42)*(XF**2)+0.5D0*P(43)*XF                        MATR0077
 H(3,3)=H(3,3)+P(20)*(X**6+3.*X**4-5.*X**2+2.)                           MATR0078
 H(3,4)=R(8)-PAR*P(19)*X                                                 MATR0079
 H(4,3)=H(3,4)                                                           MATR0080
 H(4,4)=R(9)+P(27)*DSQRT(XB)-P(28)*XB+PAR*0.5D0*P(29)*X                  MATR0081
 H(4,4)=H(4,4)+0.5D0*P(49)*(XD+XE**2)+0.5D0*P(50)*XE+P(51)               MATR0082
 H(4,4)=H(4,4)+P(25)*(DSQRT(XB))**3                                      MATR0083
 H(4,4)=H(4,4)-0.5D0*P(53)*(X-0.5D0)*(X+0.5D0)*XE                        MATR0084
 H(4,6)=R(10)-PAR*P(30)*X                                                MATR0085
 H(6,4)=H(4,6)                                                           MATR0086
 H(6,6)=R(14)+P(16)*(X**2)-PAR*0.5D0*P(38)*X+0.5D0*P(34)*(XE**2)-P(      MATR0087
135)*(X**4)                                                              MATR0088
 H(6,6)=H(6,6)+0.5D0*P(44)*(XF**2)+0.5D0*P(45)*XF                        MATR0089
 H(6,6)=H(6,6)+P(21)*(X**6+3.*X**4-5.*X**2+2.)                           MATR0090
 H(8,8)=R(21)+X**2*R(22)-PAR*0.5D0*P(66)*X+0.5D0*P(60)*XE**2-P(61)*      MATR0091
1X**4                                                                    MATR0092
 H(8,8)=H(8,8)+0.5D0*P(64)*XF**2+0.5D0*P(67)*XF                          MATR0093
 H(8,8)=H(8,8)+P(65)*(X**6+3.*X**4-5.*X**2+2.)                           MATR0094
 H(4,8)=P(70)+P(68)*XE                                                   MATR0095
 H(8,4)=H(4,8)                                                           MATR0096
 H(1,8)=P(55)+P(54)*XE                                                   MATR0097
 H(8,1)=H(1,8)                                                           MATR0098
 RETURN                                                                  MATR0099
 END                                                                     MATR0100
```

BAO A1S V=0 DATA FROM LAGERQVIST ET AL, MODR AND OODP

INITIAL PARAMETERS

E1S	0.16722180D+05	CM
E1P	0.17515000D+05	CM
E3P	0.17398000D+05	CM
BR1S	0.25783000D+00	CM
BR1P	0.22370000D+00	CM
BR3P	0.22370000D+00	CM
DR1S	0.27344698D-06	CM
DR1P	0.84000000D-02	MC
DR3P	0.84000000D-02	MC
A3P	-0.10000000D+03	CM
AJ3P	0.0	MC
C3P	0.0	MC
GAM3P	0.0	MC
C3PD	0.0	MC
QVP	0.0	MC
PVP	0.0	MC
B10+	0.50170000D-01	CM
A01+	-0.72886000D+01	CM
A11	-0.13000000D+03	CM
E1S-	0.0	MC
BR1S-	0.0	MC
DR1S-	0.0	MC
H1S	0.0	MC
H1P	0.0	MC
H1S-	0.0	MC
QV1P	0.0	MC
E3SGM+	0.0	MC
B3SGM+	0.0	MC
D3SGM+	0.0	MC
C3SGM+	0.0	MC
G3SGM+	0.0	MC
A27	0.0	MC
ALPHA0	0.0	MC
BETA0	0.0	MC
E2S	0.0	MC
BR2S	0.0	MC
DR2S	0.0	MC
2B10+	0.0	MC
2A01+	0.0	MC
B10+J	0.0	MC
E3P2	0.0	MC
B3P2	0.0	MC
D3P2	0.0	MC
A3P2	0.0	MC
A01+2	0.0	MC
0	0.0	MC
0	0.0	MC
0	0.0	MC
0	0.0	MC
0	0.0	MC
0	0.0	MC
0	0.0	MC
0	0.0	MC
0	0.0	MC
0	0.0	MC

0	0.0	MC
0	0.0	MC
0	0.0	MC
0	0.0	MC
0	0.0	MC
0	0.0	MC
0	0.0	MC
0	0.0	MC
0	0.0	MC
0	0.0	MC
0	0.0	MC
0	0.0	MC
0	0.0	MC
0	0.0	MC
0	0.0	MC
0	0.0	MC
0	0.0	MC
0	0.0	MC
0	0.0	MC
0	0.0	MC

THE LSQ FIT

VARIANCE OF THE FIT 0.1454497D+02

COSINE: 0.7244585E+00 LAMBDA: 0.100E-01
VARB: 0.7661504D-01 STEP: 0.1000000E+01

AFTER LSQ PASS 1 THE FITTED VALUES ARE

1	E1S	0.16722370D+05	CM
2	BR1S	0.25783680D+00	CM
3	DR1S	0.27426991D-06	CM

VARIANCE OF THE FIT 0.7661504D-01

COSINE: 0.8458719E+00 LAMBDA: 0.100E-02
VARB: 0.7396077D-01 STEP: 0.1000000E+01

AFTER LSQ PASS 2 THE FITTED VALUES ARE

1	E1S	0.16722373D+05	CM
2	BR1S	0.25783692D+00	CM
3	DR1S	0.27435127D-06	CM

VARIANCE OF THE FIT 0.7396077D-01

COSINE: 0.4967288E+00 LAMBDA: 0.100E-03
VARB: 0.7396072D-01 STEP: 0.1000000E+01

CONVERGENCE/VARIANCE

OUTPUT FROM LAST LSQ PASS

NUMBER	NAME	FINAL VALUE	STANDARD DEVIATION	
1	E1S	0.16722373D+05	0.2682E-02	CM
	E1P	0.17515000D+05		CM
	E3P	0.17388000D+05		CM
2	BR1S	0.25783692D+00	0.1492E-05	CM
	BR1P	0.22370000D+00		CM
	BR3P	0.22370000D+00		CM
3	DR1S	0.27435127D-06	0.1653E-09	CM
	DR1P	0.84000000D-02		MC
	DR3P	0.84000000D-02		MC
	A3P	-0.10000000D+03		CM
	AJ3P	0.0		MC
	C3P	0.0		MC
	GAM3P	0.0		MC
	C3PD	0.0		MC
	QVP	0.0		MC
	PVP	0.0		MC
	B10+	0.50170000D-01		CM
	A01+	-0.72886000D+01		CM
	A11	-0.10000000D+03		CM
	E1S-	0.0		MC
	BR1S-	0.0		MC
	DR1S-	0.0		MC
	H1S	0.0		MC
	H1P	0.0		MC
	H1S-	0.0		MC
	QV1P	0.0		MC
	B3SGM+	0.0		MC
	B3SGM+	0.0		MC
	D3SGM+	0.0		MC
	C3SGM+	0.0		MC
	G3SGM+	0.0		MC
	A27	0.0		MC
	ALPHA0	0.0		MC
	BETA0	0.0		MC
	E2S	0.0		MC
	BR2S	0.0		MC
	DR2S	0.0		MC
	2B10+	0.0		MC
	2A01+	0.0		MC
	E10+J	0.0		MC
	E3P2	0.0		MC
	B3P2	0.0		MC
	D3P2	0.0		MC
	A3P2	0.0		MC
	A01+2	0.0		MC
	C	0.0		MC
	C	0.0		MC
	O	0.0		MC
	C	0.0		MC
	C	0.0		MC
	O	0.0		MC
	O	0.0		MC
	O	0.0		MC

0	0.0	MC
0	0.0	MC
0	0.0	MC
0	0.0	MC
0	0.0	MC
0	0.0	MC
0	0.0	MC
0	0.0	MC
0	0.0	MC
0	0.0	MC
0	0.0	MC
0	0.0	MC
0	0.0	MC
0	0.0	MC
0	0.0	MC
0	0.0	MC
0	0.0	MC
0	0.0	MC
0	0.0	MC
0	0.0	MC
0	0.0	MC
0	0.0	MC

COVARIANCE MATRIX
ELEMENTS ARE ARRANGED BY PARAMETER NUMBERS

0.6467131330D+04	-0.2597771196D+01	-0.2175968152D-03
-0.2597771196D+01	0.2001581854D-02	0.2101545344D-06
-0.2175968152D-03	0.2101545344D-06	0.2456921758D-10

CORRELATION MATRIX
ELEMENTS ARE ARRANGED BY PARAMETER NUMBERS

0.1000000000D+01	-0.7220352147D+00	-0.5458848372D+00
-0.7220352147D+00	0.1000000000D+01	0.9476684543D+00
-0.5458848372D+00	0.9476684543D+00	0.1000000000D+01

EIGENVALUES OF SCALED CURVATURE MATRIX

PARAMETER	EIGENVALUE	SQRT	SCALE FACTOR
1	0.2475378E-01	0.1573334E+00	0.6270822D-02
2	0.4029179E+00	0.6347582E+00	0.2958189D+02
3	0.2572328E+01	0.1603848E+01	0.2204760D+06

EIGENVECTORS OF SCALED CURVATURE MATRIX
COLUMNS ARE IND COMBINATIONS IN THE ORDER OF EIGENVALUES ABOVE

E1S	0.2320	0.8227	-0.5314
BR1S	-0.7615	-0.2092	-0.6134
DR1S	-0.6158	0.5286	0.5842

NUMBER OF LSQ PASSES = 2

FIT TO EXPERIMENTAL POINTS

TRANSITION BETWEEN LEVELS 1 AND 2

J1	STATE1	PARITY1	J2	STATE2	PARITY2	EXPT	CALC	EXPT-CALC	EXPTL STD DEV	UNITS
3.0	5	E	2.0	5	E	46376.00000	46375.39655	0.60345	2.00000	MC
2.0	5	E				16723.75500	16723.78124	-0.02624	0.05400	CM
3.0	5	E				16725.29600	16725.32816	-0.03216	0.07400	CM
4.0	5	E				16727.34500	16727.39068	-0.04568	0.05800	CM
5.0	5	E				16729.92700	16729.96879	-0.04179	0.06500	CM
6.0	5	E				16733.03200	16733.06244	-0.03044	0.06500	CM
7.0	5	E				16736.68200	16736.67161	0.01039	0.06100	CM
8.0	5	E				16740.77900	16740.79623	-0.01723	0.05300	CM
9.0	5	E				16745.45600	16745.43627	0.01973	0.05200	CM
10.0	5	E				16750.60400	16750.59166	0.01234	0.05200	CM
11.0	5	E				16756.25200	16756.26233	-0.01033	0.05200	CM
12.0	5	E				16762.43600	16762.44822	-0.01222	0.05500	CM
13.0	5	E				16769.15500	16769.14923	0.00577	0.05400	CM
14.0	5	E				16776.36800	16776.36530	0.00270	0.05400	CM
15.0	5	E				16784.08400	16784.09632	-0.01232	0.05400	CM
16.0	5	E				16792.33000	16792.34219	-0.01219	0.05400	CM
17.0	5	E				16801.10200	16801.10282	-0.00082	0.05400	CM
18.0	5	E				16810.36900	16810.37809	-0.00908	0.05400	CM
19.0	5	E				16820.16900	16820.16787	0.00113	0.05400	CM
20.0	5	E				16830.46600	16830.47204	-0.00604	0.05200	CM
21.0	5	E				16841.29600	16841.29048	0.00552	0.05400	CM
22.0	5	E				16852.63200	16852.62304	0.00896	0.05400	CM
23.0	5	E				16864.48700	16864.46959	0.01741	0.05400	CM
24.0	5	E				16876.84500	16876.82995	0.01505	0.05400	CM
25.0	5	E				16889.71600	16889.70399	0.01201	0.05400	CM
26.0	5	E				16903.08500	16903.09153	-0.00653	0.05200	CM
27.0	5	E				16916.99300	16916.99240	0.00060	0.05400	CM
28.0	5	E				16931.40300	16931.40642	-0.00342	0.05400	CM
29.0	5	E				16946.33600	16946.33341	0.00259	0.05400	CM
30.0	5	E				16961.78500	16961.77318	0.01182	0.05400	CM
31.0	5	E				16977.73300	16977.72552	0.00748	0.05400	CM
32.0	5	E				16994.20400	16994.19025	0.01375	0.05400	CM
33.0	5	E				17011.17800	17011.16713	0.01087	0.05400	CM
34.0	5	E				17028.66600	17028.65596	0.01004	0.05400	CM
35.0	5	E				17046.66300	17046.65651	0.00649	0.05400	CM
36.0	5	E				17065.19400	17065.16855	0.02545	0.05400	CM
37.0	5	E				17084.21100	17084.19184	0.01916	0.05400	CM
38.0	5	E				17103.74500	17103.72614	0.01886	0.05400	CM
39.0	5	E				17123.78300	17123.77120	0.01180	0.05400	CM
40.0	5	E				17144.34200	17144.32676	0.01524	0.05400	CM
41.0	5	E				17165.39500	17165.39255	0.00245	0.05500	CM
42.0	5	E				17186.96000	17186.96830	-0.00830	0.05500	CM
43.0	5	E				17209.06000	17209.05375	0.00625	0.05400	CM
44.0	5	E				17231.66700	17231.64859	0.01841	0.05400	CM
45.0	5	E				17254.76500	17254.75255	0.01245	0.05400	CM
46.0	5	E				17278.38000	17278.36533	0.01467	0.05400	CM
47.0	5	E				17302.48800	17302.48661	0.00139	0.05400	CM
48.0	5	E				17327.12900	17327.11610	0.01290	0.05400	CM
49.0	5	E				17352.27200	17352.25346	0.01854	0.05400	CM
50.0	5	E				17377.90700	17377.89839	0.00861	0.05400	CM
51.0	5	E				17404.06400	17404.05055	0.01345	0.05400	CM
52.0	5	E				17430.71500	17430.70960	0.00540	0.05200	CM
53.0	5	E				17457.88800	17457.87520	0.01280	0.05200	CM
54.0	5	E				17485.54200	17485.54700	-0.00500	0.05200	CM
55.0	5	E				17513.74100	17513.72464	0.01636	0.05200	CM
56.0	5	E				17542.40300	17542.40776	-0.00476	0.05200	CM
57.0	5	E				17571.59100	17571.59598	-0.00498	0.05200	CM
58.0	5	E				17601.29200	17601.28894	0.00306	0.05200	CM

59.0	5	E
60.0	5	E
61.0	5	E
62.0	5	F
63.0	5	E
64.0	5	E
65.0	5	E
66.0	5	E
67.0	5	E
68.0	5	E
69.0	5	E
70.0	5	E
71.0	5	E
72.0	5	E
73.0	5	E
74.0	5	E
75.0	5	E
76.0	5	E
77.0	5	E
78.0	5	F
79.0	5	E
80.0	5	E
81.0	5	E
82.0	5	E
83.0	5	F
84.0	5	E
85.0	5	E
86.0	5	E
87.0	5	E
88.0	5	E
89.0	5	E
90.0	5	E
91.0	5	E
92.0	5	E
93.0	5	E
94.0	5	E
95.0	5	E
96.0	5	E
97.0	5	F
98.0	5	E
99.0	5	F

17631.48600	17631.48624	-0.00024	0.05200	CM
17662.17800	17662.18750	-0.00950	0.05200	CM
17693.38300	17693.39231	-0.00931	0.05200	CM
17725.08400	17725.10029	-0.01629	0.05200	CM
17757.31500	17757.31101	0.00399	0.05200	CM
17790.01300	17790.02406	-0.01106	0.05000	CM
17823.22800	17823.23901	-0.01101	0.05000	CM
17856.95800	17856.95544	0.00256	0.05000	CM
17891.16600	17891.17291	-0.00691	0.05000	CM
17925.86800	17925.89097	-0.02297	0.05000	CM
17961.09100	17961.10918	-0.01818	0.05000	CM
17996.80900	17996.82707	-0.01807	0.05000	CM
18033.03300	18033.04418	-0.01118	0.05000	CM
18069.74400	18069.76005	-0.01605	0.05000	CM
18106.95400	18106.97419	-0.02019	0.05000	CM
18144.69800	18144.68612	0.01188	0.05000	CM
18182.90300	18182.89534	0.00766	0.05000	CM
18221.61100	18221.60137	0.00963	0.05000	CM
18260.79500	18260.80370	-0.00870	0.05000	CM
18300.48400	18300.50181	-0.01781	0.05000	CM
18340.67100	18340.69519	-0.02419	0.05000	CM
18381.36500	18381.38331	-0.01831	0.05000	CM
18422.55800	18422.56564	-0.00764	0.05000	CM
18464.23400	18464.24164	-0.00764	0.05000	CM
18506.40100	18506.41077	-0.00977	0.05000	CM
18549.10300	18549.07247	0.03053	0.07800	CM
18592.21900	18592.22618	-0.00718	0.05000	CM
18635.88900	18635.87133	0.01767	0.05000	CM
18680.02600	18680.00736	0.01864	0.05000	CM
18724.65300	18724.63368	0.01932	0.05000	CM
18769.75000	18769.74970	0.00030	0.05000	CM
18815.35700	18815.35483	0.00217	0.05000	CM
18861.45600	18861.44846	0.00754	0.05000	CM
18908.02700	18908.02999	-0.00299	0.05000	CM
18955.09100	18955.09880	-0.00780	0.05000	CM
19002.64900	19002.65426	-0.00526	0.05000	CM
19050.68300	19050.69574	-0.01274	0.05000	CM
19099.25200	19099.22261	0.02939	0.05000	CM
19148.24100	19148.23420	0.00680	0.05000	CM
19197.73300	19197.72988	0.00312	0.05000	CM
19247.71200	19247.70897	0.00303	0.05000	CM

OBSERVED-CALCULATED

NO. OF POINTS ON ABSCISSA = 99
NO. OF INTERVALS ON ORDINATE = 118, INCREMENT = 0.600E-02

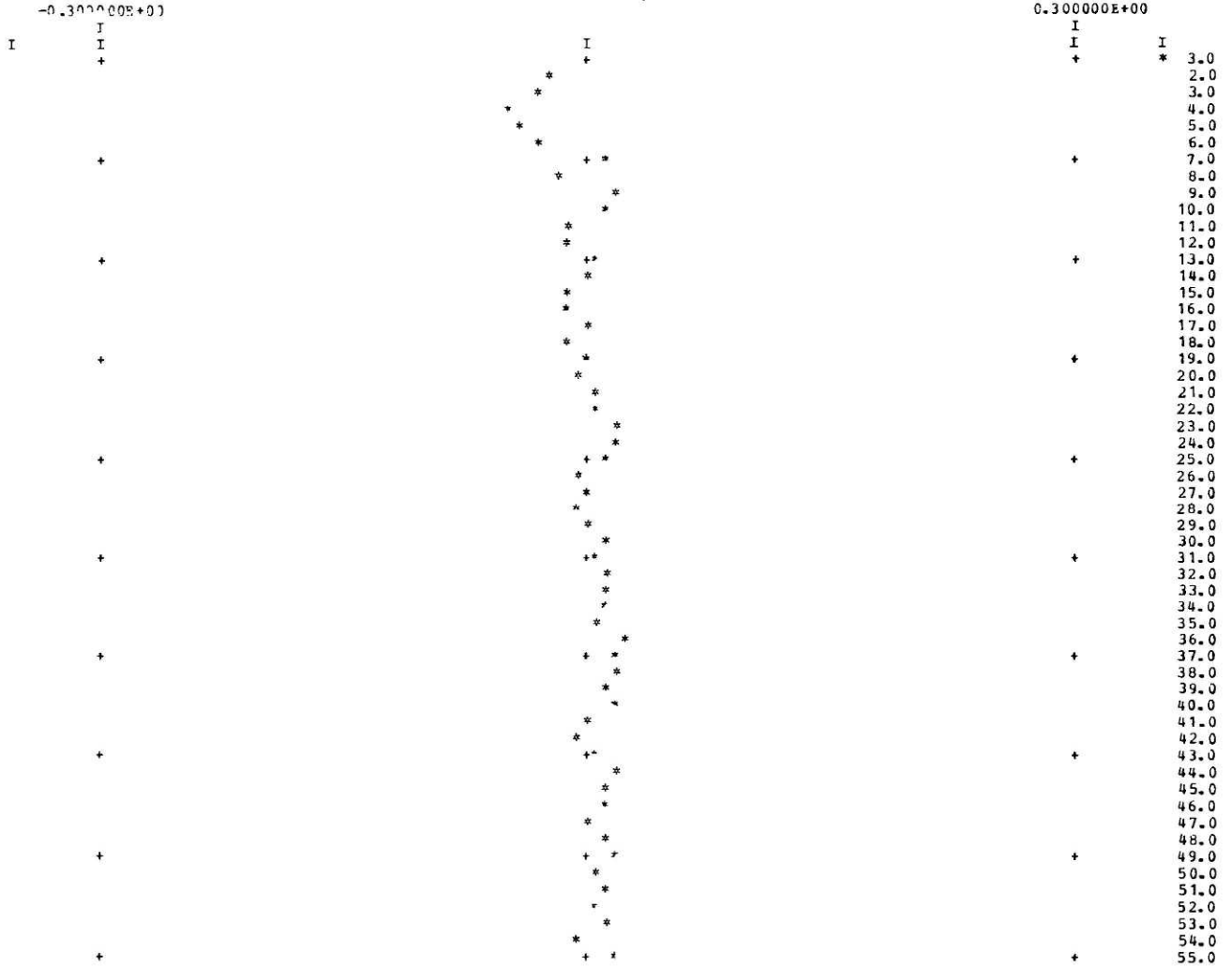

56.0
57.0
58.0
59.0
60.0
61.0
62.0
63.0
64.0
65.0
66.0
67.0
68.0
69.0
70.0
71.0
72.0
73.0
74.0
75.0
76.0
77.0
78.0
79.0
80.0
81.0
82.0
83.0
84.0
85.0
86.0
87.0
88.0
89.0
90.0
91.0
92.0
93.0
94.0
95.0
96.0
97.0
98.0
99.0

TERM ENERGIES PLUS PARITY

0.0	17488.36241	16722.23431	0.00002	0.00001	0.00001	
	PI.000SIG.000	PI.000SIG****	PI.0 SIG.0	PI.0 SIG.0	PI***SIG.000	PI
1.0	17570.28601	17488.81024	17333.60837	16722.74995	0.00002	
	PI.767SIG.000	PI.000SIG.000	PI.233SIG.000	PI.000SIG****	PI.0 SIG.0	PI
2.0	17571.18228	17489.70591	17334.50788	17288.66406	16723.78124	
	PI.767SIG.000	PI.000SIG.000	PI.233SIG.000	PI.000SIG.000	PI.000SIG****	PI
3.0	17572.52667	17491.04939	17335.85713	17289.99570	16725.32816	
	PI.767SIG.000	PI.000SIG.000	PI.233SIG.000	PI.000SIG.000	PI.000SIG****	PI
4.0	17574.31915	17492.84067	17337.65608	17291.77118	16727.39068	
	PI.767SIG.000	PI.000SIG.000	PI.233SIG.000	PI.000SIG.000	PI.000SIG****	PI
5.0	17576.55971	17495.07972	17339.90471	17293.99050	16729.96879	
	PI.767SIG.000	PI.000SIG.000	PI.232SIG.000	PI.000SIG.000	PI.000SIG****	PI
6.0	17579.24831	17497.76650	17342.60298	17296.65362	16733.06244	
	PI.767SIG.000	PI.000SIG.000	PI.232SIG.000	PI.000SIG.000	PI.000SIG****	PI
7.0	17582.38490	17500.90098	17345.75084	17299.76052	16736.67161	
	PI.767SIG.000	PI.000SIG.000	PI.232SIG.000	PI.000SIG.000	PI.000SIG****	PI
8.0	17585.96944	17504.48310	17349.34823	17303.31115	16740.79623	
	PI.767SIG.000	PI.000SIG.000	PI.232SIG.000	PI.000SIG.000	PI.000SIG****	PI
9.0	17590.00188	17508.51282	17353.39509	17307.30547	16745.43627	
	PI.767SIG.000	PI.001SIG.000	PI.232SIG.000	PI.001SIG.000	PI.000SIG****	PI
10.0	17594.48215	17512.99007	17357.89135	17311.74343	16750.59166	
	PI.767SIG.000	PI.001SIG.000	PI.232SIG.000	PI.001SIG.000	PI.000SIG****	PI
11.0	17599.41019	17517.91478	17362.83693	17316.62499	16756.26233	
	PI.767SIG.000	PI.001SIG.000	PI.232SIG.000	PI.001SIG.000	PI.000SIG****	PI
12.0	17604.78593	17523.28688	17368.23174	17321.95008	16762.44822	
	PI.767SIG.000	PI.001SIG.000	PI.232SIG.000	PI.001SIG.000	PI.000SIG****	PI
13.0	17610.60927	17529.10630	17374.07568	17327.71863	16769.14923	
	PI.766SIG.000	PI.001SIG.000	PI.231SIG.000	PI.001SIG.000	PI.000SIG****	PI
14.0	17616.88014	17535.37293	17380.36866	17333.93059	16776.36530	
	PI.766SIG.000	PI.001SIG.000	PI.231SIG.000	PI.001SIG.000	PI.000SIG****	PI
15.0	17623.59844	17542.08669	17387.11055	17340.58585	16784.09632	
	PI.766SIG.000	PI.001SIG.000	PI.231SIG.000	PI.001SIG.000	PI.000SIG****	PI
16.0	17630.76406	17549.24747	17394.30124	17347.68436	16792.34219	
	PI.766SIG.000	PI.002SIG.000	PI.231SIG.000	PI.002SIG.000	PI.000SIG****	PI
17.0	17638.37691	17556.85517	17401.94061	17355.22602	16801.10282	
	PI.766SIG.000	PI.002SIG.000	PI.231SIG.000	PI.002SIG.000	PI.000SIG****	PI
18.0	17646.43686	17564.90968	17410.02851	17363.21075	16810.37808	
	PI.766SIG.000	PI.002SIG.000	PI.230SIG.000	PI.002SIG.000	PI.000SIG****	PI
19.0	17654.94379	17573.41086	17418.56482	17371.63843	16820.16787	
	PI.765SIG.000	PI.002SIG.000	PI.230SIG.000	PI.002SIG.000	PI.000SIG****	PI
20.0	17663.89758	17582.35859	17427.54937	17380.50897	16830.47204	
	PI.765SIG.000	PI.003SIG.000	PI.230SIG.000	PI.002SIG.000	PI.000SIG****	PI
21.0	17673.29809	17591.75274	17436.98200	17389.82226	16841.29048	
	PI.765SIG.000	PI.003SIG.000	PI.230SIG.000	PI.003SIG.000	PI.000SIG****	PI
22.0	17683.14518	17601.59316	17446.86257	17399.57818	16852.62304	
	PI.765SIG.000	PI.003SIG.000	PI.229SIG.000	PI.003SIG.000	PI.000SIG****	PI
23.0	17693.43870	17611.87970	17457.19088	17409.77661	16864.46959	
	PI.764SIG.000	PI.003SIG.000	PI.229SIG.000	PI.003SIG.000	PI.000SIG****	PI
24.0	17704.17849	17622.61222	17467.96677	17420.41742	16876.82995	
	PI.764SIG.000	PI.004SIG.000	PI.229SIG.000	PI.003SIG.000	PI.000SIG****	PI
25.0	17715.36439	17633.79054	17479.19004	17431.50049	16889.70399	
	PI.764SIG.000	PI.004SIG.000	PI.228SIG.000	PI.004SIG.000	PI.000SIG****	PI
26.0	17726.99624	17645.41450	17490.86050	17443.02566	16903.09153	
	PI.764SIG.000	PI.004SIG.000	PI.228SIG.000	PI.004SIG.000	PI.000SIG****	PI
27.0	17739.07385	17657.48392	17502.97795	17454.99280	16916.99240	
	PI.763SIG.000	PI.005SIG.000	PI.228SIG.000	PI.004SIG.000	PI.000SIG****	PI
28.0	17751.59705	17669.99862	17515.54217	17467.40175	16931.40642	
	PI.763SIG.000	PI.005SIG.000	PI.227SIG.000	PI.004SIG.000	PI.000SIG****	PI
29.0	17764.56565	17682.95841	17528.55296	17480.25236	16946.33341	

	PI.763SIG.000	PI.005SIG.000	PI.227SIG.000	PI.005SIG.000	PI.000SIG**** PI
30.0	17777.97944	17696.36310	17542.01038	17493.54447	16961.77318
	PI.762SIG.000	PI.006SIG.000	PI.227SIG.000	PI.005SIG.000	PI.000SIG**** PI
31.0	17791.83823	17710.21248	17555.91331	17507.27790	16977.72552
	PI.762SIG.000	PI.006SIG.000	PI.226SIG.000	PI.005SIG.000	PI.000SIG**** PI
32.0	17806.14182	17724.50633	17570.26240	17521.45247	16994.19025
	PI.762SIG.000	PI.007SIG.000	PI.226SIG.000	PI.006SIG.000	PI.000SIG**** PI
33.0	17820.88997	17739.24445	17585.05711	17536.06802	17011.16713
	PI.762SIG.000	PI.007SIG.000	PI.226SIG.000	PI.006SIG.000	PI.000SIG**** PI
34.0	17836.08247	17754.42662	17600.29720	17551.12434	17028.65596
	PI.761SIG.000	PI.007SIG.000	PI.225SIG.000	PI.006SIG.000	PI.000SIG**** PI
35.0	17851.71909	17770.05259	17615.98239	17566.62124	17046.65651
	PI.761SIG.000	PI.008SIG.000	PI.225SIG.000	PI.007SIG.000	PI.000SIG**** PI
36.0	17867.79959	17786.12214	17632.11243	17582.55853	17065.16855
	PI.760SIG.000	PI.008SIG.000	PI.224SIG.000	PI.007SIG.000	PI.000SIG**** PI
37.0	17884.32373	17802.63503	17648.68703	17598.93599	17084.19184
	PI.760SIG.000	PI.009SIG.000	PI.224SIG.000	PI.007SIG.000	PI.000SIG**** PI
38.0	17901.29126	17819.59099	17665.70592	17615.75341	17103.72614
	PI.760SIG.000	PI.009SIG.000	PI.224SIG.000	PI.008SIG.000	PI.000SIG**** PI
39.0	17918.70193	17836.98978	17683.16881	17633.01057	17123.77120
	PI.759SIG.000	PI.010SIG.000	PI.223SIG.000	PI.008SIG.000	PI.000SIG**** PI
40.0	17936.55546	17854.83113	17701.07541	17650.70724	17144.32676
	PI.759SIG.000	PI.010SIG.000	PI.223SIG.000	PI.008SIG.000	PI.000SIG**** PI
41.0	17954.85159	17873.11477	17719.42541	17668.84320	17165.39255
	PI.758SIG.000	PI.011SIG.000	PI.222SIG.000	PI.009SIG.000	PI.000SIG**** PI
42.0	17973.59005	17891.84043	17738.21851	17687.41820	17186.96830
	PI.758SIG.000	PI.011SIG.000	PI.222SIG.000	PI.009SIG.000	PI.000SIG**** PI
43.0	17992.77054	17911.00781	17757.45439	17706.43198	17209.05375
	PI.758SIG.000	PI.012SIG.000	PI.222SIG.000	PI.009SIG.000	PI.000SIG**** PI
44.0	18012.39278	17930.61663	17777.13273	17725.88431	17231.64859
	PI.757SIG.000	PI.012SIG.000	PI.221SIG.000	PI.010SIG.000	PI.000SIG**** PI
45.0	18032.45647	17950.66660	17797.25320	17745.77492	17254.75255
	PI.757SIG.000	PI.013SIG.000	PI.221SIG.000	PI.010SIG.000	PI.000SIG**** PI
46.0	18052.96131	17971.15740	17817.81548	17766.10355	17278.36533
	PI.756SIG.000	PI.013SIG.000	PI.220SIG.000	PI.010SIG.000	PI.000SIG**** PI
47.0	18073.90698	17992.09873	17838.81920	17786.86991	17302.48661
	PI.756SIG.000	PI.014SIG.000	PI.220SIG.000	PI.011SIG.000	PI.000SIG**** PI
48.0	18095.29317	18013.46028	17860.26404	17808.07374	17327.11610
	PI.755SIG.000	PI.014SIG.000	PI.219SIG.000	PI.011SIG.000	PI.000SIG**** PI
49.0	18117.11956	18035.27175	17882.14962	17829.71474	17352.25346
	PI.755SIG.000	PI.015SIG.000	PI.219SIG.000	PI.011SIG.000	PI.000SIG**** PI
50.0	18139.38581	18057.52268	17904.47560	17851.79262	17377.89839
	PI.754SIG.000	PI.016SIG.000	PI.218SIG.000	PI.012SIG.000	PI.000SIG**** PI
51.0	18162.09158	18080.21288	17927.24160	17874.30709	17404.05055
	PI.754SIG.000	PI.016SIG.000	PI.218SIG.000	PI.012SIG.000	PI.000SIG**** PI
52.0	18185.23653	18103.34195	17950.44725	17897.25782	17430.70960
	PI.753SIG.000	PI.017SIG.000	PI.217SIG.000	PI.013SIG.000	PI.000SIG**** PI
53.0	18208.82032	18126.90954	17974.09217	17920.64452	17457.87520
	PI.753SIG.000	PI.017SIG.000	PI.217SIG.000	PI.013SIG.000	PI.000SIG**** PI
54.0	18232.84257	18150.91529	17998.17596	17944.46685	17485.54700
	PI.752SIG.000	PI.018SIG.000	PI.217SIG.000	PI.013SIG.000	PI.000SIG**** PI
55.0	18257.30293	18175.35885	18022.69825	17968.72450	17513.72464
	PI.752SIG.000	PI.019SIG.000	PI.216SIG.000	PI.014SIG.000	PI.000SIG**** PI
56.0	18282.20103	18200.23983	18047.65862	17993.41712	17542.40776
	PI.751SIG.000	PI.019SIG.000	PI.216SIG.000	PI.014SIG.000	PI.000SIG**** PI
57.0	18307.53648	18225.55786	18073.05666	18018.54438	17571.59598
	PI.750SIG.000	PI.020SIG.000	PI.215SIG.000	PI.014SIG.000	PI.000SIG**** PI
58.0	18333.30890	18251.31255	18098.89198	18044.10592	17601.28894
	PI.750SIG.000	PI.021SIG.000	PI.215SIG.000	PI.015SIG.000	PI.000SIG**** PI
59.0	18359.51790	18277.50352	18125.16413	18070.10140	17631.48624
	PI.749SIG.000	PI.021SIG.000	PI.214SIG.000	PI.015SIG.000	PI.000SIG**** PI
60.0	18386.16309	18304.13037	18151.87271	18096.53044	17662.18750
	PI.749SIG.000	PI.022SIG.000	PI.214SIG.000	PI.015SIG.000	PI.000SIG**** PI
61.0	18413.24405	18331.19268	18179.01727	18123.39268	17693.39231
	PI.748SIG.000	PI.023SIG.000	PI.213SIG.000	PI.016SIG.000	PI.000SIG**** PI
62.0	18440.76037	18358.69006	18206.59738	18150.68775	17725.10029

	PI.747SIG.000	PI.024SIG.000	PI.213SIG.000	PI.016SIG.000	PI.000SIG**** PI
63.0	18468.71163	18386.62208	18234.61259	18178.41526	17757.31101
	PI.747SIG.000	PI.024SIG.000	PI.212SIG.000	PI.017SIG.000	PI.000SIG**** PI
64.0	18497.09742	18414.98831	18263.06245	18206.57481	17790.02406
	PI.746SIG.000	PI.025SIG.000	PI.212SIG.000	PI.017SIG.000	PI.000SIG**** PI
65.0	18525.91729	18443.78833	18291.94651	18235.16602	17823.23901
	PI.746SIG.000	PI.026SIG.000	PI.211SIG.000	PI.017SIG.000	PI.000SIG**** PI
66.0	18555.17081	18473.02169	18321.26428	18264.18848	17856.95544
	PI.745SIG.000	PI.027SIG.000	PI.211SIG.000	PI.018SIG.000	PI.000SIG**** PI
67.0	18584.85754	18502.68796	18351.01532	18293.64178	17891.17291
	PI.744SIG.000	PI.027SIG.000	PI.210SIG.000	PI.018SIG.000	PI.000SIG**** PI
68.0	18614.97701	18532.78668	18381.19913	18323.52549	17925.89097
	PI.744SIG.000	PI.028SIG.000	PI.210SIG.000	PI.018SIG.000	PI.000SIG**** PI
69.0	18645.52877	18563.31739	18411.81524	18353.83920	17961.10918
	PI.743SIG.000	PI.029SIG.000	PI.209SIG.000	PI.019SIG.000	PI.000SIG**** PI
70.0	18676.51235	18594.27963	18442.86315	18384.58247	17996.82707
	PI.742SIG.000	PI.030SIG.000	PI.209SIG.000	PI.019SIG.000	PI.000SIG**** PI
71.0	18707.92729	18625.67293	18474.34237	18415.75487	18033.04418
	PI.741SIG.000	PI.031SIG.000	PI.209SIG.000	PI.019SIG.000	PI.000SIG**** PI
72.0	18739.77309	18657.49680	18506.25240	18447.35593	18069.76005
	PI.741SIG.000	PI.031SIG.000	PI.208SIG.000	PI.020SIG.000	PI.000SIG**** PI
73.0	18772.04928	18689.75077	18538.59272	18479.38523	18106.97419
	PI.740SIG.000	PI.032SIG.000	PI.208SIG.000	PI.020SIG.000	PI.000SIG**** PI
74.0	18804.75537	18722.43434	18571.36283	18511.84228	18144.68612
	PI.739SIG.000	PI.033SIG.000	PI.207SIG.000	PI.020SIG.000	PI.000SIG**** PI
75.0	18837.89084	18755.54702	18604.56219	18544.72663	18182.89534
	PI.739SIG.000	PI.034SIG.000	PI.207SIG.000	PI.021SIG.000	PI.000SIG**** PI
76.0	18871.45520	18789.08830	18638.19029	18578.03780	18221.60137
	PI.738SIG.000	PI.035SIG.000	PI.206SIG.000	PI.021SIG.000	PI.000SIG**** PI
77.0	18905.44793	18823.05767	18672.24658	18611.77539	18260.80370
	PI.737SIG.000	PI.036SIG.000	PI.206SIG.000	PI.021SIG.000	PI.000SIG**** PI
78.0	18939.86852	18857.45461	18706.73053	18645.93866	18300.50181
	PI.736SIG.000	PI.037SIG.000	PI.205SIG.000	PI.022SIG.000	PI.000SIG**** PI
79.0	18974.71643	18892.27860	18741.64158	18680.52737	18340.69519
	PI.736SIG.000	PI.037SIG.000	PI.205SIG.000	PI.022SIG.000	PI.000SIG**** PI
80.0	19009.99113	18927.52911	18776.97920	18715.54094	18381.38331
	PI.735SIG.000	PI.038SIG.000	PI.204SIG.000	PI.022SIG.000	PI.000SIG**** PI
81.0	19045.69208	18963.20560	18812.74281	18750.97884	18422.56564
	PI.734SIG.000	PI.039SIG.000	PI.204SIG.000	PI.023SIG.000	PI.000SIG**** PI
82.0	19081.81874	18999.30753	18848.93185	18786.84057	18464.24164
	PI.733SIG.000	PI.040SIG.000	PI.203SIG.000	PI.023SIG.000	PI.000SIG**** PI
83.0	19118.37054	19035.83435	18885.54575	18823.12561	18506.41077
	PI.733SIG.000	PI.041SIG.000	PI.203SIG.000	PI.023SIG.000	PI.000SIG.999 PI
84.0	19155.34694	19072.78549	18922.58393	18859.83341	18549.07247
	PI.732SIG.000	PI.042SIG.000	PI.203SIG.000	PI.023SIG.000	PI.000SIG.999 PI
85.0	19192.74736	19110.16041	18960.04580	18896.96345	18592.22618
	PI.731SIG.000	PI.043SIG.000	PI.202SIG.000	PI.024SIG.000	PI.000SIG.999 PI
86.0	19230.57123	19147.95852	18997.93078	18934.51518	18635.87133
	PI.730SIG.000	PI.044SIG.000	PI.202SIG.000	PI.024SIG.000	PI.000SIG.999 PI
87.0	19268.81796	19186.17926	19036.23826	18972.48804	18680.00736
	PI.729SIG.000	PI.045SIG.001	PI.201SIG.000	PI.024SIG.000	PI.000SIG.999 PI
88.0	19307.48698	19224.82204	19074.96764	19010.88148	18724.63368
	PI.729SIG.000	PI.046SIG.001	PI.201SIG.000	PI.025SIG.000	PI.000SIG.999 PI
89.0	19346.57769	19263.88628	19114.11832	19049.69493	18769.74970
	PI.728SIG.000	PI.047SIG.001	PI.200SIG.000	PI.025SIG.000	PI.000SIG.999 PI
90.0	19386.09948	19303.37137	19153.68967	19088.92782	18815.35483
	PI.727SIG.000	PI.048SIG.001	PI.200SIG.000	PI.025SIG.000	PI.000SIG.999 PI
91.0	19426.02175	19343.27672	19193.68107	19128.57957	18861.44846
	PI.726SIG.000	PI.049SIG.001	PI.199SIG.000	PI.026SIG.000	PI.000SIG.999 PI
92.0	19466.37388	19383.60172	19234.09189	19168.64960	18908.02999
	PI.725SIG.000	PI.050SIG.001	PI.199SIG.000	PI.026SIG.000	PI.000SIG.999 PI
93.0	19507.14526	19424.34576	19274.92150	19209.13730	18955.09890
	PI.724SIG.000	PI.051SIG.001	PI.199SIG.000	PI.026SIG.000	PI.000SIG.999 PI
94.0	19548.33525	19465.50822	19316.16926	19250.04208	19002.65426
	PI.724SIG.000	PI.052SIG.001	PI.198SIG.000	PI.026SIG.000	PI.000SIG.999 PI
95.0	19589.94322	19507.08848	19357.83451	19291.36333	19050.69574

	PI.723SIG.000	PI.053SIG.001	PI.198SIG.000	PI.027SIG.000	PI.000SIG.999	PI
96.0	19631.96854	19549.08589	19399.91661	19333.10043	19099.22251	
	PI.722SIG.000	PI.054SIG.001	PI.197SIG.000	PI.027SIG.000	PI.000SIG.999	PI
97.0	19674.41055	19591.49984	19442.41489	19375.25277	19148.23420	
	PI.721SIG.000	PI.055SIG.001	PI.197SIG.000	PI.027SIG.000	PI.000SIG.999	PI
98.0	19717.26959	19634.32966	19485.32868	19417.81972	19197.72988	
	PI.720SIG.000	PI.056SIG.001	PI.196SIG.000	PI.027SIG.000	PI.000SIG.999	PI

TERM ENERGIES MINUS PARITY

0.0	17488.22370	0.00002	0.00021	0.00001	0.0	
	PI.0 SIG.0	PI.0 SIG.0	PI.0 SIG.0	PI****SIG.0	PI.0 SIG****	PI
1.0	17570.28600	17488.67152	17333.60837	0.00002	0.0	
	PI.767SIG.0	PI.000SIG.0	PI.233SIG.0	PI.0 SIG.0	PI.0 SIG****	PI
2.0	17571.18226	17489.56714	17334.50788	17288.66406	0.0	
	PI.767SIG.0	PI.000SIG.0	PI.233SIG.0	PI.000SIG.0	PI.0 SIG****	PI
3.0	17572.52664	17490.91057	17335.85712	17289.99570	0.0	
	PI.767SIG.0	PI.000SIG.0	PI.233SIG.0	PI.000SIG.0	PI.0 SIG****	PI
4.0	17574.31911	17492.70176	17337.65607	17291.77118	0.0	
	PI.767SIG.0	PI.000SIG.0	PI.233SIG.0	PI.000SIG.0	PI.0 SIG****	PI
5.0	17576.55965	17494.94071	17339.90470	17293.99150	0.0	
	PI.767SIG.0	PI.000SIG.0	PI.232SIG.0	PI.000SIG.0	PI.0 SIG****	PI
6.0	17579.24822	17497.62737	17342.60296	17296.65362	0.0	
	PI.767SIG.0	PI.000SIG.0	PI.232SIG.0	PI.000SIG.0	PI.0 SIG****	PI
7.0	17582.38478	17500.76171	17345.75082	17299.76052	0.0	
	PI.767SIG.0	PI.000SIG.0	PI.232SIG.0	PI.000SIG.0	PI.0 SIG****	PI
8.0	17585.96929	17504.34367	17349.34820	17303.31115	0.0	
	PI.767SIG.0	PI.000SIG.0	PI.232SIG.0	PI.000SIG.0	PI.0 SIG****	PI
9.0	17590.00169	17508.37321	17353.39506	17307.30547	0.0	
	PI.767SIG.0	PI.001SIG.0	PI.232SIG.0	PI.001SIG.0	PI.0 SIG****	PI
10.0	17594.48191	17512.85026	17357.89131	17311.74343	0.0	
	PI.767SIG.0	PI.001SIG.0	PI.232SIG.0	PI.001SIG.0	PI.0 SIG****	PI
11.0	17599.40991	17517.77475	17362.83688	17316.62499	0.0	
	PI.767SIG.0	PI.001SIG.0	PI.232SIG.0	PI.001SIG.0	PI.0 SIG****	PI
12.0	17604.78559	17523.14661	17368.23168	17321.95008	0.0	
	PI.767SIG.0	PI.001SIG.0	PI.232SIG.0	PI.001SIG.0	PI.0 SIG****	PI
13.0	17610.60887	17528.96576	17374.07561	17327.71863	0.0	
	PI.766SIG.0	PI.001SIG.0	PI.231SIG.0	PI.001SIG.0	PI.0 SIG****	PI
14.0	17616.87968	17535.23211	17380.36857	17333.93058	0.0	
	PI.766SIG.0	PI.001SIG.0	PI.231SIG.0	PI.001SIG.0	PI.0 SIG****	PI
15.0	17623.59791	17541.94556	17387.11045	17340.58585	0.0	
	PI.766SIG.0	PI.001SIG.0	PI.231SIG.0	PI.001SIG.0	PI.0 SIG****	PI
16.0	17630.76347	17549.10602	17394.30113	17347.68436	0.0	
	PI.766SIG.0	PI.002SIG.0	PI.231SIG.0	PI.002SIG.0	PI.0 SIG****	PI
17.0	17638.37624	17556.71337	17401.94048	17355.22602	0.0	
	PI.766SIG.0	PI.002SIG.0	PI.231SIG.0	PI.002SIG.0	PI.0 SIG****	PI
18.0	17646.43611	17564.76750	17410.02837	17363.21074	0.0	
	PI.766SIG.0	PI.002SIG.0	PI.230SIG.0	PI.002SIG.0	PI.0 SIG****	PI
19.0	17654.94296	17573.26829	17418.56466	17371.63843	0.0	
	PI.765SIG.0	PI.002SIG.0	PI.230SIG.0	PI.002SIG.0	PI.0 SIG****	PI
20.0	17663.89666	17582.21561	17427.54919	17380.50897	0.0	
	PI.765SIG.0	PI.003SIG.0	PI.230SIG.0	PI.002SIG.0	PI.0 SIG****	PI
21.0	17673.29707	17591.60932	17436.98181	17389.82226	0.0	
	PI.765SIG.0	PI.003SIG.0	PI.230SIG.0	PI.003SIG.0	PI.0 SIG****	PI
22.0	17683.14406	17601.44928	17446.86236	17399.57817	0.0	
	PI.765SIG.0	PI.003SIG.0	PI.229SIG.0	PI.003SIG.0	PI.0 SIG****	PI
23.0	17693.43748	17611.73534	17457.19065	17409.77660	0.0	
	PI.764SIG.0	PI.003SIG.0	PI.229SIG.0	PI.003SIG.0	PI.0 SIG****	PI
24.0	17704.17716	17622.46735	17467.96652	17420.41742	0.0	
	PI.764SIG.0	PI.004SIG.0	PI.229SIG.0	PI.003SIG.0	PI.0 SIG****	PI
25.0	17715.36295	17633.64515	17479.18977	17431.50048	0.0	
	PI.764SIG.0	PI.004SIG.0	PI.228SIG.0	PI.004SIG.0	PI.0 SIG****	PI
26.0	17726.99468	17645.26855	17490.86021	17443.02565	0.0	
	PI.764SIG.0	PI.004SIG.0	PI.228SIG.0	PI.004SIG.0	PI.0 SIG****	PI

27.0	17739.07217	17657.33740	17502.97763	17454.99279	0.0	
	PI.763SIG.0	PI.005SIG.0	PI.228SIG.0	PI.004SIG.0	PI.0	SIG**** PI
28.0	17751.59524	17669.85150	17515.54183	17467.40175	0.0	
	PI.763SIG.0	PI.005SIG.0	PI.227SIG.0	PI.004SIG.0	PI.0	SIG**** PI
29.0	17764.56370	17682.81066	17528.55259	17480.25236	0.0	
	PI.763SIG.0	PI.005SIG.0	PI.227SIG.0	PI.005SIG.0	PI.0	SIG**** PI
30.0	17777.97736	17696.21470	17542.00969	17493.54446	0.0	
	PI.762SIG.0	PI.006SIG.0	PI.227SIG.0	PI.005SIG.0	PI.0	SIG**** PI
31.0	17791.83600	17710.06339	17555.91289	17507.27789	0.0	
	PI.762SIG.0	PI.006SIG.0	PI.226SIG.0	PI.005SIG.0	PI.0	SIG**** PI
32.0	17806.13944	17724.35655	17570.26195	17521.45246	0.0	
	PI.762SIG.0	PI.007SIG.0	PI.226SIG.0	PI.006SIG.0	PI.0	SIG**** PI
33.0	17820.88743	17739.09394	17585.05664	17536.06800	0.0	
	PI.761SIG.0	PI.007SIG.0	PI.226SIG.0	PI.006SIG.0	PI.0	SIG**** PI
34.0	17836.07977	17754.27535	17600.29669	17551.12432	0.0	
	PI.761SIG.0	PI.007SIG.0	PI.225SIG.0	PI.006SIG.0	PI.0	SIG**** PI
35.0	17851.71623	17769.90054	17615.98186	17566.62122	0.0	
	PI.761SIG.0	PI.008SIG.0	PI.225SIG.0	PI.007SIG.0	PI.0	SIG**** PI
36.0	17867.79656	17785.96928	17632.11186	17582.55851	0.0	
	PI.760SIG.0	PI.008SIG.0	PI.224SIG.0	PI.007SIG.0	PI.0	SIG**** PI
37.0	17884.32052	17802.48132	17648.68643	17598.93596	0.0	
	PI.760SIG.0	PI.009SIG.0	PI.224SIG.0	PI.007SIG.0	PI.0	SIG**** PI
38.0	17901.28787	17819.43641	17665.70528	17615.75338	0.0	
	PI.760SIG.0	PI.009SIG.0	PI.224SIG.0	PI.008SIG.0	PI.0	SIG**** PI
39.0	17918.69835	17836.83430	17683.16814	17633.01054	0.0	
	PI.759SIG.0	PI.010SIG.0	PI.223SIG.0	PI.008SIG.0	PI.0	SIG**** PI
40.0	17936.55169	17854.67472	17701.07470	17650.70721	0.0	
	PI.759SIG.0	PI.010SIG.0	PI.223SIG.0	PI.008SIG.0	PI.0	SIG**** PI
41.0	17954.84762	17872.95740	17719.42467	17668.84317	0.0	
	PI.758SIG.0	PI.011SIG.0	PI.222SIG.0	PI.009SIG.0	PI.0	SIG**** PI
42.0	17973.58587	17891.68206	17738.21772	17687.41816	0.0	
	PI.758SIG.0	PI.011SIG.0	PI.222SIG.0	PI.009SIG.0	PI.0	SIG**** PI
43.0	17992.76615	17910.84842	17757.45357	17706.43194	0.0	
	PI.757SIG.0	PI.012SIG.0	PI.222SIG.0	PI.009SIG.0	PI.0	SIG**** PI
44.0	18012.38817	17930.45619	17777.13187	17725.88427	0.0	
	PI.757SIG.0	PI.012SIG.0	PI.221SIG.0	PI.010SIG.0	PI.0	SIG**** PI
45.0	18032.45163	17950.50507	17797.25230	17745.77497	0.0	
	PI.757SIG.0	PI.013SIG.0	PI.221SIG.0	PI.010SIG.0	PI.0	SIG**** PI
46.0	18052.95624	17970.99474	17817.81452	17766.10349	0.0	
	PI.756SIG.0	PI.013SIG.0	PI.220SIG.0	PI.010SIG.0	PI.0	SIG**** PI
47.0	18073.90167	17991.92491	17838.81820	17786.86986	0.0	
	PI.756SIG.0	PI.014SIG.0	PI.220SIG.0	PI.011SIG.0	PI.0	SIG**** PI
48.0	18095.28762	18013.29526	17860.26299	17808.07368	0.0	
	PI.755SIG.0	PI.014SIG.0	PI.219SIG.0	PI.011SIG.0	PI.0	SIG**** PI
49.0	18117.11375	18035.10545	17882.14853	17829.71467	0.0	
	PI.755SIG.0	PI.015SIG.0	PI.219SIG.0	PI.011SIG.0	PI.0	SIG**** PI
50.0	18139.37974	18057.35516	17904.47446	17851.79255	0.0	
	PI.754SIG.0	PI.016SIG.0	PI.218SIG.0	PI.012SIG.0	PI.0	SIG**** PI
51.0	18162.08524	18080.04404	17927.24041	17874.30791	0.0	
	PI.754SIG.0	PI.016SIG.0	PI.218SIG.0	PI.012SIG.0	PI.0	SIG**** PI
52.0	18185.22992	18103.17176	17950.44600	17897.25774	0.0	
	PI.753SIG.0	PI.017SIG.0	PI.218SIG.0	PI.013SIG.0	PI.0	SIG**** PI
53.0	18208.81342	18126.73796	17974.09086	17920.64442	0.0	
	PI.753SIG.0	PI.018SIG.0	PI.217SIG.0	PI.013SIG.0	PI.0	SIG**** PI
54.0	18232.83539	18150.74228	17998.17461	17944.46675	0.0	
	PI.752SIG.0	PI.018SIG.0	PI.217SIG.0	PI.013SIG.0	PI.0	SIG**** PI
55.0	18257.29545	18175.18436	18022.69683	17968.72439	0.0	
	PI.751SIG.0	PI.019SIG.0	PI.216SIG.0	PI.014SIG.0	PI.0	SIG**** PI
56.0	18282.19324	18200.06381	18047.65714	17993.41700	0.0	
	PI.751SIG.0	PI.019SIG.0	PI.216SIG.0	PI.014SIG.0	PI.0	SIG**** PI
57.0	18307.52837	18225.38028	18073.05513	18018.54425	0.0	
	PI.750SIG.0	PI.020SIG.0	PI.215SIG.0	PI.014SIG.0	PI.0	SIG**** PI
58.0	18333.30047	18251.13336	18098.89037	18044.10579	0.0	
	PI.750SIG.0	PI.021SIG.0	PI.215SIG.0	PI.015SIG.0	PI.0	SIG**** PI
59.0	18359.50914	18277.32266	18125.16247	18070.10125	0.0	
	PI.749SIG.0	PI.022SIG.0	PI.214SIG.0	PI.015SIG.0	PI.0	SIG**** PI

60.0	18386.15399	18303.94779	18151.87097	18096.53029	0.0	
	PI.749SIG.0	PI.022SIG.0	PI.214SIG.0	PI.015SIG.0	PI.0	SIG**** PI
61.0	18413.23459	18331.00834	18179.01547	18123.39252	0.0	
	PI.748SIG.0	PI.023SIG.0	PI.213SIG.0	PI.016SIG.0	PI.0	SIG**** PI
62.0	18440.75056	18358.50391	18206.59551	18150.68757	0.0	
	PI.747SIG.0	PI.024SIG.0	PI.213SIG.0	PI.016SIG.0	PI.0	SIG**** PI
63.0	18468.70145	18386.43414	18234.61064	18178.41507	0.0	
	PI.747SIG.0	PI.024SIG.0	PI.212SIG.0	PI.017SIG.0	PI.0	SIG**** PI
64.0	18497.08686	18414.79835	18263.06043	18206.57461	0.0	
	PI.746SIG.0	PI.025SIG.0	PI.212SIG.0	PI.017SIG.0	PI.0	SIG**** PI
65.0	18525.90634	18443.59638	18291.94440	18235.16581	0.0	
	PI.745SIG.0	PI.026SIG.0	PI.211SIG.0	PI.017SIG.0	PI.0	SIG**** PI
66.0	18555.15946	18472.82769	18321.26210	18264.18825	0.0	
	PI.745SIG.0	PI.027SIG.0	PI.211SIG.0	PI.018SIG.0	PI.0	SIG**** PI
67.0	18584.84578	18502.49185	18351.01305	18293.64154	0.0	
	PI.744SIG.0	PI.028SIG.0	PI.210SIG.0	PI.018SIG.0	PI.0	SIG**** PI
68.0	18614.96482	18532.58839	18381.19677	18323.52524	0.0	
	PI.743SIG.0	PI.028SIG.0	PI.210SIG.0	PI.018SIG.0	PI.0	SIG**** PI
69.0	18645.51615	18563.11686	18411.81279	18353.83893	0.0	
	PI.743SIG.0	PI.029SIG.0	PI.210SIG.0	PI.019SIG.0	PI.0	SIG**** PI
70.0	18676.49929	18594.07679	18442.86061	18384.58218	0.0	
	PI.742SIG.0	PI.030SIG.0	PI.209SIG.0	PI.019SIG.0	PI.0	SIG**** PI
71.0	18707.91377	18625.46770	18474.33974	18415.75456	0.0	
	PI.741SIG.0	PI.031SIG.0	PI.209SIG.0	PI.019SIG.0	PI.0	SIG**** PI
72.0	18739.75910	18657.28912	18506.24966	18447.35561	0.0	
	PI.741SIG.0	PI.032SIG.0	PI.208SIG.0	PI.020SIG.0	PI.0	SIG**** PI
73.0	18772.03481	18689.54055	18538.58988	18479.38488	0.0	
	PI.740SIG.0	PI.032SIG.0	PI.208SIG.0	PI.020SIG.0	PI.0	SIG**** PI
74.0	18804.74040	18722.22151	18571.35988	18511.84191	0.0	
	PI.739SIG.0	PI.033SIG.0	PI.207SIG.0	PI.020SIG.0	PI.0	SIG**** PI
75.0	18837.87536	18755.33149	18604.55913	18544.72624	0.0	
	PI.738SIG.0	PI.034SIG.0	PI.207SIG.0	PI.021SIG.0	PI.0	SIG**** PI
76.0	18871.43920	18788.86999	18638.18711	18578.03738	0.0	
	PI.738SIG.0	PI.035SIG.0	PI.206SIG.0	PI.021SIG.0	PI.0	SIG**** PI
77.0	18905.43139	18822.83648	18672.24329	18611.77486	0.0	
	PI.737SIG.0	PI.036SIG.0	PI.206SIG.0	PI.021SIG.0	PI.0	SIG**** PI
78.0	18939.85142	18857.23046	18706.72711	18645.93819	0.0	
	PI.736SIG.0	PI.037SIG.0	PI.205SIG.0	PI.022SIG.0	PI.0	SIG**** PI
79.0	18974.69876	18892.05138	18741.63804	18680.52688	0.0	
	PI.735SIG.0	PI.038SIG.0	PI.205SIG.0	PI.022SIG.0	PI.0	SIG**** PI
80.0	19009.97288	18927.29872	18776.97552	18715.54941	0.0	
	PI.735SIG.0	PI.039SIG.0	PI.204SIG.0	PI.022SIG.0	PI.0	SIG**** PI
81.0	19045.67322	18962.97194	18812.73900	18750.97829	0.0	
	PI.734SIG.0	PI.040SIG.0	PI.204SIG.0	PI.023SIG.0	PI.0	SIG**** PI
82.0	19081.79926	18999.07049	18848.92789	18786.83999	0.0	
	PI.733SIG.0	PI.040SIG.0	PI.204SIG.0	PI.023SIG.0	PI.0	SIG**** PI
83.0	19118.35043	19035.59381	18885.54164	18823.12499	0.0	
	PI.732SIG.0	PI.041SIG.0	PI.203SIG.0	PI.023SIG.0	PI.0	SIG**** PI
84.0	19155.32616	19072.54134	18922.57967	18859.83275	0.0	
	PI.732SIG.0	PI.042SIG.0	PI.203SIG.0	PI.024SIG.0	PI.0	SIG**** PI
85.0	19192.72591	19109.91251	18960.04138	18896.96275	0.0	
	PI.731SIG.0	PI.043SIG.0	PI.202SIG.0	PI.024SIG.0	PI.0	SIG**** PI
86.0	19230.54908	19147.70675	18997.92618	18934.51444	0.0	
	PI.730SIG.0	PI.044SIG.0	PI.202SIG.0	PI.024SIG.0	PI.0	SIG**** PI
87.0	19268.79509	19185.92348	19036.23349	18972.48726	0.0	
	PI.729SIG.0	PI.045SIG.0	PI.201SIG.0	PI.024SIG.0	PI.0	SIG**** PI
88.0	19307.46337	19224.56211	19074.96269	19010.88065	0.0	
	PI.728SIG.0	PI.046SIG.0	PI.201SIG.0	PI.025SIG.0	PI.0	SIG**** PI
89.0	19346.55331	19263.62234	19114.11317	19049.69406	0.0	
	PI.727SIG.0	PI.047SIG.0	PI.200SIG.0	PI.025SIG.0	PI.0	SIG**** PI
90.0	19386.06431	19303.10267	19153.68432	19088.92689	0.0	
	PI.727SIG.0	PI.048SIG.0	PI.200SIG.0	PI.025SIG.0	PI.0	SIG**** PI
91.0	19425.99577	19343.00339	19193.67551	19128.57859	0.0	
	PI.726SIG.0	PI.049SIG.0	PI.200SIG.0	PI.026SIG.0	PI.0	SIG**** PI
92.0	19466.34706	19383.32358	19234.08611	19168.64955	0.0	
	PI.725SIG.0	PI.050SIG.0	PI.199SIG.0	PI.026SIG.0	PI.0	SIG**** PI

```
93.0   19507.11757   19424.06263   19274.91549   19209.13619        0.0
       PI.724SIG.0   PI.051SIG.0   PI.199SIG.0   PI.026SIG.0   PI.0  SIG**** PI
94.0   19548.30667   19465.21991   19316.16300   19250.04091        0.0
       PI.723SIG.0   PI.052SIG.0   PI.198SIG.0   PI.026SIG.0   PI.0  SIG**** PI
95.0   19589.91371   19506.79478   19357.82800   19291.36208        0.0
       PI.722SIG.0   PI.053SIG.0   PI.198SIG.0   PI.027SIG.0   PI.0  SIG**** PI
96.0   19631.93807   19548.78659   19399.90983   19333.09911        0.0
       PI.721SIG.0   PI.054SIG.0   PI.197SIG.0   PI.027SIG.0   PI.0  SIG**** PI
97.0   19674.37909   19591.19470   19442.40782   19375.25137        0.0
       PI.720SIG.0   PI.055SIG.0   PI.197SIG.0   PI.027SIG.0   PI.0  SIG**** PI
98.0   19717.23611   19634.01845   19485.32131   19417.81822        0.0
       PI.720SIG.0   PI.056SIG.0   PI.197SIG.0   PI.027SIG.0   PI.0  SIG**** PI
```

Appendix 3:

Reprinted from J. Mol. Spectrosc. 58, 394-413 (1975).

Observed and Calculated Interactions between Valence States of the NO Molecule

ROBERT W. FIELD[1] AND RICHARD A. GOTTSCHO

Department of Chemistry, Massachusetts Institute of Technology, Cambridge, Massachusetts 02139

AND

E. MIESCHER

Institute of Physics, University of Basel, Basel, Switzerland

No perturbation between two valence states of NO has ever been identified, although many valence–Rydberg and several Rydberg–Rydberg perturbations have been extensively studied. The first valence–valence crossing to be experimentally documented for NO is reported here and occurs between the $^{15}N^{18}O$ $B\ ^2\Pi$ ($v = 18$) and $B'\ ^2\Delta$ ($v = 1$) levels. No level shifts larger than the detection limit of 0.1 cm^{-1} are observed at the crossings near $J = 6.5$ [$B\ ^2\Pi(F_1) \sim B'\ ^2\Delta(F_2)$] and $J = 12.5$ [$B\ ^2\Pi(F_1) \sim B'\ ^2\Delta(F_1)$]; two crossings involving higher rotational levels could not be examined. Semi-empirical calculations of spin–orbit and Coriolis perturbation matrix elements indicate that although the electronic part of the $B\ ^2\Pi \sim B'\ ^2\Delta$ interaction is large, a small vibrational factor renders the $^{15}N^{18}O$ B ($v = 18$) $-$ B' ($v = 1$) perturbation unobservable. Semi-empirical estimates are given for all perturbation matrix elements of the operators $\sum_i \hat{a}_i l_i \cdot s_i$ and $B(L_{\pm}S_{\mp} - J_{\pm}L_{\mp})$ which connect states belonging to the configurations $(\sigma 2p)^2(\pi 2p)^4(\pi^* 2p)$, $(\sigma 2p)(\pi 2p)^4(\pi^* 2p)^2$, and $(\sigma 2p)^2(\pi 2p)^3(\pi^* 2p)^2$.

I. INTRODUCTION

The excited states of the NO molecule have been extensively studied (*1*). Although numerous perturbations (configuration mixing) exist between Rydberg (R) and valence (NR) states, classification into $nl\lambda$ R-states and into NR-states of Σ^+, Σ^-, Π, and Δ symmetry has been possible by various deperturbation techniques. Configurationally mixed (observed) vibronic levels appear in the absorption spectrum as violet-degraded R-bands and red-degraded NR-bands. When two bands cross or approach each other, their structure usually appears strongly perturbed. Homogeneous R $\sim$ NR interactions of the type $np\pi$, $^2\Pi \sim B\ ^2\Pi$ and $nd\delta$, $^2\Delta \sim B'\ ^2\Delta$ have been evaluated in detail (*2, 3*). Band crossings of the type R $\sim$ R and NR $\sim$ NR, however, are rare because the bands are degraded in the same direction. Nevertheless, $3d\sigma \sim 5s\sigma$ and $3p\sigma \sim 3s\sigma$ R $\sim$ R crossings have been observed and small perturbations noticed (*4*). To date not one NR $\sim$ NR crossing has been reported for NO. Perturbations between two valence states are well known in many other molecules. The absence of observed NR $\sim$ NR

[1] Alfred P. Sloan Fellow.

perturbations in NO is not due to vanishing perturbation matrix elements (spin–orbit and Coriolis matrix elements in NO should be comparable in magnitude to those in CO or NO^+), rather to the complexity of the NO spectrum and the accidental nesting of NR potential energy curves.

When the absorption spectra of four different isotopic species of NO are examined, only one example of an observable NR $\sim$ NR crossing can be found. The nearly degenerate vibrational levels are $^{15}N^{18}O$ $B\,^2\Pi$ ($v = 18$) and $B'\,^2\Delta$ ($v = 1$). The corresponding overlapping $B\,^2\Pi$–$X\,^2\Pi(18, 0)$ and $B'\,^2\Delta$–$X\,^2\Pi(1, 0)$ bands occur near 163.5 nm and are reproduced in Fig. 1.

The observed $^{15}N^{18}O$ $B\,^2\Pi$ ($v = 18$) $\sim$ $B'\,^2\Delta$ ($v = 1$) crossing is described in Section II. No level shifts due to perturbations are detected. In order to explain this null result and to determine whether it has any bearing on other possible NR $\sim$ NR interactions in NO, semi-empirical estimates are given in Section III of all spin–orbit and Coriolis matrix elements which connect states belonging to the three lowest-energy valence electronic configurations of NO. It is shown that the electronic part of the $B\,^2\Pi \sim B'\,^2\Delta$ matrix element is not small, thus the undetectability of the $^{15}N^{18}O$ B ($v = 18$) $\sim$ B' ($v = 1$) perturbation must be due to a small vibrational factor. In Section IV the vibrational factor is, in fact, shown to be small. A strong R $\sim$ NR interaction between $C\,^2\Pi$ ($v = 4$) and $B\,^2\Pi$ ($v = 18$) is shown to have only a minor effect on the $B \sim B'$ matrix element. A perturbation matrix element above the 0.1 cm^{-1} detection threshold is predicted for the $B(F_2) \sim B'(F_1)$ crossing near $J = 30.5$; however, lines corresponding to rotational levels above $J' = 14.5$ do not appear in the available low-temperature absorption spectra.

II. THE CROSSING BANDS $B\,^2\Pi$–$X\,^2\Pi(18, 0) \sim B'\,^2\Delta$–$X\,^2\Pi(1, 0)$ of $^{15}N^{18}O$

The absorption spectrum of $^{15}N^{18}O$ (98.3% ^{15}N, 95.5% ^{18}O) was photographed several years ago at the 10.5 m vacuum spectrograph of the National Research Council of Canada, Ottawa. The NO gas was maintained at -180°C. Room-temperature spectra are useless for analysis because of the abundance of unresolved rotational lines. Analysis of the low-temperature bands is striaghtforward and results in the total energy curves shown in Fig. 2. Two crossings between the $B\,^2\Pi$ ($v = 18$) and $B'\,^2\Delta$ ($v = 1$) curves fall in the observable range of J: the F_1 component of the regular $B\,^2\Pi$ level crosses the F_2 component of the inverted $B'\,^2\Delta$ level near $J = 6.5$; the second crossing is between F_1 of $B\,^2\Pi$ and F_1 of $B'\,^2\Delta$ very close to $J = 12.5$. The arrows in Fig. 1 mark the rotational lines closest to the crossing points in the R and P branches of the B–X and B'–X bands. Plotted in Fig. 3 are the measured differences between lines of the relevant branches near the crossing points:

$$\text{Curve I:} \quad B\,^2\Pi\ P_{11}(J+1) - B'\,^2\Delta\ P_{21}(J+1);$$

$$\text{Curve II:} \quad \text{Mean of} \begin{cases} B\,^2\Pi\ R_{11}(J-1) - B'\,^2\Delta\ R_{11}(J-1), \\ B\,^2\Pi\ P_{11}(J+1) - B'\,^2\Delta\ P_{11}(J+1). \end{cases}$$

These curves show that at both crossings *no* level shift due to perturbations exists which is larger than the experimental accuracy of 0.1 cm^{-1}. This null effect will be discussed in Section IV.

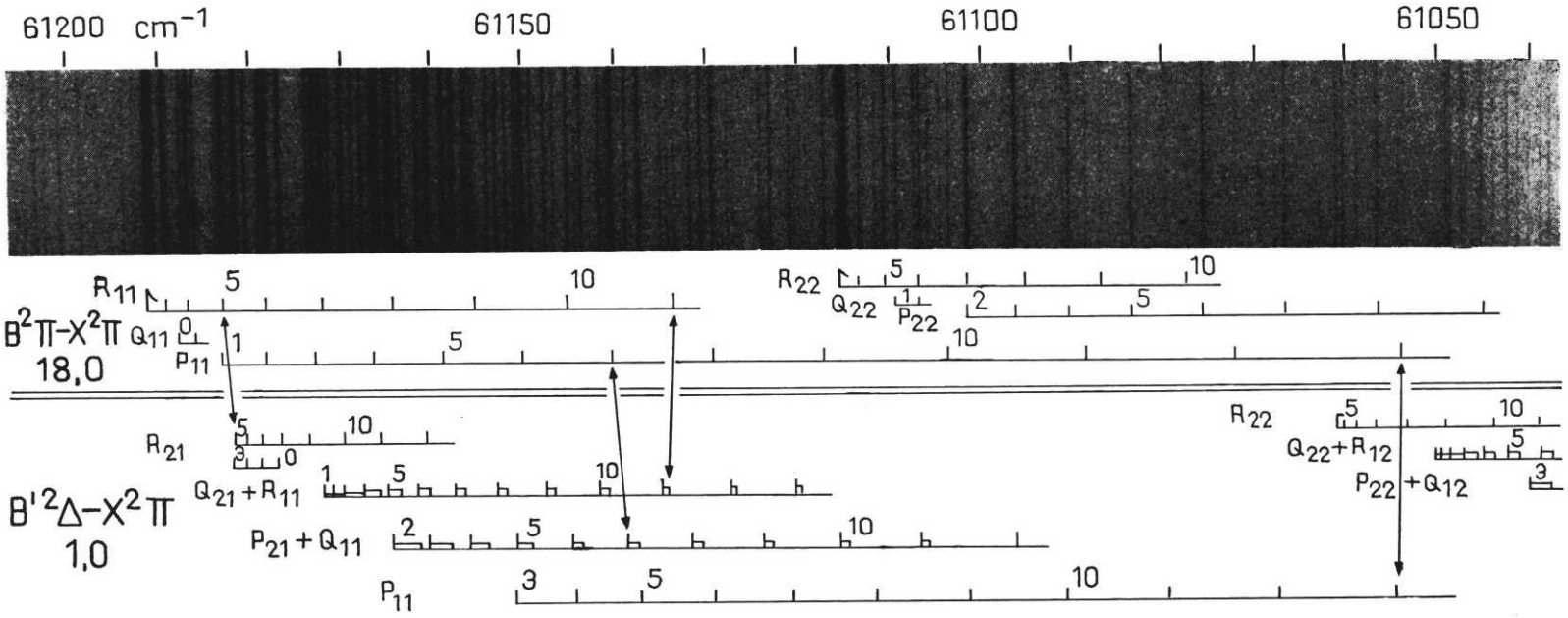

FIG. 1. Crossing bands $B'\ ^2\Delta$–$X\ ^2\Pi_{\frac{1}{2}}(1, 0)$ and $B\ ^2\Pi$–$X\ ^2\Pi_{\frac{1}{2}}$ (18, 0) in the absorption spectrum of cold $^{15}N^{18}O$ gas.

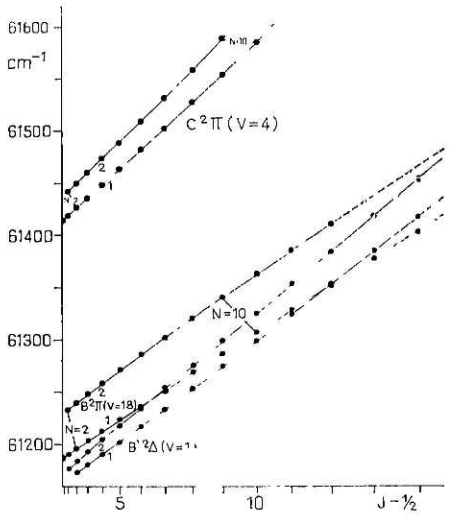

FIG. 2. Total energies of the levels $B'\ ^2\Delta$ ($v = 1$), $B\ ^2\Pi$ ($v = 18$), and $C\ ^2\Pi$ ($v = 4$) of $^{15}N^{18}O$. Energy refers to the level $X\ ^2\Pi_{\frac{1}{2}}$ ($J = \frac{1}{2}$, $v = 0$).

A rotational constant is easily calculated for the $B'\ ^2\Delta$ ($v = 1$) level. $B_1(^{15}N^{18}O) = 1.185\ cm^{-1}$ is obtained which is isotopically consistent with $B_1(^{14}N^{16}O) = 1.302\ cm^{-1}$ determined previously (*3*). However, a rotational *constant* for the $B\ ^2\Pi$ ($v = 18$) level does not, in the traditional usage, exist. This point requires clarification in view of the discussion of vibrational overlap integrals in Section IV. The observed level which we label "$B\ ^2\Pi$ ($v = 18$)" is not a pure NR-level and $v = 18$ is not a *good* vibrational quantum number. The observed level is a mixture of $B\ ^2\Pi$ ($v = 18$) with $^2\Pi$ R-levels, primarily the nearby $3p\pi$, $C\ ^2\Pi$ ($v = 4$) level. The observed $C\ ^2\Pi$ ($v = 4$) level with its complementary admixture of $B\ ^2\Pi$ ($v = 18$) is plotted in the upper part of Fig. 2. The total energy curves for $B\ ^2\Pi$ ($v = 18$) and $C\ ^2\Pi$ ($v = 4$) are not straight, but are markedly bent away from each other as J increases. The mean of the slopes of the $B\ ^2\Pi$ curves decreases from 1.10 to 0.95 cm^{-1} within the observed J range and is much larger than the calculated deperturbed value of $B_{18}(^{15}N^{18}O) = 0.82\ cm^{-1}$ (*2*). The total energy curves for the $C\ ^2\Pi$ ($v = 4$) level show a slope which increases with J and a doublet spin–splitting (15 cm^{-1} for $N = 2$) far too large for the $3p\pi$ Rydberg configuration. In

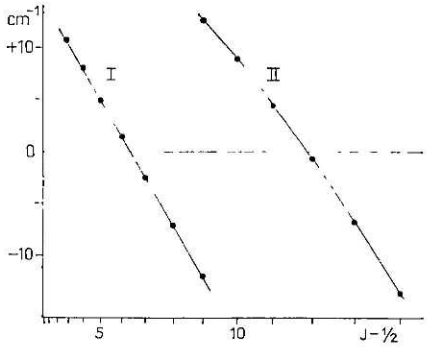

FIG. 3. Differences in energy near the two $\Delta J = 0$ crossing points for the curves in Fig. 2.

Section IV a $B\ ^2\Pi$ ($v = 18$) $\sim$ $C\ ^2\Pi$ ($v = 4$) mixing coefficient is estimated from the difference between observed and deperturbed values of the rotational constants for the B and C states. (An identical mixing coefficient is also obtained from the B and C state spin–orbit splittings). That this mixing coefficient is slightly J-dependent is evident from the changing slopes in Fig. 2. Nevertheless, it should suffice to remark that each observed $B\ ^2\Pi$ ($v = 18$) rotational level corresponds to a rovibronic wavefunction which is composed predominantly of two additive parts, $B\ ^2\Pi$ ($v = 18$) and $C\ ^2\Pi$ ($v = 4$), for which the vibrational and electronic wavefunctions are well defined.

The NO $C\ ^2\Pi$ ($v = 4$) $\sim$ $B\ ^2\Pi$ ($v = 18$) interaction is by itself a remarkable example of a homogeneous perturbation in a band spectrum (*2*, *5*). Figure 4 shows this perturbation for four NO isotopes. With increasing mass, the NR-band B–$X(18, 0)$ moves gradually to lower energy across the C–$X(4, 0)$ R-band and eventually reaches the B'–$X(1, 0)$ NR-band in the $^{15}N^{18}O$ spectrum, where it raises the problem treated in this paper.

III. SPIN–ORBIT AND CORIOLIS MATRIX ELEMENTS

Semi-empirical estimates of spin–orbit and Coriolis matrix elements are made in two steps, the first being considerably more rigorous than the second. First, relative magnitudes of matrix elements between many-electron functions are obtained by reducing intra- and interconfigurational matrix elements to products between trivially calculable numerical factors and one-electron orbital integrals. In the present work, more than 100 nonzero matrix elements between the NO valence states listed in Table I are expressed in terms of only six orbital integrals. Second, these orbital integrals are estimated from observed matrix elements. When experimental observations are not sufficient to determine all of the relevant orbital integrals, some rather drastic approximations (such as pure precession) must be made. Nevertheless, reliable upper bounds for all matrix elements and factor of two estimates for matrix elements expressed in terms of nonzero pure precession orbital integrals are expected.

The simplified microscopic form of the spin–orbit operator commonly used for semi-empirical calculations (*6*, *7*) is

$$H^{SO} = \sum_i \hat{a}_i l_i \cdot s_i, \tag{1}$$

$$\hat{a}_i = \sum_K \frac{Z_K}{r_{Ki}^3}, \tag{2}$$

where l_i = orbital angular momentum of electron i, s_i = spin angular momentum of electron i, Z_K = *effective* charge on nucleus K, r_{Ki} = distance between electron i and nucleus K. Spin–other-orbit interactions between electrons which are both in partially filled orbitals are neglected. Coriolis operators can also be expressed in terms of one- and two-electron operators (*6*):

$$-B(J_+L_- + J_-L_+) = -\left(\frac{\hbar}{4\pi c\mu r^2}\right)[J_+(\sum_i l_{i-}) + J_-(\sum_i l_{i+})], \tag{3}$$

$$B(L_+S_- + L_-S_+) = \left(\frac{\hbar}{4\pi c\mu r^2}\right)[(\sum_i l_{i+})\cdot(\sum_j s_{j-}) + (\sum_i l_{i-})\cdot(\sum_j s_{j+})]. \tag{4}$$

Table I

Configurations Giving Rise To Low-Lying Valence States of NO

Configuration	Derived States
$KK(\sigma 2s)^2(\sigma^*2s)^2(\sigma 2p)^2(\pi 2p)^4(\pi^*2p)$	$X^2\Pi$
$KK(\sigma 2s)^2(\sigma^*2s)^2(\sigma 2p)\ (\pi 2p)^4(\pi^*2p)^2$	$G^2\Sigma^-, I^2\Sigma^+, b^4\Sigma^-, B'^2\Delta$
$KK(\sigma 2s)^2(\sigma^*2s)^2(\sigma 2p)^2(\pi 2p)^3(\pi^*2p)^2$	$B^2\Pi, L^2\Pi, P^2\Pi, a^4\Pi, L'^2\Phi$

Evaluation of matrix elements of these one- and two-electron operators is facilitated by representing electronic states as antisymmetrized products of one-electron molecular orbitals (Slater determinants). The configurations giving rise to the ground state and low-lying valence states of NO are listed in Table I. Determinantal wavefunctions which have the proper values of Λ and Σ and which transform properly under σ_v are constructed for each state.

In order to maintain a consistent phase convention, a standard order is defined:

$$(1^+1^- - 1^+ - 1^-0^+0^-1^{+*}1^{-*} - 1^{+*} - 1^{-*}),$$

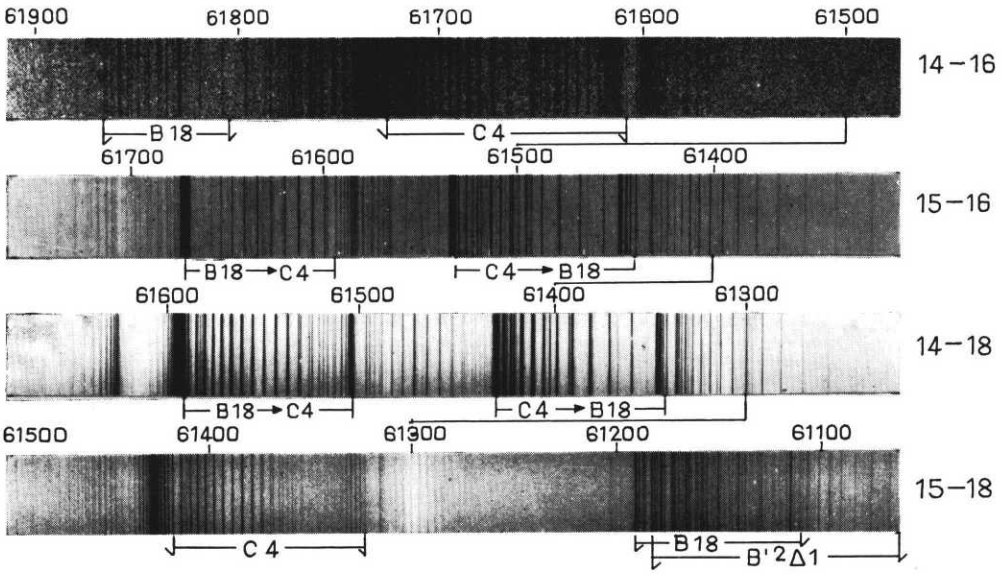

FIG. 4. Interacting R ~ NR pair of doublet bands in the absorption spectra of four different NO isotopes. The NR- and R-levels $B\ ^2\Pi$ ($v = 18$) and $C\ ^2\Pi$ ($v = 4$), are labeled, respectively, $B18$ and $C4$. Isotopic masses of N and O appear to the right of the corresponding spectrum. $B18 \rightarrow C4$ means that low rotational levels are NR, high rotational levels are R, and vice versa for $C4 \rightarrow B18$. The $^{14}N^{16}O$ spectrum was obtained with the 3 m NRC instrument (*2*), the others with the 10.5 m NRC instrument (*17*).

where numerals denote the value of λ (projection of one-electron orbital angular momentum, l, on internuclear axis), $\pm$ denotes $\sigma = \pm\frac{1}{2}$ (projection of one-electron spin angular momentum, s, on internuclear axis), and an asterisk denotes antibonding character. Each state is represented by the main diagonal of a Slater determinant. Linear combinations of Slater determinants which exhibit proper reflection symmetry are constructed for the $G\,^2\Sigma^-$ and $I\,^2\Sigma^+$ states. In the calculation of observable properties of real states, it is necessary to use wavefunctions which not only exhibit the same symmetry as that state but for which the electrostatic Hamiltonian is diagonal (*8*). When more than one eigenfunction of the same symmetry and electronic configuration exist, mixing of basis functions by the interelectronic repulsion operator, $1/r_{ij}$, must be taken into account. In calculating the lifetime of the $a\,^4\Pi$ state of NO, Lin (*9*) did not construct wavefunctions for the $A\,^2\Sigma^+$ state which exhibit the proper reflection symmetry (*10*) and also failed to use an eigenfunction of the electrostatic Hamiltonian for the $B\,^2\Pi$ state. Walker (*11*),[2] in calculating reduced matrix elements of the spin–orbit and Coriolis operators for the $(\pi)(\pi^*)^2$ configuration [which is analogous to $(\pi)^3(\pi^*)^2$] uses $^1\Sigma^+$, $^3\Sigma^-$, $^1\Delta$ $(\pi^*)^2$ parentage wavefunctions to represent the three $^2\Pi$ states; these parentage $^2\Pi$ functions are not eigenfunctions of the electrostatic $(\pi)^3(\pi^*)^2\,^2\Pi$ Hamiltonian. Eigenstates calculated for NO by Lefebvre-Brion and Moser (*12*) have been used here for the three real $^2\Pi$ states: $B\,^2\Pi$, $L\,^2\Pi$, and $P\,^2\Pi$.

Since parity is a good quantum number, wavefunctions are written in a parity basis. The proper parity linear combinations are derived with the use of the operator:

$$\sigma_v|\Lambda S\Sigma\rangle|\Omega J\rangle = (-1)^{J+S-2\Omega+\tilde{\sigma}}|-\Lambda S-\Sigma\rangle|-\Omega J\rangle, \tag{5}$$

where $\tilde{\sigma} = 1$ for Σ^- states, $\tilde{\sigma} = 0$ for all other states (*13*). $|\Lambda S\Sigma\rangle$ is represented by a Slater determinant; the form of $|\Omega J\rangle$ is not explicitly considered. The reflection operator is written as a product of one-electron operators when operating on $|\Lambda S\Sigma\rangle$:

$$\sigma_v = \prod_i \sigma_{vi}, \tag{6a}$$

where

$$\sigma_{vi}|\lambda s\sigma\rangle = (-1)^{\lambda+s-\sigma}|-\lambda s-\sigma\rangle. \tag{6b}$$

Determinantal wavefunctions in the parity basis for states arising from configurations in Table I are listed in Table II.

Matrix elements of the spin–orbit operator between Slater determinants vanish if the two determinants differ by more than one spin–orbital (*14*). Nonzero matrix elements are reduced to matrix elements between single molecular orbitals. Matrix elements of $\hat{a}$ and $\hat{a}l_\pm$ are not evaluated explicitly but are left as parameters to be determined from experimental data and are assumed to be independent of internuclear distance. The one-electron orbital angular momentum, l, is not a good quantum number, so that matrix elements of $l_\pm$ are also left as unevaluated parameters. The adequacy of this r-independent, equivalent-orbital single configuration, one-electron treatment is discussed in Ref. (*15*).

[2] Two typographical errors have been discovered in Ref. (*11*, Table IV): Under "One electron outside closed shells" the first $\sigma\pi^2(^2\Sigma^-)$ should read $\sigma\pi^2(^4\Sigma^-)$ and under "Three electrons outside closed shells" the diagonal matrix element of $\pi^2\pi(^4\Pi)$ should read $\sqrt{10}/3\ A'$.

Nonzero matrix elements of spin–orbit and Coriolis operators are listed in Table III, expressed in terms of six one-electron orbital integrals:

$$a_1 = \langle \pi 2p | \hat{a} | \pi 2p \rangle,$$
$$a_2 = \langle \pi^* 2p | \hat{a} | \pi^* 2p \rangle,$$
$$a_3 = \langle \pi 2p | \hat{a} l_+ | \sigma 2p \rangle,$$
$$a_4 = \langle \pi^* 2p | \hat{a} l_+ | \sigma 2p \rangle,$$
$$b_1 = \langle \pi 2p | l_+ | \sigma 2p \rangle,$$
$$b_2 = \langle \pi^* 2p | l_+ | \sigma 2p \rangle.$$

Only two of these six parameters can be directly evaluated from observed matrix elements:

$$\langle X\, {}^2\Pi_{\frac{1}{2}}^{\pm} | H^{SO} | X\, {}^2\Pi_{\frac{1}{2}}^{\pm} \rangle = -\tfrac{1}{2} a_2 = -\tfrac{1}{2} A(X\, {}^2\Pi), \tag{7a}$$

where $A(X\, {}^2\Pi) = 124$ cm^{-1} (*16*),

$$\langle B\, {}^2\Pi_{\frac{3}{2}}^{\pm} | H^{SO} | B\, {}^2\Pi_{\frac{3}{2}}^{\pm} \rangle = 0.312 a_1 - 0.144 a_2 = \tfrac{1}{2} A(B\, {}^2\Pi), \tag{7b}$$

where $A(B\, {}^2\Pi) = 31$ cm^{-1} (*17*). Thus,

$$a_1 = 107 \text{ cm}^{-1}, \tag{8a}$$

$$a_2 = 124 \text{ cm}^{-1}. \tag{8b}$$

Many-electron matrix elements calculated using the diagonal orbital integrals a_1 and a_2 are expected to be accurate to within a factor of 2. Comparison with observed spin–orbit splittings is given in Table IV.

In order to estimate the four remaining nondiagonal orbital integrals, a pure precession approach is adopted. In the pure precession limit, l is assigned an integral value (in this case $l = 1$, assuming that $\pi 2p$, $\pi^* 2p$, and $\sigma 2p$ molecular orbitals are comprised predominantly of $2p$ atomic orbitals) and the LCAO coefficients of bonding and antibonding orbitals differ only in phase so that

$$\langle \pi 2p | l_+ | \sigma 2p \rangle = \langle \pi^* 2p | l_+ | \sigma^* 2p \rangle = 0,$$
$$\langle \pi^* 2p | l_+ | \sigma 2p \rangle = \langle \pi 2p | l_+ | \sigma^* 2p \rangle = \sqrt{2}.$$

Thus

$$a_3 = 0,$$
$$a_4 = \sqrt{2}\, a_2 = 175 \text{ cm}^{-1}, \tag{8c}$$
$$b_1 = 0,$$
$$b_2 = \sqrt{2}. \tag{8d}$$

In a real molecule, corresponding orbitals from two configurations are not identical, orbital overlap integrals will be ≤ 1, and equations (8c) and (8d) will be good estimates *and* upper bounds for a_4 and b_2. In a real molecule, $|\pi 2p\rangle$ and $|\pi^* 2p\rangle$ differ by more than the phases of their atomic orbital coefficients, $l_+ |\sigma 2p\rangle$ will not be orthogonal to $|\pi 2p\rangle$, and a_3 and b_1 will be nonzero:

$$0 < a_3 < a_4 \simeq \sqrt{2}\, a_2, \tag{8e}$$

$$0 < |b_1| < b_2 \simeq \sqrt{2}. \tag{8f}$$

Table II

Determinantal Wavefunctions for Electronic States of NO

$$|X^2\Pi^{\pm}_{3/2}> = \frac{1}{\sqrt{2}}\{|\Lambda=1,S=1/2,\Sigma=1/2>|\Omega=3/2,J>\mp(-1)^{J-3/2}|\Lambda=-1,S=1/2,\Sigma=-1/2>|\Omega=-3/2,J>\}$$

$$|X^2\Pi^{\pm}_{1/2}> = \frac{1}{\sqrt{2}}\{|\Lambda=1,S=1/2,\Sigma=-1/2>\pm(-1)^{J-1/2}|\Lambda=-1,S=1/2,\Sigma=1/2>\}^a$$

$$|L'^2\Phi^{\pm}_{7/2}> = \frac{1}{\sqrt{2}}\{|\Lambda=3,S=1/2,\Sigma=1/2>\mp(-1)^{J-7/2}|\Lambda=-3,S=1/2,\Sigma=-1/2>\}$$

$$|L'^2\Phi^{\pm}_{5/2}> = \frac{1}{\sqrt{2}}\{|\Lambda=3,S=1/2,\Sigma=-1/2>\pm(-1)^{J-5/2}|\Lambda=-3,S=1/2,\Sigma=1/2>\}$$

$$|B'^2\Delta^{\pm}_{5/2}> = \frac{1}{\sqrt{2}}\{|\Lambda=2,S=1/2,\Sigma=1/2>\pm(-1)^{J-5/2}|\Lambda=-2,S=1/2,\Sigma=-1/2>\}$$

$$|B'^2\Delta^{\pm}_{3/2}> = \frac{1}{\sqrt{2}}\{|\Lambda=2,S=1/2,\Sigma=-1/2>\mp(-1)^{J-3/2}|\Lambda=-2,S=1/2,\Sigma=1/2>\}$$

$$|a^4\Pi^{\pm}_{5/2}> = \frac{1}{\sqrt{2}}\{|\Lambda=1,S=3/2,\Sigma=3/2>\mp(-1)^{J-5/2}|\Lambda=-1,S=3/2,\Sigma=-3/2>\}$$

$$|a^4\Pi^{\pm}_{3/2}> = \frac{1}{\sqrt{6}}\{|a>+|b>+|c>\pm(-1)^{J-3/2}(|a->+|b->+|c->)\}^b$$

$$|a^4\Pi^{\pm}_{1/2}> = \frac{1}{\sqrt{6}}\{|e>+|f>+|g>\pm(-1)^{J-1/2}(|e->+|f->+|g->)\}$$

$$|a^4\Pi^{\pm}_{-1/2}> = \frac{1}{\sqrt{2}}\{|\Lambda=1,S=3/2,\Sigma=-3/2>\pm(-1)^{J+1/2}|\Lambda=-1,S=3/2,\Sigma=3/2>\}$$

$$|B^2\Pi^{\pm}_{3/2}> = \frac{1}{\sqrt{2}}\{-0.558|a>+0.408|b>+0.149|c>-0.707|d> \pm(-1)^{J-3/2}(-0.558|a->+0.408|b->+0.149|c->-0.707|d->)\}^c$$

$$|B^2\Pi^{\pm}_{1/2}> = \frac{1}{\sqrt{2}}\{0.558|e>-0.150|f>-0.409|g>-0.707|h> \pm(-1)^{J-1/2}(0.558|e->-0.150|f->-0.409|g->-0.707|h->)\}^c$$

$$|L^2\Pi^{\pm}_{3/2}> = \frac{1}{\sqrt{2}}\{-0.149|a>+0.708|b>-0.558|c>+0.408|d> \pm(-1)^{J-3/2}(-0.149|a->+0.708|b->-0.558|c->+0.408|d->)\}^c$$

$$|L^2\Pi^{\pm}_{1/2}> = \frac{1}{\sqrt{2}}\{0.149|e>+0.558|f>-0.708|g>+0.408|h> \pm(-1)^{J-1/2}(0.149|e->+0.558|f->-0.708|g->+0.408|h->)\}^c$$

---

[a] Except for $|X\ ^2\Pi_{\frac{1}{2}}^{\pm}\rangle$, the $|\Omega J\rangle$ part of the wavefunction has been suppressed for conciseness.

[b] Slater determinants are symbolized by $|\Lambda S\Sigma\rangle$ when only one Slater determinant can be constructed with the specified values of Λ, S, Σ. Otherwise, letters are used as labels.

[c] The $B\ ^2\Pi$, $L\ ^2\Pi$, and $P\ ^2\Pi$ wavefunctions are taken from Ref. (*12*) after correcting two typographical errors [H. Lefebvre-Brion, private communication: replace the orbital part of the ϕ_2 and ϕ_2' functions by $(\omega\pi^+)^2(v\pi^+)(\omega\pi^-)(v\pi^-)$ and replace $\psi(P\ ^2\Pi)$ by $-(1/\sqrt{3})\phi_1 - (\frac{2}{3})^{\frac{1}{2}}\phi_2$]. The $^2\Pi$ functions of Ref. (*12*) are $\phi_1 = -|d\rangle$, $\phi_2 = 1/\sqrt{2}(|a\rangle - |c\rangle)$, $\phi_2' = 1/\sqrt{6}(|a\rangle + |c\rangle - 2|b\rangle)$.

Table II. Continued.

$$|P^2\Pi^{\pm}_{3/2}> = \frac{1}{\sqrt{2}}\{-0.577|a>+0.577|c>+0.577|d> \pm(-1)^{J-3/2}(-0.577|a->+0.577|c->+0.577|d->)\}^{c}$$

$$|P^2\Pi^{\pm}_{1/2}> = \frac{1}{\sqrt{2}}\{0.577|e>-0.577|f>+0.577|h> \pm(-1)^{J-1/2}(0.577|e->-0.577|f->+0.577|h->)\}^{c}$$

$$|b^4\Sigma^{-\pm}_{3/2}> = \frac{1}{\sqrt{2}}\{|\Lambda=0,S=3/2,\Sigma=3/2>\mp(-1)^{J-3/2}|\Lambda=0,S=3/2,\Sigma=-3/2>\}$$

$$|b^4\Sigma^{-\pm}_{1/2}> = \frac{1}{\sqrt{6}}\{|i>+|j>+|k>\pm(-1)^{J-1/2}(|i->+|j->+|k->)\}$$

$$|G^2\Sigma^{-\pm}_{1/2}> = \frac{1}{2\sqrt{3}}\{2|i>-|j>-|k>\pm(-1)^{J-1/2}(2|i->-|j->-|k->)\}$$

$$|I^2\Sigma^{+\pm}_{1/2}> = \frac{1}{2}\{|j>-|k>\pm(-1)^{J-1/2}(|j->-|k->)\}$$

where,

$$\sigma_v|\Lambda=1,S=1/2,\Sigma=1/2>=\sigma_v|1^+1^--1^+-1^-0^+0^-1^{+*}> = (-1)\ |\Lambda=-1,S=1/2,\Sigma=-1/2>$$
$$\sigma_v|\Lambda=1,S=1/2,\Sigma=-1/2>=\sigma_v|1^+1^--1^+-1^-0^+0^-1^{-*}> = \ |\Lambda=-1,S=1/2,\Sigma=1/2>$$
$$\sigma_v|\Lambda=3,S=1/2,\Sigma=1/2>=\sigma_v|1^+1^--1^+0^+0^-1^{+*}1^{-*}> = (-1)\ |\Lambda=-3,S=1/2,\Sigma=-1/2>$$
$$\sigma_v|\Lambda=3,S=1/2,\Sigma=-1/2>=\sigma_v|1^+1^--1^-0^+0^-1^{+*}1^{-*}> = \ |\Lambda=-3,S=1/2,\Sigma=1/2>$$
$$\sigma_v|\Lambda=2,S=1/2,\Sigma=1/2>=\sigma_v(-1)|1^+1^--1^+-1^-0^+1^{+*}1^{-*}> = \ |\Lambda=-2,S=1/2,\Sigma=-1/2>$$
$$\sigma_v|\Lambda=2,S=1/2,\Sigma=-1/2>=\sigma_v(-1)|1^+1^--1^+-1^-0^-1^{+*}1^{-*}> = (-1)\ |\Lambda=-2,S=1/2,\Sigma=1/2>$$
$$\sigma_v|\Lambda=1,S=3/2,\Sigma=3/2>=\sigma_v|1^+1^--1^+0^+0^-1^{+*}-1^{+*}> = (-1)\ |\Lambda=-1,S=3/2,\Sigma=-3/2>$$
$$\sigma_v|\Lambda=1,S=3/2,\Sigma=-3/2>=\sigma_v|1^+1^--1^-0^+0^-1^{-*}-1^{-*}> = \ |\Lambda=-1,S=3/2,\Sigma=3/2>$$
$$\sigma_v|\Lambda=0,S=3/2,\Sigma=3/2>=\sigma_v(-1)|1^+1^--1^+-1^-0^+1^{+*}-1^{+*}> = (-1)\ |\Lambda=0,S=3/2,\Sigma=-3/2>$$

$$\sigma_v|a> = \sigma_v|1^+1^--1^-0^+0^-1^{+*}-1^{+*}> = |a->$$
$$\sigma_v|b> = \sigma_v|1^+1^--1^+0^+0^-1^{-*}-1^{+*}> = |b->$$
$$\sigma_v|c> = \sigma_v|1^+1^--1^+0^+0^-1^{+*}-1^{-*}> = |c->$$
$$\sigma_v|d> = \sigma_v|1^+-1^+-1^-0^+0^-1^{+*}1^{-*}> = |d->$$
$$\sigma_v|e> = \sigma_v|1^+1^--1^+0^+0^-1^{-*}-1^{-*}> = |e->$$
$$\sigma_v|f> = \sigma_v|1^+1^--1^-0^+0^-1^{-*}-1^{+*}> = |f->$$
$$\sigma_v|g> = \sigma_v|1^+1^--1^-0^+0^-1^{+*}-1^{-*}> = |g->$$
$$\sigma_v|h> = (-1)\sigma_v|1^-1^+-1^-0^+0^-1^{+*}1^{-*}> = |h->$$
$$\sigma_v|i> = (-1)\sigma_v|1^+1^--1^+-1^-0^-1^{+*}-1^{+*}> = |i->$$
$$\sigma_v|j> = (-1)\sigma_v|1^+1^--1^+-1^-0^+1^{-*}-1^{+*}> = |j->$$
$$\sigma_v|k> = \sigma_v|1^+1^--1^+-1^-0^+1^{+*}-1^{-*}> = |k->$$

Table III

Nonzero Matrix Elements of Spin-Orbit and Coriolis Operators[a,b]

$$\langle v, X^2\Pi^{\pm}_{3/2}|H^{SO}|X\,^2\Pi^{\pm}_{3/2}, v'\rangle = \frac{1}{2}a_2\,\delta_{vv'}{}^{c}$$

$$\langle v, X^2\Pi^{\pm}_{1/2}|H^{SO}|X\,^2\Pi^{\pm}_{1/2}, v'\rangle = -\frac{1}{2}a_2\,\delta_{vv'}{}^{c}$$

$$\langle v, X^2\Pi^{\pm}_{3/2}|H^{SO}|b\,^4\Sigma^{-\pm}_{3/2}, v'\rangle = \frac{1}{2}a_4\langle v|v'\rangle{}^{d}$$

$$\langle v, X^2\Pi^{\pm}_{1/2}|H^{SO}|b\,^4\Sigma^{-\pm}_{1/2}, v'\rangle = \frac{\sqrt{3}}{6}a_4\langle v|v'\rangle$$

$$\langle v, X^2\Pi^{\pm}_{1/2}|H^{SO} + B(L_+S_- + L_-S_+ - J_+L_- - J_-L_+)|G^2\Sigma^{-\pm}_{1/2}, v'\rangle =$$
$$-\frac{\sqrt{6}}{12}a_4\langle v|v'\rangle - \frac{\sqrt{6}}{2}B_{vv',b_2}[1 \pm (-1)^{J-1/2}\sqrt{J(J+1)+1/4}\,]$$

$$\langle v, X^2\Pi^{\pm}_{1/2}|H^{SO} + B(L_+S_- + L_-S_+ - J_+L_- - J_-L_+)|I^2\Sigma^{+\pm}_{1/2}, v'\rangle =$$
$$\frac{\sqrt{2}}{4}a_4\langle v|v'\rangle - \frac{\sqrt{2}}{2}B_{vv',b_2}[1 \mp (-1)^{J-1/2}\sqrt{J(J+1)+1/4}\,]$$

$$\langle v, X^2\Pi^{\pm}_{3/2}|H^{SO} + B(L_+S_- + L_-S_+)|B'\,^2\Delta^{\pm}_{3/2}, v'\rangle = -\frac{1}{2}a_4\langle v|v'\rangle\quad B_{vv',b_2}$$

$$\langle v, X^2\Pi^{\pm}_{3/2}|-B(J_+L_- + J_-L_+)|G^2\Sigma^{-\pm}_{1/2}, v'\rangle = \frac{\sqrt{6}}{2}\sqrt{J(J+1)-3/4}\;B_{vv',b_2}$$

$$\langle v, X^2\Pi^{\pm}_{3/2}|-B(J_+L_- + J_-L_+)|I^2\Sigma^{+\pm}_{1/2}, v'\rangle = \frac{\sqrt{2}}{2}\sqrt{J(J+1)-3/4}\;B_{vv',b_2}$$

$$\langle v, X^2\Pi^{\pm}_{3/2}|-B(J_+L_- + J_-L_+)|B'^2\Delta^{\pm}_{5/2}, v'\rangle = -\sqrt{J(J+1)-15/4}\;B_{vv',b_2}$$

$$\langle v, X^2\Pi^{\pm}_{1/2}|-B(J_+L_- + J_-L_+)|B'^2\Delta^{\pm}_{3/2}, v'\rangle = -\sqrt{J(J+1)-3/4}\;B_{vv',b_2}$$

$$\langle v, b^4\Sigma^{-\pm}_{1/2}|H^{SO}|I^2\Sigma^{+\pm}_{1/2}, v'\rangle = -\frac{\sqrt{6}}{3}a_2\langle v|v'\rangle$$

$$\langle v, b^4\Sigma^{-\pm}_{3/2}|H^{SO} + B(L_+S_- + L_-S_+)|a^4\Pi^{\pm}_{3/2}, v'\rangle = -\frac{\sqrt{3}}{6}a_3\langle v|v'\rangle + \sqrt{3}\,B_{vv',b_1}$$

---

[a] This table includes *every* nonzero matrix element of $H' = H^{SO} + B(L_+S_- + L_-S_+ - J_+L_- - J_-L_+)$ between all case "*a*" basis functions listed in Table II.

[b] To facilitate the calculation of matrix elements involving analogous $^2\Pi$ states in other molecules, a table of matrix elements involving the Slater determinants which comprise the $^2\Pi$ states has been prepared and is available from the authors upon request.

[c] Lefebvre-Brion and Moser (*12*) report semi-empirical calculations of spin–orbit constants for the $X\,^2\Pi$, $B\,^2\Pi$, $L\,^2\Pi$, and $P\,^2\Pi$ states of NO. Calculation (A) of (*12*) is nearly identical to the method used here. In (*12*), the matrix element $\langle\phi_2|H^{SO}|\phi_2'\rangle = 1/(12)^{\frac{1}{2}}(a_1 - a_2)$ is arbitrarily set equal to zero. Consequently the spin–orbit constants for $B\,^2\Pi$ and $L\,^2\Pi$ are defined slightly differently: $A(B\,^2\Pi) = \frac{1}{3}a_1$ (*12*) vs $(0.624a_1 - 0.288a_2)$ and $A(L\,^2\Pi) = -\frac{1}{3}a_1 - \frac{2}{3}a_2$ (*12*) vs $(-0.624a_1 - 0.380a_2)$.

Table III. Continued.

$$\langle v,b\,^4\Sigma^{-\pm}_{1/2}|H^{SO} + B(L_+S_- + L_-S_+ - J_+L_- + J_-L_+)|a\,^4\Pi^{\pm}_{1/2},v'\rangle =$$
$$-\tfrac{1}{3}a_3\langle v|v'\rangle + B_{vv',b_1}[2 \mp (-1)^{J-1/2}\sqrt{J(J+1)+1/4}]$$

$$\langle v,b\,^4\Sigma^{-\pm}_{3/2}|-B(J_+L_- + J_-L_+)|a\,^4\Pi^{\pm}_{5/2},v'\rangle = -\sqrt{J(J+1)-15/4}\,B_{vv',b_1}$$

$$\langle v,b\,^4\Sigma^{-\pm}_{1/2}|-B(J_+L_- + J_-L_+)|a\,^4\Pi^{\pm}_{3/2},v'\rangle = -\sqrt{J(J+1)-3/4}\,B_{vv',b_1}$$

$$\langle v,b\,^4\Sigma^{-\pm}_{1/2}|H^{SO} + B(L_+S_- + L_-S_+)|a\,^4\Pi^{\pm}_{-1/2},v'\rangle = \pm(-1)^{J+1/2}\sqrt{3}\,(\tfrac{1}{6}a_3\langle v|v'\rangle + \tfrac{2}{3}B_{vv',b_1})$$

$$\langle v,b\,^4\Sigma^{-\pm}_{3/2}|-B(J_+L_- + J_-L_+)|a\,^4\Pi^{\pm}_{-1/2},v'\rangle = \mp(-1)^{J+1/2}\sqrt{J(J+1)-3/4}\,B_{vv',b_1}$$

$$\langle v,b\,^4\Sigma^{-\pm}_{3/2}|H^{SO}|B\,^2\Pi^{\pm}_{3/2},v'\rangle = 0.279a_3\langle v|v'\rangle$$

$$\langle v,b\,^4\Sigma^{-\pm}_{1/2}|H^{SO}|B\,^2\Pi^{\pm}_{1/2},v'\rangle = 0.161a_3\langle v|v'\rangle$$

$$\langle v,b\,^4\Sigma^{-\pm}_{3/2}|H^{SO}|L\,^2\Pi^{\pm}_{3/2},v'\rangle = 0.0745a_3\langle v|v'\rangle$$

$$\langle v,b\,^4\Sigma^{-\pm}_{1/2}|H^{SO}|L\,^2\Pi^{\pm}_{1/2},v'\rangle = 0.0433a_3\langle v|v'\rangle$$

$$\langle v,b\,^4\Sigma^{-\pm}_{3/2}|H^{SO}|P\,^2\Pi^{\pm}_{3/2},v'\rangle = 0.288a_3\langle v|v'\rangle$$

$$\langle v,b\,^4\Sigma^{-\pm}_{1/2}|H^{SO}|P\,^2\Pi^{\pm}_{1/2},v'\rangle = 0.166a_3\langle v|v'\rangle$$

$$\langle v,G^2\Sigma^{-\pm}_{1/2}|H^{SO}|I\,^2\Sigma^{+\pm}_{1/2},v'\rangle = \sqrt{\tfrac{3}{3}}\,a_2\langle v|v'\rangle$$

$$\langle v,G^2\Sigma^{-\pm}_{1/2}|H^{SO}|a\,^4\Pi^{\pm}_{1/2},v'\rangle = \sqrt{\tfrac{2}{6}}\,a_3\langle v|v'\rangle$$

$$\langle v,G^2\Sigma^{-\pm}_{1/2}|H^{SO}|a\,^4\Pi^{\pm}_{-1/2},v'\rangle = \pm(-1)^{J+1/2}\tfrac{\sqrt{6}}{6}a_3\langle v|v'\rangle$$

$$\langle v,G^2\Sigma^{-\pm}_{1/2}|H^{SO} + B(L_+S_- + L_-S_+ - J_+L_- - J_-L_+)|B\,^2\Pi^{\pm}_{1/2},v'\rangle =$$
$$-0.118a_3\langle v|v'\rangle - 0.684B_{vv',b_1}[1 \pm (-1)^{J-1/2}\sqrt{J(J+1)+1/4}]$$

$$\langle v,G^2\Sigma^{-\pm}_{1/2}|-B(J_+L_- + J_-L_+)|B\,^2\Pi^{\pm}_{3/2},v'\rangle = 0.684\sqrt{J(J+1)-3/4}\,B_{vv',b_1}$$

---

[d] Lefebvre-Brion and Guerin (*10*) estimate this matrix element to be 70 cm^{-1}. Using a value $a_4 = 175$ cm^{-1}, we obtain a value of 87 cm^{-1}. A similar estimate of this matrix element for the isovalent molecule SiF has been given by R. W. Martin and A. J. Merer [*Can. J. Phys.* **51**, 634 (1973)].

Table III. Continued.

$$\langle v, G^2\Sigma^{-\pm}_{1/2} | H^{SO} + B(L_+S_- + L_-S_+ - J_+L_- - J_-L_+) | L^2\Pi^{\pm}_{1/2}, v' \rangle =$$
$$- 0.0306a_3 \langle v|v' \rangle - 0.183\, B_{vv',b_1}[1 \pm (-1)^{J-1/2}\sqrt{J(J+1)+1/4}\,]$$

$$\langle v, G^2\Sigma^{-\pm}_{1/2} | -B(J_+L_- + J_-L_+) | L\,^2\Pi^{\pm}_{3/2}, v' \rangle = 0.183\sqrt{J(J+1)-3/4}\, B_{vv',b_1}$$

$$\langle v, G^2\Sigma^{-\pm}_{1/2} | H^{SO} + B(L_+S_- + L_-S_+ - J_+L_- - J_-L_+) | P\,^2\Pi^{\pm}_{1/2}, v' \rangle =$$
$$- 0.118a_3 \langle v|v' \rangle - 0.707\, B_{vv',b_1}\,[1 \pm (-1)^{J-1/2}\sqrt{J(J+1)+1/4}\,]$$

$$\langle v, G^2\Sigma^{-\pm}_{1/2} | -B(J_+L_- + J_-L_+) | P\,^2\Pi^{\pm}_{3/2}, v' \rangle = 0.707\sqrt{J(J+1)-3/4}\, B_{vv',b_1}$$

$$\langle v, I^2\Sigma^{+\pm}_{1/2} | H^{SO} + B(L_+S_- + L_-S_+ - J_+L_- - J_-L_+) | B\,^2\Pi^{\pm}_{1/2}, v' \rangle =$$
$$- 0.0916a_3 \langle v|v' \rangle + 0.183\, B_{vv',b_1}\,[1 \mp (-1)^{J-1/2}\sqrt{J(J+1)+1/4}\,]$$

$$\langle v, I^2\Sigma^{+\pm}_{1/2} | -B(J_+L_- + J_-L_+) | B\,^2\Pi^{\pm}_{3/2}, v' \rangle = - 0.183\sqrt{J(J+1)-3/4}\, B_{vv',b_1}$$

$$\langle v, I^2\Sigma^{+\pm}_{1/2} | H^{SO} + B(L_+S_- + L_-S_+ - J_+L_- - J_-L_+) | L\,^2\Pi^{\pm}_{1/2}, v' \rangle =$$
$$- 0.448a_3 \langle v|v' \rangle + 0.895\, B_{vv',b_1}\,[1 \mp (-1)^{J-1/2}\sqrt{J(J+1)+1/4}\,]$$

$$\langle v, I^2\Sigma^{+\pm}_{1/2} | -B(J_+L_- + J_-L_+) | L\,^2\Pi^{\pm}_{3/2}, v' \rangle = - 0.895\sqrt{J(J+1)-3/4}\, B_{vv',b_1}$$

$$\langle v, I^2\Sigma^{+\pm}_{1/2} | H^{SO} + B(L_+S_- + L_-S_+ - J_+L_- - J_-L_+) | P\,^2\Pi^{\pm}_{1/2}, v' \rangle =$$
$$0.204a_3 \langle v|v' \rangle - 0.408\, B_{vv',b_1}\,[1 \mp (-1)^{J-1/2}\sqrt{J(J+1)+1/4}\,]$$

$$\langle v, I^2\Sigma^{+\pm}_{1/2} | -B(J_+L_- + J_-L_+) | P\,^2\Pi^{\pm}_{3/2}, v' \rangle = 0.408\sqrt{J(J+1)-3/4}\, B_{vv',b_1}$$

$$\langle v, a^4\Pi^{\pm}_{5/2} | H^{SO} | a^4\Pi^{\pm}_{5/2}, v' \rangle = -\frac{1}{2}a_1\,\delta_{vv'}$$
$$\langle v, a^4\Pi^{\pm}_{3/2} | H^{SO} | a^4\Pi^{\pm}_{3/2}, v' \rangle = -\frac{1}{6}a_1\,\delta_{vv'}$$
$$\langle v, a^4\Pi^{\pm}_{1/2} | H^{SO} | a^4\Pi^{\pm}_{1/2}, v' \rangle = \frac{1}{6}a_1\,\delta_{vv'}$$
$$\langle v, a^4\Pi^{\pm}_{-1/2} | H^{SO} | a^4\Pi^{\pm}_{-1/2}, v' \rangle = \frac{1}{2}a_1\,\delta_{vv'}$$

Table III. Continued.

$$\langle v,a^4\Pi^{\pm}_{3/2}|H^{SO}|B\ ^2\Pi^{\pm}_{3/2},v'\rangle = \langle v,a^4\Pi^{\pm}_{1/2}|H^{SO}|B^2\Pi^{\pm}_{1/2},v'\rangle = -(0.322a_1 + 0.149a_2)\ \langle v|v'\rangle$$

$$\langle v,a^4\Pi^{\pm}_{3/2}|H^{SO}|L\ ^2\Pi^{\pm}_{3/2},v'\rangle = \langle v,a^4\Pi^{\pm}_{1/2}|H^{SO}|L^2\Pi^{\pm}_{1/2},v'\rangle = -(0.0863a_1 + 0.730a_2)\ \langle v|v'\rangle$$

$$\langle v,a^4\Pi^{\pm}_{3/2}|H^{SO}|P\ ^2\Pi^{\pm}_{3/2},v'\rangle = \langle v,a^4\Pi^{\pm}_{1/2}|H^{SO}|P^2\Pi^{\pm}_{1/2},v'\rangle = -(0.333a_1 - 0.333a_2)\ \langle v|v'\rangle$$

$$\langle v,B^2\Pi^{\pm}_{3/2}|H^{SO}|B\ ^2\Pi^{\pm}_{3/2},v'\rangle = (0.312a_1 - 0.144a_2)\ \delta_{vv'}{}^{c}$$

$$\langle v,B^2\Pi^{\pm}_{1/2}|H^{SO}|B\ ^2\Pi^{\pm}_{1/2},v'\rangle = -(0.312a_1 - 0.144a_2)\ \delta_{vv'}{}^{c}$$

$$\langle v,B^2\Pi^{\pm}_{3/2}|H^{SO}|L\ ^2\Pi^{\pm}_{3/2},v'\rangle = -(0.206a_1 + 0.372a_2)\ \langle v|v'\rangle$$

$$\langle v,B^2\Pi^{\pm}_{1/2}|H^{SO}|L\ ^2\Pi^{\pm}_{1/2},v'\rangle = (0.206a_1 + 0.372a_2)\ \langle v|v'\rangle$$

$$\langle v,B^2\Pi^{\pm}_{3/2}|H^{SO}|P\ ^2\Pi^{\pm}_{3/2},v'\rangle = -(0.0860a_1 - 0.0860a_2)\langle v|v'\rangle$$

$$\langle v,B^2\Pi^{\pm}_{1/2}|H^{SO}|P\ ^2\Pi^{\pm}_{1/2},v'\rangle = (0.0860a_1 - 0.0860a_2)\langle v|v'\rangle$$

$$\langle v,B^2\Pi^{\pm}_{3/2}|H^{SO} + B(L_+S_- + L_-S_+)|B'^2\Delta^{\pm}_{3/2},v'\rangle = 0.354a_3\ \langle v|v'\rangle + 0.707\ B_{vv'}b_1$$

$$\langle v,B^2\Pi^{\pm}_{3/2}|-B(J_+L_- + J_-L_+)|B'^2\Delta^{\pm}_{5/2},v'\rangle = 0.707\ \sqrt{J(J+1)-15/4}\ B_{vv'}b_1$$

$$\langle v,B^2\Pi^{\pm}_{1/2}|-B(J_+L_- + J_-L_+)|B'^2\Delta^{\pm}_{3/2},v'\rangle = 0.707\ \sqrt{J(J+1)-3/4}\ B_{vv'}b_1$$

$$\langle v,L^2\Pi^{\pm}_{3/2}|H^{SO}|L^2\Pi^{\pm}_{3/2},v'\rangle = -(0.312a_1 + 0.190a_2)\ \delta_{vv'}{}^{c}$$

$$\langle v,L^2\Pi^{\pm}_{1/2}|H^{SO}|L^2\Pi^{\pm}_{1/2},v'\rangle = (0.312a_1 + 0.190a_2)\ \delta_{vv'}{}^{c}$$

$$\langle v,L^2\Pi^{\pm}_{3/2}|H^{SO}|P^2\Pi^{\pm}_{3/2},v'\rangle = (0.322a_1 - 0.322a_2)\ \langle v|v'\rangle$$

$$\langle v,L^2\Pi^{\pm}_{1/2}|H^{SO}|P^2\Pi^{\pm}_{1/2},v'\rangle = -(0.322a_1 - 0.322a_2)\ \langle v|v'\rangle$$

Table III. Continued.

$$\langle v, L^2\Pi^{\pm}_{3/2} | H^{SO} + B(L_+S_- + L_-S_+) | B'^2\Delta^{\pm}_{3/2}, v' \rangle = -0.204a_3 \langle v|v'\rangle - 0.408\, B_{vv'}b_1$$

$$\langle v, L^2\Pi^{\pm}_{3/2} | -B(J_+L_- + J_-L_+) | B'^2\Delta^{\pm}_{5/2}, v' \rangle = -0.408 \sqrt{J(J+1)-15/4}\, B_{vv'}b_1$$

$$\langle v, L^2\Pi^{\pm}_{1/2} | -B(J_+L_- + J_-L_+) | B'^2\Delta^{\pm}_{3/2}, v' \rangle = -0.408 \sqrt{J(J+1)-3/4}\, B_{vv'}b_1$$

$$\langle v, P^2\Pi^{\pm}_{3/2} | H^{SO} | P^2\Pi^{\pm}_{3/2}, v' \rangle = (0.166a_1 + 0.333a_2)\, \delta_{vv'}{}^{c}$$

$$\langle v, P^2\Pi^{\pm}_{1/2} | H^{SO} | P^2\Pi^{\pm}_{1/2}, v' \rangle = -(0.166a_1 + 0.333a_2)\, \delta_{vv'}{}^{c}$$

$$\langle v, P^2\Pi^{\pm}_{3/2} | H^{SO} + B(L_+S_- + L_-S_+) | B'^2\Delta^{\pm}_{3/2}, v' \rangle = -0.288a_3 \langle v|v'\rangle - 0.577\, B_{vv'}b_1$$

$$\langle v, P^2\Pi^{\pm}_{3/2} | -B(J_+L_- + J_-L_+) | B'^2\Delta^{\pm}_{5/2}, v' \rangle = -0.577 \sqrt{J(J+1)-15/4}\, B_{vv'}b_1$$

$$\langle v, P^2\Pi^{\pm}_{1/2} | -B(J_+L_- + J_-L_+) | B'^2\Delta^{\pm}_{3/2}, v' \rangle = -0.577 \sqrt{J(J+1)-3/4}\, B_{vv'}b_1$$

$$\langle v, B'^2\Delta^{\pm}_{5/2} | H^{SO} + B(L_+S_- + L_-S_+) | L'^2\Phi^{\pm}_{5/2}, v' \rangle = -\tfrac{1}{2}a_3 \langle v|v'\rangle - B_{vv'}b_1$$

$$\langle v, B'^2\Delta^{\pm}_{5/2} | -B(J_+L_- + J_-L_+) | L'^2\Phi^{\pm}_{7/2}, v' \rangle = -\sqrt{J(J+1)-35/4}\, B_{vv'}b_1$$

$$\langle v, B'^2\Delta^{\pm}_{3/2} | -B(J_+L_- + J_-L_+) | L'^2\Phi^{\pm}_{5/2}, v' \rangle = -\sqrt{J(J+1)-15/4}\, B_{vv'}b_1$$

$$\langle v, L'^2\Phi^{\pm}_{7/2} | H^{SO} | L'^2\Phi^{\pm}_{7/2}, v' \rangle = -\tfrac{1}{2}a_1\, \delta_{vv'}$$

$$\langle v, L'^2\Phi^{\pm}_{5/2} | H^{SO} | L'^2\Phi^{\pm}_{5/2}, v' \rangle = \tfrac{1}{2}a_1\, \delta_{vv'}$$

where

$a_1 \equiv \langle \pm 1 | \hat{a} | \pm 1 \rangle$

$a_2 \equiv \langle \pm 1^* | \hat{a} | \pm 1^* \rangle$

$a_3 \equiv \langle \pm 1 | \hat{a}\ell_{\pm} | 0 \rangle = \langle 0 | \hat{a}\ell_{-}^{+} | \pm 1 \rangle$

$a_4 \equiv \langle \pm 1^* | \hat{a}\ell_{\pm} | 0 \rangle = \langle 0 | \hat{a}\ell_{-}^{+} | \pm 1^* \rangle$

$b_1 \equiv \langle \pm 1 | \ell_{\pm} | 0 \rangle = \langle 0 | \ell_{-}^{+} | \pm 1 \rangle$

$b_2 \equiv \langle \pm 1^* | \ell_{\pm} | 0 \rangle = \langle 0 | \ell_{-}^{+} | \pm 1^* \rangle$

Table IV

Spin-Orbit Coupling Constants (in cm^{-1})

	A (estimated)[a]	A (observed)
$B'^2\Delta$	0	- 2.2[b]
$a^4\Pi$	- 36 cm^{-1}	- 20 cm^{-1} [c]
$L^2\Pi$	- 114 cm^{-1}	- 80 cm^{-1} [d]

a) Estimated using the semi-empirical equations (7a), (7b), (8) and matrix elements from Table III.

b) Reference [3]. Mulliken [18] has attributed this spin-orbit splitting to a spin-other-orbit interaction. Lefebvre-Brion and Bessis have calculated a value of -3.6 cm^{-1} by considering spin-other-orbit interactions [19].

c) This value comes from incompletely resolved spectra reported by Ogawa [20].

d) Reference [17].

Short of a full ab initio calculation, nothing more than the above nonrigorous but quite conservative upper bounds for a_3 and b_1 can be stated. H. Lefebvre-Brion (private communication) has computed ab initio values

$$a_3 = 50\ \text{cm}^{-1}, \qquad a_4 = 152\ \text{cm}^{-1},$$
$$b_1 = -0.1\ \text{cm}^{-1}, \qquad b_2 = 1.5,$$

using orbitals from NO $X\ ^2\Pi$ ($R = 1.9694$ a.u.) by the method described in Ref. (*15*).

IV. THE $B'\ ^2\Delta$ ($v = 1$) $\sim$ $B\ ^2\Pi$ ($v = 18$) INTERACTION IN $^{15}N^{18}O$

Matrix elements listed in Table III have been derived within a single configuration approximation and in a Hund's case "*a*" basis. In order to use these matrix elements to calculate the perturbation interaction energy at the $B'\ ^2\Delta \sim B\ ^2\Pi$ crossing points, two additional effects must be considered: configuration interaction [the strong Rydberg–non-Rydberg $C\ ^2\Pi$ ($v = 4$) $\sim$ $B\ ^2\Pi$ ($v = 18$) perturbation] and spin-uncoupling (intermediate case "*a*"–"*b*" coupling).

An estimate of configuration mixing between $B\ ^2\Pi$ ($v = 18$) and $C\ ^2\Pi$ ($v = 4$) of $^{15}N^{18}O$ is achieved by comparing constants for the diabatic (deperturbed)[3] $B(18)$ and

[3] Diabatic constants may be obtained either by deperturbation (*2, 17*) or by extrapolation from vibrational levels which are relatively free of perturbations.

$C(4)$ levels against constants for the observed levels. Similar configuration-mxing coefficients are obtained from both rotational and spin–orbit constants. Mean values of these constants, B_{18} and A_{18}, for the observed $B\,^2\Pi$ ($v = 18$) level are

$$B_{18} = 1.012\ \text{cm}^{-1}, \qquad A_{18} = 46\ \text{cm}^{-1},$$

while the constants for the diabatic NR-$B\,^2\Pi$ ($v = 18$) and R-$C\,^2\Pi$ ($v = 4$) levels are

$$\begin{aligned} B_{\text{NR}} &= 0.82\ \text{cm}^{-1} && (2),\\ A_{\text{NR}} &= 60\ \text{cm}^{-1} && (17),^4\\ B_{\text{R}} &= 1.70\ \text{cm}^{-1} && (2),\\ A_{\text{R}} &= 2.5\ \text{cm}^{-1} && (23). \end{aligned}$$

Constants with subscripts 18, NR, and R correspond, respectively, to the vibronic functions Ψ_{18} (adiabatic), Ψ_{NR} (diabatic), and Ψ_{R} (diabatic). Ψ_{18}, the vibronic function to which the observed $B\,^2\Pi$ ($v = 18$) level belongs, *cannot* be expressed as the product of a configuration-mixed electronic part with a complex and poorly determined vibrational part; rather, it may be expressed as the sum of two vibronic parts for which the vibrational factors are simply the vibrational eigenfunctions obtained from diabatic potential energy curves:

$$\Psi_{18} = c_{\text{NR}}\Psi_{\text{NR}} + c_{\text{R}}\Psi_{\text{R}}, \tag{9}$$

where

$$|c_{\text{NR}}|^2 + |c_{\text{R}}|^2 = 1. \tag{10}$$

Contributions to Ψ_{18} from R-levels other than $C\,^2\Pi$ ($v = 4$) are neglected. The observed constants, B_{18} and A_{18}, will depend on the mixing coefficients, c_{NR} and c_{R}:

$$B_{18} = |c_{\text{NR}}|^2 B_{\text{NR}} + |c_{\text{R}}|^2 B_{\text{R}}, \tag{11a}$$

$$A_{18} = |c_{\text{NR}}|^2 A_{\text{NR}} + |c_{\text{R}}|^2 A_{\text{R}}. \tag{11b}$$

Thus

$$|c_{\text{NR}}| = 0.88, \qquad |c_{\text{R}}| = 0.48.^5$$

Assuming that $B'\,^2\Delta$ ($v = 1$) is not significantly mixed with any other states, the $B'\,^2\Delta$ ($v = 1$) $\sim B\,^2\Pi$ ($v = 18$) matrix element is

$$\langle v = 1, B'\,^2\Delta|H'|\Psi_{18}\rangle = c_{\text{NR}}\langle v = 1, B'|H'|B, v' = 18\rangle + c_{\text{R}}\langle v = 1, B'|H'|C, v' = 4\rangle, \tag{12}$$

where

$$H' = H^{\text{SO}} + B(L_+S_- + L_-S_+ - J_+L_- - J_-L_+).$$

[4] Taken from (*17*, Fig. 5) after reexpressing $A(v)$ as a function of the mass reduced quantum number $\eta \equiv (v + \frac{1}{2})\mu^{-\frac{1}{2}}$ (*22*).

[5] These mixing coefficients are calculated using Eqs. (10) and (11a) or (10) and (11b). The perturbation matrix element, $H_{\text{R}\sim\text{NR}}$, between $C\,^2\Pi$ ($v = 4$) and $B\,^2\Pi$ ($v = 18$) and the zero-order energy separation, $C \equiv E(C\,^2\Pi) - E(B\,^2\Pi)$, may be determined from the mixing coefficients and the observed energy difference at $J = 1.5$ of 218 cm^{-1} between the average energies of the $C(4)$ and $B(18)$ levels: $H_{\text{R}\sim\text{NR}} = 92\ \text{cm}^{-1}$, $C = 118\ \text{cm}^{-1}$. Matrix elements for the $B(18) \sim C(4)$ interaction in the other NO isotopes are 49, 70, and 80 cm^{-1}, respectively, for $^{14}\text{N}^{16}\text{O}$, $^{15}\text{N}^{16}\text{O}$, and $^{14}\text{N}^{18}\text{O}$ (*17*). Since the vibrational overlap between $B(18)$ and $C(4)$ for $^{15}\text{N}^{18}\text{O}$ is 0.125 [calculated from diabatic RKR potential energy curves constructed using the constants from Ref. (*25*)], the electronic factor of the perturbation matrix element is $\sim$740 cm^{-1}, in fair agreement with the ab initio value from Felenbok and Lefebvre-Brion (*24*) but significantly smaller than the value obtained by Bartholdi *et al.* (*25*).

The second term in Eq. (12) vanishes because the $\Delta\Lambda = \pm 1$ part of H' is a one-electron operator and the diabatic $C\,^2\Pi$ and $B'\,^2\Delta$ states arise from configurations which differ by more than one spin-orbital.[6] The effect of the $B \sim C$ interaction on the possible $B \sim B'$ perturbation is simply one of dilution; $B\,^2\Pi$ character is removed from the $B\,^2\Pi$ ($v = 18$) level and replaced by $C\,^2\Pi$ character which cannot interact with $B'\,^2\Delta$.

It now remains to evaluate the interaction matrix element

$$\langle v = 1, J, F_i, B'\,^2\Delta | H' | \Psi_{18}, J, F_j \rangle = c_{\mathrm{NR}} \langle v = 1, J, F_i, B' | H' | B, J, F_j, v = 18 \rangle \quad (13)$$

for intermediate Hund's case "*a*"–"*b*" $^2\Delta$ and $^2\Pi$ functions at the four J values where crossings occur between the $B'\,^2\Delta(F_i)$ and $B\,^2\Pi(F_j)$ spin components. Using a transformation similar to that given by Kovacs (*26*, Eqs. (2.1.3-5) and (2.1.3-6)), intermediate case functions are constructed in the case "*a*" basis at the following crossings.

$J = 6.5$, $B'\,^2\Delta(F_2) \sim B\,^2\Pi(F_1)$

$$|B'\,^2\Delta, F_2\rangle = 0.87|B'\,^2\Delta_{\frac{3}{2}}\rangle - 0.49|B'\,^2\Delta_{\frac{5}{2}}\rangle, \quad (14a)$$

$$|B\,^2\Pi, F_1\rangle = 0.99|B\,^2\Pi_{\frac{1}{2}}\rangle + 0.16|B\,^2\Pi_{\frac{3}{2}}\rangle. \quad (14b)$$

$J = 12.5$, $B'\,^2\Delta(F_1) \sim B\,^2\Pi(F_1)$

$$|B'\,^2\Delta, F_1\rangle = 0.59|B'\,^2\Delta_{\frac{3}{2}}\rangle + 0.81|B'\,^2\Delta_{\frac{5}{2}}\rangle. \quad (15a)$$

$$|B\,^2\Pi, F_1\rangle = 0.96|B\,^2\Pi_{\frac{1}{2}}\rangle + 0.27|B\,^2\Pi_{\frac{3}{2}}\rangle. \quad (15b)$$

$J = 17.5$, $B'\,^2\Delta(F_2) \sim B\,^2\Pi(F_2)$

$$|B'\,^2\Delta, F_2\rangle = 0.78|B'\,^2\Delta_{\frac{3}{2}}\rangle - 0.62|B'\,^2\Delta_{\frac{5}{2}}\rangle, \quad (16a)$$

$$|B\,^2\Pi, F_2\rangle = -0.34|B\,^2\Pi_{\frac{1}{2}}\rangle + 0.94|B\,^2\Pi_{\frac{3}{2}}\rangle. \quad (16b)$$

$J = 30.5$, $B'\,^2\Delta(F_1) \sim B\,^2\Pi(F_2)$

$$|B'\,^2\Delta, F_1\rangle = 0.66|B'\,^2\Delta_{\frac{3}{2}}\rangle + 0.75|B'\,^2\Delta_{\frac{5}{2}}\rangle, \quad (17a)$$

$$|B\,^2\Pi, F_2\rangle = -0.46|B\,^2\Pi_{\frac{1}{2}}\rangle + 0.89|B\,^2\Pi_{\frac{3}{2}}\rangle. \quad (17b)$$

Crossings at $J = 17.5$ and $J = 30.5$ are predicted by extrapolation of Fig. 2, but could not be observed in absorption spectra available for this work. Using the case "*a*" matrix elements listed in Table III, *upper bounds* for the electronic perturbation parameters,

$$a_3 = 175\ \mathrm{cm}^{-1}, \qquad b_1 = 1.41,$$

and vibrational matrix elements (calculated from RKR potential energy curves constructed using spectroscopic constants for the $B'\,^2\Delta$ and $B\,^2\Pi$ states given in Refs. (*3*, *25*)),

$$\langle v = 18 | v' = 1 \rangle = -7.9 \times 10^{-3},$$

$$B_{vv'} = \langle v = 18 | B | v' = 1 \rangle = -1.3 \times 10^{-2}\ \mathrm{cm}^{-1},$$

[6] $C\,^2\Pi$ belongs to the $KK(\sigma 2s)^2(\sigma^* 2s)(\sigma 2p)^2(\pi 2p)^4(3p\pi)$ configuration. The vibrational overlap between $C\,^2\Pi$ ($v = 4$) and $B'\,^2\Delta$ ($v = 1$) is -0.160; thus the second term of Eq. (12) is $(0.48)(-0.160) \times \langle B'\,^2\Delta | H' | C\,^2\Pi \rangle$. It is unlikely that the configurationally forbidden $B' \sim C$ electronic factor could be larger than 1 cm^{-1}; thus the $C(4) \sim B'(1)$ matrix element should be smaller than 0.1 cm^{-1}.

interactions between $B\,^2\Pi$ and $B'\,^2\Delta$ are estimated:

$$J = 6.5, \quad c_{\mathrm{NR}}\langle v = 18, F_1, B\,^2\Pi | H' | B'\,^2\Delta, F_2, v = 1\rangle \leq -0.12\ \mathrm{cm}^{-1}, \quad (14c)$$

$$J = 12.5, \quad c_{\mathrm{NR}}\langle v = 18, F_1, B\,^2\Pi | H' | B'\,^2\Delta, F_1, v = 1\rangle \leq -0.19\ \mathrm{cm}^{-1}, \quad (15c)$$

$$J = 17.5, \quad c_{\mathrm{NR}}\langle v = 18, F_2, B\,^2\Pi | H' | B'\,^2\Delta, F_2, v = 1\rangle \leq -0.15\ \mathrm{cm}^{-1}, \quad (16c)$$

$$J = 30.5, \quad c_{\mathrm{NR}}\langle v = 18, F_2, B\,^2\Pi | H' | B'\,^2\Delta, F_1, v = 1\rangle \leq -0.39\ \mathrm{cm}^{-1}. \quad (17c)$$

The matrix elements at the observed perturbation-free $J = 6.5$ and 12.5 crossings are predicted to be below the detection threshold, but a level shift might be just detectable at the not yet observed $J = 30.5$ crossing.

The variation in the magnitude of the calculated matrix elements arises from spin uncoupling combined with competition between $\Delta\Omega = 0$ spin–orbit and $\Delta\Omega = \pm 1$ Coriolis matrix elements. At the $J = 17.5$ crossing the spin–orbit and Coriolis contributions to Eq. (16c) partially cancel; at the $J = 6.5$, 12.5, and 30.5 crossings, the contributions to Eqs. (14c), (15c), and (17c) add.[7] This interference between two kinds of perturbation is real and not due to an arbitrary phase choice.

It should be noted that Eqs. (14c) and (15c) represent upper bounds to the $J = 6.5$ and 12.5 matrix elements since the spin–orbit and Coriolis contributions add and are overestimated by pure precession arguments. In addition, in order for a level shift of 0.1 cm^{-1} to be observed at $J = 6.5$ and $J = 12.5$, the matrix elements (14c) and (15c) would have to be larger than ± 0.27 and ± 0.18 cm^{-1}, respectively.[8]

V. CONCLUSION

NR $\sim$ NR perturbations $B\,^2\Pi$ ($v = 18$) $\sim$ $B'\,^2\Delta$ ($v = 1$) in $^{15}N^{18}O$ are shown to be neither observable nor expected at two $B \sim B'$ crossing points. The absence of observed NR $\sim$ NR perturbations in NO in general and at the observed $B \sim B'$ crossings in particular does not imply that valence states of NO cannot perturb each other. The specific interaction examined here is undetectable because the $B \sim B'$ vibrational integrals $\langle v | v' \rangle$ and $\langle v | B | v' \rangle$ are both quite small. A strong $B\,^2\Pi$ ($v = 18$) $\sim$ $C\,^2\Pi$ ($v = 4$) interaction is shown to have only a slight diminishing effect on the possible $B\,^2\Pi$ ($v = 18$) $\sim$ $B'\,^2\Delta$ ($v = 1$) interaction.

Although local rotational perturbations between valence states of NO have not been observed, interactions between states which are energetically far apart and do not exhibit crossings undoubtedly exist. These interactions will contribute to the Λ-doubling of the $X\,^2\Pi$, $B\,^2\Pi$, $L\,^2\Pi$, $P\,^2\Pi$, and $a\,^4\Pi$ states and to the spin-splitting of $G\,^2\Sigma^-$, $I\,^2\Sigma^+$, and $b\,^4\Sigma^-$ states. The matrix elements listed in Table III and the electronic perturbation parameters defined in equations (8a)–(8f) should facilitate calculation of NR $\sim$ NR contributions to these second-order interactions.

[7] The $\langle {}^2\Pi_{\frac{1}{2}} | H^{\mathrm{SO}} | {}^2\Delta_{\frac{1}{2}} \rangle$ spin–orbit contributions to Eqs. (14c)–(17c) are -0.060, -0.069, -0.32, and -0.25 cm^{-1}. The Coriolis contributions include effects of three case "a" matrix elements: $\langle {}^2\Pi_{\frac{1}{2}} | BL_-S_+ | {}^2\Delta_{\frac{1}{2}} \rangle$, $\langle {}^2\Pi_{\frac{1}{2}} | -BL_-J_+ | {}^2\Delta_{\frac{1}{2}} \rangle$, and $\langle {}^2\Pi_{\frac{1}{2}} | -BL_-J_+ | {}^2\Delta_{\frac{1}{2}} \rangle$.

[8] *Note added in proof.* Reexamination of plates of the NO absorption spectrum has led to discovery of another NR $\sim$ NR crossing. This crossing, $^{14}N^{16}O$ $B^2\Pi(v = 19) \sim G^2\Sigma^-$ ($v = 0$) between $J = 12.5$ and 13.5, also displays undetectably small level shifts. Although the electronic part of the $B \sim G$ perturbation matrix element is shown in Table III to be nonzero, calculated vibrational factors are even smaller than for the $^{15}N^{18}O$ $B(v = 18) \sim B'(v = 1)$ crossing. Detectable level shifts at the $B \sim G$ crossing are neither observed nor predicted.

ACKNOWLEDGMENTS

We are grateful to Dr. A. E. Douglas and F. Alberti of the National Research Council of Canada (Ottawa) for the NO spectra and to M. E. Liard for measurement of the spectra. Discussions with Professors J. L. Kinsey and R. J. Silbey have been of considerable value. We are particularly indebted to Dr. H. Lefebvre-Brion for helpful criticism and for providing us with ab initio perturbation matrix elements.

RECEIVED: June 6, 1975

REFERENCES

1. E. MIESCHER AND K. P. HUBER, "Spectroscopy" (D. A. Ramsay, Ed.), MTP International Review of Science, Ser. 2, Vol. 3, Butterworths, London, 1975.
2. A. LAGERQVIST AND E. MIESCHER, *Helv. Phys. Acta* **31**, 221 (1958).
3. CH. JUNGEN, *Can. J. Phys.* **44**, 3197 (1966).
4. E. MIESCHER, *Can. J. Phys.* **49**, 2350 (1971).
5. K. DRESSLER AND E. MIESCHER, *Astrophys. J.* **141**, 1266 (1965).
6. R. W. FIELD, B. G. WICKE, J. D. SIMMONS, AND S. G. TILFORD; *J. Mol. Spectrosc.* **44**, 383 (1972).
7. K. KAYAMA AND J. C. BAIRD, *J. Chem. Phys.* **46**, 2604 (1967).
8. J. RAFTERY, P. R. SCOTT, AND W. G. RICHARDS; *J. Phys. B* **5**, 1293 (1972).
9. S. H. LIN, *J. Chem. Phys.* **46**, 279 (1967).
10. H. LEFEBVRE-BRION AND F. GUERIN, *J. Chem. Phys.* **49**, 1446 (1968).
11. T. E. H. WALKER, *Mol. Phys.* **23**, 489 (1972).
12. H. LEFEBVRE-BRION AND C. M. MOSER, *J. Chem. Phys.* **44**, 2951 (1966).
13. JON T. HOUGEN, *Nat. Bur. Stand. US Monogr.* 115, June 1970.
14. E. U. CONDON AND G. H. SHORTLEY, "The Theory of Atomic Spectra," Cambridge University Press, Cambridge, 1951.
15. J. A. HALL, J. SCHAMPS, J. M. ROBBE, AND H. LEFEBVRE-BRION, *J. Chem. Phys.* **59**, 3271 (1973); T. E. H. WALKER AND W. G. RICHARDS, *J. Chem. Phys.* **52**, 1311 (1970).
16. M. D. OLMAN, M. D. MCNELIS, AND C. D. HANSE, *J. Mol. Spectrosc.* **14**, 62 (1964).
17. A. LAGERQVIST AND E. MIESCHER, *Can. J. Phys.* **44**, 1525 (1966).
18. R. S. MULLIKEN, *Rev. Mod. Phys.* **4**, 1 (1932).
19. H. LEFEBVRE-BRION AND N. BESSIS, *Can. J. Phys.* **47**, 2727 (1969).
20. M. OGAWA, *Sci. Light Tokyo* **3**, 39 (1954).
21. G. HERZBERG, "Molecular Spectra and Molecular Structure, I. Spectra of Diatomic Molecules," Van Nostrand Reinhold, New York, 1950.
22. K. R. WAY AND W. C. STWALLEY, *J. Chem. Phys.* **59**, 5298 (1973).
23. F. ACKERMAN AND E. MIESCHER, *Chem. Phys. Lett.* **2**, 351 (1968).
24. P. FELENBOK AND H. LEFEBVRE-BRION, *Can. J. Phys.* **44**, 1677 (1966).
25. E. BARTHOLDI, M. LEONI, AND K. DRESSLER, *J. Appl. Math Phys.* **22**, 797 (1971).
26. I. KOVACS, "Rotational Structure in the Spectra of Diatomic Molecules," American Elsevier, New York, 1969.

Appendix 4:

Reprinted from J. Mol. Spectrosc. 70, 420-431 (1978).

Ab Initio and Semiempirical Estimates of PN Valence State Interactions

RICHARD A. GOTTSCHO AND ROBERT W. FIELD

Department of Chemistry, Massachusetts Institute of Technology, Cambridge, Massachusetts 02139

AND

H. LEFEBVRE-BRION

Centre de Mécanique Ondulatoire Appliquée, 23 rue du Maroc 75019, Paris, France and Laboratoire de Photophysique Moléculaire, Bâtiment 213 Université Paris-Sud 91405, Orsay, France

Hartree–Fock wavefunctions for the valence states of PN arising from the lowest energy open shell configurations, $2\pi^4 7\sigma 3\pi$ and $2\pi^3 7\sigma^2 3\pi$, are generated and used in *ab initio* calculations of diagonal spin–orbit, off-diagonal spin–orbit, and rotation-electronic matrix elements. These results are compared with those from two semiempirical methods, one based on atomic orbital populations and the other dependent solely on atomic spin–orbit splittings. The latter method is found to be surprisingly successful in predicting the $^3\Delta$ spin–orbit constant for a series of isovalent molecules. Semiempirical estimates of the $^3\Delta$ and $^3\Pi$ spin–orbit constants of AsN are given. The Hartree–Fock values of the a and b perturbation parameters are found to be 50 cm^{-1} and 0.60 (unitless), respectively. A previously reported perturbation in the $A^1\Pi$–$X^1\Sigma^+$ band system is shown to arise from a $^3\Sigma^- \sim {}^1\Pi$ spin–orbit interaction.

I. INTRODUCTION

This paper reports the results of *ab initio* and semiempirical estimates of spin–orbit and rotation-electronic matrix elements for the PN molecule and may be viewed as a continuation of previous studies of the isovalent species CO, SiO, CS, SiS, and NO^+ (*1–12*).

The purpose of this work is twofold: to provide initial estimates of A_Π, A_Δ, and perturbation parameters for PN; and to develop semiempirical methods for extrapolation, within an isovalent group, to heavier molecules, such as AsN, for which *ab initio* calculations are either unreliable or prohibitively costly. Initial estimates of spin–orbit, spin–spin, and perturbation parameters are valuable in utilizing the fragmentary information provided by perturbations in order to assign and characterize perturbing states.

In light of these *ab initio* results we have reexamined the lines of the PN $A^1\Pi$–$X^1\Sigma^+$ band system reported by Curry *et al.* (*13*) who observed perturbations in $A^1\Pi$ ($v' = 1$). We show below (Sect. VE) that the perturbing state symmetry is $^3\Sigma^-$.

TABLE I

Configurations of the Lowest Valence States of PN

$(1\sigma - 6\sigma)^2\ 1\pi^4\ 2\pi^4\ 7\sigma^2$	$X^1\Sigma^+$	I
$(1\sigma - 6\sigma)^2\ 1\pi^4\ 2\pi^4\ 7\sigma\ 3\pi$	$^3\Pi$, $A^1\Pi$	II
$(1\sigma - 6\sigma)^2\ 1\pi^4\ 2\pi^3\ 7\sigma^2\ 3\pi$	$^3\Delta$, $^3\Sigma^+$, $^3\Sigma^-$, $^1\Sigma^-$, $^1\Delta$, $^1\Sigma^+$	III

II THEORY

The lowest energy valence states of PN arising from the $7\sigma 2\pi^4 3\pi$ and $7\sigma^2 2\pi^3 3\pi$ configurations are given in Table I. Matrix elements between these states may be reduced to matrix elements of one-electron operators between one-electron molecular orbitals (*2, 3, 14, 15*).

The one-electron spin–orbit operator may be written as:

$$H^{SO} = \sum_i \hat{a}_i l_i \cdot s_i, \tag{1}$$

where

$$\hat{a}_i = \sum_K (\alpha^2/2)\zeta_K / r_{iK}^3,$$

ζ_K is the effective charge on nucleus K, r_{iK} is the distance between nucleus K and electron i, l_i is the orbital angular momentum of electron i, and s_i is the spin angular momentum of electron i. $\alpha^2/2$ is a factor equal to 5.84 cm^{-1} if the unit length is the atomic unit (*14, 16*). Selection rules for this operator are:

$$\Delta\Lambda = 0, \pm 1, \qquad \Delta\Sigma = -\Delta\Lambda, \qquad \Delta\Omega = 0, \qquad \text{and} \qquad \Delta S = 0, \pm 1;$$

or in terms of one-electron quantum numbers: $\Delta\lambda = 0, \pm 1$, $\Delta\sigma = -\Delta\lambda$, and $\Delta s = 0$.

The one-electron rotation-electronic operator may be written as:

$$H^{RE} = B(\sum_i l_{i\pm})(\sum s_{j\mp}) - BJ_{\pm}(\sum_i l_{i\mp}), \tag{2}$$

where $B = h/(8\pi^2 c\mu R^2)$, $l_{i\pm}$, $s_{i\pm}$, and $J_{\mp}$ are the orbital, spin, and total angular momenta raising and lowering operators, respectively, μ is the molecular reduced mass, R is the internuclear distance, and all other constants have their conventional meanings. Selection rules are: $\Delta\Lambda = -\Delta\Sigma = \pm 1$ (or $\Delta\Lambda = \pm 1$, $\Delta\Sigma = 0$), $\Delta S = 0$, and $\Delta\Omega = 0, \pm 1$.

The matrix elements of the configuration II $^1\Pi$ state with all states of configuration III may be written in terms of two parameters (*2, 3, 14, 16*):

$$a \equiv \langle 2\pi | a l_+ | 7\sigma \rangle, \tag{3}$$
$$b \equiv \langle 2\pi | l_+ | 7\sigma \rangle.$$

These elements are derived in Ref. (*2*) and are listed here in Table II. It is implicit in Table II that a and b are independent of the vibrational coordinate R. The matrix elements are factored into a product of vibrational, rotational, and electronic terms in the spirit of the Born–Oppenheimer approximation. The validity of this approximation is discussed in Ref. (*3*).

TABLE II

Perturbation Matrix Elements Involving PN $A^1\Pi$[a]

$$\langle {}^1\Pi, J, v|H^{SO}|{}^3\Sigma_1^+, J, v'\rangle^{e,f} = \tfrac{1}{4}\, a\langle v|v'\rangle^b$$
$$\langle {}^1\Pi, J, v|H^{SO}|{}^3\Sigma_1^-, J, v'\rangle^{e,f} = -\tfrac{1}{4}\, a\langle v|v'\rangle$$
$$\langle {}^1\Pi, J, v|H^{SO}|{}^3\Delta, J, v'\rangle^{e,f} = -\tfrac{1}{8}\sqrt{\tfrac{1}{2}}\, a\langle v|v'\rangle$$
$$\langle {}^1\Pi, J, v|H^{RE}|{}^1\Sigma^-, J, v'\rangle^{f} = -B_{vv'}\, bx^{\frac{1}{2}}$$
$$\langle {}^1\Pi, J, v|H^{RE}|{}^1\Delta, J, v'\rangle^{e,f} = B_{vv'}\, b(x-2)^{\frac{1}{2}}$$

where $x = J(J+1)$, $a = \langle 2\pi|\hat{a}l_+|7\sigma\rangle$, and $b = \langle 2\pi|l_+|7\sigma\rangle$.

[a] Matrix elements are taken from Ref. (*2*).
[b] H^{SO} and H^{RE} are defined in the text.

In calculating *ab initio* values for the a and b parameters, it is not necessary to assume that they are R independent if wavefunctions are calculated as a function of internuclear distance. As pointed out in Ref. (*3*) these parameters are in fact R dependent and may be expressed as a function of the R centroid between the two interacting vibronic levels, where

$$R_{\text{centroid}} = \langle v|R|v'\rangle/\langle v|v'\rangle. \tag{4}$$

Schamps (*17*) has shown that for pairs of near-degenerate interacting levels, R centroid is dependent only on v'–v and approximately equal to the internuclear distance for which the potential energy curves of the two interacting states intersect.

III. METHOD

Hartree–Fock wavefunctions for the states of configurations I, II, and III in Table I were calculated as a function of internuclear distance using the program ALCHEMY written by Bagus, McLean, Yoshimine, and Liu. The atomic basis set of Slater-type orbitals, taken in part from Clementi and Roetti (18) is specified in Table III.

These wavefunctions were then used as input in a second program written by Hall (*3*) in calculating the a and b perturbation parameters, the $^3\Pi$ and $^3\Delta$ diagonal spin–orbit

TABLE III

Atomic Basis Set Used for Calculation of PN Ground and Valence States

Number	Orbital	Center	Exponent
1	1s	P	16.14890
2	1s	P	23.28360
3	2s	P	5.60322
4	2s	P	14.52140
5	3s	P	2.39990
6	3s	P	1.48370
7	3s	P	4.69535
8	2p	P	6.51465
9	2p	P	12.37150
10	3p	P	2.02705
11	3p	P	1.19796
12	3p	P	4.87455
13	3dσ	P	2.42260
14	3dπ	P	1.70459
15	1s	N	10.34240
16	1s	N	5.68298
17	2s	N	2.43875
18	2s	N	1.45349
19	3s	N	7.04041
20	2p	N	6.21698
21	2p	N	2.56988
22	2p	N	1.28261
23	3dσ	N	1.90668
24	3dπ	N	2.04556

TABLE IV

Atomic p Orbital Coefficients[a]

Molecular Orbital	7σ				2π				3π			
Atomic Orbitals[b]	10	11	21	22	10	11	21	22	10	11	21	22
State												
$^1\Pi$					.296 .294	.148 .202	.328 .310	.476 .483	-0.423 -0.449	-0.631 -0.566	0.165 0.191	0.473 0.471
$^3\Pi$									-.412 -.431	-.613 -.552	.210 .236	.477 .468
$^3\Sigma^+$	0 .389	0 .109	.187 -.296	.178 -.474								
$^3\Sigma^-$	.106 .398	0 .117	.170 -.296	.155 -.470								
$^3\Delta$	0 .393	0 .112	.180 -.296	.168 -.472	—— .322	—— .246	—— .296	—— .443	—— .416	—— .557	—— -.247	—— -.496

[a]Only the largest p-orbital coefficients are given. The upper coefficients are for R = 2.818 a.u. and the lower are for 3.1 a.u.

[b]The numbers refer to the atomic p orbital basis functions given in Table III.

constants, and the $^1\Pi$–$^3\Pi$ spin–orbit interaction energy as a function of internuclear distance.

IV. RESULTS

A. Hartree–Fock Wavefunctions

In considering spin–orbit interactions, it is sufficient to examine the atomic p orbital character in the valence molecular orbitals. The P $3p$ and N $2p$ orbital characters in the 2π, 3π, and 7σ molecular orbitals are given in Table IV for $R = 2.82$ and 3.10 a.u. These coefficients are useful in interpreting the magnitudes of calculated spin–orbit interaction energies (see Sect. V below). The states within a given configuration have very similar atomic composition and will, therefore, have similar potential energy curves. In general the N $2p$ and P $3p$ orbitals are equally important in the make-up of the $^1\Pi$ and $^3\Pi$ states and these coefficients change little from $R = 2.82$ to 3.10 a.u. However, for the configuration III states the P $3p$ orbital character is larger than N $2p$ for small internuclear distances but near the potential minima both N $2p$ and P $3p$ are equally important.

B. Hartree–Fock Energies

HF energies as a function of internuclear distance are given for the states of configurations I, II, and III in Table V. The $X^1\Sigma^+$ equilibrium distance is seen to be approximately 2.82 a.u. which is consistent with the results of McLean and Yoshimine (*19*) and the experimental value of 2.81732 a.u. (*20*). The total $X^1\Sigma^+$ energy calculated here is lower than the theoretical value reported by Boyd (*21*) and nearly equal to but slightly higher than the value reported by McLean and Yoshimine (*19*).

Using the calculated energies given in Table V, Morse potential energy functions (Fig. 1) were generated for the configuration II and III states and yield the spectroscopic

TABLE V

Hartree–Fock Energies (in a.u.) for Valence States of PN

R(a.u.)	2.65	2.818	3.10	3.30
$X^1\Sigma^+$	-395.17877	-395.18061	-395.13990	-395.09414
$^3\Pi$	-395.03257	-395.04789	-395.03293	—
$A^1\Pi$	-395.00107	-395.01475	-394.99811	—
$^3\Delta$	—	-395.06714	-395.07440	-395.05900
$^3\Sigma^+$	—	-395.09472	-395.10283	-395.08780
$^3\Sigma^-$	—	-395.04120	-395.04742	-395.03154
$^1\Sigma^-$	—	-395.04120	-395.04742	-395.03154
$^1\Delta$	—	-395.029853	-395.033256	-395.015962

constants given in Table VI. From Fig. 1 the $^3\Pi$ and $^1\Pi$ minima are estimated to lie near 2.82 a.u. compared with the experimental $A^1\Pi$ R_e of 2.9147 a.u. (*13*). T_e for $A^1\Pi$ from Table V is 36402 cm^{-1} compared with the experimental value of 39805.66 cm^{-1} (*13*). From Fig. 1, R_e for the configuration III states is 3.00 a.u. As in the isovalent species CO, CS, SiO, SiS, and NO^+ (*1–12*) these states are more weakly bound than the configuration II states.

C. Ab Initio Matrix Elements

Figures 2, 3, and 4 illustrate the R dependence of the a and b parameters and the $^3\Pi$ and $^3\Delta$ spin–orbit constants (A_Π and A_Δ, respectively). For example, at $R = 2.82$ a.u.,

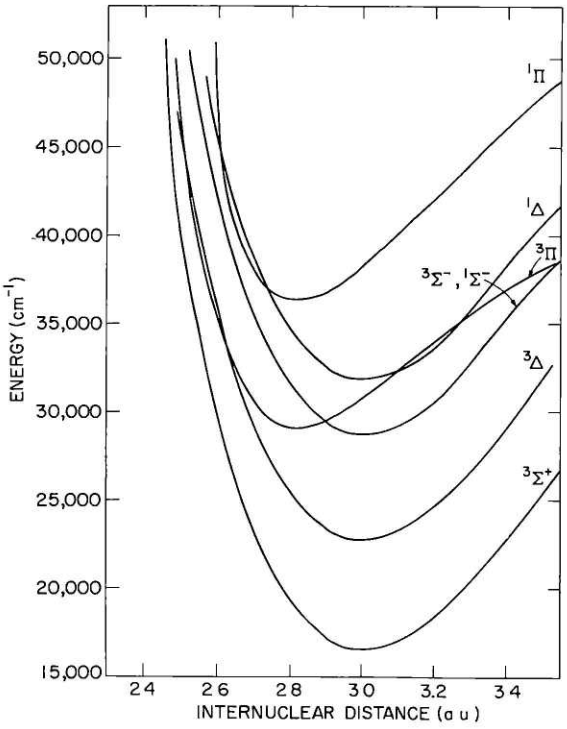

FIG. 1. Morse potential energy functions for the lowest valence states of PN generated from Hartree–Fock energies.

TABLE VI

Spectroscopic Constants for PN Valence States[a,b]

	$T_e(cm^{-1})$	$\omega_e(cm^{-1})$	$\omega_e x_e(cm^{-1})$	$B_e(cm^{-1})$	$\alpha_e(cm^{-1})$	$r_e(\AA)$	$D_e(cm^{-1})$
$^1\Pi$	36402	1380	21	0.785	0.01	1.492	23050
	(39805.66)	(1103.09)	(7.222)	(0.7307)	(0.00663)	(1.5424)	(41500)
$^1\Delta$	31804	1190	5.7	0.692	0.004	1.587	62500
$^3\Pi$	29129	1390	34	0.785	0.01	1.492	14300
$^3\Sigma^-, ^1\Sigma^-$	28696	1190	5.7	0.692	0.004	1.587	62500
$^3\Delta$	22774	1190	5.7	0.692	0.004	1.587	62500
$^3\Sigma^+$	16534	1190	5.7	0.692	0.004	1.587	62500

[a]Experimental values from Ref. (13) are given in parentheses.

[b]Morse potential constants. Within the accuracy of our calculations, the configuration III states have identical potential energy curves.

$a = 44$ cm^{-1} determined from the $^1\Pi$–$^3\Sigma^+$ matrix element and $b = 0.64$ determined from the $^1\Pi$–$^1\Delta$ matrix element (see Table II). The $^3\Pi \sim {}^1\Pi$ interaction energy ranges from -85 cm^{-1} at $R = 2.65$ a.u. to -94 cm^{-1} at 3.10 a.u. and is seen to be nearly equal in magnitude to the $^3\Pi$ spin–orbit constant as expected (*14*, p. 435).

V. DISCUSSION

A. Hartree–Fock Calculations

Although the Hartree–Fock calculations yield accurate ($\pm 5\%$) equilibrium internuclear distances when compared with experiment, the $A^1\Pi$ T_e value is significantly low. HF functions are expected (*9*) to yield accurate ($\pm \sim 20\%$) values for diagonal and

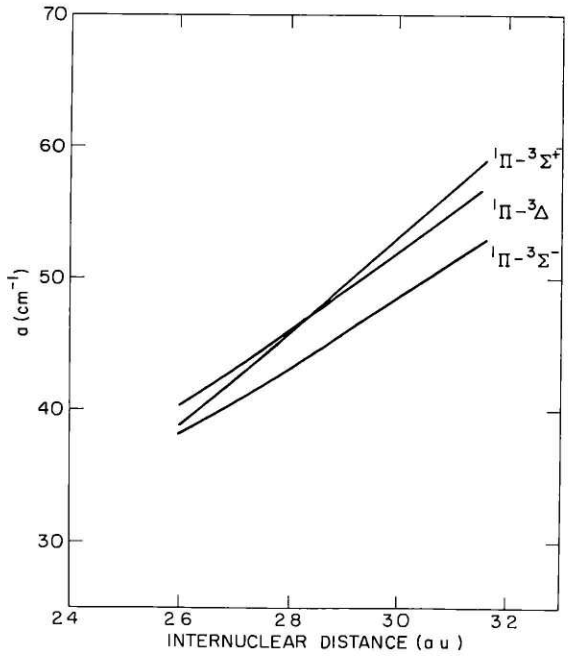

FIG. 2. R dependence of the a spin–orbit perturbation parameter, where $a \equiv \langle 2\pi | \hat{a} l_+ | 7\sigma \rangle$.

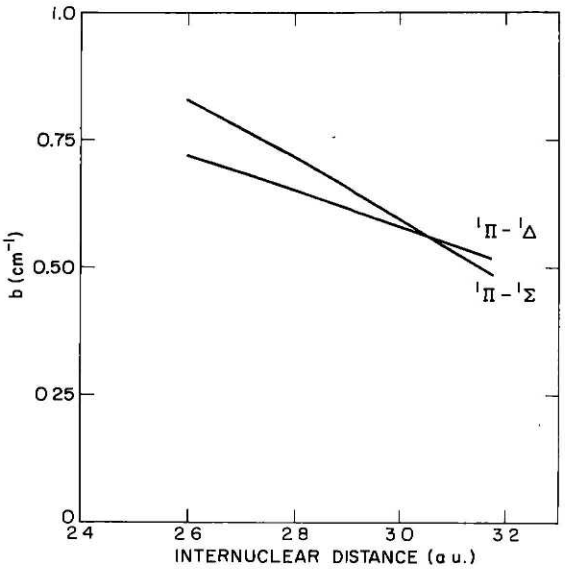

FIG. 3. R dependence of the b rotation–electronic perturbation parameter, where $b \equiv \langle 2\pi | l_+ | 7\sigma \rangle$.

nondiagonal spin–orbit and rotation-electronic interaction energies. Although configuration interaction (CI) wavefunctions should improve the agreement between calculated and experimental energies and provide more accurate estimates of spin–orbit and rotation electronic energies (*9*), the single configuration approximation is expected to

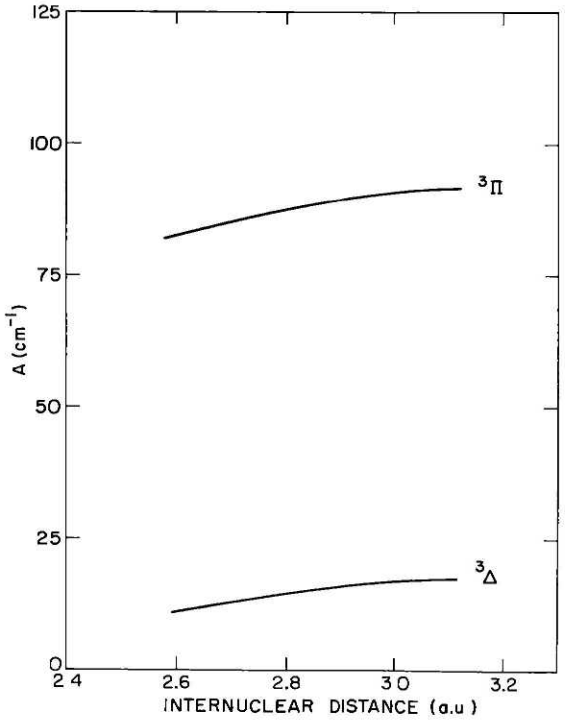

FIG. 4. R dependence of $^3\Pi$ and $^3\Delta$ spin–orbit constants (A_Π and A_Δ, respectively).

be valid for the configuration III states. A_Δ calculated here, in particular, should be within $\pm 10\%$ of the true value.

B. Comparison with Isovalent Molecules

As stated and illustrated in Ref. (*5*), a wealth of information concerning the lowest valence states of 10 valence electron molecules exists. In Ref. (*5*), a comparison of configurationally averaged properties for most of these molecules was presented. In Table VII we have extended the work of Ref. (*5*) to include P_2 and PN which are contrasted with SiO.

The energies of the configuration II states may be approximately represented in terms of three interelectronic integrals and a configurational energy as defined by Recknagel (*22*):

$$
\begin{aligned}
&^3\Sigma^+ \quad E(\pi^3\pi') - a,\\
&^3\Delta \quad E(\pi^3\pi'),\\
&^3\Sigma^-, {}^1\Sigma^- E(\pi^3\pi') + a,\\
&^1\Delta \quad E(\pi^3\pi') + 2b,\\
&^1\Sigma^+ \quad E(\pi^3\pi') - a + 4c,
\end{aligned}
$$

TABLE VII

Isovalent Comparison of Configurationally Averaged Properties

	P_2[a]	PN[b]	SiO[c,d]
$E(\pi^3\pi')\times 10^{-3}$ cm^{-1}	24	23	36
$a \times 10^{-3}$ cm^{-1}	4.8	6.1	2.4
$b \times 10^{-3}$ cm^{-1}	3.1	4.6	1.3
$c \times 10^{-3}$ cm^{-1}	2.8	—	4.4
$r_e(\pi^3\pi')/r_e(X)$	1.04	1.04	1.14
$\omega_e(\sigma\pi^4\pi')/\omega_e(X)$	0.81	0.82	.060
$E(\sigma\pi^4\pi')\times 10^{-3}$ cm^{-1}	31	33	38
$E(^1\Pi)-E(3\Pi)\times 10^{-3}$ cm^{-1}	6.3	7.3	8.9
$r_e(\sigma\pi^4\pi')/r_e(X)$	1.09	1.07	1.05
$\omega_e(\sigma\pi^4\pi')/\omega_e(X)$	0.76	0.89	0.74

[a] All values taken from J. Brion, Radical P_2: Etude des transitions $C^1\Sigma_u^+ - X^1\Sigma_g^+$, $A^1\Pi_g - X^1\Sigma_g^+$, $B^1\Pi_u - A^1\Pi_g$ et de la transition $c^3\Pi_u - b^3\Pi_g$. Etude et interprétation des perturbations observées dans les états $C^1\Sigma_u^+$ et $^3\Pi_u$. Thesis, University of Reims, France (1977).

[b] This work except for the $r_e(\pi^3\pi')/r_e(X)$ and $\omega_e(\pi^3\pi')/\omega_e(X)$ ratios which were taken from Ref. (13).

[c] Values for $b^3\Pi$ and $a^3\Sigma^+$ from G. Hager, R. Harris, and S.G. Hadley, J. Chem. Phys. 63, 2810 (1975).

[d] Ref. (5).

where for PN π and π' stand for 2π and 3π, respectively. Similarly the configuration II $^1\Pi$ and $^3\Pi$ states may be written in terms of one interelectronic integral and a configurational energy, $E(\sigma\pi')$. As discussed in Ref. (*5*), an increase in spatial separation of the π and π' orbitals leads to a reduction of the a, b, and c integrals. An increase in the spatial separation of these orbitals may arise from an increase in the molecular polarity so that the $\pi(\pi')$ orbital is localized on the more electronegative (electropositive) atom or from an increase in atomic size. These effects are nicely illustrated in the P_2, PN, SiO sequence shown in Table VI. PN and P_2 are essentially nonpolar so that the relative sizes of P to N dictate the magnitudes of a, b, and c which are all larger for PN than for P_2. SiO, on the other hand, is significantly more polar than P_2 or PN and the values of a, b, and c for SiO are smallest. Localization of σ and π' orbitals increases with increasing ionicity (*5*) so that $E(^1\Pi)$–$E(^3\Pi)$ increases from $P_2 \rightarrow$ PN $\rightarrow$ SiO.

C. Semiempirical Calculations

Knowledge of the molecular and atomic HF wavefunctions and atomic spin–orbit energies provide estimates for A_Π and A_Δ without recourse to full *ab initio* calculations. The first method which we employ (called method I) is essentially that described by Ishiguro and Kobori (*23*). We illustrate method I by computing A_Δ (*5*, *15*):

$$A_\Delta = \tfrac{1}{4}[\langle 3\pi|\hat{a}|3\pi\rangle - \langle 2\pi|\hat{a}|2\pi\rangle] \equiv \tfrac{1}{4}[a(3\pi) - a(2\pi)]. \tag{5}$$

We make the approximation

$$a(2\pi) = |\langle P3p|2\pi\rangle|^2\zeta_P(3p) + |\langle N2p|2\pi\rangle|^2\zeta_N(2p), \tag{6}$$

where $|\langle P3p|2\pi\rangle|^2$ is the phosphorus $3p$ atomic character in the PN 2π molecular orbital and $\zeta_P(3p)$ and $\zeta_N(2p)$ are calculated atomic spin–orbit parameters (*24*). Overlap between P $3p$ and N $2p$ is neglected.[1] We obtain $A_\Delta \sim 31$ cm^{-1} which is to be compared with the *ab initio* value at $R = 3.10$ a.u. of 15 cm^{-1}. Similarly, $A_\Pi = a(3\pi) \sim 100$ cm^{-1} at $R = 2.818$ a.u. is semiempirically estimated and compared with the *ab initio* value of 88 cm^{-1}. It should be noted that $\zeta_N(2p)$ is irrelevant in the calculation of A_Δ because the N $2p$ character in 3π and 2π is nearly equal (see Tables II and IV).

Field *et al.* (*4*, *5*) have proposed an alternative semiempirical method (method II) for the calculation of A which may be viewed as a special case of method I. An upper bound is placed on the difference $|a(3\pi) - a(2\pi)|$ from known experimental atomic $\zeta(np)$ parameters. We restate their arguments here for comparison. The $3\pi(2\pi)$ orbital is considered to be localized on the more electropositive (electronegative) atom since it is less (more) stable. Thus, if the more electropositive atom has the smaller $\zeta(np)$ the Δ state will be inverted and vice versa. For inverted states then, an upper bound for A_Δ is given by

$$0 > A > \tfrac{1}{4}(\zeta_A(np) - \zeta_B(np)) \tag{7a}$$

and for regular states A is given by

$$0 < A < \tfrac{1}{4}\zeta_{A^+}(np) - \zeta_{B^-}(np). \tag{7b}$$

[1] Because each atomic orbital is written in terms of more than one function (e.g., there are three $3p$ phosphorous basis functions given in Table III) overlaps between these functions must be considered. These are calculated using the formula given in (*25*).

where $A(A^+)$ is the more electropositive atom (ion) (*4, 5*). The ionic $\zeta(np)$ parameters are used for the regular $^3\Delta$ states to magnify the difference between the ζ's and provide an upper bound for A_Δ. Negative(positive) ions exhibit smaller(larger) spin–orbit matrix elements than neutrals because there is less (more) interaction between the electrons and the nucleus. Except for the use of ionic ζ's this method is simply a limiting case of method I, where

$$\begin{aligned} &|\langle P3p|2\pi\rangle|^2 \quad \text{and} \quad |\langle N2p|3\pi\rangle|^2 \to 0 \\ \text{and} \qquad &|\langle P3p|3\pi\rangle|^2 \quad \text{and} \quad |\langle N2p|2\pi\rangle|^2 \to 1. \end{aligned} \tag{8}$$

The recommended value for A_Δ is one-half the upper bound given in Eq. (7) (*4, 5*) so that PN $A_\Delta \sim 20$ cm^{-1}. In that method II requires no knowledge of atomic or nuclear wavefunctions it is superior to method I for the calculation of A_Δ. The agreement between method II and experiment is seen to be very good for SiO, CS, and CO (*4, 5*). This is due to a cancellation of errors in the subtraction of $a(2\pi)$ from $a(3\pi)$ in Eq. (5). On the other hand, no such cancellation occurs in the method II estimation of A_Π which is proportional to $a(3\pi)$. We expect method II to be less reliable for A_Π than A_Δ.

D. Semiempirical Predictions

If we make the drastic assumption that the atomic orbital coefficients for AsN, and PN are identical, estimates for A_Π and A_Δ may be made for AsN without recourse to additional *ab initio* calculations by replacing the appropriate ζ parameters in Eq. (6) (*23*). Method I yields for AsN, $A_\Delta \sim 190$ cm^{-1}, and $A_\Pi \sim 670$ cm^{-1}. Method II gives, from Eq. (7), $0 < A_\Delta < 410$ cm^{-1} or $A_\Delta \sim 205$ cm^{-1} for AsN.

E. Perturbations in the PN $A^1\Pi$–$X^1\Sigma^+$ Band System

From the Morse curves generated above (see Fig. 1), vibrational overlaps between $A^1\Pi$ and all possible perturbers have been calculated. Since a is calculated to be $\sim$50 cm^{-1}, a vibrational overlap >0.002 would be necessary to produce a readily detectable level shift of 0.1 cm^{-1}. We conclude from these overlap calculations that $^1\Pi \sim {}^3\Sigma^+$ perturbations will be definitely unobservable for $A^1\Pi$ $v = 0 - 20$; however, $A^1\Pi \sim {}^3\Sigma^-$, $^1\Sigma^-$, and $^1\Delta$ perturbations may not be ruled out for the lowest vibrational levels of $A^1\Pi$. $^1\Sigma^-$ and $^1\Delta$ perturbations will be weaker than $^3\Sigma^-$ perturbations at J values <82 (see Table II, Figs. 1 and 2) so that the observation of $A^1\Pi \sim {}^3\Sigma^-$ perturbations is most likely for low v, J $A^1\Pi$ levels.

In fact, Curry *et al.* (*13*) have observed perturbations in the PN (1, 0), (1, 2), and (1, 3) $A^1\Pi$–$X^1\Sigma^+$ bands. Figure 5 illustrates the level shifts observed in $A^1\Pi$ $v' = 1$; plotted are the observed minus calculated transitions as a function of J' for both e and f parity. The latter were generated using the constants from Ref. (*13*). The perturbations are obvious but there appears to be a problem with the e parity data derived from the P and R branches. Neglecting the two e parity data points for $J' = 46$ and 47 which do not fit on a smooth curve through the other points, the perturbation seems to culminate around $J' = 45$–46 for the e parity levels and around $J' = 52$–53 for the f parity levels. This is precisely the pattern expected for $^1\Pi \sim {}^3\Sigma^-$ interactions. From our calculated vibrational overlaps we expect a *minimum* overlap between $A^1\Pi$ and

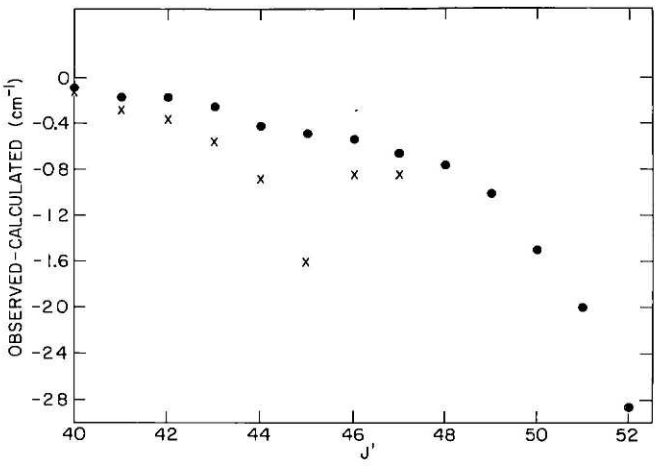

FIG. 5. Observed minus calculated $A^1\Pi$–$X^1\Sigma^+$ transitions as a function of J'. ● denotes f parity upper levels taken from the (1, 0), (1, 2), and (1, 3) Q-branch lines of Ref. (*21*). × denotes e parity levels taken from the P and R branches. Two perturbations are observed culminating at $J'_0 \sim 45.5$ and $J'_0 \sim 52.5$ for the e and f levels, respectively.

$^3\Sigma^-$ in this region to be ~0.05. Therefore, the *minimum* vibronic interaction matrix element observable is ~0.6 cm^{-1} (See Table II and Fig. 2). From the maximum level shift in the f parity levels,[2] an experimental lower bound for the vibronic spin–orbit matrix element is found to be ~2.8 cm^{-1}.

Other $^1\Pi \sim {}^3\Sigma^-$ perturbations should be present and observable. It is hoped that this work will stimulate their eventual characterization.

ACKNOWLEDGMENTS

We gratefully acknowledge the assistance of J. Schamps and J. M. Robbe in performing the PN *ab initio* perturbation parameter calculations. We also thank Drs. Bagus, McLean, Yoshimine, and Liu for making their program ALCHEMY available to us. This work was supported in part by NATO Grant No. 1177.

RECEIVED: December 28, 1977

REFERENCES

1. R. W. FIELD, S. G. TILFORD, R. A. HOWARD, AND J. D. SIMMONS, *J. Mol. Spectrosc.* **44**, 347–382 (1972).
2. R. W. FIELD, B. G. WICKE, J. D. SIMMONS, AND S. G. TILFORD, *J. Mol. Spectrosc.* **44**, 383–399 (1972).
3. J. A. HALL, J. SCHAMPS, J. M. ROBBE, AND H. LEFEBVRE-BRION, *J. Chem. Phys.* **59**, 3271–3283 (1973).
4. R. W. FIELD, A. LAGERQVIST, AND I. RENHORN, *J. Chem. Phys.* **66**, 868–869 (1977).
5. R. W. FIELD, A. LAGERQVIST, AND I. RENHORN, *Physica Scripta* **14**, 298–319 (1977).
6. J. M. ROBBE, J. SCHAMPS, AND H. LEFEBVRE-BRION, "Electronic Structure and Perturbations: Interpretation in the SiO Valence States," to be published.
7. R. W. FIELD, *J. Mol. Spectrosc.* **47**, 194–203 (1973).
8. D. COSSART AND T. BERGEMAN, *J. Chem. Phys.* **65**, 5462–5468 (1976).

[2] The $^3\Sigma_0^-$ and $^3\Sigma_1^-$ e levels are nearly equally mixed (Hund's case "b"), so the $^1\Pi \sim {}^3\Sigma^-$ f parity matrix element is correspondingly $2^{\frac{1}{2}}$ larger than the $^1\Pi \sim {}^3\Sigma^-$ e parity matrix element.

9. J. M. Robbe and J. Schamps, *J. Chem. Phys.* **65**, 5420–5426 (1976).
10. B. Fémelat and W. E. Jones, *J. Mol. Spectrosc.* **49**, 388–400 (1974).
11. S. Harris, R. Barrow, R. W. Field, and R. A. Gottscho, "The $D^1\Pi$–$X^1\Sigma^+$ Band System of SiS," to be published.
12. J. M. Robbe, J. Schamps, and R. A. Gottscho, "The Valence States of SiS," to be published.
13. J. Curry, L. Herzberg, and G. Herzberg, *Z. Phys.* **86**, 348–366 (1933).
14. H. Lefebvre-Brion, Perturbations in the spectra of diatomic molecules in "Atoms, Molecules, and Lasers," pp. 411–448, International Atomic Energy Agency Vienna, 1974.
15. J. Schamps, Thesis, L'Université des Sciences et des Techniques de Lille, 1973.
16. R. W. Field, R. A. Gottscho, and E. Miescher, *J. Mol. Spectrosc.* **58**, 394–413 (1975).
17. J. Schamps, *J. Quant. Spectrosc. Radiat. Transfer* **17**, 685–694 (1977).
18. E. Clementi and C. Roetti, *Atomic Data Nucl. Data Tables* **14**, 177–478 (1974).
19. A. D. McLean and M. Yoshimine, "Tables of Linear Molecule Wave Functions," Supplement to IBM J. Res. Developm, Vol. 12, p. 206 1968.
20. F. C. Wyse, E. L. Manson, and W. Gordy, *J. Chem. Phys.* **57**, 1106–1108 (1972).
21. D. B. Boyd, *J. Chem. Phys.* **52**, 4845–4852 (1970).
22. A. Recknagel, *Z. Phys.* **87**, 375–398 (1934).
23. E. Ishiguro and M. Kobori, *J. Phys. Soc. Japan* **22**, 263–270 (1967).
24. C. Froese-Fischer, "Tables of Hartree-Fock Results," Thesis, U. of British Columbia, Vancouver, 1968.
25. H. Lefebvre-Brion and C. M. Moser, *J. Chem. Phys.* **44**, 2951–2954 (1966).

Appendix 5

Reprinted from J. Chem. Phys. 68, 4110-4122 (1978).

OODR spectroscopy of BaO. II. New observations of $a\,^3\Pi$ and $A'\,^1\Pi$ and re-examination of the Parkinson band system

Richard A. Gottscho, J. Brooke Koffend, and Robert W. Field[a)]

Department of Chemistry, Massachusetts Institute of Technology, Cambridge, Massachusetts 02139

John R. Lombardi

Department of Chemistry, City College of New York, New York, New York 10031
(Received 28 September 1977)

One and two dye lasers have been used in an optical–optical double resonance (OODR) study of the excited $B\,^1\Pi$ and $C\,^1\Sigma^+$ states as well as the low-lying, long-lived $A'\,^1\Pi$ and $a\,^3\Pi_1$ electronic states of BaO. $C\,^1\Sigma^+$ ($v=0$) is shown to be the upper level in the $v'=0$ progression of the Parkinson band system. Intensity anomalies in $C\,^1\Sigma^+$–$X\,^1\Sigma^+$ emission, due to an interference effect between parallel and perpendicular transition amplitudes, have proved to be a sensitive indication of $\Delta\Omega=\pm1$ perturbations. Emission from $C\,^1\Sigma^+$, which is populated by absorption of two photons via a real intermediate $A\,^1\Sigma^+$ vibronic level, into $A'\,^1\Pi$ ($v=0,1$, and 2) and $a\,^3\Pi_1$ ($v=0,1$, and 2) has been observed. A scheme is presented by which the relative populations of the $A'\,^1\Pi$ and $a\,^3\Pi$ "reservoir states" could be monitored.

I. INTRODUCTION

This paper is the second in a series reporting an investigation of the electronic spectrum of BaO by the technique of optical–optical double resonance (OODR) spectroscopy. The results reported here were obtained using one and two cw dye lasers to excite BaO molecules in two steps from $X\,^1\Sigma^+$ to $A\,^1\Sigma^+$ and then to $C\,^1\Sigma^+$ or $B\,^1\Pi$. The main difference from the first BaO OODR investigation,[1] hereafter referred to as OODR I, is that tunable lasers are used for both excitation steps,

$$v', J' \leftarrow v'', J'' ,$$

$$v^*, J^* \leftarrow v', J' ,$$

and that states other than $X\,^1\Sigma^+$ are observed as the terminal level in

$$v^*, J^* \rightarrow v, J$$

OODR photoluminescence.[2]

Results reported here may be divided into four categories: new spectroscopic observations on the BaO $a\,^3\Pi$ ($v=0$–2), $A'\,^1\Pi$ ($v=0$–2) and mutually perturbing $C\,^1\Sigma^+(v^*=0)$ and $B\,^1\Pi$ ($v^*=?$) levels; an excitation spectroscopic scheme for monitoring populations in the long-lived "reservoir levels" $a\,^3\Pi$ and $A'\,^1\Pi$; a quantum mechanical interference effect which manifests itself in anomalous relative intensities of P and R transitions originating from a common v^*, J^* level and which is a sensitive probe for $\Delta\Omega=\pm1$ perturbations; applications of new OODR techniques including OODR with two tunable lasers, OODR detected as a decrease in fluorescence from the intermediate v', J' levels,[3] and accidental double coincidence OODR spectroscopy using only one (tunable) laser. A detailed analysis, including deperturbed constants, of all spectral data pertaining to the mutually interacting $A\,^1\Sigma^+$, $a\,^3\Pi$, and $A'\,^1\Pi$ states is deferred to OODR III.[4] The high energy BaO states, $B\,^1\Pi$, $C\,^1\Sigma^+$, other $^1\Sigma^+$ states (observed in OODR I[1] and by Pruett and Torres-Filho[5]), and various perturbers will be more fully discussed in OODR IV.[6]

This research was stimulated in part by the observation in OODR I of a large number of v^* levels *all* of apparent $^1\Sigma^+$ symmetry. In an attempt to solve the riddles of the numerous $^1\Sigma^+$ levels and the missing non-$^1\Sigma^+$ states and to locate the as yet unobserved, low-lying $^3\Sigma^+$ state, OODR experiments employing two tunable lasers were initiated. As might be expected, two new questions arose. How was it possible for a single red dye laser to excite strong blue and ultraviolet fluorescence? What could explain the intensity behavior of the R, P doublets in the long $v^*, J^* \rightarrow X\,^1\Sigma^+ v'', J''=J^*\pm1$ fluorescence progression? Sometimes the P line would be stronger than R and then *vice versa* in the adjacent doublet. In fact, the two longest wavelength doublets were actually singlets!

The anti-Stokes fluorescence is explained by accidental coincidences of the frequencies of rotational transitions in the $A\,^1\Sigma^+$–$X\,^1\Sigma^+$ (0, 1) band with rotationally linked transitions in the $C\,^1\Sigma^+$–$A\,^1\Sigma^+$ (0, 0) band. Four strong coincidences were found corresponding to the four possible excitation schemes: *RR*, *RP*, *PR*, and *PP*. The $C\,^1\Sigma^+$ ($v^*=0$) level is the upper level of the $v'=0$ progression of the Parkinson band system of BaO.[7] The R, P intensity anomalies are the result of $C\,^1\Sigma^+ \sim B\,^1\Pi$ perturbations and are a quantum mechanical interference effect between parallel ($\Delta\Omega=0$) and perpendicular ($\Delta\Omega=\pm1$) transition amplitudes. Two-laser OODR experiments permit a complete characterization of the $C(v^*=0)\sim B$ perturbation.

The one-laser OODR fluorescence in the red region was very complex and probably could not have been assigned if more than one v^*, J^* level had been simultaneously excited. An unexpected dividend was observation of $C\,^1\Sigma^+$–$A'\,^1\Pi$ and $C\,^1\Sigma^+$–$a\,^3\Pi_1$ P, Q, R fluorescence triplets. The C–$a(\Omega=1)$ fluorescence intensity was primarily borrowed from the C–A' transition by the known[8] strong $^1\Pi \sim {}^3\Pi_1$ $\Delta v=0$ spin–orbit interaction. The C–A'

a)Alfred P. Sloan Fellow.

 0021-9606/78/6809-4110$01.00

and $C-a$ bands are important because they provide a method for monitoring populations of the metastable $A'^1\Pi$ and $a^3\Pi$ states.

There have been many reports in the recent literature concerning the reactions of Ca, Sr, and Ba atoms with various oxidants (CO, CO_2, N_2O, NO_2, O_2, and O_3).[9–26] Particular attention has been focused on the $a^3\Pi$ and $A'^1\Pi$ states. Although BaO $a^3\Pi$ has been shown to be a precursor[27] to high quantum yield radiation from $A^1\Sigma^+$ in reactions such as

$$Ba + N_2O \rightarrow BaO^* + N_2, \quad (1)$$

how $a^3\Pi$ is populated remains a question which has stirred some controversy.[20,21] Several states exist which might act as energy reservoirs in Reaction (1): $X^1\Sigma^+$, $a^3\Pi$, $A'^1\Pi$, and $^3\Sigma^+$. In order to answer such questions as whether or not high vibrational levels of $X^1\Sigma^+$ are precursors to $a^3\Pi$ it would be necessary to measure cross sections for intersystem crossing between these two states. This requires a method for monitoring the populations of both states and for selective population of one or the other. Modeling of the population flow among reservoir levels must entail a detailed understanding of $a^3\Pi \sim X^1\Sigma^+$, $a^3\Pi \sim {}^3\Sigma^+$, and $a^3\Pi \sim A^1\Sigma^+$ perturbations likely responsible for efficient transfer.[28–31]

To date little information has been obtained for the low-lying $^3\Pi$ and $^1\Pi$ states of Ca, Sr, and Ba monoxides. Although rotational and vibrational constants are known for these states of all three molecules from the analysis of $A^1\Sigma^+ \sim A'^1\Pi$ and $A^1\Sigma^+ \sim a^3\Pi$ perturbations[8,32–34] and from direct experimental observations of the $^1\Pi$ states,[9,17,35–38] this work reports the *first* observation of BaO $a^3\Pi$ ($v = 0$, 1, and 2) and $A'^1\Pi$ ($v = 0$) rotational levels which are *not* perturbed by $A^1\Sigma^+$.[39]

II. EXPERIMENTAL

A. Apparatus

The OODR experimental apparatus and procedure for producing BaO have been described elsewhere.[1,13,40] Ba vapor was entrained in a flow of Ar (99.998% purity) and mixed with CO_2 (99.8% purity), which reacted spontaneously, resulting in a very weak reddish flame. CO_2 was chosen as an oxidant instead of N_2O, NO_2, O_3, or O_2 so as to minimize the chemiluminescence. Operating pressures were usually 1–3 torr; the gas mixture was typically 95% Ar, 5% CO_2.

Folded cavity, rhodamine 6G, jet stream dye lasers with intracavity three stage birefringent filters[41–43] provided radiation with spectral width (FWHM) of ~ 1 cm^{-1} throughout their tuning ranges from 570–630 nm. Conversion efficiencies when pumped with the 514.5 nm line of an Ar^+ laser were 20%; typical dye laser powers were 0.5–1 W. A 1.0 mm, 97% reflecting, solid quartz etalon with a free spectral range of 3.057 cm^{-1} was used to measure the laser frequency relative to atomic neon with a relative precision of 0.2 cm^{-1} and absolute accuracy of 1.0 cm^{-1}.

Laser induced fluorescence was viewed perpendicular to the laser beam by focusing the fluorescence onto the slit of a Spex 1704X monochromator (6 Å/mm reciprocal dispersion) for photoelectric work or onto the slit of a Spex 1802 spectrograph (18 Å/mm reciprocal dispersion) for photographic work. A Hamamatsu R818 red sensitive photomultiplier tube operated at 600 V was used with the 1704X; Kodak type IIIF photographic plates were used with the 1802. $C^1\Sigma^+ - X^1\Sigma^+$ uv emission was monitored using a Corning 7-37 uv passing-visible absorbing colored glass filter and a 480 nm cut-off interference filter with 70% average transmission from 400.0 to 475.0 nm (Ditric Optics Inc.) placed in front of an RCA 1P28 photomultiplier tube at 600 V. Total uv fluorescence was detected perpendicular to both the laser beam and the optic axis of the monochromator. For both photoelectric and photographic work, Hg and Ne pen lamps were used as frequency standards.

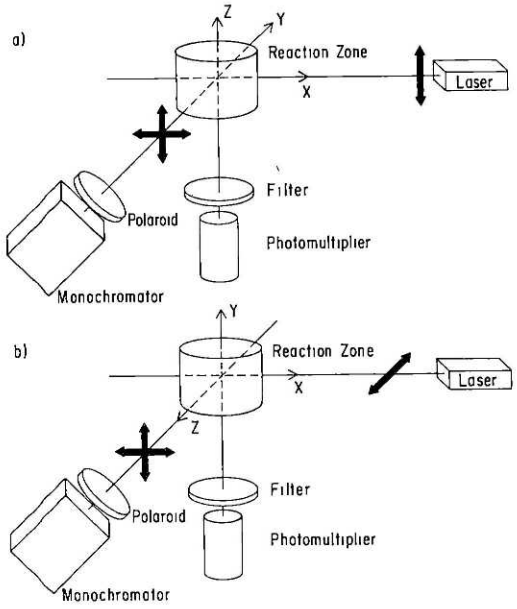

FIG. 1. Schematic representation of apparatus used to monitor OODR photoluminescence as a function of wavelength and polarization. (a) Laser is polarized in Z direction. Using a polaroid in front of monochromator slit, either X or Z linearly polarized light may be selected. (b) Laser polarized in Z direction, but the coordinate system has been rotated so that only X or Y fluorescence can be detected.

B. Polarization experiments

Two equivalent methods were used to monitor the polarization dependence of OODR transitions (see Fig. 1). The laser plane of polarization could be rotated using first a Fresnel rhomb which produced circularly polarized light and then a rotatable calcite polarizer to select linearly polarized light along any direction (with a loss of 50%). Alternatively, a polaroid sheet was placed in front of the monochromator slit passing only X or Z polarized light but not both (see Fig. 1). If we always consider the laser to be polarized in the Z direction (for simplicity in calculations below) and propagat-

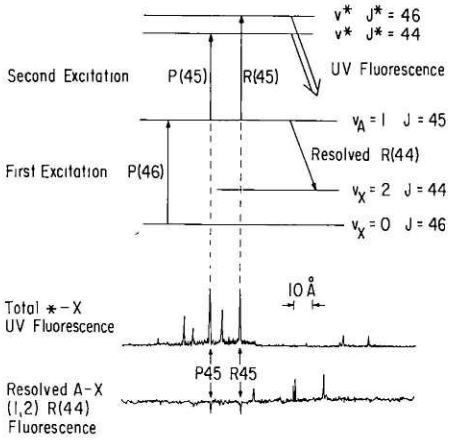

FIG. 2. Portion of an OODR excitation spectrum and corresponding excitation scheme illustrating two means by which OODR transitions may be detected. The first laser excites $A\,^1\Sigma^+(v'=1,\ J'=45) \leftarrow X\,^1\Sigma^+(v''=0,\ J''=46)$. The upper trace is a recording of uv fluorescence; the lower trace is resolved $A\,^1\Sigma^+(v'=1,\ J'=45) \rightarrow X\,^1\Sigma^+(v''=2,\ J''=44)$ fluorescence. Increases in the lower trace are caused by the second laser exciting $A\,^1\Sigma^+ \leftarrow X\,^1\Sigma^+$ followed by $A\,^1\Sigma^+$ emission whose frequency is coincidentally within the spectral width of the monochromator

ing in the X direction, then rotation of the plane of polarization of the laser corresponds to a 90° rotation about the X axis so that $X+Y$ polarized light is detected as opposed to $X+Z$ (see Fig. 1). X and Y polarized fluorescence are identical,[44] so that X-only, Y-only, and $X+Y$ unpolarized detection schemes should be equivalent. X or Y to Z intensity ratios, obtained either by rotating the laser or detector polarization, are found to be identical (see Secs. III.A and III.D) when the polarization dependence of the monochromator grating was considered.

C. OODR detection

Several methods exist by which OODR transitions may be detected: (1) $v^*, J^* \rightarrow v'', J''$ photoluminescence[1]; (2) $v^*, J^* \rightarrow v', J'$ photoluminescence[45-49]; (3) decreases in fluorescence from the intermediate v', J' levels[3]; and (4) total OODR photoluminescence. Each of these methods of detection provides different types and quantities of spectroscopic information. The first two schemes employ broad band filters to pass only certain frequency emission (here we detect uv $C\,^1\Sigma^+ \rightarrow X\,^1\Sigma^+$ OODR photoluminescence, for example). The third method listed above is the most versatile in that it samples OODR transitions into not only radiating but also nonradiating v^*, J^* levels. In BaO, for example, a perturbed level with 50% $A\,^1\Sigma^+$ and 50% $a\,^3\Pi$ character [for example, $J=45$ of $A\,^1\Sigma^+(v=1) \sim a\,^3\Pi_2(v=0)$] could be populated from $X\,^1\Sigma^+$ with the first photon; then, access to excited triplets as well as singlets should be equally probable, all other factors being equal. The singlets should radiate in the uv back down to $X\,^1\Sigma^+$ while the triplets will usually not radiate in the uv; thus, monitoring decreases in v', J' fluorescence without concomitant increases in uv fluorescence simplifies detection of OODR transitions into triplet states. An example of this type of detection scheme is illustrated in Fig. 2, where the first photon pumped $A\,^1\Sigma^+(v'=1, J'=45)$ which has 44.2% $a\,^3\Pi$ character.[4] No transitions to triplet states have yet been detected; every decrease in the pumped level fluorescence as the second laser is tuned is accompanied by uv fluorescence. There are, however, differences in the visible to uv branching ratio. It is clear from Fig. 2 that although this fluorescence decrease (flop out) method is versatile it lacks the sensitivity of the fluorescence increase (flop in) methods. Detection of total OODR photoluminescence is versatile and especially useful in a system where the emission frequencies are unknown. Total OODR fluorescence can be distinguished from single resonance fluorescence excited by either laser by modulating both lasers at different frequencies and detecting all fluorescence (no filters) at the sum or difference frequencies using a phase sensitive detector.

III. RESULTS AND ANALYSIS

In Table I we present a summary of the various emission systems observed in the single laser OODR experiments showing the fluorescence structure and how this information was used to sort out and assign all the spectral features. Below, we discuss each band system in detail.

A. $C\,^1\Sigma^+ - X\,^1\Sigma^+$ band system

1. *Single laser OODR excitation spectrum*

Figure 3 shows a *single laser* excitation spectrum where ultraviolet fluorescence intensity is recorded as a function of laser frequency. A red degraded band with a head at 16 030.3 cm^{-1} is observed with four strong lines standing alone above many weaker transitions; fluorescence from only these four strong transitions is considered.

2. *OODR photoluminescence*

Figure 4 shows a portion of the ultraviolet emission spectrum from these levels extending from 320 nm to 480 nm and consisting primarily of P and R doublets characteristic of either $^1\Sigma^+ \rightarrow {}^1\Sigma^+$ or $^1\Pi \rightarrow {}^1\Sigma^+$ emission.[50] Seventeen doublets corresponding to emission into $X\,^1\Sigma^+$

TABLE I. Summary of emission observed.

Band system	Structure	Information obtained
$C\,^1\Sigma^+ \rightarrow X\,^1\Sigma^+$	PR doublets in uv with large intensity anomalies	Isotopic assignment J^* $B\,^1\Pi \sim C\,^1\Sigma^+$ perturbation
$C\,^1\Sigma^+ \rightarrow A\,^1\Sigma^+$	PR doublets in visible	J^*
$A\,^1\Sigma^+ \rightarrow X\,^1\Sigma^+$	Pairs of PR doublets	J', v' Assignment of intermediate state
$C\,^1\Sigma^+ \rightarrow a\,^3\Pi_1$	PQR triplets Intensity anomalies	Characterization of $a\,^3\Pi_1$. $C\,^1\Sigma^+ \sim {}^3\Sigma_0^-$ perturbation. Alignment of $C\,^1\Sigma^+$.
$C\,^1\Sigma^+ \rightarrow A'\,^1\Pi$	PQR triplets Intensity anomalies	Characterization of $A'\,^1\Pi$. Alignment of $C\,^1\Sigma^+$. Proof of $C\,^1\Sigma^+$ symmetry.

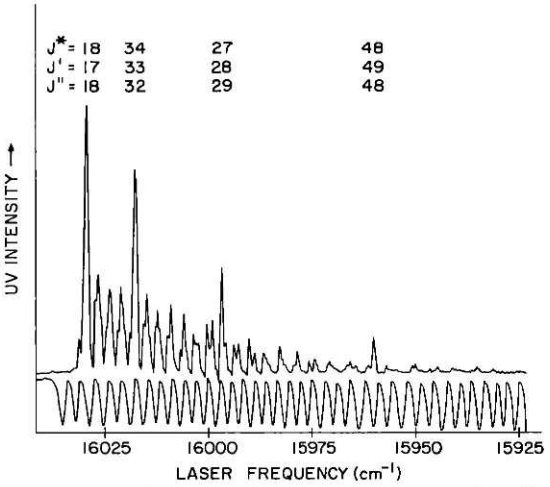

FIG. 3. Single laser OODR excitation spectrum resulting from the absorption of two photons from $X\,^1\Sigma^+(v''=1)$ via $A\,^1\Sigma^+(v'=0)$ to $C\,^1\Sigma^+(v^*=0)$. The four strongest transitions are labelled according to J^*, J', and J''. The lower trace is a series of interference fringes from a 97% reflecting, 3.057 cm^{-1} free spectral range external cavity etalon used for frequency calibration.

($v''=1$ to $v''=17$) are observed for each of the four excited J^* levels. Three features should be noted: (1) there is a broad Franck–Condon maximum between $v''=8$ and 10; (2) emission into $v''=0$ is not observed because of a small Franck–Condon factor; and (3) the relative intensities of P and R lines vary from doublet to doublet and generally deviate from expected 1:1 ratios.[50] The appearance of only a single Franck–Condon maximum suggests that $v^*=0$. J^* is determined from the frequency difference between P and R lines and known ground state rotational constants[1]:

$$\Delta PR = (4B_v'' - 6D_v'')(J^*+1/2) - 8D_v''(J^*+1/2)^3 , \qquad (2)$$

where B_v'' and D_v'' have their usual meanings.[50] ΔPR was determined to ± 0.3 cm^{-1} from photographic plates of $*\rightarrow X\,^1\Sigma^+$ emission.

From examination of fluorescence at and near the laser frequency, it is possible to assign an excitation scheme for each double resonance transition. Measurement of the laser frequency and observation of $A\,^1\Sigma^+(v'=0)\rightarrow X\,^1\Sigma^+(v'')$ emission (see below) indicates that the first photon excites the $A\,^1\Sigma^+\leftarrow X\,^1\Sigma^+(0,1)$ band; $A\,^1\Sigma^+\rightarrow X\,^1\Sigma^+$ fluorescence consists of P and R transitions with the R branch always at higher energy. Examination of $A\,^1\Sigma^+\rightarrow X\,^1\Sigma^+(0,1)$ fluorescence therefore determines whether the laser is exciting a P or an R branch. Similarly, from $*\rightarrow A\,^1\Sigma^+$ emission (see below) in the same frequency region, the second step can be determined to be either a P or an R transition. Table II summarizes the excitation schemes for each of the four transitions.

TABLE II. Single laser OODR excitation schemes.

		Branch	
J^*	$\tilde{\nu}_{laser}$ (cm^{-1})	$A\,^1\Sigma^+(v'=0)$ $\leftarrow X\,^1\Sigma^+(v''=1)$	$C\,^1\Sigma^+(v^*=0)$ $\leftarrow A\,^1\Sigma^+(v'=0)$
18	16029.6 ± 0.5	$P(18)$	$R(17)$
27	15995.6	$P(29)$	$P(28)$
34	16016.8	$R(32)$	$R(33)$
48	15957.5	$R(48)$	$P(49)$

It should be noted here that there are five naturally abundant isotopes of Ba: ^{138}Ba(71.66%), ^{137}Ba(11.32%), ^{136}Ba(7.81%), ^{135}Ba(6.59%), and ^{134}Ba(2.42%). In order to correctly assign J^* it is necessary to determine which isotopic species is observed since B_v'' and D_v'' are isotopically dependent.[50] This was done by examining $*\rightarrow X\,^1\Sigma^+$ emission into two different ground state vibrational levels, $v_1''=12$ and $v_2''=6$. The separation between P or R lines in these two bands depends only on ground state rotational and vibrational constants[50]

$$\Delta\nu_{v1b} = \omega_e(v_2''-v_1'') - \omega_e x_e[v_2''(v_2''+1) - v_1''(v_1''+1)] - \alpha_e J''(J''+1)(v_2''-v_1'') , \qquad (3)$$

where ω_e, $\omega_e x_e$, and α_e have their usual meanings. The isotopic dependence of these constants is well known[50]:

$$\omega_e^i = \rho\omega_e ,$$
$$\omega_e x_e^i = \rho^2\omega_e x_e ,$$
$$\alpha_e^i = \rho^3\alpha_e , \qquad (4)$$

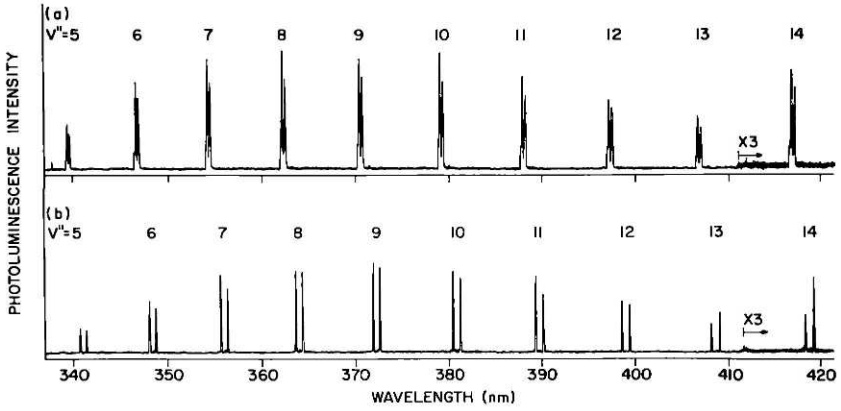

FIG. 4. (a) A portion of the resolved $C\,^1\Sigma^+(v^*=0,\ J^*=18)\rightarrow X\,^1\Sigma^+(v'',\ J''=17 \text{ or } 19)$ ultraviolet photoluminescence spectrum consisting of P and R doublets and exhibiting anomalous $P:R$ intensity ratios. (b) Same as (a) except $C\,^1\Sigma^+(v^*=0,\ J^*=48)\rightarrow X\,^1\Sigma^+(v'',\ J''=47 \text{ or } 49)$. Note the reversal of intensities for $v''=13$ and 14 due to the $B\sim C$ perturbation.

TABLE III. The nonvanishing direction cosine matrix elements $\langle \Omega' J' M' | \alpha_{Rs} | \Omega J M \rangle$, where $R = X$, Y, or Z and $s = x$, y, or z are given by the product of three factors: $f(J';J) g_s(J', \Omega'; J, \Omega) \times h_R(J', M'; J, M)$. The factors f, g_s, h_R for a given matrix element are taken from different rows of the same column of this table. The choice of columns depends on the value of $J' - J$. The choice of rows depends on R and s. In all cases, the first factor f is taken from row one; the second factor g_s is chosen from rows two or three; and the third factor h_R is chosen from rows four or five.[a]

Factor	$J' = J+1$	$J' = J$	$J' = J-1$
$f(J';J)$	$\{4(J+1)[(2J+1)(2J+3)]^{1/2}\}^{-1}$	$[4J(J+1)]^{-1}$	$\{4J[(2J+1)(2J-1)]^{1/2}\}^{-1}$
$g_z(J', \Omega; J, \Omega)$	$2[(J+\Omega+1)(J-\Omega+1)]^{1/2}$	2Ω	$2[(J+\Omega)(J-\Omega)]^{1/2}$
$g_x(J', \Omega \pm 1; J, \Omega)$ or $\pm i g_y(J', \Omega \pm 1; J, \Omega)$	$\mp[(J \pm \Omega + 1)(J \pm \Omega + 2)]^{1/2}$	$[(J \pm \Omega)(J \pm \Omega + 1)]^{1/2}$	$\pm[(J \mp \Omega)(J \mp \Omega - 1)]^{1/2}$
$h_Z(J', M; J, M)$	$2[(J+M+1)(J-M+1)]^{1/2}$	$2M$	$2[(J+M)(J-M)]^{1/2}$
$h_X(J', M \pm 1; J, M)$ or $\pm i h_Y(J', M \pm 1; J, M)$	$\mp[(J \pm M + 1)(J \pm M + 2)]^{1/2}$	$[(J \pm M)(J \pm M + 1)]^{1/2}$	$\pm[(J \mp M)(J \mp M - 1)]^{1/2}$

[a]This table was taken directly from Ref. 56 and was originally published in Ref. 57. Capital (lower case) letters refer to space (molecule) fixed coordinates.

where $\rho = (\mu/\mu')^{1/2}$, and μ is the molecular reduced mass. Thus $\Delta\nu_{vib}$ may be calculated for all isotopes and compared with experiment. For example, for $J'' = 26$,

$$\Delta\nu_{vib}^{calc} = 3773.85 \text{ cm}^{-1} \quad \text{for } {}^{138}\text{Ba}^{16}\text{O},$$

$$\Delta\nu_{vib}^{calc} = 3775.23 \text{ cm}^{-1} \quad \text{for } {}^{137}\text{Ba}^{16}\text{O},$$

and

$$\Delta\nu_{vib}^{meas} = 3773.8 \pm 0.3 \text{ cm}^{-1}.$$

In this fashion we were able to determine that only $^{138}Ba^{16}O$ was observed in *each* of the four transitions.

Once J^* is known, energies relative to $v'' = 0$ and $J'' = 0$ are easily obtained[51]:

$$E(v^*, J^*) = E(A\,{}^1\Sigma^+, J', v' = 0) + E_{laser}, \tag{5}$$

where $E(A\,{}^1\Sigma^+, J', v' = 0)$ was calculated from $A\,{}^1\Sigma^+ - X\,{}^1\Sigma^+$ transition energies given in Ref. 32 and $X\,{}^1\Sigma^+$ ground state constants in OODR I.[1] In order to obtain further information from these energies a physical model must be employed which is consistent with all of the data described above.

3. *Intensity anomalies*

As seen in Fig. 4, intensity anomalies are observed in $* - X\,{}^1\Sigma^+$ P and R branch emission. The magnitude and sign of these anomalies depend on J^* as well as v'' as shown in Fig. 4; and, at times, branches even disappear. Upon rotation of the laser plane of polarization or use of a polaroid in front of the monochromator slit as described above in Sec. II, no change in the relative intensity of P to R emission could be detected within experimental error. The vibrational and rotational dependence of these anomalies is overwhelmingly suggestive of a perturbation; in other words, the * state is a mixture of two Born–Oppenheimer basis states since $X\,{}^1\Sigma^+$ ($v'' = 1$ to $v'' = 17$) are known to be completely free of perturbations.[1,8] Similar interferences due to Coriolis interaction in polyatomic molecules[52] and rotation–electronic interaction in diatomic molecules[53,54] have been observed previously. In fact, interference between transition amplitudes associated with a mixture of two Born–Oppenheimer states has led to the annihilation of normally fully allowed bands as well as branches in the NO molecule.[55]

We represent the * state as a linear combination of $^1\Sigma^+$ and $^1\Pi$ basis states:

$$|*\rangle = c\,|{}^1\Sigma^+\rangle + (1 - c^2)^{1/2}\,|{}^1\Pi\rangle, \tag{6}$$

where c is a mixing coefficient. The transition intensity is proportional to the electric dipole, μ, matrix element squared:

$$I \sim |\langle *, J^*, v^* | \mu | X\,{}^1\Sigma^+, v'', J'' \rangle|^2. \tag{7}$$

Explicitly treating $\langle *, J^*, v^* |$ as a mixed state one obtains

$$I \sim |c|^2 |\mu_{\Sigma X}|^2 + |(1 - c^2)|\,|\mu_{\Pi X}|^2 + c'(1 - c^2)^{1/2} \mu'_{\Sigma X} \mu_{\Pi X}, \tag{8}$$

where a prime denotes a complex conjugate and $\mu_{\Lambda X} = \langle *, \Lambda, J^* | \mu | X\,{}^1\Sigma^+, v'', J'' \rangle$. The last term in Eq. (8) is responsible for interference between P and R branches. In order to explain the observed vibrational and rotational dependence of these anomalies we factor the matrix elements of μ in the spirit of the Born–Oppenheimer approximation:

$$\mu_{\Sigma X} \sim \langle v_\Sigma | v_X \rangle\, \alpha(J^*, J'', \Delta\Omega = 0) R_e^{\Sigma X},$$

$$\mu_{\Pi X} \sim \langle v_\Pi | v_X \rangle\, \alpha(J^*, J'', \Delta\Omega = 1) R_e^{\Pi X}, \tag{9}$$

where $\langle v_\Lambda | v_X \rangle$ is a vibrational overlap, α is a direction cosine matrix element, $R_e^{\Lambda X}$ is an electronic transition moment integral, and Ω is the projection of J onto the internuclear axis. It is seen from Eq. (9) that both $R_e^{\Lambda X}$ and $\langle v_\Lambda | v_X \rangle$ must be nonzero for *both* $\Lambda = \Sigma$ and Π in order to account for the observed intensity anomalies. The interference effect varies in magnitude and sign from band to band because of the independent variation of $\langle v_\Sigma | v_X \rangle$ and $\langle v_\Pi | v_X \rangle$ with v_X. Only $^1\Sigma^+$ and $^1\Pi$ states may have nonzero electronic transition moments with $X\,{}^1\Sigma^+$. An examination of α (see Table III) shows that only matrix elements for $\Delta\Omega = \pm 1$ have opposite signs for P and R transitions so that * is a mixture of at least one $^1\Sigma^+$ and one $^1\Pi$ state.

Intensity anomalies in a particular band should become more severe as the two perturbing states become

degenerate and $c^2 \rightarrow 0.5$. As seen in Fig. 4, these anomalies get larger as J^* increases. From second order perturbation theory,

$$c(J^*) \sim \frac{H(J^*)}{\Delta E(J^*)}, \tag{10}$$

where $H(J^*)$ is the interaction matrix element between the two states and $\Delta E(J^*)$ is the energy difference as a function of J^*. Thus when the two states cross, ΔE changes sign, c changes sign and the sense of the PR interference changes. This crossover is observed between $J^* = 34$ and 48 assuming that *both* transitions into $J^* = 34$ and 48 observed are either main or extra lines. If the transition into $J^* = 34$ is a main line and the transition into $J^* = 48$ is an extra line (or *vice versa*) a change in sign of the PR interference would be observed when the crossover is *not* between $J^* = 34$ and 48. A more systematic investigation of this region is therefore required.

4. Two laser OODR excitation spectra

In order to verify the above analysis and unambiguously determine the J value of the $^1\Sigma^+ \sim {}^1\Pi$ crossing, we have used *two* dye lasers to *systematically* probe the * state in the region of $J^* = 34$ to 48. In these experiments, the $A\,^1\Sigma^+ \leftarrow X\,^1\Sigma^+$ (0, 0) band was excited with the first laser which was amplitude modulated at 200 Hz. The second laser then excited $^* \leftarrow A\,^1\Sigma^+$ (0, 0) and uv fluorescence was detected using a phase sensitive detector in order to eliminate interference from single laser OODR effects.[58] Not only main but also extra lines were observed between $J^* = 34$ and 48. Figure 5 shows a two laser OODR excitation spectrum exhibiting main and extra P and R branch lines[59,60] and indicating that the crossing is near $J^* = 42$. The $J^* = 34$ and 48 levels observed in the single laser OODR spectrum are composed of mostly the same basis state, $C\,^1\Sigma^+$ ($v^* = 0$).

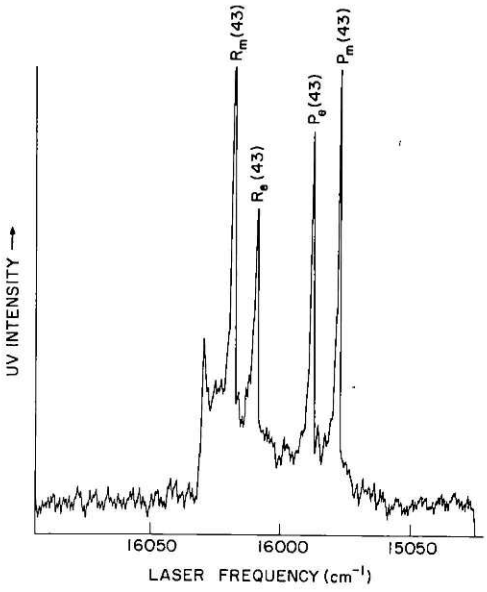

FIG. 5. Two laser OODR excitation spectrum. First laser excites $A\,^1\Sigma^+$ ($v' = 0$, $J' = 43$) $\leftarrow X\,^1\Sigma^+$ ($v'' = 0$, $J'' = 44$). The second laser is scanned exciting both main (m) and extra (e) P and R branches in the $C\,^1\Sigma^+ \leftarrow A\,^1\Sigma^+$ (0, 0) band as $C\,^1\Sigma^+ \rightarrow X\,^1\Sigma^+$ ultraviolet photoluminescence is recorded.

TABLE IV. $B\,^1\Pi(v) - C\,^1\Sigma^+$ ($v^* = 0$) Hamiltonian matrix[a] and fitted parameters.

$H_{11} = E_\Sigma + B_\Sigma J(J+1) - D_\Sigma [J(J+1)]^2$

$H_{22} = E_\Pi + B_\Pi [J(J+1) - 1] - D_\Pi [J(J+1) - 1]^2$

$H_{12} = H_{21} = \beta [2J(J+1)]^{1/2}$ [b]

Parameter	Fitted Value (cm^{-1})[c]
E_Σ	33 084.0 (10)[d]
B_Σ	0.23846 (30)
D_Σ	2.8×10^{-7}[e]
E_Π	33 105.1 (10)[d]
B_Π	0.2266 (6)
D_Π	2.8×10^{-7}[e]
β	0.1001 (15)

[a] Only the e-parity[64] matrix is considered here.

[b] $\beta = b \langle v_\Pi | B | v_\Sigma \rangle$, where b and $\langle v_\Pi | B | v_\Sigma \rangle$ are defined in Ref. 8.

[c] Uncertainties in the last figure of one standard deviation are listed in parentheses.

[d] Energy relative to the $X\,^1\Sigma^+$ potential minimum.

[e] Arbitrarily held constant at the D_e value for $A\,^1\Sigma^+$.[32]

5. Theoretical interpretation and comparison with the Parkinson band system

We are now able to return to the energy levels measured and employ a model involving two states which we shall designate $C\,^1\Sigma^+$ and $B\,^1\Pi$[61] in obtaining rotational constants for these two vibrational levels. Using a weighted, nonlinear, least squares program[62,63] (originally written by R. Stern with modifications by T. Bergeman and A. Kotlar) to fit these eigenvalues to a diagonalized Hamiltonian matrix given in Table IV, we obtained the rotational constants and perturbation matrix element which are also given in Table IV. Using constants from Table IV for $C\,^1\Sigma^+$ ($v^* = 0$) and those of OODR I[1] for $X\,^1\Sigma^+$ we have calculated the positions of $C\,^1\Sigma^+ - X\,^1\Sigma^+$ bandheads given in Table V. These bandheads are found to be in excellent agreement with those reported previously by Parkinson,[7] who attributed these transitions to the $v' = 0$ progression of the $B(^1\Pi) - X\,^1\Sigma^+$ system. Parkinson chose the assignment of $^1\Pi$ for the upper state because of "the complex rotational structure."[7] We have seen that the rotational structure for this state is complex because of $^1\Sigma^+ \sim {}^1\Pi$ perturbations, but in fact the state is best characterized as $^1\Sigma^+$; therefore, we adopt the notation of $C\,^1\Sigma^+$ for this system and retain the notation $B\,^1\Pi$ for the perturbing state.

6. Explanation of single laser OODR effect

In the single laser OODR experiment, $C\,^1\Sigma^+$ can be populated only when $\nu_{A-X}(J' \leftarrow J'') = \nu_{C-A}(J^* \leftarrow J')$ and

TABLE V. $C\,^1\Sigma^+(v^*=0)$–$X\,^1\Sigma^+(v'')$ bandheads.

v''	$\tilde{\nu}_{head}(cm^{-1})$	$\lambda^{air}_{head}(Å)$
0	32 751	3052.5 (0)[a]
1	32 085	3115.8 (1)
2	31 423	3181.4 (3)
3	30 766	3249.5 (5)
4	30 113	3319.9 (7)
5	29 463	3393.0 (8)
6	28 818	3469.0 (9)
7	28 178	3547.9 (10)
8	27 541	3629.9 (10)
9	26 909	3715.1 (10)
10	26 281	3803.9 (9)
11	25 658	3896.4 (8)
12	25 038	3992.7 (7)
13	24 424	4093.2 (5)
14	23 814	4198.1 (3)
15	23 208	4307.7 (2)
16	22 607	4422.2 (1)
17	22 010	4542.0 (1)
18	21 418	4667.6 (0)

[a]Relative intensities uncorrected for instrument response are given in parentheses. Zero intensity transitions were *not* observed in this work.

$J^* = J' \pm 1 = J'' \pm 2$ or J''. Figures 6 and 7 illustrate how $C\,^1\Sigma^+$–$A\,^1\Sigma^+$ and $A\,^1\Sigma^+$–$X\,^1\Sigma^+$ transitions come into and go out of resonance. From Fig. 7 it is seen that there are only four coincidences possible corresponding to the excitation schemes given in Table II. This is not a general conclusion concerning $^1\Sigma^+$–$^1\Sigma^+$ double coincidence spectra; depending on B^*, B', B'', and the vibronic energies of the three states it may be possible to have less than four coincidences. Two mechanisms may be responsible for the weaker transitions in the single laser OODR excitation spectrum (see Fig. 3) resulting in the formation of a bandhead[65]: (1) rotational relaxation in the relatively long-lived $A\,^1\Sigma^+$ state ($\tau_{rad} = 3.56\times10^{-7}$ sec for $v'=0$)[66]; or (2) two photon transitions via a *virtual* intermediate state enhanced by near resonance transitions. Two observations indicate that the latter mechanism is relatively unimportant:

(1) The weaker transitions decrease in intensity faster than the four strong double coincidence lines with decreasing Ar carrier gas pressure; and

(2) Fluorescence from one of these weaker transitions has been observed and partially assigned to excitation via a specific $A\,^1\Sigma^+$ ($v'=0$) rotational level.

TABLE VI. $A\,^1\Sigma^+$–$X\,^1\Sigma^+$ bands observed in single laser OODR experiments.

Band	$\tilde{\nu}_{head}(cm^{-1})$[a]	$\lambda^{air}_{head}(Å)$[a]	Relative intensity[b]	Source of fluorescence
(3,0)	18201.0	5492.69	1	Cascade
(2,0)	17712.7	5644.13	1	Cascade
(1,0)	17221.3	5805.15	1	Cascade
(2,1)	17047.0	5864.51	1	Cascade
(0,0)	16728.1	5976.28	5	Direct
(1,1)	16552.7	6039.64	1	Cascade
(0,1)	16060.7	6224.66	10[c]	Direct
(0,2)	15396.7	6493.09	9	Direct
(0,3)	14739.1	6782.79	9	Direct
(0,4)	14085.8	7097.41	8	Direct
(0,5)	13436.4	7440.42	6	Direct
(0,6)	12792.1	7815.20	3	Direct

[a]Taken from Ref. 67.
[b]Intensities relative to laser band.
[c]Laser band.

B. $A\,^1\Sigma^+$–$X\,^1\Sigma^+$ band system

For each of the four single laser OODR transitions discussed above, 12 $A\,^1\Sigma^+$–$X\,^1\Sigma^+$ bands were observed (see Table VI). The strongest emission arose from $v'=0$, which was directly populated by absorption of the first photon. Quartets of rotational lines were observed in every $A\,^1\Sigma^+$–$X\,^1\Sigma^+$ band in addition to many weaker transitions from collisionally populated levels resulting in the formation of bandheads.

Line quartets arose in two distinct ways: (1) simultaneous excitation of two different $A\,^1\Sigma^+$ ($v'=0$) rotation-

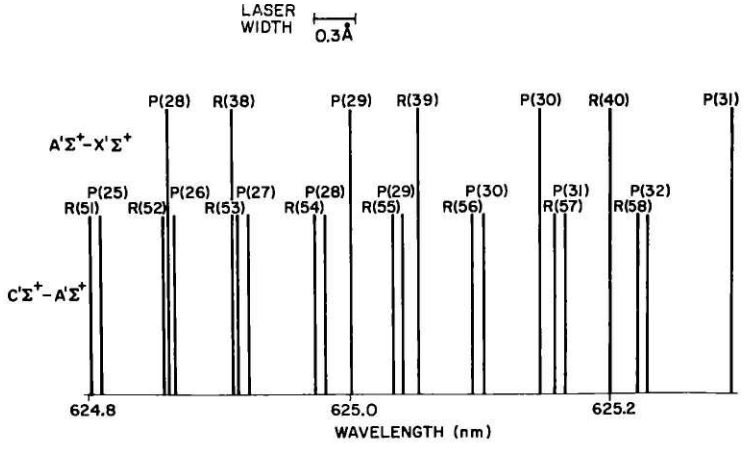

FIG. 6. OODR coincidence spectrum illustrating how the $C\,^1\Sigma^+$–$A\,^1\Sigma^+$ (0,0) and $A\,^1\Sigma^+$–$X\,^1\Sigma^+$ (0,1) bands come into and go out of resonance. When $J^* = J' \pm 1 = J'' \pm 2$ or J'' and $\nu_{C-A} = \nu_{A-X}$ within the laser spectral width an OODR transition occurs.

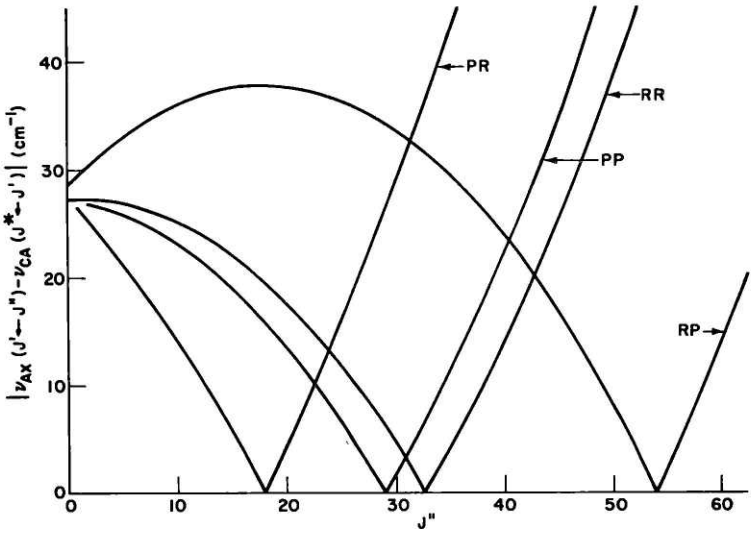

FIG. 7. Differences between $A\,^1\Sigma^+$–$X\,^1\Sigma^+$ (0, 1) and $C\,^1\Sigma^+$–$A\,^1\Sigma^+$ (0, 0) transition frequencies are plotted as a function of J'' for each of four possible excitation schemes: PR, PP, PR, and RP. Four zeroes are calculated corresponding to the four strong coincidences in Fig. 3. Effects of a $C\,^1\Sigma^+ \sim B\,^1\Pi$ perturbation can be seen in the shifting of the RP coincidence from the zero interaction calculated value of $J'' = 53$ to the observed value of $J'' = 48$.

al levels; and (2) P and R cascade fluorescence from $C\,^1\Sigma^+$ ($v^* = 0, J^*$) into $A\,^1\Sigma^+$ ($v', J' = J^* \pm 1$) levels. Quartets from the former consisted of two PR doublets with different intensities and PR spacings because the J' levels populated were very different: for $A\,^1\Sigma^+$–$X\,^1\Sigma^+$ (0, 1), transitions into two levels differing in J' by 10 occurred within the laser spectral width. Cascade quartets consisted of two PR doublets with nearly the same intensities and PR spacings since they resulted from $A\,^1\Sigma^+$ (v') rotational levels differing in J' by two and populated from the same initial $C\,^1\Sigma^+$ (v^*, J^*) state. Cascade fluorescence from $A\,^1\Sigma^+$ ($v' = 0$) was too weak to be detected in the presence of laser induced $A\,^1\Sigma^+ - X\,^1\Sigma^+$ ($v' = 0, v''$) fluorescence.

C. $C\,^1\Sigma^+$–$A\,^1\Sigma^+$ band system

Emission into $A\,^1\Sigma^+$ ($v' = 0$, 1, 2, and 3) was observed and consisted of P and R doublets resulting in the cascade fluorescence discussed above and summarized in Table VI. Contrary to the situation for $C\,^1\Sigma^+ - X\,^1\Sigma^+$ emission, no intensity anomalies were observed in these bands presumably because of small R_e^{BA} and/or small $\langle v_B | v_A \rangle$ factors; this observation is consistent with the lack of Q branches in the two laser OODR excitation spectra.[59]

TABLE VII. Experimental and calculated intensity ratios for the $C\,^1\Sigma^+ \rightarrow a\,^3\Pi_1$ (0, 0) band.

	Intensity ratios			
J^* excitation[a] scheme	$X+Z$ detection[b] $P/(P+R)$	$Q/(P+R)$	$X+Y$ Detection[b] $P/(P+R)$	$Q/(P+R)$
18 PR	0.67 (0.53)[c]	0.93 (0.63)	0.62 (0.50)	1.44 (1.70)
27 PP	0.59 (0.53)	0.71 (0.68)	0.59 (0.50)	1.29 (1.55)
34 RR	0.67 (0.53)	0.67 (0.63)	0.71 (0.50)	1.21 (1.60)
48 RP	0.67 (0.53)	0.80 (0.63)	0.71 (0.50)	1.21 (1.55)

[a]See Table II.
[b]See Fig. 1.
[c]Values in parentheses are calculated (see text and Table VIII).

D. $C\,^1\Sigma^+$–$A'\,^1\Pi$ and $C\,^1\Sigma^+$–$a\,^3\Pi_1$ band systems

1. Experimental observations

For each of the four J^* levels populated in the single laser OODR experiment, a progression consisting of three approximately equally spaced bands[68] with an average spacing of 438 cm^{-1} was observed from 655 nm to 700 nm; the bands decreased in intensity with increasing wavelength. Each band consisted of three nearly equally spaced P, Q, and R branch lines the relative intensities of which differed significantly from expected $P/(P+R) = 0.5$ and $Q/(P+R) = 1$ ratios (see Fig. 8). Although these ratios varied only slightly with the lower vibrational level and J^*, dramatic changes were observed in the $Q/(P+R)$ ratio as a function of detection geometry (see Fig. 1 and Table VII). The $P/(P+R)$ intensity ratio was on the average 0.65 (see Table VII) and changed insignificantly with detection geometry; the Q

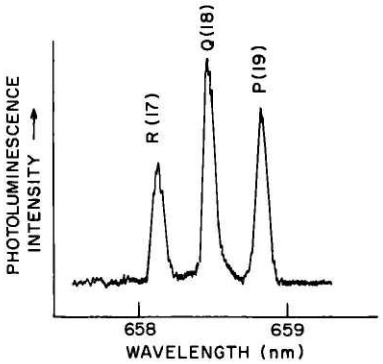

FIG. 8. $C\,^1\Sigma^+ (v^* = 0, J^* = 18) \rightarrow A'\,^1\Pi (v = 0)$ emission consisting of P, Q, and R branches whose relative intensities deviate markedly from the expected[50] 1:2:1 ratio. X and Z polarized fluorescence is recorded with the laser polarized in the Z direction.

branch intensity was anomalously weak relative to P and R for $X+Z$ detection but anomalously strong for $X+Y$ detection.

A second progression identical in structure to the above emission although 2.5 times weaker (after correcting for instrumental response) was observed an average of 235 cm^{-1} to higher frequency. Splittings between bands and P, Q, and R branch lines differed slightly from the above emission; however, the same relative intensities and anomalies were observed.

Energies for the lower states of these transitions were calculated directly from $E(v^*=0, J^*)$ calculated above and the $C^1\Sigma^+ - v, J$ transition energy.

2. Expectations from previous work

In addition to $X^1\Sigma^+$ and $A^1\Sigma^+$ three low-lying bound states of BaO might be considered in interpreting emission spectra from $C^1\Sigma^+$ ($v^*=0$): $a^3\Pi$, $A'^1\Pi$, and $^3\Sigma^+$.[8] $a^3\Pi$ and $A'^1\Pi$ energies relative to $X^1\Sigma^+$ as well as rotational and vibrational constants have been determined from deperturbation of $A^1\Sigma^+ - X^1\Sigma^+$ spectra[4,8] and, for $A'^1\Pi$, from the experimental work of Hsu *et al.*[10] and Zare *et al.*[35] Thus, the energies for these states are readily calculated as a function of v and J. From Ref. 8 we calculate $E(a^3\Pi_1, v=0) - E(A'^1\Pi, v=0) = 236$ cm^{-1} and $E(a^3\Pi_1, v=1) - E(a^3\Pi_1, v=0) = 443.5$ cm^{-1} and note that vibrational and rotational constants for $A'^1\Pi$ and $a^3\Pi_1$ are nearly identical.[8,35] There are, to date, no observations of the $^3\Sigma^+$ state.

Emission into $A'^1\Pi$ must be accompanied by emission into $a^3\Pi_1$. Spin–orbit interaction between $A'^1\Pi$ and $a^3\Pi_1$ results in an approximately J independent mixing such that $A'^1\Pi$ has an average 23% $a^3\Pi_1$ character and *vice versa*.[4,8] If the emitting state has oscillator strength to only $A'^1\Pi$ or $a^3\Pi_1$ but not to both, then the relative intensities of the two band systems must be consistent with the mixed nature of these two states: if only $C^1\Sigma^+ - A'^1\Pi$ emission is allowed then emission into $a^3\Pi_1$ will be 3.3 times weaker than emission into $A'^1\Pi$. Although spin–uncoupling[69] results in a J-dependent mixture of Hund's case a $^3\Pi_0$, $^3\Pi_1$, and $^3\Pi_2$ basis states, for $v=0$ and $J=50$ the percentage $A'^1\Pi$ in $a^3\Pi_2$ and $a^3\Pi_0$ is 2%; therefore, emission into these other spin components would be 12 times weaker than emission into $a^3\Pi_1$ for an allowed transition into only $A'^1\Pi$.

3. Comparison between predictions and observations

The agreement between predicted $A'^1\Pi$ and $a^3\Pi_1$ vibrational spacings and the $a^3\Pi_1 - A'^1\Pi$ splittings with the observation above is highly suggestive that the lower states of these transitions are $a^3\Pi_1$ and $A'^1\Pi$, with $a^3\Pi_1$ 2.5 times weaker and 235 cm^{-1} to higher frequency. A further comparison between calculated and observed energies for the lower states of these transitions yields a rms difference between observed and calculated energies of 0.5 cm^{-1}. On this basis we assign the lower levels of these transitions to $a^3\Pi_1$ ($v=0$, 1, and 2) and $A'^1\Pi$ ($v=0$, 1, and 2).

Although the agreement between theoretical and experimental energies is very good, significant discrepancies between expected and observed intensities exist: (1) emission into $a^3\Pi_1$ is 30% stronger than expected for an allowed transition into only $A'^1\Pi$; (2) P branch emission is always stronger than expected relative to R branch emission; and (3) Q branch intensity, relative to P and R, is strongly dependent on detection geometry.

It is apparent from the first of these discrepancies that $C^1\Sigma^+$ must have an admixture of triplet character and, therefore, a finite transition probability into $a^3\Pi_1$. Since exhaustive searches for emission into $a^3\Pi_0$ and $a^3\Pi_2$ proved fruitless, it is concluded that this triplet state must be $^3\Sigma_0^-$ (F_1 and F_3 levels) which can both perturb $C^1\Sigma^+$ and preferentially radiate into $a^3\Pi_1$.[50] A $^3\Pi_1$ perturber which might also interact with $C^1\Sigma^+$ via $B^1\Pi$ may be eliminated because $C^1\Sigma^+ - a^3\Pi_1$ Q branch intensities are in proportion to P and R branch intensities. $^3\Pi_1 - {}^3\Pi_1$ Q branches are weak and decrease rapidly in intensity as J increases[50] so that $C^1\Sigma^+ - a^3\Pi_1$ Q branches would be weak compared with P and R branches.

The fact that the P branches are always stronger than the R branches is suggestive of interference between $\Delta\Omega=0$ (parallel) and $\Delta\Omega=\pm1$ (perpendicular) transition moments in the $C^1\Sigma^+ - A'^1\Pi$ or $a^3\Pi_1$ emission. We already know of two participating $\Delta\Omega=1$ transition moments: $^1\Sigma_0^+ - {}^1\Pi_1$ and $^3\Sigma_0^- - {}^3\Pi_1$. Thus, either an $\Omega=1$ state or an $\Omega=0$ state could be mixed with the upper or lower levels, respectively. Although a $B^1\Pi - A'^1\Pi$ transition moment is a logical choice for causing this interference, from Table VII no change in the $P/(P+R)$ ratio is seen between $J^*=34$ and 48 as would be expected (see Sec. II.A). It is concluded, therefore, that the $B-A'$ transition moment is negligibly small. Admixture of $A^1\Sigma^+$ into $A'^1\Pi$ or $a^3\Pi_1$ is known to be negligible for the values of v and J observed here from deperturbation of the $A^1\Sigma^+ - X^1\Sigma^+$ band system.[37] Moreover, any PR interference in $C^1\Sigma^+ - a^3\Pi_1$ or $A'^1\Pi$ emission due to mixing between $A^1\Sigma^+$, $a^3\Pi_1$, and $A'^1\Pi$ would necessarily also appear in a complementary fashion in $C^1\Sigma^+ - A^1\Sigma^+$ emission for which no anomalies have been observed (see Sec. III.C). We are forced therefore to include yet another perturbing state: $^3\Pi_1$ or $^1\Pi$ in $C^1\Sigma^+$ or $^3\Sigma^+$ in $a^3\Pi_1$ and $A'^1\Pi$. It is not surprising that so many states need be considered in interpreting emission from a highly excited electronic state but it is dissatisfying that no simple picture can be presented. It should be noted that effects of these perturbing states have not yet been observed in the form of $C^1\Sigma^+$, $a^3\Pi$, or $A'^1\Pi$ level shifts. This is indicative of the sensitivity of intensity anomalies in signaling the presence of perturbations.

4. Polarization effects

It is straightforward albeit tedious to calculate P, Q, and R branch intensities as a function of detection geometry, excitation scheme, and J^* for the $C^1\Sigma^+ - A'^1\Pi$ and $a^3\Pi_1$ emission observed. We employ the following assumptions: (1) $A^1\Sigma^+$ and $C^1\Sigma^+$ $\Delta J=0$, $\Delta M\neq0$ collisional transitions are neglected; (2) upper and lower state perturbations are ignored; and (3) optical pumping[70,71] of $X^1\Sigma^+$ and $A^1\Sigma^+$ is not considered. First, the $C^1\Sigma^+$ population distribution $P(J^*, M^*)$ as a function of J^*, M^*,

TABLE VIII. J^*, M^* population distributions and calculated $C\,^1\Sigma^+ \rightarrow A'\,^1\Pi(^3\Sigma_0^- \rightarrow a\,^3\Pi_1)$ relative intensities.[a,b]

Excitation[c] scheme	$P(J,M)$[d]
$P(J'')R(J')$	$\frac{(J^2-M^2)^2}{(4J^2-1)^2}$
$P(J'')P(J')$	$\frac{(J+M+2)(J-M+2)(J+M+1)(J-M+1)}{(2J+3)^2(2J+1)(2J+5)}$
$R(J'')R(J')$	$\frac{(J+M-1)(J-M-1)(J^2-M^2)}{(2J-1)^2(2J-3)(2J+1)}$
$R(J'')P(J')$	$\left[\frac{(J+M+1)(J-M+1)}{(2J+1)(2J+3)}\right]^2$

$$I_X^Q(J)^{d,e} = \sum_{M=-J}^{J}\left[\frac{(J^2+J-M^2)}{16J(J+1)}P(J,M)\right], \quad I_Z^Q(J)^{d,e} = \sum_{M=-J}^{J}\frac{M^2P(J,M)}{4J(J+1)}$$

[a]All J'' populations were considered to be equal for the purpose of these calculations since only relative intensities of P, Q, and R branches are considered for one J level. To obtain a more accurate distribution useful in comparing intensities from one J level to another, $P(J,M)$ must be multiplied by a Boltzmann factor.

[b]Results of these calculations are presented in Table VII.

[c]See Table II.

[d]Asterisks indicative of the OODR populated level have been suppressed for conciseness.

[e]Similar expressions for P and R branch fluorescence may be obtained by using Table III.

and excitation scheme must be calculated. This is simply a product of two squared direction cosine matrix elements (see Table III), one for each transition in the OODR excitation of $C\,^1\Sigma^+$; since the laser is always taken to be polarized in the Z direction only $\Delta M = 0$ transitions need be considered. $C\,^1\Sigma^+ \rightarrow A'\,^1\Pi$ or $a\,^3\Pi_1$ P, Q, and R branch intensity polarized in the X, Y, or Z direction is then a summation over M^* of the product of $P(J^*,M^*)$ with the square of the appropriate direction cosine matrix element. In Table VIII we list $P(J^*,M^*)$ for each excitation scheme in Table II and give as an example Q branch intensities. Table VII shows the agreement between the results of these calculations and experiment. Levels with different $|M^*|$ are predicted to be populated unequally resulting in the production of an aligned state[70] and a spatial dependence of the $Q/(P+R)$ ratio. In every case the experimental $Q/(P+R)$ ratios are nearer to unity than the calculated values, indicating a partial equalization of the M^* level populations. This is reasonable if one remembers the assumptions made in these calculations. Ground state levels are depleted at a rate approximately inversely proportional to $|M''|$ (see Table III). This, of course, is the same mechanism by which an aligned upper state is produced; however, if relaxation into these levels is comparable or less than the induced absorption rate, a steady state situation exists where the ground state is said to be optically pumped[70,71] and the upper state alignment will be diminished relative to the situation without optical pumping. In addition, any relaxation among M' or M^* levels will tend to create a $P(J^*,M^*)$ which is independent of M^*.

Neglect of upper and lower state perturbations can only result in discrepancies between observed and calculated $P/(P+R)$ ratios which we have already discussed.

In short, we make the following observations. Anomalously intense $C\,^1\Sigma^+ - a\,^3\Pi_1$ with no $C\,^1\Sigma^+ - a\,^3\Pi_0$ or $a\,^3\Pi_2$ emission suggests an admixture of $^3\Sigma_0^-$ character into $C\,^1\Sigma^+$. PR intensity anomalies sensitively indicate the presence of at least one more Π perturbation in the upper level or one more Σ perturbation in the lower levels. Finally, the fluorescence polarization tells us that OODR pumping produces an aligned upper state.

TABLE IX. $C\,^1\Sigma^+(v=0) - a\,^3\Pi(v)$ bandheads.[a]

	$\tilde{\nu}_{head}(cm^{-1})$			$\lambda_{head}^{air}(Å)$		
v	$^3\Pi_0$	$^3\Pi_1$	$^3\Pi_2$	Π_0	$^3\Pi_1$	$^3\Pi_2$
0	15269	15414	15463	6547.4 (0)[b]	6485.8 (10)	6465.3 (0)
1	14826	14971	15020	6743.0 (0)	6677.8 (4)	6656.0 (0)
2	14387	14532	14581	6948.8 (0)	6879.5 (1)	6856.3 (0)
3	13954	14099	14148	7165.0 (0)	7090.7 (0)	7066.2 (0)

[a]Data used for $a\,^3\Pi$ taken from Ref. 8. The $A'\,^1\Pi \sim a\,^3\Pi_1$ induced asymmetry in the $a\,^3\Pi$ spin–orbit splitting has been taken into account in calculating these bandheads.[8]

[b]Relative intensities are given in parentheses. Zero intensity transitions were *not* observed in this work.

TABLE X. $C\,^1\Sigma^+(v^*=0) - A'\,^1\Pi(v)$ bandheads.[a]

v	$\tilde{\nu}_{head}(cm^{-1})$	$\lambda_{head}^{air}(Å)$
0	15178	6586.7 (10)[b]
1	14735	6784.8 (4)
2	14296	6992.9 (1)
3	13863	7211.6 (0)

[a]Data used for $A'\,^1\Pi$ taken from Ref. 8.

[b]Relative intensities are given in parentheses. Zero intensity transitions were not observed in this work.

IV. CONCLUSION

The importance of using a narrow bandwidth ($\Delta\nu \sim 1$ cm^{-1}) laser in a two photon process cannot be overstated. A narrow frequency source allowed population of a single $C\,^1\Sigma^+$ J^* level which greatly simplified the emission spectrum permitting detection of the low-lying $a\,^3\Pi$ and $A'\,^1\Pi$ states.

It must be admitted that the single laser OODR experiments rely upon fortuitous coincidences; however, these coincidences can be and should be expected in other molecules with a large density of excited vibronic levels in the proper energy range. In fact, similar transitions have been observed in CaCl.[72] Polyatomic molecules should almost invariably exhibit similar phenomena. The single laser experiments are experimentally simpler but two laser OODR spectra are less ambiguous, simpler to interpret, and allow a *systematic* interrogation of a highly excited electronic state.

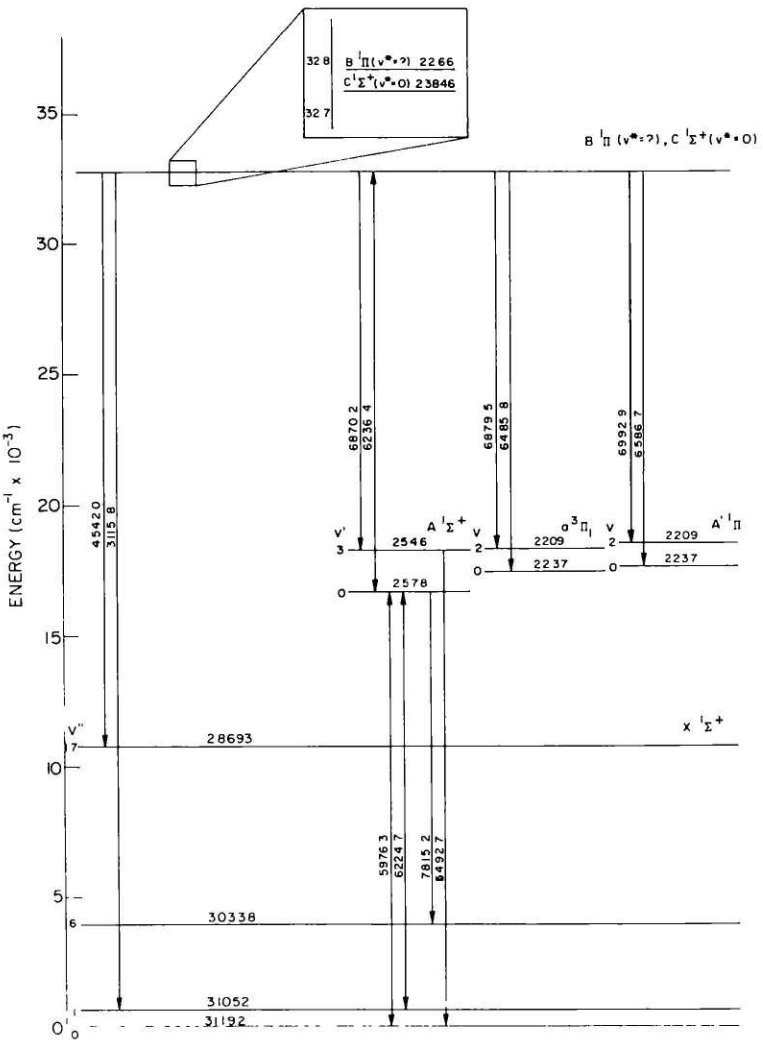

FIG. 9. Known electronic states of BaO illustrating the limits of laser induced fluorescence and absorption observed in this work. For example, the single headed arrows indicate fluorescence was observed from $C\,^1\Sigma^+ (v^* = 0)$ and $B\,^1\Pi (v^* = ?)$ to $X\,^1\Sigma^+ (v'' = 1$ to 17), the double headed arrows indicate that the $A\,^1\Sigma^+ - X\,^1\Sigma^+$ (0,0) and (0,1) bands were laser excited as well as observed in fluorescence. Bandhead positions in air wavelengths are given on each arrow. The number written on a vibrational level is the rotational constant for that level.

This paper reports the first rotational analysis of the $C\,^1\Sigma^+$ and $B\,^1\Pi$ electronic states, participants in the Parkinson[7] band system of BaO. Results of OODR interrogations of higher $C\,^1\Sigma^+$ and $B\,^1\Pi$ vibrational levels as well as new data on $A'\,^1\Pi$ and $a\,^3\Pi$ will be presented subsequently.[4,6]

The $C\,^1\Sigma^+ - a\,^3\Pi$ and $C\,^1\Sigma^+ - A'\,^1\Pi$ band systems could be used to probe the populations of these reservoir states. To aid such investigations, positions of strongest $C-a$ and $C-A'$ bandheads observed here are given in Tables IX and X.

Figure 9 summarizes the experimental work discussed here and the relative energies of all known electronic states of BaO.

Major and as yet elusive goals of BaO OODR spectroscopy are locating the missing $^3\Sigma^+$ state and characterizing the $X\,^1\Sigma^+ \sim a\,^3\Pi$ and $a\,^3\Pi \sim {}^3\Sigma^+$ perturbations. The failure to observe $^3\Sigma^+$ perturbations in $a\,^3\Pi$ and $A'\,^1\Pi$ implies that the $^3\Sigma^+$ state lies above $A\,^1\Sigma^+$, in agreement with a prediction by Michels.[73]

ACKNOWLEDGMENTS

We gratefully acknowledge the experimental aid of J. Manni, P. Brucat, and M. Dulick. Discussions with I.M. Mills and J.C. Lehmann were particularly fruitful in our analysis of P and R branch intensity anomalies. We thank J.G. Pruett, A. Torres-Filho, D. Cossart, M. Horani, J. Rostas, D.J. Eckstrom, J.R. Barker, J.G. Hawley, J.P. Reilly, and D.L. Huestis for conveying results prior to publication. We are especially indebted to J.G. Pruett for insights into the $C\,^1\Sigma^+$ vibrational numbering, interpretation of the single laser OODR bandhead, and a critical reading of this manuscript. We are also grateful to A. Lagerqvist for inspiring Fig. 9.

This research was conducted using equipment pro-

vided by the M.I.T. Chemistry Department, The Research Corporation, and the National Science Foundation, and individual support was provided by the following grants: National Science Foundation 7505959-CHE (RAG), Air Force Office of Scientific Research 76-3056 (RAG, JBK, and RWF), and the petroleum Research Fund 8408-AC5, 6 (JRL).

[1]R. W. Field, G. A. Capelle, and M. A. Revelli, J. Chem. Phys. **63**, 3228 (1975).

[2]Quantum numbers with a double prime, single prime, asterisk, or no prime refer, respectively, to initial level (here $X\,^1\Sigma^+$), intermediate level (here $A\,^1\Sigma^+$), two step excited level ($B\,^1\Pi$ or $C\,^1\Sigma^+$), and final level populated by spontaneous fluorescence.

[3]M. E. Kaminsky, R. T. Hawkins, F. V. Kowalski, and A. L. Schawlow, Phys. Rev. Lett. **36**, 671 (1976). These authors referred to OODR as modulated-population spectroscopy (MPS) type 2.

[4]J. B. Koffend, R. A. Gottscho, and R. W. Field, (to be published).

[5]J. G. Pruett and A. Torres-Filho, Symp. Mol. Spectrosc., 32nd, Columbus, OH, June 1977 (1977).

[6]J. G. Pruett and R. A. Gottscho (to be published).

[7]W. H. Parkinson, Proc. Phys. Soc. **78**, 705 (1961).

[8]R. W. Field, J. Chem. Phys. **60**, 2400 (1974).

[9]R. H. Obenauf, C. J. Hsu, and H. B. Palmer, J. Chem. Phys. **57**, 5607 (1972).

[10]C. J. Hsu, W. D. Krugh, H. B. Palmer, R. H. Obenauf, and C. F. Aten, J. Mol. Spectrosc. **53**, 273 (1974).

[11]H. B. Palmer, W. D. Krugh, and C. J. Hsu, Symp. Combust., 15th, Tokyo, Japan, 1974 (1975), p. 951.

[12]C. J. Hsu, W. D. Krugh, and H. B. Palmer, J. Chem. Phys. **60**, 5118 (1974).

[13]C. R. Jones and H. P. Broida, J. Chem. Phys. **60**, 4369 (1974).

[14]R. W. Field, C. R. Jones, and H. P. Broida, J. Chem. Phys. **60**, 4377 (1974).

[15]D. J. Eckstrom, S. A. Edelstein, and S. W. Benson, J. Chem. Phys. **60**, 2930 (1974); D. J. Eckstrom, S. A. Edelstein, D. L. Huestis, B. E. Perry, and S. W. Benson, J. Chem. Phys. **63**, 3828 (1975).

[16]D. J. Eckstrom, J. R. Barker, J. G. Hawley, and J. P. Reilly, Appl. Opt. **16**, 2102 (1977); D. J. Eckstrom and D. L. Huestis, J. Chem. Phys. (to be published).

[17]F. Engleke, R. K. Sander, and R. N. Zare, J. Chem. Phys. **65**, 1146 (1976).

[18]J. B. West and H. M. Poland, J. Chem. Phys. **66**, 2139 (1977).

[19]D. J. Wren and M. Menzinger, Chem. Phys. Lett. **25**, 378 (1974); D. J. Wren and M. Menzinger, J. Chem. Phys. **63**, 4557 (1975).

[20]D. Husain and J. R. Wiesenfield, J. Chem. Phys. **62**, 2010 (1975).

[21]R. W. Field, C. R. Jones, and H. P. Broida, J. Chem. Phys. **62**, 2012 (1975).

[22]B. G. Wicke, M. A. Revelli, and D. O. Harris, J. Chem. Phys. **63**, 3120 (1975).

[23]M. A. Revelli, B. G. Wicke, and D. O. Harris, Chem. Phys. Lett. **39**, 454 (1976).

[24]R. W. Field, in *Molecular Spectroscopy: Modern Research, Volume II*, edited by K. N. Rao (Academic, New York, 1976), p. 261.

[25]D. J. Benard, W. D. Slafer, and J. Hecht, J. Chem. Phys. **66**, 1012 (1977); D. J. Benard and W. D. Slafer, J. Chem. Phys. **66**, 1017 (1977).

[26]W. Felder, R. K. Gould, and A. Fontijn, J. Chem. Phys. **66**, 3256 (1977).

[27]As pointed out in Ref. 10, any discussion of $a\,^3\Pi$ as a precursor to radiation from $A\,^1\Sigma^+$ must also imply the same role for $A'\,^1\Pi$ since these states are strongly mixed owing to spin–orbit interaction.

[28]T. G. Slanger and G. Black, J. Chem. Phys. **63**, 969 (1975).

[29]M. Lavolée and A. Tramer, Symp. Mol. Struct. Spectrosc., 32nd, Columbus, OH, June, 1977 (1977).

[30]H. E. Radford and H. P. Broida, J. Chem. Phys. **38**, 644 (1963); K. M. Evenson and H. P. Broida, J. Chem. Phys. **44**, 1637 (1966).

[31]W. M. Gelbart and K. F. Freed, Chem. Phys. Lett. **18**, 470 (1973).

[32]A. Lagerqvist, E. Lind, and R. F. Barrow, Proc. Phys. Soc. London Sect. A **63**, 1132 (1950).

[33]M. Hultin and A. Lagerqvist, Ark. Fys. **2**, 471 (1950).

[34]G. Almkvist and A. Lagerqvist, Ark. Fys. **2**, 233 (1950).

[35]J. G. Pruett and R. N. Zare, J. Chem. Phys. **62**, 2050 (1975).

[36]J. C. Wyss and H. P. Broida, J. Mol. Spectrosc. **59**, 235 (1976).

[37]R. W. Field, G. A. Capelle, and C. R. Jones, J. Mol. Spectrosc. **54**, 156 (1975).

[38]G. A. Capelle, H. P. Broida, and R. W. Field, J. Chem. Phys. **62**, 3131 (1975).

[39]CaO $a\,^3\Pi$ has also been observed in single resonance experiments. R. A. Gottscho and R. W. Field (unpublished).

[40]J. B. West, R. S. Bradford, Jr., J. D. Eversole, and C. R. Jones, Rev. Sci. Instrum. **46**, 164 (1975).

[41]D. Jennings and R. Barger, National Bureau of Standards, Boulder, CO.

[42]A. L. Bloom, J. Opt. Soc. **64**, 447 (1974).

[43]H. W. Kogelnik, E. P. Ippen, A. Dienes, and C. V. S. Shank, IEEE J. Quant. Electron. **QE-8**, 373 (1972).

[44]In the absence of an external field we are free to choose a quantization direction coincident with the direction of laser polarization so that no coherent superposition state (a linear combination of different M levels) is created. Each M level has a random phase with respect to every other level and no interference between X and Y polarized fluorescence exists. R. N. Zare, Acc. Chem. Res. **4**, 361 (1974); P. A. Franken, Phys. Rev. **121**, 508 (1969).

[45]D. L. Rousseau and P. F. Williams, Phys. Rev. Lett. **33**, 1368 (1974).

[46]R. H. Barnes, C. E. Moeller, J. F. Kircher, and C. M. Verber, Appl. Phys. Lett. **24**, 610 (1974).

[47]M. D. Danyluk and G. W. King, Chem. Phys. Lett. **43**, 1 (1976).

[48]M. D. Danyluk and G. W. King, Chem. Phys. Lett. **44**, 440 (1976).

[49]M. D. Danyluk and G. W. King, Chem. Phys. **22**, 59 (1977).

[50]G. Herzberg, *Molecular Spectra and Molecular Structure I. Spectra of Diatomic Molecules* (Van Nostrand Reinhold, New York, 1950).

[51]Alternatively, * rotational energies could have been determined from $E(J^*) = 2E_{\text{laser}} + E(X\,^1\Sigma^+, v'', J'')$; however, this introduces a larger uncertainty due to the 1 cm^{-1} laser spectral width.

[52]I. M. Mills, Chim. Pure Appl. **11**, 325 (1965); I. M. Mills, W. L. Smith, and J. L. Duncan, J. Mol. Spectrosc. **16**, 349 (1965); C. diLauro and I. M. Mills, J. Mol. Spectrosc. **21**, 386 (1966).

[53]D. Cossart, M. Horani, and J. Rostas, J. Mol. Spectrosc. **67**, 283 (1977).

[54]T. C. James, J. Mol. Spectrosc. **40**, 545 (1971).

[55]A. Lagerqvist and E. Miescher, Can. J. Phys. **44**, 1525(1966).

[56]J. T. Hougen, Natl. Bur. Stand. U. S. Monogr. **115** (1970).

[57]C. H. Townes and A. L. Schawlow, *Microwave Spectroscopy* (McGraw-Hill, New York, 1955).

[58]Single laser OODR is inherently more sensitive than two laser OODR since the overlap of the "two beams" is perfect

in the former; the collisional satellites shown in Fig. 3 obscure the two laser OODR signal.

[59]The lack of Q branches in the $B\,^1\Pi \leftarrow A\,^1\Sigma^+$ two laser OODR excitation spectrum can be explained in two ways: (1) R_e^{BA} and/or (2) $\langle v_B \mid v_A \rangle$ may be negligible so that only the Σ character of a level is sampled and therefore, only e levels[64] are observed. Q branch transitions would populate f levels which do not exist for a $^1\Sigma^+$ state.

[60]Examination of photoluminescence from these extra lines revealed the same spectra (albeit weaker) as the main lines.

[61]Although $B\,^1\Pi(v)$ lies above $C\,^1\Sigma^+(v^* = 0)$, see Table IV, it is unlikely that the $B\,^1\Pi$ vibrational level perturbing $C\,^1\Sigma^+(v^* = 0)$ is also $v = 0$.

[62]W. E. Wentworth, J. Chem. Ed. **42**, 96 (1965).

[63]D. W. Marquardt, J. Soc. Ind. Appl. Math. **11**, 431 (1963).

[64]J. M. Brown, J. T. Hougen, K. P. Huber, J. W. C. Johns, I. Kopp, H. Lefebvre-Brion, A. J. Merer, D. A. Ramsay, J. Rostas, and R. N. Zare, J. Mol. Spectrosc. **55**, 500 (1975).

[65]Because both $C\,^1\Sigma^+$–$A\,^1\Sigma^+$ and $A\,^1\Sigma^+$–$X\,^1\Sigma^+$ band systems are red degraded and the C–A head is to the red of A–X, a head is formed in the single laser OODR excitation spectrum which is equivalent to the $C\,^1\Sigma^+$–$A\,^1\Sigma^+$ bandhead.

[66]S. E. Johnson, J. Chem. Phys. **56**, 149 (1972).

[67]P. C. Mahanti, Proc. Phys. Soc. London **48**, 51 (1934).

[68]Spacings between rotational lines of different bands depend on J and v.

[69]Spin uncoupling results from the interaction of different $^3\Pi$ spin components via the operator $BJ_\pm S_\mp$.

[70]R. E. Drullinger and R. N. Zare, J. Chem. Phys. **51**, 5532 (1969).

[71]J. C. Lehmann, Comments At. Mol. Phys. **4**, 129 (1973).

[72]P. Domaille and D. Harris (private communication).

[73]H. Michels (private communication).

Appendix 6

The Lowest Energy Excited Electronic State of BaO

J. Chem. Phys. (in press).

The only known triplet state of BaO has been $a^3\Pi$, which was characterized by analysis of $a^3\Pi \sim A^1\Sigma^+$ perturbations appearing in the $A^1\Sigma^+ - X^1\Sigma^+$ band system.[1,2] However, the $z\sigma^2y\sigma x\sigma w\pi^4$ electronic orbital configuration which yields $A^1\Sigma^+$ also gives rise to a $^3\Sigma^+$ state which, in the single configuration approximation and in accordance with Hund's rules,[3,4] is expected to lie below $A^1\Sigma^+$.

This communication reports observation of optical-optical double resonance (OODR) induced $C^1\Sigma^+ \rightarrow {}^3\Sigma^+$ photoluminescence. Analysis of these emission spectra, which include $^3\Sigma^+ \sim A'^1\Pi$ spin-orbit perturbations, indicates that this $^3\Sigma^+$ state is the lowest energy excited state of BaO. In accordance with these observations, the lowest triplet states of BaO are renamed $a^3\Sigma^+$ and $b^3\Pi$ (formerly known as $a^3\Pi$).

Emission into $b^3\Pi$(v = 0 to 11), $A'^1\Pi$(v = 0 to 10), $A^1\Sigma^+$ (v=0 to 9), and $X^1\Sigma^+$ (v=0 to 24) is also observed. A more complete manuscript which will include transition line frequencies as well as a detailed description of the least squares, deperturbation analysis procedure is in preparation.[5]

The advantages of OODR over traditional and single laser spectroscopy have been amply demonstrated.[6-11] Recently,[11] OODR induced BaO $C^1\Sigma^+ \rightarrow b^3\Pi$, $A'^1\Pi$ emission was observed using broadband ($\Delta\nu_{FWHM} \sim 1\ cm^{-1}$) lasers to pump $A^1\Sigma^+ \leftarrow X^1\Sigma^+$ and then probe $C^1\Sigma^+ \leftarrow A^1\Sigma^+$; no $C^1\Sigma^+ \rightarrow a^3\Sigma^+$ emission was detectable. This emission is now observed as a direct consequence of using narrow line width

($\Delta\nu_{FWHM} \sim 1$ MHz), frequency stabilized lasers (Coherent Radiation Model CR599, 50 mW single mode power; Exciton rhodamine 590 dye).

The instantaneous spectrum of a broadband dye laser consists of a frequency comb corresponding to longitudinal cavity modes. Because of mode competition as well as thermal and mechanical fluctuations, these modes lase erratically and drift in frequency. With such lasers, OODR results only when there is a fortuitous coincidence of modes from the two lasers each capable of exciting identical velocity groups and connected rovibronic transitions. A 50-fold increase in $C^1\Sigma^+ \rightarrow X^1\Sigma^+$ UV fluorescence intensity as well as $C^1\Sigma^+ \rightarrow a^3\Sigma^+$ emission resulting from more efficient pumping is obtained with single mode, stabilized lasers.

BaO was prepared by resistively melting Ba metal (Alfa 99.999% purity), entraining it in Ar (Airco, 99.998% purity), and reacting with CO_2 (Airco, 99.8% purity). Typical steady state pressures were 1.0 torr Ar, 5×10^{-2} torr CO_2 and 1×10^{-4} torr Ba. Only $^{138}Ba^{16}O$ was selected by the pump laser. The experimental details are described more completely elsewhere.[8,12,13]

OODR induced fluorescence was detected perpendicular to the laser propagation direction by focussing the fluorescence image onto the slit of a Spex 1802 monochromator (1200 grooves /mm, blazed at 1.2μ) equipped with an RCA 31034A photomultiplier tube operated at-1400VDC and cooled to -20.0°C mounted on the exit slit.

Five $C^1\Sigma^+ \rightarrow a^3\Sigma^+$ bands were observed in fluorescence; two $a^3\Sigma^+$ vibrational levels were detected only via perturbations in $C^1\Sigma^+ \rightarrow A'^1\Pi$ emission spectra. Calculated $C^1\Sigma^+ - a^3\Sigma^+$ bandheads[14] and measured $a^3\Sigma^+$

vibrational energies and rotational constants derived from bands observed are given in Table I. Table II compares $a^3\Sigma^+$ and $A^1\Sigma^+$ equilibrium vibrational and rotational constants.[2,17]

Assignment of the bands listed in Table I and illustrated in Fig. 1 as $C^1\Sigma^+ \rightarrow a^3\Sigma^+$ emission was based on three factors: 1) the pattern of emission is that corresponding to a $^1\Sigma^+ \rightarrow {}^3\Sigma^+$ transition[15] (see Fig. 1); assignment to none of the previously known lower states ($X^1\Sigma^+$, $A^1\Sigma^+$, $b^3\Pi$, or $A'^1\Pi$) could account for the observed fluorescence structure or frequencies[5,16]; and 3) the pattern of perturbations in $C^1\Sigma^+$ - $A'^1\Pi$ and $C^1\Sigma^+$ - $a^3\Sigma^+$ spectra are identically those expected for $^3\Sigma^+ \sim {}^1\Pi$ spin-orbit interactions.[5,18] Rotational assignments were made from known pump and probe transitions.[2,8,16] Vibrational assignments were made by matching observed with calculated vibrational variations of $a^3\Sigma^+ \sim A'^1\Pi$ interaction matrix elements.[1,19-22] Vibronic matrix elements are factored into rotational, vibrational, and electronic factors:

$$\langle A'^1\Pi, v' | H^{SO} | v, a^3\Sigma^+ \rangle = H_{el}^{SO} \langle v' | v \rangle \qquad (1)$$

where H^{SO} is the spin-orbit operator, H_{el}^{SO} is a constant electronic factor, and $\langle v|v' \rangle$ is a calculated vibrational overlap integral. $a^3\Sigma^+ \sim A'^1\Pi$ vibrational overlaps were calculated for a family of $a^3\Sigma^+$ potential energy curves (each having vibrational energies and rotational constants identical with those in Table II). The $a^3\Sigma^+$ potential energy function resulting in a constant H_{el}^{SO} was adopted (Table III) and yields the equilibrium constants of Table II. The validity of this method is discussed in Refs. 20 and 22.

Table I: $C^1\Sigma^+ - a^3\Sigma^+$ Bandheads[a] and $a^3\Sigma^+$ Vibrational Constants

Band	Head		$E^b(a^3\Sigma^+)$	$B(a^3\Sigma^+)$
(v_C, v_a)	$\nu(cm^{-1})$	$\lambda_{air}(Å)$		
(3,6)	14 813	6 749.0	19 245.4 (06)[c]	0.2505 (04)
(3,7)	14 362	6 960.7	19 696.1 (06)	0.2487 (04)
(3,8)	13 916	7 184.2	20 143.5 (12)	0.2479 (10)
(2,11)	12 166	8 217.1	21 461.5 (06)	0.2425 (04)
(2,12)	11 735	8 519.2	21 893.4 (06)	0.2414 (04)

[a]Calculated (see Ref. 15, p. 171) from $a^3\Sigma^+$ constants in Table II and $C^1\Sigma^+$ constants from Ref. 16. To precision quoted the ^RR and ^RQ heads would be unresolvable.

[b]Relative to $X^1\Sigma^+$ (v" = 0, J" = 0) and equal to energy of J = 0 level minus 2B.

[c]Uncertainties in the last digit corresponding to one standard deviation are given in parentheses.

Table II: BaO $a^3\Sigma^+$ and $A^1\Sigma^+$ Spectroscopic Constants

	$a^3\Sigma^+$		$A^1\Sigma^+$
T_e	16 558.	(10)[a]	16 807.20[b]
ω_e	477.0	(20)	499.7[b]
$\omega_e x_e$	1.88	(12)	1.64[b]
B_e	0.2602	(08)	0.25832[c]
α_e	0.00152	(08)	0.001070[c]

[a] Uncertainties of one standard deviation in the last digit are enclosed in parentheses.

[b] From Ref. 2.

[c] From Ref. 15.

Figure 1:

$C^1\Sigma^+ - a^3\Sigma^+$ (2,12) emission spectrum and schematic energy level diagram for J = 16. The splittings between levels for given N result from spin-spin and second order spin-orbit interactions; a discussion of these is deferred to Ref. 5. See Ref. 15 for definitions of spectroscopic notation.

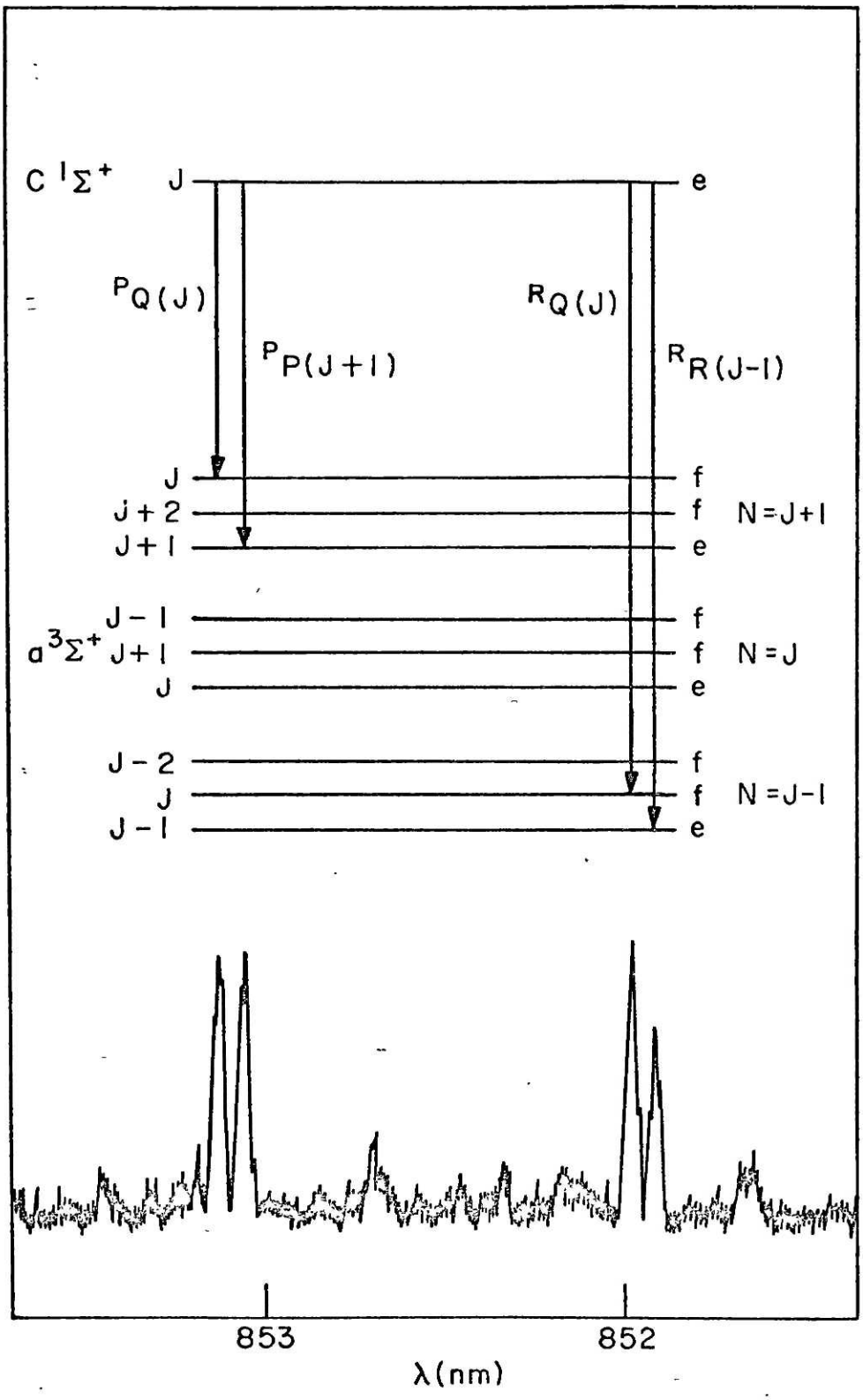
C $^1\Sigma^+$
J
e
$P_Q(J)$
$P_P(J+1)$
$R_Q(J)$
$R_R(J-1)$
J
J + 2
J + 1
f
f
e
N = J+1
J - 1
J + 1
J
$a^3\Sigma^+$
f
f
e
N = J
J - 2
J
J - 1
f
f
e
N = J-1
853
852
λ(nm)

Table III. $A'^1\Pi \sim a^3\Sigma^+$ Spin-Orbit Perturbations[a]

$A'^1\Pi(v)$	$a^3\Sigma^+(v)$	$\lvert H^{SO}\rvert$[b]	H_{el}^{SO} a = 1	a = 2	a = 3	a = 4
0	a	42 (06)	83 (12)	76 (11)	84 (12)	106 (15)
1	a + 1	25 (10)	306 (122)	105 (42)	58 (23)	52 (21)
4	a + 4	21 (02)	143 (14)	63 (06)	88 (08)	1750 (170)
5	a + 5	21 (02)	414 (39)	87 (08)	66 (08)	133 (13)
6	a + 6	9 (03)	45 (15)	94 (31)	30 (10)	33 (11)
7	a + 7	2.2 (10)	8 (4)	39 (18)	10 (05)	7 (03)
		$\langle H_{el}^{SO}\rangle$[c] =	29 (52)	71 (14)	42 (33)	19 (106)
			reject	adopt	alternate	reject

[a]Uncertainties in the last digit of one standard deviation are given in parentheses.

[b]$\lvert H^{SO}\rvert \equiv \lvert\langle A'^1\Pi, v' \lvert H^{SO} \rvert v, a^3\Sigma^+\rangle\rvert$

[c]Weighted average

The BaO $A^1\Sigma^+$ - $a^3\Sigma^+$ vibrationless (v = 0) energy splitting (249 cm^{-1}) is comparable to the deperturbed $A'^1\Pi$ - $b^3\Pi$ splitting (151 cm^{-1})[1] as expected when the single configuration approximation is valid and the $y\sigma$, $w\pi$ orbitals are comprised mostly of O 2p and $x\sigma$ is mostly comprised of Ba 6s.[1,3]

Acknowledgements

The experimental assistance of Dr. Roger Bacis and Mr. Paul Weiss are gratefully acknowledged. Many thanks go to Mr. Warren Weintraub for his expert instruction on the use of the CR599 dye laser. I am especially indebted to Professor Robert Field for originally suggesting this experiment as well as for many enlightening discussions. This research was supported by grants from the National Science Foundation (CHE-7505959 and CHE-7519410).

1. R.W. Field, J. Chem. Phys. 60, 2400 (1974).
2. A. Lagerqvist, E. Lind, and R.F. Barrow; Proc. Phys. Soc. A 63, 1132 (1950).
3. J. Raftery, P.R. Scott, W.G. Richards; J. Phys. B 5, 1293 (1972).
4. F. Hund, Z. Phys. 33, 345 (1925).
5. R.A. Gottscho, J.B. Koffend, and R.W. Field, "The Low-Lying States of BaO" (in preparation).
6. R.H. Barnes, C.E. Moeller, J.F. Kircher, and C.M. Verber, Appl. Phys. Lett. 24, 610 (1974).
7. D.L. Rousseau and P.F. Williams, Phys. Rev. Lett. 33, 1368 (1974).
8. R.W. Field, G.A. Capelle, and M.A. Revelli; J. Chem. Phys. 63, 3228 (1975).
9. M.D. Danyluk and G.W. King, Chem. Phys. Lett. 43, 1 (1976); Chem. Phys. Lett. 44, 440 (1976); Chem. Phys. 22, 59 (1977).
10. M.E. Kaminsky, R.T. Hawkins, F.V. Kowalski, and A.L. Schawlow, Phys. Rev. Lett. 36, 67 (1976).
11. R.A. Gottscho, J.B. Koffend, R.W. Field, and J.R. Lombardi; J. Chem. Phys. 68, 4110 (1978).
12. C.R. Jones and H.P. Broida, J. Chem. Phys. 60, 4369 (1974).
13. J.B. West, R.S. Bradford, Jr., J.D. Eversole, and C.R. Jones; Rev. Sci. Instrum. 46, 164 (1975).
14. Bandheads are not observed since emission comes from a single $C^1\Sigma^+$ rovibronic level for each pump and probe laser frequency. There is no evidence of $C^1\Sigma^+$ relaxation.
15. G. Herzberg, Molecular Spectra and Molecular Structure I. Spectra of Diatomic Molecues. (Van Nostrand, Reinhold Co., New York, 1950).

16. R.A. Gottscho, P.S. Weiss, J.G. Pruett, "The High Energy States of BaO", (in preparation).

17. R.W. Field, A.D. English, T. Tanaka, D.O. Harris, and D.A. Jennings; J. Chem. Phys. 59, 2191 (1973).

18. I. Kovacs, Rotational Structure in the Spectra of Diatomic Molecules, (American Elsevier, New York, 1969).

19a. R.W. Field, S.G. Tilford, R.A. Howard, and J.D. Simmons; J. Mol. Spectrosc. 44, 347-382 (1972).

19b. R.W. Field, B.G. Wicke, J.D. Simmons, and S.G. Tilford, J. Mol. Spectrosc. 44, 383-399 (1972).

20. J.A. Hall, J. Schamps, J.M. Robbe, and H. Lefebvre-Brion; J. Chem. Phys. 59, 3271-3283 (1973).

21a. D. Cossart and T. Bergeman, J. Chem. Phys. 65, 5462 (1976).

21b. J.M. Robbe and J. Schamps, J. Chem. Phys. 65, 5420 (1976).

22. J. Schamps, J. Quant. Spectrosc. Radiat. Transfer 17, 685 (1977).

Appendix 7

Reprinted from Chem. Phys. Lett. 60, 65-68 (1978).

ASSIGNMENT OF EXTRA LINES IN A PERTURBED BAND SPECTRUM USING POWER BROADENED LINE WIDTHS

Richard A. GOTTSCHO and Robert W. FIELD
Department of Chemistry, Massachusetts Institute of Technology, Cambridge, Massachusetts 02139, USA

Received 4 August 1978

Sub-Doppler optical–optical double resonance (OODR) spectroscopy using two tuneable, 1 MHz width, dye lasers is shown to enehance detection, assignment, and frequency measurement of extra lines in perturbed band spectra. Perturbations of the BaO $C\,^1\Sigma^+$ ($v = 3, J = 50$) level are recognized by the appearance of narrow ($\Delta\nu \approx 60$ MHz) extra lines.

The regular patterns exhibited by band spectra are often interrupted by missing, shifted, and extra lines. These anomalies are collectively labelled as perturbations and result from the interaction of two or more Born–Oppenheimer basis functions. This interaction is characterized by mixing of basis functions and repulsion of unperturbed energy levels.

Transitions involving levels which have borrowed oscillator strength via the perturbation mechanism are called extra lines. Though perturbation induced shifts of main lines (allowed transitions in the absence of perturbation) provide information about the perturbing state structure, assignment of extra lines is a more direct and precise means by which the constants of the perturber and the value of the perturbation matrix element may be determined.

Detection of extra lines is often hampered by their inherent weakness and by overlapping with other transitions. Described below is a sub-Doppler optical–optical double resonance (OODR) experiment by which extra lines may be easily recognized by the narrowness of their power broadened widths despite their weak intensities and in the presence of overlapping transitions.

The essential experimental details have been described by several authors [1–5]. Two copropagating, single mode, frequency stabilized ($\Delta\nu_{\mathrm{fwhm}} \approx 1$ MHz, Coherent Radiation model 599-21) rhodamine 6G dye lasers are used to sequentially pump the BaO $A\,^1\Sigma^+ \leftarrow X\,^1\Sigma^+$ and then probe the $C\,^1\Sigma^+ \leftarrow A\,^1\Sigma^+$ band systems (fig. 1) [6–9]. BaO is produced in an Ar + Ba + CO_2 → BaO + CO + Ar flame. This system is described

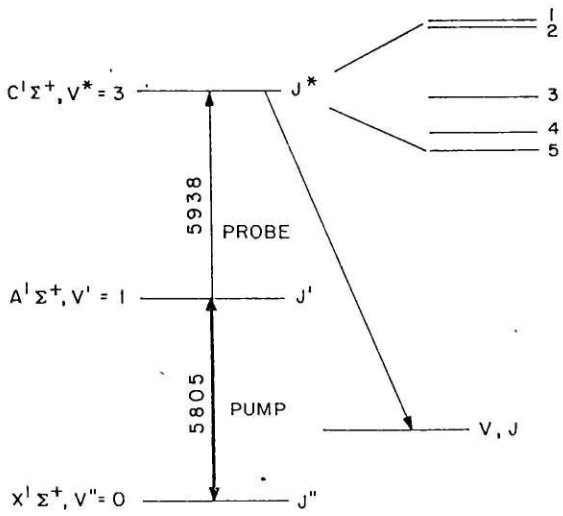

Fig. 1. Energy level diagram illustrating OODR excitation scheme ($v^*, J^* \leftarrow v', J' \leftarrow v'', J''$). $C\,^1\Sigma^+(v^*, J^*) \rightarrow X\,^1\Sigma^+(v, J)$ UV emission is detected as the probe laser is scanned. A–X(1, 0) and C–A(3, 1) bandheads (air wavelengths in nm) are indicated for the pump and probe transitions. For $C\,^1\Sigma^+$ the energy level structure for $v^* = 3, J^* = 50$ is expanded and drawn to scale illustrating the five perturbing energy levels detected.

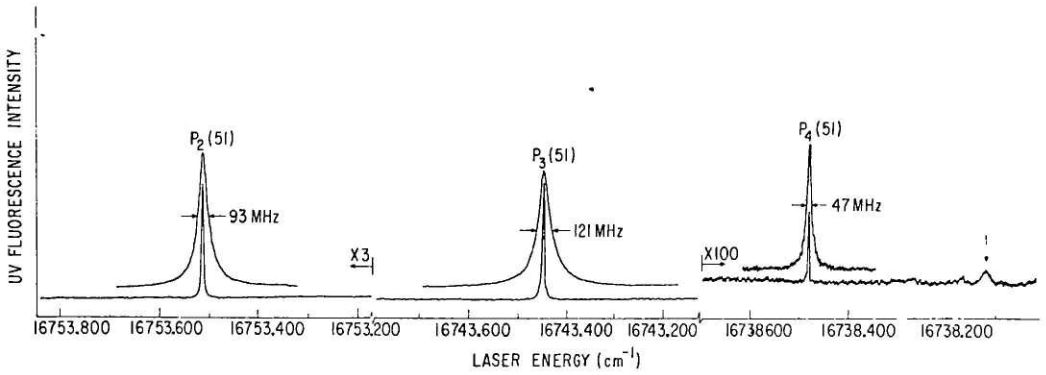

Fig. 2. OODR excitation spectrum $A\,^1\Sigma^+ \leftarrow X\,^1\Sigma^+$ (1, 0) R(50) is pumped, $C\,^1\Sigma^+ \leftarrow A\,^1\Sigma^+$ (3, 1) is probed while $C\,^1\Sigma^+ \rightarrow X\,^1\Sigma^+$ UV fluorescence is recorded. Shown are the C ← A P(51) main line and two of the four extra lines, each peak is expanded to further illustrate line width variations. The unassigned collisional satellite marked with an arrow is equally intense as the P_4 (51) extra line.

elsewhere [10]. As the probe laser is scanned, $C\,^1\Sigma^+ \rightarrow X\,^1\Sigma^+$ ultraviolet fluorescence intensity is recorded to produce an OODR excitation spectrum. A single $A\,^1\Sigma^+$ rovibronic level is prepared possessing only a narrow velocity distribution along the laser propagation direction. This non-Boltzmann velocity distribution is sampled by the probe laser [11–13] and displayed as the OODR line shape (fig. 2).

Both lasers are focussed with a 30.5 cm focal length lens so that the intensity in the observation region is approximately 10^8 W/m^2. The observed main line widths are 123 ± 3 MHz at 1 torr Ar; extra line widths range from 46 to 93 MHz (see table 1).

The OODR line shapes are a function of the laser

Table 1
Transition frequencies, term values, relative intensities, and line widths for $J = 50$ main and extra lines in the $C\,^1\Sigma^+$–$A\,^1\Sigma^+$ (3,1) band of BaO. Pressure ≈1 torr Ar, laser intensity ≈10^8 W/m^2. Uncertainties in parentheses are one standard deviation estimates

Transition [a]	Transition frequency [b] (cm^{-1})	Upper level term value [b] (cm^{-1})	$\Delta\nu$fwhm (MHz)	$(I_j/I_3)^{1/2}$	W [d]
$P_5(51)$	16735.989 (6)	34631.20 (2)	δ [c]	δ	δ
$R_5(49)$	16787.436 (3)	34631.20 (2)	52 (6)	0.037 (7)	0.14 (5)
$P_4(51)$	16738.485 (3)	34633.70 (2)	47 (6)	0.071 (7)	0.09 (4)
$R_4(49)$	16789.933 (3)	34633.70 (2)	46 (6)	0.035 (7)	0.07 (3)
$P_3(51)$	16743.448 (3)	34638.66 (2)	121 (3)	1.0	1.0
$R_3(49)$	16794.898 (3)	34638.66 (2)	125 (3)	1.0	1.0
$P_2(51)$	16753.500 (3)	34648.72 (2)	93 (3)	0.520 (30)	0.65 (10)
$R_2(49)$	16804.947 (3)	34648.71 (2)	91 (3)	0.490 (25)	0 60 (9)
$P_1(51)$	16754.467 (3)	34649.68 (2)	54 (6)	0.200 (10)	0.17 (3)
$R_1(49)$	16805.937 (6)	34649.70 (2)	δ	δ	δ

a) Transitions are labelled as P_j $(J + 1)$ and R_j $(J - 1)$ where J is the $C\,^1\Sigma^+$ ($v = 3$) rotational quantum number and j is a relative energy index. $j = 3$ corresponds to main line transitions which were assigned as such on the basis of their intensities and widths.

b) See ref. [8]. Term values are relative to $^{138}Ba^{16}O\ X\,^1\Sigma^+$ ($v'' = 0, J'' = 0$) and are less precise than the corresponding transition frequencies owing to less precise measurements of the intermediate $A\,^1\Sigma^+$ levels [6]. The difference between main and extra term values is nonetheless precise to ±0.004 cm^{-1}.

c) δ denotes a blended line from which accurate intensity and width measurements could not be made.

d) See text for definition. W is determined from linewidths after correcting for residual broadening and should be identical to the intensity ratio in the preceding column.

line width, the A $^1\Sigma^+$ and C $^1\Sigma^+$ spontaneous radiation lifetimes, collisions of BaO with Ar [14], laser power, interference between two-photon (Raman-type) excitation via a virtual level and step-wise (resulting in population of A $^1\Sigma^+$) transition probabilities [15,16]. Here, the radiative lifetimes of intermediate, perturbed, and perturbing states are long compared with the light induced (Rabi) oscillation period:

$$\tau_{\text{rad}} \gg h/\mu E \,. \tag{1}$$

Thus the observed line shapes are dominated by saturation broadening and interference between two-photon and step-wise transition amplitudes [15,16]. The latter effect is only weakly power dependent [15] and is neglected. Pressure broadening, natural lifetime broadening, and finite laser width result in a power independent width of ≈40 MHz at 1 torr Ar.

As defined above, extra lines are partially forbidden transitions and, therefore, exhibit *narrower* line widths than their main line counterparts when stimulated by an intense, resonant, electromagnetic field (providing eq. (1) is satisfied) [‡]. In this fashion sub-Doppler OODR provides a sensitive and unambiguous means by which extra lines can be identified as such.

Experimentally, two lines of equal intensity but with different widths will not be detected with equal sensitivity: the narrower, taller line is more easily observed. In the OODR excitation spectrum there are many lines. In addition to the direct main and extra transitions, lines result from collisional relaxation in the intermediate state [14]. These collisional satellite lines are significantly broader (from 0.2 to 1 GHz) than the direct transitions owing to partial velocity randomization upon relaxation [14]. Comparing a weak extra line ($\Delta\nu \approx 60$ MHz, see table 1) with a collisional satellite ($\Delta\nu \approx 300$ MHz) of equal integrated intensity, the extra line is necessarily five times *higher* and is thus more readily detected and immediately recognized as an extra line (see fig. 2).

Theoretically, extra line widths and intensities may be understood in terms of the perturbation induced mixing of basis functions. If the upper state is perturbed but the lower state is not,

$$|U_j\rangle = \sum_{i=1}^{m} c_{ij}|\chi_i\rangle \,, \tag{2a}$$

$$\langle U_j|\mu|L\rangle = \sum_{i=1}^{m} c_{ij}\langle\chi_i|\mu|L\rangle \,, \tag{2b}$$

where $|U_j\rangle$ is the jth upper eigenstate written as a linear combination of m $|\chi_i\rangle$ basis functions as prescribed by the c_{ij} mixing coefficients. $|L\rangle$ is the lower eigenstate. If all $\langle\chi_i|\mu|L\rangle = 0$ except for $i = 3$ ($i = 3$ is chosen for reasons given in table 1),

$$\langle U_j|\mu|L\rangle = c_{3j}\langle\chi_3|\mu|L\rangle \,. \tag{3}$$

$|\chi_3\rangle$ is the perturbed (main) basis state; all other $|\chi_{i\neq 3}\rangle$'s are perturbing (extra) states. The jth extra to main power broadened line width ratio is simply given by:

$$\Delta\nu_j^{\text{p}}/\Delta\nu_3^{\text{p}} = |c_{3j}|/|c_{33}| \,. \tag{4}$$

Similarly, the ratio of the integrated line intensities, proportional to $|\langle U_j|\mu|L\rangle|^2$ is given by:

$$I_j/I_3 = (|c_{3j}|/|c_{33}|)^2 = (\Delta\nu_j^{\text{p}}/\Delta\nu_3^{\text{p}})^2 \,. \tag{5}$$

Perturbations in BaO C $^1\Sigma^+$ ($v = 3$) are considered. Four extra lines are observed at $J' = 50$ in both P ($\Delta J = -1$) and R ($\Delta J = +1$) branches for excitation into the C $^1\Sigma^+$ ($v = 3$) level. Each extra line observed in the P branch is verified by finding the corresponding line in the R branch with comparable intensity and width and identical term energy (see table 1). At least three different perturbing vibronic levels are needed to account for the positions and intensities of main and extra lines [8]. Fig. 2 illustrates the variation in intensities and widths of P branch main and extra transitions; table 1 summarizes the observations.

Because of the residual ≈40 MHz pressure and Doppler width, the simple relationship between line width and intensity ratios [eq. (5)] is not valid for weak, narrow extra lines. The observed line widths are approximated by:

[‡] Kaminsky et al. [5] report broader lines at a perturbation in Na_2 A $^1\Sigma_u^+$ ($v' = 22$, $J' = 14$) in a similar sub-Doppler experiment the perturbed line width observed was 500 MHz while other comparable line widths ranged from 60 to 150 MHz. This is clearly a case where eq. (1) is not satisfied for the perturbing state which is most likely predissociated and short-lived so that the observed width in this case is a measure of the accidental predissociation lifetime $\tau \approx 4.5 \times 10^{-10}$ s.

$$\Delta\nu_j = c_{3j}\Delta\nu_3^p/c_{33} + \Delta\nu^r , \quad (6)$$

where $\Delta\nu_j$ is the total observed line width for transitions into the jth eigenstate and $\Delta\nu^r$ is the residual line width which is assumed constant for all basis states.

To compare line width and line intensity ratios, it is necessary to correct for residual power-independent broadening. $\Delta\nu^r$ could be subtracted from both $\Delta\nu_j$ and $\Delta\nu_3$; however, when $\Delta\nu_j \approx \Delta\nu^r$ the error associated with their difference is approximately twice the magnitude of this difference. A more precise measure of the mixing coefficient ratio is obtained from the empirical quantity W:

$$W \equiv 1 - (\Delta\nu_3 - \Delta\nu_j)/(\Delta\nu_3 - \Delta\nu^r) , \quad (7)$$

where $W \approx (I_j/I_3)^{1/2} \approx |c_{3j}/c_{33}|$. W and $(I_j/I_3)^{1/2}$ (table 1) agree within the relatively large experimental errors. As the ratio of c_{3j} to c_{33} approaches zero, the perturbation mixing and resultant extra line intensity become weak. However, extra lines are nonetheless sensitively detected because of their unusual narrowness and height. As the c_{3j} to c_{33} ratio approaches unity, main and extra lines become indistinguishable.

If any of the $\langle\chi_{j\neq 3}|\mu|L\rangle$ matrix elements assumed zero in eq. (3) are non-negligible, the relationship between mixing coefficients and intensities becomes more complicated: quantum mechanical interference between the different transition moments can be expected.

Because of large experimental errors associated with measuring widths and intensities, these quantities provide little precise quantitative information about perturbation mixing coefficients. This is of no consequence, however, because mixing coefficients are best determined from level shifts. Extra and main line transition frequencies to only 0.1 cm^{-1} are sufficient to more accurately determine interaction matrix elements and mixing coefficients than linewidth or radiative lifetime measurements; the lines reported in table 1 are measured with precision of 3×10^{-3} cm^{-1}. The sub-Doppler width of OODR extra lines not only facilitates their detection and assignment but also enhances the precision of subsequent frequency measurements.

The experimental assistance of Dr. Roger Bacis and the expert instruction on the use of the CR599-21 dye laser by Mr. Warren Weintraub are gratefully acknowledged. This work was supported in part by grants from the National Science Foundation (CHE-7505959) and the Air Force Office of Scientific Research (AFOSR-76-3056).

References

[1] M.D. Danyluk and G.W. King, Chem. Phys. Letters 43 (1976) 1; 44 (1976) 440; Chem. Phys. 22 (1977) 59.
[2] D.L. Rousseau and P.F. Williams, Phys. Rev. Letters 33 (1974) 1368.
[3] R.H. Barnes, C.E. Moeller, J.F. Kircher and C.M. Verber, Appl. Phys. Letters 24 (1974) 610.
[4] R.W. Field, G.A. Capelle and M.A. Revelli, J. Chem. Phys. 63 (1975) 3228.
[5] M.E. Kaminsky, R.T. Hawkins, F.V. Kowalski and A.L. Schawlow, Phys. Rev. Letters 36 (1976) 671.
[6] A. Lagerqvist, E. Lind and R.F. Barrow, Proc. Phys. Soc (London) A63 (1950) 1132.
[7] R.A. Gottscho, J.B. Koffend, R.W. Field and J.R. Lombardi, J. Chem. Phys. 68 (1978), to be published
[8] R.A. Gottscho and J.G. Pruett, in preparation.
[9] J.G. Pruett and A. Torres-Filho, 32nd Symposium on Molecular Spectroscopy, Columbus, Ohio, 1977 (1977)
[10] J.B. West, R.S. Bradford Jr., J.D. Eversole and C.R. Jones, Rev. Sci. Instr. 46 (1975) 164.
[11] W.D. Phillips and D. Pritchard, Phys. Rev. Letters 33 (1974) 1254.
[12] J.L. Kinsey, J. Chem. Phys. 66 (1977) 2560.
[13] S.M. Freund, J.W.C. Johns, A.R.W. McKellar and T. Oka, J. Chem. Phys. 59 (1973) 3445.
[14] R.A. Gottscho, R.W. Field and R. Bacis, to be published
[15] I.M. Beterov, Yu.A. Matyugin and V.P. Chebotaev, Zh. Eksperim. i Teor. Fiz. 64 (1973) 1495 [English transl Soviet Phys. JETP 37 (1973) 756].
[16] M.S. Feld, Fundamental and Applied Laser Physics, Proceedings of the Esfahan Symposium, August 29 – September 5, 1971, eds. M.S. Feld, A. Javan and N. Kurnit (Wiley, New York, 1973) p. 369.